TECHNISCHE UNIVERSITÄT DARMSTADT
INSTITUT FÜR MASSIVBAU

51

Dominik Müller

Probabilistic Assessment of Existing Masonry Structures

The Influence of Spatially Variable Material Properties and a Bayesian Method for Determining Structure-Specific Partial Factors

DISSERTATION

Heft 51 **Darmstadt 2022**

Probabilistic Assessment of Existing Masonry Structures

The Influence of Spatially Variable Material Properties and a Bayesian Method for Determining Structure-Specific Partial Factors

Vom Fachbereich Bau- und Umweltingenieurwissenschaften
der Technischen Universität Darmstadt
zur Erlangung des akademischen Grades eines
Doktor-Ingenieurs (Dr.-Ing.)
genehmigte

DISSERTATION

von

Dominik Müller M.Sc.

aus
Usingen

D 17

Darmstadt 2022

Referent:	Prof. Dr.-Ing. Carl-Alexander Graubner
Korreferent:	Prof. dr. ir. Robby Caspeele
Korreferent:	Prof. Dr.-Ing. Jens Schneider
Tag der Einreichung:	26. Oktober 2021
Tag der mündlichen Prüfung:	31. Januar 2022

Herausgeber:

Prof. Dr.-Ing. Carl-Alexander Graubner

Anschrift:

Technische Universität Darmstadt
Institut für Massivbau
Franziska-Braun-Straße 3
64287 Darmstadt

https://www.massivbau.tu-darmstadt.de

Müller, Dominik:

Probabilistic Assessment of Existing Masonry Structures
The Influence of Spatially Variable Material Properties and a
Bayesian Method for Determining Structure-Specific Partial Factors

Dissertation // Institut für Massivbau, Technische Universität Darmstadt; Heft 51

ISBN 978-3-942886-28-4

Online veröffentlicht bei TUprints

URN: urn:nbn:de:tuda-tuprints-229972
URI: https://tuprints.ulb.tu-darmstadt.de/id/eprint/22997

VORWORT

Die vorliegende Arbeit entstand während meiner Tätigkeit als wissenschaftlicher Mitarbeiter am Institut für Massivbau der Technischen Universität Darmstadt. Die Förderung des Forschungsprojektes „Modifizierte Teilsicherheitsbeiwerte für Mauerwerkswände im Bestand“ durch das Bundesinstitut für Bau-, Stadt- und Raumforschung im Auftrag des Bundesministeriums des Innern, für Bau und Heimat aus Mitteln des Innovationsprogramms Zukunft Bau hat wesentliche Teile dieser Arbeit ermöglicht.

Meinem Doktorvater Herrn Prof. Dr.-Ing. Carl-Alexander Graubner danke ich herzlich für das mir entgegengebrachte Vertrauen, die wertvollen fachlichen Diskussionen und Impulse bei der Erstellung der Arbeit sowie die vielen Möglichkeiten, die er mir im Rahmen meiner Tätigkeit am Institut für Massivbau eröffnet hat.

Herrn Prof. dr. ir. Robby Caspeele und Herrn Prof. Dr.-Ing. Jens Schneider danke ich herzlich für das Interesse an meiner Arbeit und die Übernahme des Korreferates.

Für die kritische Durchsicht der Entwurfsfassung dieser Arbeit und spannende wissenschaftliche Diskussionen danke ich den Herren Dr.-Ing. habil. Ngoc Linh Tran, Dr.-Ing. Tilo Proske, Dr.-Ing. Valentin Förster, Dr.-Ing. Redouan El Ghadioui, Lukas Bujotzek M.Sc., Maximilian Brinkmann M.Sc. und Dominik Hiesch M.Sc.

Dank gilt auch den Prüflaboren, die mir Daten aus der Materialprüfung von Bestandsmauerwerk zur Verfügung gestellt haben. Für den damit verbundenen fachlichen Austausch sei insbesondere Herrn Dipl.-Ing. Jonny Henkel und Herrn Dipl.-Ing. (FH) Maik Kramer gedankt.

Danken möchte ich zudem den Mitarbeitern des Forschungs- und Prüflabors für Massivbau, ohne die die experimentellen Untersuchungen nicht möglich gewesen wären, sowie allen Studierenden, die mich im Rahmen ihrer Abschlussarbeiten bei der Forschung unterstützt haben.

Meine Zeit am Institut für Massivbau habe ich sehr genossen. Allen Kolleginnen und Kollegen danke ich daher für das freundschaftliche und hilfsbereite Miteinander sowie für die vielen schönen Erlebnisse, die mir immer in guter Erinnerung bleiben werden.

Zu guter Letzt danke ich meinen Eltern Simone und Bernd von Herzen für ihre liebevolle Unterstützung und den immer vorhandenen Rückhalt. Auch meiner lieben Freundin Julia danke ich, denn ohne ihre große Geduld mir gegenüber wäre die Erstellung dieser Arbeit so nicht möglich gewesen.

Darmstadt, Januar 2022 Dominik Müller

ABSTRACT

For the assessment of existing masonry structures, a safety concept is required that takes into account the differences compared to the design of new masonry structures, such as the possibility of material testing, high variability of material properties, and a potentially reduced target reliability level. Therefore, a method for determining characteristic values, structure-specific partial factors, and assessment values for the compressive strength of existing masonry is developed.

For this purpose, the influence of spatially variable material properties within a masonry wall is investigated first: Based on experiments on clay brick masonry, a finite element model is developed and then used in Monte Carlo simulations for quantifying the effect of spatial material variability on the probability distribution of the load-bearing capacity of masonry walls under compression. The statistical uncertainty resulting from small sample sizes in material testing is considered through Bayesian statistical procedures. Prior distributions for unit, mortar, and masonry compressive strength are modelled utilising a test database for existing solid clay brick masonry. Finally, the findings are implemented in a practice-oriented method for determining assessment values of masonry compressive strength, which is validated through reliability analyses.

ZUSAMMENFASSUNG

Für die Nachrechnung bestehenden Mauerwerks ist ein Sicherheitskonzept erforderlich, welches die Unterschiede zur Bemessung von Neubauten aus Mauerwerk, wie die Möglichkeit der Materialprüfung, hohe Streuungen der Materialeigenschaften und ein gegebenenfalls reduziertes Zielzuverlässigkeitsniveau, berücksichtigt. Es wird daher eine Methode zur Ermittlung charakteristischer Werte, bauwerksspezifischer Teilsicherheitsbeiwerte und Nachrechnungswerte für die Druckfestigkeit von Bestandsmauerwerk entwickelt.

Hierzu wird zunächst der Einfluss einer räumlichen Streuung der Materialeigenschaften innerhalb einer Mauerwerkswand untersucht: Aufbauend auf experimentellen Untersuchungen an Ziegelmauerwerk wird ein Finite-Elemente-Modell entwickelt, das für Monte-Carlo-Simulationen zur Quantifizierung der Auswirkung räumlicher Materialstreuungen auf die Wahrscheinlichkeitsverteilung der Tragfähigkeit von Mauerwerkswänden unter Druckbeanspruchung verwendet wird. Die aus kleinen Stichprobenumfängen bei der Materialprüfung resultierende statistische Unsicherheit wird mittels Verfahren der bayesschen Statistik berücksichtigt. A-priori-Verteilungen für die Stein-, Mörtel- und Mauerwerksdruckfestigkeit werden hierzu auf Grundlage einer Prüfdatenbank für bestehendes Vollziegelmauerwerk ermittelt. Die Erkenntnisse münden schließlich in eine praxisgerechte Methode zur Bestimmung von Nachrechnungswerten der Mauerwerksdruckfestigkeit, welche durch Zuverlässigkeitsanalysen validiert wird.

CONTENTS

Notations and Abbreviations V

1 Introduction 1

1.1 Motivation 1

1.2 Research Objective 3

1.3 Thesis Organisation 3

1.4 Related Publications 5

2 Basics of Statistics and Structural Reliability 7

2.1 Introduction 7

2.2 Aleatory and Epistemic Uncertainty 7

2.3 Stochastic Modelling of Random Variables 8

2.3.1 General Definitions and Stochastic Moments 8

2.3.2 Multivariate Distributions 11

2.3.3 Functions of Random Variables 12

2.3.4 Selected Probability Distribution Types 13

2.3.5 Modelling Spatial Variability 17

2.3.6 Parameter Estimation 20

2.3.7 Goodness-of-Fit Testing 24

2.3.8 Definition of Populations 26

2.4 Bayesian Statistics 27

2.4.1 General and Bayesian Interpretation of Probability 27

2.4.2 Bayesian Updating of Distribution Parameters 28

2.5 Structural Reliability 31

2.5.1 General 31

2.5.2 First-Order Reliability Method 34

2.5.3 Monte Carlo Simulation 38

2.5.4 Calibration of Partial Factors 39

2.5.5 Reliability of Structural Systems 44

2.6 Reliability of Existing Structures 47

2.6.1 General 47

2.6.2 Target Reliability for Existing Structures 49

2.6.3 Concepts for Modified Partial Factors 52

2.6.4 Concepts for Considering Statistical Uncertainty 55

3 Structural Behaviour and Assessment of Masonry 57

3.1 Introduction 57

3.2 Overview of the History of Masonry Construction 57
3.3 Structural Behaviour of Masonry under Compression 62
3.3.1 General Failure Mechanism of Masonry under Compression 62
3.3.2 Stress-Strain Relationship of Masonry under Compression 62
3.3.3 Slender Masonry Walls under Eccentric Compression 66
3.3.4 Influence of Inhomogeneity 69
3.3.5 Further Influences on the Resistance of Masonry 70
3.4 Methods for Testing the Compressive Strength of Masonry 72
3.4.1 General 72
3.4.2 Unit Compressive Strength 74
3.4.3 Mortar Compressive Strength 74
3.4.4 Masonry Compressive Strength 75
3.5 Prediction of Masonry Compressive Strength based on Component Properties 79
3.5.1 General 79
3.5.2 Models Based on Mechanical Principles 79
3.5.3 Empirical Power Equation 81
3.5.4 Analysis of the Power Equation Concerning Stochastic Extension 82
3.5.5 Influence of Mortar Joint Thickness 86
3.6 Finite Element Modelling Strategies for Masonry Structures 88
3.7 Safety Format in Eurocode 6 89

4 Experimental Investigations on Clay Brick Masonry 91
4.1 Introduction 91
4.2 Testing of the Components 91
4.2.1 Clay Bricks 91
4.2.2 Mortar 92
4.3 Tests on Masonry Specimens 97
4.4 Tests on Masonry Walls 100
4.4.1 Testing Programme and Procedure 100
4.4.2 Results 102
4.5 Summary 110

5 Finite Element Modelling of Clay Brick Masonry Walls 111
5.1 Introduction 111
5.2 Description of the Finite Element Model 111
5.2.1 General and Modelling Strategy 111
5.2.2 Geometry, Mesh, and Iteration Method 112
5.2.3 Material Modelling 113

5.3 Validation of the Finite Element Model 120
5.3.1 Comparison with Analytical Model for the Resistance of Slender Walls 120
5.3.2 Comparison with Experimental Results 121
5.4 Summary 124

6 Monte Carlo Simulation of Masonry Walls with Spatially Variable Material Properties 125

6.1 Introduction 125
6.2 Investigation Procedure 126
6.2.1 Stochastic Model for Spatial Variability 126
6.2.2 Selection of Stochastic Parameters 128
6.2.3 Generation of Random Material Properties 129
6.2.4 Evaluation Procedure 131
6.3 Parameter Studies 133
6.3.1 Overview 133
6.3.2 Results for the Reference Wall 134
6.3.3 Investigation of Different Options for Mortar Property Assignment 137
6.3.4 Influence of Material Variability 140
6.3.5 Influence of Spatial Correlation 142
6.3.6 Influence of Wall Length 145
6.3.7 Influence of Slenderness 148
6.3.8 Influence of Load Eccentricity 152
6.3.9 Influence of Masonry Bond 155
6.3.10 Influence of Unit Format 156
6.4 Summary 157

7 Bayesian Framework for Statistical Uncertainty and Prior Modelling 159

7.1 Introduction 159
7.2 Bayesian Framework 159
7.3 Test Database for Material Properties of Existing Masonry 163
7.4 Modelling Prior Distributions 169
7.4.1 General 169
7.4.2 Procedure for Estimating the Prior Hyperparameters 170
7.4.3 Building-Related Prior Distributions 171
7.4.4 Location-Related Prior Distributions 173
7.4.5 Correlation of Strength at a Sampling Location 175
7.4.6 Statistical Uncertainty in the Estimation of Prior Hyperparameters 176
7.4.7 Prior Distribution for the Compressive Strength of Masonry 179
7.5 Summary 181

8 Method for Determining Assessment Values of Masonry Compressive Strength 183
8.1 Introduction 183
8.2 Approach and Assumptions 184
8.2.1 General 184
8.2.2 Selection of Populations, Material Sampling, and Testing 184
8.2.3 Definition of Safety Elements 185
8.2.4 Consideration of Statistical Uncertainty 188
8.2.5 Target Reliability 188
8.2.6 Partial Factors for Actions 188
8.2.7 Further Influences on Masonry Compressive Strength 190
8.3 Model Uncertainties 191
8.3.1 Uncertainty in the Resistance Model 191
8.3.2 Uncertainty in Masonry Compressive Strength Prediction 192
8.4 Combination of the Different Types of Uncertainty and Approximation 199
8.4.1 General 199
8.4.2 Simulation Procedure for Combining the Different Types of Uncertainty 199
8.4.3 Simulation Results and Approximation for the Reference Case 203
8.4.4 Considerations for Walls with Small Cross-Sections 208
8.4.5 Considerations for Slender Walls 210
8.4.6 Considerations for Direct Testing of Masonry Compressive Strength 212
8.5 Validation of the Developed Method by Reliability Analyses 214
8.5.1 Procedure of the Reliability Analyses 214
8.5.2 Resulting Level of Reliability 218
8.5.3 FORM Sensitivity Factors 220
8.6 Summary 225
9 Practice-Oriented Proposal for Determining Assessment Values and Partial Factors 227
9.1 Introduction 227
9.2 General and Equations for Determining Assessment Values 227
9.3 Diagrams for Determining Assessment Values 230
9.4 Typical Characteristic-to-Mean Ratios and Partial Factors 236
9.5 Alternative Assessment Procedures in the Absence of Test Results 238
10 Summary and Outlook 243
References 248
Annex 266

NOTATIONS AND ABBREVIATIONS

The most important symbols, notations, and abbreviations are defined below. Symbols that are not listed here are explained in the text.

Frequent Indices

1a	Reference period of one year
50a	Reference period of 50 years
a	Assessment value
b	Unit (brick)
d	Design value
j	Mortar (joint)
k	Characteristic value
ln	Parameter related to the natural logarithms of the single values of a sample or the natural logarithm of a random variable
m	Mean value
ma	Masonry
spat	Parameter related to spatial variability (= unit-to-unit variability)
wall	Parameter related to wall-to-wall variability

Notations for Probability Distributions

Inv-χ^2 (v, s^2)	Scaled inverse-χ^2 distribution with v degrees of freedom and scale s^2
LN (μ_Y, σ_Y^2)	Log-normal distribution with parameters μ_Y and σ_Y^2
N (μ, σ^2)	Normal distribution with mean μ and variance σ^2
t_v	t-distribution with v degrees of freedom
W (k, λ)	Weibull distribution with shape parameter k and scale parameter λ
χ_v^2	χ^2-distribution with v degrees of freedom

Latin Characters

A	Cross-sectional area

a, b, c	Parameters in approximate equations for the influence of spatially variable material properties on the resistance of a masonry wall
$\mathrm{Cov}\,(X,Y)$	Covariance of random variables X and Y
E	Load effect
$\mathrm{E}\,(X)$	Expected value of random variable X
E_{ma}	Modulus of elasticity of masonry
$F\,(x)$	Cumulative distribution function of random variable X
$F^{-1}(p)$	Inverse cumulative distribution function
$f\,(x)$	Probability density function of random variable X
f_{b}	Unit compressive strength
f_{bt}	Unit tensile strength
f_{j}	Mortar compressive strength
f_{ma}	Masonry compressive strength
f_{t}	Tensile strength of mortar joint
G	Permanent load effect
$g\,(\mathbf{X})$	Limit state function of the random variables $\mathbf{X}$
h	Height
K	Parameter of the power equation for masonry compressive strength
k	Stress-strain parameter (total to elastic strain at peak stress)
$L\,(\boldsymbol{\theta}\|\mathbf{x})$	Likelihood of the parameters $\boldsymbol{\theta}$ given the outcome $\mathbf{x}$
l	Length
m	Arithmetic mean
m'	Prior hyperparameter (one of two parameters for the distribution of the expectation of a normal random variable for a given variance, equivalent to the arithmetic mean of a hypothetical prior test series)
m''	Posterior hyperparameter resulting from an update of m'
$m_{\mathrm{ln,b}}$	Arithmetic mean of the logarithms of unit compressive strength
$m_{\mathrm{ln,j}}$	Arithmetic mean of the logarithms of mortar compressive strength
n	Sample size, number of particular items

n'	Prior hyperparameter (one of two parameters for the distribution of the expectation of a normal random variable for a given variance, equivalent to the sample size of a hypothetical prior test series)
n''	Posterior hyperparameter resulting from an update of n'
$P(A)$	Probability of event A
P_f	Probability of failure
p	Level of significance, probability for specifying a p fractile
Q	Variable load effect
R	Resistance
$R_\mathrm{a,hom}$	Assessment value of the resistance assuming homogeneity
R_det	Resistance obtained deterministically with mean material properties
$r_{x,y}$	Sample correlation coefficient of realisations of X and Y
s'^2	Prior hyperparameter (one of two parameters for the distribution of the variance of a normal random variable, equivalent to the sample variance of a hypothetical prior test series)
s''^2	Posterior hyperparameter resulting from an update of s'^2
s	Sample standard deviation
s^2	Sample variance
$s_{\ln,\mathrm{b}}^2$	Sample variance of the logarithms of unit compressive strength
$s_{\ln,\mathrm{j}}^2$	Sample variance of the logarithms of mortar compressive strength
$s_{\ln,\mathrm{ma}}^2$	Sample variance of the logarithms of masonry compressive strength
t	Thickness
V	Sample coefficient of variation
$\mathrm{Var}(X)$	Variance of X
V_b	Sample coefficient of variation of unit compressive strength
V_j	Sample coefficient of variation of mortar compressive strength
V_ma	Sample coefficient of variation of masonry compressive strength
X	Random variable
$\mathbf{X}$	Random vector
x	Realisation of the random variable X

$\mathbf{x}$	Realisation of the random vector $\mathbf{X}$
$\bar{x}$	Arithmetic mean of realisations of X

Greek Characters

α	Parameter of the power equation for masonry compressive strength
α_X	Sensitivity factor of the random variable X
β	Parameter of the power equation for masonry compressive strength
β	Reliability index
β_t	Target reliability index
$\Gamma(\cdot)$	Gamma function
γ_{Ed}, γ_{Ea}	Partial factor for the uncertainty of the load effect model
γ_G	Partial factor for permanent actions
γ_Q	Partial factor for variable actions
γ_M	Partial factor for the resistance of masonry
γ_m	Partial factor for the resistance of masonry without consideration of resistance model uncertainty
γ_{Rd}, γ_{Ra}	Partial factor for the uncertainty of the resistance model
ε	Strain
ε_f	Compressive strain at reaching compressive strength
ζ	Factor for considering effects of sustained loading on masonry compressive strength
θ	Parameter of a probability distribution
$\hat{\theta}$	Estimate of parameter θ
$\hat{\theta}^*$	Bootstrap estimate of parameter θ
θ_E	Uncertainty factor of load effect model
θ_f	Uncertainty factor of strength model
θ_R	Uncertainty factor of resistance model
λ	Material-related slenderness
μ_b	Expected value of unit compressive strength
μ_j	Expected value of mortar compressive strength

$\mu_{\ln,b}$	Expected value of the logarithm of unit compressive strength
$\mu_{\ln,j}$	Expected value of the logarithm of mortar compressive strength
$\mu_{\ln,ma}$	Expected value of the logarithm of masonry compressive strength
μ_{ma}	Expected value of masonry compressive strength
μ_X	Expected value of random variable X
ν	Degrees of freedom
ν'	Prior hyperparameter (one of two parameters for the distribution of the variance of a normal random variable, equivalent to the degrees of freedom in calculating the sample variance of a hypothetical prior test series)
ν''	Posterior hyperparameter resulting from an update of ν'
ρ_{spat}	Spatial coefficient of correlation
$\rho_{X,Y}$	Correlation coefficient of the random variables X and Y
σ	Stress
$\sigma_{\ln,b}^2$	Variance of the natural logarithm of unit compressive strength
$\sigma_{\ln,j}^2$	Variance of the natural logarithm of mortar compressive strength
$\sigma_{\ln,ma}^2$	Variance of the natural logarithm of masonry compressive strength
σ_X	Standard deviation of random variable X
σ_X^2	Variance of random variable X
υ_b	Coefficient of variation of unit compressive strength
υ_E	Coefficient of variation of the elastic modulus of masonry
υ_j	Coefficient of variation of mortar compressive strength
υ_{ma}	Coefficient of variation of masonry compressive strength
υ_t	Coefficient of variation of the tensile strength of the mortar joint
υ_X	Coefficient of variation of random variable X
$\Phi(z)$	Standard normal cumulative distribution function of Z
$\Phi^{-1}(p)$	Inverse standard normal cumulative distribution function
Φ_{red}	Capacity reduction factor for masonry walls addressing slenderness and load eccentricity
$\varphi(z)$	Standard normal probability density function of Z

Other Abbreviations

APFM	Adjusted partial factor method
CC	Consequence class
CoV	Coefficient of variation
CDF	Cumulative distribution function
DVM	Design value method
FORM	First-order reliability method
LHS	Latin hypercube sampling
LVDT	Linear variable displacement transducer
MCS	Monte Carlo simulations
MLE	Maximum likelihood estimation
NA	National Annex
PDF	Probability density function
SCBM	Solid clay brick masonry

1 INTRODUCTION

1.1 Motivation

The refurbishment, conversion, and extension of existing buildings are steadily gaining importance. Almost 70 % of the revenue in housing construction in Germany is currently attributable to activities on existing buildings (BBSR 2020). To save resources and avoid CO_2 emissions in the production of building materials, increasing the service life of existing buildings is necessary. If the conversion or extension of a building increases the load effects on existing structural members, structural safety must be re-evaluated. Current standards for verifying structural safety, most notably the Eurocodes, primarily address the design of new structures. Consequently, many issues concerning the assessment of existing structures are not standardised, which leads to a lack of practical guidance and potentially poor decision-making. Therefore, closing these regulatory gaps through standards or guidelines that explicitly target the assessment of existing structures is a matter of great urgency.

Among other issues, the reliability concept underlying the assessment of existing structures is an important aspect. In some cases, the partial factors calibrated for the design of new structures are inappropriate for existing structures. In the assessment of existing structures, the actual material properties, including their variability, can be measured, allowing for the consideration of additional information to determine structure-specific partial factors for material properties or member resistances. Furthermore, the appropriate target reliability level for the assessment of existing structures may be lower than for the design of new structures, which tends to lead to a reduction of suitable partial factors (Diamantidis 2001; DBV-Heft 24 2013; Steenbergen et al. 2015). The application of partial factors calibrated for the design of new structures can lead to inappropriate decisions concerning existing structures: If, on the one hand, the partial factors are too low due to a high material variability in a particular existing structure, safety deficits may not be identified; on the other hand, if the partial factors calibrated for new structures are too high, the assessment may wrongly indicate the need for expensive upgrading measures, which can lead to the decision to demolish existing structures and build new ones instead.

For existing concrete structures, concepts for determining modified partial factors have already been developed; see, for example, DBV-Merkblatt "*Modifizierte Teilsicherheitsbeiwerte für Stahlbetonbauteile*" (2013) and fib bulletin 80 (2016). However, a large share of existing buildings, especially residential buildings, are made of masonry. In 2019, masonry was the predominant building material for over 70 % of completed residential buildings in Germany (Destatis 2020). Concerning the entire existing building stock in Germany, the exterior walls of almost 90 % of residential buildings are made of masonry (Cischinsky and

Diefenbach 2018, data from 2016). A method is hence required for modifying partial factors addressing the special features of masonry construction.

One such feature of masonry is its composition of masonry units (i.e. bricks or blocks) and mortar, which leads to the speciality that the material properties of masonry can be tested either on the composite material masonry or on the two components separately. Another speciality is the old age of many masonry buildings: 12 % of the existing residential buildings in Germany were built until 1918, and another 12 % between 1919 and 1948 (Cischinsky and Diefenbach 2018). Many of the existing masonry buildings were thus built before the introduction of the first German brick standard DIN 105 (1922) or the first German structural design standard for masonry DIN 1053 (1937). Among artificial units for masonry construction, solid clay bricks dominated until about 1950 (Loga et al. 2015). With the manufacturing techniques that were common until the beginning of the 20th century, it was not possible to precisely achieve specified strengths of clay bricks, which resulted in a high variability of their strength (Franke and Goretzky 2004; Neumann 2017).

The high variability from brick to brick, as well as between mortar joints, leads to an inhomogeneity of masonry, that is, spatial variability of material properties within existing masonry walls. This raises the question of how spatial variability affects the resulting load-bearing capacity. Goretzky (2000) demonstrated that the variability of material properties within a masonry wall leads to a reduction of the mean load-bearing capacity (i.e. a lower load-bearing capacity than obtained by a deterministic calculation based on mean material properties as input values). Regarding the reliability of existing masonry walls and suitable partial factors, lower quantiles of the load-bearing capacity are relevant. Hence, to determine suitable partial factors γ_M for the resistance of existing masonry, the relationship between the probability distribution of the spatially variable material properties and the resulting probability distribution of the load-bearing capacity must be known.

Another challenge in the assessment of existing masonry structures are small sample sizes in the testing of the material properties. For economic and structural reasons and, in some cases, to preserve cultural heritage, the number of specimens taken from an existing structure is usually kept to a minimum, which leads to statistical uncertainty regarding the tested material properties. Statistical uncertainty must thus be addressed when characteristic values of material properties and structure-specific partial factors are determined based on test results. The statistical uncertainty in the assessment of a particular structure can be reduced by considering information from the previous assessment of similar structures. Mathematically, this can be achieved by modelling prior distributions for the stochastic parameters of material properties. By applying Bayesian statistical methods, these prior distributions can be incorporated into the assessment procedure, as described in Diamantidis (2001), Caspeele and Taerwe (2012), and ISO 2394 (2015), for example.

For the verification of existing masonry structures under compression loading, assessment values of masonry compressive strength are needed. These values are equivalent to design values as defined in EN 1990 (2010) for the verification of new structures. In principle, assessment values are hence obtained by dividing characteristic values by respective partial factors. The term “assessment value” emphasises that the assessment of existing structures differs from the design of new structures. It is used in the draft standard prEN 1990-2 (2021) for the assessment of existing structures, and it is also adopted in this thesis.

1.2 Research Objective

The goal of the following investigations is the development of a method to determine suitable assessment values of masonry compressive strength based on available test results. The method to be developed includes the determination of both characteristic values for masonry compressive strength and structure-specific partial factors for the resistance of masonry under predominant compression loading.

As the method will consider both the influence of the spatial variability of material properties and the statistical uncertainty from limited sample sizes, two questions must be answered:

1. What is the influence of the spatial variability of material properties on the probability distribution of the load-bearing capacity of masonry walls under compression?
2. How can statistical uncertainty be considered in the assessment of existing masonry structures, and what are suitable prior distributions for reducing statistical uncertainty in the estimation of stochastic parameters for masonry compressive strength?

The focus of these investigations is on unreinforced, solid clay brick masonry.

The final method will enable practising engineers to obtain assessment values of masonry compressive strength depending on a specified target reliability level as well as the type, number, and results of conducted compression tests.

1.3 Thesis Organisation

Chapter 2 presents the basics of statistics and structural reliability as well as selected topics regarding the reliability assessment of existing structures. Chapter 3 then provides relevant background knowledge concerning masonry construction in general, the load-bearing behaviour of masonry under compression, related testing procedures, and the design and assessment of masonry structures.

Chapter 4 illustrates the procedure and results of experimental investigations on the stress redistribution capability of solid clay brick masonry walls with local weaknesses. The experimental results serve as a basis for validating a finite element model, which is described in Chapter 5.

Thereafter, in Chapter 6, the validated finite element model is utilised to perform Monte Carlo simulations of masonry walls under compression loading considering spatially variable material properties. In various parameter studies, the relationship between the probability distribution of the material properties and the resulting distribution of the wall resistance is quantified.

Chapter 7 first presents a Bayesian framework for statistically evaluating the results of compression tests on specimens extracted from existing masonry. This framework allows for the inclusion of prior information on the typical variability of unit, mortar, and masonry compressive strength. For modelling corresponding prior distributions, a database with results of compression tests on unit and mortar specimens extracted from existing masonry buildings is set up. After a description of the database, suitable hyperparameters of the prior distributions are determined.

In Chapter 8, the method for determining characteristic values, partial factors, and assessment values for masonry compressive strength is finally developed. First, the fundamental approach of the method, the underlying assumptions and the application conditions are described. Then, the model uncertainties to be taken into account are examined. The different types of present uncertainties (i.e. spatial material variability, statistical uncertainty, and model uncertainty) are combined through stochastic simulations. Based on the simulation results, simplifications are made to attain a practice-oriented method. The chapter closes with a validation of the developed method by means of reliability analyses.

Chapter 9 presents the developed method in its final, practice-oriented form. In addition to a summary that provides the equations required to determine characteristic values, partial factors, and assessment values for masonry compressive strength in engineering practice, diagrams are presented that allow for a graphical application of the proposed method. Furthermore, typical characteristic-to-mean ratios and partial factors resulting from the proposed method are displayed, and suggestions for alternative assessment procedures in the absence of test results are made.

Finally, a summary of the thesis and an outlook on further research needs are provided in Chapter 10.

1.4 Related Publications

The following list contains publications that are related to this thesis and have previously been published by the author.

Müller, D.; Bujotzek, L.; Proske, T.; Graubner, C.-A. (2022): Influence of Spatially Variable Material Properties on the Resistance of Masonry Walls under Compression. Materials & Structures, 55 (2), 84.

Müller, D.; Graubner, C.-A. (2021): Assessment of Masonry Compressive Strength in Existing Structures Using a Bayesian Method. ASCE-ASME Journal of Risk and Uncertainty in Engineering Systems, Part A: Civil Engineering, 7 (1), 04020057.

Müller, D.; Proske, T.; Graubner, C.-A. (2021): Stochastic Simulation of Clay Brick Masonry Walls with Spatially Variable Material Properties. In Matos et al. (Eds.): 18th International Probabilistic Workshop. Lecture Notes in Civil Engineering, 153. Cham: Springer, pp. 779-791.

Müller, D.; Graubner, C.-A. (2019): Modification of the Partial Safety Factor for Compressive Strength of Existing Masonry Using a Bayesian Method. In Yurchenko, Proske (Eds.): Proceedings of the 17th International Probabilistic Workshop. Edinburgh, United Kingdom, 11-13 September 2019, pp. 133-138.

Müller, D.; Graubner, C.-A. (2018): Uncertainties in the Assessment of Existing Masonry Structures. In Caspeele, Taerwe, Frangopol (Eds.): Proceedings of the 6th International Symposium on Life-Cycle Civil Engineering. London: Taylor & Francis, pp. 369-376.

Müller, D; Förster, V.; Graubner, C.-A. (2017): Influence of Material Spatial Variability on Required Safety Factors for Masonry Walls in Compression. Mauerwerk – European Journal of Masonry, 21 (4), pp. 209-222.

Müller, D; Förster, V.; Graubner, C.-A. (2017): Influence of Material Spatial Variability on the Reliability of Masonry Walls in Compression. In Liu, Banting (Eds.): 13th Canadian Masonry Symposium Proceedings. Halifax, Canada, 4-7 June 2017.

2 BASICS OF STATISTICS AND STRUCTURAL RELIABILITY

2.1 Introduction

This chapter introduces selected topics of statistics, structural reliability theory, and the reliability assessment of existing structures. The illustration is limited to concepts that are essential in the further course of this thesis. For more information, the reader is referred to the standard literature covering the broad topic of structural reliability, such as Spaethe (1992), Melchers and Beck (2018), and Nowak and Collins (2013), as well as textbooks for the related background in probability and statistics, for example Hedderich and Sachs (2020), Wasserman (2011), and Gelman et al. (2013).

Section 2.2 introduces the two main types of uncertainty. Then, Section 2.3 presents the essential concepts in the stochastic modelling of random variables, including information about the stochastic moments of random variables, probability distribution types, the modelling of spatially variable properties, parameter estimation methods, goodness-of-fit testing, and the choice of populations for statistical evaluation. In Section 2.4, the basic concepts of Bayesian statistics and the Bayesian updating of probability distribution parameters are presented. Section 2.5 addresses the topic of structural reliability, covering the general concept, methods of reliability analysis, the calibration of partial factors for structural design standards and system reliability. Finally, Section 2.6 presents some of the specialities related to the reliability of existing structures. In addition to illustrating the general differences between the design of new structures and the assessment of existing ones, the topic of appropriate target reliability levels for existing structures, concepts for modified partial factors, and approaches for considering statistical uncertainty are treated.

2.2 Aleatory and Epistemic Uncertainty

Uncertainties are the reason for having to deal with the probability of structural failure. Uncertainties are present both in the design phase of new structures and in the assessment of existing structures, and they can be categorised into two types: aleatory and epistemic uncertainty (Faber 2005; Der Kiureghian and Ditlevsen 2009). The term “aleatory” comes from the Latin word “*alea*”, meaning die (plural: dice). *Aleatory uncertainties* are inherent in a physical process and cannot be reduced by the modeller of the engineering problem. The situation is equivalent to rolling the dice, where the person rolling the dice cannot increase the odds of obtaining a six. The physical process can be the construction of a building, including the production of the construction materials, for example. In this case, the structural engineer cannot reduce the variability of material properties. Aleatory uncertainties in the design of structures include the variability of material properties, geometrical dimensions, imposed loads, and climatic actions.

In contrast, the word "epistemic" has its origin in the ancient Greek word "*ἐπιστήμη*", which means knowledge or understanding. *Epistemic uncertainties* are caused by a lack of knowledge and can be reduced by extending this knowledge. In engineering, epistemic uncertainties arise due to limited data, leading to statistical uncertainty; the scattering of testing methods, causing testing uncertainty; and the use of models that are, by definition, a simplification of reality and thus introduce model uncertainty. The engineer can reduce these epistemic uncertainties by gaining more data, using more accurate testing methods, and applying more refined models.

Both types of uncertainty can be described by random variables, as explained in Section 2.3. In the case of aleatory uncertainties, these random variables usually represent actual physical properties. In contrast, auxiliary, non-physical variables are typically introduced to model epistemic uncertainties (Der Kiureghian and Ditlevsen 2009). Such a non-physical variable can be a model uncertainty factor θ, for example, representing the ratio of experimental results to model predictions. Statistical uncertainty can be treated by Bayesian methods, in which probability distribution parameters are modelled as random variables (see Section 2.4).

The differentiation between aleatory and epistemic uncertainty helps to point out one of the fundamental differences between the design of new structures and the assessment of existing structures: Since an existing structure has already been built, random properties of the structure, such as material strengths or geometrical dimensions, have been realised. In other words: The dice have been rolled. Therefore, these uncertainties shift from aleatory to epistemic with the realisation of the building. In quantitative terms, the uncertainty after the realisation is initially still the same as before. However, the uncertainty now exists only due to a lack of knowledge, which can be reduced by measuring geometrical dimensions or testing material properties, for example. Hence, the uncertainties associated with the existing structural properties depend on the available information. If, in addition to the knowledge from the design phase, information from measurements is obtained, then the uncertainty is smaller than in the design phase. However, design and construction documents might not be available in the assessment phase. In this case, the epistemic uncertainty associated with the structural properties can be much higher than the respective aleatory uncertainty during structural design.

2.3 Stochastic Modelling of Random Variables

2.3.1 General Definitions and Stochastic Moments

All processes and phenomena in nature and technology are subject to randomness. Therefore, quantities in nature and technology are random variables, which are variables whose values depend on the outcome of a random experiment. More formally, a random variable

is a function assigning a real number to each outcome (Wasserman 2011). Random variables are hereafter denoted by the capital letter X. A possible realisation of the random variable (i.e. a random value of X) is denoted by the small letter x. If the possible realisations are countable, the random variable is a discrete random variable. Each possible realisation x of a discrete random variable possesses a certain probability $P(X = x)$ of occurrence. In contrast, a continuous random variable can take values from an uncountable set: Any value within a defined interval can be the realisation x. Thus, the probability $P(X = x)$ of observing a particular value x is zero; non-zero probabilities can only be given for intervals.

All random variables can be described by their *cumulative distribution function* (CDF) $F_X(x)$, which gives the probability P that X takes a value smaller than or equal to a value x:

$$F_X(x) = P(X \leq x) \qquad \textit{Eq. 2-1}$$

The probability that a continuous random variable X takes a value x in the interval (a, b) is defined by its *probability density function* (PDF) $f_X(x)$:

$$P(a < X < b) = \int_a^b f_X(x)\,dx \qquad \textit{Eq. 2-2}$$

Due to the above definition, integrating a PDF over its whole domain yields one. Probability density functions are usually chosen according to certain probability distribution types, some of which are introduced in Section 2.3.4. The CDF of a continuous random variable can be received through the integration of its PDF:

$$F_X(x) = \int_{-\infty}^{x} f_X(t)\,dt \qquad \textit{Eq. 2-3}$$

The inverse $F_X^{-1}(p)$ of the CDF is also called the "quantile function" as it allows for calculating p fractiles of the respective random variable (i.e. values x_p that are not exceeded with probability p). In the course of this thesis, for brevity, the CDF and PDF are usually denoted as F and f, respectively, instead of F_X and f_X.

Random variables can be characterised by their *stochastic moments*. The i-th moment of a random variable is defined as

$$\mu_i = \int_{-\infty}^{+\infty} (x - c)^i \, f_X(x)\,dx \qquad \textit{Eq. 2-4}$$

If stochastic moments are not further specified, c equals zero. For the i-th central moment, c is equal to the mean. The *mean*, which is also called the *expectation* or *expected value* and is denoted by $\mathrm{E}(X)$ or μ_X, is the first moment and is hence defined as

$$\mathrm{E}(X) = \mu_X = \int_{-\infty}^{+\infty} x\, f_X(x)\, dx \qquad \textit{Eq. 2-5}$$

The mean is a measure of the central tendency of X (Melchers and Beck 2018). Other central tendency measures are the median, which is the 50 % fractile, and the mode, which is the location of the maximum of the PDF.

A measure for the spread of a random variable is given by its *variance*, denoted $\mathrm{Var}(X)$ or σ_X^2. The variance is the second central moment (i.e. the second moment about the mean):

$$\mathrm{Var}(X) = \sigma_X^2 = \int_{-\infty}^{+\infty} (x - \mu_X)^2\, f_X(x)\, dx \qquad \textit{Eq. 2-6}$$

The square root of the variance is the *standard deviation* σ_X. If the standard deviation is related to the mean, the *coefficient of variation* (CoV) v_X is received, which is a dimensionless measure of the spread:

$$v_X = \frac{\sigma_X}{\mu_X} \qquad \textit{Eq. 2-7}$$

The *skewness* γ_1 is a measure of the asymmetry of a probability distribution. It is defined as the third central moment, standardised through division by σ_X^3:

$$\gamma_1 = \frac{\int_{-\infty}^{+\infty} (x - \mu_X)^3\, f_X(x)\, dx}{\sigma_X^3} \qquad \textit{Eq. 2-8}$$

If the skewness γ_1 is positive, the distribution is right-tailed (i.e. the right tail of the distribution is longer). For $\gamma_1 < 0$, the opposite is true. The skewness of symmetrical distributions equals zero. The standardised fourth central moment is the *kurtosis*. Instead of the kurtosis itself, the excess kurtosis γ_2 is often given. The excess kurtosis is defined as the kurtosis of the considered probability distribution minus the kurtosis of a normal distribution, which equals three:

$$\gamma_2 = \frac{\int_{-\infty}^{+\infty} (x - \mu_X)^4\, f_X(x)\, dx}{\sigma_X^4} - 3 \qquad \textit{Eq. 2-9}$$

The kurtosis can be interpreted as the tail extremity of a probability distribution (Westfall 2014). If $\gamma_2 > 0$, then outliers (i.e. extreme values strongly deviating from the mean) are more likely than for a normally distributed random variable with equal variance.

2.3.2 Multivariate Distributions

In many cases, the joint probability distribution (or multivariate distribution) of n random variables $X_1, X_2, \ldots, X_n$ is of interest. The vector $\mathbf{X}$ containing all the random variables X_i is a *random vector* (or multivariate random variable). If the random variables X_i are continuous, $\mathbf{X}$ can be described by the joint PDF $f_{\mathbf{X}}(x_1, x_2, \ldots, x_n)$. The probability that the random outcomes x_i fall within particular intervals (a_i, b_i) is given by

$$P\left(a_1 < X_1 < b_1 \cap \ldots \cap a_n < X_n < b_n\right) = \int_{a_n}^{b_n} \ldots \int_{a_2}^{b_2} \int_{a_1}^{b_1} f_{\mathbf{X}}\left(x_1, x_2, \ldots, x_n\right) dx_1 dx_2 \ldots dx_n \qquad \textit{Eq. 2-10}$$

By definition, integrating $f_{\mathbf{X}}(x_1, x_2, \ldots, x_n)$ over the entire domain of all variables X_i yields one. If only two continuous random variables X and Y are of interest, their bivariate distribution can be described by the joint PDF $f_{X,Y}(x, y)$. The corresponding *marginal densities* f_X and f_Y, which are the PDFs of the single random variables, are obtained by

$$f_X(x) = \int_{-\infty}^{+\infty} f_{X,Y}\left(x, y\right) dy \quad \text{and} \quad f_Y(y) = \int_{-\infty}^{+\infty} f_{X,Y}\left(x, y\right) dx \qquad \textit{Eq. 2-11}$$

For general multivariate distributions, marginal densities can be computed accordingly. The random variables X and Y are *independent*, if and only if

$$f_{X,Y}\left(x, y\right) = f_X(x)\ f_Y(x) \quad \text{for all } x \text{ and } y \qquad \textit{Eq. 2-12}$$

If $Y = y$ is observed, the *conditional distribution* of X given $Y = y$ is obtained as

$$f_{X|Y}(x|y) = \frac{f_{X,Y}\left(x, y\right)}{f_Y(y)} \qquad \textit{Eq. 2-13}$$

The *covariance* is a measure of how strong the linear relationship between two random variables X and Y is. It is defined as

$$\mathrm{Cov}\left(X, Y\right) = \mathrm{E}\left[\left(X - \mu_X\right)\left(Y - \mu_Y\right)\right] = \int_{-\infty}^{+\infty} \int_{-\infty}^{+\infty} \left(x - \mu_X\right)\left(y - \mu_Y\right) f\left(x, y\right) dxdy \qquad \textit{Eq. 2-14}$$

The covariance $\mathrm{Cov}(X, X)$ of a random variable with itself is the variance of X. If the covariance is standardised with regard to the standard deviations σ_X and σ_Y, the *correlation coefficient* ρ is received:

$$\rho_{X,Y} = \frac{\mathrm{Cov}\left(X, Y\right)}{\sigma_X\ \sigma_Y} \qquad \textit{Eq. 2-15}$$

If a perfect linear relationship between X and Y exists, given by $Y = a\,X + b$, then $\rho = 1$ for $a > 0$ and $\rho = -1$ for $a < 0$. If X and Y are independent, the covariance and the correlation

coefficient are zero. However, a correlation coefficient of zero does not automatically imply that two variables are independent.

2.3.3 Functions of Random Variables

A random variable Y is often a function of other random variables. The probability distribution of this function $Y(X_1, X_2,\ldots, X_n)$ might not be easy to determine, and the distribution of Y is not necessarily of a specific probability distribution type in general cases. Exceptions for the latter (i.e. cases where the probability distribution type of the function Y is known) are pointed out in Section 2.3.4. However, in many cases, the mean and variance of Y can be determined analytically (Melchers and Beck 2018).

If Y is a linear function of random variables X_i defined by

$$Y = a_0 + \sum_{i=1}^{n} a_i X_i \qquad \textit{Eq. 2-16}$$

then the mean and variance of Y can be obtained as

$$\mu_Y = a_0 + \sum_{i=1}^{n} a_i \mu_{X_i} \quad \text{and} \quad \sigma_Y^2 = \sum_{i=1}^{n} a_i^2 \sigma_{X_i}^2 + \sum_{j \neq i}^{n} \sum_{i=1}^{n} a_i a_j \mathrm{Cov}\left(X_i, X_j\right) \qquad \textit{Eq. 2-17}$$

If Y is the product of two independent random variables X_1 and X_2, which means

$$Y = X_1 X_2 \quad \text{and} \quad \rho_{X_1, X_2} = 0 \qquad \textit{Eq. 2-18}$$

then the mean μ_Y and CoV v_Y are

$$\mu_Y = \mu_{X_1} \mu_{X_2} \quad \text{and} \quad v_Y^2 = v_{X_1}^2 + v_{X_2}^2 + v_{X_1}^2 v_{X_2}^2 \qquad \textit{Eq. 2-19}$$

For small CoVs, the term ${v_{X_1}}^2 {v_{X_2}}^2$ is negligible.

Suppose that Y is a more complex function for that an analytical solution for the mean and variance is difficult or impossible to obtain. In that case, approximate solutions can be found utilising the respective first-order Taylor polynomial about the means of the random variables X_i (Melchers and Beck 2018):

$$\mu_Y \approx Y\left(\mu_{X_1}, \mu_{X_2}, ..., \mu_{X_n}\right) \qquad \textit{Eq. 2-20}$$

$$\sigma_Y^2 = \sum_{i=1}^{n} c_i^2 \sigma_{X_i}^2 + \sum_{j \neq i}^{n} \sum_{i=1}^{n} c_i c_j \mathrm{Cov}\left(X_i, X_j\right) \qquad \textit{Eq. 2-21}$$

$$\text{where} \quad c_i = \left.\frac{\partial Y}{\partial X_i}\right|_{\mu_{X_1}, \mu_{X_2}, ..., \mu_{X_n}} \qquad \textit{Eq. 2-22}$$

Due to the first-order Taylor approximation, the equations are identical to those for a linear combination, except for the constants a_i being replaced by the factors c_i, which are the partial derivatives of Y with respect to the corresponding X_i evaluated at the point given by the means.

2.3.4 Selected Probability Distribution Types

In this thesis, various types of probability distribution functions are used to model random variables. These distribution types are briefly introduced regarding definitions of their PDFs, corresponding distribution parameters, and typical applications.

Normal (Gaussian) distribution

The importance of the normal distribution results from the central limit theorem, which states that the distribution of a sum of n independent and identically distributed random variables X_1, X_2,…, X_n converges towards a normal distribution for $n \to \infty$. The random variables X_i can have any distribution as long as their mean μ and variance σ^2 exist (Wasserman 2011). Since many phenomena in nature result from random effects adding up, they are approximately normally distributed. The PDF of a normal distribution is

$$f(x) = \frac{1}{\sqrt{2\pi\sigma^2}} \exp\left[-\frac{1}{2}\left(\frac{x-\mu}{\sigma} \right)^2 \right], \quad x \in \mathbb{R} \qquad \textit{Eq. 2-23}$$

where x can take any real number. The two parameters of the normal distribution are the mean μ and the variance σ^2, where $\mu \in \mathbb{R}$ and $\sigma > 0$. The PDF of a normal distribution is symmetric. Consequently, the skewness γ_1 is zero.

The normal distribution with $\mu = 0$ and $\sigma = 1$ is called *standard normal distribution*. Standard normal random variables are usually denoted by Z, and their PDF and CDF are denoted by $\varphi(z)$ and $\Phi(z)$, respectively. There is no closed-form solution for the CDF of a normal distribution. Since values of $\Phi(z)$ are commonly given in tables in probability and statistics literature, the CDF is often expressed via the standard normal CDF:

$$F(x) = \Phi\left(\frac{x-\mu}{\sigma} \right), \quad x \in \mathbb{R} \qquad \textit{Eq. 2-24}$$

Due to the central limit theorem, the linear combination of normal random variables is also normally distributed.

Log-normal distribution

Normally distributed random variables can take negative values x, which can be a disadvantage when negative values do not make physical sense. In such cases, a log-normal

distribution can be used instead. If X is log-normally distributed, denoted as $X \sim \text{LN}$, then $Y = \ln X$ is normally distributed, written as $Y \sim \text{N}$. Therefore, the PDF is given by

$$f(x) = \frac{1}{\sqrt{2\pi\sigma_Y^2}} \exp\left[-\frac{1}{2}\left(\frac{\ln x - \mu_Y}{\sigma_Y} \right)^2 \right], \quad x > 0 \qquad \textit{Eq. 2-25}$$

The two parameters of the log-normal distribution are the mean μ_Y and the variance σ_Y^2 of the related normal random variable Y. If the mean μ_X and the variance σ_X^2 of the random variable X are known, μ_Y and σ_Y^2 can be calculated by

$$\mu_Y = \ln \mu_X - 0.5\,\sigma_X^2 \qquad \textit{Eq. 2-26}$$

$$\sigma_Y^2 = \ln\left(1 + \frac{\sigma_X^2}{\mu_X^2} \right) = \ln\left(1 + v_X^2 \right) \qquad \textit{Eq. 2-27}$$

For $v_X < 0.2$, σ_Y is approximately equal to v_X. Due to the central limit theorem as well as the relationship between the log-normal and the normal distribution, the product of n positive, independent, and identically distributed random variables converges towards a log-normal distribution for $n \to \infty$. Hence, phenomena resulting from a product of random effects can be well described by a log-normal distribution, and the product of log-normal variables is also log-normally distributed. Further analogies between normal and log-normal distributions are described in Limpert et al. (2001). In contrast to the symmetric PDF of the normal distribution, the log-normal PDF has a positive skewness γ_1 (i.e. it is right-skewed; see Fig. 2-1).

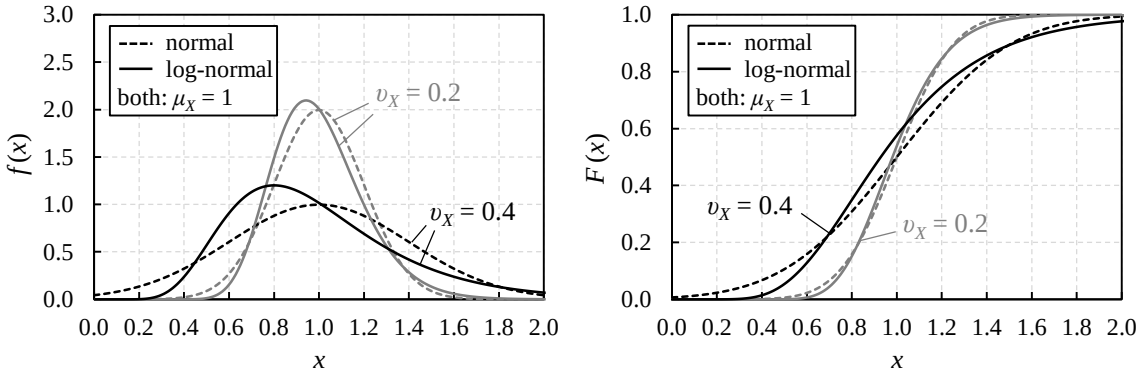

Fig. 2-1 Comparison of normal and log-normal distribution (left: probability density function, right: cumulative distribution function)

Gumbel distribution (extreme value distribution type I)

The maximum (and minimum) of n random variables X_i converges towards a Gumbel distribution for $n \to \infty$ if the distribution of X_i has an exponentially decreasing tail in the direction of the extreme (Gumbel 1958; Ang and Tang 1984). The normal distribution, among

others, fulfils this condition. As a result, the Gumbel distribution is well suited for modelling random variables that are the maximum of several random variables. A typical example in structural engineering is the maximum load over a specific time period. For the distribution of maxima, the PDF and CDF are

$$f(x) = a \exp\left[-a(x-u) - \exp\left(-a(x-u)\right)\right], \quad x \in \mathbb{R} \qquad \textit{Eq. 2-28}$$

$$F(x) = \exp\left[-\exp\left(-a(x-u)\right)\right], \quad x \in \mathbb{R} \qquad \textit{Eq. 2-29}$$

where the location parameter $u \in \mathbb{R}$ is the mode of the distribution, and the parameter $a > 0$ is a measure of the spread of the distribution. The mean μ and variance σ^2 of a Gumbel distribution can be calculated from the distribution parameters by

$$\mu = u + \frac{\gamma}{a} \quad \text{and} \quad \sigma^2 = \frac{\pi^2}{6\,a^2} \qquad \textit{Eq. 2-30}$$

where $\gamma \approx 0.5772$ is the Euler-Mascheroni constant. The skewness and excess kurtosis of a Gumbel distribution are $\gamma_1 \approx 1.14$ and $\gamma_2 = 2.4$, irrespective of the selected parameters a and u. The quantile function of a Gumbel distribution is given by

$$F^{-1}(p) = u - \frac{1}{a}\ln(-\ln p) \approx \mu - \sigma\left[0.45 + 0.78\ln(-\ln p)\right] \qquad \textit{Eq. 2-31}$$

with p being the probability that X takes a value smaller than the calculated quantile.

The maximum of n Gumbel-distributed random variables is also Gumbel distributed, which is convenient if a random variable represents the maximum load for a particular reference period t_0. If the reference period is changed to t_{ref}, the resulting random variable is Gumbel distributed with unchanged parameter a and thus unchanged standard deviation σ. The location parameter u_{ref} and mean μ_{ref} for the reference period t_{ref} can be obtained from the original parameter u_0 and mean μ_0 by

$$u_{\text{ref}} - u_0 = \mu_{\text{ref}} - \mu_0 = \frac{1}{a}\ln\frac{t_{\text{ref}}}{t_0} \approx 0.78\,\sigma\ln\frac{t_{\text{ref}}}{t_0} \qquad \textit{Eq. 2-32}$$

Hence, as illustrated in Fig. 2-2, the PDF of the maximum of n Gumbel-distributed variables is obtained by shifting the PDF of the original Gumbel distribution.

Weibull distribution (extreme value distribution type III)

As with the Gumbel distribution, the extreme value distribution type III (EVD III) is also an asymptotic distribution of the maximum or minimum of many independent and identically distributed random variables X_i. The exact conditions for the random variables X_i leading to convergence to the EVD III are given in Gumbel (1958). In contrast to the Gumbel distribution, the EVD III has a limiting value in the direction of the extreme value (i.e.

an upper bound for maxima and a lower bound for minima). The EVD III distribution for the minimum of random variables is known as the Weibull distribution. In its most common form, it is defined with a lower limit of zero, leading to the following PDF and CDF:

$$f(x) = \frac{k}{\lambda}\left(\frac{x}{\lambda}\right)^{k-1} \exp\left[-\left(\frac{x}{\lambda}\right)^{k}\right], \quad x \geq 0 \qquad \textit{Eq. 2-33}$$

$$F(x) = 1 - \exp\left[-\left(\frac{x}{\lambda}\right)^{k}\right], \quad x \geq 0 \qquad \textit{Eq. 2-34}$$

where $\lambda > 0$ is the scale parameter, and $k > 0$ is the shape parameter. Due to its background, the Weibull distribution is particularly suited for modelling materials or structural members whose failure is determined by their weakest link (Weibull 1939). The minimum of n Weibull-distributed random variables is also Weibull distributed. The corresponding PDF equals a scaled version of the original PDF (see Fig. 2-2).

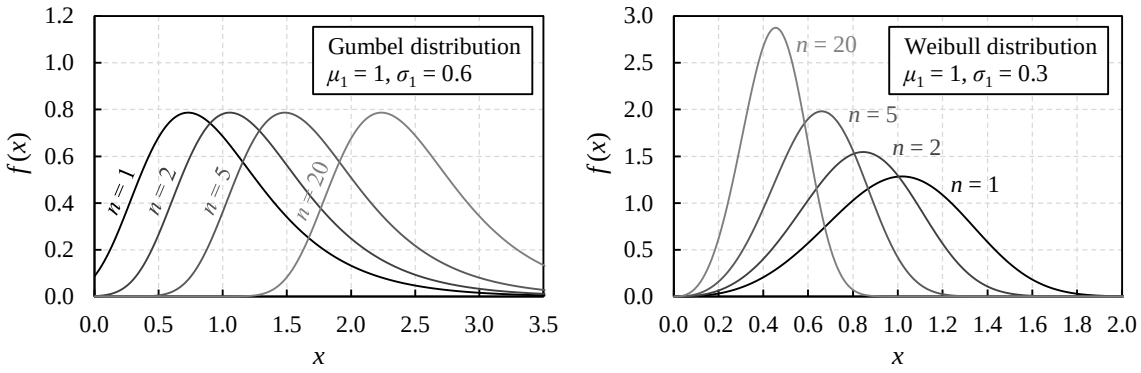

Fig. 2-2 Left: Probability density of the maximum of n Gumbel-distributed variables Right: Probability density of the minimum of n Weibull-distributed variables

Student's *t*-distribution

Student's *t*-distribution (short: *t*-distribution) arises when the mean of a normal distribution is estimated, and the variance is unknown (see Section 2.3.6). In Bayesian statistics, the predictive distribution of a normal random variable with uncertain variance is a *t*-distribution (see Section 2.4.2). If X is *t*-distributed, written as $X \sim t_\nu$, then the PDF is

$$f(x) = \frac{\Gamma\left(\frac{\nu+1}{2}\right)}{\sqrt{\pi\nu}\,\Gamma(\nu/2)}\left(1+\frac{x^2}{\nu}\right)^{-\frac{\nu+1}{2}}, \quad x \in \mathbb{R} \qquad \textit{Eq. 2-35}$$

where $\Gamma(\cdot)$ is the gamma function and the parameter $\nu > 0$ is the number of degrees of freedom. For $\nu \to \infty$, the *t*-distribution is identical to the standard normal distribution. With decreasing ν, both the variance and the excess kurtosis γ_2 increase. Hence, there is more weight in the tails compared to a normal distribution (see Fig. 2-3).

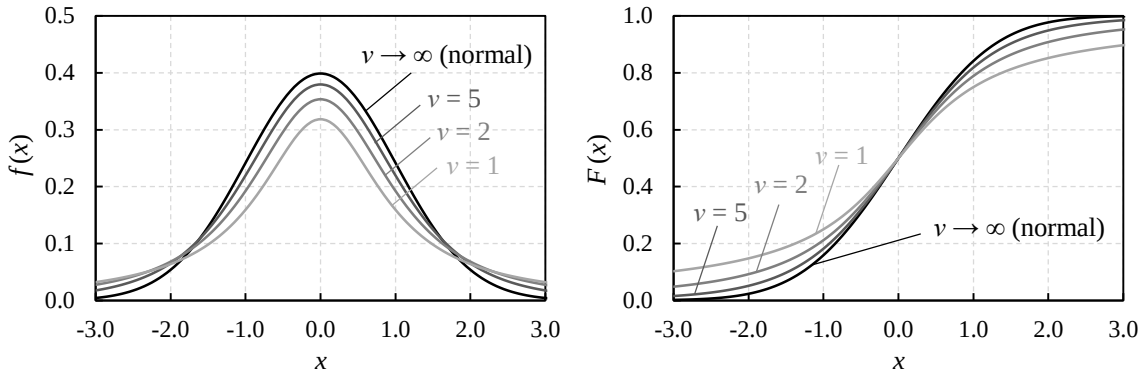

Fig. 2-3 Comparison of Student's t and standard normal distribution (left: probability density function, right: cumulative distribution function)

Chi-squared distribution

The chi-squared distribution (or χ^2-distribution) arises in the estimation of the variance of a normal distribution (see Section 2.3.6). If X is the sum of the squares of v independent standard normal random variables, then X is χ^2-distributed, written as $X \sim \chi_v^2$. The PDF is

$$f\left(x\right) = \frac{1}{2^{v/2}\,\Gamma\left(v/2\right)} x^{v/2-1} \exp\left(-\frac{x}{2}\right), \quad x > 0 \qquad \textit{Eq. 2-36}$$

where the parameter $v > 0$ is the number of degrees of freedom.

Scaled inverse chi-squared distribution

In Bayesian statistics, the scaled inverse χ^2-distribution is of importance, as it is the conjugate prior for the variance of a normal distribution (see Section 2.4.2). If X is scaled inverse χ^2-distributed with $v > 0$ degrees of freedom and scale parameter $s^2 > 0$, written as $X \sim \text{Inv-}\chi^2\,(v, s^2)$, then the PDF of X is

$$f\left(x\right) = \frac{\left(s^2\, v/2\right)^{v/2}}{\Gamma\left(v/2\right)} \frac{\exp\left(-\frac{vs^2}{2x}\right)}{x^{v/2+1}}, \quad x > 0 \qquad \textit{Eq. 2-37}$$

2.3.5 Modelling Spatial Variability

Single random variables cannot adequately describe the material properties within structural members since this would falsely assume homogeneity (i.e. perfect correlation of these properties at different points). Instead, material properties vary spatially within a structural member. This random variation in space must be modelled if it influences the investigated problem. Two main approaches of modelling spatial variability are illustrated next.

Random fields

A random field $X(\mathbf{t})$ can be viewed as a collection of random variables (Sudret and Der Kiureghian 2000). At each point given by the vector $\mathbf{t} \in \mathbb{R}^n$, which defines the coordinates of the point in n-dimensional space, $X(\mathbf{t})$ is a random variable. The realisation of a random field, denoted by $x(\mathbf{t})$, is a deterministic function assigning a specific value x to each location $\mathbf{t}$. The correlation between two random variables $X(\mathbf{t}_1)$ and $X(\mathbf{t}_2)$ at locations $\mathbf{t}_1$ and $\mathbf{t}_2$ is given by the autocorrelation function $\rho(\mathbf{t}_1, \mathbf{t}_2)$ of the random field. If a random field is homogeneous and isotropic, the autocorrelation function only depends on the distance between $\mathbf{t}_1$ and $\mathbf{t}_2$; that is, the correlation function is given by $\rho(\|\mathbf{t}_1 - \mathbf{t}_2\|)$; see Vanmarcke (1983). Such a random field can be suitable for modelling the compressive strength of concrete within a structural member, for example.

For many computational applications (e.g. for generating random realisations), random fields need to be discretised. In this context, discretisation means that the random field is approximated by a finite set of random variables (Sudret and Der Kiureghian 2000). If random fields are utilised in combination with finite element simulations, an obvious approach is to discretise the random field according to the spatial discretisation given by the finite element mesh. However, other approaches can be more efficient in terms of the required number of random variables; see Sudret and Der Kiureghian (2000) for a comprehensive description of discretisation methods. If the random field is discretised at the midpoints $\mathbf{t}_1$, $\mathbf{t}_2$,…, $\mathbf{t}_n$ of each of the n finite elements, the random field reduces to a random vector $\mathbf{X}$ consisting of n random variables X_i with n x n correlation matrix $\mathbf{R}_{XX}$. If the random field is homogeneous and isotropic, $\mathbf{R}_{XX}$ can be written as

$$\mathbf{R}_{XX} = \begin{pmatrix} 1 & \rho(\|\mathbf{t}_1-\mathbf{t}_2\|) & \rho(\|\mathbf{t}_1-\mathbf{t}_3\|) & \cdots & \rho(\|\mathbf{t}_1-\mathbf{t}_n\|) \\ & 1 & \rho(\|\mathbf{t}_2-\mathbf{t}_3\|) & \dots & \rho(\|\mathbf{t}_2-\mathbf{t}_n\|) \\ & & 1 & \dots & \rho(\|\mathbf{t}_3-\mathbf{t}_n\|) \\ & & & \ddots & \vdots \\ \text{symmetric} & & & & 1 \end{pmatrix} \qquad \textit{Eq. 2-38}$$

If $X(\mathbf{t})$ is a Gaussian random field (i.e. the variables at a location $\mathbf{t}$ are normal random variables), a realisation $\mathbf{x}$ of the random vector $\mathbf{X}$ can be created by first generating realisations y_i of independent normal random variables Y_i, which are then transformed utilising the matrix containing the eigenvectors of the correlation matrix $\mathbf{R}_{XX}$ (Tran et al. 2015).

Component-to-component variability

The spatial discretisation of a structural member is sometimes naturally given, which is the case if the structural member itself consists of several components. Examples are a cable consisting of multiple wires, a truss girder composed of several members, or a masonry wall made of many units. In these cases, the spatial variability of material properties can

predominantly consist of variability from component to component. If the components are placed in the member without a known pattern, it is unreasonable to assume that the correlation between the material properties X_i and X_j within the *i*-th and *j*-th component depends on their relative location to each other. However, modelling a particular material property within one component as independent of the same material property within another component might also be inappropriate since the material properties of different components can be influenced by effects from a common source (Song and Kang 2009). If, for example, the components within one member are from the same production batch, the material properties of different components are correlated due to common production conditions.

If the spatial variability between components is dominating, it can be reasonable to neglect spatial variability within the component and assume perfect correlation at this lower level. In such cases, a specific material property can be modelled by a random vector **X**, where all random variables X_i contained by the vector are mutually correlated with the same correlation coefficient ρ_{spat}. For instance, X_i and X_j could be the compressive strength within the *i*-th and *j*-th component, respectively. The correlation matrix is given by

$$\mathbf{R}_{XX} = \begin{pmatrix} 1 & \rho_{\text{spat}} & \rho_{\text{spat}} & \cdots & \rho_{\text{spat}} \\ & 1 & \rho_{\text{spat}} & \cdots & \rho_{\text{spat}} \\ & & 1 & \cdots & \rho_{\text{spat}} \\ & & & \ddots & \vdots \\ \text{symmetric} & & & & 1 \end{pmatrix} \qquad \textit{Eq. 2-39}$$

Such a correlation structure can be modelled utilising a common *parent variable* for all X_i (see Song and Kang 2009; Schneider et al. 2015; Vereecken et al. 2020). This parent variable represents the effects of a common source and is included in the formulation of the respective component properties: If **X** is a normal random vector with equal mean μ_X and σ_X for all X_i, the equi-correlated random variables X_i can be expressed as

$$X_i = M + C_i + \mu_X \quad \text{with } M \sim N\left(0, \rho_{\text{spat}}\sigma_X^2\right) \text{ and } C_i \sim N\left(0, \left(1-\rho_{\text{spat}}\right)\sigma_X^2\right) \qquad \textit{Eq. 2-40}$$

where M is the parent variable shared by all components within the member, and C_i is a variable considering the additional variability of the *i*-th component arising from an individual source. The variance of the parent variable M represents the variability from member to member. It is equal to the covariance of two random variables X_i and X_j, describing the same material property within different components. In contrast, the variance of C_i represents the component-to-component variability (i.e. the spatial variability of this material property within the structural member). A similar approach with parent variables is usually employed to model the spatial correlation of imposed loads (i.e. live loads) in a building (see Rackwitz 1997; JCSS 2001b; Tran et al. 2017).

2.3.6 Parameter Estimation

In the real world, the parameters of probability distributions are never given or known but must be estimated from data. Parameter estimation belongs to the field of *statistical inference*. The term "statistical inference" describes the process of analysing data to draw conclusions about the properties of the underlying probability distribution. In the following, a parameter is denoted by θ, and the corresponding *estimator* and *estimate* by $\hat{\theta}$. The estimator is the rule (usually a function) leading to a particular estimate for θ. First, some basic principles of parameter estimation are explained based on the parameters μ and σ^2 of a normal distribution. In this special case, the parameters are equal to the mean and variance of the random variable. The mean and variance of random variables are usually estimated by the *arithmetic mean* $\bar{x}$ and the *sample variance* s^2:

$$\bar{x} = \frac{1}{n}\sum_{i=1}^{n} x_i \qquad \textit{Eq. 2-41}$$

$$s^2 = \frac{1}{n-1}\sum_{i=1}^{n}\left(x_i - \bar{x}\right)^2 \qquad \textit{Eq. 2-42}$$

The arithmetic mean of a sample is also denoted by m in this thesis. The *sample coefficient of variation* V_x (sample CoV) is then defined as

$$V_x = \frac{s}{\bar{x}} \qquad \textit{Eq. 2-43}$$

The arithmetic mean $\bar{x}$, the sample variance s^2, and the sample CoV V_x are *statistics*; that is, they are functions of the data x_1, x_2,…, x_n. Since the random values x_i are random outcomes of the random variables X_i, the statistics $\bar{x}$ and s^2 are also random outcomes. Hence, the estimators $\hat{\mu} = \bar{X}$ and $\hat{\sigma} = S^2$ are random variables with a particular distribution. In the case of a normal distribution with given parameters μ and σ, $\bar{X}$ is t-distributed and S^2 is χ^2-distributed with $\nu = n - 1$ degrees of freedom if standardised as follows:

$$\frac{\bar{X} - \mu}{S/\sqrt{n}} \sim t_{n-1} \qquad \textit{Eq. 2-44}$$

$$\left(n-1\right)\frac{S^2}{\sigma^2} \sim \chi^2_{n-1} \qquad \textit{Eq. 2-45}$$

An estimator is *unbiased* if its mean is equal to the true value θ; that is, $\mathrm{E}(\hat{\theta}) = \theta$. The arithmetic mean and the sample variance as defined in Eq. 2-41 and Eq. 2-42 are unbiased estimators for the mean μ and the variance σ^2. In contrast, the sample standard deviation s (i.e. the square root of the sample variance s^2) is a biased estimator of the standard deviation σ. The same applies to estimating the CoV v_X of a probability distribution by the sample

CoV V_x. Another example of an unbiased estimator is the *sample covariance* $s_{x,y}$ with respect to estimating the covariance of two random variables X and Y:

$$s_{x,y} = \frac{1}{n-1}\sum_{i=1}^{n}\left(x_i - \bar{x}\right)\left(y_i - \bar{y}\right) \qquad \textit{Eq. 2-46}$$

In contrast, the corresponding *sample correlation coefficient* $r_{x,y}$ is a biased estimator of the true correlation coefficient $\rho_{X,Y}$. It is defined as

$$r_{x,y} = \frac{s_{x,y}}{s_x \, s_y} \qquad \textit{Eq. 2-47}$$

More important than being unbiased is that an estimator is *consistent*, which means that it converges to the true parameter if the sample size n is increased (Wasserman 2011). All of the estimators introduced above are consistent.

The most common parameter estimation methods are the method of moments and the maximum likelihood method, which are briefly explained next. Both methods are frequentist statistical methods. Parameters can also be estimated by Bayesian procedures, as described in Section 2.4, including a differentiation between the two approaches.

Method of moments

The method of moments is the easiest and perhaps most apparent approach for estimating probability distribution parameters. First, the stochastic moments μ_j of the distribution are estimated by the sample moments $\hat{\mu}_j$. The j-th sample moment is defined as

$$\hat{\mu}_j = \frac{1}{n}\sum_{i=1}^{n} x_i^j \qquad \textit{Eq. 2-48}$$

If the distribution function has k parameters, the first k stochastic moments are estimated by the sample moments. Since the stochastic moments can also be expressed as a function of the k unknown parameters of the probability distribution, k equations can be set up. Solving for the k parameters yields the parameter estimates. Most of the probability distributions presented in Section 2.3.4 are two-parameter distributions. In this case, the mean and the variance are usually estimated first. Since the mean and variance of a probability distribution can be calculated based on its parameters, the parameter estimates are given by the values that lead to the estimated mean and variance.

Maximum likelihood estimation

Although the method of moments is appealing due to its simplicity, maximum likelihood estimation (MLE) is more commonly used because the related estimators have more favourable properties. Since a discussion of these properties is beyond the scope of this brief

introduction, refer to Wasserman (2011) for more information. According to MLE, the distribution parameters are estimated by the values that maximise the *likelihood*. The likelihood is equal to the joint probability density of the observed values x_i; however, it is viewed as a function of the parameters θ_i since the data is given. The likelihood L is hence defined as

$$L\left(\boldsymbol{\theta}|\mathbf{x}\right) = \prod_{i=1}^{n} f\left(x_i|\boldsymbol{\theta}\right) \qquad \textit{Eq. 2-49}$$

where $\mathbf{x}$ is a vector containing the data x_1, x_2,…, x_n, and the vector $\boldsymbol{\theta}$ contains the parameters θ_i to be estimated. In some cases, the maximum of the likelihood function can be found analytically. If the analytical approach fails, the maximum of the likelihood function and thus the estimates for the parameters θ_i can be found numerically.

Confidence intervals

The use of confidence intervals can be helpful if the uncertainty involved in parameter estimation is to be quantified. Instead of giving only a point estimate (i.e. a single value for the parameter), an interval with a certain confidence level $1 - \alpha$ is constructed. If the confidence level is, for example, 95 %, the interval is called a "95 % confidence interval". The confidence intervals for the mean and variance of a normal distribution are defined as follows if both mean and variance are unknown:

Mean: $$C_{1-\alpha} = \left(\bar{x} + t_{n-1,\alpha/2} \frac{s}{\sqrt{n}}, \bar{x} + t_{n-1,1-\alpha/2,} \frac{s}{\sqrt{n}} \right) \qquad \textit{Eq. 2-50}$$

Variance: $$C_{1-\alpha} = \left(\frac{(n-1)s^2}{\chi^2_{n-1,1-\alpha/2}}, \frac{(n-1)s^2}{\chi^2_{n-1,\alpha/2}} \right) \qquad \textit{Eq. 2-51}$$

where $\bar{x}$ and s^2 are the arithmetic mean and the sample variance calculated from the data, and $t_{\nu,p}$ and $\chi^2_{\nu,p}$ are the p fractiles of the t- and χ^2-distribution, respectively, with ν degrees of freedom. The confidence intervals as presented above directly follow from the distribution of the arithmetic mean and the sample variance as given by Eq. 2-44 and Eq. 2-45.

The confidence level should not be misunderstood as the probability that the true value of the parameter lies in a constructed confidence interval. Such a statement is not possible since the parameter itself is not viewed as a random variable in frequentist (i.e. classical) statistics, and no probability statements can thus be made about it. However, a different interpretation is possible: In 95 % of the cases, where a 95 % confidence interval is constructed, the interval contains the true parameter (Wasserman 2011).

Bootstrap confidence intervals

If the distribution type of a random variable is unknown or the analytical derivation of a confidence interval is too complex or even impossible, the bootstrap (Efron 1979) is a helpful method for quantifying the uncertainty in parameter estimation and constructing confidence intervals. A comprehensive description of bootstrap procedures can be found in Efron and Tibshirani (1993).

Suppose that a sample $x_1, x_2, \ldots, x_n$ of size n is observed and a particular distribution parameter θ is estimated by $\hat{\theta}$. The parameter could be, for example, the mean μ, which would make the arithmetic mean $\bar{x}$ the statistic for estimating the parameter. For constructing confidence intervals, the probability distribution of $\bar{x}$ given μ, $f(\bar{x} \mid \mu)$, is required. Therefore, in the general case, the probability distribution $f(\hat{\theta} \mid \theta)$ is needed. The bootstrap method approximates this probability distribution by utilising the following procedure.

From the data $x_1, x_2, \ldots, x_n$, values $x_1^*, x_2^*, \ldots, x_n^*$ are randomly drawn with replacement. As a result of drawing with replacement, a particular value x_i can appear multiple times in the resampled data. Based on the resampled data $x_1^*, x_2^*, \ldots, x_n^*$, which is called a *bootstrap sample*, a bootstrap estimate $\hat{\theta}^*$ is calculated using the same function as for $\hat{\theta}$. The resampling is repeated m times, resulting in m bootstrap samples of size n. Thus, m bootstrap estimates $\hat{\theta}^*$ can be calculated from the respective bootstrap samples. The bootstrap principle states that the probability distribution of $\hat{\theta}$ given θ can be approximated by the probability distribution of $\hat{\theta}^*$ given the data $x_1, x_2, \ldots, x_n$. If the probability distribution type of X is known or assumed, the resampling can also be performed based on the corresponding probability function with the unknown parameter θ being set to $\hat{\theta}$, which is called *parametric bootstrap* (Efron and Tibshirani 1993).

Since a bootstrap estimate $\hat{\theta}^*$ can be generated any number of times, the standard deviation and percentiles of $\hat{\theta}^*$ can be determined with any desired accuracy. The standard deviation of $\hat{\theta}^*$ is the *bootstrap standard error*, which approximates the standard deviation of $\hat{\theta}$ given θ (i.e. the actual standard error in estimating θ). Furthermore, bootstrap confidence intervals can be constructed based on the simulated bootstrap distribution of $\hat{\theta}^*$ following different procedures. Mathematical justifications and a discussion of the advantages and disadvantages of the procedures for setting up bootstrap confidence intervals can be found in Efron (1987) and Hesterberg (2015). In the course of this thesis, bootstrap percentile intervals are utilised, which are shortly described next.

The *bootstrap percentile interval* with confidence level $1 - \alpha$ is given by

$$C_{1-\alpha} = \left(\hat{\theta}^*_{\alpha/2}, \hat{\theta}^*_{1-\alpha/2}\right) \qquad \textit{Eq. 2-52}$$

where $\hat{\theta}^*_{\alpha/2}$ and $\hat{\theta}^*_{1-\alpha/2}$ are the $\alpha/2$ and $1-\alpha/2$ fractiles of the simulated bootstrap estimates $\hat{\theta}^*$. Compared to other bootstrap confidence intervals, percentile intervals have the property of being transformation-respecting (Efron and Tibshirani 1993), which means that percentile intervals obtained for a particular parametrisation are equal to those that are first determined for a different parametrisation and subsequently transformed by applying the transformation function to the endpoints of the interval. Furthermore, percentile intervals are range-preserving; that is, they do not fall outside the range that the parameter θ can take. If, for example, θ is the expectation μ of a log-normal random variable, only positive values of μ are allowed. The accuracy of the bootstrap percentile interval can be improved by a bias correction (Efron and Tibshirani 1986). The bias-corrected percentile interval is defined as

$$C = \left(\hat{\theta}^*_{\alpha_1}, \hat{\theta}^*_{\alpha_2} \right) \qquad \textit{Eq. 2-53}$$

where the values α_1 and α_2 that define the fractiles can be determined by

$$\alpha_1 = \Phi\left[2z_0 + \Phi^{-1}\left(\frac{\alpha}{2} \right) \right] \quad \text{and} \quad \alpha_2 = \Phi\left[2z_0 + \Phi^{-1}\left(1 - \frac{\alpha}{2} \right) \right] \qquad \textit{Eq. 2-54}$$

$$\text{with} \quad z_0 = \Phi^{-1}\left[P(\hat{\theta}^* \le \hat{\theta}) \right]$$

If the median of $\hat{\theta}^*$ is equal to $\hat{\theta}$, then $z_0 = 0$ is obtained, and the bias-corrected percentile interval is equal to the percentile interval as defined by Eq. 2-52.

2.3.7 Goodness-of-Fit Testing

The purpose of goodness-of-fit testing is to check whether observed data is the outcome of a specific probability distribution function. The hypothesis that the sample originates from a particular distribution is called the "null hypothesis". It is rejected if the occurrence of the observed discrepancy between the data and the tested probability distribution is very improbable under the null hypothesis. "Very improbable" is defined quantitatively by selecting a significance level *p*. Various methods exist for testing the goodness of fit of a probability distribution for a given data set. Common methods include the chi-squared test (Pearson 1900) and the Kolmogorov-Smirnov test (Smirnov 1948). In the following investigations, the Anderson-Darling test (Anderson and Darling 1952) is employed, which is more sensitive to data in the tails of the probability distribution. This tail-sensitivity makes the test particularly suited for application in the context of structural reliability.

As with the Kolmogorov-Smirnov test, the Anderson-Darling test is based on the discrepancy between the *empirical distribution function* (EDF) of the observed data and the distribution function that is tested. For a random sample of size n with realisations $x_1 < x_2 < \ldots < x_n$, the EDF is defined as follows (Stephens 1986):

$$F_n(x) = \frac{\text{number of observations } \le x}{n} \qquad \textit{Eq. 2-55}$$

The difference between the EDF $F_n(x)$ and the tested distribution function $F(x)$ can be measured by, for example, a quadratic statistic:

$$Q = n\int_{-\infty}^{+\infty}\left[F_n(x) - F(x)\right]^2 \psi(x)\, dF(x) \qquad \textit{Eq. 2-56}$$

where $\psi(x)$ is a weighting function. The Anderson-Darling statistic A^2 is obtained if the weighting function is chosen as $\psi(x) = [F(x)\,(1 - F(x))]^{-1}$, which assigns more weight to both tails of the distribution. The statistic A^2 can be obtained by

$$A^2 = -n - \frac{1}{n}\sum_{i=1}^{n}(2i-1)\left[\ln F(x_i) + \ln\left(1 - F(x_{n+1-i})\right)\right] \qquad \textit{Eq. 2-57}$$

The null hypothesis is rejected if A^2 exceeds a critical value that depends on the chosen significance level p. Critical values for a modified test statistic A^{*2} are tabulated in Stephens (1974) for $F(x)$ being a normal distribution and in Stephens (1977) for $F(x)$ being a Gumbel distribution. The critical values are based on the assumption that the unknown parameters μ and σ^2 of a normal distribution are estimated by the arithmetic mean $\bar{x}$ and the unbiased sample variance s^2. In the case of a Gumbel distribution, it is assumed that the corresponding parameters are obtained by MLE. If both the mean and the variance of the distribution are unknown, the modified statistic A^{*2} is obtained by

Normal distribution: $$A^{*2} = A^2\left(1 + \frac{4}{n} - \frac{25}{n^2}\right) \qquad \textit{Eq. 2-58}$$

Gumbel distribution: $$A^{*2} = A^2\left(1 + \frac{0.2}{\sqrt{n}}\right) \qquad \textit{Eq. 2-59}$$

Instead of comparing the modified test statistic A^{*2} to a critical value belonging to a chosen significance level p, the actual significance level p corresponding to the observed statistic A^{*2} can be computed. Suitable functions for determining the observed significance level p are given in MIL-HDBK-17-1F (2002):

Normal distribution: $$p = \frac{1}{1 + \exp(-0.48 + 0.78\ln A^{*2} + 4.58A^{*2})} \qquad \textit{Eq. 2-60}$$

Gumbel distribution: $$p = \frac{1}{1 + \exp(-0.1 + 1.24\ln A^{*2} + 4.48A^{*2})} \qquad \textit{Eq. 2-61}$$

Anderson-Darling tests for log-normal distribution functions can be performed analogously to the procedure for a normal distribution if, instead of the observations x_i, the logarithms

ln x_i of the observed values are used. The equations for the Gumbel distribution can also be used if the test is to be performed for a two-parameter Weibull distribution (Stephens 1986). This is possible due to the relationship between the Gumbel and the two-parameter Weibull distribution: If X is Weibull distributed, then $Y = -\ln X$ is Gumbel distributed.

2.3.8 Definition of Populations

Before applying statistical methods of inference, the *population* for that the inference is performed must be clearly defined. A statistical population can be understood as a set of similar objects, and the properties of these objects can be described by probability distributions related to this particular population. Suppose that statistical inference is made about the properties of clay bricks, for example. In this case, it must be specified whether the considered population consists of all the bricks in a particular masonry wall, all the bricks in a building, all bricks belonging to the same production batch, or all clay bricks that were produced in a specific country and year, to name a few possibilities. Each of these definitions can lead to a different probability distribution for the properties of the bricks. Populations can be defined based on the physical phenomena influencing the considered random variables. Hence, the nature and origin of a random quantity, as well as spatial and temporal conditions, can be characterising criteria for a population (ISO 2394 2015). Dividing a population into sub-populations is often helpful, as it enables the estimation of variability within and between these sub-populations (JCSS 2001a). The selection of populations depends on the goal of the statistical evaluation and is therefore up to the modellers who want to draw conclusions. In the brick example above, the choice would be up to the engineers, who must make decisions based on the evaluation results, and their engineering judgement regarding the origin of uncertainties.

Statistical tests can sometimes help in defining populations. A *two-sample t-test* can be used to test whether two populations, each with a sample with size n, arithmetic mean $\overline{x}$, and variance s^2, have the same mean $\mu_1 = \mu_2$. If the hypothesis of equal means is rejected, this indicates that the two populations should not be merged into one population. The two-sample t-test assumes that both populations have the same variance $\sigma_1^2 = \sigma_2^2$. Furthermore, either the underlying random variables must be normally distributed, or the sample sizes must be large enough that the arithmetic means are approximately normally distributed according to the central limit theorem. The test statistic is defined as (Hedderich and Sachs 2020)

$$t = \frac{\left|\overline{x}_1 - \overline{x}_2\right|}{\sqrt{\frac{n_1 + n_2}{n_1\, n_2} \frac{\left(n_1 - 1\right) s_1^2 + \left(n_2 - 1\right) s_2^2}{n_1 + n_2 - 2}}} \qquad \textit{Eq. 2-62}$$

The hypothesis of equal means $\mu_1 = \mu_2$ is rejected with significance level p if t is larger than the $1 - p / 2$ fractile of the t-distribution with $n_1 + n_2 - 2$ degrees of freedom.

2.4 Bayesian Statistics

2.4.1 General and Bayesian Interpretation of Probability

Within statistics, two branches with differing philosophies and methods have evolved: frequentist and Bayesian statistics. The term "Bayesian" refers to the fundamental role of Bayes' theorem in Bayesian statistics. However, although Bayes' theorem dates back to 1763 (Bayes 1763), the adjective "Bayesian" for describing a particular category of statistical methods was uncommon until the 1950s (Fienberg 2006).

The main difference between Bayesian and frequentist statistics lies in their interpretation of probability. According to frequentist interpretation, probabilities are the limits of relative frequencies: If a random experiment is repeated many times, the relative frequency of the occurrence of an event A converges to the probability $P(A)$. In contrast, a probability represents a *degree of belief* in the Bayesian view. As a result, Bayesian probability statements can also be made about singular events, which are not subject to random variation (anymore) and cannot be described by a limiting relative frequency. The following is an example given by Wasserman (2011): "The probability that Albert Einstein drank a cup of tea on August 1, 1948, is .35." Such a probability is the expression of a person's degree of belief that this statement is true. It is conditional on the person's knowledge regarding this proposition and is updated if the person gains new information.

Although the Bayesian interpretation of probability causes controversy because it is sometimes perceived as too subjective, Bayesian methods offer some essential advantages over frequentist methods. The JCSS Probabilistic Model Code (JCSS 2001a) and ISO 2394 (2015) explicitly state that, with respect to structural reliability and the corresponding stochastic modelling of uncertainties, probabilities should be interpreted in a Bayesian way. Particularly for assessing existing structures, the Bayesian interpretation of probability and the resulting methods can be beneficial, as illustrated next.

Bayesian statistics offers a consistent framework for deriving answers to questions that frequentist methods cannot capture due to their different interpretation of probability. By definition, questions such as "What is the probability that the average compressive strength in this particular existing concrete column is below 20 N/mm²?" cannot be answered by frequentist inference. In contrast, Bayesian inference allows for the mathematical derivation of probability statements regarding singular events mostly subjected to epistemic uncertainty.

Using Bayesian methods requires the definition of *prior probability distributions* (short: priors) that reflect the prior information available before any data for answering a specific question is received. The need for prior distributions is sometimes stated as a main critique of Bayesian statistics since different inferential results from the same data can be obtained if two persons use different priors. There are also approaches for defining *non-informative priors*, which are priors that have minimal influence on the obtained results and, hence, aim at letting "the data speak for themselves" (Gelman et al. 2013). However, the possible incorporation of prior information can also be viewed as one of the main advantages of Bayesian methods. If an existing structure is assessed, the prior can be based on previous experience with similar structures. Thereby, the uncertainty can be strongly reduced.

According to the Bayesian philosophy, probability distributions are updated whenever new data is received. This consequent updating of prior experience in the light of new information reflects the process of assessing an existing structure well, regardless of whether Bayesian methods are explicitly used. Bayesian updating is, in principle, based on Bayes' theorem, which is usually given in the following form:

$$P\left(A|B\right)=\frac{P\left(B|A\right)P\left(A\right)}{P\left(B\right)}=\frac{P\left(B|A\right)P\left(A\right)}{P\left(B|A\right)P\left(A\right)+P\left(B|\bar{A}\right)P\left(\bar{A}\right)} \qquad \textit{Eq. 2-63}$$

In the context of Bayesian updating, the probability $P(A)$ is the prior probability of event A, which is updated to obtain the posterior probability $P(A|B)$, that is, the probability of A given the observance of B. For this update, the prior is multiplied by the likelihood $P(B|A)$ that B is observed if A is true and divided by $P(B)$, which ensures that the posterior probability $P(A|B)$ and the probability $P(\bar{A}|B)$ of the complementary event $\bar{A}$ add up to $P = 1$.

2.4.2 Bayesian Updating of Distribution Parameters

In contrast to frequentist methods, the Bayesian interpretation allows modelling distribution parameters θ as random variables. The parameters themselves can hence be described by probability distributions. If a stochastic model for the distribution of a random variable X is selected via a PDF $f(x|\theta)$ with parameter θ, and a prior distribution $f(\theta)$ for this parameter is chosen, the distribution of θ can be updated using Bayes' theorem in its continuous form:

$$f\left(\theta|\mathbf{x}\right)=\frac{f\left(\mathbf{x}|\theta\right)f\left(\theta\right)}{\int f\left(\mathbf{x}|\theta\right)f\left(\theta\right)d\theta}\propto L\left(\theta|\mathbf{x}\right)f\left(\theta\right) \qquad \textit{Eq. 2-64}$$

where $f(\theta|\mathbf{x})$ is the posterior distribution, $\mathbf{x}$ is the data, and $L(\theta|\mathbf{x}) = f(\theta|\mathbf{x})$ is the likelihood (see Section 2.3.6). The sign "$\propto$" denotes that the expressions are equal except for multiplication by a constant. Here, this constant is given by the term in the denominator, which is only needed for scaling the posterior PDF along the vertical axis such that it integrates to one.

If the probability distribution assigned to the parameter θ has parameters itself, these are called "hyperparameters". In many cases, the prior PDF can be chosen such that the resulting posterior PDF is of the same distribution type; then, the prior is a *conjugate prior* (Raiffa and Schlaifer 1961). The choice of conjugate priors is beneficial, as it reduces an update of the prior distribution to an update of the hyperparameters. For example, in the case of a normal distribution of X with parameters μ and σ^2, the joint conjugate prior is a normal-inverse-χ^2 distribution with prior hyperparameters n', m', v', and s'^2. This means that the variance is scaled inverse-χ^2 distributed with v' degrees of freedom and scale s'^2, and for a given variance σ^2, μ is normally distributed with mean m' and variance σ^2 / n':

$$\sigma^2 \sim \text{Inv-}\chi^2\left(v', s'^2\right) \qquad \textit{Eq. 2-65}$$

$$\mu \middle| \sigma^2 \sim \mathrm{N}\left(m', \sigma^2 / n'\right) \qquad \textit{Eq. 2-66}$$

As a result, the marginal (i.e. unconditional) prior distribution of μ is as follows:

$$\frac{\mu - m'}{\sqrt{s'^2 / n'}} \sim t_{v'} \qquad \textit{Eq. 2-67}$$

Since the normal-inverse-χ^2 distributed prior is conjugate, it can be shown that applying Eq. 2-64 leads to a joint posterior of μ and σ^2 that is also normal-inverse-χ^2 distributed. If data with sample size n, arithmetic mean m, and sample variance s^2 is acquired, the posterior hyperparameters n'', m'', v'', and s''^2 can be determined as (Gelman et al. 2013)

$$n'' = n' + n \qquad \textit{Eq. 2-68}$$

$$m'' = \frac{n'}{n''} m' + \frac{n}{n''} m \qquad \textit{Eq. 2-69}$$

$$v'' = v' + n \qquad \textit{Eq. 2-70}$$

$$s''^2 = \frac{1}{v''}\left[v' s'^2 + (n-1) s^2 + \frac{n\, n'}{n''} \left(m - m'\right)^2 \right] \qquad \textit{Eq. 2-71}$$

From these equations, it follows that the hyperparameters n' and v' can be interpreted as the number and degrees of freedom, respectively, of two hypothetical prior samples, one for estimating the mean and one for estimating the variance, where m' is the arithmetic mean, and s'^2 is the sample variance of the corresponding prior samples (ISO 2394 2015). The process of updating the normal distribution parameters is illustrated by Fig. 2-4 with specific values of the prior hyperparameters and sample results that serve as an example.

If no reasonable informative prior can be set up, a non-informative prior can be used instead. For normally distributed data **x**, the following non-informative prior is usually chosen (Gelman et al. 2013):

$$f\left(\mu,\sigma^2\right) \propto \frac{1}{\sigma^2} \quad \text{with } \mu \in \mathbb{R} \text{ and } \sigma^2 > 0 \qquad \textit{Eq. 2-72}$$

The non-informative prior distribution defined by Eq. 2-72 is an *improper prior*, as integrating over the domains of μ and σ^2 does not yield one but infinity (Wasserman 2011). However, the update according to Eq. 2-64 leads to a posterior distribution that is normal-inverse-χ^2 as in the case of a conjugate prior and thus proper. When applying the non-informative prior, the resulting posterior hyperparameters are $n'' = n$, $m'' = m$, $\nu'' = n - 1$, and $s''^2 = s^2$. Therefore, the posterior hyperparameters only depend on the data.

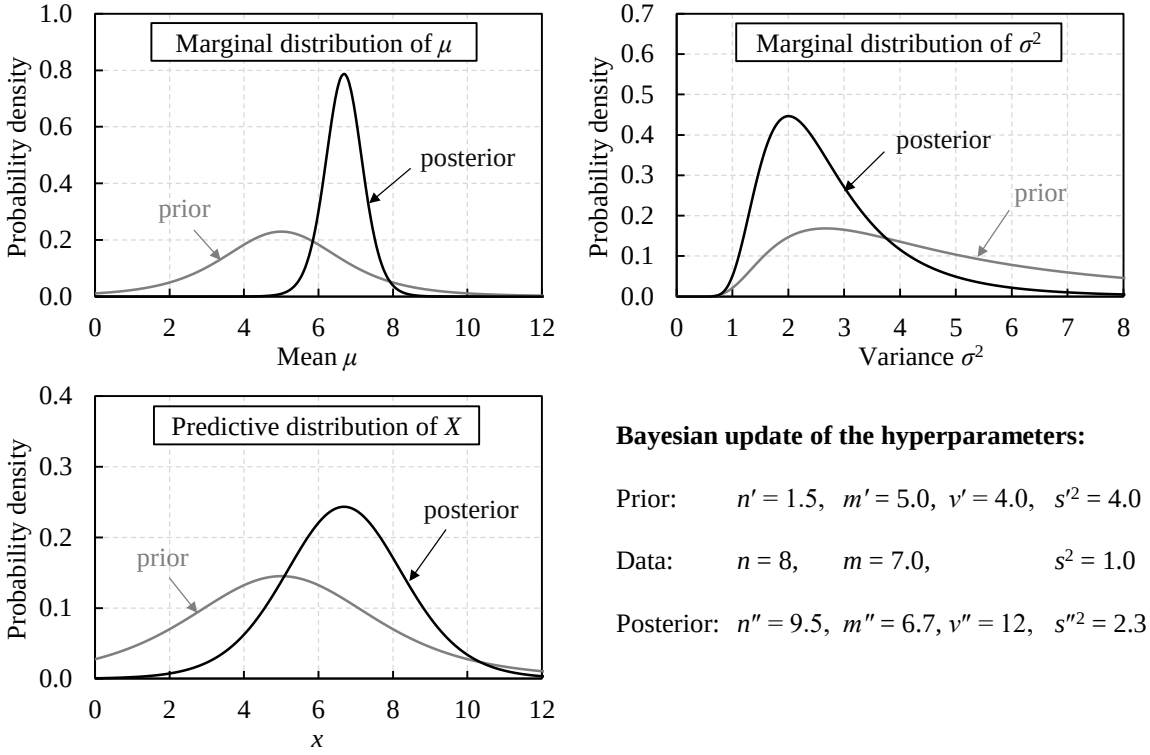

Fig. 2-4 Illustration of updating the parameters of a normally distributed random variable

In many cases, the probability distribution of the parameters μ and σ^2 is not of primary interest but the probability distribution of a future observation x of X, which is the *predictive distribution*. The data $\mathbf{x}$ can represent the outcome of compressive strength tests on bricks extracted from an existing masonry wall, for example. Then, the probability distribution for the compressive strength of the remaining bricks is of interest. The posterior predictive distribution is received by first formulating the joint distribution of X, μ, and σ^2 and then integrating out the unknown parameters μ and σ^2:

$$f\left(x|\mathbf{x}\right) = \int_{-\infty}^{+\infty}\int_{0}^{+\infty} f\left(x,\mu,\sigma^2|\mathbf{x}\right)d\sigma d\mu = \int_{-\infty}^{+\infty}\int_{0}^{+\infty} f\left(x\middle|\mu,\sigma^2\right) f\left(\mu,\sigma^2|\mathbf{x}\right)d\sigma d\mu \qquad \textit{Eq. 2-73}$$

The predictive distribution for the variable X thereby combines both material (aleatory) and statistical (epistemic) uncertainty in one probability distribution (see also Fig. 2-4). If shifted by m'' and scaled by $s''\,(1 + 1 / n'')^{0.5}$, the posterior predictive distribution of X is a t-distribution with ν'' degrees of freedom:

$$\frac{X - m''}{s''\sqrt{1+1/n''}} \sim t_{\nu''} \qquad \textit{Eq. 2-74}$$

2.5 Structural Reliability

2.5.1 General

Structural reliability can be defined as the probability that a structure satisfies a specified requirement over a defined period of time (Schneider 1996; EN 1990 2010). Since the complementary event of satisfying the requirement is failure, reliability can also be defined as $1 - P_\mathrm{f}$, where P_f is the *probability of failure*. According to this definition, the term "failure" does not necessarily refer to a structural collapse but can also relate to not meeting serviceability requirements. Determining the probability of failure is termed "reliability analysis".

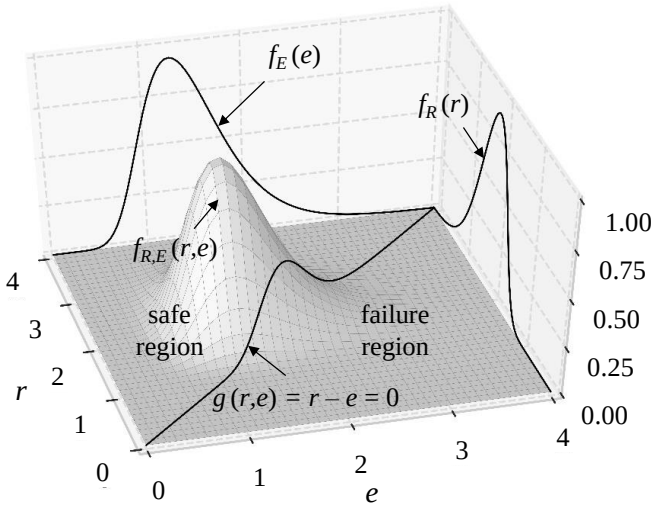

Fig. 2-5 Illustration of the joint probability density of R and E, the corresponding marginal distributions, the limit state function and the failure region

The transition between satisfying and not satisfying a specific requirement is called "limit state" and can be defined by a *limit state function* $g\,(\mathbf{X})$. Here, the vector $\mathbf{X}$ represents the *basic variables* $X_1, X_2, \ldots, X_n$, which are the random variables that influence the satisfaction or violation of the limit state. Violation of the limit state is usually defined by $g\,(\mathbf{x}) \leq 0$ (Melchers and Beck 2018). Hence, the limit state (hyper-)surface $g\,(\mathbf{x}) = 0$ divides the n-dimensional domain of the basic variables into a safe and a failure region, as illustrated in Fig. 2-5. The probability of failure is defined as the integral of the joint PDF $f_\mathbf{X}\,(\mathbf{x})$ over the failure region (e.g. Spaethe 1992; Melchers and Beck 2018):

$$P_\mathrm{f} = P\left[g\left(\mathbf{X}\right) \le 0 \right] = \int\int ... \int_{g(\mathbf{x}) \le 0} f_\mathbf{X}\left(x_1, x_2, ..., x_n\right) dx_1 dx_2 ... dx_n \qquad \textit{Eq. 2-75}$$

If the limit state function can be defined as $g(R, E) = R - E$, where the two random variables R and E are independent and represent the resistance of a structural member and the corresponding load effect, respectively, Eq. 2-75 simplifies to

$$P_\mathrm{f} = P\left(R - E \le 0\right) = \int_{-\infty}^{+\infty} \int_{-\infty}^{e} f_R\left(r\right) f_E\left(e\right) dr\, de \qquad \textit{Eq. 2-76}$$

The failure probability according to Eq. 2-76 can be interpreted as the volume under the joint PDF in the failure region (see Fig. 2-5).

Typical values of P_f for the ultimate limit state (i.e. for the collapse) of a structure are in the range of 10^{-7} to 10^{-3}. Due to these small values, the probability of failure is not a convenient measure for reliability. Therefore, structural reliability is typically expressed via the *reliability index* β, which is defined as

$$\beta = \Phi^{-1}\left(1 - P_\mathrm{f}\right) \quad \Leftrightarrow \quad P_\mathrm{f} = \Phi\left(-\beta\right) \qquad \textit{Eq. 2-77}$$

For the reliability index, standards for structural design and assessment often define target values β_t, which are considered an optimum compromise between the costs for achieving a particular reliability and the potential consequences of failure. For example, Table 2-1 lists the target reliability levels specified by EN 1990 (2010) for ultimate limit states and different consequence classes CC 1 to CC 3. The target reliability levels are defined for a reference period of both one and 50 years.

Table 2-1 Target reliability indices β_t in EN 1990 (2010)

Consequence class	**Target reliability index β_t for a reference period of**	
	1 year	**50 years**
CC 1 (low failure consequences)	4.2 ($P_\mathrm{f} = 1.3 \cdot 10^{-5}$)	3.3 ($P_\mathrm{f} = 4.8 \cdot 10^{-4}$)
CC 2 (medium failure consequences)	4.7 ($P_\mathrm{f} = 1.3 \cdot 10^{-6}$)	3.8 ($P_\mathrm{f} = 7.2 \cdot 10^{-5}$)
CC 3 (high failure consequences)	5.2 ($P_\mathrm{f} = 1.0 \cdot 10^{-7}$)	4.3 ($P_\mathrm{f} = 8.5 \cdot 10^{-6}$)

Assuming that the uncertainty of the outcome of the limit state function is dominated by time-variant load effects with independent maxima in subsequent years, the reliability index β_n for any reference period of n years can be determined by (EN 1990 2010)

$$\Phi\left(\beta_n\right) = \left[\Phi\left(\beta_{1\mathrm{a}}\right)\right]^n \qquad \textit{Eq. 2-78}$$

Based on Eq. 2-78, the target reliability indices $\beta_{\mathrm{t,1a}} = 4.7$ and $\beta_{\mathrm{t,50a}} = 3.8$ specified for CC 2 can be converted into each other. If, however, the uncertainty also originates from permanent load effects and time-invariant resistance parameters, the reliability indices related to one and 50 years are closer to each other than given by Eq. 2-78. In the theoretical case that

the limit state function only includes time-invariant variables, the reliability indices for the reference periods of one and 50 years are equal (i.e. $\beta_{1a} = \beta_{50a}$).

If the target reliability index $\beta_{t,50a} = 3.8$ for 50 years is viewed as the reference target reliability level, $\beta_{t,1a} = 4.7$ only gives an upper boundary for the suitable target reliability index for one year. In JCSS (2001a) and ISO 2394 (2015), the target reliability index for a reference period of one year, medium failure consequences, and medium relative costs of safety measures is specified as $\beta_{t,1a} = 4.2$. Investigations by Meinen and Steenbergen (2018) suggest that structural design according to the current Eurocodes leads to an average reliability of structural members close to $\beta_{t,50a} = 3.8$ for a reference period of 50 years and close to $\beta_{t,1a} = 4.2$ for a reference period of one year. These findings indicate that $\beta_{t,1a} = 4.2$ can be viewed as a suitable target reliability index for one year that corresponds to $\beta_{t,50a} = 3.8$. The theoretical background of target values β_t is illustrated in Section 2.6.2, where differences between appropriate target reliability levels for the design of new and the assessment of existing structures are discussed.

Table 2-2 Levels of probabilistic methods for structural design and assessment

Level		**Calculation methods**	**Limit state function**	**Uncertainty modelling**	**Verification format**	**Typical application**
I	semi-probabilistic	according to code	-	fixed partial factors	$E_d \leq R_d$	standard design and assessment situations
II$^-$	approximate probabilistic methods	as above but with adjusted partial factors	fixed sensitivity factors	any random variables	$E_d \leq R_d$	calibration of partial factors, special design and assessment situations
II		first-order second-moment method (FOSM)	approximated as linear	mean and variance considered	$\beta_{approx} \geq \beta_t$	
		first- or second-order reliability method (FORM/SORM)	approximated as linear or quadratic	random variables approximated as normal	$\beta_{approx} \geq \beta_t$	
III	exact probabilistic methods	analytical or numerical integration, Monte Carlo simulation	any	any random variables	$\beta \geq \beta_t$	
IV	risk-informed	decision-theoretic methods	see level II or III	see level II or III plus modelling of risks	minimum costs	derivation of target reliability, exceptional design and assessment situations

References: Melchers and Beck (2018), Glowienka (2007), ISO 2394 (2015), König and Hosser (1982), EN 1990 (2010), prEN 1990 (2020)

Structural design could theoretically be performed based on the general expression for the probability of failure as given in Eq. 2-75 by varying structural properties, such as cross-sectional areas or nominal material strengths, until the probability of failure complies with the target reliability index. Accordingly, the assessment of existing structures could be performed by determining the probability of failure with Eq. 2-75 and comparing the result to an appropriate target value. However, this is often not feasible for the following two reasons: First, calculating the probability of failure requires modelling all basic variables stochastically, which is too complex for everyday engineering practice; second, solving the integral in Eq. 2-75 analytically can be complicated or even impossible, depending on the limit state function and the joint PDF of the basic variables. Therefore, it is essential to differentiate between the various levels of probabilistic methods, each being justified in different situations (see Table 2-2). Most of these methods are illustrated in more depth in the following sections.

2.5.2 First-Order Reliability Method

The first-order reliability method (FORM) is an approximate method for calculating the failure probability P_f if the solution of the integral in Eq. 2-75 is too complex. The term "first-order" refers to a first-order Taylor series expansion of the limit state function, which is the main approximation of FORM. The development of FORM lead to the definition of key concepts in reliability theory, such as the design point and sensitivity factors. In this section, the main principles of FORM are presented in three chronological steps, which lead to the methodology currently understood as FORM.

The development of FORM began with so-called "second-moment" concepts, which only considered the first two stochastic moments of the basic variables, that is, their means and (co)variances (Melchers and Beck 2018). Within those concepts, the limit state function $g(\mathbf{X})$ is usually represented by a random variable Z with mean μ_Z and standard deviation σ_Z. If $g(\mathbf{X})$ is linear, μ_Z and σ_Z can be computed easily (see Section 2.3.3). Otherwise, μ_Z and σ_Z can be determined based on the first-order Taylor polynomial about the mean value. If, regardless of their actual probability distribution, all basic variables are viewed as normally distributed random variables and $g(\mathbf{X})$ is approximated as linear, then Z is also normally distributed, and the approximate probability of failure is

$$P_\mathrm{f} = P\left(Z \le 0\right) = \Phi\left(\frac{0-\mu_Z}{\sigma_Z}\right) \quad \Rightarrow \quad \beta = \frac{\mu_Z}{\sigma_Z} \qquad \textit{Eq. 2-79}$$

where the relationship for β results from the definition in Eq. 2-77. If the limit state function can be represented by $Z = R - E$, where R and E are independent, the reliability index is obtained as

$$\beta = \frac{\mu_R - \mu_E}{\sqrt{\sigma_R^2 + \sigma_E^2}} \qquad \textit{Eq. 2-80}$$

In the case of actually linear limit state functions and normally distributed basic variables X_i, the failure probability according to Eq. 2-79 is mathematically exact.

One main disadvantage of the early second-moment concepts is their lack of invariance regarding the formulation of the limit state function: The resulting probability of failure depends on the formulation of $g(\mathbf{X})$ if $g(\mathbf{X})$ is nonlinear. This disadvantage was overcome by the developments of Hasofer and Lind (1974), which resulted in the *Hasofer-Lind method*, sometimes also referred to as the first-order second-moment method (FOSM; see e.g. Melchers and Beck 2018). Hasofer and Lind (1974) suggested transforming the basic variables X_i, which are assumed to be normally distributed with mean μ_{Xi} and standard deviation σ_{Xi}, into standard normal variables Y_i:

$$Y_i = \frac{X_i - \mu_{X_i}}{\sigma_{X_i}} \qquad \textit{Eq. 2-81}$$

If the basic variables X_i are correlated, then they must first be transformed into independent variables. The transformation to standard normal variables leads to the transformed limit state function $h(\mathbf{Y})$. In Fig. 2-6, a reliability problem with two basic variables and corresponding limit state lines $g(x_1, x_2) = 0$ and $h(y_1, y_2) = 0$ is depicted in original space (left) and in transformed standard normal space (right), respectively. In standard normal space, all points with equal distance from the origin have equal probability density. According to Hasofer and Lind (1974), the reliability index β corresponds to the shortest distance from the origin to the limit state surface $h(\mathbf{y}) = 0$ in transformed space, which can be expressed as

$$\beta = \min\left\{ \left(\sum_{i=1}^{n} y_i^2 \right)^{1/2} \middle| \, h(\mathbf{y}) = 0 \right\} \qquad \textit{Eq. 2-82}$$

The point on the limit state surface with the highest joint probability density (i.e. the point closest to the origin in standard normal space) is the *design point* $\mathbf{y}^*$. Its coordinates y_i^* are the design values of the basic variables, which are given by

$$y_i^* = -\alpha_i \, \beta \qquad \textit{Eq. 2-83}$$

where the *sensitivity factors* α_i are the direction cosines of the vector $\mathbf{y}^*$ (see also Fig. 2-6). The sensitivity factors are a measure of the stochastic importance of the respective basic variables concerning the exceedance of the limit state condition $g(\mathbf{X}) = 0$. By definition, the sum of the squared sensitivity factors α_i^2 equals one.

If the limit state function is nonlinear, the reliability index β as defined by Hasofer and Lind (1974) can be found through an iterative procedure. The approximate failure probability P_f can then be determined via the relationship $P_f = \Phi^{-1}(\beta)$. This approximation of the failure probability is based on the first-order Taylor approximation of $g(\mathbf{y})$ about the design point $\mathbf{y}^*$ (see Fig. 2-6). In contrast to earlier second-moment methods, which are based on a Taylor expansion about the means of the basic variables, the expansion about the design point leads to the invariance of the resulting β with respect to the formulation of the limit state.

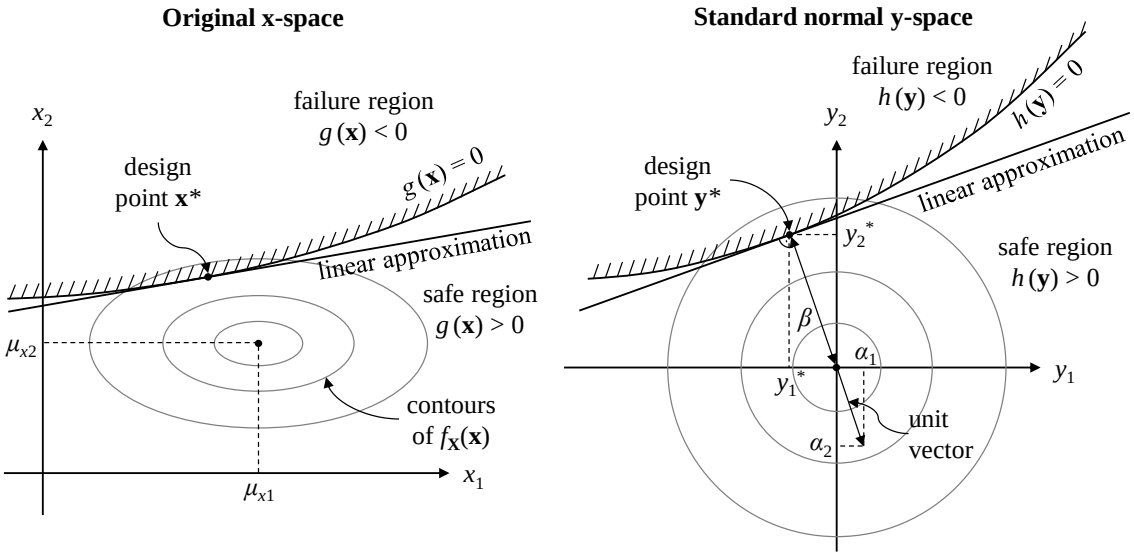

Fig. 2-6 Illustration of transformation into standard normal space, design point, reliability index β, and sensitivity factors α_i (two-dimensional case)

One disadvantage of the Hasofer-Lind method is that the probability distribution types of the basic variables are not considered. As an improvement, Rackwitz and Fießler (1976) suggested taking into account the actual distributions of the basic variables within the iteration procedure for finding the reliability index β. While the original distributions are still approximated by normal distributions, the corresponding means $\mu_{Xi,N}$ and variances $\sigma_{Xi,N}^2$ are now chosen such that, in the design point $\mathbf{x}^*$, both the PDFs and the CDFs of the normal distributions take the same values as the original distributions:

$$\Phi^{-1}\left(\frac{x_i^* - \mu_{X_i,\mathrm{N}}}{\sigma_{X_i,\mathrm{N}}}\right) = F\left(x_i^*\right) \quad \text{and} \quad \frac{1}{\sigma_{X_i,\mathrm{N}}}\varphi^{-1}\left(\frac{x_i^* - \mu_{X_i,\mathrm{N}}}{\sigma_{X_i,\mathrm{N}}}\right) = f\left(x_i^*\right) \qquad \textit{Eq. 2-84}$$

This type of approximation is also known as “normal tail transformation”. If included in the iteration procedures, it results in the *Rackwitz-Fiessler algorithm*. Due to the consideration of the actual probability distributions, the Rackwitz-Fiessler algorithm is no longer a second-moment method but belongs to the methods nowadays known as FORM.

For independent basic variables X_i, the algorithm for finding the design point $\mathbf{x}^*$, the reliability index β, and the sensitivity factors α_i can be formulated as follows (see Melchers and Beck 2018):

(1) Choose an initial design point $\mathbf{x}^* = \mathbf{x}^{(1)}$. An initial point can be $\mathbf{x}^{(1)} = \boldsymbol{\mu}_\mathbf{X}$.

(2) Calculate the means and standard deviations of the normal distributions that approximate the original distributions at $\mathbf{x}^{(m)}$, which is the current estimate of the design point:

$$\mu_{X_i,\mathrm{N}}^{(m)} = x_i^{(m)} - \sigma_{X_i,\mathrm{N}}^{(m)} \, \Phi^{-1}\left[F\left(x_i^{(m)}\right)\right] \qquad \textit{Eq. 2-85}$$

$$\sigma_{X_i,\mathrm{N}}^{(m)} = \frac{\varphi\left[\Phi^{-1}\left(F\left(x_i^{(m)}\right)\right)\right]}{f\left(x_i^{(m)}\right)} \qquad \textit{Eq. 2-86}$$

(3) Calculate the sensitivity factors α_i based on the partial derivatives of the limit state function at the current estimate $\mathbf{x}^{(m)}$ of the design point:

$$\alpha_i^{(m)} = \frac{\sigma_{X_i,\mathrm{N}}^{(m)} \left.\dfrac{\partial g}{\partial x_i}\right|_{\mathbf{x}^{(m)}}}{l} \quad \text{with} \quad l = \sqrt{\sum_{i=1}^{n}\left(\sigma_{X_i,\mathrm{N}}^{(m)} \left.\frac{\partial g}{\partial x_i}\right|_{\mathbf{x}^{(m)}}\right)^2} \qquad \textit{Eq. 2-87}$$

(4) Calculate the current estimate of the reliability index β:

$$\beta^{(m)} = -\sum_{i=1}^{n} \frac{x_i^{(m)} - \mu_{X_i,\mathrm{N}}^{(m)}}{\sigma_{X_i,\mathrm{N}}^{(m)}} \alpha_i^{(m)} \qquad \textit{Eq. 2-88}$$

(5) Determine a new estimate for the design point. In standard normal space, this new design point is given by the shortest connection from the origin to the current first-order Taylor approximation of the limit state hypersurface $g(\mathbf{y}) = 0$.

$$x_i^{(m+1)} = \mu_{X_i,\mathrm{N}}^{(m)} - \sigma_{X_i,\mathrm{N}}^{(m)} \, \alpha_i^{(m)} \left[\beta^{(m)} + \frac{g\left(\mathbf{x}^{(m)}\right)}{l}\right] \qquad \textit{Eq. 2-89}$$

Steps (2) to (5) are repeated until the differences between two successive estimates for $\mathbf{x}^*$ and β are lower than a predefined threshold.

FORM can be extended to the second-order reliability method (SORM) if, in addition to the linear terms of the Taylor expansion, the curvature of the limit state function is considered. For highly nonlinear limit state functions, SORM can be helpful to increase the accuracy in estimating the failure probability (Breitung 1984).

2.5.3 Monte Carlo Simulation

The Monte Carlo method belongs to the mathematically exact level III approaches for determining the failure probability. Performing reliability analyses by means of Monte Carlo simulations (MCS) is, at least in its simplest form, straightforward: In each of many stochastic simulation runs, random values for the basic variables are generated according to their probability distributions. A check is then performed to determine whether these random values lead to failure, given by $g(\mathbf{x}) \leq 0$. An unbiased estimate $\hat{P}_\mathrm{f}$ of the probability of failure is given by the number of simulation runs n_fail that lead to failure divided by the total number of simulation runs n_sim:

$$\hat{P}_\mathrm{f} = \frac{n_\mathrm{fail}}{n_\mathrm{sim}} \qquad \textit{Eq. 2-90}$$

The variance and CoV of the estimator $\hat{P}_\mathrm{f}$ are as follows (Lemaire 2009):

$$\mathrm{Var}\left(\hat{P}_\mathrm{f}\right) = \frac{P_\mathrm{f}\left(1-P_\mathrm{f}\right)}{n_\mathrm{sim}} \approx \frac{P_\mathrm{f}}{n_\mathrm{sim}} \quad \Rightarrow \quad v_{\hat{P}_\mathrm{f}} \approx \frac{1}{\sqrt{n_\mathrm{sim}\, P_\mathrm{f}}} \qquad \textit{Eq. 2-91}$$

Hence, for $n \to \infty$, the estimate converges to the true failure probability P_f. However, this "crude" version of the Monte Carlo method requires a large number of simulation runs. For example, for $P_\mathrm{f} = 10^{-6}$, the number of simulation runs must be higher than 10^8 to reach a CoV below 10 %. If the limit state function $g(\mathbf{X})$ is given in analytical form, such a number of simulation runs is feasible for modern computers. However, if the limit state function is given only implicitly, for example through a finite element model, and each evaluation of $g(\mathbf{x})$ thus requires a finite element simulation, reliability analysis via the crude Monte Carlo method becomes practically impossible. Therefore, many variance reduction techniques have been developed to minimise the required number of either simulation runs or direct evaluations of the limit state function. Such techniques include adaptive importance sampling (Bucher 1988), the response surface method (Bucher and Bourgund 1990), and subset simulation (Au and Beck 2001), among others. For further information on variance reduction techniques, see Lemaire (2009) and Rubinstein and Kroese (2017).

The generation of random values in each simulation run is typically based on *pseudorandom numbers*. The term "pseudorandom" denotes that these numbers are obtained via a deterministic code that produces a sequence of numbers that only appear to be random. If produced by a good pseudorandom number generator, the most important statistical properties of such sequences are equivalent to those of actual random sequences (Rubinstein and Kroese 2017). The deterministic code starts with a particular *seed*, which is an arbitrary number specified by the user. Pseudorandom numbers can hence be reproduced by selecting the same seed again. Random number generators usually produce samples of random

variables U_i that are uniformly distributed between 0 and 1. Therefore, random samples of a specific random variable X_i can be generated by applying the inverse CDF:

$$x_i = F^{-1}(u_i) \qquad \textit{Eq. 2-92}$$

In addition to the Monte Carlo method being utilised for estimating the failure probability P_f, a more general application is drawing random samples from a function $Y(\mathbf{X})$ of several random variables to determine the distribution of Y. This approach can be helpful if the function $Y(\mathbf{X})$ is only given by a finite element model, for example, and, thus, neither the function itself nor its probability distribution can be described analytically. Then, the stochastic moments of Y can be estimated based on the random sample generated by Monte Carlo simulation. In such a case, *Latin hypercube sampling* (LHS) can be a helpful variance reduction technique (see e.g. Olsson and Sandberg 2002).

If LHS is applied, the number n_{sim} of performed simulation runs must be chosen beforehand. Then, the range of each of k random variables X_i is divided into n_{sim} equally probable intervals. The interval (0, 1) of the possible outcomes of the uniform random variables U_i is hence divided into n_{sim} intervals of equal length. For each of these intervals, a random value is generated, thereby ensuring that the whole range of possible values of the random variables is well covered. These n_{sim} random values for each of the k random variables are then randomly permuted to receive n_{sim} combinations with one random value for each random variable. As an example, a sampling plan for $k = 2$ random variables and $n_{sim} = 5$ simulation runs is illustrated in Fig. 2-7. Each of the five sample points represents one combination of u_1 and u_2. By definition, each row and line must contain exactly one point. LHS can be further improved by ensuring that the sample points do not form clusters but cover the whole k-dimensional sampling space more uniformly (Olsson and Sandberg 2002).

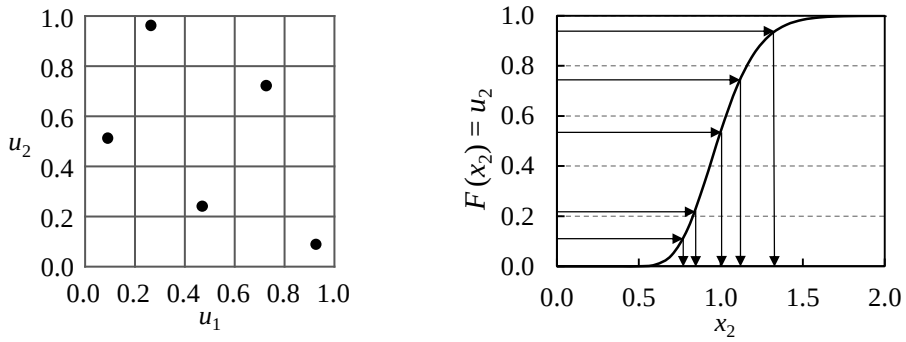

Fig. 2-7 Latin hypercube sampling plan (two random variables, five simulation runs) and subsequent transformation of u_2 to values x_2 of the desired distribution

2.5.4 Calibration of Partial Factors

Probabilistic approaches of level II and III are too complex for ordinary structural engineering projects. Therefore, semi-probabilistic approaches have been developed, in which

the basic variables are no longer represented by random variables but by characteristic values and corresponding partial factors. The partial factors reflect the uncertainty associated with the random variable and the importance of the basic variable regarding the considered limit state. The reliability-based verification format $\beta \geq \beta_t$ is replaced by the verification format $E_d \leq R_d$, where E_d and R_d are the design values of the load effect and the resistance, respectively. In principle, those design values reflect the FORM design point.

In EN 1990 (2010), the general definition of E_d and R_d for the verification of ultimate limit states is as follows:

$$E_d = \gamma_{Ed} E\left\{\gamma_{g,j} G_{k,j};\ \gamma_{q,1} Q_{k,1};\ \gamma_{q,i}\psi_{0,i} Q_{k,i}\right\} \quad j \geq 1;\ i > 1$$
$$R_d = \frac{1}{\gamma_{Rd}} R\left\{\eta_i \frac{X_{k,i}}{\gamma_{m,i}}; a_d\right\} \quad i \geq 1 \qquad \textit{Eq. 2-93}$$

where $E\{\cdot\}$ and $R\{\cdot\}$ represent the load effect and resistance, respectively, which are functions of the enclosed variables; γ_{Rd} and γ_{Ed} are partial factors addressing model uncertainty; $G_{k,j}$, $Q_{k,i}$ and $X_{k,i}$ are the characteristic values of permanent loads, variable loads, and material properties, respectively; and $\gamma_{g,j}$, $\gamma_{q,i}$, and $\gamma_{m,i}$ are the corresponding partial factors. The combination factor $\psi_{0,i}$ is applied to non-dominant variable loads and considers the unlikeliness of the simultaneous occurrence of the variable load maxima. The factor η_i addresses a potentially required conversion of a material property to represent the actual material behaviour in the structure, and a_d denotes the design values of geometrical properties. In typical cases, however, geometrical properties are applied as their nominal values a_{nom}, and the corresponding variability is covered by the partial factors addressing model uncertainty. Furthermore, γ_{Rd} and γ_{Ed} are usually merged with γ_m, γ_g, and γ_q by multiplication. Instead of separately considering γ_{Rd} and γ_m, for example, a partial factor $\gamma_M = \gamma_m \gamma_{Rd}$ is applied, which covers both model uncertainty and material variability.

The characteristic values denoted by the index "k" are defined as specified fractiles of the corresponding basic variables. By applying the partial factors and, if applicable, the combination factor ψ_0 and the conversion factor η, the design values X_d, G_d and Q_d are obtained. The fundamental problem of calibrating partial factors is that they are defined as a set of fixed values, although they are applied to different design situations in which different sensitivity factors α_i for the basic variables occur. Since the design value of a basic variable is defined by its probability distribution and its sensitivity factor according to FORM, the design values obtained by fixed partial factors can never exactly lead to the FORM design values in all cases. As a result, fixed partial factors can never lead to a constant reliability level equal to the target β_t. In NABau (1981), for example, a minimum reliability index of $\beta_{min} = \beta_t - 0.5$ is accepted when sets of fixed partial factors are derived.

There are two main ways to derive fixed sets of partial factors (ISO 2394 2015). The first approach is the *design value method* (DVM), which is based on fixed sensitivity factors that are meant to cover a wide range of typical design situations. The second option is *reliability-based code optimisation*, which aims at setting up partial factors such that the deviation of the resulting reliability level from the target reliability index is minimised for the most typical design situations.

Due to the choice of fixed sensitivity factors, the concept behind the DVM is also referred to as the *simplified level II method* or *level II⁻ method* (König and Hosser 1982). One of the first appearances of the DVM was in NABau (1981), and the DVM is also given as a method for deriving partial factors in EN 1990 (2010). If load effect E and resistance R are each represented by a single random variable, and the sensitivity factors α_E and a_R as well as the target reliability index β_t are given, the corresponding design values can be obtained as follows:

$$\begin{aligned} P\left(E > E_\mathrm{d}\right) &= \Phi\left(\alpha_E \beta_\mathrm{t}\right) \quad \Leftrightarrow \quad E_\mathrm{d} = F_E^{-1}\left[\Phi\left(-\alpha_E \beta_\mathrm{t}\right)\right] \\ P\left(R \le R_\mathrm{d}\right) &= \Phi\left(-\alpha_R \beta_\mathrm{t}\right) \quad \Leftrightarrow \quad R_\mathrm{d} = F_R^{-1}\left[\Phi\left(-\alpha_R \beta_\mathrm{t}\right)\right] \end{aligned} \qquad \textit{Eq. 2-94}$$

In EN 1990 (2010), fixed sensitivity factors $\alpha_E = -0.7$ and $a_R = 0.8$ are proposed for typical design situations. Usually, E and R are functions of several random variables. In this more general case, the design value Y_d of a particular random variable Y can be obtained as

$$Y_\mathrm{d} = F_Y^{-1}\left[\Phi\left(-\alpha_Y \beta_\mathrm{t}\right)\right] \qquad \textit{Eq. 2-95}$$

In this general case, $\alpha_Y = \alpha_R = 0.8$ can be applied for dominant resistance variables and $\alpha_Y = \alpha_E = -0.7$ for dominant load variables. For non-dominant variables, $0.4\ \alpha_E = -0.28$ and $0.4\ \alpha_R = 0.32$ are applicable (ISO 2394 2015). Partial factors can then be determined as the ratio of characteristic value to design value for resistance variables and the ratio of design value to characteristic value for load variables.

The background of fixed sensitivity factors is illustrated in König and Hosser (1982) and König et al. (1982). Here, fixed values for α_R and α_E are derived based on normal distributions for E and R and an accepted minimum reliability index of $\beta_\mathrm{min} = \beta_\mathrm{t} - 0.5$, leading to $\beta_\mathrm{min} / \beta_\mathrm{t} = 0.89$ for $\beta_\mathrm{t} = 4.7$. If a typical range for the ratio σ_E / σ_R of the standard deviations of E and R is defined, fixed sensitivity factors α_E and α_R can be determined according to

$$\alpha_E = -\frac{\beta_\mathrm{min}}{\beta_\mathrm{t}} \frac{\sqrt{1+\left(\max \sigma_E/\sigma_R\right)^2} - \sqrt{1+\left(\min \sigma_E/\sigma_R\right)^2}}{\max \sigma_E/\sigma_R - \min \sigma_E/\sigma_R} \qquad \textit{Eq. 2-96}$$

$$\alpha_R = \frac{\beta_\mathrm{min}}{\beta_\mathrm{t}} \sqrt{1+\left(\min \sigma_E/\sigma_R\right)^2} + \alpha_E \ \min \sigma_E/\sigma_R \qquad \textit{Eq. 2-97}$$

For $\beta_{min} / \beta_t = 0.89$, the established sensitivity factors $\alpha_E = -0.7$ and $a_R = 0.8$ can be obtained based on an application range of $0.15 \leq \sigma_E / \sigma_R \leq 3.48$ (König and Hosser 1982). At the limits of this application range, the actual sensitivity factors would be $\alpha_E = -0.148$ and $\alpha_R = 0.989$ as well as $\alpha_E = -0.961$ and $\alpha_R = 0.276$. Hence, the fixed sensitivity factors are applicable to a wide range of actual sensitivity factors. The relationship between the accepted minimum reliability index, the application range concerning the ratio σ_E / σ_R and the resulting fixed sensitivity factors are illustrated in Fig. 2-8. It is evident that in the middle of the accepted range of σ_E / σ_R, the values $\alpha_E = -0.7$ and $a_R = 0.8$ lead to a reliability index β that is larger than the target value β_t since the sum of the squared sensitivity factors is greater than one. The maximum reliability index is $\beta_{max} = 1.063\ \beta_t$.

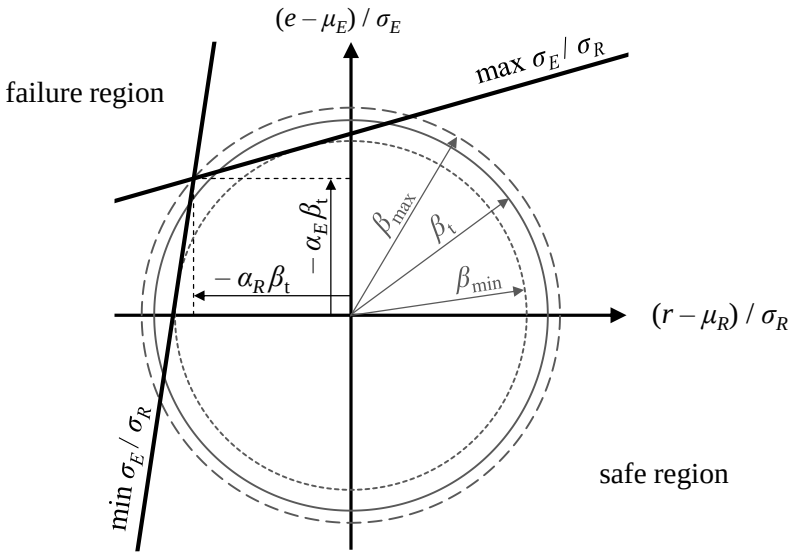

Fig. 2-8 Illustration of the boundaries for the fixed sensitivity factors $\alpha_R = 0.8$ and $\alpha_E = -0.7$ according to König and Hosser (1982)

In contrast to the range for σ_E / σ_R defined in König and Hosser (1982), EN 1990 (2010) defines the application limits for the fixed sensitivity factors $\alpha_E = -0.7$ and $a_R = 0.8$ as $0.16 \leq \sigma_E / \sigma_R \leq 7.6$. Based on these limits, $0.9\ \beta_t$ and $0.8\ \beta_t$ can be computed as implicitly accepted minimum reliability indices at the lower and upper limit of the application range, respectively. EN 1990 (2010) specifies that, outside of the application range, $\alpha_i = \pm 1.0$ should be used for the variable with the larger standard deviation and $\alpha_i = \pm 0.4$ for the variable with the smaller standard deviation.

The fixed sensitivity factors $\alpha_E = -0.7$ and $a_R = 0.8$ are usually applied in combination with the target reliability index $\beta_{t,50a}$ for a reference period of 50 years; see, for example, Annex D.7.3 of EN 1990 (2010) and fib bulletin 80 (2016). Therefore, for CC 2 with $\beta_{t,50a} = 3.8$, the design value of a dominant resistance variable approximately corresponds to the 0.1 % fractile of this variable:

$$P\left(R \le R_{\mathrm{d}}\right) = \Phi\left(-\alpha_R\, \beta_{\mathrm{t,50a}}\right) = \Phi\left(-0.8 \cdot 3.8\right) = 0.12\,\% \qquad \textit{Eq. 2-98}$$

There are two main reasons why different fixed sensitivity factors should be applied when the reference period for the target reliability index is changed from 50 years to one year. First, the actual FORM sensitivity factors α_R for the resistance are, on average, lower if the reliability analysis is performed for a reference period of one instead of 50 years (Meinen and Steenbergen 2018). Second, changing the sensitivity factors is needed for compatibility. If the fixed sensitivity factors were independent of the reference period, applying $\beta_{\mathrm{t,50a}} = 3.8$ and $\beta_{\mathrm{t,1a}} = 3.8$ would lead to the same design resistance, although $\beta_{\mathrm{t,1a}} = 3.8$ actually represents a lower target reliability level. Meinen and Steenbergen (2018) determined the suitable fixed sensitivity factor $\alpha_{R,\mathrm{1a}}$ for a one-year reference period based on the requirement that the design resistances obtained by the simplified level II approach should be equal for both reference periods. Assuming that $\beta_{\mathrm{t,50a}} = 3.8$ corresponds to $\beta_{\mathrm{t,1a}} = 4.2$ (see Section 2.5.1), $\alpha_{R,\mathrm{1a}}$ is obtained as follows:

$$\alpha_{R,\mathrm{1a}}\, \beta_{\mathrm{t,1a}} = \alpha_R\, \beta_{\mathrm{t,50a}} \quad \Rightarrow \quad \alpha_{R,\mathrm{1a}} = \alpha_R\, \frac{\beta_{\mathrm{t,50a}}}{\beta_{\mathrm{t,1a}}} = 0.8\, \frac{3.8}{4.2} \approx 0.7 \qquad \textit{Eq. 2-99}$$

If $\alpha_R = 0.8$ is changed to $\alpha_{R,\mathrm{1a}} = 0.7$, then the sensitivity factor α_E must also be adjusted (see e.g. Sykora and Diamantidis 2021). Instead of $\alpha_E = -0.7$, $\alpha_{E,\mathrm{1a}} = -0.8$ should be applied to keep the sum of the squared sensitivity factors constant.

One advantage of the simplified level II approach is that no reliability analyses are needed to derive partial factors, thus making its application straightforward as soon as stochastic models for the random variables are available. The simplified level II approach can hence be convenient when deriving partial factors for existing structures based on newly acquired statistical information about the respective random variables (see Section 2.6.3). However, the set of partial factors derived through the DVM is not optimal concerning the resulting reliability level. Therefore, reliability-based optimisation can be viewed as the preferred method for calibrating the whole set of partial factors $\boldsymbol{\gamma}$ (and all other safety elements) within structural design codes.

The steps of the reliability-based optimisation procedure are, for example, described in ISO 2394 (2015) and prEN 1990 (2020) and are as follows:

(1) Define a set of representative structures and corresponding design situations.
(2) Select the target reliability index β_{t}.
(3) Specify the general verification format, including the type and number of safety elements and rules for load combinations.
(4) Formulate limit state equations for the relevant failure modes, and select stochastic models for the involved basic variables.

(5) Calibrate the partial factors $\boldsymbol{\gamma}$ iteratively such that the following expression is minimised:

$$\sum_{i=1}^{n} w_i \left[\beta_i(\boldsymbol{\gamma}) - \beta_t \right]^2 \qquad \textit{Eq. 2-100}$$

where w_i is a weighting factor addressing the relative frequency or importance of the i-th design situation, and $\beta_i(\boldsymbol{\gamma})$ is the reliability index for the i-th design situation given the current set of partial factors $\boldsymbol{\gamma}$.

Hence, reliability-based code optimisation leads to a minimum deviation from the target reliability index for a predefined verification format and a given number of safety elements. Eq. 2-100 can also be extended by assigning more weight to reliability indices smaller than the target or by defining a lower limit of resulting reliability indices. The more safety elements included in the code, the smaller the deviations from β_t can become.

2.5.5 Reliability of Structural Systems

Structures usually consist of several members, which form a structural system with various possible failure mechanisms. Depending on the type of system and its inherent redundancy, the failure of one member does not necessarily lead to the failure of the whole system. The failure probability of a structural system can consequently be higher or lower than the failure probabilities of its single members. In general, system reliability analysis is complex due to many possible failure modes, each represented by a corresponding limit state function, possible correlations between load effects and between member resistances, and an influence of the loading sequence, to name a few challenges (Melchers and Beck 2018). Given this complexity, the reliability requirements as currently specified by EN 1990 (2010) are related to structural members instead of structural systems. However, the behaviour of structural systems is essential with regard to possible failure consequences. Idealisations of structural systems can be beneficial to understanding the general influence of system effects on structural reliability. Furthermore, the upper and lower bounds of system reliability can be defined based on suitable system idealisations. Since structural members that consist of several components, for example members with component-to-component variability of material properties (see Section 2.3.5), can be viewed as structural systems themselves, the explanations in this section also apply at this lower level.

Two categories of idealised systems can be defined: series systems and parallel systems. *Series systems* are also called “weakest link systems” since the failure of a single element leads to the failure of the whole system. If a series system is equivalent to a chain consisting of several links (i.e. all elements are subjected to the same load effect E), and the resistances R_i of the single elements are independent and identically distributed (see Fig. 2-9), the CDF of the system resistance R_{sys} is

$$F_{R_{sys}}(r) = 1 - P(R_{sys} > r) = 1 - P(R_i > r)^n = 1 - \left[1 - F_{R_i}(r)\right]^n \qquad \textit{Eq. 2-101}$$

In contrast, *parallel systems* only fail if every single element fails. For parallel structural systems, the material behaviour of the elements must be further specified. A lower and upper bound of the element behaviour after reaching the element resistance R_i is given by the perfectly brittle and the perfectly ductile behaviour (Nowak and Collins 2013). In Fig. 2-9, both cases are illustrated in combination with linear elastic behaviour before reaching the element resistance. The following considerations correspond to idealised parallel systems subjected to a single load that leads to equal strain ε in all elements (see Fig. 2-9).

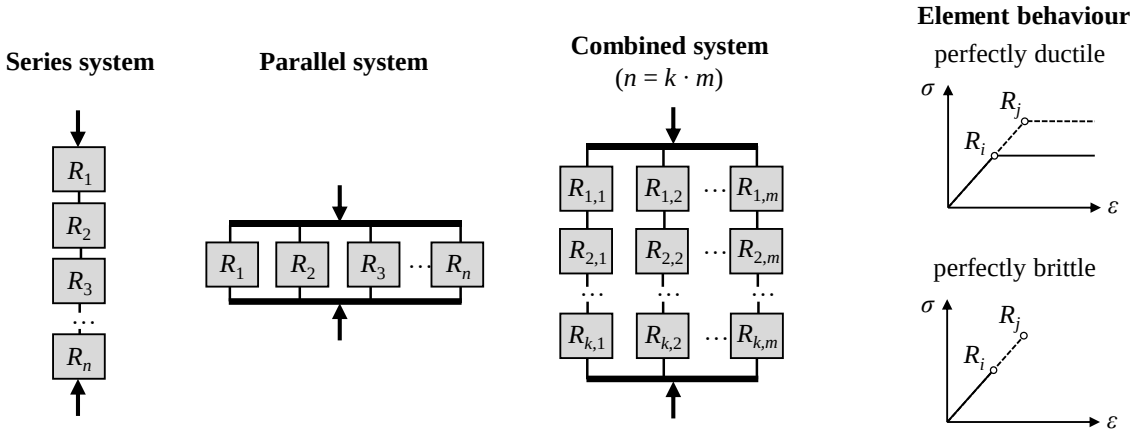

Fig. 2-9 Idealised systems and elements

In the case of perfectly ductile elements, the system resistance is given by the sum of the element resistances. For independent and identically distributed element resistances with mean μ and variance σ^2, the system resistance R_{sys} and its mean and variance are

$$R_{sys} = \sum_{i=1}^{n} R_i \quad \Rightarrow \quad \mu_{sys} = \sum_{i=1}^{n} \mu_i = n\,\mu \qquad \sigma_{sys}^2 = \sum_{i=1}^{n} \sigma_i^2 = n\,\sigma^2 \qquad \textit{Eq. 2-102}$$

The mean and variance of the system resistance directly follow from the relationships for functions of random variables given in Section 2.3.3.

If an element behaves in a perfectly brittle manner, its contribution to the system resistance reduces to zero as soon as the element resistance is reached. After each element failure, the system load can only be further increased if the load that acted on the failed element can be redistributed to the remaining intact elements. If each element has the same stiffness, this type of system is also referred to as a "Daniels system" (see Daniels 1945). Its resistance is given by (Hohenbichler and Rackwitz 1983)

$$R_{sys} = \max\left\{nR_1, (n-1)R_2, (n-2)R_3, ..., R_n\right\} \quad \text{with} \quad R_1 \le R_2 \le ... \le R_n \qquad \textit{Eq. 2-103}$$

The behaviour of real structural elements lies between the two idealised cases of perfectly ductile and perfectly brittle behaviour. Furthermore, real systems are usually a combination of parallel and series systems. Such a combination could be a parallel system, for example, in which the elements themselves are series systems (see Fig. 2-9).

In Fig. 2-10, the effect of the system configuration on the PDF of the system resistance R_{sys} is illustrated for the previously mentioned idealisations. The PDFs are obtained by MCS for $n = 10$ independent elements, each having a log-normally distributed resistance with a CoV of $\upsilon = 0.2$. The PDF is normalised by the mean element resistance μ_{el} and the number n_{par} of parallel elements. It is noted that the PDF of the element resistance is equivalent to the PDF of the normalised resistance of a system with perfectly correlated elements.

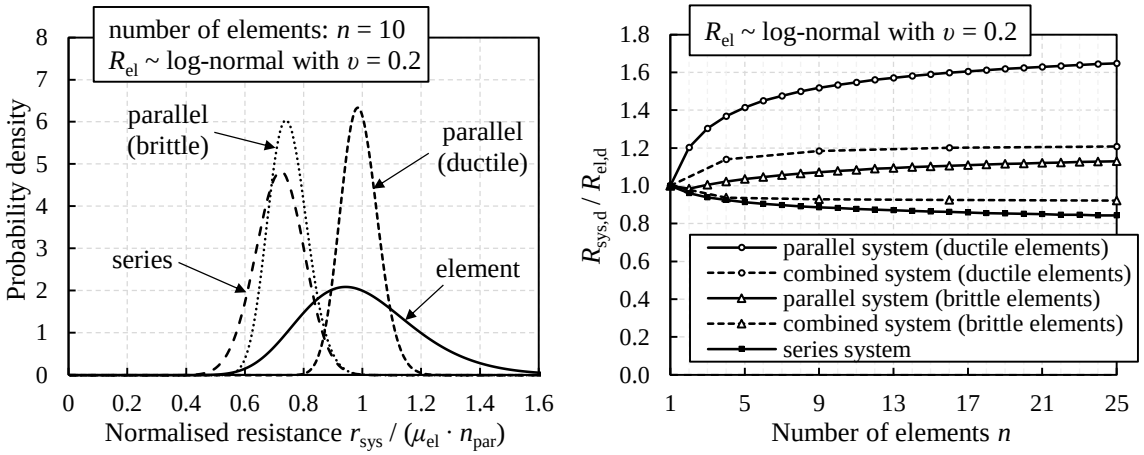

Fig. 2-10 Probability density (left) and design values (right) for the resistance of different idealised systems

Compared to the PDF of the element resistance, two main effects on the system resistance are evident. First, the CoVs of the system resistances are lower than the CoV of the element resistance. Second, except for the parallel system with perfectly ductile elements, the mean of the normalised system resistance is lower than the mean of the element resistance. Since the area under the left tail of the PDF is essential with respect to structural reliability, the two effects have an opposite influence on system reliability.

The comparison of lower quantiles of the system resistance to lower quantiles of the element resistance illustrates whether the configurations in Fig. 2-9 have a positive or negative effect on the system reliability. For this purpose, level II^{-} design values of the system resistance are presented in Fig. 2-10 (right) based on a target reliability of $\beta_t = 3.8$ and a sensitivity factor $\alpha_R = 0.8$. The resulting design resistances $R_{sys,d}$ thus approximately equal the 0.1 % fractiles of the system resistance (see Eq. 2-98). They are displayed in relation to the design resistance $R_{el,d}$ of a single element. An increase in $R_{sys,d}$ with an increasing number of elements in the system indicates a positive influence of system effects on the reliability and vice versa. An upper and lower bound are given, one the one hand, by the parallel

system with ductile elements, which shows the most positive influence, and, on the other hand, by the series system, for which the most negative influence is found. It appears that for some intermediate cases, the influence of system effects on the design value is negligible, which indicates that system and element reliability are approximately equal.

2.6 Reliability of Existing Structures

2.6.1 General

The assessment of an existing structure might become necessary for one of the following reasons (Ellingwood 1996; ISO 13822 2010):

- Planned change of use, modification of the structure, or extension of design service life
- Discovery of design or construction errors
- Complaints by tenants regarding serviceability
- Appearance of structural damage (e.g. after extreme environmental events)
- Observed structural deterioration due to time-dependent actions
- Reliability check required by authorities, insurance companies, or owners

Regardless of whether reliability-based or semi-probabilistic verification formats are applied, the assessment of existing structures is fundamentally different from the design of new structures. The main differences are summarised in Table 2-3 and described next.

Table 2-3 Differences between designing new and assessing existing structures

Differences regarding	Design of new structures	Assessment of existing structures
Material properties	choice of nominal values; assumption of mean and variance	mean and variance measurable
Geometrical dimensions	choice of nominal values	measurable
Design and construction documents	under preparation	available or unavailable
Type of uncertainty	mostly aleatory	mostly epistemic
Structural verification	according to current standards	according to former standards, current standards, or more advanced methods
Partial factors	partial factors according to standards	adjusted partial factors possible
Design service life	design service life according to standards	remaining service life possibly shorter than the usual design service life
Proof-loading	–	proof-loading possible; increased reliability of service-proven structures
Relative costs of measures for increasing reliability	low to medium	high

In the design of new structures, materials with specified nominal material properties can be chosen, whereas in the assessment of existing structures, the materials are already present, and their properties can be tested. The same applies to geometrical dimensions. If design or construction documents no longer exist, the assessment of an existing structure must rely exclusively on the inspection and measurements of geometrical dimensions and material properties, which can be difficult if structural members are not easily accessible. As a result, epistemic uncertainties can be the dominant type of uncertainty in assessing existing structures (see Section 2.2). Therefore, statistical uncertainty related to a limited number of measurements must be considered. Corresponding approaches are presented in Section 2.6.4.

New structures are to be designed according to currently valid standards. In most cases, these standards did not exist when the structure under assessment was constructed, and existing structures might hence not comply with current standards, even if they are free of structural damages and deterioration. In the context of an extension of an existing structure or a change of use leading to higher loads, this can lead to obstacles if compliance with the current standard is required. In these cases, the German building authority allows unchanged parts of the existing structure to be verified according to former standards that were in force at the time of construction (ARGEBAU 2008). If verification according to both former and current standards is not possible, more advanced methods can help to avoid costly retrofitting works or demolition. Such methods can be more advanced in terms of the probabilistic level (see Table 2-2) or the methods of structural analysis (e.g. physically nonlinear finite element simulations; see BMVBS 2011). Concerning the level of probabilistic methods, the first logical step is to apply adjusted partial factors instead of those defined in standards for the design of new structures. Concepts for adjusted partial factors are described in Section 2.6.3.

In addition to the previously mentioned methods, proof load testing of existing structures can be beneficial for verifying sufficient reliability (see e.g. Moses et al. 1994; Ellingwood 1996). In principle, proof-loading an existing structure (or structural member) demonstrates that its resistance is at least as high as the applied load. The higher the proof load (i.e. the higher the probability of failure due to proof-loading itself), the higher the gain in structural reliability if the structure survives the proof-loading. The satisfactory past performance of a structure for a long time (i.e. its survival under all the loads having occurred since it was erected) has a similar effect on structural reliability (Hall 1988; Val and Stewart 2002). Such a structure is sometimes referred to as “service-proven”. However, the actual loads that have occurred in the past service life are uncertain, and the gain in reliability for a service-proven structure is hence usually much lower than in the case of proof load testing (Melchers and Beck 2018). The effect of satisfactory past performance and proof-loading strongly depends on the present uncertainties: The most positive effect on reliability occurs

if the present uncertainty mainly originates from the resistance and if the ratio of variable load to permanent load is low. Satisfactory past performance also indicates that gross human errors (e.g. due to oversight or ignorance) are less likely to have been made during construction or design (Hall 1988). Human errors are usually not explicitly included in the derivation of reliability requirements and corresponding uncertainty modelling, as stated in prEN 1990 (2020), for example. However, in reality, they influence observed failure rates and thus the actual failure probability of a structure. Therefore, the "actual" probability of failure might be more strongly reduced by satisfactory past performance than the "nominal" probability of failure without considering human error.

A further difference between the design of new and the assessment of existing structures lies in the costs of measures for increasing reliability: In the design of new structures, reliability can easily be increased by, for example, choosing larger cross-sections or materials with higher strengths. If an existing structure needs to be upgraded, the relative costs for increasing the reliability are usually much higher. This directly influences the optimum reliability for existing structures, which is further discussed in Section 2.6.2.

2.6.2 Target Reliability for Existing Structures

The target reliability indices specified in EN 1990 (2010) – see Table 2-1 – were primarily derived for the design of new structures. Appropriate target reliability indices for existing structures can differ from these recommended values, as illustrated next. The considerations mainly focus on target reliability levels for ultimate limit states.

In general, optimal reliability levels can be found by economic optimisation. For new structures, this corresponds to finding the maximum of the following objective function (Rackwitz 2000):

$$Z(d) = B(d) - C_{\text{con}}(d) - F(d) \qquad \textit{Eq. 2-104}$$

where $B(d)$ is the expected benefit from the existence of the structure, $C_{\text{con}}(d)$ are the expected costs for design and construction, and the expected failure costs $F(d)$ address the risk of structural failure. $F(d)$ can be expressed as the product of the probability of failure $P_{\text{f}}(d)$ and the expected costs C_{f} given failure. The costs C_{f} must account for the replacement of the structure, expected economic losses due to non-availability of the structure, environmental and psychological effects, and expected fatalities and injuries in the case of a failure (Steenbergen et al. 2015). To express the risk of fatalities in monetary units, the so-called "societal willingness to pay" (SWTP) can be used, which is the amount of money a society is willing to spend to save an additional anonymous life (Fischer et al. 2019). The SWTP can be derived from social indicators such as the life quality index (Lind 2002; Rackwitz 2002). Since all potential failure costs occur in the future, they must be discounted to their worth at the time of construction, which is neglected in the following expressions for the

sake of simplicity. The parameter d is the decision parameter, which can represent physical parameters, such as the cross-section of a structural member. However, the parameter d can also be the reliability index β that results from selecting particular physical parameters. The benefit $B(d)$ is usually almost independent of d; therefore, the optimisation is equivalent to minimising the total costs $C_{\text{tot,new}}$. If the reliability index β is the decision parameter, the following expression is received for new structural members:

$$C_{\text{tot,new}}(\beta) = C_{\text{con}}(\beta) + P_{\text{f}}(\beta)\, C_{\text{f}} \qquad \textit{Eq. 2-105}$$

The optimum reliability index $\beta_{\text{opt,new}}$, which minimises $C_{\text{tot,new}}$, depends on two parameters: First, the magnitude of possible failure consequences C_{f}, and, second, the marginal costs of measures for increasing the reliability, that is, the steepness of the curve $C_{\text{con}}(\beta)$; see Fig. 2-11.

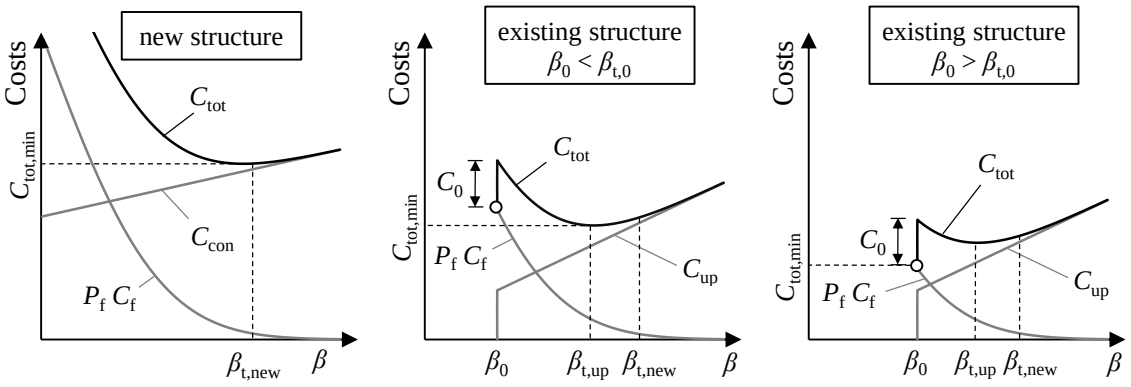

Fig. 2-11 Optimisation of reliability index for new and existing structures

For an existing structural member, the decision-making regarding the optimum reliability consists of two steps. First, based on the reliability index β_0 of the structural member in its current condition, a decision must be made on whether the structural member should be kept in this condition or upgraded to a reliability index β_{up}. Second, in the case of an upgrade, a decision concerning the optimum reliability index β_{up} must be made. The total costs $C_{\text{tot,exist}}$ to be minimised can be expressed as (Steenbergen et al. 2015)

$$C_{\text{tot,exist}}(\beta) = \begin{cases} C_0 + C_1(\beta_{\text{up}}) + P_{\text{f}}(\beta_{\text{up}})\, C_{\text{f}} & \text{in case of an upgrade} \\ P_{\text{f}}(\beta_0)\, C_{\text{f}} & \text{in case of no upgrade} \end{cases} \qquad \textit{Eq. 2-106}$$

Here, C_0 represents upgrade costs independent of the decision parameter β_{up} (e.g. costs related to surveys, design, administration, and economic losses due to business interruptions). The upgrade costs that depend on β_{up} are represented by $C_1(\beta_{\text{up}})$. The optimum reliability level $\beta_{\text{t,up}}$ in case of an upgrade does not depend on C_0 but only on the steepness of $C_1(\beta_{\text{up}})$. The initial costs C_0, however, influence whether the upgrade is beneficial: If the initial reliability index β_0 is close to $\beta_{\text{t,up}}$, then the initial investment C_0 cannot be compensated by the subsequent decrease in the expected failure costs $P_{\text{f}}\, C_{\text{f}}$ (see Fig. 2-11).

If $C_{tot,exist}$ is minimised for a set of typical existing structures, two generalised target values can be derived: A reliability index $\beta_{t,0}$, below which the upgrade of the structure is usually beneficial, and a target reliability $\beta_{t,up}$ for the upgrade. For general application, Steenbergen et al. (2015) propose the selection of $\beta_{t,0}$ and $\beta_{t,up}$ by reducing the target reliability indices in EN 1990 (2010) by $\Delta\beta = 1.5$ and $\Delta\beta = 0.5$, respectively (see Table 2-4). The values $\beta_{t,0}$ and $\beta_{t,up}$ are valid for a reference period equal to the remaining service life of the existing structure and are also proposed in fib bulletin 80 (2016).

Table 2-4 Target reliability indices (remaining service life) for existing structures based on economic optimisation (Steenbergen et al. 2015)

Consequence class	**$\beta_{t,new,50a}$ (EN 1990)**	**$\beta_{t,up}$**	**$\beta_{t,0}$**
CC 1	3.3	3.3 − 0.5 = 2.8	3.3 − 1.5 = 1.8
CC 2	3.8	3.8 − 0.5 = 3.3	3.8 − 1.5 = 2.3
CC 3	4.3	4.3 − 0.5 = 3.8	4.3 − 1.5 = 2.8

In the current draft of fib Model Code 2020 (2020), the recommended target reliability levels for the design of new and the assessment of existing structures are aligned with the target reliability levels given by ISO 2394 (2015), which are specified for a one-year reference period and are equal to those in the JCSS Probabilistic Model Code (2001a). Apart from a differentiation between different consequence classes, the target reliability indices in ISO 2394 (2015) also depend on the relative costs of safety measures (see Table 2-5). For the assessment of existing structures, fib Model Code 2020 (2020) recommends applying the reliability indices for large relative costs of safety measures. Hence, for moderate failure consequences, which corresponds to CC 2 in EN 1990 (2010), $\beta_{t,0} = 3.3$ is specified for the assessment of existing structures. Compared to $\beta_{t,new} = 4.2$, which is specified for the design of new structures, the target reliability for the assessment of existing structures is thus reduced by $\Delta\beta = 0.9$. If the reliability index β_0 of the existing structural member is smaller than $\beta_{t,0} = 3.3$, fib Model Code 2020 (2020) recommends upgrading towards the same target reliability as for the design of new structures (i.e. $\beta_{t,up} = \beta_{t,new} = 4.2$).

Table 2-5 Target reliability indices $\beta_{t,1a}$ (one-year reference period) based on economic optimisation (JCSS 2001a; ISO 2394 2015)

Relative costs of safety measures	**Minor consequences of failure**	**Moderate consequences of failure**	**Large consequences of failure**
Large	3.1	**3.3**	3.7
Medium	3.7	**4.2**	4.4
Small	4.2	4.4	4.7

It is important to note that the target reliability indices specified in Table 2-5 are based on economic optimisation. In some cases, higher reliability is required due to *human safety criteria*, which set a lower limit to the target reliability index. One such criterion is the requirement that, for occupants of buildings, the individual risk from the possibility of a

structural collapse should be lower than the risk of other daily-life activities (fib bulletin 80 2016). According to ISO 2394 (1998), the overall lethal accident rate is approximately 10^{-4} per year. Steenbergen and Vrouwenvelder (2010) suggested setting the maximum acceptable probability of being killed by structural collapse to 10^{-5} per year (i.e. one order of magnitude lower), which is also specified by the Swiss standard SIA 269 (2011). If the conditional probability of a casualty given failure is estimated, upper bounds for the target failure probability per year can be calculated (Steenbergen et al. 2015). Furthermore, if structural failure can lead to the collapse of large areas, an additional check of group risk criteria can be required to avoid high probabilities of failure events with a large number of fatalities. For more information about group risk criteria, refer to Tanner and Hingorani (2015), Steenbergen et al. (2015), and fib bulletin 80 (2016).

When assessment values are determined in the course of this thesis, a target reliability level of $\beta_{t,1a} = 3.3$ is applied in most cases. As illustrated above, this value corresponds to the target reliability specified by ISO 2394 (2015) for high relative costs of safety measures and medium failure consequences based on economic optimisation.

2.6.3 Concepts for Modified Partial Factors

Suitable partial factors for the assessment of existing structures can differ from those for the design of new structures for two reasons: First, reduced target reliability indices β_t for existing structures should also lead to a reduction in the partial factors. Second, the stochastic models for the basic variables might differ from those considered in the partial factors for new structures. For example, information about the actual variability of material properties can be obtained by measurements, which can justify an increase or a reduction of partial factors compared to those for new structures. Three available approaches for determining modified partial factors for existing structures are briefly presented next. All of them were mainly developed for existing concrete structures.

Design value method (DVM)

The DVM, as defined by EN 1990 (2010), can also be used to derive partial factors for existing concrete structures, which is described in Caspeele et al. (2013) and fib bulletin 80 (2016). As explained in Section 2.5.4, the DVM is based on the simplified level II approach proposed by König and Hosser (1982). Therefore, fixed sensitivity factors α_R and α_E are applied to enable a simplified determination of partial factors based on a specified target reliability level β_t and stochastic models for the relevant basic variables. The DVM is also included in the draft standard prEN 1990-2 (2021), where design values are referred to as "assessment values" with index "a" instead of "d". When using the design/assessment value method, determining partial factors is not necessarily required, as assessment values can be

directly evaluated as specific fractiles of the basic variables. The assessment value method for existing structures is, in principle, identical to the DVM for new structures.

Adjusted partial factor method (APFM)

The adjusted partial factor method (APFM) is proposed as an alternative to the DVM in fib bulletin 80 (2016) and Caspeele et al. (2013). The APFM is also based on the simplified level II approach; however, in contrast to the DVM, it only specifies adjustment factors ω_γ for the partial factors defined in the Eurocodes, thereby guaranteeing consistency with the Eurocode regulations for new structures. Adjusted partial factors for material properties (index X), permanent loads (G), and variable loads (Q) are obtained by multiplying the partial factors for new structures by adjustment factors:

$$\gamma_X = \omega_{\gamma,X}\,\gamma_{X,\text{new}} \quad \gamma_G = \omega_{\gamma,G}\,\gamma_{G,\text{new}} \quad \gamma_Q = \omega_{\gamma,Q}\,\gamma_{Q,\text{new}} \qquad \textit{Eq. 2-107}$$

The adjustment factors ω_γ address differences between parameters for existing structures (marked by ″) and reference parameters for new structures (marked by ′) that are relevant concerning suitable partial factors. These differences include a different target reliability level β_t'' for the considered existing structure compared to the target reliability index β_t' for new structures, and different CoVs v'' of the basic variables compared to the CoVs v' implicitly included in the partial factors for new structures. For variable loads, a reference period t_ref deviating from the standard design working life of 50 years can also be considered. The adjustment factors ω_γ for material properties (log-normal distribution), permanent loads (normal), and variable loads (Gumbel) can be calculated by

$$\omega_{\gamma,X} = \frac{\gamma_{\text{Rd},X}\left(\beta_\text{t}''\right)}{\gamma_{\text{Rd},X}\left(\beta_\text{t}'\right)} \exp\left[\alpha_R\left(\beta_\text{t}''\,v_X'' - \beta_\text{t}'\,v_X'\right) - 1.645\left(v_X'' - v_X'\right)\right] \qquad \textit{Eq. 2-108}$$

$$\omega_{\gamma,G} = \frac{\gamma_{\text{Ed},G}\left(\beta_\text{t}''\right)}{\gamma_{\text{Ed},G}\left(\beta_\text{t}'\right)} \frac{1-\alpha_E\,\beta_\text{t}''\,v_G''}{1-\alpha_E\,\beta_\text{t}'\,v_G'} \qquad \textit{Eq. 2-109}$$

$$\omega_{\gamma,Q} = \frac{\gamma_{\text{Ed},Q}\left(\beta_\text{t}''\right)}{\gamma_{\text{Ed},Q}\left(\beta_\text{t}'\right)} \frac{1-v_{Q,50\text{a}}''\left[0.45+0.78\ln\left(-\ln\left(\Phi\left(-\alpha_E\beta_\text{t}''\right)\right)\right)\right]}{1-v_{Q,50\text{a}}'\left[0.45+0.78\ln\left(-\ln\left(\Phi\left(-\alpha_E\beta_\text{t}'\right)\right)\right)\right]} \qquad \textit{Eq. 2-110}$$

The target reliability level β_t' is to be chosen according to EN 1990 (2010) for a reference period of 50 years (i.e. as $\beta_\text{t}' = 3.8$), and the sensitivity factors should be selected as $\alpha_E = -0.7$ and $\alpha_R = 0.8$. The specified reference CoVs are $v_X' = v_\text{c}' = 0.15$ for concrete strength, $v_X' = v_\text{s}' = 0.05$ for the yield strength of reinforcement steel, $v_G' = 0.1$ for permanent loads, and $v_{Q,50\text{a}}' = 0.25$ for imposed loads. For information about other variable loads, see fib bulletin 80 (2016). Calculating the adjustment factor for variable loads according to Eq. 2-110 implies that the reference period is either 50 years or considered by adjusting the

characteristic value. The partial factors for considering model uncertainties, γ_{Rd} and γ_{Ed}, are to be calculated by

$$\gamma_{Rd}(\beta_t) = \frac{1}{1 - 0.4\,\alpha_R\,\beta_t\,\upsilon_\theta} \qquad \gamma_{Ed}(\beta_t) = 1 - 0.4\,\alpha_E\,\beta_t\,\upsilon_\theta \qquad \textit{Eq. 2-111}$$

where $\upsilon_{\theta G} = 0.065$ and $\upsilon_{\theta Q} = 0.11$ are suggested in fib bulletin 80 (2016) for permanent and variable loads, respectively. The partial factor for resistance model uncertainty γ_{Rd} is obtained as the product of γ_{Rd1} for the actual model uncertainty and γ_{Rd2} for geometrical uncertainty. Both partial factors can be calculated with Eq. 2-111 using $\upsilon_{\theta,Rd1,c} = \upsilon_{\theta,Rd2,c} = 0.075$ for concrete compressive strength, as well as $\upsilon_{\theta,Rd1,s} = 0.02$ and $\upsilon_{\theta,Rd2,s} = 0.04$ for the yield strength of reinforcement steel. Eq. 2-111 is based on a normal distribution of model uncertainty. Concerning the resulting partial factors γ_{Rd} and γ_{Ed}, the difference to a log-normal distribution is negligible due to the small CoVs υ_θ.

One advantage of the APFM is that the ratio υ'' / υ' can be set to one if no additional information regarding the CoVs of the basic variables is available for the existing structure. In doing so, the isolated influence of an adjusted target reliability level β_t'' on partial factors can be considered, as displayed in Fig. 2-12 for the partial factors for permanent and imposed loads according to EN 1990 (2010), and for concrete and reinforcement strength according to EN 1992-1-1 (2010).

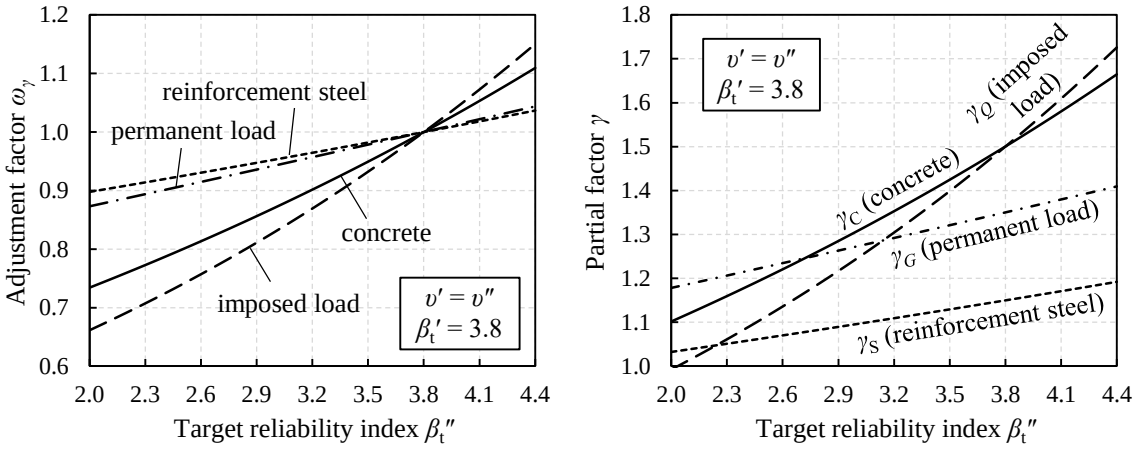

Fig. 2-12 Influence of target reliability β_t on adjustment factors (left) and partial factors (right) obtained by the adjusted partial factor method

Modified partial factors according to DBV-Merkblatt

In the DBV-Merkblatt (2013), titled "*Modifizierte Teilsicherheitsbeiwerte für Stahlbetonbauteile*" (Modified partial factors for reinforced concrete members), partial factors for concrete and reinforcement steel strength are specified depending on the respective CoVs. Since modified partial factors are only given in a table (see Table 2-6), the modification method is less transparent than the DVM and APFM. Related background information is

given in DBV-Heft 24 (2013). The partial factors are based on a target reliability level of $\beta_{t,\,50a} = 3.2$. The reduction of the normative target reliability of $\beta_{t,50a} = 3.8$ for CC 2 is justified by arguments related to satisfactory past performance: If the structure has been in use for at least five years without showing any damage, then the assumption is that the probability of gross human errors, which might have been made during design and construction and could lead to structural failure, is significantly reduced. Therefore, the authors argue that the nominal target reliability level β_t, which does not consider human error, can be reduced without leading to a higher actual failure probability compared to new structures.

In contrast to the DVM and the APFM, modified partial factors are only given for the resistance parameters: concrete ($\gamma_{C,mod}$) and reinforcement strength ($\gamma_{S,mod}$). The potential reduction of the partial factors for actions, which originates from the reduced target reliability level of $\beta_{t,50} = 3.2$, is addressed by further reducing the modified partial factors $\gamma_{C,mod}$ and $\gamma_{S,mod}$. Consequently, the modified partial factors may not be used if favourable load effects are involved in the verification. According to DBV-Heft 24 (2013), the partial factor $\gamma_C = 1.50$ includes a factor of 1.15 for considering that, due to insufficient compaction and other influences during construction, the concrete strength in the structural member might be lower than that obtained from normative test specimens. Therefore, another reason for reducing the normative partial factor γ_C is seen in neglecting this conversion factor if concrete strength is obtained from tests on drill cores. The modified partial factors are based on a reference period and a remaining working life of 50 years. For the detailed application conditions of the modified partial factors in Table 2-6, refer to DBV-Merkblatt (2013).

Table 2-6 Modified partial factors for reinforced concrete members according to DBV-Merkblatt (2013)

Concrete (persistent and transient design situations)					
$\upsilon_{R,C}$[1]	≤ 0.2	0.25	**0.30**	0.35	0.40
$\gamma_{C,mod}$[2]	1.2	1.25	**1.30**[4]	1.40[3]	1.50[3]
Reinforcement steel (persistent and transient design situations)					
$\upsilon_{R,S}$[1]	0.06		0.08	**0.10**	
$\gamma_{S,mod}$[2]	1.05		1.10	**1.10**[4]	

Intermediate values may be interpolated.
[1] *The coefficients of variation $\upsilon_{R,C}$ and $\upsilon_{R,S}$ must include material, model, and geometrical uncertainty.*
[2] *Not to be applied for verification of vertical members of the bracing system*
[3] *To be increased by 20 % for verification of $V_{Rd,max}$ (compressive strut resistance for shear transfer)*
[4] *Assumption for preliminary/conceptual design without material testing*

2.6.4 Concepts for Considering Statistical Uncertainty

If the material properties of an existing structure are obtained by material testing, the statistical uncertainty resulting from the limited sample size must be considered. A general method for determining the characteristic values and design values of material properties based on limited test data is given in Annex D of EN 1990 (2010). The method is based on

a Bayesian approach with non-informative prior distribution. The characteristic value X_k and the design value X_d are determined based on the posterior predictive distribution: X_k is obtained as the 5 % fractile, and the p fractile that corresponds to X_d is defined by the simplified level II approach. Assessment values X_a for existing structures can be determined accordingly (see prEN 1990-2 2021). Based on a log-normal distribution and an unknown CoV, X_k and X_d can be obtained as

$$X_k = \exp\left(m_y - k_n\, s_y\right) \quad \text{with} \quad k_n = -t_{n-1,5\%}\sqrt{1+1/n} \qquad \textit{Eq. 2-112}$$

$$X_d = \exp\left(m_y - k_{d,n}\, s_y\right) \quad \text{with} \quad k_{d,n} = -t_{n-1,p}\sqrt{1+1/n}, \quad p = \Phi\left(-\alpha_R \beta_t\right) \qquad \textit{Eq. 2-113}$$

where m_y and s_y are the arithmetic mean and standard deviation of the natural logarithms of the test results, respectively, n is the sample size, and $t_{n-1,p}$ is the p fractile of the t-distribution with $n - 1$ degrees of freedom. In EN 1990 (2010), the factors k_n and $k_{d,n}$ are given in tables instead of by equations.

The method described in Annex D of EN 1990 (2010) is applicable for all material types. Therefore, material-specific standards and guidelines for determining the characteristic material properties of existing structures are often based on this method; see, for example, EN 13791 (2019) for existing concrete and WTA 7-4 (2021) for existing masonry structures. The characteristic values derived by applying the Bayesian approach with non-informative prior distribution can be quite low for small sample sizes. Less conservative results can be obtained if informative prior distributions are used in the assessment, as demonstrated in Caspeele and Taerwe (2012) for the characteristic concrete compressive strength.

The DVM and the APFM, as presented in fib bulletin 80 (2016), as well as the modification of partial factors according to DBV-Merkblatt (2013) do not consider the number of conducted material tests in the derivation of partial factors. However, in both documents, it is emphasised that statistical uncertainty should be considered when characteristic values for the material properties are determined, and Annex D of EN 1990 (2010) is referred to for this purpose. In contrast, Val and Stewart (2002) present a Bayesian method for determining partial factors of resistance parameters that depend on the number of conducted tests. The method follows the simplified level II approach and is, in principle, similar to the DVM. However, the partial factors are derived from the posterior predictive distribution of the considered material property. In this way, information from material testing and, if available, prior information are considered, including the corresponding statistical uncertainty. Val and Stewart (2002) show that too conservative partial factors for small sample sizes can be avoided by considering prior information.

3 STRUCTURAL BEHAVIOUR AND ASSESSMENT OF MASONRY

3.1 Introduction

General knowledge regarding the structural behaviour and assessment of masonry is presented in this chapter. Due to the scope of this thesis, the focus is on existing masonry under compression loading. Masonry is designed according to Eurocode 6 in most European countries: General design rules are specified in EN 1996-1-1 (2012), and simplified calculation methods are included in EN 1996-3 (2009). The National Annexes (NAs) DIN EN 1996-1-1/NA (2019) and DIN EN 1996-3/NA (2019) additionally apply in Germany. The current generation of Eurocode 6 primarily aims at the design of new masonry structures and is therefore not fully applicable to the assessment of existing masonry structures. However, reference is made to Eurocode 6 and its German NAs throughout this chapter, as no comprehensive European standard for assessing existing masonry is available at present.

In the assessment of existing masonry structures, basic knowledge about the history of masonry construction, including the evolution of masonry unit and mortar types and respective construction techniques, is beneficial. Hence, a short overview of the history of masonry construction, emphasising clay brick masonry construction in Germany, is provided in Section 3.2. The overview also includes information on the typology of masonry. In Section 3.3, the behaviour of the composite material masonry under compression and the structural behaviour of masonry walls are illustrated. The section briefly discusses not only general information but also influences on masonry strength that become important in the assessment of existing masonry structures, such as inhomogeneity, defects, and deterioration.

If no documents with reliable information regarding material strength are available for a masonry structure under assessment, the compressive strength of masonry is usually determined experimentally. Section 3.4 deals with the different methods for testing masonry compressive strength. If unit and mortar properties are tested separately, the compressive strength of masonry must subsequently be predicted by applying appropriate models, which are described in Section 3.5. Finally, different approaches for the finite element modelling of masonry are presented in Section 3.6, and the safety format for the design of masonry structures according to Eurocode 6 is discussed in Section 3.7.

3.2 Overview of the History of Masonry Construction

Masonry construction has a history of more than 10,000 years, as evidence was found of stone masonry buildings built in the Levant and Mesopotamia in the ninth millennium BC (Kurapkat 2017). Around the same time, construction with hand-moulded and air-dried clay

bricks began in the early civilisations in western Asia. Although the firing of clay for producing ceramic products had been common in those civilisations since the seventh millennium BC, the use of fired clay bricks did not gain dominance over the use of unfired bricks due to the shortage of firewood and thus the high price of fired clay bricks. Therefore, fired clay bricks were only used for the parts of structures that required resistance to wet conditions (Sievertsen 2017).

One of the first civilisations to use fired clay bricks to a larger extent was the Indus Valley Culture, where fired bricks were a common building material between 2600 to 1600 BC (Khan and Lemmen 2014). The dimensions of Indus Valley bricks had the proportions 4 : 2 : 1 (length : width : height), which are still typical today. Well-known written evidence of the early manufacturing of fired clay bricks is the story of the Tower of Babel in the Hebrew and Christian Bible: "And they said to one another, 'Come, let us make bricks, and burn them thoroughly.' And they had brick for stone, and bitumen for mortar." (Genesis 11,3, English Standard Version). The historical inspiration for this story might have been the Etemenanki, a Babylonian temple structure built around 600 BC, which presumably had a height of around 90 m (Streck 2006). While in ancient Egypt and Greece, the use of fired clay bricks was still limited to structural members that needed resistance to moisture, fired clay bricks became a common building material in the Roman Empire, which enabled their spread over large parts of Europe (Osthues 2017).

The general techniques for manufacturing fired clay bricks did not substantially change until the end of the 18th century (Egermann and Mayer 1989). The clay was first watered, kneaded, and, depending on its consistency, mixed with sand before being pushed into wooden moulds. The excess material was then wiped off. After being air-dried, the bricks were stacked on top of one another with fuel, such as wood, turf, or straw, in between to form a brick clamp. The bricks were then fired for several days or weeks, ideally reaching temperatures between 800 and 1,000 °C during the burning process. Due to the different positions of the fired bricks in the kiln and hence different maximum temperatures, this firing technique led to high variability of the brick properties. Bricks that were only weakly fired (< 573 °C) or that melted (> 1,200 °C) were usually sorted out. Based on their visual appearance, the bricks were sometimes further separated into bricks of higher and lower quality (i.e. higher and lower strength and water resistance) to be used at the outer surface or interior of a masonry wall, respectively (Neumann 2017).

During the 19th century, several inventions changed the procedure of clay brick production. Concerning the shaping of bricks, a significant invention was the screw extrusion press by Carl Schlickeysen in 1854, which allowed for the extrusion of a continuous strand of clay that was then cut into single bricks. One characteristic of extruded clay bricks, which are still state of the art today, is their anisotropy: The extrusion causes an alignment of the clay

minerals, leading to a higher compressive strength of bricks parallel to the extrusion direction, which is usually the vertical direction in the completed masonry wall (Egermann and Mayer 1989).

With regard to the firing, the invention of the ring-shaped kiln by Hoffmann and Licht, patented in 1858 (Rupp and Friedrich 1993), brought clay brick production a further step forward. The so-called "Hoffmann kiln" allowed all stages of the process (i.e. heating-up, firing, and cooling down) to be executed simultaneously in several interconnected chambers, thereby enabling the kiln to be operated in a never-ending, much more efficient process and leading to less variability of brick strength compared to the firing in a brick clamp. The last significant step concerning the production techniques for clay bricks was the implementation of tunnel kilns. Although initially invented in the middle of the 19th century, tunnel kilns did not become common in Germany until around 1950 and are – in further developed forms – still state of the art today (Rupp and Friedrich 1993). In a tunnel kiln, the bricks are placed on a wagon moving through the kiln sections, each with different temperatures. In addition to a more efficient production compared to previous kiln types, all the bricks moving through the tunnel kiln are subjected to approximately the same temperature, leading to a further reduction in strength variability.

Historical mortars for masonry construction include mortars with lime, gypsum, clay, and bitumen as binding material. Lime mortars have been used for construction since the ninth millennium BC. Hence, the technology of first burning limestone (calcium carbonate) and then slaking the burnt lime (calcium oxide) to receive calcium hydroxide had already been applied on a larger scale before the firing of clay to produce ceramics became common (Kurapkat 2017). Concerning lime mortars, a distinction must be made between hydraulic and non-hydraulic lime. While non-hydraulic lime (air lime) hardens by carbonation if exposed to carbon dioxide, hydraulic lime contains additional components, such as clay minerals or pozzolans, leading to hardening by hydration and thus higher mortar strengths. From around 1870, the use of the historical mortar types began to decline in Germany, being gradually replaced by cement-lime and cement mortars (Ahnert and Krause 2009). The application of Portland cement as a binder allowed for much higher mortar strengths.

An important step regarding the standardisation of masonry construction in Germany was the introduction of the *Reichsformat* in Prussia in 1872, specifying the brick dimensions of 25 x 12 x 6.5 cm³ (length x width x height) as mandatory for public buildings (Bender 2004). Soon, this format spread throughout the whole German Reich. Up to this time, many different regional brick formats had been used; however, they did not substantially differ from the *Reichsformat*, as these small brick dimensions enabled good handling of bricks without further technical support. In contrast to larger masonry units commonly used in Germany nowadays, these small-sized bricks resulted in walls with a thickness of more

than one brick width. While single wythe masonry, which is masonry with a thickness of one unit, is commonly constructed in a stretcher bond, the bricks in bonded masonry can be placed as stretchers (longer side parallel to the wall face) or headers (longer side perpendicular to the wall), as depicted in Fig. 3-1. A wide variety of different masonry bonds is hence possible, with the English bond (German: *Blockverband*) and the cross bond (German: *Kreuzverband*) having been the most common types for bonded masonry in Germany since the 16th century (Maier 2012).

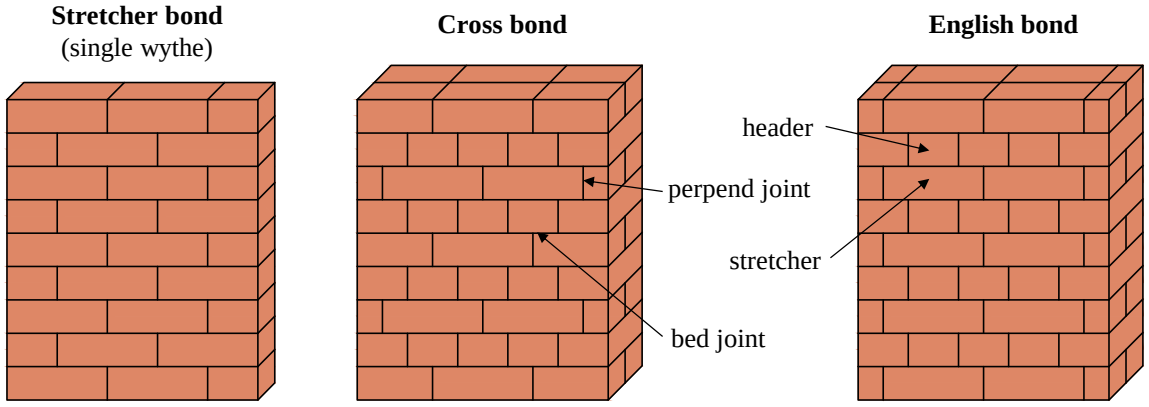

Fig. 3-1 Common masonry bond types in Germany

The first German brick standard, DIN 105 "*Mauerziegel (Backsteine)*", was introduced in 1922. According to this standard, second-class clay bricks had to achieve a compressive strength of at least 10 N/mm² and first-class clay bricks of at least 15 N/mm² on average. The first German standard for the structural design of masonry, DIN 1053, was then published in 1937. Later, in 1951, a new set of standard construction dimensions was introduced by DIN 4172, according to which building dimensions should be multiples of 25/3 or 25/4 cm. This rule led to new standardised unit dimensions: the *Normalformat* (NF) of 24 x 11.5 x 7.1 cm³ (length x width x height) and the *Dünnformat* (DF) of 24 x 11.5 x 5.2 cm³; see DIN 105 (1952) for clay bricks and DIN 106 (1952) for calcium silicate bricks. The difference between the specified dimensions and a multiple of 25/3 or 25/4 results from a nominal perpend joint thickness of 10 mm and bed joint thicknesses of 1.23 cm and 1.05 cm, respectively. In the past decades, typical units for masonry construction in Germany have gained in size. However, the dimensions are still based on the same system, with unit dimensions being named by multiples of the dimensions DF or NF according to the volume of the units including one of the neighbouring mortar joint thicknesses in each direction.

Table 3-1 provides an overview of the most common masonry types in the existing residential building stock in Germany based on a typology by Loga et al. (2015), who categorised the existing buildings by particular age classes. Masonry buildings and half-timbered buildings were the most common construction types until 1859. Since then, masonry has

been the dominating material for vertical structural members in German residential buildings. With regard to horizontal load-bearing members, the standard construction type shifted from timber joist floors to reinforced concrete slabs between 1919 and 1957. Apart from the common construction types, the share of the number of buildings belonging to the respective building age classes is presented as given in Cischinsky and Diefenbach (2018).

Natural stone masonry and fired solid clay brick masonry dominated masonry construction in Germany until around 1950 (Loga et al. 2015). Then, other masonry types started to gain in importance (see Table 3-1). In the 1950s, many buildings were constructed using concrete blocks, with the aggregate consisting of recycled rubble from buildings destroyed in World War II. Due to their better insulating properties compared to solid bricks, perforated bricks became more popular in the 1960s. By the end of that decade, calcium silicate bricks, made of sand and burnt lime under increased temperature and pressurised steam in autoclaves and first patented in 1880 (Bundesverband Kalksandsteinindustrie e.V. 2018), had become one of the most common units for masonry construction in Germany. Since around 1980, autoclaved aerated concrete blocks have been among the three most popular masonry unit types in Germany aside from perforated clay and calcium silicate bricks.

Table 3-1 Construction types in the existing German residential building stock (Loga et al. 2015; Cischinsky and Diefenbach 2018)

<table>
<tr><th>Building age class</th><th>Share of buildings (data of 2016)</th><th>Most common masonry unit types</th><th>Most common floor types</th></tr>
<tr><td>Until 1859</td><td rowspan="2">12 %</td><td>natural stones, solid clay bricks</td><td rowspan="2">timber joists</td></tr>
<tr><td>1860 – 1918</td><td rowspan="2">solid clay bricks,
natural stones</td></tr>
<tr><td>1919 – 1948</td><td>12 %</td><td rowspan="2">timber joists,
reinforced concrete slabs</td></tr>
<tr><td>1949 – 1957</td><td>9 %</td><td>solid clay bricks,
hollow rubble concrete blocks</td></tr>
<tr><td>1958 – 1968</td><td>12 %</td><td>hollow concrete blocks,
perforated clay bricks</td><td rowspan="7">reinforced concrete slabs</td></tr>
<tr><td>1969 – 1978</td><td>14 %</td><td>perforated clay bricks,
perforated calcium silicate bricks</td></tr>
<tr><td>1979 – 1983</td><td>8 %</td><td>perforated clay bricks,
perforated calcium silicate bricks,
autoclaved aerated concrete blocks</td></tr>
<tr><td>1984 – 1994</td><td>13 %</td><td rowspan="4">perforated clay bricks,
solid calcium silicate bricks,
autoclaved aerated concrete blocks</td></tr>
<tr><td>1995 – 2001</td><td>10 %</td></tr>
<tr><td>2001 – 2009</td><td>7 %</td></tr>
<tr><td>Since 2010</td><td>4 %</td></tr>
</table>

In the following course of this thesis, the term “historical masonry” refers to masonry from a past period, in which typical masonry types and production techniques substantially differed from today. Based on the previously presented development steps in masonry construction in Germany, the term can be viewed as applicable to masonry from the time before about 1950.

3.3 Structural Behaviour of Masonry under Compression

3.3.1 General Failure Mechanism of Masonry under Compression

Since masonry is a composite material consisting of units and mortar, the compressive strength f_{ma} of masonry results from the properties of its components. For typical unit-mortar combinations, the uniaxial compressive strength of mortar is smaller than the compressive strength of the units. Furthermore, if unit and mortar were separately subjected to the same uniaxial compressive stress, the mortar would show higher transverse strains, as the elastic modulus E divided by Poisson's ratio v is usually smaller for the mortar. If the composite material masonry is loaded perpendicular to the bed joints (i.e. vertically in the case of regular walls), the mutual constraint of the transverse strains thus leads to a triaxial compression state within the mortar joint and transverse (i.e. horizontal) tensile stresses in the units (see Fig. 3-2).

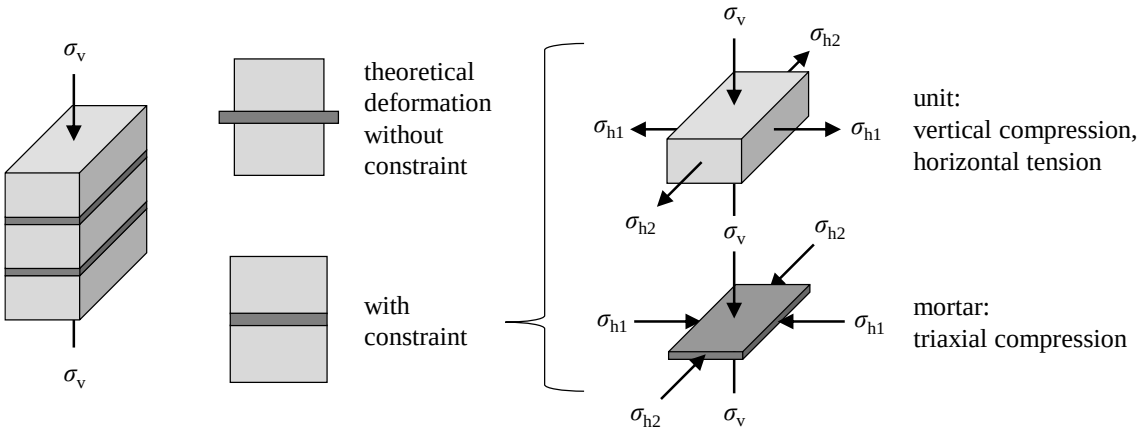

Fig. 3-2 Stresses within unit and mortar joint of masonry under uniaxial compression

Due to the triaxial compression state, the mortar joint can resist compressive stresses higher than the uniaxial (i.e. unconfined) mortar compressive strength. For the units, the opposite is the case: The horizontal tensile stresses reduce the resistible vertical stress of the units, thereby initiating the failure, which is accompanied by vertical cracks. Throughout the past decades, several researchers have investigated the details of this failure mechanism (see e.g. Hilsdorf 1969; Khoo 1972; Probst 1981; Goretzky 2000). More details are presented in Section 3.5, which deals with the prediction of masonry compressive strength based on the properties of unit and mortar.

3.3.2 Stress-Strain Relationship of Masonry under Compression

The uniaxial stress-strain relationship of masonry depends on the particular combination of unit and mortar. According to EN 1996-1-1 (2012), the stress-strain curve of masonry under compression is generally nonlinear. For structural design, it may be approximated as linear, parabolic, parabolic rectangular, or rectangular. However, different stress-strain curves for

different types of masonry are not explicitly specified in EN 1996-1-1 (2012). To describe the actual shape of the stress-strain relationship, it is convenient to introduce the stress-strain parameter k:

$$k = \frac{E_{\mathrm{ma},0}\ \varepsilon_f}{f_{\mathrm{ma}}} \qquad \textit{Eq. 3-1}$$

where $E_{\mathrm{ma},0}$ is the modulus of elasticity, defined as the tangential modulus in the origin, and ε_f is the compressive strain at reaching the compressive strength f_{ma}. The stress-strain parameter k can thus be viewed as the normalised tangential modulus of elasticity in the origin. Furthermore, it describes the ratio between the total strain ε_f and elastic strain $\varepsilon_{f,\mathrm{el}}$ at reaching the compressive strength f_{ma}. In this context, the elastic strain $\varepsilon_{f,\mathrm{el}}$ equals the compressive strength f_{ma} divided by the elastic modulus $E_{\mathrm{ma},0}$. According to EN 1996-1-1 (2012), the elastic modulus of masonry E_{ma} is defined as the secant modulus $E_{\mathrm{ma},0\text{-}33}$ at one-third of the compressive strength. Depending on the mathematical formulation of the stress-strain curve, the tangential modulus $E_{\mathrm{ma},0}$ can be slightly larger or equal to the secant modulus $E_{\mathrm{ma},0\text{-}33}$. For $k = 1$, the stress-strain curve is perfectly linear, whereas for $k \to \infty$, the curve converges to a rigid-plastic behaviour. In the case of $k = 2$, the curve is similar to a quadratic parabola. For an arbitrary parameter k, the stress-strain curve can be formulated according to the formulation given in EN 1992-1-1 (2010), for example (Glock 2004; Förster 2018):

$$\frac{\sigma_{\mathrm{c}}}{f_{\mathrm{ma}}} = \frac{k\,\eta - \eta^2}{1 + (k-2)\,\eta} \quad \text{for } 0 \le \eta \le \eta_{\mathrm{u}} \quad \text{with } \eta = \frac{\varepsilon_{\mathrm{c}}}{\varepsilon_f} \qquad \textit{Eq. 3-2}$$

where σ_{c} is the compressive stress, and $\eta = \varepsilon_{\mathrm{c}} / \varepsilon_f$ is the normalised compressive strain. The maximum compressive strain is usually limited by the ultimate compressive strain ε_{u} or, in normalised form, by η_{u}. Fig. 3-3 illustrates the introduced terms taking the stress-strain relationship according to Eq. 3-2 as an example.

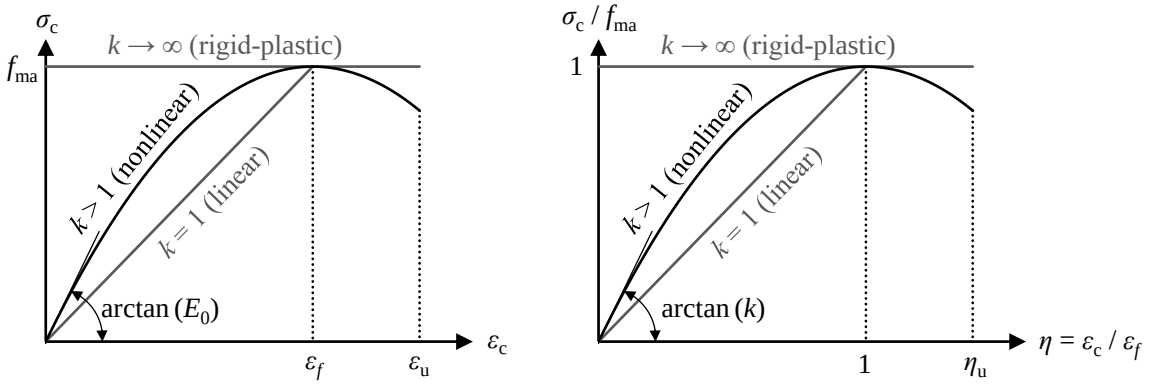

Fig. 3-3 Stress-strain curve of masonry under compression according to Glock (2004) (left: original, right: normalised)

Depending on the masonry type, Meyer and Schubert (1992) proposed modelling the stress-strain behaviour either as linear or as parabolic rectangular: For masonry made of perforated clay bricks, autoclaved aerated concrete blocks, or lightweight concrete blocks, a linear stress-strain curve is proposed, whereas, for calcium silicate bricks, a parabolic rectangular stress-strain curve is recommended. In Schubert (2010), the nonlinearity of the stress-strain relationship for different masonry types is specified by the parameter α_0, which is defined as the integral of the normalised stress-strain curve for $0 \leq \eta \leq 1$. Assuming a stress-strain curve according to Eq. 3-2, the stress-strain parameter k can be calculated from α_0. The parameter $k = 1$ follows from $\alpha_0 = 0.5$, for example, and $k = 2$ corresponds to $\alpha_0 = 2/3$. Parameters k for different masonry types are displayed in Table 3-2.

Table 3-2 Nonlinearity of the stress-strain relationship of masonry under compression for different unit types according to Schubert (2010)

Stress-strain parameter	Perforated clay bricks	Calcium silicate bricks	Lightweight concrete blocks	Concrete blocks	Autoclaved aerated concrete blocks
α_0	0.55	0.65	0.60	0.65	0.55
k	1.15	1.80	1.40	1.80	1.15

Since solid clay brick masonry (SCBM) no longer plays a significant role in contemporary masonry construction in Germany, no specifications regarding the stress-strain curve of SCBM are given in Meyer and Schubert (1992) and Schubert (2010). However, for the assessment of existing masonry structures, knowledge about SCBM is essential. Investigations by Kaushik et al. (2007), Lumantarna et al. (2014), and Thamboo and Dhanasekar (2019) indicate that a quadratic parabola until reaching the compressive strength (i.e. $k = 2$) is suited to represent the stress-strain curve of SCBM.

In addition to a mathematical formulation for the shape of the stress-strain curve, a value for the elastic modulus of masonry E_{ma} is needed to define the stress-strain relationship. If no experimental results are available, EN 1996-1-1 (2012) allows for the determination of E_{ma} by multiplying the characteristic compressive strength $f_{\mathrm{ma,k}}$ of masonry by a factor K_E:

$$E_{\mathrm{ma}} = K_E \; f_{\mathrm{ma,k}} \qquad \textit{Eq. 3-3}$$

A value of $K_E = 1{,}000$ is recommended regardless of the specific masonry type in EN 1996-1-1 (2012). In the corresponding German National Annex DIN EN 1996-1-1/NA (2019), different values K_E are given for different masonry types to calculate deformations and internal forces (see Table 3-3). However, for the verification of masonry walls against buckling failure, $K_E = 700$ is specified for all masonry types. A comparison between the normative ratio $E_{\mathrm{ma}} / f_{\mathrm{ma,k}} = 1{,}100$ for clay brick masonry and typical ratios for SCBM from the literature indicates that the normative ratio is only suited for contemporary perforated clay brick masonry. For existing SCBM, the typical ratio $E_{\mathrm{ma}} / f_{\mathrm{ma}}$ is much lower because of the solid geometry of the bricks, the higher ratio of joint thickness to unit height in the

case of small-sized bricks, and the softness of historical mortars (Neuwald-Burg and Bohne 1999; Pech et al. 2018). For this reason, the Danish NA, DS/EN 1996-1-1 DK NA (2013), explicitly specifies different factors K_E for lime and cement mortars used in combination with calcium silicate or clay units:

lime mortar: $K_E = 150\, f_{\mathrm{j,m}}$

mortars with other binders: $K_E = \min\left\{400\, f_{\mathrm{j,m}};\ 20\, f_{\mathrm{b,m}};\ 1{,}000\right\}$ *Eq. 3-4*

where $f_{\mathrm{b,m}}$ and $f_{\mathrm{j,m}}$ are the mean unit and mortar compressive strength in N/mm², respectively. With this differentiation, the low modulus of elasticity of masonry with historical lime mortars having a compressive strength of around 1 N/mm² – see, for example, Neuwald-Burg and Bohne (1999) in Table 3-3 – are covered much better than by factors K_E that are specified independently of the mortar type.

Table 3-3 Ratio of modulus of elasticity to masonry compressive strength for different masonry types

Reference	Unit type	$E_{\mathrm{ma}} / f_{\mathrm{ma}}$	
		proposed	range
EN 1996-1-1 (2012)	all types	1,000[1]	-
DIN EN 1996-1-1/NA (2019)	clay bricks	1,100[1,2]	950 – 1,250
	calcium silicate bricks	950[1,2]	800 – 1,250
	lightweight concrete blocks	950[1,2]	800 – 1,100
	concrete blocks	2,400[1,2]	2050 – 2,700
	autoclaved aerated concrete blocks	550[1,2]	500 – 650
	all types	700[1,3]	-
Kaushik et al. (2007)	solid clay bricks	550	250 – 1,100
Lumantarna et al. (2014)		294[4]	89 – 433
Neuwald-Burg and Bohne (1999)		-	80 – 260
Pech et al. (2018)		300[1]	-

[1] *Ratio of E_{ma} to characteristic masonry compressive strength $f_{ma,k}$*
[2] *For calculation of internal forces*
[3] *For verification against buckling*
[4] *Chord modulus between 0.05 and 0.7 f_{ma}*

As indicated by the large range of ratios $E_{\mathrm{ma}} / f_{\mathrm{ma}}$, the use of a constant factor K_E might not be suited for the assessment of existing SCBM. Therefore, if the elastic modulus E_{ma} is essential for the verification of the structure, suitable values for E_{ma} should be chosen carefully. If the elastic modulus of masonry cannot be tested directly, which is usually the case, the ratio $E_{\mathrm{ma}} / f_{\mathrm{ma}}$ can be conservatively selected based on the literature. Alternatively, the elastic modulus of masonry can be estimated based on the elastic moduli of unit and mortar utilising a simple spring model, where the unit and the mortar joint are viewed as two springs with stiffness $E_{\mathrm{b}} / h_{\mathrm{b}}$ and $E_{\mathrm{j}} / h_{\mathrm{j}}$, respectively, that are arranged in series:

$$\frac{h_b + h_j}{E_{ma}} = \frac{h_b}{E_b} + \frac{h_j}{E_j} \quad \Leftrightarrow \quad E_{ma} = \frac{h_b + h_j}{h_b / E_b + h_j / E_j} \qquad \textit{Eq. 3-5}$$

where E_b and E_j are the elastic moduli of unit and mortar, respectively, h_b is the unit height, and h_j is the mortar joint thickness. The spring model according to Eq. 3-5 can be found in the German guideline for the assessment of existing road bridges ("*Nachrechnungsrichtline*", BMVBS 2011), for example. Pelà et al. (2016) and Segura et al. (2018) present an extension of the spring model that considers the influence of vertical mortar joints. Furthermore, they compare the model with experimental results and thereby demonstrate that the spring model is well suited to predict the modulus of elasticity of masonry.

3.3.3 Slender Masonry Walls under Eccentric Compression

To consider the influence of the load eccentricity e and the wall slenderness λ on the vertical resistance R of a masonry wall under compression, EN 1996-1-1 (2012) introduces the reduction factor Φ_{red}:

$$R = \Phi_{red} \, A \, f_{ma} \quad \Leftrightarrow \quad \Phi_{red} = \frac{R}{A \, f_{ma}} \qquad \textit{Eq. 3-6}$$

where A is the cross-sectional area of the masonry wall, and f_{ma} is the compressive strength of masonry. The reduction factor Φ_{red} can therefore be viewed as a normalised vertical resistance. Following EN 1996-1-1 (2012), a masonry wall must be verified at its top, bottom, and mid-height. In the usual case with horizontal supports at the top and bottom of the wall, second-order effects and thus the slenderness are only relevant for the verification at mid-height. According to EN 1996-1-1 (2012), the effect of the eccentricity on the cross-sectional resistance may be determined by assuming a rectangular stress block with stress f_{ma} (i.e. rigid-plastic behaviour without tensile strength). Hence, the reduction factor $\Phi_{red,cs,EC6}$ for the cross-sectional capacity corresponds to a theoretical upper bound for Φ_{red}:

$$\Phi_{red,cs,EC6} = 1 - 2\frac{e}{t} \qquad \textit{Eq. 3-7}$$

where e is the eccentricity of the compression loading (here: perpendicular to wall length), and t is the thickness of the wall.

Concerning the failure mode of a masonry wall under compression, a distinction must be made between material failure at the critical cross-section and stability failure due to buckling. The difference is illustrated in Fig. 3-4. When the acting compression force N is increased, the first-order moment M_I at a particular cross-section rises proportionally. The lateral displacement Δe_{II} causes an additional second-order moment ΔM_{II}. In the case of material failure, the load N can be increased until the combination of N and M_{II} at the critical cross-section reaches the respective cross-sectional capacity. If the compressive strength is

homogeneously distributed within the wall and both the cross-section and the normal force are constant over the wall height, the critical cross-section is the cross-section with the largest moment M_{II}, which is the cross-section at mid-height for the structural system in Fig. 3-4. In the case of stability failure, the wall fails before the cross-sectional capacity is reached at any section of the wall. Due to the nonlinear material behaviour under compression and potential cracking at the tension side of the wall, the overall flexural stiffness of the wall reduces with increasing compression loading. Stability failure occurs as soon as the marginal flexural stiffness of the wall is no longer large enough to enable an equilibrium for a further increase of the compression loading. At this point, the *N*-*M* curve describing the normal force and second-order moment acting at the critical cross-section becomes horizontal before reaching the envelope representing the cross-sectional capacity (see Fig. 3-4).

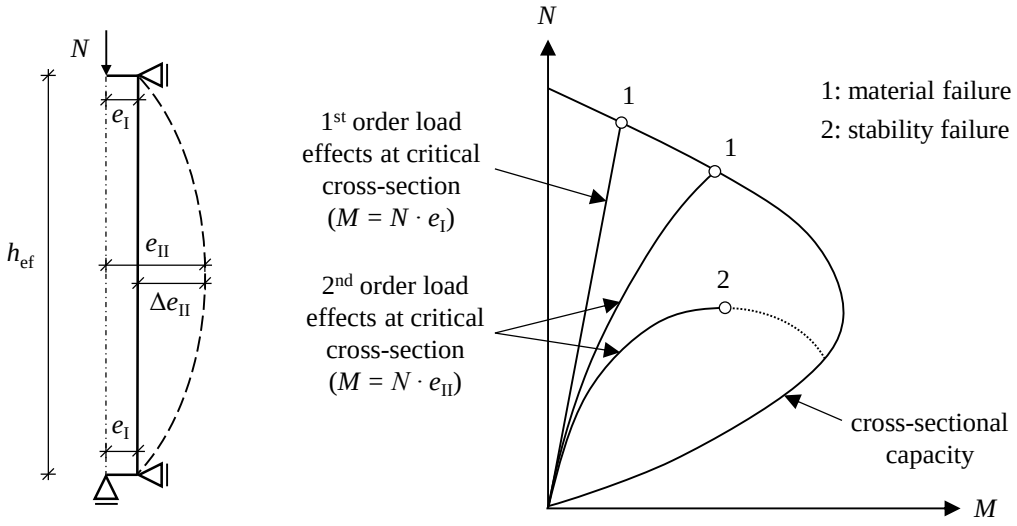

Fig. 3-4 Idealised system of a masonry wall and differentiation between material and stability failure

EN 1996-1-1 (2012), DIN EN 1996-1-1/NA (2019), and EN 1996-3 (2009) define different reduction factors Φ_{red} accounting for eccentricity and slenderness, each representing different degrees of approximation. While the reduction factors for considering slenderness according to DIN EN 1996-1-1/NA (2019) and EN 1996-3 (2009) do not allow for the explicit consideration of a specific elastic modulus E_{ma}, the reduction factor according to Annex G of EN 1996-1-1 (2012) is a function of E_{ma}.

If the vertical resistance of an unreinforced masonry wall shall be determined precisely to obtain results close to the exact solution of the differential equation defining the stability problem, the closed-form expression derived by Glock (2004) can be used. Fig. 3-5 displays the reduction factor Φ_{red} according to Glock (2004) for varying slenderness λ and different load eccentricities e_I. The material-related slenderness λ is defined as

$$\lambda = \frac{h_{ef}}{t}\sqrt{\varepsilon_f} = \frac{h_{ef}}{t}\sqrt{k\,\frac{E_{ma,0}}{f_{ma}}} \qquad \textit{Eq. 3-8}$$

where h_{ef} is the buckling length of the wall.

The model proposed by Glock (2004) allows for the consideration of different stress-strain parameters k. After reaching the peak stress f_{ma} at strain ε_f, a horizontal stress-strain curve until reaching the ultimate strain $\varepsilon_u = \eta_u\,\varepsilon_f$ is assumed. In Fig. 3-5, the reduction factors are displayed for $k = 2$ combined with $\eta_u = 1.75$ and for $k = 1$ with $\eta_u = 1$. For a given value of ε_f, a higher nonlinearity of the stress-strain curve, represented by a higher value k, leads to a higher load-bearing capacity. Employing the model by Glock (2004), the flexural tensile strength of masonry can also be considered. The respective stress-strain behaviour is taken as linear until reaching the tensile strength f_t, followed by a sudden drop to zero. The reduction factors in Fig. 3-5 are given with and without considering the tensile strength f_t.

As evident from Fig. 3-5, f_t is only influential for high slenderness combined with a large eccentricity of the load. For a theoretical slenderness $\lambda = 0$, the resistance R is proportional to the compressive strength f_{ma} and independent of E_{ma}. In the case of stability failure, $k = 1$, and $f_t = 0$, the resistance is directly proportional to E_{ma} and independent of f_{ma}.

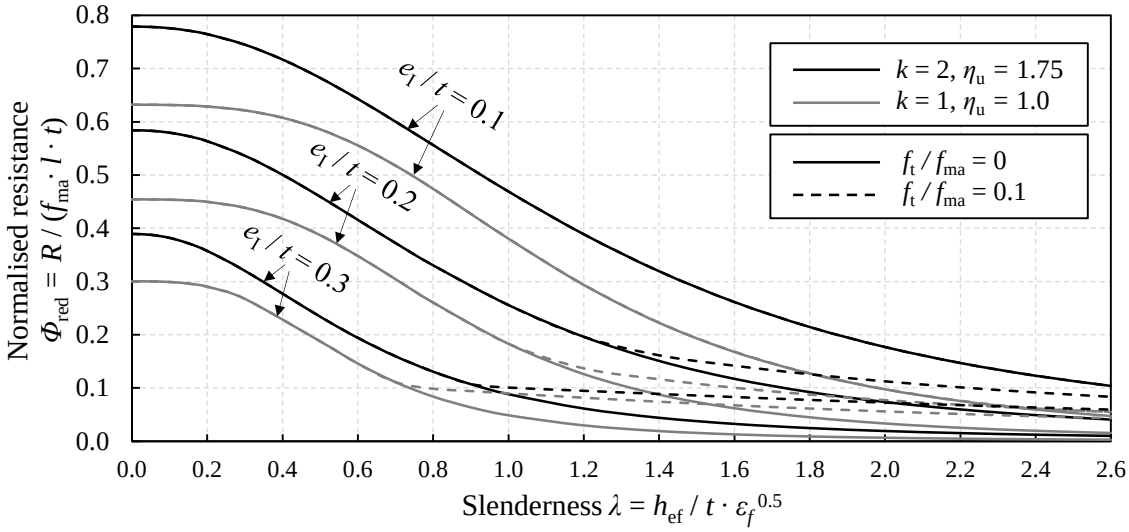

Fig. 3-5 Normalised load-bearing capacity for varying slenderness, eccentricity, and nonlinearity of the stress-strain relationship according to Glock (2004)

Another closed-form expression for the vertical load-bearing capacity of slender unreinforced masonry walls was developed by Bakeer (2015). In contrast to the model by Glock (2004), however, the closed-form expression by Bakeer (2015) does not allow for the consideration of the post-peak behaviour of the stress-strain curve nor for the consideration of the tensile strength (i.e. it is valid for the special case of $\eta_u = 1$ and $f_t / f_{ma} = 0$). In Bakeer (2016a), a simplified version of the expression is proposed that, for $h / t \rightarrow 0$, converges to

the cross-sectional capacity given rigid-plastic behaviour (see Eq. 3-7). Thereby, consistency with the cross-sectional capacity as defined in EN 1996-1-1 (2012) is obtained. In slightly altered form, the proposal by Bakeer (2016a) is also included in the current draft standard FprEN 1996-1-1 (2020).

3.3.4 Influence of Inhomogeneity

One main objective of this thesis is to investigate the influence of spatially varying unit and mortar properties and thus inhomogeneity on the load-bearing capacity of masonry under compression. Stochastic finite element simulations have already been performed to study the influence of spatially variable material properties on the out-of-plane flexural resistance and the in-plane shear resistance of masonry walls (Li et al. 2014; Gooch et al. 2021; Isfeld et al. 2021). The results of these investigations have in common that the consideration of spatially variable material properties leads to a reduction in the mean resistance compared to a non-spatial analysis, in which unit and mortar properties are modelled as homogeneous within a masonry wall. Furthermore, the coefficient of variation (CoV) of the resistances obtained by the spatial analysis is much lower than the input CoVs of the influential material properties. Concerning masonry under compression loading, two existing studies regarding the influence of inhomogeneity are briefly described next.

Kirtschig and Meyer (1990) performed compression tests on walls made of calcium silicate bricks, which contained specific percentages of bricks with either a higher or a lower unit compressive strength. The experiments were conducted for several unit dimensions, varying wall lengths, and different percentages of weaker bricks within the wall. The main goal of the investigations was to find an experimental justification for the higher global safety factor of $\gamma = 2.5$ for masonry pillars (cross-section $A < 0.1$ m² or < 2 units per course) compared to $\gamma = 2.0$ for masonry walls ($A \geq 0.1$ m² and ≥ 2 units per course) as introduced by DIN 1053-2 (1984) based on theoretical considerations. The investigations did not reveal a significant difference between the mean resistances of pillars and walls. Higher variability of the resistance of pillars, which would also justify the higher safety factor, is not evident from the results, due to the small number of tests (only two) per wall configuration. Nevertheless, the experimental series revealed one main issue regarding the influence of inhomogeneity: The inhomogeneous walls and pillars consisting of specific shares of stronger and weaker units showed a lower load-bearing capacity than obtained by linear interpolation between the capacities of the two homogeneous reference walls. Hence, if spatial variability is present, the strength of the masonry wall is lower than the average masonry compressive strength within the wall, which is due to an imperfect capability of stress redistribution.

Goretzky (2000) performed Monte Carlo simulations (MCS) of masonry walls under compression loading to investigate the influence of the spatial variability of unit and mortar

properties within historical masonry, which is typically higher than in modern masonry. To reduce the computational effort compared to using a finite element model, a simplified model was developed that displays masonry as a set of vertical prisms. Each prism consists of several unit-mortar elements, whose number is equal to the number of courses. The deformation and cracking of the unit-mortar elements are determined based on the properties of unit and mortar. A prism fails if, after the appearance of the first crack, the stress is further increased up to a critical stress value, which depends on the lengths of the existing vertical cracks. If the remaining prisms can additionally resist the load of the failed prism, the load acting on the masonry wall can be further increased. Based on the results of the MCS, reduction factors for the mean and the 5 % fractile of the wall resistance are proposed for historical masonry with a high CoV v_b of unit compressive strength. The factors represent the relative reduction compared to the mean and 5 % fractile of the wall resistance for modern masonry, for which a reference CoV of v_b = 10 % is assumed. The reduction factor f_I for the mean is given by

$$f_I = 1.1 - v_b \qquad \textit{Eq. 3-9}$$

and the reduction factor ξ_I for the 5 % fractile is given by

$$\xi_I = 1 + 0.33\left(0.1 - v_b\right) \qquad \textit{Eq. 3-10}$$

The investigations by Goretzky (2000) can be viewed as a significant step towards understanding the influence of spatially varying material properties on the vertical load-bearing capacity of masonry walls. However, the simulations were only performed for a masonry wall with concentric compression loading and a height of only seven courses, with six units per course. Second-order effects were not considered. For a deeper understanding, investigations with varying wall length, slenderness, and load eccentricity are thus needed (see Chapter 6 of this thesis). Furthermore, for the reliability of masonry walls, neither the mean nor the 5 % fractile of the resistance is decisive. Instead, lower fractile values, namely design/assessment values, are essential, which were not evaluated by Goretzky (2000).

3.3.5 Further Influences on the Resistance of Masonry

Some other influences on the resistance of masonry under compression, namely high sustained loading, physicochemical deterioration, incompletely filled mortar joints, and increased moisture content, are briefly described next. The importance of considering their respective effects on masonry strength is not limited to the assessment of existing structures but is also given for the design of new structures. However, some of the following influences result from structural defects due to poor workmanship or mechanisms overlooked during design; therefore, the need to consider these influences becomes more apparent in the assessment of existing masonry.

Sustained loading

Due to the creep-related development of micro-cracks, high sustained compressive stress levels can lead to a failure of masonry, even if the stress level is below the masonry compressive strength as determined in short-term testing. For concrete, this phenomenon is also known as the "Rüsch effect", as it was made known through investigations by Rüsch (1960). The same effect has also been identified for masonry structures (Hierl et al. 1973; Binda 2008; Verstrynge 2010). To consider the influence of high sustained stress levels, DIN EN 1996-1-1/NA (2019) specifies a reduction factor of $\zeta = 0.85$ that is to be applied to the short-term strength.

Deterioration

The term "deterioration" refers to processes leading to an irreversible and gradual change in one or more of the structural properties, thereby reducing the ability of the structure to perform according to a defined standard (Maes et al. 1999). Detailed descriptions of masonry-related deterioration mechanisms can be found in Franke and Schumann (1998), Larbi (2004), Maier (2012), and Ghiassi and Lourenço (2019). A categorisation of common deterioration mechanisms is listed in Table 3-4, focusing on mechanisms that lead to a reduction of the resistance, which is usually due to a reduced effective cross-section. As evident, deterioration is mostly caused by insufficient protection against water penetration. If deterioration mechanisms are identified in the assessment of an existing structure, the processes should be either stopped by suitable measures or considered via time-dependent deterioration models to evaluate structural reliability within the remaining service life (Maes et al. 1999).

Table 3-4 Typical deterioration mechanisms for masonry structures (Franke and Schumann 1998; Maes et al. 1999; Larbi 2004; Ghiassi and Lourenço 2019)

Type	Cause	Possible consequences
Freeze-thaw cycles	Increased moisture content and temperature changes	Spalling of unit parts, disintegration of mortar joints, loss of adhesion between unit and mortar, cracking
Salt crystallisation	Intrusion of moisture-transported salts, crystallisation	Spalling or powdering of units, sanding of mortar, cracking
Attacks by chemicals	Intrusion of chemicals (e.g. sulphates, acids) dissolved in water, chemical reaction	Disintegration of mortar joints due to volume increase, leaching of constituents of unit and mortar
Biological mechanisms	Growth of biological agents (e.g. plants, fungi, micro-organisms)	Disintegration of mortar joints, cracking
Erosion	Particles transported by wind	Abrasion of unit and mortar

Incompletely filled mortar joints

In the assessment of existing structures, bed joints that are imperfectly filled with mortar are frequently found. They can be the result of either poor workmanship or deterioration processes. In the structural assessment, the incomplete filling of bed joints must be considered, as it results in a reduced masonry compressive strength if related to the complete cross-section of the wall. Investigations by Kirtschig and Meyer (1989) show that the reduced masonry strength is approximately proportional to the ratio of the filled area to the total area of the bed joints, which can be applied as a helpful rule of thumb in practical assessment situations. The same approach is also recommended in the Swiss standard SIA 269/6-2 (2014) for the assessment of existing masonry structures.

Increased moisture content

The compressive strength of masonry is moisture-dependent (Witzany et al. 2010; Franzoni et al. 2015). Compared to air-dry masonry (i.e. masonry under standard environmental conditions), masonry compressive strength reduces with increased moisture content. For practical applications, WTA 7-4 (2021) recommends reducing the compressive strength of masonry by up to 20 %, depending on the degree of saturation. A similar approach is proposed by the Czech standard ČSN 73 0038 (2019), according to which the masonry compressive strength obtained for standard environmental conditions is to be divided by a reduction factor, which is determined by linear interpolation between 1.0 and 1.25 for a mass-related moisture content between 4 % and 20 %.

3.4 Methods for Testing the Compressive Strength of Masonry

3.4.1 General

For the assessment of existing structures, not all of the standardised testing methods for the compressive strength of masonry and its components (i.e. unit and mortar) are feasible, as illustrated in this section. Selecting the most suitable testing procedure for existing masonry (and the corresponding sample size) involves finding the best compromise between the accuracy of the procedure on the one hand and the effort and damage to the structure on the other (see Fig. 3-6). Concerning experimental procedures for determining the compressive strength of masonry, a distinction must be made between direct and indirect testing as well as destructive and non-destructive testing (Henkel 2016).

In *direct tests*, the compressive strength of masonry is directly obtained by performing tests on masonry specimens (i.e. composite specimens consisting of unit and mortar), as described in Section 3.4.4. If *indirect testing* is performed, unit and mortar compressive strength are tested separately (see Sections 3.4.2 and 3.4.3), and the compressive strength

of masonry is subsequently predicted based on the results of the separate component tests (see Section 3.5).

Destructive testing usually involves extracting specimens from existing masonry that are then tested in the laboratory. *Non-destructive* testing procedures are mainly available for the separate testing of unit and mortar. With regard to the masonry units, rebound hammer tests or ultrasonic pulse velocity tests can be applied, for example (Vasanelli et al. 2016; Sýkora et al. 2018; Noor-E-Khuda and Albermani 2019). Since non-destructive tests do not measure the compressive strength itself but only yield a substituting quantity (e.g. a rebound value or a pulse velocity), complementary destructive testing should usually be performed to find suitable structure-specific relationships between the results of non-destructive tests and the actual unit compressive strength (Sykora et al. 2022). Concerning mortar, the most common non-destructive testing procedures are different versions of penetration tests, where the penetration depths of indenters with defined impact speed are measured to draw conclusions about mortar compressive strength (Henkel 2016; Sýkora et al. 2018). A direct testing procedure that is only moderately destructive – and is thus sometimes also categorised as non-destructive – is flat-jack testing (Gregorczyk and Lourenço 2000). Flat-jacks are thin envelopes that, after removing the mortar, are placed within the joints of existing masonry and then filled with pressurised oil. If two flat-jacks are placed in the wall, and the masonry strain in between is measured for increasing oil pressure, the elastic modulus can be determined, and, by extrapolating the stress-strain curve, the compressive strength can be estimated.

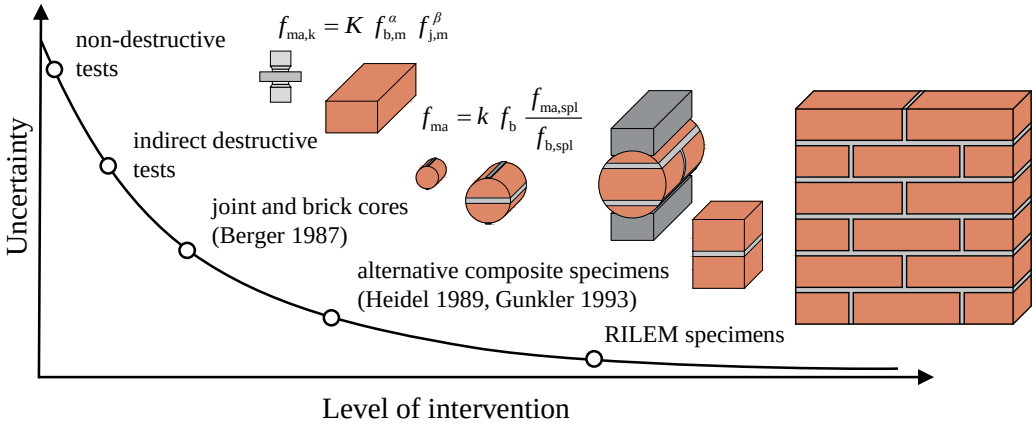

Fig. 3-6 Uncertainty and level of intervention associated with different procedures for testing masonry compressive strength (see Gigla 2020)

Non-destructive testing is connected with much more uncertainty than destructive testing, which is one reason why destructive testing is currently much more common in Germany (see Gigla 2020). Therefore, the rest of this section and this thesis in general focus on destructive tests. Concerning destructive tests, indirect testing currently represents the default

method for assessing existing masonry in Germany, which, at least to some degree, is because standards covering feasible testing procedures are better developed for this case. In Sections 3.4.2 to 3.4.4, the common destructive testing methods for unit compressive strength, mortar compressive strength, and masonry compressive strength are described.

3.4.2 Unit Compressive Strength

In Europe, unit compressive strength is usually tested according to EN 772-1 (2011), which is equally suited for new masonry units and units removed from existing masonry. The prepared specimens, which can be either whole units or parts thereof, are tested by applying a uniformly distributed load that is increased until failure. For details regarding the conditioning and capping or grinding of the test specimens, see EN 772-1 (2011). Due to the influence of the specimen geometry on the obtained results, the obtained strength must be converted into a normalised unit compressive strength f_b by applying suitable shape factors. EN 772-1 (2011) defines these shape factors as a function of the height and width of the test specimens, where the normalised strength corresponds to a test specimen with a height of 100 mm and a width of 100 mm. According to DIN EN 1996-1-1/NA (2019), the converted mean unit compressive strength f_{st} is to be used for all further applications instead of the normalised unit compressive strength f_b. The main difference between f_{st} and f_b consists of different shape factors that are to be applied. For clay bricks, the shape factors for obtaining f_{st} are specified in DIN 20000-401 (2017). In the following, the symbol f_b is used for the normalised unit strength, irrespective of the applied shape factor.

3.4.3 Mortar Compressive Strength

EN 1996-1-1 (2012) specifies that mortar compressive strength must be tested on mortar prisms according to EN 1015-11 (2019). The prisms are made in metal moulds with interior dimensions 160 x 40 x 40 mm³. First, a three-point flexural tensile strength test is usually performed, by which the prisms are broken into two parts. Each half is then loaded via 40 mm long and 40 mm wide platens. The standard mortar compressive strength is then defined as the maximum load divided by the loading plate area. Further details (e.g. on curing conditions) are defined in EN 1015-11 (2019).

Standard mortar testing cannot be performed on mortar specimens extracted from existing masonry since ordinary mortar joint thicknesses are much lower than 40 mm. Therefore, different procedures for the destructive testing of mortar extracted from masonry were developed, three of which are included in the German standard DIN 18555-9 (2019). The three procedures differ regarding the geometry of the specimens and loading platens. Procedure III, presented in its first version by Henzel and Karl (1987), is the most suitable approach for determining the mortar compressive strength of existing masonry (DIN 18555-9 2019; WTA 7-4 2021). Following procedure III, specimens with a width and length (or diameter) of approximately 50 mm and a height equal to the joint thickness are

extracted from masonry. The load is then applied by platens with a diameter of 20 mm (see Fig. 3-7). The advantage of not loading the entire area is that the specimen dimensions may slightly deviate from the specified dimensions, and defective spots at the edges are not influential. This is a significant benefit, as specimens of weak mortar cannot be prepared with high geometrical accuracy (Henzel and Karl 1987). The testing procedure is also named the "double punch test" in the international literature (Sassoni et al. 2015; Marastoni et al. 2016).

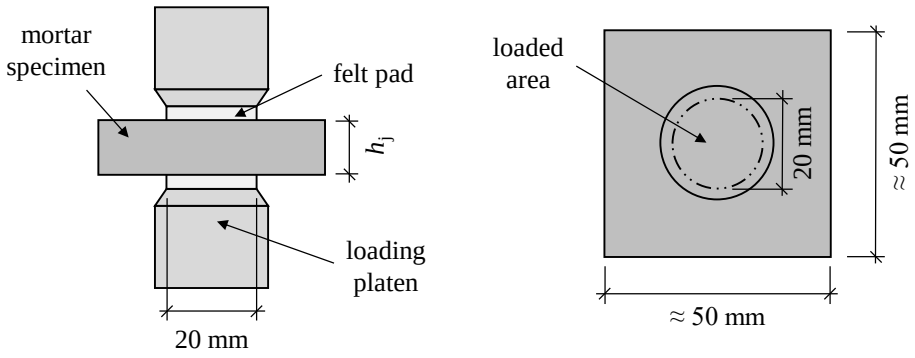

Fig. 3-7 Double punch testing on mortar specimens extracted from existing masonry according to procedure III of DIN 18555-9 (2019)

Compared to standard mortar testing on moulded prisms, the mortar strength obtained by double punch tests on specimens extracted from masonry might differ for two reasons: First, the different geometry of specimens and loading platens and, second, the different curing conditions can lead to different strengths. However, the standard prism strength is typically needed to determine masonry compressive strength based on unit and mortar compressive strength (see Section 3.5). Reliable research results are still lacking concerning generally valid approaches for converting double punch strengths into standard prism strengths (WTA 7-4 2021). Regarding the influence of the geometry, a shape factor of 1.0 can approximately be applied to convert double punch strengths into standard prism strengths (Riechers et al. 1998). The influence of the curing conditions, however, depends on the particular type of unit and mortar. According to Schubert (1995), the different curing conditions, particularly the influence of water absorption by the units, lead to a conversion factor of about 0.5 to 1.5. Hence, due to the curing conditions in the joint, the mortar compressive strength is 0.7 to two times the strength that develops in moulded prisms. For a conservative conversion, Schubert (1995) recommends a factor of 0.5. Investigations by Henzel and Karl (1987) also indicate that a factor of about 0.5 is suited.

3.4.4 Masonry Compressive Strength

EN 1052-1 (1998) specifies the experimental determination of masonry compressive strength and the modulus of elasticity of masonry, which is defined as the secant modulus at one-third of the maximum stress. The corresponding test specimens have a height of at

least five and a length of at least two units in the case of small-sized units. For distinction from wall-high specimens and stack-bonded masonry specimens with a cross-section of one unit and no vertical joints, these specimens are usually referred to as "RILEM specimens" (see RILEM 1994). More detailed requirements on the specimen dimensions are defined in EN 1052-1 (1998). The requirements usually lead to a slenderness of roughly $h / t = 5$. EN 1052-1 (1998) requires at least $n = 3$ tests. For $n < 5$, the characteristic masonry compressive strength $f_{\mathrm{ma,k}}$ is given by the average strength divided by 1.2 or the minimum strength, whichever is smaller:

$$f_{\mathrm{ma,k}} = \min \left\{ \frac{1}{n} \sum_{i=1}^{n} f_{\mathrm{ma},i} \Big/ 1.2, \;\; f_{\mathrm{ma},i,\mathrm{min}} \right\} \qquad \textit{Eq. 3-11}$$

For $n \geq 5$ tests, the characteristic compressive strength is to be determined as the 5 % fractile with a confidence level of 95 %. The obtained characteristic compressive strength $f_{\mathrm{ma,k}}$ may then be used as an input parameter for structural verification according to EN 1996-1-1 (2012), which defines the characteristic strength as the 5 % fractile of masonry compressive strength for the theoretical slenderness of $h / t = 0$. It is noted that the factor 1.2 defined for determining the 5 % fractile in EN 1052-1 (1998) – see Eq. 3-11 – is only suited if the CoV of strength is small and hence not for the general case of assessing an existing masonry structure. Up to the slenderness of $h / t = 5$, the difference between the obtained strength and the strength corresponding to $h / t = 0$ is small and can conservatively be neglected (Jäger and Pflücke 2006; Graubner et al. 2020). If specimens with higher slenderness, for example wall-high specimens, are tested, then a conversion to $h / t = 5$ is usually conducted as proposed by Mann (1983); see also Graubohm and Brameshuber (2016):

$$f_{\mathrm{ma},h/t=5} = f_{\mathrm{ma,test}} \left[0.966 + 0.00136 \left(\frac{h}{t} \right)^2 \right] \qquad \textit{Eq. 3-12}$$

Some international standards, for example ASTM C1314 (2018), define tests on stack-bonded masonry prisms for determining masonry compressive strength. Due to the missing influence of vertical mortar joints on the obtained strength, it is reasonable to assume that this strength should be reduced to attain a strength representative of the actual masonry bond. In Thamboo and Dhanasekar (2019), estimating the RILEM specimen strength as 0.75 times the stack-bonded prism strength is recommended. In contrast, investigations by Mann and Betzler (1996) indicate that the difference between the strength obtained on either RILEM specimens or stack-bonded prisms is negligible. It can thus be concluded that the influence of vertical mortar joints strongly depends on the particular combination of unit and mortar.

In the assessment of existing masonry, the extraction of RILEM specimens is usually not feasible, as this would result in significant damage to the existing structure. Therefore, alternative testing methods have been developed that allow for the direct determination of masonry compressive strength on smaller composite specimens (see WTA 7-4 2021).

Berger (1987) discovered that the ratio $f_{ma,spl} / f_{b,spl}$ between the splitting tensile strengths of a masonry core with a centred mortar bed joint and a brick core is approximately equal to the ratio f_{ma} / f_b between the compressive strengths of masonry and brick (see Fig. 3-8). Masonry compressive strength f_{ma} can hence be evaluated if the three other material properties are obtained:

$$f_{ma} = k \; f_b \frac{f_{ma,spl}}{f_{b,spl}} \quad \text{with } k = \frac{1+3.24\sqrt{h_j/\left(d_{jc}-h_j\right)}}{1+3.24\sqrt{h_j/h_b}} \qquad \textit{Eq. 3-13}$$

where k is a correction factor considering the specific joint thickness h_j and unit height h_b (Wenzel et al. 2000). The drilled masonry cores should have a diameter of d_{jc} = 10 cm and a length of 10 cm (WTA 7-4 2021). Although three different material properties must be tested before calculating masonry compressive strength, the method by Berger can still be beneficial since the required specimens are much smaller than RILEM specimens. Despite the testing of composite specimens, the method is not a direct testing procedure in a strict sense, as material properties other than masonry compressive strength itself are tested. Since masonry compressive strength must be calculated based on the model given by Eq. 3-13, the method is connected with non-negligible model uncertainty (see Fig. 3-6).

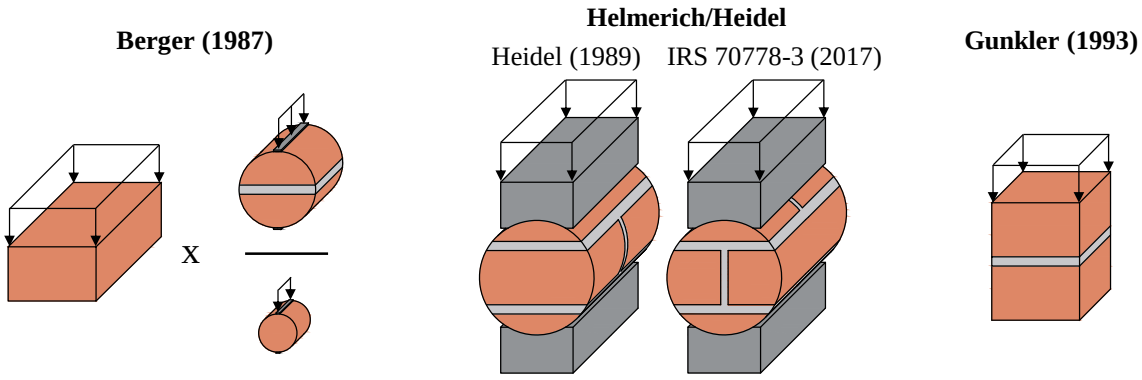

Fig. 3-8 *Alternative procedures for testing masonry compressive strength on composite specimens extracted from existing masonry*

Helmerich and Heidel developed a direct testing procedure, which requires the horizontal extraction of masonry drill cores with a diameter of 15 cm, a length equal to one unit length, and an arrangement of joints as displayed in Fig. 3-8 (Heidel 1989). With a slightly different recommended joint arrangement, the procedure can also be found in the guideline IRS 70778-3 (2017). The compression tests are then performed in the same direction as the load

acts in the existing masonry wall. For this purpose, curved loading platens are used to apply the load to the lateral surface of the specimens over a width of 7.5 cm (WTA 7-4 2021). The compressive strength of masonry can then be determined as

$$f_{ma} = k_{RILEM}\, k_s\, \frac{F_{max}}{A_{mid}} \qquad \textit{Eq. 3-14}$$

where the factor $k_s = 1.3$ considers the non-uniformity of the stress distribution within the cylindrical specimen, F_{max} is the failure load, and A_{mid} is the cross-sectional area in the middle of the cylinder (i.e. diameter times length). The factor k_{RILEM} for converting the results to a strength equivalent to the RILEM specimen strength is given in Heidel (1989) as $k_{RILEM} = 0.8$ for solid clay bricks with $f_b \leq 25$ N/mm² and 0.7 for solid clay bricks with $f_b \geq 35$ N/mm². Due to its high practicality, the direct testing of masonry compressive strength on drilled cores has recently gained research attention again (Sassoni et al. 2014; Pelà et al. 2016; Segura et al. 2019; Henkel and Neuwald-Burg 2021). Most investigations aim at finding suitable relationships between the obtained strength and the standardised masonry compressive strength for different unit-mortar combinations and test setups.

Gunkler (1993) developed direct tests on small rectangular prisms containing one mortar bed joint in the middle. The height of the prism should equate to two unit heights plus the joint thickness, and the width and length should approximately equal the unit width. In the case of the brick format investigated by Gunkler (1993), this leads to dimensions of 12.5 x 12.5 x 15 mm³ (length x width x height). Conversion factors to RILEM strength, which are limited to the solid clay brick format and strength ($25 \leq f_b \leq 28$ N/mm²) used in the corresponding investigations, are given as a function of mortar compressive strength in Gunkler (1993).

In conclusion, the presented direct test methods provide a significant advantage over indirect testing, as the model uncertainty in calculating masonry compressive strength based on unit and mortar properties is avoided. However, the above summary of procedures for direct tests on alternative composite specimens suggests that, concerning the current state of research, converting the obtained results to the standard RILEM strength is still associated with considerable uncertainty if the particular unit-mortar combination deviates from that in the respective research projects.

3.5 Prediction of Masonry Compressive Strength based on Component Properties

3.5.1 General

Since the start of research on masonry structures, predicting masonry compressive strength based on the properties of unit and mortar has been a steady research topic. Models for masonry strength prediction can be categorised into models based on a mechanical description of the interaction of unit and mortar within masonry (see Section 3.5.2) and empirical models derived from test databases, most notably the power equation (see Section 3.5.3). In Section 3.5.4, the power equation is further analysed and compared with a model with a mechanical background to evaluate its suitability for stochastic applications. Most empirical models do not take the unit dimensions and the mortar thickness into account; therefore, the influence of mortar thickness is briefly discussed in Section 3.5.5.

3.5.2 Models Based on Mechanical Principles

The model by Hilsdorf (1965; 1969) is one of the earliest models with a mechanical background for predicting masonry compressive strength. Since many models that were developed later are based on the general ideas of Hilsdorf's model, it is illustrated in more detail here, serving as an example.

As explained in Section 3.3.1, the mortar joints are subjected to lateral compressive stresses, whereas the units receive lateral tensile stresses if masonry is loaded perpendicular to the bed joints (i.e. vertically in typical cases). Hilsdorf (1969) assumes that the horizontal stresses acting in the two different lateral directions are equal; that is, $\sigma_{h1} = \sigma_{h2}$. For the failure criterion of the unit, Hilsdorf applies a linear relationship, according to which the maximum vertical stress $\sigma_{v,max}$ in the units is given by

$$\sigma_{v,max} = f_b \left(1 - \frac{\sigma_{h,b}}{f_{bt}} \right) \qquad \textit{Eq. 3-15}$$

where f_b is the uniaxial unit compressive strength, $\sigma_{h,b}$ is the biaxial lateral tensile stress in the unit, and f_{bt} is the tensile strength of the unit. With increasing vertical load, the horizontal tensile stresses in the brick increase (see Fig. 3-9). When the unit failure criterion is reached, a local crack appears, resulting in a reduction of the horizontal tensile stresses $\sigma_{h,b}$ in the unit, which are in equilibrium with the horizontal compressive stresses $\sigma_{h,j}$ in the mortar joint. For simplicity, Hilsdorf (1969) assumes a uniform distribution of the lateral stresses over unit height and mortar joint thickness, resulting in the following condition:

$$\sigma_{h,j} \, h_j = \sigma_{h,b} \, h_b \qquad \textit{Eq. 3-16}$$

where h_j is the bed joint thickness, and h_b is the unit height. If the vertical stress is higher than the uniaxial mortar compressive strength, lateral confining stresses are needed in the

mortar joint to enable the resistance against the vertical stress. Hence, due to the equilibrium, the tensile stresses in the unit cannot fall below a minimum lateral stress without leading to failure of the mortar. Hilsdorf (1969) approximates the maximum vertical stress $\sigma_{v,max}$ for confined mortar with the following relationship initially derived for confined concrete:

$$\sigma_{v,max} = f_j + 4.1\,\sigma_{h,j} \qquad \textit{Eq. 3-17}$$

As illustrated in Fig. 3-9, further cracks appear with increasing load, each followed by a reduction of the lateral stresses until the failure of masonry is reached at the intersection of the two failure curves for unit and mortar. According to Hilsdorf (1969), the vertical stresses are distributed non-uniformly over the cross-section. An empirical non-uniformity factor U was thus introduced by Hilsdorf, ranging from 1.35 to 2.18 for the tests presented in Hilsdorf (1969). From Eq. 3-15 to Eq. 3-17, it follows that

$$f_{ma} = \frac{\sigma_{v,max}}{U} = \frac{f_b}{U} \cdot \frac{f_{bt} + a\ f_j}{f_{bt} + a\ f_b} \quad \text{with } a = \frac{h_j}{4.1 h_b} \qquad \textit{Eq. 3-18}$$

If the unit tensile strength f_{bt} is unknown, as only the compressive strength f_b of the units is tested, Eq. 3-18 can still be applied by estimating f_{bt} based on f_b using typical relationships for the particular unit type.

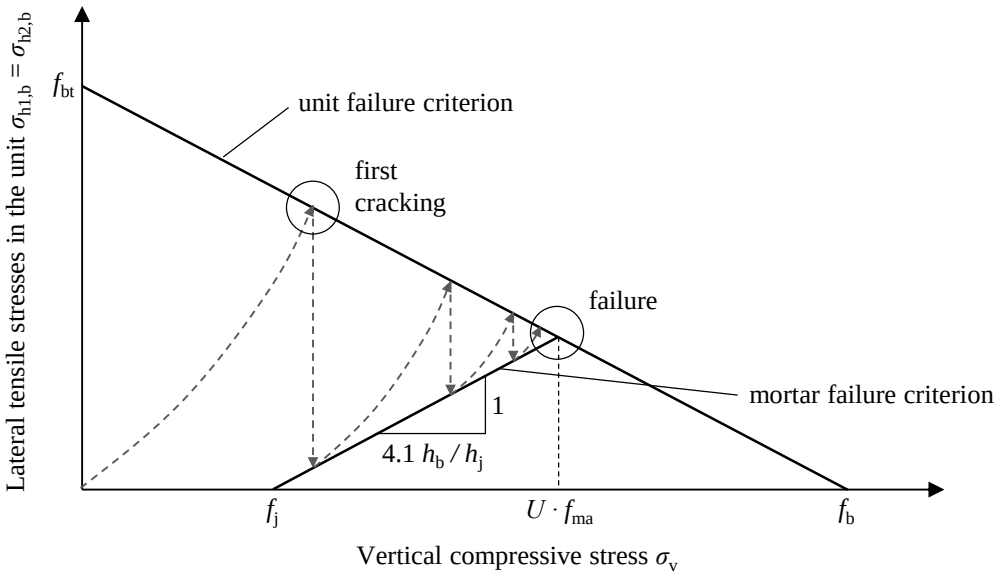

Fig. 3-9 Compressive strength of masonry according to Hilsdorf (1969)

Several other models with a mechanical background for predicting masonry compressive strength have been developed, for example the models by Khoo (1972), Ohler (1986), and Sabha (Wenzel et al. 2000; WTA 7-4 2021). Most of these models are based on similar principles as the model by Hilsdorf (1969) but include more refined failure curves for unit and mortar and more complex descriptions of the stress distribution. Despite these research

efforts, models with a mechanical background are only rarely used in engineering practice. Empirical models, as covered in Section 3.5.3, are much more common.

3.5.3 Empirical Power Equation

Empirical models for predicting masonry compressive strength based on the properties of unit and mortar are most commonly formulated through a power equation, which was proposed by Mann (1983). In EN 1996-1-1 (2012), the power equation is given in the following form:

$$f_{\mathrm{ma,k}} = K \; f_{\mathrm{b,m}}^{\alpha} \; f_{\mathrm{j,m}}^{\beta} \qquad \textit{Eq. 3-19}$$

where $f_{\mathrm{b,m}}$ and $f_{\mathrm{j,m}}$ are the mean values of unit and mortar compressive strength, and $f_{\mathrm{ma,k}}$ is the characteristic masonry compressive strength. Suitable values for the parameters K, α, and β can be evaluated via a regression analysis based on data from compression tests on masonry and accompanying compression tests on unit and mortar specimens, which has been conducted by numerous researchers. Since the model is purely empirical and lacks any mechanical background, the accuracy of the model highly depends on whether the combination of unit and mortar types included in the respective database is representative of the unit-mortar combinations to which the model is applied. Therefore, derived values for K, α, and β are only applicable for a particular range of boundary conditions. For $\alpha + \beta \neq 1$, the dimensional correctness of the power equation is violated, and the dimensions of the material strengths must thus be explicitly specified.

Since the mean values of unit and mortar compressive strength are the input values according to the formulation in EN 1996-1-1 (2012), whereas the resulting compressive strength of masonry is a characteristic value, the power equation contains a conversion from the mean values to a 5 % fractile value. According to Brameshuber et al. (2012), the conversion factor is implicitly included in the parameter K and equals 0.8, which approximately matches 1 / 1.2 = 0.83 as included in the testing standard EN 1052-1 (1998). Due to this fixed conversion from mean to characteristic values, the power equation as defined by EN 1996-1-1 (2012) is not suited for existing masonry with high material variability without further modification. EN 1996-1-1 (2012) explicitly states that the power equation may only be used if the CoV of unit compressive strength is below $v_{\mathrm{b}} = 25$ %.

For masonry made with general purpose mortar, EN 1996-1-1 (2012) specifies $\alpha = 0.7$ and $\beta = 0.3$, whereas the parameter K depends on the unit type. For solid clay bricks, $K = 0.55$ is defined. According to the German NA DIN EN 1996-1-1/NA (2019), all of the parameters K, α, and β depend on the type of unit and mortar. $K = 0.95$, $\alpha = 0.585$, and $\beta = 0.162$ are given for solid clay brick masonry with general purpose mortar. Since $\alpha + \beta \neq 1$, the parameters are only valid for the specified dimension of strength, which is N/mm².

more, both sets of parameter values are related to single wythe masonry. For bonded masonry (i.e. masonry with vertical mortar joints parallel to the face of the wall), K must be multiplied by 0.8.

Fig. 3-10 displays the masonry compressive strength $f_{ma,k}$ resulting from Eq. 3-19 as a function of $f_{b,m}$ and $f_{j,m}$. The displayed contour lines for $f_{ma,k}$ are valid for solid clay brick masonry arranged in a single wythe. Due to the included factor of 0.8 for converting the mean to the characteristic compressive strength, which is equal to the factor of 0.8 for the conversion from single wythe to bonded masonry, the displayed values can also be understood as mean values $f_{ma,m}$ for bonded masonry. The values according to EN 1996-1-1 (2012) are displayed on the left, while the right diagram shows the values according to DIN EN 1996-1-1/NA (2019). Both EN 1996-1-1 (2012) and the German NA define boundaries regarding applicable input values for $f_{b,m}$ and $f_{j,m}$. Combinations outside the boundaries are highlighted in grey in Fig. 3-10. The boundary conditions for the German NA are shown as specified in DIN EN 1996-1-1/NA/A1 (2014). The red line in both diagrams marks the combination of $f_{b,m}$ and $f_{j,m}$, for which the compressive strengths according to both sets of parameters are equal. The masonry strength $f_{ma,k}$ according to the German NA is more conservative if unit or mortar compressive strength is high. In contrast, for low unit or mortar strengths, which largely lie outside the application range, the parameters according to the German NA yield higher characteristic compressive strengths of masonry.

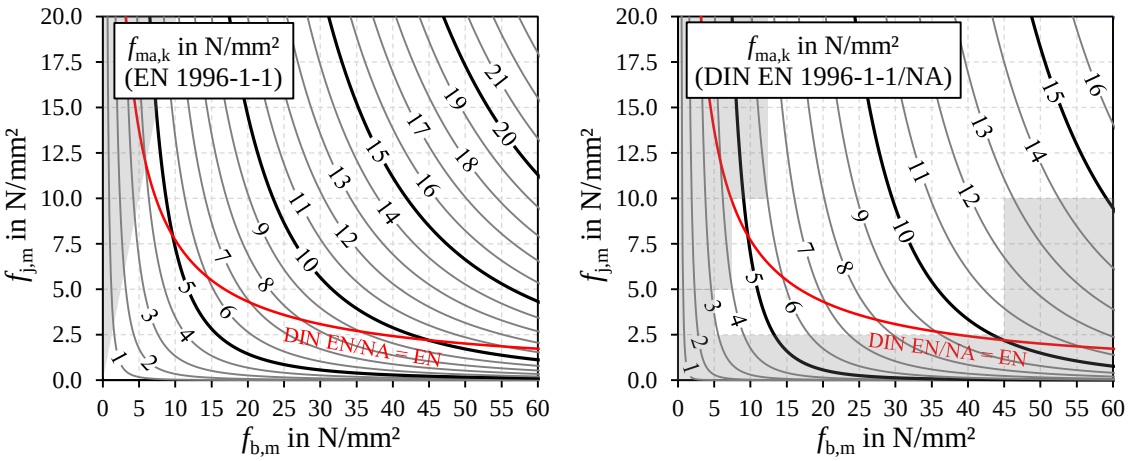

Fig. 3-10 Characteristic compressive strength of masonry according to the power equation (single wythe masonry, solid clay bricks)

3.5.4 Analysis of the Power Equation Concerning Stochastic Extension

In this section, the power equation is further analysed to check its suitability for a stochastic extension. If the suitability is given, the power equation can also be used to determine the probability distribution of masonry compressive strength based on the distribution of the input parameters. Since empirical models often do not include all relevant influencing parameters, the variance contributed by these parameters might be neglected. The starting

point of the analysis is a model with a mechanical background, namely the model by Hilsdorf (1969), as illustrated in Section 3.5.2, which is then transformed into the structure of the power equation. As demonstrated next, this transformation also allows for determining the parameters K, α, and β analytically. The same procedure is applicable to other models with a mechanical background as well.

The general structure of the power equation is convenient for probabilistic applications: Assuming a log-normal distribution for unit and mortar compressive strength, masonry compressive strength is also log-normally distributed. This is because the power equation (Eq. 3-19) can be transformed into a linear relationship for the logarithms of strengths, which, given the log-normal distribution of strength, are normally distributed:

$$\ln f_{\mathrm{ma}} = \ln K_{\mathrm{prob}} + \alpha \ln f_{\mathrm{b}} + \beta \ln f_{\mathrm{j}} \qquad \textit{Eq. 3-20}$$

As the original parameter K according to EN 1996-1-1 (2012) relates mean unit and mortar strength and characteristic masonry compressive strength, K_{prob} is introduced for probabilistic purposes to define the relationship between the random variables f_{ma}, f_{b}, and f_{j}.

Since Eq. 3-20 is a linear function, Hilsdorf's model can be converted to the same structure by a first-order Taylor approximation, which is equivalent to a linearisation. As described in Section 2.3.3, the linearisation of functions is a common approach if approximate stochastic moments for arbitrary functions are needed and no analytical solutions are available. The linearisation hence leads to a first-order approximation of the exact stochastic extension. Since the linear function is expressed in terms of the logarithms of strength, Hilsdorf's model is first written in logarithmic form:

$$\ln f_{\mathrm{ma}} = \ln f_{\mathrm{b}} - \ln U + \ln\left(e^{\ln f_{\mathrm{bt}}} + a\, e^{\ln f_{\mathrm{j}}}\right) - \ln\left(e^{\ln f_{\mathrm{bt}}} + a\, e^{\ln f_{\mathrm{b}}}\right) \qquad \textit{Eq. 3-21}$$

where $a = h_{\mathrm{j}} / (4.1\, h_{\mathrm{b}})$. In addition to f_{b} and f_{j}, unit tensile strength f_{bt} and the ratio of joint thickness to unit height $h_{\mathrm{j}} / h_{\mathrm{b}}$ also influence the compressive strength of masonry, which is not explicitly considered in the original power equation. The additional influence of $h_{\mathrm{j}} / h_{\mathrm{b}}$ is discussed in Section 3.5.5 and neglected here. To include the influence of unit tensile strength, the structure of the linear function to be obtained by the first-order Taylor approximation is as follows:

$$\ln f_{\mathrm{ma}} = \ln K^{*}_{\mathrm{prob}} + \alpha_1 \ln f_{\mathrm{b}} + \alpha_2 \ln f_{\mathrm{bt}} + \beta \ln f_{\mathrm{j}} \qquad \textit{Eq. 3-22}$$

where α_1, α_2 and β are obtained as the partial derivatives of Eq. 3-21 at a reference point (with coordinates $f_{\mathrm{bt,ref}}$, $f_{\mathrm{b,ref}}$ and $f_{\mathrm{j,ref}}$) that is selected for the first-order Taylor approximation:

$$\alpha_1 = \frac{\partial \ln f_{ma}}{\partial \ln f_b} = \frac{f_{bt,ref}}{f_{bt,ref} + a\ f_{b,ref}} \qquad \textit{Eq. 3-23}$$

$$\alpha_2 = \frac{\partial \ln f_{ma}}{\partial \ln f_{bt}} = \frac{f_{bt,ref}}{f_{bt,ref} + a\ f_{j,ref}} - \frac{f_{bt,ref}}{f_{bt,ref} + a\ f_{b,ref}} \qquad \textit{Eq. 3-24}$$

$$\beta = \frac{\partial \ln f_{ma}}{\partial \ln f_j} = \frac{a\ f_{j,ref}}{f_{bt,ref} + a\ f_{j,ref}} \qquad \textit{Eq. 3-25}$$

The parameter K_{prob}^* is determined by equating Hilsdorf's model and the desired power equation at the reference point:

$$K_{prob}^* = \left(\frac{f_{b,ref}}{U} \frac{f_{bt,ref} + a\ f_{j,ref}}{f_{bt,ref} + a\ f_{b,ref}} \right) \Big/ \left(f_{b,ref}^{\alpha_1}\ f_{bt,ref}^{\alpha_2}\ f_{j,ref}^{\beta} \right) \qquad \textit{Eq. 3-26}$$

Expressed as a power equation, Eq. 3-22 becomes

$$f_{ma} = K_{prob}^*\ f_b^{\alpha_1}\ f_{bt}^{\alpha_2}\ f_j^{\beta} \qquad \textit{Eq. 3-27}$$

With the exception of the term for f_{bt}, Eq. 3-27 is similar to the original power equation. Eq. 3-23 to Eq. 3-25 demonstrate that deriving the power equation based on a model with a mechanical background leads to exponents for the strength variables that sum up to one:

$$\alpha_1 + \alpha_2 + \beta = 1 \qquad \textit{Eq. 3-28}$$

Tensile tests on the units are usually not conducted within the assessment of existing masonry. Next, unit tensile strength f_{bt} is thus expressed as unit compressive strength multiplied by a deterministic factor (i.e. as $c \cdot f_b$; see Schubert 2010) which includes two approximations. First, a perfect correlation between the tensile strength and compressive strength of the units is assumed, which increases the resulting variance of masonry compressive strength and is therefore a conservative assumption. Second, the CoV of unit tensile strength is assumed to be equal to the CoV of unit compressive strength, which matches experimental results by Egermann (1992) for splitting tensile and compressive strength tests on historical solid clay bricks. It follows that

$$f_{ma} = K_{prob}^*\ f_b^{\alpha_1}\ (c\ f_b)^{\alpha_2}\ f_j^{\beta} = \left(K_{prob}^*\ c^{\alpha_2}\right) f_b^{\alpha_1+\alpha_2}\ f_j^{\beta} = K_{prob}\ f_b^{\alpha}\ f_j^{\beta} \qquad \textit{Eq. 3-29}$$

Hilsdorf's model is thereby completely transformed to the same structure as the empirical power equation. The parameters K_{prob}, α, and β of the power equation can be determined analytically if a typical ratio for unit tensile strength to unit compressive strength c is selected, and reference ratios $h_{j,ref} / h_{b,ref}$ and $f_{j,ref} / f_{b,ref}$ are chosen for the Taylor approximation. The reference ratios should represent typical values for the application range. With c = 0.04 (Schubert 2010), $h_{b,ref}$ = 71 mm and $h_{j,ref}$ = 12 mm (standard unit format NF), and

a ratio $f_{j,ref} / f_{b,ref} = 0.3$, which is assumed to be in the middle of the general application range of the power equation, the following parameters are obtained:

$$\alpha = \alpha_1 + \alpha_2 = \frac{c}{c + a\left(f_{j,ref} / f_{b,ref}\right)} = 0.76 \qquad \textit{Eq. 3-30}$$

$$\beta = \frac{a\left(f_{j,ref} / f_{b,ref}\right)}{c + a\left(f_{j,ref} / f_{b,ref}\right)} = 0.24 \qquad \textit{Eq. 3-31}$$

$$K_{prob} = K^*_{prob}\, c^{\alpha_2} = \frac{c + a\left(f_{j,ref} / f_{b,ref}\right)}{U\,(a+c)\left(f_{j,ref} / f_{b,ref}\right)^{\beta}} = 0.57 \qquad \textit{Eq. 3-32}$$

The obtained parameters are quite close to those defined by EN 1996-1-1 (2012). Concerning a comparison, however, it should be noted that the power equation with parameters according to Eq. 3-30 to Eq. 3-32 directly connects the random variables of strength, whereas the normative power equation connects mean component strengths with a characteristic masonry strength. One benefit of the presented analytical equations is that they offer an explanation for the differences between the empirical parameters derived for different boundary conditions. Furthermore, since the power equation can be viewed as a first-order Taylor polynomial of the model by Hilsdorf (1969) – or similar models with a mechanical background – for a particular reference point, the power equation can be considered suitable for probabilistic applications. As obtained in the analysis above, the recommendation is to choose the exponents α and β such that they fulfil $\alpha + \beta = 1$. The same recommendation is made by Ferretti (2020) in the context of dimensional analysis. For $\alpha + \beta < 1$, the resulting variance might be underestimated.

For probabilistic purposes, the power equation should be further extended by a model uncertainty factor θ_f:

$$f_{ma} = \theta_f\; K_{prob}\; f_b^{\alpha}\; f_j^{\beta} \quad \Leftrightarrow \quad \ln f_{ma} = \ln\theta_f + \ln K_{prob} + \alpha \ln f_b + \beta \ln f_j \qquad \textit{Eq. 3-33}$$

The variance $\sigma_{ln,ma}^2$ of the logarithm of f_{ma} is thus obtained as

$$\sigma^2_{ln,ma} = \sigma^2_{ln\theta f} + \alpha^2\; \sigma^2_{ln,b} + \beta^2\; \sigma^2_{ln,j} \qquad \textit{Eq. 3-34}$$

It is noted that the expectation of the power equation (i.e. the mean masonry compressive strength $f_{ma,m}$) is slightly overestimated if it is calculated by evaluating the power equation at the means of unit and mortar compressive strength:

$$\mu_{\theta f}\; K_{prob}\; f^{\alpha}_{b,m}\; f^{\beta}_{j,m} > f_{ma,m} = \mathrm{E}\left(\theta_f\; K_{prob}\; f_b^{\alpha}\; f_j^{\beta}\right) \quad \text{for } \alpha < 1 \text{ and } \beta < 1 \qquad \textit{Eq. 3-35}$$

If the expectation $\mu_{\theta f}$ of the model uncertainty factor is one, the relationship between the mean value of masonry compressive $f_{\mathrm{ma,m}}$ and the mean values of the component strengths $f_{\mathrm{b,m}}$ and $f_{\mathrm{j,m}}$ can be expressed via a parameter K_{m} as follows:

$$f_{\mathrm{ma,m}} = K_{\mathrm{m}} \; f_{\mathrm{b,m}}^{\alpha} \; f_{\mathrm{j,m}}^{\beta} \qquad \textit{Eq. 3-36}$$

$$K_{\mathrm{m}} = K_{\mathrm{prob}} \exp\left[-0.5\left(\sigma_{\ln,\mathrm{b}}^2\left(\alpha-\alpha^2\right)+\sigma_{\ln,\mathrm{j}}^2\left(\beta-\beta^2\right)\right)\right] \qquad \textit{Eq. 3-37}$$

Eq. 3-37 is derived from the relationship between the parameters and stochastic moments of a log-normal distribution (see Section 2.3.4), and the relations for the stochastic moments of a linear function (see Section 2.3.3). If the CoVs of f_{b} and f_{j} are $v_{\mathrm{b}} = v_{\mathrm{j}} = 35$ %, which is typical for historical masonry (see Section 7.3), and if the exponents are selected as $\alpha = 0.7$ and $\beta = 0.3$ according to EN 1991-1-1 (2009), K_{m} is only 2 % lower than K_{prob}. Hence, the difference is negligible. Since the normative parameter K includes a factor of approximately 0.8 for the conversion from mean to characteristic masonry compressive strength (Graubohm and Brameshuber 2016), the following relationship can be applied if the normative parameters are used for probabilistic purposes:

$$K_{\mathrm{prob}} \approx K_{\mathrm{m}} = 1.25\,K \qquad \textit{Eq. 3-38}$$

3.5.5 Influence of Mortar Joint Thickness

The empirical power equation for predicting masonry compressive strength as specified in EN 1996-1-1 (2012) does not allow for the consideration of mortar joint thicknesses that deviate from the normatively specified dimensions, for example from a bed joint thickness of 12 mm as specified in DIN EN 1996-1-1/NA (2019) for general purpose mortar. In the assessment of existing masonry, however, higher mortar joint thicknesses are often found. According to experimental results (Francis et al. 1971; Kirtschig and Meyer 1989) and models with a mechanical background, masonry compressive strength reduces if the bed joint thickness is increased. Kirtschig and Meyer (1989) proposed the following modification factor η to take into account the bed joint thickness h_{j}:

$$\eta = \frac{2}{1 + h_{\mathrm{j}} / 12\,\mathrm{mm}} \qquad \textit{Eq. 3-39}$$

where 12 mm is the reference bed joint thickness.

According to the mechanical principles of the model by Hilsdorf (1969), it is not the bed joint thickness h_{j} itself that is decisive but the ratio of h_{j} to unit height h_{b}. In principle, the empirical power equation can be extended by a corresponding correction term:

$$f_{\mathrm{ma}} = \theta_f \; K_{\mathrm{prob}} \; f_{\mathrm{b}}^{\alpha} \; f_{\mathrm{j}}^{\beta} \left(\frac{h_{\mathrm{j}}/h_{\mathrm{b}}}{\left(h_{\mathrm{j}}/h_{\mathrm{b}}\right)_{\mathrm{ref}}} \right)^{\gamma} \qquad \textit{Eq. 3-40}$$

The determination of suitable values for the parameter γ could be included in the general regression analysis for deriving the power equation. However, the corresponding test databases usually do not contain a wide variety of bed joint thicknesses. The exponent γ can also be determined by a first-order Taylor approximation of the model by Hilsdorf (1969), as demonstrated in the previous section:

$$\gamma = \frac{\partial \ln f_{\mathrm{ma}}}{\partial \ln \frac{h_{\mathrm{j}}}{h_{\mathrm{b}}}} = \frac{1}{1 + 4.1\, c \frac{h_{\mathrm{b,ref}}}{h_{\mathrm{j,ref}}} \frac{f_{\mathrm{b,ref}}}{f_{\mathrm{j,ref}}}} - \frac{1}{1 + 4.1\, c \frac{h_{\mathrm{b,ref}}}{h_{\mathrm{j,ref}}}} \qquad \textit{Eq. 3-41}$$

The higher the difference between unit and mortar compressive strength, the larger the influence of the ratio $h_{\mathrm{j}} / h_{\mathrm{b}}$. With $c = 0.04$, $h_{\mathrm{b,ref}} = 71$ mm, and $h_{\mathrm{j,ref}} = 12$ mm as in the previous section, $\gamma = -0.27$ is obtained for $f_{\mathrm{j,ref}} / f_{\mathrm{b,ref}} = 0.3$, and $\gamma = -0.41$ for $f_{\mathrm{j,ref}} / f_{\mathrm{b,ref}} = 0.1$. A bed joint thickness twice as high as the reference thickness consequently leads to a decrease in f_{ma} of 17 % and 25 %, respectively. According to Eq. 3-40, the reduction would be 33 %. An average mortar bed joint thickness that is considerably larger than the standardised dimensions should thus be considered in the assessment.

Grimm (1988) analysed the bed joint thickness variation within brick masonry walls. For 24 investigated buildings constructed in Austin, Texas, between 1894 and 1985, he found a median CoV of the bed joint thickness of 13.6 %. Moreover, Mojsilović and Stewart (2015) evaluated the bed joint thickness variation of four masonry buildings constructed in 2012 in Switzerland and found CoVs of the bed joint thickness of 19.2 % to 35.5 % within one building. If the variability of $h_{\mathrm{j}} / h_{\mathrm{b}}$ is considered in determining the variability of masonry compressive strength, Eq. 3-34 can be extended accordingly:

$$\sigma_{\ln,\mathrm{ma}}^2 = \sigma_{\ln\theta f}^2 + \alpha^2 \; \sigma_{\ln,\mathrm{b}}^2 + \beta^2 \; \sigma_{\ln,\mathrm{j}}^2 + \gamma^2 \; \sigma_{\ln\left(h_{\mathrm{j}}/h_{\mathrm{b}}\right)}^2 \qquad \textit{Eq. 3-42}$$

The CoV of masonry compressive strength is obtained as $v_{\mathrm{ma}} = 26.3$ % if, in a first step, the model uncertainty and the variance of $h_{\mathrm{j}} / h_{\mathrm{b}}$ are neglected, α and β are set to 0.7 and 0.3, respectively, and the CoVs of log-normally distributed unit and mortar compressive strength are assumed as $v_{\mathrm{b}} = v_{\mathrm{j}} = 35$ %, which is typical for the component strengths of solid clay brick masonry within historical masonry buildings (see Section 7.3). The conversion between the variance of the logarithm $\sigma_{\ln}^2$ and the CoV v is done through Eq. 2-27.

The units can usually be produced with reasonable geometrical precision, whereas the mortar joint thickness strongly depends on the workmanship on site. Hence, the variability of $h_{\mathrm{j}} / h_{\mathrm{b}}$ for a particular type of masonry is mainly influenced by the variability of the bed

joint thickness h_j (see Mojsilović and Stewart 2015). Even if the variability of h_j / h_b is additionally considered through a log-normal variable with a CoV of 25 % – a value much higher than the median CoV for h_j in the investigations by Grimm (1988) – and the exponent is conservatively selected as $\gamma = -0.41$, the CoV of masonry compressive strength increases only slightly, namely, to $v_{ma} = 28.3$ %. It can hence be concluded that the influence of the variability of the bed joint thickness on the variability of masonry compressive strength for a particular masonry type within one building is almost negligible compared to the influence of the variability of unit and mortar compressive strength.

3.6 Finite Element Modelling Strategies for Masonry Structures

For modelling masonry structures by means of the finite element method, various strategies are available, which differ regarding their level of detail (see Fig. 3-11). Selecting the best modelling strategy for a particular application involves finding the right balance between the accuracy and the level of detail of the results on the one hand and the modelling and computational efforts on the other (Lourenço 1996; Schlegel 2004).

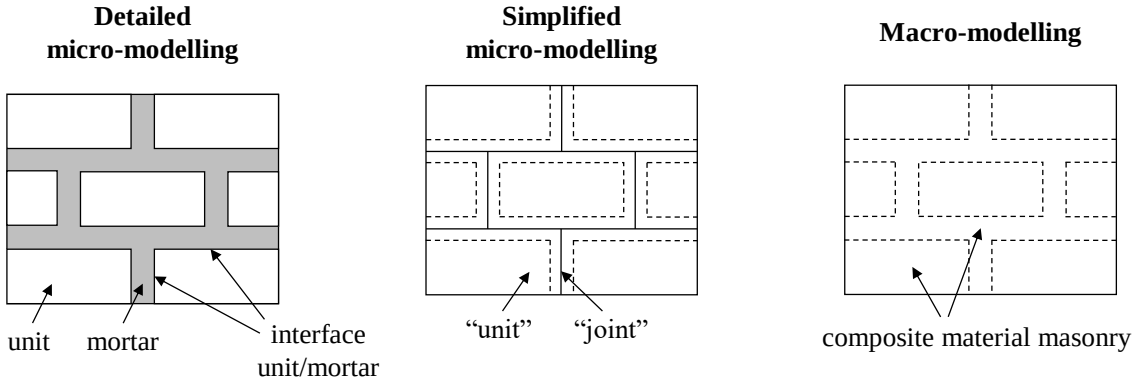

Fig. 3-11 Modelling strategies for masonry structures according to Lourenço (1996)

In a *detailed micro-model*, both the units and the mortar joints are modelled separately according to their original dimensions using continuum elements that represent the actual material behaviour of unit and mortar. Interface elements are placed between the units and mortar joints to model the corresponding bond behaviour. If all material properties are chosen adequately, the detailed micro-modelling enables the display and prediction of the actual failure mechanisms of masonry in detail, for example the interaction of unit and mortar that determines the compressive strength of masonry.

According to the *macro-modelling* approach, no distinction is made between the units and the mortar joints in the masonry member. Instead, masonry is represented by only one type of continuum elements, to which the properties of the composite material masonry (e.g. the compressive strength of masonry) are assigned. The actual local failure mechanisms are

thus not displayed in detail, but the behaviour on a larger scale (i.e. at the structural member or system level) is reflected with sufficient precision.

The *simplified micro-modelling* approach is a compromise between the two former approaches. The model consists of expanded "units", whose dimensions equal the original unit dimensions plus one half of the adjacent mortar joint thicknesses, and "joints" represented by interface elements with zero thickness. The separation into "units" and "joints" allows for the modelling of discrete failure mechanisms, such as the discrete cracking in the mortar joints under flexural tension. However, the actual failure mechanism of masonry under compression, which results from the interaction between unit and mortar, is not displayed by the simplified micro-model. Instead, the nonlinear compression behaviour of the composite material masonry, including masonry compressive strength, is assigned to either the "joints" (i.e. the interface elements) or the "units" consisting of continuum elements.

3.7 Safety Format in Eurocode 6

For unreinforced masonry walls mainly subjected to vertical compression loading, the verification format according to EN 1996-1-1 (2012) is as follows:

$$E_\mathrm{d} \le R_\mathrm{d} = \Phi_\mathrm{red}\ A\ f_\mathrm{ma,d} = \frac{1}{\gamma_\mathrm{M}}\ \Phi_\mathrm{red}\ A\ f_\mathrm{ma,k} = \frac{1}{\gamma_\mathrm{M}}\ R_\mathrm{k} \qquad \textit{Eq. 3-43}$$

where E_d is the design value of the normal force acting on the wall, determined according to EN 1990 (2010) and EN 1991-1-1 (2009); R_d is the design value of the vertical resistance of the wall; Φ_red is the reduction factor for the influence of slenderness and load eccentricity; and A is the cross-sectional area. The design value $f_\mathrm{ma,d}$ of masonry compressive strength is obtained by dividing the characteristic compressive strength $f_\mathrm{ma,k}$ by the partial factor γ_M. If A is smaller than 0.1 m², the design value $f_\mathrm{ma,d}$ is to be additionally reduced by

$$0.7 + 3\,A \le 1 \quad \text{with } A \text{ in m}^2 \qquad \textit{Eq. 3-44}$$

which accounts for the smaller stress redistribution capability of walls with a small cross-sectional area.

The reduction factor Φ_red is (at least implicitly) a function of the ratio between elastic modulus E_ma and masonry compressive strength f_ma if second-order effects are considered (see Section 3.3.3). Since the variability of the elastic modulus E_ma is not accounted for within Φ_red, it must also be covered by the partial factor γ_M. Therefore, although applied to the characteristic masonry compressive strength $f_\mathrm{ma,k}$, the partial factor γ_M actually serves as a global safety factor for the characteristic resistance R_k, as demonstrated by Eq. 3-43 and also described in Bakeer (2016b).

In EN 1996-1-1 (2012), recommendations for the partial factor γ_M are given for different unit categories (I or II depending on statistical quality assurance), different types of mortar (designed or prescribed mortar), and five execution classes that may be specified by the NAs. The respective values for the partial factor range from γ_M = 1.5 to 3.0. Based on these recommendations, the NAs to EN 1996-1-1 specify very different values for the partial factors γ_M, as illustrated for the NAs of 11 countries in Fig. 3-12, based on a review by Graubner and Koob (2015). The specified partial factors are valid for unreinforced masonry walls subjected to mainly compression loading with units of category I. Furthermore, they correspond to consequence class 2. Where a range is given, the partial factor γ_M depends on the execution class and/or the choice of designed or prescribed mortar. Concerning the relatively low value γ_M = 1.5 for Germany (DE), it is noted that only the German NA specifies a reduction factor for considering the effect of sustained loads, namely ζ = 0.85, which increases the ratio of characteristic to design compressive strength to approximately 1.76. The significant differences between the nationally defined values for γ_M can be attributed to national traditions and the high diversity of typical masonry types in the different countries.

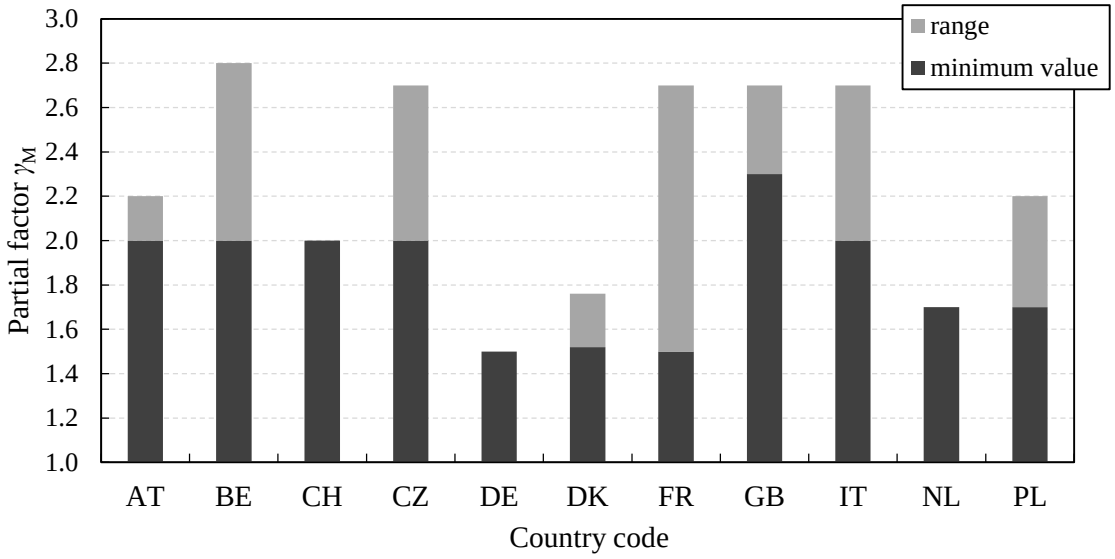

Fig. 3-12 Partial factors γ_M for the compressive strength of unreinforced masonry specified by National Annexes to EN 1996-1-1 for unit category I and consequence class 2 (see Graubner and Koob 2015)

The large variation of partial factors γ_M between the NAs indicates that further research into the reliability of masonry walls is needed. It should be noted that the partial factors γ_M as given in EN 1996-1-1 (2012) and its NAs are intended for the design of new masonry structures. For assessing existing masonry, suitable partial factors γ_M might differ due to a lack of knowledge (i.e. epistemic uncertainty) about the masonry properties within the existing structure, higher variability of the material properties than assumed for new masonry, and a lower target reliability level compared to that for structural design.

4 EXPERIMENTAL INVESTIGATIONS ON CLAY BRICK MASONRY

4.1 Introduction

The main objective of the conducted experiments, which are presented in this chapter, is to investigate the behaviour of clay brick masonry walls with local weaknesses. As a result, a basis is established for validating the finite element model in Chapter 5. The main experiments consisted of 24 compression tests conducted on clay brick masonry walls, which were either constructed as single wythe masonry or arranged in cross bond. In addition to tests on reference walls without weaknesses, walls with local weaknesses were also constructed and tested. The first type of weakness was realised by means of a missing brick in the masonry bond. The second type of weakness was introduced by placing a specific percentage of perforated clay bricks in the wall, which had a significantly lower compressive strength than the reference solid clay bricks in the rest of the wall. Apart from the main tests on masonry walls, complementary compression tests on bricks, mortar, and masonry specimens were carried out. With respect to mortar compressive strength, the experimental program included standard testing of the mortar on prisms and double punch tests. Thereby, the influence of the testing method on the obtained mortar strength was investigated.

Section 4.2 describes the types of bricks and mortar for the experimental investigations and the results of corresponding compressive strength tests. In Section 4.3, the tests on masonry specimens are illustrated. Finally, the main tests on masonry walls and their results are presented and analysed in Section 4.4.

4.2 Testing of the Components

4.2.1 Clay Bricks

As presented in Section 3.2, masonry made of small-sized solid clay bricks was the most common type of masonry in Germany before 1950 and therefore represents a large share of the masonry to be dealt with in the assessment of existing buildings. For this reason, small-sized solid clay bricks were chosen for the experimental investigations. The solid clay bricks had nominal dimensions of 240 x 115 x 71 mm³ corresponding to the German standard format NF according to DIN 20000-401 (2017). The bricks were newly produced by extrusion and firing in a tunnel kiln. The variability of brick properties is hence much lower than that of bricks in historical masonry buildings, which is beneficial for the accuracy of the experimental results. As weaknesses in several of the investigated walls, perforated bricks were used. Perforated bricks were favoured over solid bricks with lower strength, as this choice ensured that the difference between the compressive strengths of the two brick types was significantly larger than the material variability within each brick

type. The perforated bricks used in the experiments can be assigned to group 2 units according to EN 1996-1-1 (2012) and unit type HLzA according to DIN 20000-401 (2017). The relative volume of holes was approximately 40 %, and the nominal outer dimensions were the same as those for the solid clay bricks. In Fig. 4-1, the solid and perforated clay bricks for the experimental investigations are shown.

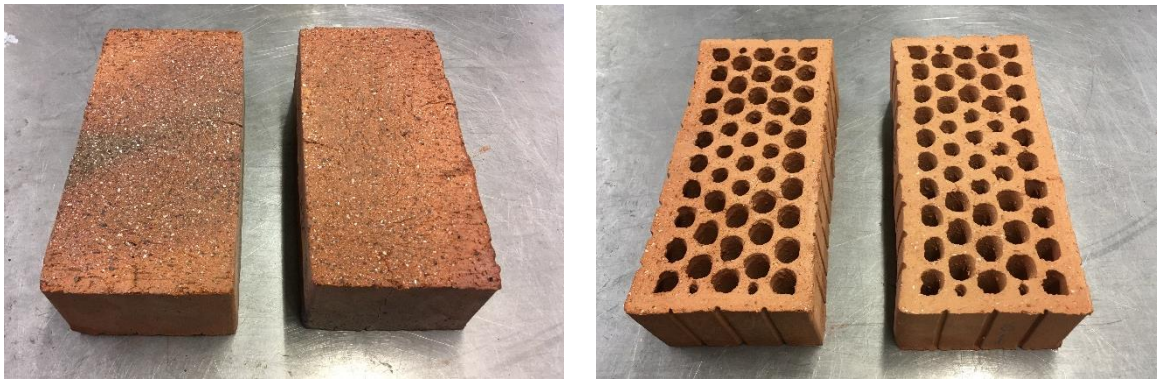

Fig. 4-1 Solid (left) and perforated (right) clay bricks for the experiments

From each of the delivered pallets, at least six bricks were taken to determine the dimensions and weight as well as to test unit compressive strength according to EN 772-1 (2011). The surface of the bricks was first ground to obtain parallel and plain surfaces at the top and bottom of the bricks. Thereafter, the bricks were stored under laboratory conditions (temperature ≥ 15 °C, relative humidity ≤ 65 %) for at least 14 days to reach the air-dry state as defined in EN 772-1 (2011). In the compression test, the load was applied with a rate of 0.3 and 0.15 (N/mm²)/s for the solid and perforated clay bricks, respectively. The results are displayed in Table 4-1. It is noted that the height includes the reduction due to grinding. The compressive strength is converted to the normalised compressive strength by applying the shape factor according to EN 772-1 (2011).

Table 4-1 Properties of the clay bricks

Brick type	Dimensions			Bulk density	Compressive strength	Shape factor	Normalised compressive strength f_b
	Length	Width	Height				
	mm	mm	mm	g/cm³	N/mm²		N/mm²
Solid	243.3 (0.003)	117.7 (0.004)	70.8 (0.01)	2.03 (0.01)	29.7 (0.08)	0.84	24.9 (0.08)
Perforated	236.4 (0.009)	111.3 (0.005)	67.8 (0.02)	0.89 (0.02)	13.8 (0.11)	0.84	11.6 (0.11)
Average values for n = 37 solid and n = 18 perforated bricks (CoVs in parentheses)							

4.2.2 Mortar

The mortar used in the experimental investigations was a factory-mixed dry mortar (Histocal by the producer Otterbein), which contained natural hydraulic lime NHL 5 according to EN 459-1 (2015), pozzolans, and sand with a maximum aggregate size of 1.2 mm. The

specified strength class was M 2.5, which corresponds to a minimum mean value of mortar compressive strength of 2.5 N/mm². This mortar type was selected to reach a mortar compressive strength typical for existing masonry structures from around 1850 to 1950 (see also Section 7.3).

Prism tests

The masonry walls were constructed and tested in four test series. For the construction of each masonry wall, several mortar mixes of 15 litres corresponding to one bag of dry mortar were needed, and a sample was taken from at least one of these mortar mixes in a wall. Each of these samples consisted of three mortar prisms according to EN 1015-11 (2019). Furthermore, at least 12 prisms were taken from one mortar mix in each test series to determine the development of mortar compressive strength over time. The amount of water added to the mortar mixes was chosen to meet the specification by the producer (i.e. 4.5 l water per 25 kg dry mortar).

The preparation of the test specimens and the tests themselves were conducted as required by EN 1015-11 (2019). After mixing, the sampled mortar was placed in a mould in two layers, each compacted by 25 strokes with a compacting bar. Then, the mould was wrapped in foil. After two days, the prisms were unmoulded and subsequently kept at a relative humidity (RH) of 95 ± 5 % and a temperature of 20 ± 2 °C for five days before they were stored in a climate chamber with an RH of 65 ± 5 % and a temperature of 20 ± 2 °C until testing. Before the compression tests, the mortar prisms with dimensions of 40 x 40 x 160 mm³ were divided into halves by conducting a flexural tensile test (see Fig. 4-2). Then, compression tests were conducted on the two halves with a loading rate of 100 N/s.

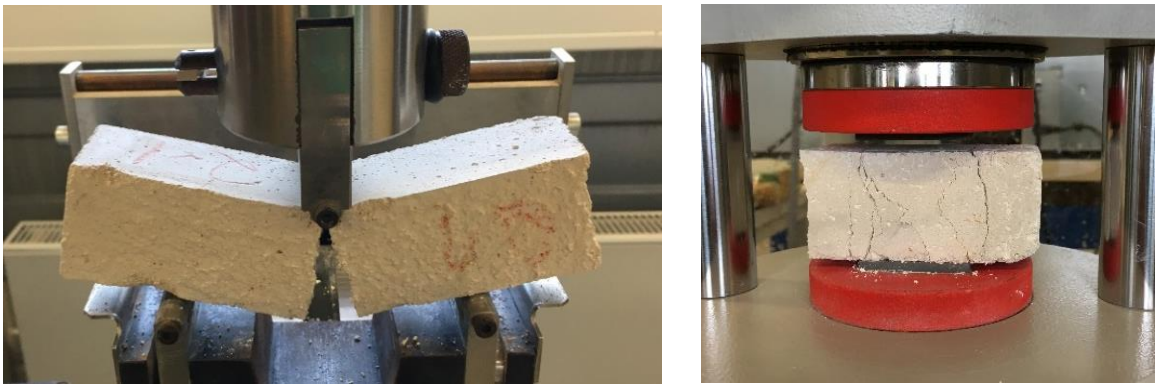

Fig. 4-2 Testing of mortar prisms (left: flexural tensile strength, right: compressive strength) according to EN 1015-11 (2019)

The results of the mortar compressive strength tests are displayed in Fig. 4-3, with each point corresponding to a test at one half of a prism. Most of the mortar compression tests were tests accompanying the main tests on the masonry walls. Hence, the mortar specimens were tested on the same day as the corresponding wall at an age between 32 and 43 days.

Additional tests were conducted after curing times of 14, 21, 28, and 56 days. In addition to the single test results, the average compressive strength for each testing age is given. To reduce the scatter between mortar mixes for pointing out the actual influence of curing time, the averages are given as a moving average for plus/minus one day (if applicable). As evident from Fig. 4-3, the increase in mortar compressive strength over curing time had already slowed down significantly after 32 days. The influence of the different curing times on the strength of the tested masonry walls can consequently be viewed as very small. The average mortar compressive strength for a curing time between 32 and 43 days was obtained as f_j = 2.71 N/mm² for n = 226 test results, and the corresponding CoV was 17 %.

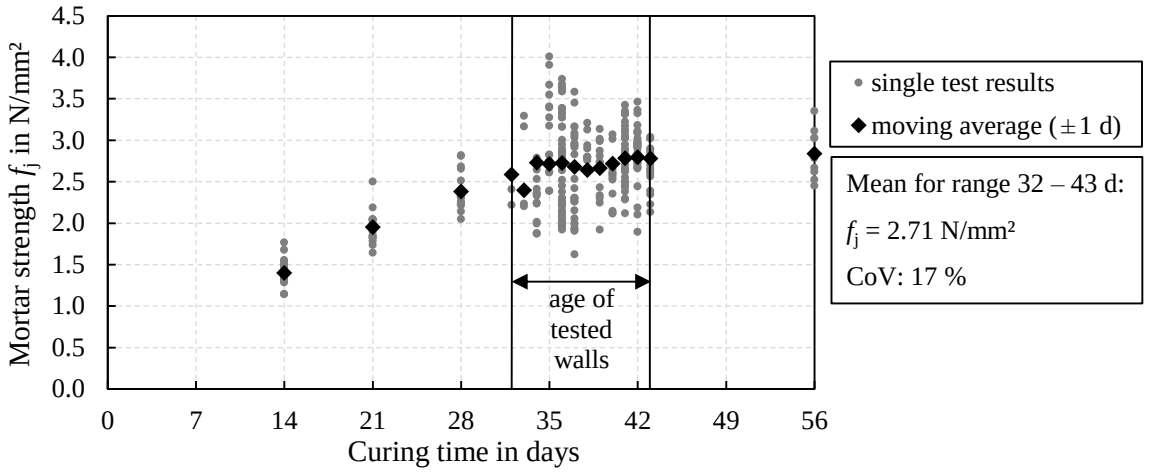

Fig. 4-3 Development of mortar compressive strength over time

Double punch tests

In addition to the tests on mortar prisms, double punch tests according to procedure III of DIN 18555-9 (2019) were performed. The motivation behind these experiments was to investigate whether the strength obtained by double punch tests is comparable to the strength obtained on standard prisms. The double punch tests were conducted on two types of specimens. The first type of specimens was extracted from masonry samples stored in the laboratory until testing. The strength obtained by this procedure corresponds to the realistic curing conditions within masonry; that is, it includes the influence of the surrounding bricks and related moisture conditions on mortar strength. The second type of specimen was cut from standard mortar prisms (see Fig. 4-4). The curing conditions were consequently identical to those of the prisms, and the isolated influence of the specimen shape and the type of load application on the obtained strength could be examined.

To achieve consistent results, the mortar prisms and the masonry specimens, which were used for extracting mortar samples, were all made from the same mortar mix. All of the specimens for the double punch test were obtained by dry cutting. The specimens from mortar prisms were cut to a thickness of 12 mm, matching the standard bed joint thickness

specified by DIN EN 1996-1-1/NA (2019). The length and width were determined by the prism dimensions of 40 x 40 mm² and therefore slightly smaller than the dimensions of 50 x 50 mm² defined by DIN 18555-9 (2019). Since the load was applied on a circular area with a diameter of only 20 mm, as specified by DIN 18555-9 (2019), the influence of the different specimen dimensions can be considered negligible in this case.

Fig. 4-4 Mortar specimens for double punch tests cut from prisms

The specimens of each type were subdivided into two further groups. The first group of specimens was tested directly after being cut, and the load was applied via a felt pad to compensate for the uneven surface of the specimens (see Fig. 4-5). The selected felt had a bulk density of 0.48 g/cm³ as required by DIN 18555-9 (2019). The specimens of the second group were capped with a thin (1 mm thick) gypsum layer. After the capping, the specimens were dried at 50° C until reaching a constant mass before they were tested. In all the cases, the loading rate was chosen to reach the maximum load between 30 s and 90 s.

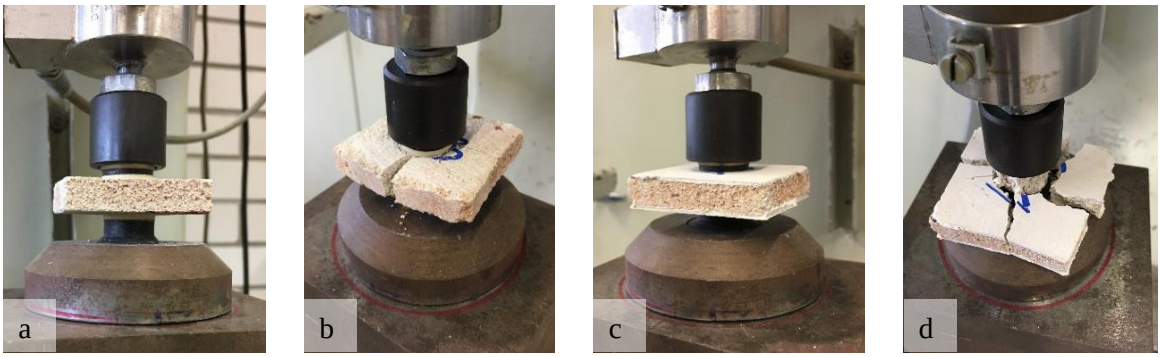

Fig. 4-5 Double punch tests (a + b: load applied via felt pad, c + d: gypsum capping)

The results of the double punch tests are presented in Table 4-2. Since all of the test results in Table 4-2 were obtained from specimens made from the same mortar mix, the CoVs of the test results are much lower than the CoV of 17 % given in Fig. 4-3. In the case of the use of felt pads, the results obtained from double punch tests on specimens cut from prisms match well with the standard prism strengths. This confirms the findings in Riechers et al. (1998), where it is concluded that no shape factor is needed to convert strengths from double punch tests to prism strengths. With gypsum capping, the obtained strengths in the double punch tests are higher by a factor of approximately 1.5 for all types of tested specimens (see Fig. 4-6). However, the conversion factor of about 1.5 cannot be viewed as valid for

all types of mortar. Therefore, double punch testing with felt pads and without gypsum capping can be recommended.

Table 4-2 Results of double punch tests on mortar

Mortar specimens from	Number of tests *n*	Dimensions			Strength $f_{j,dpt}$	
		Length	Width	Thickness	Felt pad	Gypsum capping
		mm	mm	mm	N/mm²	N/mm²
Mortar prisms cut in pieces	10	40	40	12	3.19 (0.08)	5.18 (0.03)
Solid clay brick masonry	12	50	50	11	6.50 (0.03)	10.76 (0.04)
Perforated clay brick masonry	12	50	50	12	7.44 (0.03)	10.11 (0.03)
Average values (CoVs in parentheses), curing time: 36 d *Corresponding standard prism strength (n = 12): 3.48 N/mm² (0.05)*						

Fig. 4-6 illustrates the ratio of the strengths $f_{j,dpt}$ obtained by double punch tests to the strength f_j obtained by prism tests. It is evident that the curing conditions within masonry have a substantial effect on the resulting mortar strength. For both brick types, the strength of the mortar cured within masonry (i.e. between bricks) is about two times higher than the strength of the mortar cured in prism shape according to EN 1015-11 (2019), which approximately aligns with the findings by Henzel and Karl (1987).

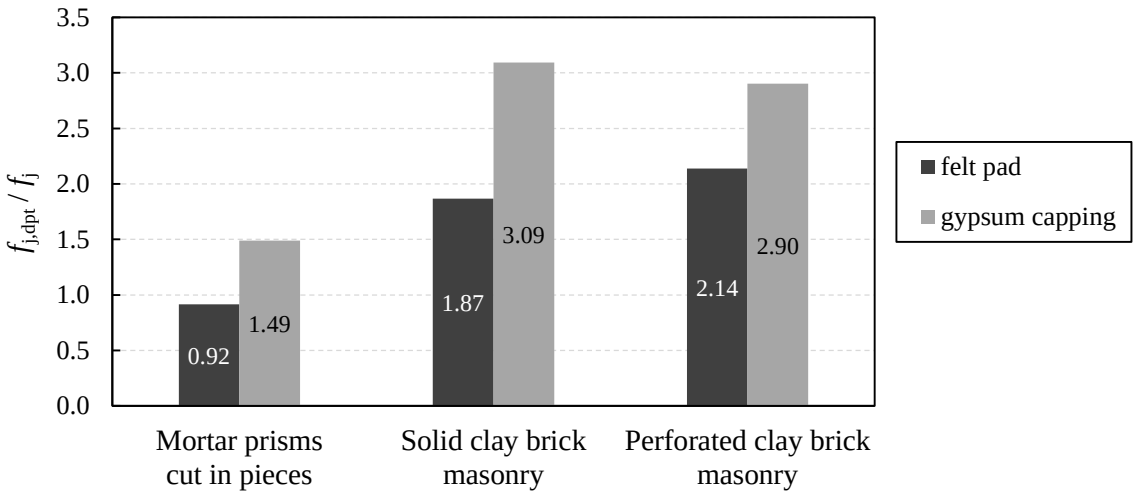

Fig. 4-6 Ratio of double punch test results $f_{j,dpt}$ to prism compressive strength f_j for specimens cut from mortar prisms and specimens extracted from masonry

Since most of the empirical formulae, for example the power equation of EN 1996-1-1 (2012), are derived based on prism strength data, masonry compressive strength might be overestimated if the results of double punch tests on specimens extracted from masonry are used as input values without modification. Therefore, the influence of curing conditions on mortar strength should be considered if masonry compressive strength is predicted based

on empirical formulae combined with double punch tests results for mortar specimens extracted from masonry. Further research is necessary to obtain reliable conversion factors for all typical combinations of units and mortar.

4.3 Tests on Masonry Specimens

In addition to the tests on brick and mortar, tests on the composite material masonry were performed to obtain the reference strength and the modulus of elasticity of masonry according to EN 1052-1 (1998). The tests were conducted for both solid and perforated clay brick masonry. Furthermore, stack-bonded masonry prisms with a height of three bricks were prepared and tested for both brick types. The masonry specimens according to EN 1052-1 (1998) – that is, RILEM specimens – and the stack-bonded masonry specimens are displayed in Fig. 4-7 and Fig. 4-8. The thicknesses of bed and perpend joints were selected as 12 mm and 10 mm, respectively, which are the standard joint thicknesses according to DIN EN 1996-1-1/NA (2019).

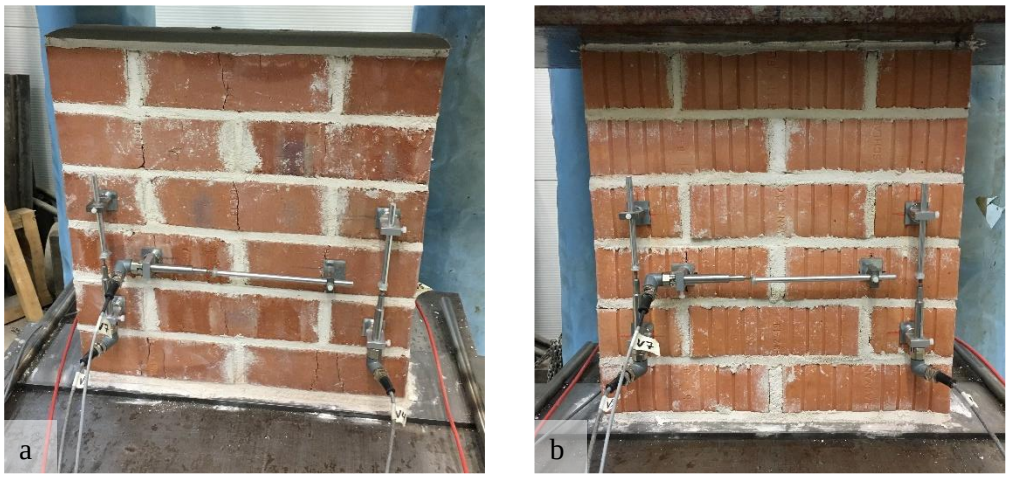

Fig. 4-7 Specimens according to EN 1052-1 (1998) for testing masonry compressive strength (a: solid clay brick masonry, b: perforated clay brick masonry)

Fig. 4-8 Stack-bonded prisms for testing masonry compressive strength

The RILEM specimens were built on steel plates, and, before testing, the top surface of the specimens was capped with a thin gypsum layer. The bottom bricks of the stack-bonded prisms were placed on a gypsum layer. Before constructing the prisms, the top of the corresponding upper bricks was ground to obtain an even surface. All specimens were covered by polyethylene sheets for the first three days of curing and stored in the laboratory until testing.

The loading in the tests according to EN 1052-1 (1998) was applied with a constant displacement rate, which was selected to reach the maximum load between 15 and 30 min. The vertical displacement of the masonry was recorded with two linear variable displacement transducers (LVDTs) on each side of the specimens, which reached over two brick and mortar joint heights. The stress-strain curve corresponding to the average displacement measured by the four LVDTs is presented in Fig. 4-9. To obtain a modulus of elasticity that corresponds to the approximately linear part of the stress-strain curve, EN 1052-1 (1998) specifies determining the modulus of elasticity as the secant modulus between 0 % and 33 % of the maximum stress. As illustrated in Fig. 4-9, some stress-strain curves first experienced hardening before the linear part of the stress-strain curve was reached. Therefore, the modulus of elasticity was determined as the chord modulus between 5 % and 33 % of the maximum stress, which is also recommended in the standard ASTM C1314 (2018). The actual linear part of the stress-strain curve can be captured more accurately by following this procedure.

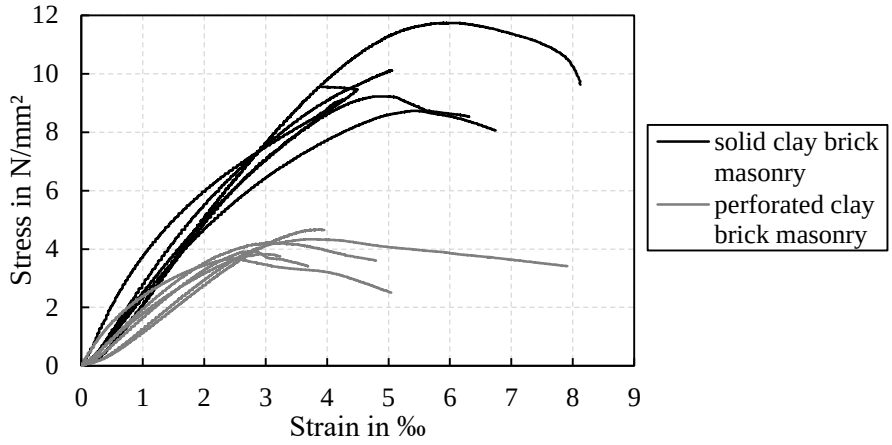

Fig. 4-9 Stress-strain curves of the compression tests according to EN 1052-1 (1998)

Since the LVDTs measure only the displacement at the surface, the strain displayed in Fig. 4-9 might not be representative for the whole cross-section as soon as cracks parallel to the surface occur (i.e. when the compressive stress is close to masonry strength). For some of the investigated specimens, the measured displacements declined after the peak stress was reached, although the displacement of the testing machine was further increased. The stress-strain curves in Fig. 4-9 are only displayed up until one of the measured displacements

began to decrease. For one specimen, this effect already occurred before the peak stress was reached, as shown in Fig. 4-9. However, since this effect is only relevant for strains corresponding to stresses close to masonry strength, it does not influence the obtained modulus of elasticity.

The compression tests on stack-bonded prisms were also conducted with a loading rate such that the maximum load occurred between 15 and 30 min. The modulus of elasticity was not determined within these tests. The results of the compression tests on RILEM specimens according to EN 1052-1 (1998) and of the tests on stack-bonded prisms are listed for solid and perforated clay brick masonry in Table 4-3. In addition to the dimensions and testing age, values for the unit and mortar compressive strength of the corresponding pallet and mix, respectively, are displayed, each being the average of at least six test results.

Table 4-3 Results of compression tests on RILEM specimens according to EN 1052-1 (1998) and three-brick high, stack-bonded masonry prisms

Specimen	Age	Dimensions			Unit strength f_b	Mortar strength f_j	Strength f_{ma}	Modulus of elasticity E_{ma}	E_{ma} / f_{ma}
		Length	Thickness	Height					
	d	mm	mm	mm	N/mm²	N/mm²	N/mm²	N/mm²	-
RIL-sol-1	41	496	115	514	24.6	2.5	10.1	3,129	309
RIL-sol-2	40	498	115	514	24.6	2.5	9.2	2,644	287
RIL-sol-3	40	497	115	514	24.6	2.5	11.7	2,860	244
RIL-sol-4	35	491	114	509	24.0	3.2	9.1	4,128	453
RIL-sol-5	36	491	114	513	24.0	3.2	8.7	2,540	291
RIL-sol-6	36	490	114	514	24.0	3.2	9.5	2,697	283
RIL-per-1	42	488	111	503	12.0	2.7	4.3	1,607	371
RIL-per-2	41	490	111	505	12.0	2.7	4.2	2,028	482
RIL-per-3	41	489	111	503	12.0	2.7	4.7	1,449	311
RIL-per-4	35	486	110	500	12.0	3.2	3.8	1,939	507
RIL-per-5	35	489	110	504	12.0	3.2	3.9	1,754	448
RIL-per-6	34	487	110	501	12.0	3.2	3.7	2,974	803
sbp-sol-1	41	243	116	244	24.6	2.4	11.0	-	-
sbp-sol-2	41	244	116	244	24.6	2.4	10.1	-	-
sbp-sol-3	41	244	115	244	24.6	2.4	8.6	-	-
sbp-sol-4	35	241	115	241	24.0	3.5	11.0	-	-
sbp-sol-5	35	240	115	242	24.0	3.5	12.1	-	-
sbp-sol-6	36	241	115	239	24.0	3.5	11.2	-	-
sbp-per-1	42	235	110	235	12.0	3.1	4.8	-	-
sbp-per-2	42	237	110	237	12.0	3.1	4.3	-	-
sbp-per-3	42	238	110	235	12.0	3.1	5.0	-	-
sbp-per-4	35	235	112	231	12.0	3.5	5.0	-	-
sbp-per-5	35	235	112	232	12.0	3.5	5.5	-	-
sbp-per-6	35	236	112	233	12.0	3.5	5.0	-	-

RIL: RILEM specimens, sbp: stack-bonded prims, sol: solid bricks, per: perforated bricks

In Table 4-4, the average results for masonry compressive strength obtained from tests on RILEM specimens and tests on stack-bonded prisms are given together with the corresponding CoV. Predictions of masonry compressive strength according to EN 1996-1-1 (2012) and DIN EN 1996-1-1/NA (2019) are also listed in Table 4-4. The predictions are based on the average unit compressive strength and the average mortar compressive strength (standard prism strength) for all test series (see Section 4.2). The corresponding empirical parameters of the power equation for solid clay brick masonry are $K = 0.55$, $\alpha = 0.7$, and $\beta = 0.3$ according to EN 1996-1-1, and $K = 0.95$, $\alpha = 0.585$, and $\beta = 0.162$ according to DIN EN 1996-1-1/NA. For perforated clay bricks, K is 0.45 for EN 1996-1-1 (units of group 2) and 0.69 for DIN EN 1996-1-1/NA, whereas α and β are the same as for solid clay bricks. Since the power equations of both standards include a conversion from the mean to the characteristic value of masonry compressive strength, the obtained values are converted back to mean values via division by 0.8 (see Section 3.5).

Table 4-4 Comparison between experimental masonry compressive strength and predictions by normative equations

Type of masonry	Masonry strength f_{ma}			
	Tests on RILEM specimens	Tests on stack-bonded prisms	EN 1996-1-1 ($f_{ma,k}$ / 0.8)	DIN EN 1996-1-1/NA ($f_{ma,k}$ / 0.8)
	N/mm²	N/mm²	N/mm²	N/mm²
Solid clay brick masonry	9.74 (0.11)	10.66 (0.11)	8.81	9.16
Perforated clay brick masonry	4.11 (0.09)	4.94 (0.08)	4.21	4.25

Average results of n = 6 tests for each type of specimen and masonry (CoVs in parentheses). Predictions based on f_b = 24.9 N/mm² (solid), f_b = 11.6 N/mm² (perforated), and f_j = 2.71 N/mm² (see Section 4.2).

The experimentally obtained masonry compressive strengths displayed in Table 4-4 match the predictions according to both standards well. Furthermore, the results of the tests on RILEM specimens and the tests on stack-bonded masonry prisms are relatively close to each other. If all test results are converted to slenderness $h / t = 5$ based on Eq. 3-12, the ratio of average strength obtained on RILEM specimens to average strength obtained on stack-bonded masonry prisms is 0.91.

4.4 Tests on Masonry Walls

4.4.1 Testing Programme and Procedure

Fig. 4-10 provides an overview of the masonry walls that were tested. The testing programme consisted of reference walls made solely out of either solid (abbreviated as “sol” in the labelling of the experiments) or perforated (“per”) clay bricks, walls with local weaknesses consisting of one missing brick in the masonry bond, and walls that contained both solid and perforated clay bricks in specific ratios. Furthermore, all these wall types were tested as single wythe masonry walls (“sw”, walls with a thickness of only one brick width),

and as walls laid in cross bond (“cb”) with a wall thickness of one brick length (= two brick widths plus one vertical mortar joint).

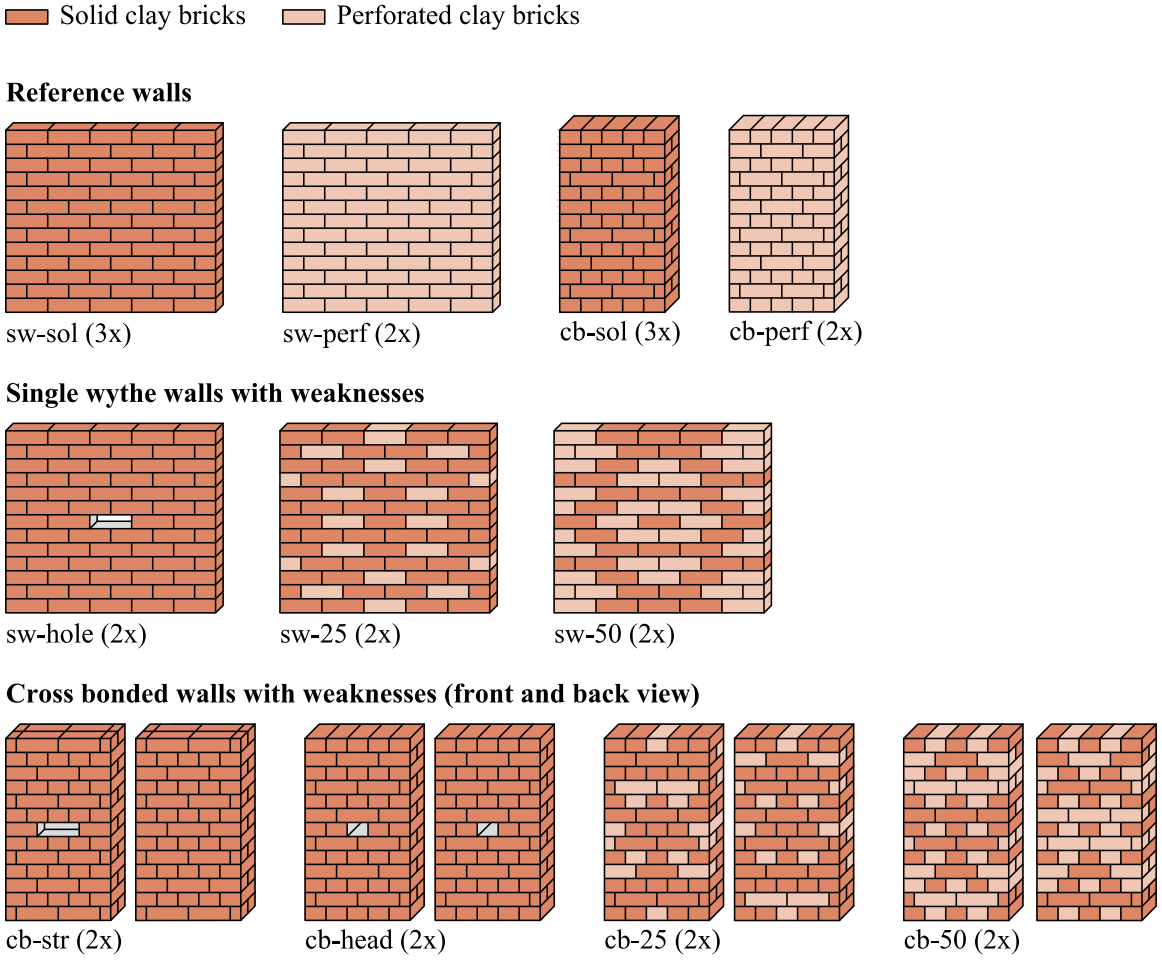

Fig. 4-10 Overview of the tested masonry walls

The walls of both bond types had a height of 13 courses with five bricks per course. The nominal perpend joint thickness was selected as 10 mm, and the nominal bed joint thickness as 12 $^1/_3$ mm. The nominal thickness of 12 $^1/_3$ mm results from the requirement of DIN 4172 (2015) that the height of three courses of brick and mortar should sum up to 0.25 m. Based on the nominal brick dimensions of 240 x 115 x 71 mm³, the nominal overall dimensions were 1240 x 115 x 1083 mm³ (length x width x height) for the single wythe walls and 615 x 240 x 1083 mm³ for those in cross bond. For the walls with missing bricks, inner bricks in the middle course were left out. Concerning the walls in cross bond, the options of a missing stretcher (“str”) and a missing header (“head”) were tested. The walls containing both solid and perforated clay bricks were erected with 25 % and 50 % perforated bricks. The positions of the perforated bricks in the walls are depicted in Fig. 4-10. The perforated bricks were arranged symmetrically on the left and right side of the wall and such that load paths from top to bottom running only through solid bricks were possible.

The walls were constructed by trained masons and erected on concrete beams to allow for easy transportation to the testing machine. After construction, the walls were covered by polyethylene sheets for three days and then stored under laboratory conditions until the day of testing. On the day before testing, the concrete beam with the wall was placed in the testing machine upon a thin mortar layer, enabling the levelling of the wall. The top of the wall was capped with a thin gypsum layer before testing. The load was applied via a steel beam, whose support allowed rotation. As an example, the test setup for the wall cb-50-1 is depicted in Fig. 4-11.

Fig. 4-11 Test setup for wall cb-50-1

Vertical displacements were measured by four cable LVDTs (two on each side) reaching over 10 brick and bed joint heights (see Fig. 4-11). Additionally, one side of the wall was prepared to enable displacement measurement by digital image correlation (DIC). For this purpose, the walls were painted white, and a speckle pattern was applied. During the tests, two cameras took images of the prepared side of the wall at a rate of one picture per second. The loading was increased with a constant displacement rate, which was chosen to reach the maximum load after 15 to 30 min. After reaching the maximum load, the displacement was further increased until the load declined to less than 90 % of its maximum.

4.4.2 Results

An overview of the test results is presented in Table 4-5. In addition to the load-bearing capacity and the respective strength (maximum load per gross cross-sectional area), the testing age, the actual dimensions of the wall, and the unit and mortar strengths of the corresponding brick pallets and mortar mixes, respectively, are displayed. Based on these unit and mortar strengths, a modification of the capacity as specified in EN 1052-1 (1998) would be possible so that all modified capacities correspond to the same unit and mortar strengths. However, the associated unit strengths do not vary greatly. The mortar variability is slightly

higher but has much less influence on the resulting strength. Furthermore, not all of the mortar mixes in one wall were tested. Therefore, the tested mortar mixes might not be representative of the whole wall, and a modification might not lead to better results. The original load-bearing capacities are hence used for further evaluation. More detailed documentation of the tests on masonry walls is given in Annex A.

Table 4-5 Results of the compression tests on masonry walls

Wall type	No.	Age	Dimensions			Unit strength f_b solid / perf.	Mortar strength f_j	Max. load	Strength	Mean strength
			Length	Thick-ness	Height					
		d	mm	mm	mm	N/mm²	N/mm²	kN	N/mm²	N/mm²
Sw-sol	1	35	1,266	115	1,122	25.7 / -	2.77	1,004	6.90	7.42
	2	36	1,265	115	1,112	25.7 / -	2.77	1,089	7.49	
	3	40	1,255	115	1,115	25.7 / -	2.77	1,136	7.87	
Sw-perf	1	34	1,234	110	1,077	- / 12.0	2.80	437	3.22	3.14
	2	37	1,245	111	1,086	- / 11.4	2.24	423	3.06	
Sw-hole	1	40	1,245	115	1,110	23.6 / -	2.40	814	5.68	5.62
	2	41	1,250	115	1,112	23.6 / -	2.40	799	5.56	
Sw-25	1	36	1,247	113	1,108	24.6 / 12.0	2.30	681	4.83	5.02
	2	35	1,248	113	1,119	24.6 / 12.0	2.03	736	5.22	
Sw-50	1	36	1,246	113	1,112	24.6 / 12.0	2.16	565	4.01	4.02
	2	36	1,248	113	1,105	24.6 / 12.0	2.03	568	4.03	
Cb-sol	1	32	620	241	1,121	25.2 / -	2.76	943	6.31	6.35
	2	39	629	241	1,091	23.1 / -	2.89	826	5.45	
	3	37	625	240	1,110	24.0 / -	2.85	1,093	7.29	
Cb-perf	1	38	622	239	1,084	- / 11.4	2.90	391	2.63	2.64
	2	41	621	239	1,083	- / 11.4	3.11	394	2.66	
Cb-str	1	33	623	242	1,114	25.2 / -	2.76	694	4.61	4.47
	2	34	624	241	1,116	25.2 / -	2.76	651	4.33	
Cb-head	1	35	617	242	1,115	25.2 / -	2.76	748	5.01	4.94
	2	36	622	242	1,117	25.2 / -	2.76	732	4.86	
Cb-25	1	41	624	239	1,098	24.0 / 11.4	3.13	721	4.83	4.77
	2	42	622	240	1,101	24.0 / 11.4	2.73	703	4.71	
Cb-50	1	42	620	239	1,093	24.0 / 11.4	3.14	501	3.38	3.32
	2	43	622	240	1,095	24.0 / 11.4	2.90	485	3.25	

Fig. 4-12 displays the stress-strain curves of the tests on masonry walls (i.e. the load-displacement curves with the load related to the cross-sectional area and the displacement related to the measurement lengths of the LVDTs). The stresses and strains are averages since the actual stresses and strains vary within the wall due to the local weaknesses. The effect of cracks parallel to the wall surface on the displacement measured by the LVDTs, described in Section 4.3 for the tests on RILEM specimens, is less problematic for tests on

masonry walls. Since the cracks that lead to failure randomly occur at different locations in the wall, the probability of large cracks at the supports of the LVDTs is much smaller.

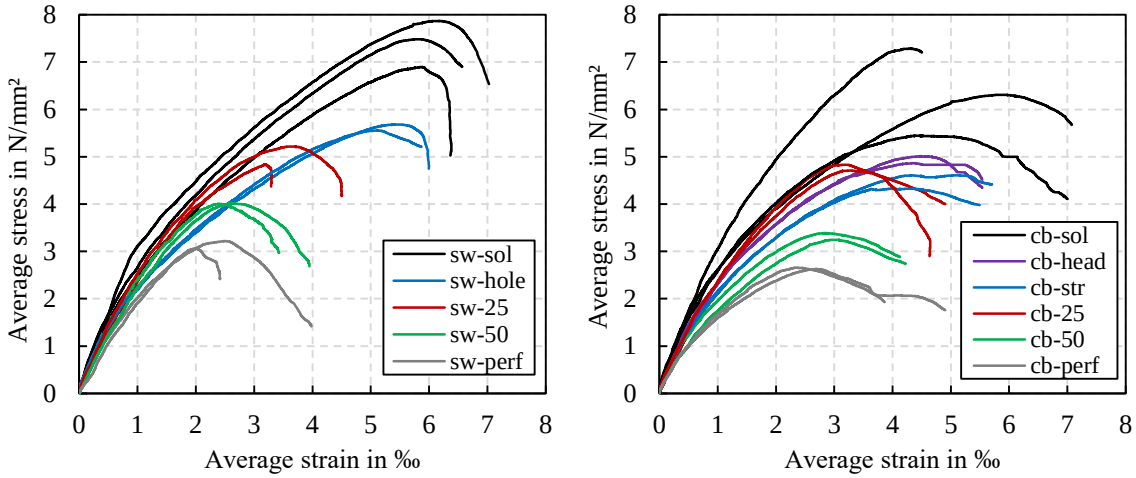

Fig. 4-12 Stress-strain curves obtained in the tests on masonry walls

Reference walls

First, the results of the reference tests on solid and perforated clay brick masonry walls are evaluated in more detail. Fig. 4-13 shows exemplary images of the most dominant cracks in the tested masonry walls. The pictures were taken after the completion of the experiments, and the typical behaviour of masonry under compression can be recognised: Transversal strain in the mortar joints causes transversal tensile stress in the bricks, leading to cracks, which form parallel to the surface of the wall. As a result of these cracks, slices of the bricks can be separated from the wall at some parts. Since the reference walls are not purposely weakened at specific locations, the most dominant cracks that lead to failure occur at random locations, where the material is the weakest.

Based on the stress-strain curves displayed in Fig. 4-12, the parameter k, which quantifies the nonlinearity of the stress-strain relationship (see Section 3.3.2), can be obtained as

$$k = \frac{\varepsilon_f \, E_{\mathrm{ma}}}{f_{\mathrm{ma}}} \qquad \textit{Eq. 4-1}$$

with f_{ma} and E_{ma} being the masonry compressive strength and modulus of elasticity, respectively, and ε_f being the strain at the maximum stress. Since the effect of initial hardening, which occurred for the tests on the RILEM specimens, did not occur for the tests on the walls, the modulus of elasticity is determined as the secant modulus $E_{\mathrm{ma,0\text{-}33}}$ between 0 % and 33 % of the maximum load. The secant modulus $E_{\mathrm{ma,0\text{-}33}}$ approximately equals the tangential modulus in the origin $E_{\mathrm{ma,0}}$, for which Eq. 4-1 is originally defined (see Eq. 3-1). Equating $E_{\mathrm{ma,0}}$ and $E_{\mathrm{ma,0\text{-}33}}$ also matches the selected material model for the finite element simulations (see Section 5.2.3). The average parameter k was obtained as 2.31 for the solid

clay brick masonry arranged as single wythe walls and as 2.38 for the solid clay brick masonry walls in cross bond. For the perforated clay brick masonry walls, *k* was 1.69 for the single wythe walls and 2.04 for the walls in cross bond.

Fig. 4-13 Crack formation in the tests on reference walls (a: sw-sol-3, b: cb-sol-2, c: sw-perf-2, d: cb-perf-2)

The experimentally obtained strengths for single wythe masonry, masonry arranged in cross bond, the RILEM specimens, and stack-bonded prisms are compared in Fig. 4-14. Note that all of the strengths have been converted to a slenderness ratio of $h / t = 5$ based on Eq. 3-12. The ratio of the strength of masonry walls in cross bond to the strength of the single wythe masonry walls is 78 % for the solid clay brick masonry and 76 % for the perforated clay brick masonry, which matches the factor of 80 % defined in EN 1996-1-1 (2012) well. The reason for the lower strength of the single wythe masonry walls compared to the RILEM specimens can be assumed to be a combination of the effects of small eccentricities due to

imperfections and a statistical size effect due to a higher number of possible failure locations in the walls. The strength ratio of perforated to solid clay brick masonry is 42 %, regardless of whether it is calculated from the results obtained on RILEM, single wythe, or cross bond specimens. Hence, there is a high consistency of the test results.

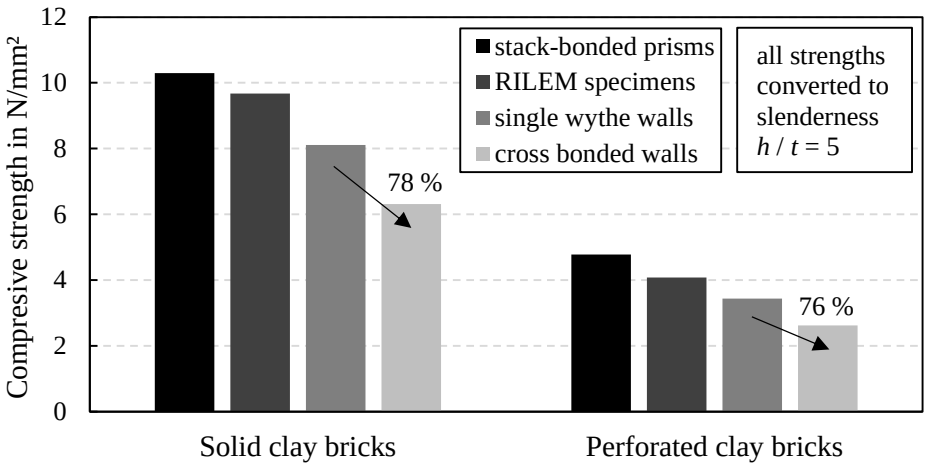

Fig. 4-14 Comparison of masonry strength obtained from different testing specimens

Walls with a missing brick

Walls with a missing brick were tested to investigate how clay brick masonry behaves under local stress concentrations. Furthermore, the corresponding results are needed to validate the finite element model in the next chapter. Due to the holes in the wall, high strains and stresses occurred in the critical cross-section next to the missing bricks. Therefore, the compressive strength of masonry was reached much earlier here than in the other parts of the wall, which is also evident by the cracking behaviour of the tested walls. The most dominant cracks formed at the edges of the holes (see Fig. 4-15).

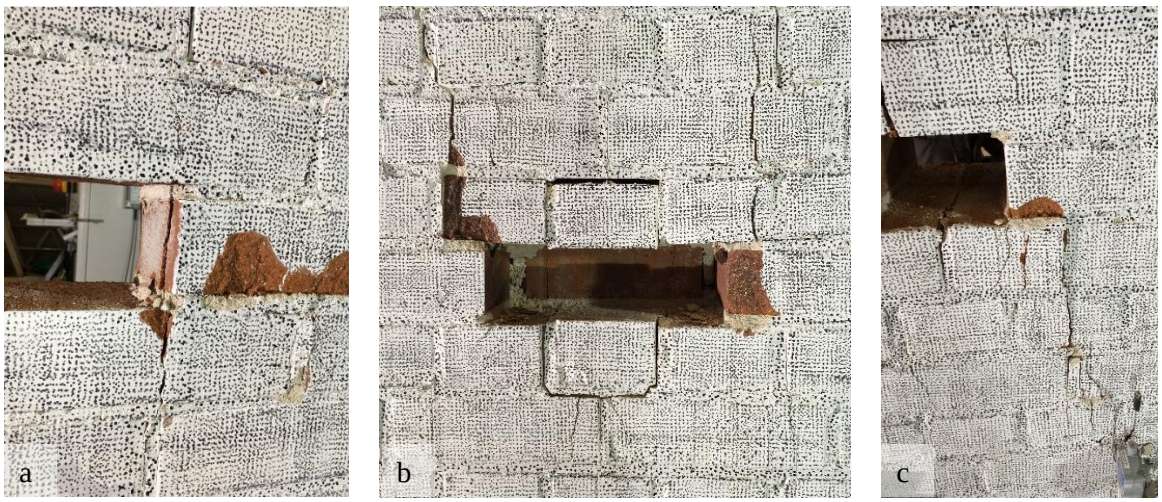

Fig. 4-15 Crack formation in the tests on walls with a missing brick (a: sw-hole-2, b: cb-str-1, c: cb-head-1)

In Table 4-6, the strengths of the walls with a missing brick are listed in relation to the strengths of the reference walls. The relative strengths of the walls with a missing brick are between 70 % and 78 %. Hence, they are only slightly lower than the relative area of the critical cross-section, which is 80 % (four instead of five bricks).

Table 4-6 Strength of walls with missing brick compared to reference strength

Specimen		Reference strength	Strength with hole	Relative strength
		N/mm²	N/mm²	
Single wythe masonry		7.42	5.62	75.8 %
Cross bond	Missing header	6.35	4.94	77.8 %
	Missing stretcher		4.47	70.4 %

If the material behaviour were perfectly ductile (i.e. the stress-strain curve continued horizontally after reaching its maximum), the relative strength would be equal to the relative area of the critical cross-section, which is illustrated in Fig. 4-16. The difference between this theoretical upper bound and the actual load-bearing capacity depends on the post-peak behaviour of the stress-strain relationship. Another influence on the actual capacity is that the maximum stress in the critical cross-section can be slightly higher than the uniaxial masonry strength (i.e. the strength of the reference walls). The reason for this lies in the interaction between neighbouring bricks. High vertical strains in the area with stress concentration also lead to high transversal strains and hence transversal compression, as these areas are constrained by surrounding bricks with a lower stress level. Since the vertical compressive strength is higher than the uniaxial strength if transversal compressive stresses are present, the relative capacity of a wall with a hole can be close to the relative area of the critical cross-section, although the stress-strain relationship is not perfectly ductile (see Fig. 4-16, right). These effects are also discussed during the validation of the finite element model in Chapter 5.

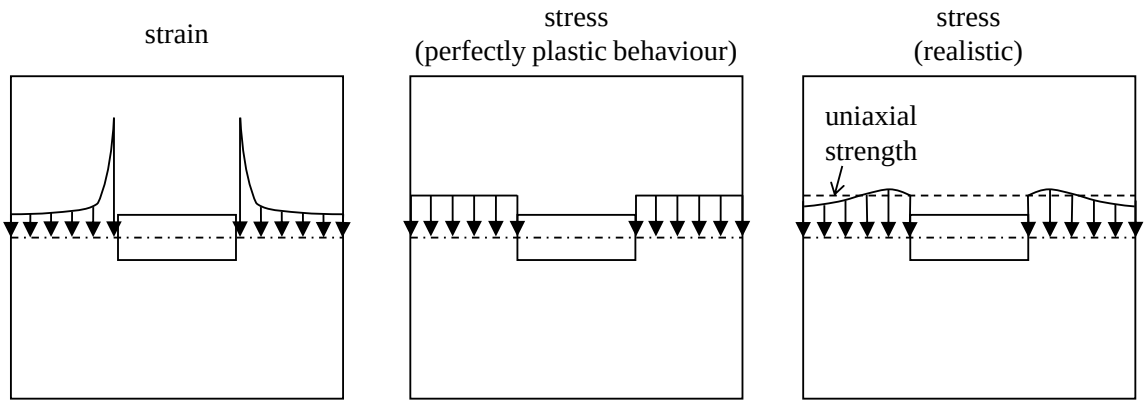

Fig. 4-16 Qualitative illustration of vertical strain and stress at maximum load in the cross-section with a missing brick

Walls with varying brick strength

Fig. 4-17 shows typical cracking patterns which occurred at the masonry walls containing both strong (i.e. solid) and weak (i.e. perforated) clay bricks. As expected, the first cracks appeared at the perforated bricks and developed from there. A further essential finding was that the first crack usually did not appear at a single perforated brick but at a conglomeration of two or more such bricks. In most cases, perforated bricks that were surrounded by solid bricks did not start to crack if there were other parts in the wall with two or more perforated bricks on top of each other (see Fig. 4-17).

Fig. 4-17 Crack formation in the tests on walls with varying brick strength (a: sw-25-1, b: cb-25-1, c: sw-50-2, d: cb-50-1)

This observation indicates that, locally, the masonry strength of a combination of perforated brick and mortar joint in the mixed walls can be higher than the uniaxial reference strength of the perforated clay brick walls. Again, this effect can be explained by the interaction

between neighbouring bricks. The horizontal strain of perforated bricks that are close to their maximum capacity is constrained by solid bricks that are much less utilised. This constraint leads to a multiaxial compression state and hence a vertical compressive strength higher than the uniaxial reference strength. Therefore, weaker bricks are supported by adjacent stronger bricks.

If the stress redistribution capability within the masonry walls were perfect, the resulting load-bearing capacity would correspond to the average masonry strength in the wall. The load-bearing capacity could consequently be obtained by linear interpolation between the reference strengths according to the percentage of solid and perforated bricks in the wall. In Fig. 4-18, the experimental strengths are displayed over the percentage of perforated clay bricks in the tested walls. Moreover, a line corresponding to linear interpolation between the reference strengths is displayed. For further illustration, the experimental results are approximated by a quadratic polynomial fitted by the method of least squares. It can be seen that the test results significantly deviate from the linear interpolation, which also aligns with the findings of Kirtschig and Meyer (1990) for calcium silicate masonry walls (see also Section 3.3.4). Hence, the load-bearing capacity cannot be determined directly by the average strength in the wall but must be further reduced. This effect reduces if, instead of the overall percentage of weak bricks in the wall, the percentage of weak bricks and respective average strength in the weakest course is considered. However, the general effect remains.

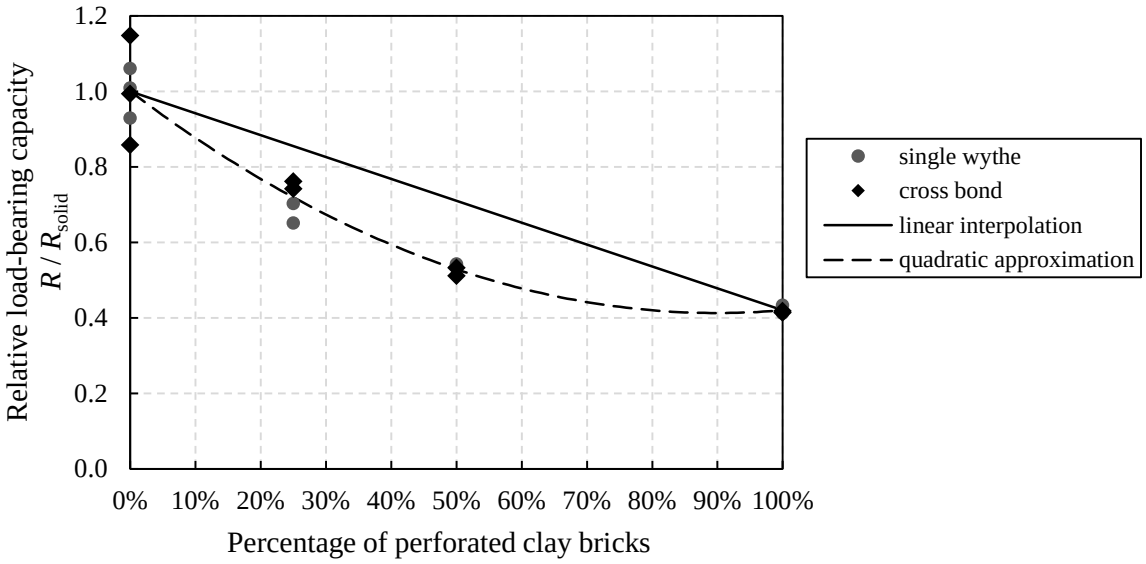

Fig. 4-18 Load-bearing capacity R of walls with varying percentages of perforated bricks in relation to the reference capacity R_{solid} of solid brick walls

4.5 Summary

This chapter described the procedure and the results of experimental investigations on clay brick masonry walls. First, complementary tests on brick and mortar were illustrated. In addition to standard testing of the mortar according to EN 1015-11 (2019), the mortar compressive strength was obtained by double punch tests according to procedure III of DIN 18555-9 (2019). The geometrical boundary conditions in the double punch test were found to approximately lead to the same mortar strength as in a standard prism test. However, due to the different curing conditions of mortar within masonry compared to the curing of the standard prisms, the strength of samples extracted from masonry can significantly deviate from that of standard prisms. For the investigated natural hydraulic lime mortar, the strength within masonry was higher by a factor of about two.

Section 4.3 presented the results of compressive strength tests on standard masonry specimens according to EN 1052-1 (1998) and on stack-bonded masonry prisms. The strengths obtained from standard masonry specimens align well with the predicted strengths according to the equations in EN 1996-1-1 (2012) and DIN EN 1996-1-1/NA (2019) based on unit and mortar compressive strength. The ratio of the masonry compressive strength obtained from standard masonry specimens (i.e. RILEM specimens) to the strength obtained from stack-bonded prims is 91 % if both strengths are converted to a slenderness $h / t = 5$.

Finally, the results of 24 tests on masonry walls were presented. In addition to reference tests on solid and perforated clay brick masonry walls, walls with weaknesses were also tested. These weaknesses consisted of either a missing brick in the masonry bond or a certain percentage of perforated clay bricks within a solid clay brick masonry wall. The tests were conducted on single wythe masonry walls and masonry walls arranged in cross bond. The ratio of the compressive strength of masonry arranged in cross bond to single wythe masonry was determined as 77 %. The tests on walls with weaknesses revealed a reasonable stress redistribution capability of the walls. Altogether, the experimental results indicate a high level of consistency; therefore, they establish a reliable basis for the validation of the finite element model in Chapter 5.

5 FINITE ELEMENT MODELLING OF CLAY BRICK MASONRY WALLS

5.1 Introduction

For the Monte Carlo simulations (MCS) presented in Chapter 6, unreinforced clay brick masonry walls under compression loading are modelled by means of the finite element method. In this chapter, the finite element model is illustrated. Section 5.2 provides a description of the model, including the selected elements, the mesh, the boundary conditions, the iteration method, and the material models. In Section 5.3, the model is validated. First, the load-bearing capacities of walls with varying eccentricities of the applied load and varying slenderness are compared to results obtained from the analytical model by Glock (2004). The second step of the validation is a comparison of the experimental results from Chapter 4 with the results of corresponding finite element simulations.

5.2 Description of the Finite Element Model

5.2.1 General and Modelling Strategy

For the finite element simulations, the software DIANA (Version 10.3) is utilised. Simplified micro-modelling (see Section 3.6) is chosen as the modelling strategy, as this approach represents an appropriate compromise between detailed micro-modelling and macro-modelling. Detailed micro-modelling would be computationally more expensive and would require additional mechanical input parameters that would also have to be modelled stochastically. For the MCS in Chapter 6, the finite element model must be suited for displaying material variability from unit to unit. With macro-modelling, there is no discretisation of a masonry wall into single units, making this modelling strategy inapplicable for walls with unit-to-unit material variability.

In the simplified micro-modelling approach described by Lourenço (1996), the expanded units behave elastically, and the inelastic behaviour of masonry is assigned to the interfaces. In contrast, the inelastic behaviour of masonry under compression is included in the expanded units in the following investigations, and the interfaces only display cracking in the mortar joints due to tensile stresses. This choice – assigning masonry compressive strength to the expanded units rather than to the interfaces – recognises that the material properties of the units have a greater influence on masonry compressive strength than the properties of the mortar joints. The variability of masonry compressive strength from expanded unit to expanded unit is hence better suited for representing the material variability within masonry than the variability from interface to interface.

For the sake of readability, the expanded units are simply called “units” in the following. The quotation marks indicate that the geometry and, in particular, the assigned material properties differ from those of the actual bricks.

5.2.2 Geometry, Mesh, and Iteration Method

The “units” are modelled by eight-node solid elements (element type HX24L in DIANA). The dimensions of the “units” that represent bricks with the German standard format NF in single wythe masonry are 250 x 115 x 83.3 mm³ (length x width x height). These dimensions result from the nominal brick dimensions plus two times half the perpend joint thickness regarding the length of the “units” and two times half the bed joint thickness regarding their height. For the walls in cross bond, the thickness of the vertical joint parallel to the wall face also has to be considered, which results in total “unit” dimensions of 250 x 120 x 83.3 mm³ for the stretchers and 240 x 125 x 83.3 mm³ for the headers. Each “unit” is discretised into 8 x 4 x 3 elements, leading to approximately cubic elements with an edge length of around 30 mm. At the position of the bed and perpend joints, interfaces are placed between the “units”. The corresponding elements are plane quadrilateral interface elements with four plus four nodes (type Q24IF in DIANA).

In the finite element model of the experiments, the load is applied displacement-controlled at the centre point of the top of the wall. The vertical displacement of this centre point is tied to all points on the centre line, leading to a uniform vertical displacement over the whole length of the wall. This corresponds to the application of the load via a beam with high stiffness in the experiments. Instead of a prescribed deformation, a uniform line load with defined eccentricity is applied at the top of the wall in the MCS. In both types of simulation, the load is then distributed from this (ec-)centric line to the whole cross-section via a thin, rigid plate. For the MCS, a similar rigid plate is provided at the bottom, which is vertically supported along a line with a specific eccentricity. The support conditions allow free rotation around the weak longitudinal axis (x-axis) at the top and bottom. In contrast, the bottom plate is vertically supported over the whole area for the simulation of the experiments, resulting in a restraint of rotations around the longitudinal axis at the bottom, which better displays the experimental boundary conditions. In both cases, the wall is supported against out-of-plane displacement at the top and bottom. The geometry, the element mesh, and an example illustration of the stress and the strain distribution are depicted in Fig. 5-1 for the reference wall of the MCS.

Since a uniform load instead of a uniform deformation is applied in the MCS, the wall can also freely tilt around the strong axis (y-axis) at the top. This is required because the random assignment of material properties leads to an asymmetric distribution of material strength and stiffness and, hence, to one side of the wall being weaker than the other. In a building,

this asymmetry can lead to a rotation around the y-axis, which is only slightly restrained by the adjacent floor.

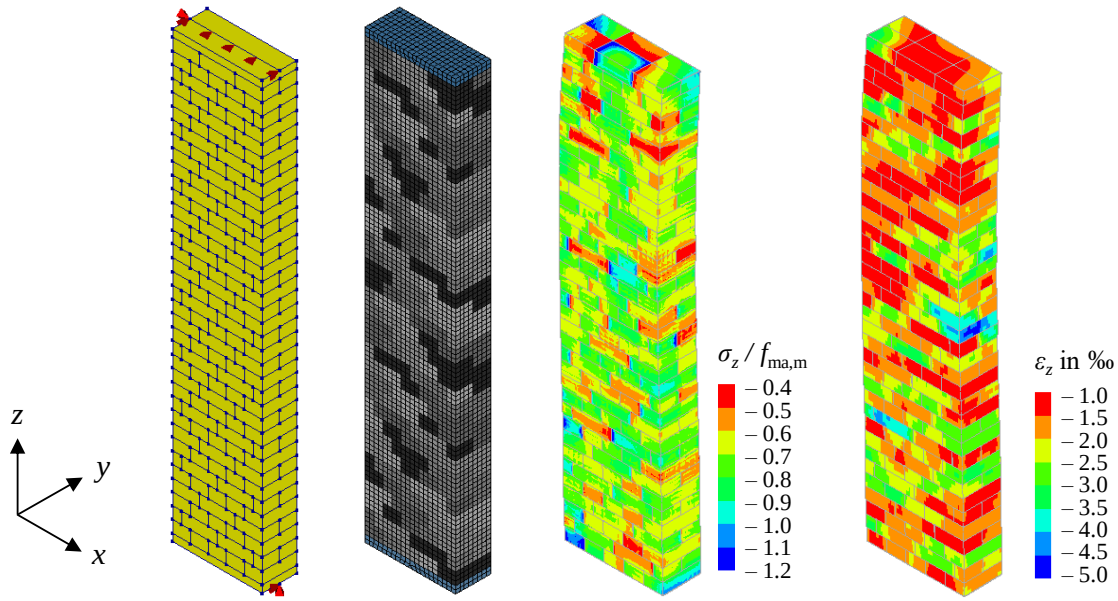

Fig. 5-1 Geometry, mesh, example stresses, and example strains of the finite element model (reference wall for the Monte Carlo simulations)

When the finite element model is used to perform MCS, the option of automatic step sizes is selected in combination with arc-length control. Using arc-length control, the additional load in each step automatically decreases as soon as the load-displacement curve becomes nonlinear and approaches the peak load. The Newton-Raphson iterative method is applied. For a successful iteration, both energy and displacement convergence norm have to be satisfied. After each simulation run, there is an automatic check whether the peak of the load-displacement curve has been reached, that is, whether the load-displacement curve has decreased in the last step of the simulation run. If the iteration has failed before reaching the peak, the simulation is repeated with a different initial step size. This procedure ensures that the maximum resistance of the masonry walls is reliably obtained in all simulation runs.

5.2.3 Material Modelling

Although the material behaviour of masonry is orthotropic in general, an isotropic material model for the “units” is chosen. In the following investigations, an isotropic material model yields sufficiently accurate results since the predominant compression stresses act in the vertical direction. The material model has to display the hardening and softening behaviour of masonry under compression when the limit of the elastic stress-strain state is reached. Furthermore, the model has to adequately represent the behaviour of masonry under vertical compression in combination with compressive or tensile stresses in the horizontal directions.

For this purpose, the material model "crack and plasticity" in DIANA is selected for the "units", which combines two material models, one for the behaviour under compression and one for tensile behaviour. Under compression, plasticity with a Drucker-Prager yield criterion and cohesion hardening/softening is selected. Under tension, the material model "crack and plasticity" includes a multi-directional fixed crack model (DIANA FEA 2019). The transition between the Drucker-Prager yield-criterion under compression and the crack model under tension is modelled by a linear, rather than a constant, tension cut-off.

For the Drucker-Prager plasticity model, the definition of the friction angle φ and the dilatancy angle ψ is required. The dilatancy angle ψ is set to equal the friction angle φ to attain an associated flow-rule (see Lourenço 1996). Since the dilatancy angle is greater than zero, plastic deformations are associated with an increase in volume. Together with the cohesion, the friction angle φ defines the yield surface. The choice of the friction angle thus determines how strongly the vertical compressive strength of masonry is increased if the vertical stress is combined with compressive stresses in the horizontal directions. Hence, the friction angle φ is an important calibration parameter. If a weak "unit" within the wall is close to reaching its maximum uniaxial strength, there are large deformations in the horizontal direction that are partly restrained by stronger "units" at the top and bottom. This leads to triaxial compression in the weak "unit" and thus an increase in its vertical compressive strength. Simultaneously, the vertical compressive strength of the stronger "units" is reduced due to horizontal tension. This effect was also observed in the experiments (see Section 4.4.2).

The choice of a friction angle of $\varphi = 12°$ yields simulation results matching well with those of the experiments. This friction angle also shows good agreement with experimental results for the biaxial compression strength of masonry, as shown next. The general definition of the Drucker-Prager yield criterion Drucker and Prager (1952) can be written as

$$\alpha_{\mathrm{f}} \left(\sigma_1 + \sigma_2 + \sigma_3\right) + \sqrt{\frac{1}{2}\left[\left(\sigma_1 - \sigma_2\right)^2 + \left(\sigma_2 - \sigma_3\right)^2 + \left(\sigma_3 - \sigma_1\right)^2\right]} = k \qquad \textit{Eq. 5-1}$$

where σ_1, σ_2, and σ_3 are the principal stresses. Based on the cohesion c and the friction angle φ, α_{f} and k can be determined as

$$\alpha_{\mathrm{f}} = \frac{2\sin\varphi}{3-\sin\varphi} \qquad \textit{Eq. 5-2}$$

$$k = \frac{6c\cos\varphi}{3-\sin\varphi} \qquad \textit{Eq. 5-3}$$

The cohesion c that corresponds to a particular uniaxial compressive strength f_{ma} can be obtained as follows (DIANA FEA 2019):

$$c = f_{ma} \frac{1-\sin\varphi}{2\cos\varphi} \qquad \textit{Eq. 5-4}$$

Based on Eq. 5-1 to Eq. 5-4, the Drucker-Prager failure criterion for a biaxial stress state ($\sigma_3 = 0$) is displayed in Fig. 5-2. Furthermore, experimental results on the biaxial compressive strength of solid clay brick masonry from Page (1981) are included in the diagram. Here, σ_2 is the compressive stress perpendicular to the bed joints, and σ_1 is the compressive stress parallel to the bed joints. Fig. 5-2 demonstrates that the assumption of isotropic material behaviour is not correct if the whole range of theoretically possible biaxial stress states is considered. However, since the investigated walls are mainly loaded vertically (i.e. perpendicular to the bed joints), horizontal compressive stresses only result from constraint by other "units". Therefore, only stress states with σ_1 significantly smaller than σ_2 are relevant for the following studies. If only the range of $\sigma_1 < 1/3\ \sigma_2$, which is not exceeded in the simulation of the experiments, is considered, excellent agreement of the Drucker-Prager criterion with the parameter $\varphi = 12°$ and the experimental results by Page (1981) is found, as shown in the right diagram of Fig. 5-2.

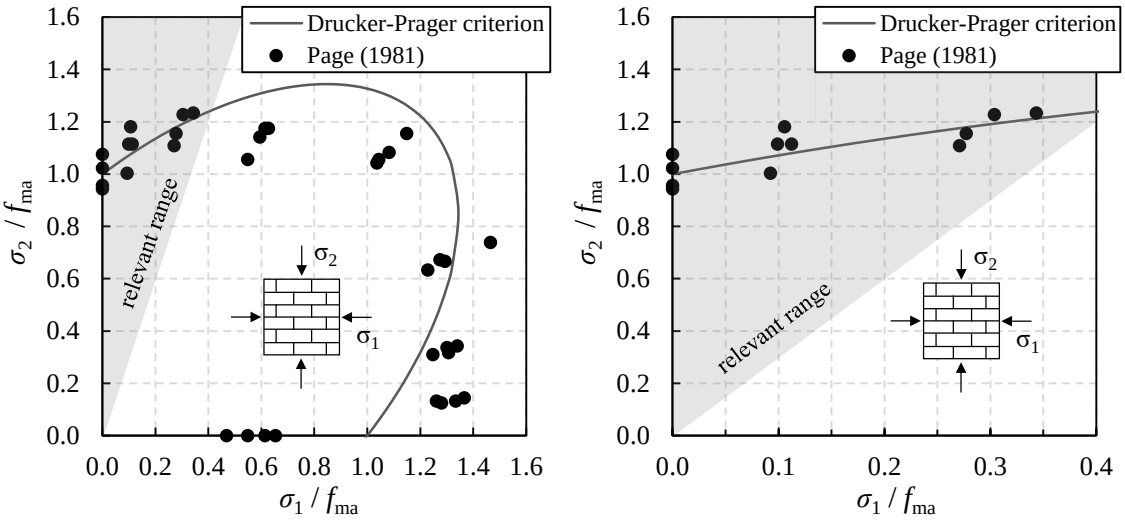

Fig. 5-2 Comparison of Drucker-Prager criterion with $\varphi = 12°$ and experimental results for biaxial compressive strength by Page (1981) (left: full range, right: lower range of σ_1)

The hardening/softening law for the relationship between plastic strain and yield stress is assigned in the form proposed by Lourenço (1996). If expressed as a uniaxial relationship between compressive stress σ_c and plastic compressive strain ε_{pl}, the hardening/softening law can be written as

$$\sigma_c\left(\varepsilon_{pl}\right)=\sigma_i+\left(\sigma_p-\sigma_i\right)\sqrt{\frac{2\,\varepsilon_{pl}}{\varepsilon_p}-\frac{\varepsilon_{pl}^2}{\varepsilon_p^2}} \qquad \text{for } \varepsilon_{pl}\le\varepsilon_p$$

$$\sigma_c\left(\varepsilon_{pl}\right)=\sigma_p+\left(\sigma_m-\sigma_p\right)\left(\frac{\varepsilon_{pl}-\varepsilon_p}{\varepsilon_m-\varepsilon_p}\right)^2 \qquad \text{for } \varepsilon_p\le\varepsilon_{pl}\le\varepsilon_m \qquad \textit{Eq. 5-5}$$

$$\sigma_c\left(\varepsilon_{pl}\right)=\sigma_r+\left(\sigma_m-\sigma_r\right)\exp\left(2\frac{\sigma_m-\sigma_p}{\varepsilon_m-\varepsilon_p}\,\frac{\varepsilon_{pl}-\varepsilon_m}{\sigma_m-\sigma_r}\right) \qquad \text{for } \varepsilon_m\le\varepsilon_{pl}$$

The parameters σ_p and ε_p are equal to the uniaxial masonry compressive strength f_{ma} and the plastic strain at reaching this strength. For $\sigma_c \le \sigma_i$, only elastic deformations occur. With the parameters σ_m and ε_m, the post-peak behaviour can be controlled, and σ_r is a residual stress required for numerical reasons (see also Fig. 5-3). In Lourenço (1996), the values $\sigma_i = 0.33\,f_{ma}$, $\sigma_m = 0.5\,f_{ma}$, and $\sigma_r = 0.1\,f_{ma}$ are recommended, which are also applied in the following simulations.

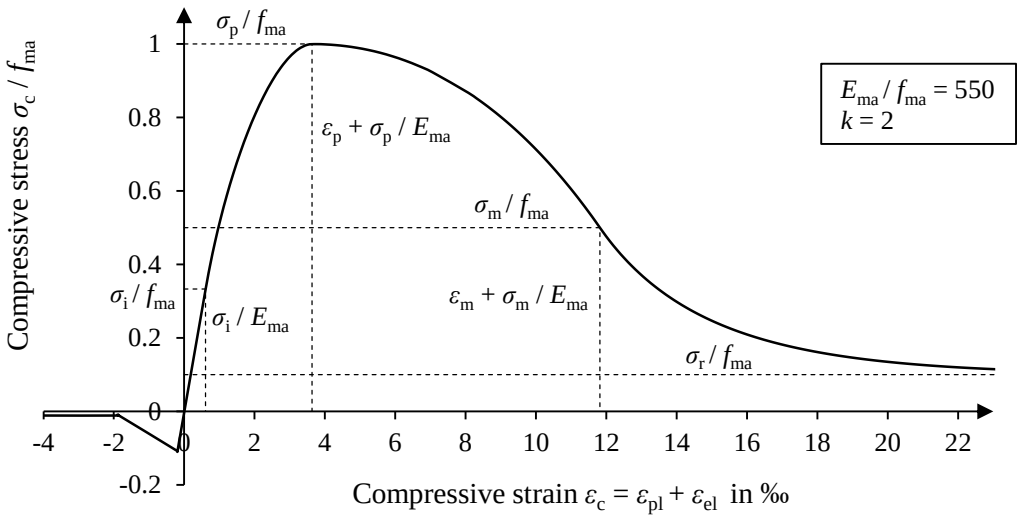

Fig. 5-3 Uniaxial stress-strain relationship for the expanded units (see Lourenço 1996)

If the modulus of elasticity and the masonry compressive strength are given, the plastic strain ε_p at peak stress can be obtained by choosing a stress-strain relationship parameter k. Here, the parameter k is defined as the ratio between total strain and elastic strain at peak stress (see Section 3.3.2). Therefore, the plastic strain at peak stress is

$$\varepsilon_p=\varepsilon_f\,\frac{k-1}{k}=\frac{f_{ma}}{E_{ma}}\left(k-1\right) \qquad \textit{Eq. 5-6}$$

where ε_f is the total strain at peak stress and E_{ma} is the modulus of elasticity of masonry. For the simulation of the experiments, the values of k determined in Chapter 4 based on the experimental results for masonry walls are used: k = 2.31 (single wythe) and 2.38 (cross

bond) for the experiments on solid clay brick masonry, and $k = 1.69$ (single wythe) and 2.04 (cross bond) for perforated clay brick masonry. The modulus of elasticity is chosen as obtained in the experiments on RILEM specimens (see Section 4.3).

For the MCS of solid clay brick masonry, $k = 2$ is chosen for both bond types, which is slightly lower than the experimentally obtained value but more representative for solid clay brick masonry in general (see Section 3.3.2). The value $E_{ma} / f_{ma} = 550$ is chosen as a reference for the ratio of elastic modulus to compressive strength of masonry within the MCS. As presented in Section 3.3.2, a wide variation for the ratio E_{ma} / f_{ma} can be found in the literature. Kaushik et al. (2007) found $E_{ma} / f_{ma} = 550$ as an average for solid clay brick masonry. In Schubert (2010), $E_{ma,m} = 5{,}000$ N/mm² is stated for a unit and mortar combination with compressive strengths $f_{b,m} = 25$ N/mm² and $f_{j,m} = 2.5$ N/mm². According to DIN EN 1996-1-1/NA (2019), the corresponding masonry compressive strength is $f_{ma,k} = 7.2$ N/mm². With $f_{ma,m} = f_{ma,k} / 0.8$ (see Section 3.5.3), this results in $E_{ma,m} / f_{ma,m} = 552.2$ and, hence, good agreement. It should be noted that lower ratios for E_{ma} / f_{ma} may be present in the assessment of existing masonry, especially in the case of weak lime mortars (see Section 3.3.2).

As the parameter ε_m defines the post-peak behaviour after reaching compressive strength, it influences the load-bearing capacity of a wall with local stress concentrations. In the calibration process, choosing the value as six times the plastic strain at peak stress, $\varepsilon_m = 6\ \varepsilon_p$, yielded good results. The hardening/softening law as described by Eq. 5-5 cannot be assigned to the material model in DIANA directly. Since the hardening/softening behaviour is defined by cohesion hardening, the uniaxial strength must be converted to an equivalent cohesion c based on Eq. 5-4. Furthermore, the cohesion hardening curve is a function of an equivalent plastic strain variable κ (DIANA FEA 2019). Based on the plastic strain ε_{pl} corresponding to uniaxial stress, the equivalent plastic strain variable κ can be obtained by

$$\kappa = -\frac{\sqrt{1+2\alpha_g^2}}{1-\alpha_g}\varepsilon_{pl} \quad \text{with} \quad \alpha_g = \frac{2\sin\psi}{3-\sin\psi} \qquad \textit{Eq. 5-7}$$

In Fig. 5-4, the uniaxial stress-strain relationship used for the MCS, the corresponding relationship between uniaxial compressive stress and plastic strain, and the resulting cohesion hardening diagram are illustrated.

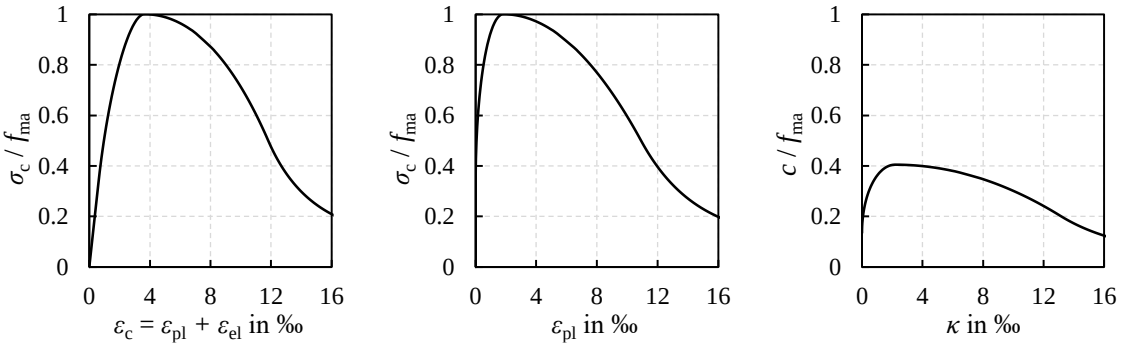

Fig. 5-4 Uniaxial compressive stress-strain relationship and cohesion hardening law for the expanded units (E_{ma} / f_{ma} = 550, k = 2)

The parameter κ_m, which is the equivalent plastic strain variable corresponding to ε_m (see Eq. 5-5), can also be determined based on the compressive fracture energy G_{fc} and an equivalent element length h. According to Lourenço (1996), the compressive fracture energy G_{fc} corresponds to the area between the descending branch and the residual strength of the σ-κ diagram multiplied by the equivalent element length h. Based on this definition, κ_m can be determined as

$$\kappa_m = \frac{75}{67} \frac{G_{fc}}{h \, f_{ma}} + \kappa_p \qquad \textit{Eq. 5-8}$$

where κ_p is the equivalent plastic strain variable corresponding to the plastic strain ε_p at the maximum compressive stress in a uniaxial test. With an equivalent element length $h = V^{1/3}$ (in which V is the volume of one element) and the calibrated ratio of $\varepsilon_m / \varepsilon_p = 6$, the ratio of fracture energy to masonry compressive strength can be obtained as $G_{fc} / f_{ma} = 0.29$ mm for $E_{ma} / f_{ma} = 550$ and $k = 2$. This aligns well with results by Schueremans (2001), who experimentally determined the compressive fracture energy on masonry walls, prisms, and cores and found ratios G_{fc} / f_{ma} of 0.45, 0.40, and 0.30 mm, respectively.

The horizontal tensile strength f_{bt} of the clay bricks is assigned as the tensile strength of the expanded units. In Schubert (2010), the horizontal unit tensile strength is provided in relation to unit compressive strength f_b. For solid clay bricks, a unit tensile strength of 0.04 f_b is specified, whereas for perforated clay bricks, 0.03 f_b is stated. For the simulation of the experiments, the experimental unit compressive strengths f_b (see Section 4.2.1) are used to calculate corresponding tensile strengths based on these ratios. For the MCS, all values are related to the masonry compressive strength. For a typical unit strength of f_b = 25 N/mm² and a typical mortar strength of f_j = 2.5 N/mm², a masonry strength of $f_{ma,m} = f_{ma,k} / 0.8$ = 9.1 N/mm² is obtained according to DIN EN 1996-1-1/NA (2019). Based on $f_{bt} / f_b = 0.04$, this results in $f_{bt} / f_{ma} = 0.11$. The tension softening is modelled as linear with a residual tensile strength of 0.1 f_{bt}, which is chosen for numerical robustness.

A material model displaying discrete cracking is assigned to the interfaces. As the elastic modulus of masonry is assigned to the “units”, the stiffness of the interface elements is

assigned a high value, leading to almost no relative displacements if uncracked. The purpose of the interfaces is to model cracking in the mortar joints if the tensile stress perpendicular to the bed joints reaches the corresponding flexural tensile strength f_{x1}. Therefore, the flexural tensile strength f_{x1} is directly assigned as tensile strength f_t of the interfaces. In Schmidt and Schubert (2004), a range from 0.23 to 1.10 N/mm² (with an average value of 0.57 N/mm²) is provided for the flexural tensile strength f_{x1} of solid clay brick masonry. Here, a value of 0.4 N/mm² is chosen for flexural tensile strength f_{x1} since the value should be representative of mortars with lower strengths. The tension softening behaviour is defined by a bilinear curve according to JSCE (2010) with specified fracture energy (see Fig. 5-5). The fracture energy is chosen according to Schueremans (2001), in which the ratio of tensile fracture energy G_{ft} to bond tensile strength f_t is specified as 0.0148 mm based on an evaluation of direct tensile tests conducted by van der Pluijm (1999).

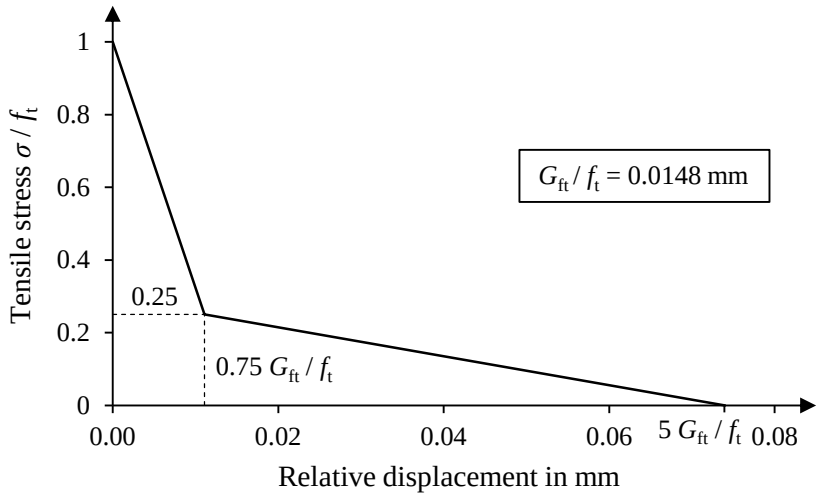

Fig. 5-5 Softening behaviour of the interface elements according to JSCE (2010)

The material properties of the finite element model are summarised in Table 5-1. The material properties for the MCS are provided in relation to masonry compressive strength f_{ma} since they are normalised with regard to mean masonry compressive strength $f_{ma,m}$ in the corresponding finite element simulations. Concerning the MCS, this relationship to masonry compressive strength f_{ma} should not be misunderstood as a stochastic dependence but as a relationship between the respective mean values of the material properties. The stochastic correlation between the particular material properties is described in Section 6.2.1.

Table 5-1 Material properties of the finite element model

Type of element		Parameter	Value	Reference
Expanded units	General	friction angle φ	12°	calibration
		dilatancy angle ψ	φ	Lourenço (1996)
		Poisson's ratio	0.19	Schueremans (2001)
	Solid clay brick masonry (experiments)	compressive strength f_{ma}	7.42 N/mm² (single wythe) 6.35 N/mm² (cross bond)	experimental
		modulus of elasticity E_{ma}	3,000 N/mm²	experimental
		stress-strain parameter k	2.31 (single wythe) 2.38 (cross bond)	experimental
		tensile strength f_{bt}	0.04 f_b = 1.0 N/mm²	Schubert (2010)
	Perforated clay brick masonry (experiments)	compressive strength f_{ma}	3.14 N/mm² (single wythe) 2.64 N/mm² (cross bond)	experimental
		modulus of elasticity E_{ma}	1,959 N/mm²	experimental
		stress-strain parameter k	1.69 (single wythe) 2.04 (cross bond)	experimental
		tensile strength f_{bt}	0.03 f_b = 0.35 N/mm²	Schubert (2010)
	Solid clay brick masonry (Monte Carlo simulation)	mean modulus of elasticity E_{ma}	550 f_{ma}[1]	Kaushik et al. (2007) and Schubert (2010)
		stress-strain parameter k	2.0	Kaushik et al. (2007) and Lumantarna et al. (2014)
		mean compressive fracture energy G_{fc}	0.29 mm · f_{ma}	calibration
		tensile strength f_{bt}	0.04 f_b = 0.11 f_{ma}[1]	Schubert (2010)
Interfaces		(mean) tensile strength f_t	0.044 f_{ma}[1]	Schmidt and Schubert (2004)
		tensile fracture energy G_{ft}	0.0148 f_t	Schueremans (2001)

[1]*Relative material properties are based on f_b = 25 N/mm², f_j = 2.5 N/mm², and f_{ma} = 9.1 N/mm².*

5.3 Validation of the Finite Element Model

5.3.1 Comparison with Analytical Model for the Resistance of Slender Walls

In the first step of the validation, results obtained by finite element simulation are compared to results obtained via the closed-form expressions provided by Glock (2004) for the load-bearing capacity of slender unreinforced masonry walls under eccentric compression loading (see Section 3.3.3). This validates that the model is suited for determining the load-bearing capacity of masonry walls with varying slenderness and various eccentricities of compression loading. Finite element simulations are conducted for three different ratios e / t of eccentricity to wall thickness and varying material-related slenderness λ. The corresponding finite element model represents a wall in cross bond with 36 courses, which results in a height of 3 m. To vary the slenderness λ, the modulus of elasticity and, thereby,

the strain ε_f at reaching the compressive strength is adjusted. The model by Glock (2004) is applied based on a parabolic-rectangular stress-strain relationship with a ratio of ultimate strain to strain at peak compressive stress of $\varepsilon_u / \varepsilon_f = 1.75$. This ratio is chosen since it is specified in FprEN 1996-1-1 (2020) for masonry composed of solid units. Furthermore, due to this choice, the obtained cross-sectional capacity is approximately equal to that resulting from the stress-strain relationship implemented in the finite element model. In Fig. 5-6, the load-bearing capacity according to the model by Glock (2004) and the results obtained by finite element simulation are illustrated. The comparison shows that the finite element model is well suited for determining the load-bearing capacity of masonry walls with increasing slenderness.

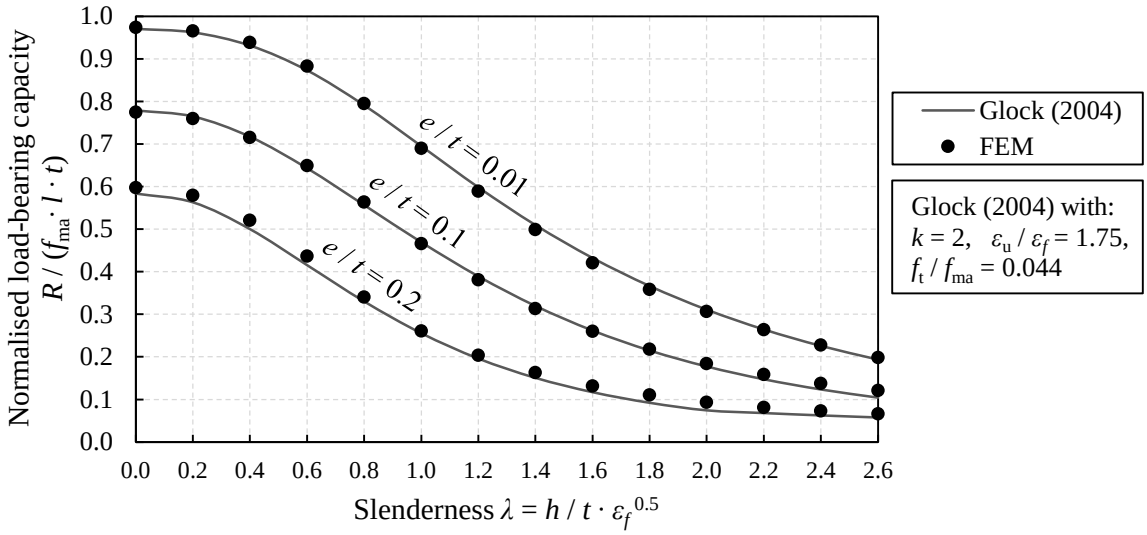

Fig. 5-6 Load-bearing capacity of slender walls obtained by finite element simulation and by the model of Glock (2004)

5.3.2 Comparison with Experimental Results

The second step of the validation is the comparison of the experimental results with the corresponding finite element simulations. This demonstrates that the finite element model represents the behaviour of masonry walls with local weaknesses sufficiently well. For this purpose, the respective reductions in the resistance relative to that of the solid clay brick reference walls without weakening are of interest. Therefore, the masonry compressive strength f_{ma} and the stress-strain parameter k, which were obtained in the experiments for the reference walls, are also applied in the simulations. The load-displacement curves obtained in the experiments and by the finite element simulations are shown in Fig. 5-6. The load is related to the cross-sectional area of the wall without weakening; that is, it is shown as average stress over the gross cross-section. The experimental displacements at the LVDTs are related to the corresponding measurement length, and the simulated displacements at the top of the wall are related to the wall height. Both displacements are hence

shown as average strain along the respective measurement lengths. Fig. 5-7 demonstrates that the finite element model reproduces the behaviour of the experimental walls very well.

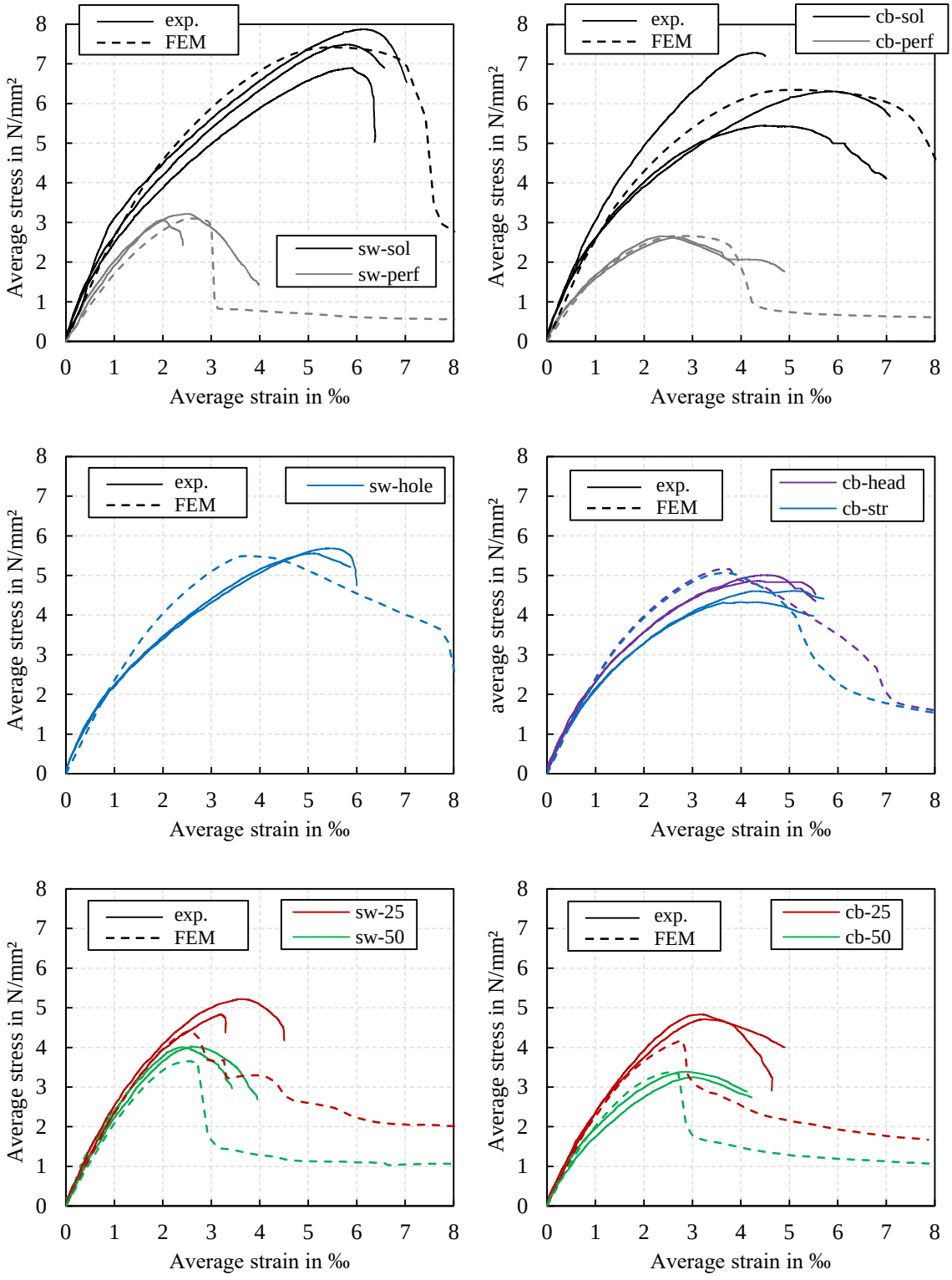

Fig. 5-7 *Stress-strain curves obtained in the experiments on masonry walls and corresponding results of finite element simulations*

For the MCS conducted in the next chapter, the finite element model must accurately capture the load-bearing capacity of masonry walls with local weaknesses. In Table 5-2, a comparison of the simulation results and the average experimental results for the load-bearing capacity is shown. The simulation results for the reference walls are equal to the experimental results since the experimental reference strengths are used as input parameters for the finite element simulations, and, without weakening, the load-bearing capacity related to the cross-section A matches the input compressive strength. The average ratio of experimental to simulation results is 1.03, and the coefficient of variation (CoV) of the ratio is 9.5 %. Since the experimental results themselves also show some scatter, the CoV of 9.5 % can be considered sufficiently low.

Table 5-2 Comparison of results from experiments and finite element simulations

Wall	Load-bearing capacity R per area A		Ratio R_{exp} / R_{cal}
	Experiment R_{exp}	Simulation R_{cal}	
	N/mm²	N/mm²	
Sw-sol	7.42		-
Sw-perf	3.14		-
Sw-hole	5.62	5.49	1.02
Sw-25	5.02	4.44	1.13
Sw-50	4.02	3.66	1.10
Cb-sol	6.35		-
Cb-perf	2.64		-
Cb-head	4.94	5.17	0.95
Cb-str	4.47	5.07	0.88
Cb-25	4.77	4.18	1.14
Cb-50	3.32	3.38	0.98
		Mean	1.03
		CoV	9.5 %

In Fig. 5-8, an example comparison of the strains measured by digital image correlation (DIC) with the strains and stresses obtained by finite element simulation is presented for the experimental wall laid in cross bond with a missing header (cb-head-2). All strains and stresses correspond to the state of reaching the maximum load. The stresses in the finite element model are normalised with respect to masonry compressive strength. Hence, a stress of one corresponds to reaching the uniaxial compressive strength.

The figure illustrates the main difference between the simplified micro model and reality. In the experiments, the strains in the mortar joints were much higher than in the bricks, which is due to the lower stiffness of the mortar. In contrast, there is no differentiation between the compression behaviour of bricks and mortar in the finite element model since the compression behaviour of the composite material masonry is included in the expanded units. However, the overall behaviour is similar: The highest strains occur besides the opening, and, from there, the region with the highest strains extends to the four corners. Under

low loads that do not lead to plastic strains, the stress distribution along the critical cross-section is equal to the strain distribution. The stress is highest next to the opening in this state; plastic strains thus occur here first. Stresses are consequently redistributed to the outer regions with increasing load, and the stress distribution gets more uniform. At the maximum load, the stress next to the opening already corresponds to the descending branch of the stress-strain relationship. Due to the constraint from surrounding bricks with lower stress, the maximum vertical stress can be slightly higher than the uniaxial strength. The results of the finite element simulations thus confirm the considerations in Section 4.4.2.

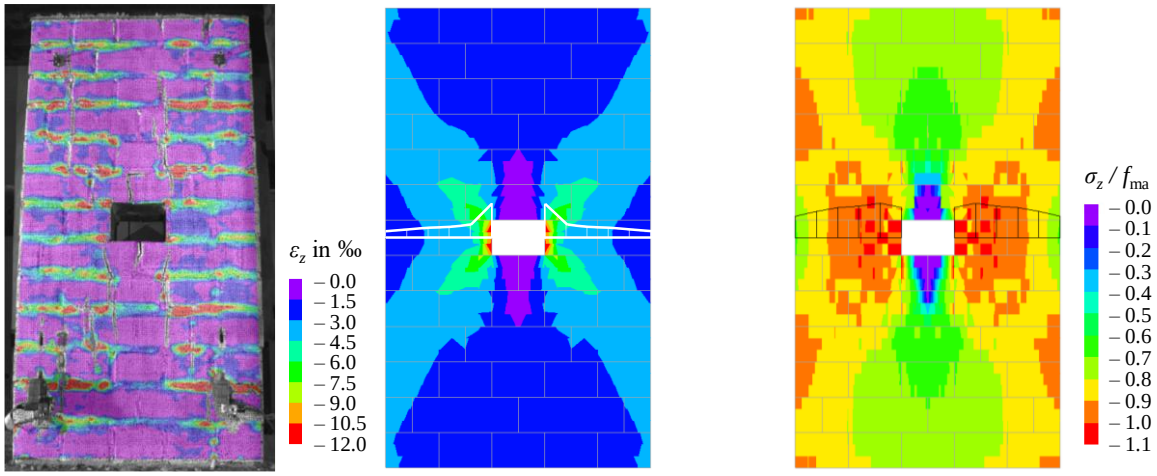

Fig. 5-8 *Wall cb-head-2 and the respective finite element model at maximum load*
Left: Vertical strain in the experiment measured by digital image correlation
Middle: Vertical strain ε_z in the finite element model
Right: Vertical stress σ_z in the finite element model

5.4 Summary

In this chapter, the finite element model created for the following investigations was presented. The finite element model follows the simplified micro-modelling approach. The geometrical boundary conditions, the finite element mesh, and the implemented material models were described. The compressive behaviour of the expanded units is modelled by Drucker-Prager plasticity, with the corresponding parameters being selected based on the experiments and information in the literature. Interfaces between the expanded units display the cracking behaviour in the joints.

In a first step of validating the finite element model, simulated load-bearing capacities of walls with varying slenderness and load eccentricity were compared to load-bearing capacities obtained with the model by Glock (2004). The second validation step was the simulation of the conducted experiments and a subsequent comparison of the simulated and experimental load-bearing capacities of clay brick masonry walls with local weaknesses. Based on both validation steps, the finite element model can be considered well suited for the following investigations.

6 MONTE CARLO SIMULATION OF MASONRY WALLS WITH SPATIALLY VARIABLE MATERIAL PROPERTIES

6.1 Introduction

Since existing masonry often shows a distinct spatial variability of material properties, the influence of spatially variable material properties on the load-bearing capacity of solid clay brick masonry walls under compression loading is investigated in this chapter. The investigations aim to find a relationship between the probability distribution of the material properties within a masonry wall and the probability distribution of the resulting load-bearing capacity.

In Fig. 6-1, the expected effect of spatial variability on the distribution of the load-bearing capacity R is illustrated. The probability density function (PDF) of R is compared to the PDF of masonry compressive strength f_{ma}, which is the most influential material property for non-slender masonry walls under compression. As masonry compressive strength is spatially variable, the PDF for f_{ma} corresponds to the strength at a particular location in the wall. In the illustration, masonry compressive strength is normalised by its mean value $f_{ma,m}$, and the load-bearing capacity is additionally normalised by the cross-sectional area A. In this example, the compression loading is applied without eccentricity, and second-order effects are neglected, which means that a deterministic calculation based on the mean value of masonry compressive strength would lead to a normalised load-bearing capacity of one. Due to the normalisation, the PDF of f_{ma} equals the PDF for the load-bearing capacity R_{hom} of a homogenous wall. In a homogenous wall, there is perfect spatial correlation between the material properties. Consequently, the overall masonry compressive strength varies from wall to wall, but there is no spatial variability within a single wall.

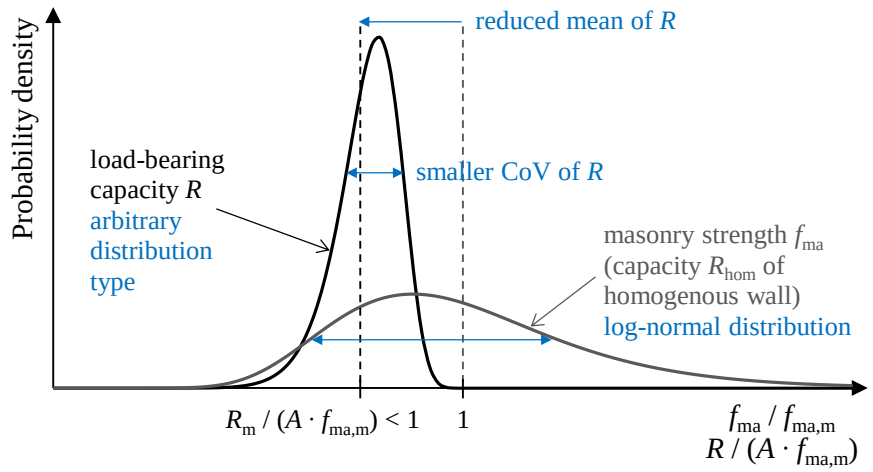

Fig. 6-1 Qualitative illustration of the effects of spatial variability on the probability distribution of the load-bearing capacity of a masonry wall under compression

Compared to the structural systems introduced in Section 2.5.5, a masonry wall under compression can be viewed as a combination of series and parallel systems. In the horizontal direction, the stresses can be redistributed between the units within a course, which resembles a parallel system. In the vertical direction, the behaviour is closer to that of a series system, as the wall fails as soon as the weakest course cannot bear any more load. Three system effects can thus be expected for a wall with spatially varying material properties (see Fig. 6-1). First, the mean value of the relative load-bearing capacity is smaller than one, which means that spatial variability leads to a reduction in the mean load-bearing capacity compared to a homogenous wall. Second, the coefficient of variation (CoV) of the load-bearing capacity is smaller than the CoV of masonry compressive strength. Third, the resulting distribution type of the load-bearing capacity differs from the distribution type of the input material properties.

In the following investigations, the mean, the CoV, and the distribution type of the load-bearing capacity of solid clay brick masonry walls with spatially varying material properties are determined by Monte Carlo simulations (MCS). Thereby, relationships are found that can be used in the development of a method for determining suitable assessment values of masonry compressive strength. In Section 6.2, the investigation procedure is described, including the stochastic model for spatial variability, the corresponding selection of stochastic parameters, the generation of random material properties, and the approach for evaluating the results. Section 6.3 presents various parameter studies to investigate the probability distribution of the load-bearing capacity of walls with spatially variable material properties. First, a reference wall is defined and investigated. In the parameter studies, the CoV of the spatially varying material properties, the spatial correlation of the material properties, the wall length and slenderness, the load eccentricity, the masonry bond type, and the dimensions and number of units in the wall are varied.

6.2 Investigation Procedure

6.2.1 Stochastic Model for Spatial Variability

In the following, spatial variability is modelled as unit-to-unit variability. The compressive strength f_{ma} of masonry, the modulus of elasticity E_{ma} of masonry, and the tensile strength f_t of the joints are modelled as random variables (see Fig. 6-2). Instead of separately considering the spatial variability of unit and mortar compressive strength, each of the expanded “units” is assigned a random value for the compressive strength and modulus of elasticity of masonry. This is in line with the simplified micro-modelling approach, which is followed in the finite element modelling. Masonry compressive strength and the masonry modulus of elasticity within one “unit” are assumed to be correlated with a correlation coefficient $\rho_{f,E}$. To assign spatially varying tensile strengths, the interfaces, which represent

the mortar joints, are discretised according to the units placed on top. This is because, during construction, the mortar is usually placed section by section for the next unit to be laid. The spatial correlation of the material properties within a particular wall is assumed to be independent of their location. For masonry compressive strength and the masonry modulus of elasticity, the spatial correlation between any two "units" in the wall is given by the spatial correlation coefficient ρ_{spat} (see Fig. 6-2).

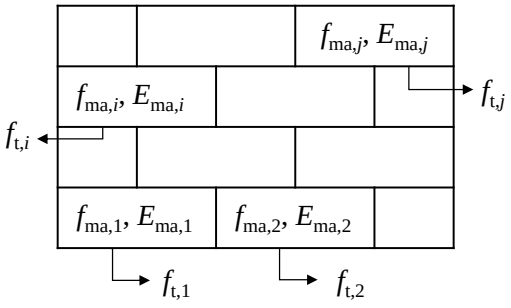

ρ	$f_{ma,i}$	$E_{ma,i}$	$f_{ma,j}$	$E_{ma,j}$	$f_{t,i}$	$f_{t,j}$
$f_{ma,i}$	1	$\rho_{f,E}$	ρ_{spat}	$\rho_{spat}\rho_{f,E}$	0	0
$E_{ma,i}$		1	$\rho_{spat}\rho_{f,E}$	ρ_{spat}	0	0
$f_{ma,j}$			1	$\rho_{f,E}$	0	0
$E_{ma,j}$				1	0	0
$f_{t,i}$					1	0
$f_{t,j}$		*symmetric*				1

Fig. 6-2 Correlation between material properties (left: material properties within the wall, right: correlation matrix)

For $\rho_{spat} = 1$, the material properties are equal at every "unit" in the wall: One randomly generated material property is assigned to all "units". In this case, the CoV of, for example, masonry compressive strength specifies a homogeneous variability of the masonry strength of all "units" in the wall. In contrast, $\rho_{spat} = 0$ corresponds to full spatial variability, which means that the CoV of masonry strength specifies the unit-to-unit variability, and each "unit" receives a masonry strength that is independent of the masonry strengths of the other "units".

This spatial correlation structure is considered suitable since the compressive strength of masonry is dominated by the material properties of the units. The units are delivered to the construction site in batches, in which their material properties are correlated because of influences from the production process. Since one wall is usually constructed with units from only one batch, the unit properties within the wall are correlated, whereas other walls may be constructed with units from a different batch. This effect is also observed in Section 7.4.5 in the evaluation test data from the material properties of existing masonry buildings. The units from a batch are placed in the wall in an arbitrary order, which makes any assumption regarding a distance-related correlation, such as a specific correlation length, very questionable.

While distance-related correlation coefficients for the material properties of the units (i.e. for the actual bricks) are not considered suitable, the material properties of the mortar joints can show a distance-related correlation in reality. Usually, several mortar mixes are used for the construction of one wall. Since the properties of mortar joints made from the same mortar mix are correlated, the mortar joint properties within one course may be more

strongly correlated. Furthermore, it may be appropriate to model the correlation of mortar joint properties along one course via a correlation function with a specific correlation length.

Heffler et al. (2008) investigated the correlation of the flexural tensile strengths of mortar joints within a masonry wall by experiments in that the flexural tensile strengths were obtained unit by unit through bond wrench testing. The correlation of the flexural tensile strengths below adjacent units was found to be low. Heffler et al. (2008) thus recommended considering the flexural tensile strengths as stochastically independent. In the present study, mortar joint tensile strength is not very influential, as masonry walls under compression are examined. Only for very slender walls with a high load eccentricity, flexural tensile strength gains influence (see Section 3.3.3). The recommendation in Heffler et al. (2008) is hence followed, and no spatial correlation is considered for the tensile strength of the interfaces in the parameter studies.

Another influence of the correlation of mortar properties might be due to the influence of the compressive strength of mortar on the compressive strength of masonry. According to Section 3.5.4, the standard deviation of the logarithm of masonry strength $\sigma_{\ln,ma}$ can be determined based on the power equation from EN 1996-1-1 (2012) as

$$\sigma_{\ln,ma}^2 = \alpha^2 \, \sigma_{\ln,b}^2 + \beta^2 \, \sigma_{\ln,j}^2 = 0.49 \, \sigma_{\ln,b}^2 + 0.09 \, \sigma_{\ln,j}^2 \qquad \textit{Eq. 6-1}$$

where $\sigma_{\ln,b}$ and $\sigma_{\ln,j}$ are the standard deviations of the logarithms of unit and mortar compressive strength, respectively. Eq. 6-1 demonstrates that the influence of the variability in mortar compressive strength is very low compared to the dominant influence of unit compressive strength. Therefore, the potentially different correlation structure of mortar joint properties is neglected in the investigations. The correlation structure of the masonry properties, which are assigned to the expanded "units", is completely based on the correlation structure for the units, that is, the actual bricks.

Further considerations regarding the assignment of masonry properties to the "units" must be addressed, as the masonry strength of one "unit" is influenced by the properties of the actual unit and both the adjacent mortar bed joints. Therefore, the masonry compressive strengths of two "units" that lie on top of each other are slightly correlated, as they share the interjacent mortar joint properties. However, the parameter study in Section 6.3.3 shows that the corresponding effects can be neglected and that the direct assignment of random masonry properties to the expanded "units" based on the variability given by Eq. 6-1 is suitable.

6.2.2 Selection of Stochastic Parameters

Within the parameter studies, the CoVs of the material properties are varied. Therefore, typical ratios between the CoVs of the different material properties need to be defined rather

than fixed values. In Schueremans (2001), CoVs of the compressive strength of masonry, the modulus of elasticity of masonry, and the tensile strength of the joints are provided as 17 %, 22 %, and 35 %, respectively. These values were determined through experiments on solid clay brick masonry: The CoVs of compressive strength and the modulus of elasticity were obtained from masonry cores with 150 mm diameter and 300 mm height, and the CoV of the tensile strength of the joints was determined in direct tensile strength tests. The values are close to those in the JCSS Probabilistic Model Code (2011), which specifies a CoV of 14 % to 20 % for masonry compressive strength, 25 % for the modulus of elasticity of masonry, and 30 % to 35 % for flexural tensile strength. Where a range is given, the value depends on the type of masonry. Solid clay brick masonry, however, is not explicitly considered. Based on the results by Schueremans (2001), typical ratios of the CoVs to the CoV of masonry compressive strength are defined (see Table 6-1). These relative CoVs are used in all the following parameter studies. When the CoV for masonry compressive strength is varied, the CoVs of the masonry modulus of elasticity and the tensile strength of the joints are varied by the same factor. The correlation between masonry compressive strength and the modulus of elasticity is set to $\rho_{f,E} = 0.72$, as stated in Schueremans (2001).

Table 6-1 Stochastic parameters of the material properties

Material property	Distribution type	Correlation	CoV in Schueremans (2001)	Relative CoV υ / υ_{ma}
Masonry compressive strength f_{ma}	LN	$\rho_{f,E} = 0.72$ (Schueremans 2001)	$\upsilon_{ma} = 17$ %	1
Masonry modulus of elasticity E_{ma}	LN		$\upsilon_E = 22$ %	≈ 1.3
Tensile strength f_t	LN	-	$\upsilon_t = 35$ %	≈ 2.0

6.2.3 Generation of Random Material Properties

For the generation of random material properties according to the correlation matrix in Fig. 6-2, the following approach has been developed. Since the product of log-normally distributed random variables is also log-normally distributed, the material properties can be modelled as the product of auxiliary log-normally distributed random variables. Random values for the compressive strength $f_{ma,i}$ and the modulus of elasticity $E_{ma,i}$ of a specific "unit" i are thus generated by the multiplication of four independent random variables:

$$f_{ma,i} = W\ f_w\ U_i\ f_{u,i} \qquad \textit{Eq. 6-2}$$

$$E_{ma,i} = W\ E_w\ U_i\ E_{u,i} \qquad \textit{Eq. 6-3}$$

where W, E_w, f_w, and U_i are parent variables for the generation of the material properties. Each of these variables is shared by certain pairs of the material properties $f_{ma,i}$ and $E_{ma,i}$, as

illustrated in Fig. 6-3. This means that the same random realisation of the parent variables is applied in calculating all the random material properties that share this parent variable. Sharing a parent variable thus results in correlation. The random variable W describes the shared deviation of the mean compressive strength and modulus of elasticity in the wall from an overall mean value. The variables f_w and E_w display the additional deviation of the mean compressive strength in the wall and the mean modulus of elasticity in the wall, respectively, from their overall mean. U_i is the shared deviation of the compressive strength and the modulus of elasticity of an individual "unit" i from the mean value of the wall. By multiplication with $f_{u,i}$ and $E_{u,i}$, the additional deviation of the specific material properties from their mean value in the wall is considered.

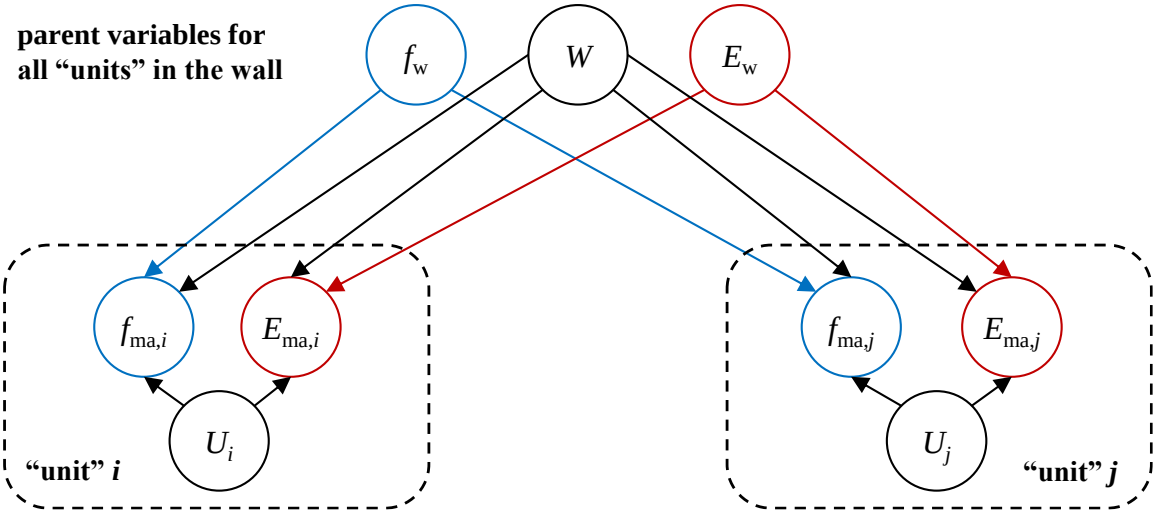

Fig. 6-3 Illustration of the generation of random material properties

The random variables W and U_i create a correlation between the compressive strength and the modulus of elasticity of a particular "unit" since the corresponding random values are the same for $f_{ma,i}$ and $E_{ma,i}$. Accordingly, W and f_w create a correlation between the compressive strengths f_{ma} of two different "units" i and j. Finally, W and E_w create a correlation between the moduli of elasticity E_{ma} of different "units".

All random variables in Eq. 6-2 and Eq. 6-3 are log-normally distributed with a mean value of one, except for $f_{u,i}$ and $E_{u,i}$, the mean values of which are set to the actual mean values of masonry compressive strength f_{ma} and the modulus of elasticity E_{ma}. To achieve the desired correlation coefficients (ρ_{spat} and $\rho_{f,E}$) and the desired overall CoV for the material properties, the CoVs for the auxiliary random variables can be determined using Eq. 6-4 to Eq. 6-9. The equations are derived based on the well-established relationships for the correlation coefficient of two random variables and for the variance of the product of random variables (see Annex B).

$$v_W = \sqrt{\rho_{spat}\ \rho_{f,E}\ v_E\ v_{ma}} \qquad \text{Eq. 6-4}$$

$$v_{f_w} = \sqrt{\frac{\rho_{spat}\left(v_{ma}^2 - \rho_{f,E}\, v_E\, v_{ma}\right)}{1+\rho_{spat}\,\rho_{f,E}\, v_E\, v_{ma}}} \qquad \textit{Eq. 6-5}$$

$$v_{E_w} = \sqrt{\frac{\rho_{spat}\left(v_E^2 - \rho_{f,E}\, v_E\, v_{ma}\right)}{1+\rho_{spat}\,\rho_{f,E}\, v_E\, v_{ma}}} \qquad \textit{Eq. 6-6}$$

$$v_{U_i} = \sqrt{\frac{\rho_{f,E}\, v_E\, v_{ma}\left(1-\rho_{spat}\right)}{1+\rho_{spat}\,\rho_{f,E}\, v_E\, v_{ma}}} \qquad \textit{Eq. 6-7}$$

$$v_{f_{u,i}} = \sqrt{\frac{\left(v_{ma}^2 - \rho_{f,E}\, v_E\, v_{ma}\right)\left(1-\rho_{spat}\right)}{\left(1+\rho_{spat}\, v_{ma}^2\right)\left(1+\rho_{f,E}\, v_E\, v_{ma}\right)}} \qquad \textit{Eq. 6-8}$$

$$v_{E_{u,i}} = \sqrt{\frac{\left(v_E^2 - \rho_{f,E}\, v_E\, v_{ma}\right)\left(1-\rho_{spat}\right)}{\left(1+\rho_{spat}\, v_E^2\right)\left(1+\rho_{f,E}\, v_E\, v_{ma}\right)}} \qquad \textit{Eq. 6-9}$$

Unit-to-unit variability is given by the variability of U_i, $f_{u,i}$, and $E_{u,i}$ alone. In contrast, the variability of W, E_w, and f_w displays the deviation of the mean material properties of a wall from overall mean values. For $\rho_{spat} = 1$, the CoVs of U_i, $f_{u,i}$, and $E_{u,i}$ are zero, which means that no unit-to-unit variability exists. In most parameter studies, the spatial correlation coefficient is set to $\rho_{spat} = 0$. In these cases, the CoVs of the random variables W, f_w, and E_w are zero. Therefore, only the shared parent variable U_i for the material properties of one "unit" remains, which is needed to create the correlation between the compressive strength and modulus of elasticity of masonry.

To model the stress-strain relationship, the stress-strain parameter k is considered as a deterministic variable, with $k = 2$. Therefore, the ascending branch of the stress-strain relationship according to Eq. 5-5 is completely defined if random values for f_{ma} and E_{ma} are given. Based on the relationship $\varepsilon_m = 6\ \varepsilon_p$, which was found in the calibration process (see Section 5.2.3), the post-peak behaviour is also defined. The tensile strength $f_{bt,i}$ of the expanded "units", which represents the tensile strength of the bricks, is modelled as a dependent variable. It is set to $0.11\ f_{ma,i}$ for each of the "units" (see Table 5-1).

Since the random material properties for the tensile strength f_t of the joints are not modelled as correlated, they can be directly generated according to the desired mean and CoV.

6.2.4 Evaluation Procedure

In the parameter studies, all material properties and the results for the load-bearing capacity are normalised by the mean compressive strength of masonry $f_{ma,m}$. This procedure is equivalent to performing all simulations based on a mean value of $f_{ma,m} = 1$. The results of the

parameter studies are thus independent of the absolute values of $f_{ma,m}$. In general, 200 simulation runs are conducted for each parameter combination. The mean R_m and the CoV v_R of the random variable R are then estimated by the arithmetic mean and the sample CoV of the simulation results. Furthermore, the deterministic load-bearing capacity R_{det} is determined through a simulation with mean material properties as input parameters:

$$R_{det} = R\left(f_{ma,m}, E_{ma,m}, f_{t,m} \right) \qquad \textit{Eq. 6-10}$$

Regarding structural reliability, lower quantiles of the load-bearing capacity are essential. Therefore, theoretical assessment values R_a of the load-bearing capacity are calculated. A target reliability index of $\beta_{t,1a} = 3.3$ and a fixed sensitivity factor of $\alpha_{R,1a} = 0.7$ are selected for this purpose (see Sections 2.5.4 and 2.6.2). Since the resulting probability distribution types of the load-bearing capacity are unknown, and the most suitable distribution type varies within the parameter studies, the theoretical assessment values are all determined assuming a log-normal distribution. However, the skewness of the resulting distribution function might differ from that of a log-normal distribution, and more weight might lie in the left tail of the distribution. Therefore, the corresponding log-normal distribution is not set up based on the method of moments. Instead, the distribution parameters $\mu_{\ln R}$ and $\sigma_{\ln R}$ are chosen such that the mean value and the 5 % fractile of the distribution match the arithmetic mean and the 5 % fractile of the random sample. The assessment value R_a is then determined as follows:

$$\begin{aligned} R_a &= R_m \exp\left(-0.5\,\sigma^2_{\ln R,5\%} - \alpha_R\,\beta_t\,\sigma_{\ln R,5\%}\right) \\ &= R_m \exp\left(-0.5\,\sigma^2_{\ln R,5\%} - 0.7 \cdot 3.3 \cdot \sigma_{\ln R,5\%}\right) \end{aligned} \qquad \textit{Eq. 6-11}$$

At this step, the assessment values R_a only serve comparative purposes. They are not suited for further application since they do not contain model and statistical uncertainties.

In addition to the theoretical assessment value considering spatial variability, assessment values $R_{a,hom}$ are calculated based on the assumption of homogeneity. This means that the reduction of the mean due to spatial variability (i.e. $R_m / R_{det} < 1$) is not considered, and the variability of masonry compressive strength is used to determine the assessment value:

$$R_{a,hom} = R_{det} \exp\left(-0.5\,\sigma^2_{ln,ma} - 0.7 \cdot 3.3 \cdot \sigma_{ln,ma}\right) \qquad \textit{Eq. 6-12}$$

where $\sigma_{ln,ma}$ is determined based on the CoV v_{ma} of masonry compressive strength (see Eq. 2-27).

Finally, Anderson-Darling goodness-of-fit tests are conducted for normal, log-normal, and Weibull distribution functions to check which probability distribution type is best suited to describe the results for the load-bearing capacity. These tests are performed as described in Section 2.3.7.

6.3 Parameter Studies

6.3.1 Overview

This section presents various parameter studies to investigate the probability distribution of the load-bearing capacity of masonry walls under compression in the case of spatially varying material properties. The parameter studies are based on a reference wall, which is illustrated in Fig. 6-4 and described next. In each study, one of the parameters of the reference wall is varied.

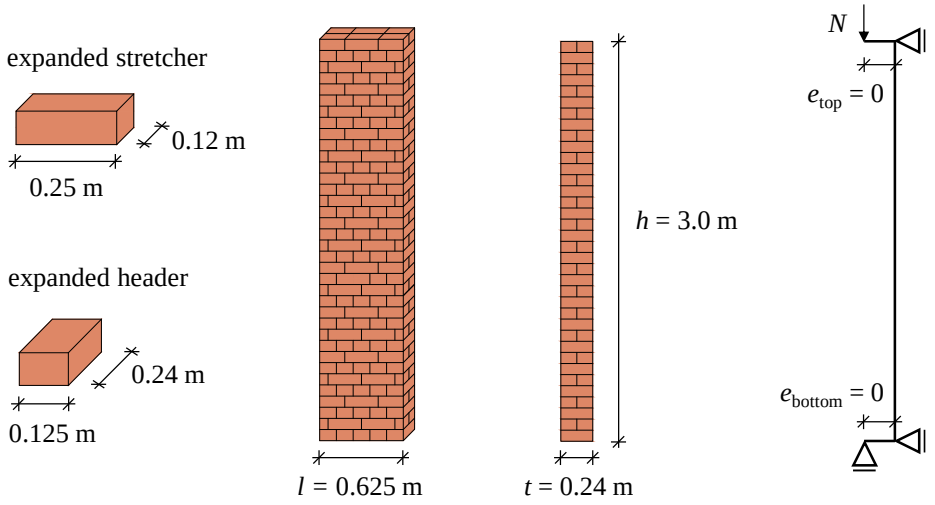

Fig. 6-4 Reference wall for the Monte Carlo simulations

The reference wall is arranged in cross bond with a thickness of two unit widths. It contains 36 courses with five units per course. The "unit" dimensions correspond to the German standard format NF, which results in dimensions 250 x 120 x 83.3 mm³ (length x width x height) for the expanded stretchers and 240 x 125 x 83.3 mm³ for the expanded headers. Hence, the overall dimensions of the reference wall are 0.625 x 0.24 x 3.0 m³. Wall height and unit dimensions are chosen to be typical for existing masonry structures. The arrangement in cross bond is selected since single wythe masonry walls are uncommon for existing load-bearing masonry made from small-sized solid clay bricks. A thickness of two unit widths is chosen, as this thickness is more critical regarding the load redistribution capability than a thickness of more than two units (see Section 6.3.9). The eccentricity of the compression loading is selected as $e / t = 0$ for the reference wall. The ratio of modulus of elasticity to compressive strength is set to $E_{ma,m} / f_{ma,m} = 550$ (see Section 5.2.3). However, this ratio is only influential for slender walls. Geometrical nonlinearity is not considered in the reference investigation, resulting in a theoretical slenderness of zero and, therefore, material failure without the influence of second-order effects (see Section 3.3.3). The choice of no eccentricity and no slenderness leads to the most critical influence of spatial variability, which is shown in the following parameter studies.

The reference CoV of masonry compressive strength is selected as υ_{ma} = 30 %, which results in CoVs of the modulus of elasticity and the joint tensile strength of υ_E = 39 % and υ_t = 60 % (see Section 6.2.2). The CoVs are chosen higher than those in Schueremans (2001) and JCSS (2011) to represent typical existing solid clay brick masonry (see Section 7.3). However, since the main results of the following investigations are provided as a function of υ_{ma}, they are applicable for a broader range of CoVs. The spatial correlation of the material properties is set to ρ_{spat} = 0, which means that the specified CoVs of the reference wall correspond to the unit-to-unit variability of the material properties.

Table 6-2 summarises the chosen values for the parameters of the reference wall and provides an overview of the parameter studies. The results for the reference wall are shown in Section 6.3.2, and those of the parameter studies are presented in the subsequent sections. In addition to the parameter studies displayed in Table 6-2, different options of considering mortar compressive strength in the generation of masonry compressive strength are investigated in Section 6.3.3, which aims to validate the selected approach for the parameter studies.

Table 6-2 Reference values for the parameters and overview of the parameter studies

Parameter	Reference value	Varied in Section
CoV of masonry compressive strength f_{ma}	υ_{ma} = 30 %	6.3.4
Spatial correlation coefficient	ρ_{spat} = 0	6.3.5
Wall length (number of units per course)	5 units	6.3.6
Wall slenderness $\lambda = h / t \cdot \varepsilon_f^{0.5}$	λ = 0	6.3.7
Relative eccentricity of compression loading	e / t = 0	6.3.8
Type of masonry bond	cross bond	6.3.9
Unit format	NF	6.3.10

6.3.2 Results for the Reference Wall

Before the results of the parameter studies are presented, the results for the reference wall are evaluated in more detail. The normalised load-bearing capacity of the reference wall based on a deterministic finite element simulation with mean material properties is

$$\frac{R_{det}}{l\ t\ f_{ma,m}} = \frac{R_{det}}{A\ f_{ma,m}} = 1 \qquad \textit{Eq. 6-13}$$

where l and t are the length and thickness of the wall, A is the cross-sectional area, and $f_{ma,m}$ is the mean of masonry compressive strength. The normalised load-bearing capacity is obtained as one, as there is no eccentricity of the load for the reference wall, and geometrical nonlinearity is not considered at this point. The normalised mean R_m of the results obtained

by the finite element simulations with spatially varying material properties is smaller than one, with a value of

$$\frac{R_{\mathrm{m}}}{A\, f_{\mathrm{ma,m}}} = 0.745 \qquad \textit{Eq. 6-14}$$

The ratio $R_{\mathrm{m}} / R_{\mathrm{det}} = 0.745$ demonstrates that spatial variability of the material properties leads to a reduction of the mean load-bearing capacity. This reduction is caused by the limited stress redistribution capability within a particular course and by the fact that the weakest of the courses within the masonry wall determines the load-bearing capacity. The CoV of the load-bearing capacity is obtained as $v_R = 5.3$ %, which is significantly smaller than the input CoV of $v_{\mathrm{ma}} = 30$ % for masonry compressive strength.

In Fig. 6-5, the Monte Carlo simulation results are displayed regarding their relative frequencies divided by bin width on the left and by their empirical distribution function (EDF) on the right. For comparison, the PDFs and cumulative distribution functions (CDFs) of different distribution types are also shown. The parameters of the normal and log-normal distributions are derived based on the method of moments. The parameters of the Weibull distribution are determined by maximum likelihood estimation. Furthermore, a second log-normal distribution is displayed (denoted by "LN,5%"), the parameters of which are selected to match the simulation results regarding their mean and 5 % fractile (see Section 6.2.4).

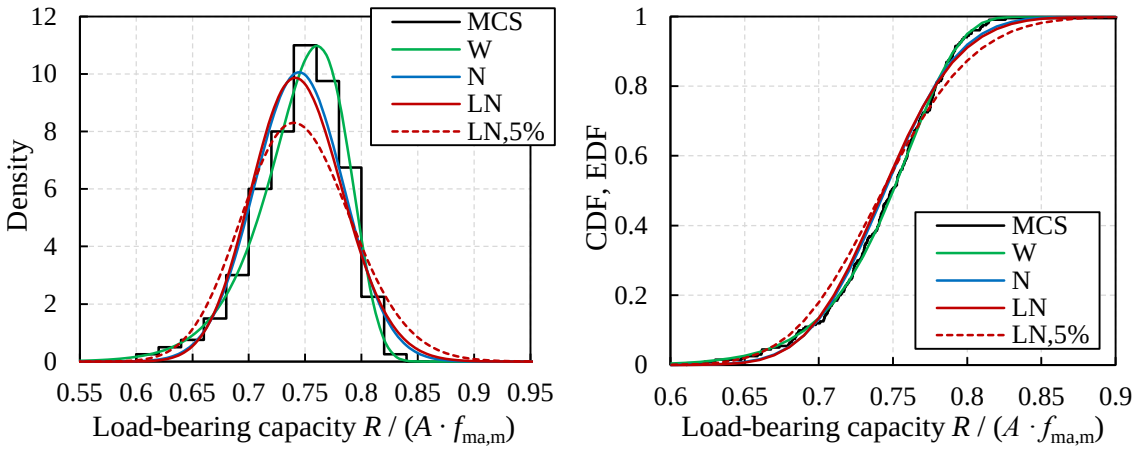

Fig. 6-5 Comparison of simulation results (MCS) with probability density functions and cumulated distribution functions of a Weibull (W), a normal (N), and log-normal (LN) distributions

The Weibull distribution appears to be most appropriate for describing the simulation results of the reference wall. Since the CoV of the distributions is small, the normal and log-normal distribution are very similar. Compared to the log-normal distribution with parameters estimated based on the method of moments, the log-normal distribution that is fitted

to match the mean and the 5 % fractile of the simulation results very well approximates the left tail of the simulated distribution.

The goodness-of-fit of the different probability distribution types is quantified utilising the Anderson-Darling test (see Section 2.3.7). In Table 6-3, the results for the three different distribution types are listed. Low values for the test statistic A^2 indicate a good fit. For low significance levels p, the results are unlikely to have originated from the hypothesised distribution. Hence, a high value p indicates a good fit. As indicated by the illustration in Fig. 6-5, the Weibull distribution is the best-fitting distribution for the reference wall. This result is comprehensible since the Weibull distribution well describes materials or structural systems failing due to the weakest link (see Weibull 1939). For the investigated masonry wall, the load-bearing capacity is dominated by the strength of the weakest course.

Table 6-3 Results of the Anderson-Darling test

Distribution type	Test statistic A^2	Modified statistic A^2*	Significance level p
Log-normal	1.79	1.83	$2.3 \cdot 10^{-4}$
Normal	1.23	1.25	$4.3 \cdot 10^{-3}$
Weibull	0.15	0.15	0.85
Modified test statistics A^2 and significance level p according to Eq. 2-58 to Eq. 2-61*			

To investigate whether the overall effect of considering spatial variability is negative (due to the decrease in the mean value) or positive (due to the decrease in the CoV), a theoretical assessment value R_a is calculated. Although the most appropriate distribution type is the Weibull distribution, the theoretical assessment value R_a is determined based on the log-normal distribution that is fitted to the arithmetic mean and the 5 % fractile of the simulation results, which results in the parameter value $\sigma_{\ln R,5\%} = 0.065 \approx \upsilon_{R,5\%}$. The CoV $\upsilon_{R,5\%}$ of this log-normal distribution is slightly higher than the CoV υ_R of the simulation results. The log-normal distribution is selected to determine assessment values since the Weibull distribution is not the most appropriate in all investigated cases, and choosing only one distribution is required for better comparability. Therefore, the theoretical assessment value R_a (see Section 6.2.4) is obtained as

$$\frac{R_a}{R_{det}} = \frac{R_m}{R_{det}} \exp\left(-0.5\,\sigma^2_{\ln R,5\%} - \alpha_R\,\beta_t\,\sigma_{\ln R,5\%}\right) = 0.745 \exp\left(-0.5 \cdot 0.065^2 - 0.7 \cdot 3.3 \cdot 0.065\right) = 0.640 \qquad \textit{Eq. 6-15}$$

The theoretical assessment value under the assumption of homogeneity is calculated as

$$\frac{R_{a,hom}}{R_{det}} = \exp\left(-0.5\,\sigma^2_{ln,ma} - \alpha_R\,\beta_t\,\sigma_{ln,ma}\right) = \exp\left(-0.5 \cdot 0.294^2 - 0.7 \cdot 3.3 \cdot 0.294\right) = 0.486 \qquad \textit{Eq. 6-16}$$

where $\sigma_{\ln,ma} = 0.294$ is obtained from $\upsilon_{ma} = 0.3$ based on Eq. 2-27. The results show that the consideration of spatial variability leads to a much higher theoretical assessment value for the reference wall.

Since the results are based on a limited number of 200 simulation runs, the arithmetic mean and the sample CoV contain a certain degree of statistical uncertainty. Therefore, confidence intervals for the population parameters R_m and υ_R are determined utilising bootstrap percentile intervals with bias correction, as described in Section 2.3.2. Based on a confidence level of 90 % and 10^6 non-parametric bootstrap samples, the confidence intervals for R_m and υ_R are as follows:

$$0.740 \leq \frac{R_m}{R_{det}} \leq 0.749 \qquad \textit{Eq. 6-17}$$

$$4.8\,\% \leq \upsilon_R \leq 5.8\,\% \qquad \textit{Eq. 6-18}$$

The mean value can be considered estimated with high precision since the confidence interval bounds are only ± 1 % away from the arithmetic mean. The absolute value for the CoV of the load-bearing capacity is small and, therefore, not very influential compared to additional uncertainties, such as model uncertainty. Thus, the precision in estimating the CoV based on 200 simulation runs can also be viewed as sufficient.

6.3.3 Investigation of Different Options for Mortar Property Assignment

Although masonry compressive strength is a function of the properties of the unit and the adjacent mortar joints, random values for masonry compressive strength are generated directly and then assigned to the "units" in the reference case above. To investigate whether this approach is suitable for the following parameter studies, it is compared to more detailed procedures in this section.

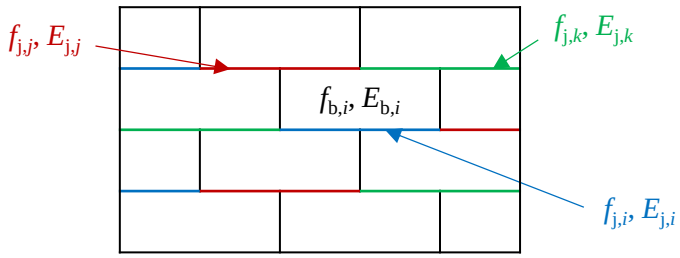

Fig. 6-6 Discretisation of mortar joint properties

Fig. 6-6 illustrates the discretisation of the mortar joint properties for single wythe masonry as an example. As mentioned in Section 6.2.1, the illustrated unit-to-unit discretisation is employed to model the spatial variability of the interface tensile strength in all the parameter studies. Here, the same discretisation is used to create random properties for the spatially variable compressive strength and elastic modulus of the mortar. These properties are

not directly assigned to the finite element model but are used to determine the compressive strength and elastic modulus of masonry, which are then assigned to the "units". By utilising the power equation for predicting masonry strength, the compressive strength of one "unit" can be determined based on the compressive strength of the respective unit *i* as well as a combination of the compressive strength of the mortar joint *i* underneath and the mortar joints *j* and *k* above the considered unit (see Fig. 6-6).

However, the question is how the different compressive strengths of the mortar joints *i*, *j*, and *k* should be considered when used as input for the power equation. Two options seem to be reasonable boundaries from a mechanical perspective. Option 1 corresponds to the assumption that masonry compressive strength is determined by the mortar strength either on top or below, whichever is smaller (see Eq. 6-19). In this option, the mortar strength on top is considered as the average of the two upper strength values. This approach of determining masonry strength via the minimum of the two mortar properties above or below the unit can be viewed as a lower boundary for the estimate of masonry strength. The second option, which provides an upper boundary, is based on the approach that unit strength combined with the average of the adjacent mortar properties determines masonry strength. The average is weighted according to the respective contact areas with the unit (see Eq. 6-20). It should be noted that Eq. 6-19 and Eq. 6-20 are displayed for single wythe masonry as depicted in Fig. 6-6. For masonry laid in cross bond, taking the average of the adjacent mortar strength values is more complex since more mortar strength values, corresponding to different contact areas, must be considered at the top of the unit. The exponents of the power equation are chosen as $\alpha = 0.7$ and $\beta = 0.3$ according to EN 1996-1-1 (2012).

Option 1: $$f_{\mathrm{ma},i} = K_{\mathrm{prob}} \; f_{\mathrm{b},i}^{0.7} \; \min\left(f_{\mathrm{j},i}, \frac{f_{\mathrm{j},j} + f_{\mathrm{j},k}}{2} \right)^{0.3} \qquad \textit{Eq. 6-19}$$

Option 2: $$f_{\mathrm{ma},i} = K_{\mathrm{prob}} \; f_{\mathrm{b},i}^{0.7} \left(\frac{f_{\mathrm{j},i} + \frac{f_{\mathrm{j},j} + f_{\mathrm{j},k}}{2}}{2} \right)^{0.3} \qquad \textit{Eq. 6-20}$$

where K_{prob} is the parameter of the power equation suitable for probabilistic purposes (see Section 3.5.4). According to Options 1 and 2, the mortar strength value of one particular mortar joint section is considered to determine the compressive strength of the "unit" above and the "units" below. Thereby, a correlation is created between these "units", which is not considered in the other parameter studies. The approach of directly assigning masonry strengths to the "units", as followed in the reference case in Section 6.3.2 and all further parameter studies, is mathematically equal to a third option. In this option, only the mortar strength value underneath the respective unit is considered in the calculation of masonry compressive strength.

Option 3: $$f_{\mathrm{ma},i} = K_{\mathrm{prob}} \; f_{\mathrm{b},i}^{0.7} \; f_{\mathrm{j},i}^{0.3} \qquad \textit{Eq. 6-21}$$

MCS according to the three options as defined by Eq. 6-19 to Eq. 6-21 are conducted for the reference wall. The same values for the mean and the CoV of unit and mortar compressive strength are selected in all options. The mean values for unit and mortar strength, $f_{\mathrm{b,m}}$ and $f_{\mathrm{j,m}}$, are chosen to obtain the same mean compressive strength $f_{\mathrm{ma,m}}$ for Option 3 as for the reference case. The results are normalised by this reference mean value $f_{\mathrm{ma,m}}$. Option 1 thus leads to a lower mean value of masonry compressive strength, which is not eliminated by the normalisation. The CoVs for mortar and unit compressive strength are set to $\upsilon_{\mathrm{b}} = \upsilon_{\mathrm{j}} = 0.4$, which results in a CoV for masonry strength of $\upsilon_{\mathrm{ma}} = 0.3$ based on the stochastic extension of Eq. 6-21.

The elastic modulus of masonry assigned to one "unit" is also determined based on the elastic moduli of the corresponding unit and the adjacent mortar joints. The random values for the elastic moduli of the unit and mortar are generated similarly to the approach described in Section 6.2.2, that is, including a correlation coefficient $\rho_{f,E} = 0.72$ and a CoV of $1.3\,\upsilon_{\mathrm{b}} = 1.3\,\upsilon_{\mathrm{j}}$. The corresponding elastic modulus of masonry is then determined based on a spring model (see Section 3.3.2). In Options 1 and 2, all of the adjacent mortar joint properties are input values for determining the elastic modulus of masonry. In Option 3, only the modulus of elasticity of the mortar joint below is used. The mean values for the elastic modulus are chosen such that the resulting modulus of elasticity for masonry corresponds to $E_{\mathrm{ma,m}} / f_{\mathrm{ma,m}} = 550$. The ratio $E_{\mathrm{b,m}} / E_{\mathrm{j,m}}$ is chosen as 2.5, which lies in a typical range for existing masonry (see Kaushik et al. 2007; Neuwald-Burg and Bohne 1999; Schubert 2010). For masonry with units of standard format NF (height 71 mm) and with standard mortar joint thickness (12 mm), this leads to a CoV υ_E for the modulus of elasticity of masonry of approximately $1.3\,\upsilon_{\mathrm{ma}}$ for Option 3 and, therefore, matches the reference approach. Based on the chosen dimensions and the selected ratio $E_{\mathrm{b,m}} / E_{\mathrm{j,m}}$, the units and mortar joints are, on average, responsible for 70 % and 30 % of the total vertical displacement, respectively.

The stochastic simulations for the three options are performed with the same seed for generating the random variables; that is, the same random properties for units and mortar joints are used. Then, these random properties are combined differently to calculate masonry compressive strength values, which are assigned to the "units". Thereby, it is avoided that statistical uncertainty dominates the obtained differences between the three options.

The results for the three different options for considering the mortar properties are given in Fig. 6-7. Regarding the mean value R_{m} and the assessment value R_{a}, Option 3 lies between the results for Options 1 and 2. The CoVs υ_R of the resulting load-bearing capacities are very close to each other, which was expected due to the small influence of the CoV of mortar compressive strength on the CoV of masonry compressive strength. Since Options

1 and 2 display a lower and upper boundary from a mechanical perspective and the results of Option 3 lie in between, Option 3 can be considered a suitable choice that yields realistic results. Option 3 is mathematically equivalent to the reference case, according to which random values for masonry properties are generated directly. This reference approach, however, is more straightforward and hence used in the subsequent parameter studies. The slight differences between Option 3 and the reference approach are due to the small statistical scatter remaining after 200 simulation runs.

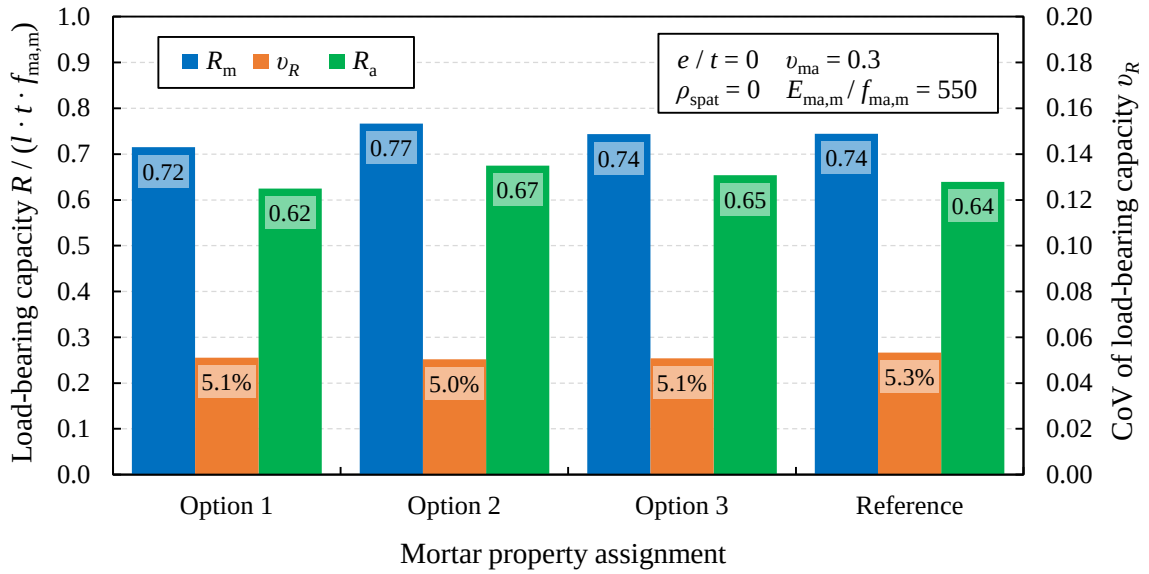

Fig. 6-7 Simulation results for different options of mortar property assignment

6.3.4 Influence of Material Variability

In this first parameter study, the influence of varying the CoV of the material properties on the resulting mean, CoV, and theoretical assessment value of the load-bearing capacity is demonstrated. Since the spatial correlation coefficient is $\rho_{spat} = 0$, the CoV of masonry compressive strength fully corresponds to unit-to-unit variability (i.e. $v_{ma} = v_{ma,spat}$). The unit-to-unit CoV for masonry compressive strength is varied between $v_{ma,spat} = 0$ and $v_{ma,spat} = 0.5$. The CoVs for the modulus of elasticity and the tensile strength of the interfaces are simultaneously varied as specified by the ratios in Table 6-1. All other parameters are the same as for the reference wall. The results are given in Fig. 6-8, where the results for the reference wall correspond to the values at $v_{ma,spat} = 0.3$. Fig. 6-9 displays load-displacement curves of the MCS for $v_{ma,spat} = 0.1$, 0.3, and 0.5. For each of these cases, the curves of 30 simulation runs are shown. The curves are truncated at their peak points.

The mean value R_m of the load-bearing capacity decreases with increasing unit-to-unit variability of masonry compressive strength. The reason for this effect is the increasing number of "units" with very low compressive strength in the walls, combined with a limited

stress redistribution capability. Concerning the theoretical assessment value R_a, the reduction in the mean value is more than compensated for by the smaller CoV v_R of the load-bearing capacity compared to the input CoV v_{ma} of masonry compressive strength. Therefore, the resulting theoretical assessment values R_a are much higher than the assessment values $R_{a,hom}$, which are calculated without considering spatial variability.

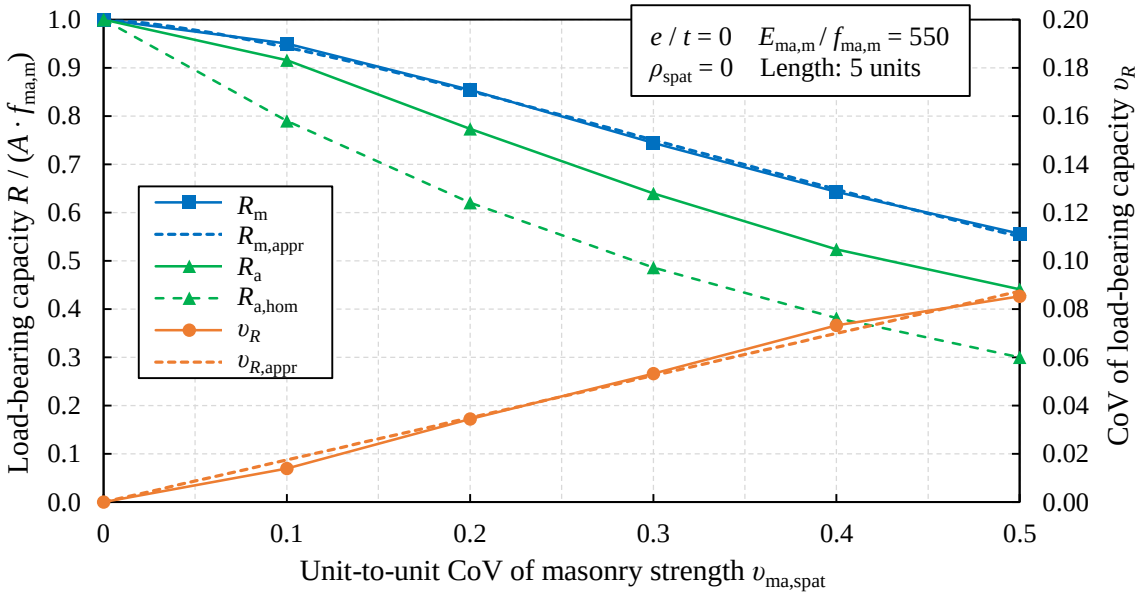

Fig. 6-8 Simulation results for varying the coefficients of variation of the material properties

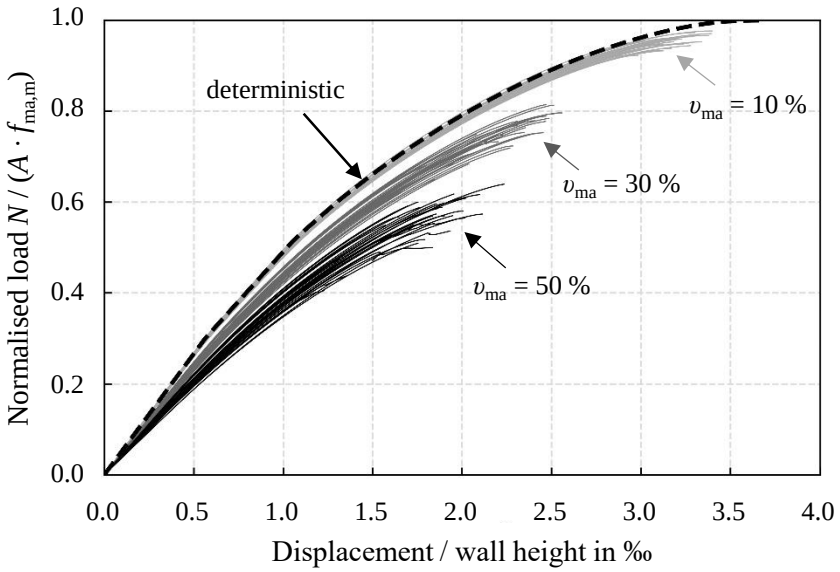

Fig. 6-9 Load-displacement curves resulting from the Monte Carlo simulations

The reduction in the mean value can be approximated by the following equation:

$$R_{\mathrm{m}} \approx R_{\mathrm{m,appr}} = R_{\mathrm{det}} \exp\left(-a\, \upsilon_{\mathrm{ma,spat}}^{b}\right) \qquad \textit{Eq. 6-22}$$

Furthermore, the CoVs $\upsilon_{R,5\%}$ and υ_R can be well approximated by linear relationships:

$$\upsilon_{R,5\%} \approx \upsilon_{R,5\%,\mathrm{appr}} = c\, \upsilon_{\mathrm{ma,spat}} \qquad \textit{Eq. 6-23}$$

$$\upsilon_R \approx \upsilon_{R,\mathrm{appr}} = d\, \upsilon_{\mathrm{ma,spat}} \qquad \textit{Eq. 6-24}$$

Utilising the method of least squares, suitable values for the parameters *a*, *b*, *c*, and *d* are found as 1.62, 1.44, 0.21, and 0.17, respectively. The approximations of R_{m} and υ_R are displayed in Fig. 6-8, demonstrating the excellent fit.

The previously presented results are also listed in Table 6-4 together with the resulting significance levels of Anderson-Darling tests for log-normal, normal, and Weibull distributions. For all investigated CoVs, the Weibull distribution is most suited for describing the resulting load-bearing capacity.

Table 6-4 Results for varying the coefficients of variation of the material properties

Unit-to-unit CoV $\upsilon_{\mathrm{ma,spat}}$	$R_{\mathrm{m}} / R_{\mathrm{det}}$	υ_R	$\upsilon_{R,5\%}$	$R_{\mathrm{a}} / R_{\mathrm{det}}$	Significance level *p*			Best fit
					Log-Normal	Normal	Weibull	
0.1	0.951	0.014	0.016	0.916	0.014	0.025	0.271	W
0.2	0.854	0.034	0.043	0.774	$4.0 \cdot 10^{-5}$	$3.6 \cdot 10^{-4}$	0.695	W
0.3	0.745	0.053	0.065	0.640	$2.3 \cdot 10^{-4}$	$4.3 \cdot 10^{-3}$	0.851	W
0.4	0.643	0.073	0.087	0.524	$3.5 \cdot 10^{-4}$	0.019	0.730	W
0.5	0.556	0.085	0.098	0.441	$1.9 \cdot 10^{-3}$	0.090	0.375	W

6.3.5 Influence of Spatial Correlation

Within the following parameter study, the spatial correlation coefficient ρ_{spat} is varied between 0 and 1. The overall CoV of masonry compressive strength is kept constant at $\upsilon_{\mathrm{ma}} = 0.3$, but the unit-to-unit CoV varies due to the different spatial correlation coefficients. For $\rho_{\mathrm{spat}} = 0$, the investigation corresponds to the reference case; that is, the unit-to-unit CoV $\upsilon_{\mathrm{ma,spat}}$ equals the total CoV υ_{ma}. In the case of $\rho_{\mathrm{spat}} = 1$, there is no spatial variability since the material properties of the "units" are perfectly correlated. Hence, the variability only consists of a variability between walls, and the CoV υ_{ma} is equal to a wall-to-wall CoV $\upsilon_{\mathrm{ma,wall}}$. Results for varying correlation coefficients ρ_{spat} are presented in Fig. 6-10 and Table 6-5. The random variables *W*, f_{w}, and E_{w} (see Section 6.2.3), which are much more influential than the random variables for the single "units", are generated using Latin hypercube sampling (LHS; see Section 2.5.3). Due to LHS, the number of simulation runs is decreased from $n = 200$ to $n = 100$ for $\rho_{\mathrm{spat}} > 0$.

For $\rho_{\mathrm{spat}} = 1$, the mean load-bearing capacity R_{m} equals the deterministically obtained load-bearing capacity R_{det}. Furthermore, the CoV of the load-bearing capacity υ_R is equal to the CoV of masonry compressive strength υ_{ma} since, due to geometrical linearity, the load-bearing capacity is proportional to masonry compressive strength, which is the only varying

material property with influence on the load-bearing capacity in the present case. For $\rho_{spat} < 1$, the "unit" properties are no longer perfectly correlated, and spatial variability is introduced. Consequently, the mean load-bearing capacity decreases due to weak spots within the wall and limited stress redistribution capability. The CoV of the load-bearing capacity also decreases since a larger share of the CoV belongs to unit-to-unit variability that is, to a certain extent, averaged out within the wall. Since the positive effect of the lower CoV dominates in the case of low spatial correlation ($\rho_{spat} < 0.5$), the theoretical assessment value is higher than for the homogeneous case. The assessment value for a homogeneous wall ($\rho_{spat} = 1$) obtained by the simulations matches the theoretical assessment value $R_{a,hom}$ determined by Eq. 6-12.

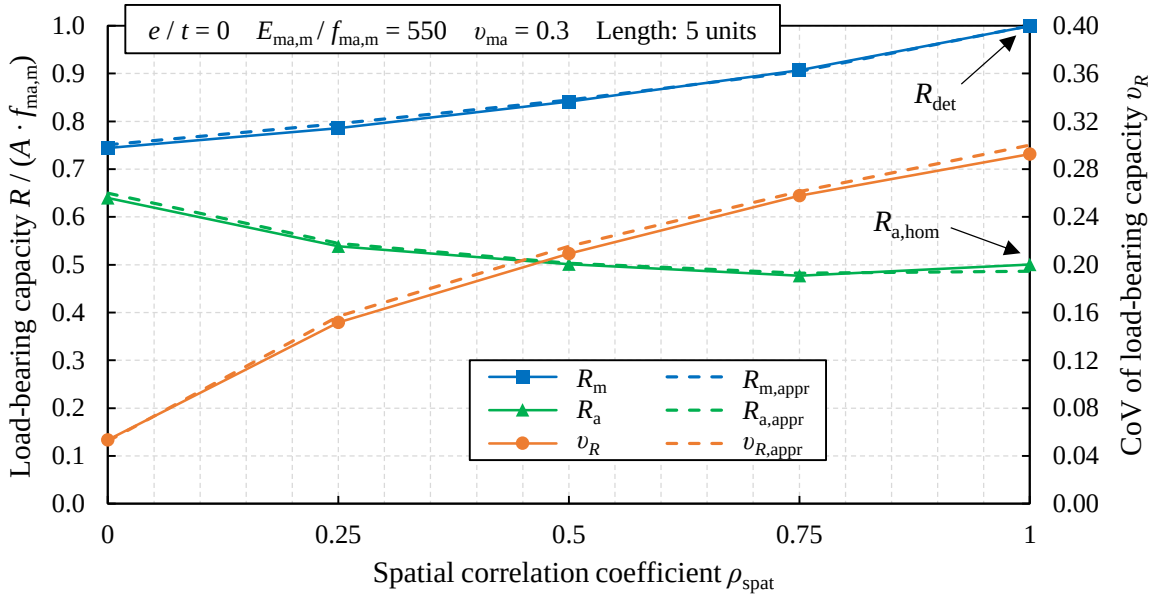

Fig. 6-10 Simulation results for varying the spatial correlation coefficient

The mean R_m and CoV υ_R of the load-bearing capacity can also be determined analytically based on the approximate relationships derived in Section 6.3.4 (see Eq. 6-22 and Eq. 6-24). For this purpose, the CoV υ_{ma} of masonry compressive strength needs to be decomposed into a unit-to-unit CoV $\upsilon_{ma,spat}$ and a wall-to-wall CoV $\upsilon_{ma,wall}$. This is achieved by the following two equations, which are based on Eq. 6-4 to Eq. 6-9 in Section 6.2.3.

$$\upsilon_{ma,wall} = \upsilon_{W \cdot f_w} = \sqrt{\upsilon_W^2 + \upsilon_{f_w}^2 + \upsilon_W^2 \, \upsilon_{f_w}^2} = \upsilon_{ma} \sqrt{\rho_{spat}} \qquad \textit{Eq. 6-25}$$

$$\upsilon_{ma,spat} = \upsilon_{U_i \cdot f_{u,i}} = \sqrt{\upsilon_{U_i}^2 + \upsilon_{f_{u,i}}^2 + \upsilon_{U_i}^2 \, \upsilon_{f_{u,i}}^2} = \upsilon_{ma} \sqrt{\frac{1 - \rho_{spat}}{1 + \rho_{spat} \, \upsilon_{ma}^2}} \qquad \textit{Eq. 6-26}$$

The reduction in the mean load-bearing capacity (see Eq. 6-22) is caused by only the spatial component $\upsilon_{ma,spat}$ of variability. In normalised form, the load-bearing capacity R can be

considered as a product of two random variables, where each of the random variables corresponds to one component of the variability (see Section 6.2.3). One random variable corresponds to a wall with $\rho_{spat} = 0$ and $\upsilon_{ma} = \upsilon_{ma,spat}$ and the other to a wall with $\rho_{spat} = 1$ and $\upsilon_{ma} = \upsilon_{ma,wall}$. Hence, based on Eq. 6-24, the CoV of the load-bearing capacity is obtained as follows:

$$\upsilon_R^2 \approx \upsilon_{R,appr}^2 = d^2\ \upsilon_{ma,spat}^2 + \upsilon_{ma,wall}^2 + d^2\ \upsilon_{ma,spat}^2\ \upsilon_{ma,wall}^2 \qquad \textit{Eq. 6-27}$$

The CoV $\upsilon_{R,5\%}$ can be obtained accordingly based on Eq. 6-23:

$$\upsilon_{R,5\%}^2 \approx \upsilon_{R,5\%,appr}^2 = c^2\ \upsilon_{ma,spat}^2 + \upsilon_{ma,wall}^2 + c^2\ \upsilon_{ma,spat}^2\ \upsilon_{ma,wall}^2 \qquad \textit{Eq. 6-28}$$

For the curves in Fig. 6-10, the parameters c and d are set to $c = 0.21$ and $d = 0.17$, as obtained in Section 6.3.4. Based on R_m from Eq. 6-22 and $\upsilon_{R,5\%}$ from Eq. 6-28, the theoretical assessment value can be determined by Eq. 6-11. The analytically determined results are also displayed in Fig. 6-10 and excellently match the simulation results. As the results for $\rho_{spat} > 0$ can be obtained analytically by decomposing variability into a unit-to-unit and a wall-to-wall component, the following parameter studies are only conducted for $\rho_{spat} = 0$.

The wall-to-wall component of the variability of strength, given by $\upsilon_{ma,wall}$, directly leads to the same amount of variability in the load-bearing capacity, as this component of the CoV is not reduced by stress redistribution (see Eq. 6-27). Therefore, the wall-to-wall variability dominates the total variability of the resistance in the considered cases with $\rho_{spat} > 0.25$. Consequently, the best-suited distribution type corresponds to the input distribution type for masonry compressive strength. These considerations are supported by the results of Anderson-Darling tests in Table 6-5, demonstrating that the log-normal distribution type provides the best fit for $\rho_{spat} > 0.25$.

Table 6-5 Results for varying spatial correlation coefficient

Correlation coefficient ρ_{spat}	R_m / R_{det}	υ_R	$\upsilon_{R,5\%}$	R_a / R_{det}	Significance level p			Best fit
					Log-Normal	Normal	Weibull	
0.00	0.745	0.053	0.065	0.640	$2.3 \cdot 10^{-4}$	$4.3 \cdot 10^{-3}$	0.851	W
0.25	0.786	0.152	0.159	0.538	0.586	0.620	0.017	N
0.50	0.841	0.209	0.217	0.501	0.617	0.382	0.010	LN
0.75	0.907	0.258	0.268	0.477	0.759	0.192	$8.2 \cdot 10^{-3}$	LN
1.00	0.999	0.293	0.288	0.500	0.733	0.024	$3.3 \cdot 10^{-3}$	LN

Fig. 6-11 displays EDFs of the simulation results together with the CDFs for masonry compressive strength. It is evident that the EDF of the simulation results for $\rho_{spat} = 1$ resembles the input CDF. The mean value R_m of the load-bearing capacity corresponds to the area between the vertical axis and the respective EDF. Fig. 6-11 thus also demonstrates the reduced mean value for the cases with spatial variability (i.e. cases with $\rho_{spat} < 1$). The high

steepness of the EDF for $\rho_{spat} = 0$ indicates the very low variability of the load-bearing capacity.

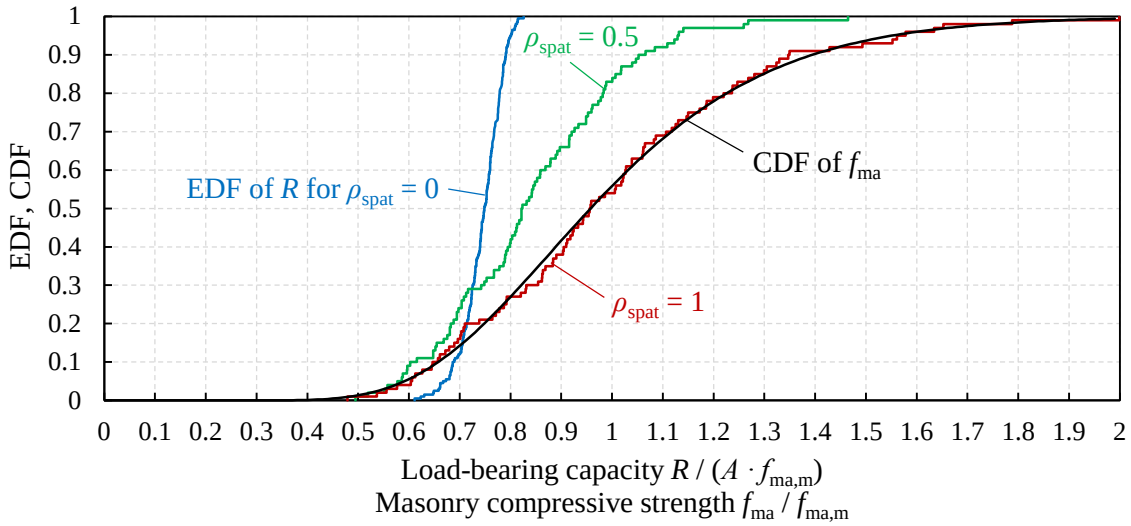

Fig. 6-11 Empirical distribution functions of the load-bearing capacity for different spatial correlation coefficients and input cumulative distribution function of masonry compressive strength

6.3.6 Influence of Wall Length

In this section, the influence of the wall length is investigated by altering the number of units per course. The investigation starts with a masonry pillar with one single, undivided unit per course; it continues with a pillar with two undivided units per course; then walls in cross bond with three, five, seven, nine, and 11 units per course are investigated (see Fig. 6-12). The wall with five units per course corresponds to the reference wall. The results are displayed in Fig. 6-13.

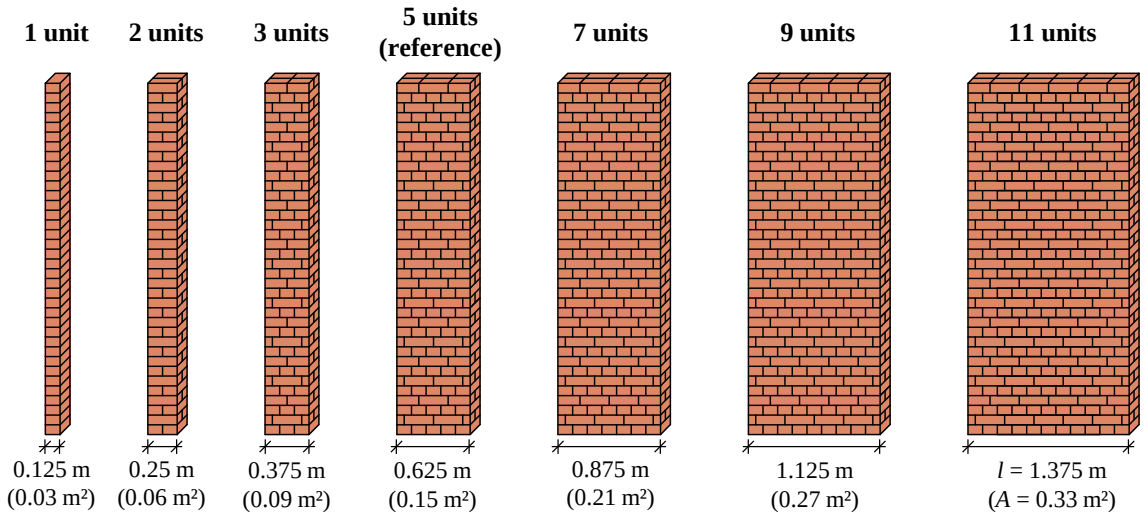

Fig. 6-12 Walls for investigating the influence of wall length

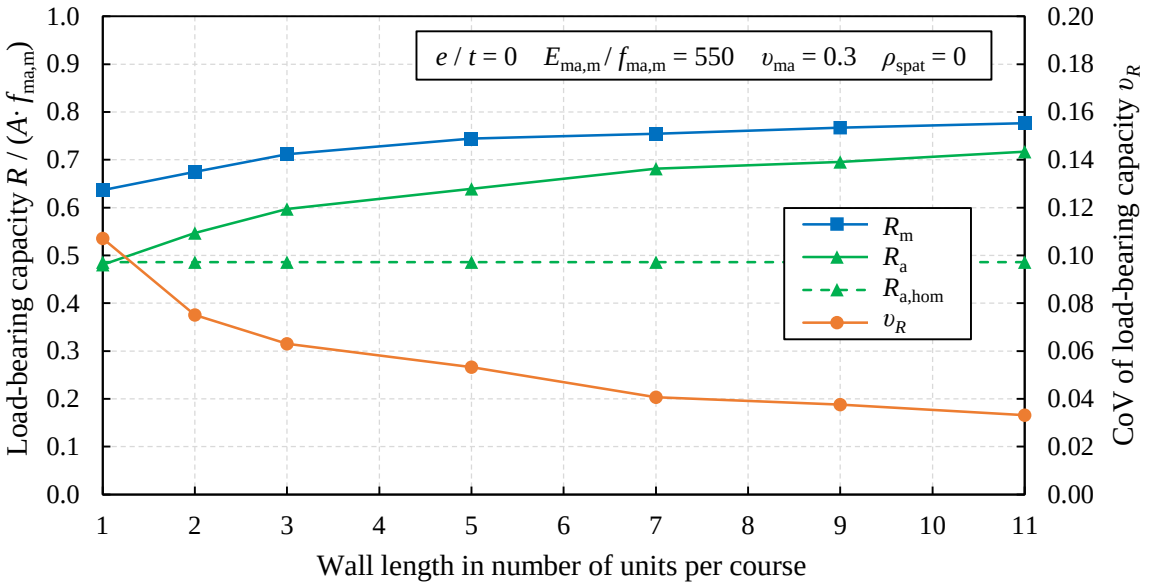

Fig. 6-13 Simulation results for varying wall length

It can be observed that the resulting mean load-bearing capacity R_m is lowest for the pillar with only one unit per course and then increases with wall length. This effect can be attributed to the higher number of units per course, which contribute to the stress redistribution when the weakest unit within the course starts to fail. For a high number of units per course, R_m appears to converge. As expected, the CoV υ_R of the load-bearing capacity decreases with higher wall length. Due to stress redistribution, the variability of the compressive strengths of the "units" is, to a certain extent, averaged out within a course. Depending on the wall length, either the Weibull or the normal distribution provide the best fit for the walls (see Table 6-6).

Table 6-6 Results for varying wall length

Units per course	R_m / R_{det}	υ_R	$\upsilon_{R,5\%}$	R_a / R_{det}	Significance level p			Best fit
					Log-Normal	Normal	Weibull	
1	0.637	0.107	0.119	0.481	0.253	0.677	$6.1 \cdot 10^{-3}$	N
2	0.675	0.075	0.089	0.547	0.257	0.542	$4.4 \cdot 10^{-3}$	N
3	0.711	0.063	0.075	0.597	0.010	0.114	0.103	N
5	0.745	0.053	0.065	0.640	$2.3 \cdot 10^{-4}$	$4.3 \cdot 10^{-3}$	0.851	W
7	0.755	0.041	0.044	0.681	0.016	0.050	0.101	W
9	0.767	0.038	0.042	0.696	0.056	0.172	$4.7 \cdot 10^{-4}$	N
11	0.777	0.033	0.034	0.717	0.019	0.063	$5.4 \cdot 10^{-3}$	N

The assessment value significantly increases with higher wall lengths. However, this effect is not captured by the assessment value $R_{a,hom}$ that is determined assuming homogeneity. In principle, the results of the parameter study thus confirm the need for a reduction factor for walls with a small cross-sectional area. In EN 1996-1-1 (2012), such a reduction factor is given for walls with cross-section area $A < 0.1$ m² as $0.7 + 3\,A$. In Chapter 8, this normative

approach for strength reduction is checked for suitability for existing solid clay brick masonry walls.

To obtain a broader basis for checking the normative reduction factor, the walls with one, two, three, and five units per course are also simulated with other CoVs of the material properties. In Fig. 6-14, the mean load-bearing capacity R_m and the resulting CoV v_R of the load-bearing capacity are shown for varying unit-to-unit CoVs $v_{ma,spat}$ of masonry compressive strength. The results display the same effects as presented before: a stronger reduction of the mean load-bearing capacity R_m and a higher CoV v_R if there is an increase in the unit-to-unit CoV $v_{ma,spat}$ or a decrease in wall length.

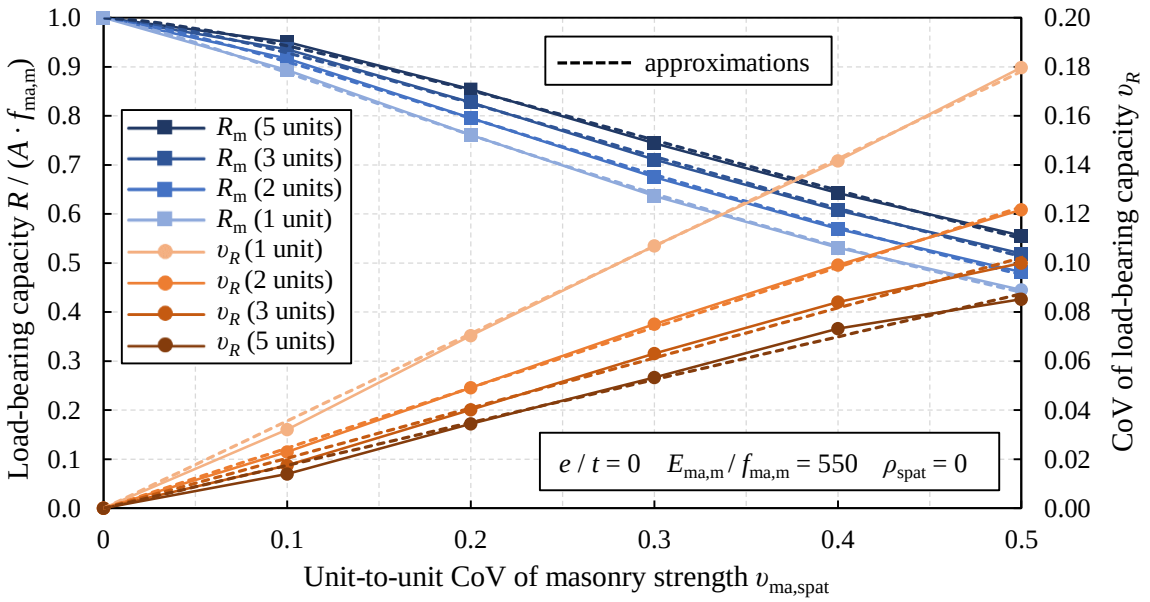

Fig. 6-14 Simulation results for varying coefficients of variation of the material properties and different wall lengths

Approximate equations for R_m and v_R depending on $v_{ma,spat}$, as given by Eq. 6-22, Eq. 6-23, and Eq. 6-24 for a wall length of five units per course, can also be derived for shorter walls based on the simulation results. Suitable values for the parameters *a*, *b*, *c*, and *d*, which are obtained by the method of least squares, can be found in Table 6-7. The approximations are also displayed in Fig. 6-14, demonstrating the excellent fit of the approximations.

Table 6-7 Parameter values for the approximate equations

Units per course	*a*	*b*	*c*	*d*
1	1.89	1.20	0.39	0.36
2	1.80	1.28	0.28	0.25
3	1.71	1.36	0.24	0.20
5	1.62	1.44	0.21	0.17

6.3.7 Influence of Slenderness

In the following parameter study, the slenderness of the investigated wall is varied and geometrical nonlinearity is considered. Thereby, the transition between material failure and stability failure is investigated. For a definition of the two failure modes, see Section 3.3.3. In the following, material-related slenderness λ is defined according to Glock (2004):

$$\lambda = \frac{h_{\mathrm{ef}}}{t}\sqrt{\varepsilon_{f,\mathrm{m}}} = \frac{h_{\mathrm{ef}}}{t}\sqrt{k\,\frac{f_{\mathrm{ma,m}}}{E_{\mathrm{ma,m}}}} \qquad \textit{Eq. 6-29}$$

where $\varepsilon_{f,\mathrm{m}}$ is the total strain at peak stress (based on the mean of f_{ma} and E_{ma}), k is the stress-strain parameter (defined as the ratio between total and elastic strain at peak stress), and h_{ef} is the effective height (i.e. buckling length) of the wall. To avoid the influence of altered unit dimensions or an increased number of units when changing the height h or thickness t of the wall, slenderness λ is varied by modifying the ratio $E_{\mathrm{ma,m}} / f_{\mathrm{ma,m}}$ of the elastic modulus to the compressive strength of masonry. First, the finite element simulations are performed assuming geometrically linearity, which corresponds to $\lambda = 0$. Then, $E_{\mathrm{ma,m}} / f_{\mathrm{ma,m}}$ is varied between 10,000 and 75. It should be noted that particularly ratios in the upper range do not represent realistic values; in reality, low slenderness also results from high wall thickness or low wall height. However, to investigate the pure effect of the transition between material and stability failure, the approach of not modifying the number or dimensions of the units but only the ratio $E_{\mathrm{ma,m}} / f_{\mathrm{ma,m}}$ is chosen here. The effective wall height h_{ef} is equal to the wall height h itself since the support at top and bottom is modelled as pinned. The eccentricity is selected as $e = 0.1\ t$ at top and bottom to create an initial eccentricity that is then increased by second-order effects at mid-height.

Fig. 6-15 shows the results of the MCS for varying wall slenderness. In addition to the mean load-bearing capacity R_{m}, the theoretical assessment values R_{a} and $R_{\mathrm{a,hom}}$, and the CoV of the load-bearing capacity v_R, the deterministic load-bearing capacity R_{det} based on a simulation with mean material properties is provided. In Fig. 6-16, the same results are displayed; however, the load-bearing capacities are related to the deterministic load-bearing capacity R_{det}. In the MCS with spatially variable material properties, the transition between material and stability failure cannot be distinctly defined in terms of a particular slenderness λ. This is because, depending on the realisations of the random material properties in a simulation run, both failure modes can occur in the transitional region between material and stability failure.

It can be observed that, at first, the ratio $R_{\mathrm{m}} / R_{\mathrm{det}}$ increases and v_R decreases when the slenderness of the wall gets higher. This trend stops at $\lambda \approx 1$, from where the curves for $R_{\mathrm{m}} / R_{\mathrm{det}}$ and v_R continue approximately horizontally. The reason for this development of the curves lies in the transition between material and stability failure. At $\lambda = 0$, no second-order effects are present, and the load-bearing capacity is primarily influenced by compressive strength.

With higher slenderness, the initial first-order eccentricity e_I is increased by an additional eccentricity Δe_{II} due to second-order effects. This additional eccentricity Δe_{II} depends on the bending stiffness of the wall and therefore is a function of the moduli of elasticity within the wall. Hence, both the compressive strength f_{ma} and the modulus of elasticity E_{ma} influence the load-bearing capacity. If the compressive strength f_{ma} is unusually low due to randomness, the effective ratio E_{ma} / f_{ma} is higher, leading to a lower effective material-related slenderness λ, which partly compensates for the low compressive strength. This results in the observed decrease in v_R and the increase in R_m / R_{det} when slenderness increases.

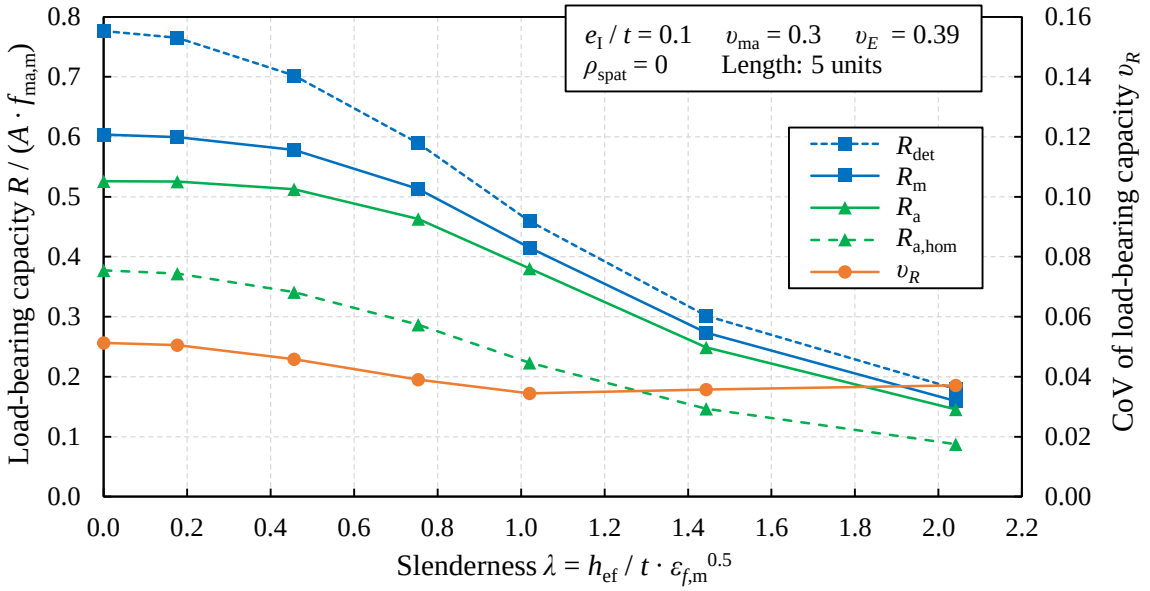

Fig. 6-15 Simulation results for varying wall slenderness

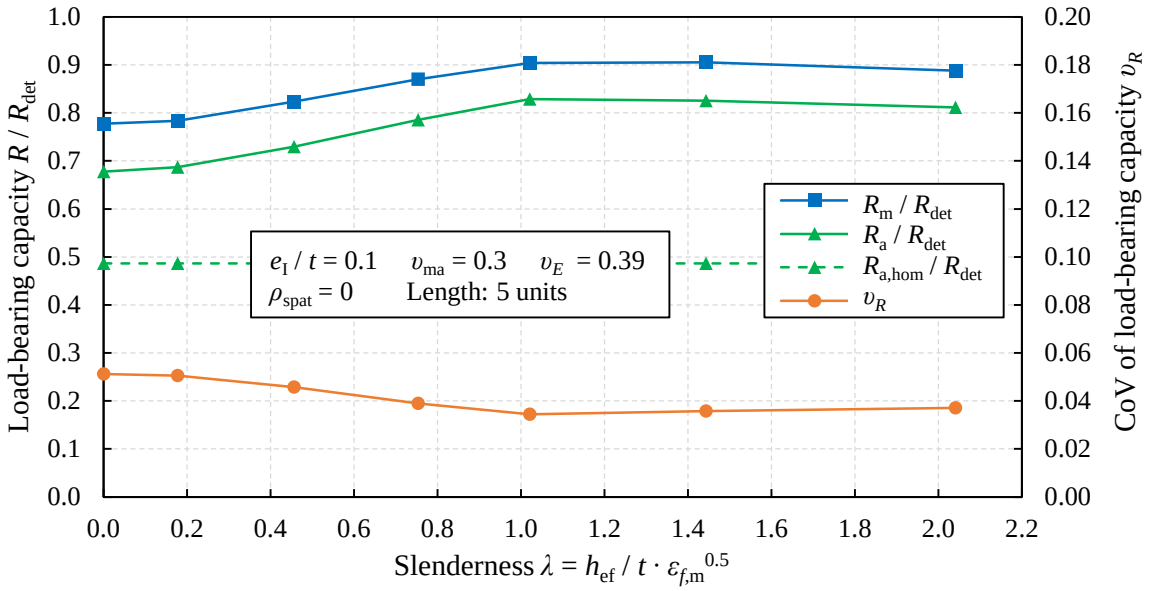

Fig. 6-16 Simulation results for varying wall slenderness (load-bearing capacity related to the result of a deterministic simulation)

For high slenderness λ, all walls fail due to buckling. In this case, the load-bearing capacity R_{buckling} depends on the bending stiffness of the wall and, hence, on the elastic moduli E_{ma} of the "units". Since the compressive strength f_{ma} does not influence the load-bearing capacity in the case of high slenderness, the ratio $E_{\text{ma,m}} / f_{\text{ma,m}}$ no longer affects the relative load-bearing capacity R / R_{det}. As a result, the curves in Fig. 6-16 become almost horizontal for high slenderness. The slight deviation from a horizontal line is caused by the fact that the flexural tensile strength f_{t}, which has a high CoV, gains influence for very high slenderness (see Section 3.3.3).

If f_{t} is neglected, the overall bending stiffness and, therefore, the load-bearing capacity R_{buckling} in the case of stability failure is proportional to an effective modulus of elasticity $E_{\text{ma,eff}}$ of the wall, which is a function of the spatially variable elastic moduli of the "units". In this context, $E_{\text{ma,eff}}$ is defined as the elastic modulus for a homogeneous wall, whose buckling load equals that of the wall with spatially varying material properties. Buckling is caused by a displacement of the wall out of its original plane. This displacement can be determined by double integration of the curvature over the wall height. Since the curvature is inversely proportional to the modulus of elasticity at the respective location, the effective modulus of elasticity can be approximately described by a weighted harmonic mean of the elastic moduli $E_{\text{ma,course},i}$ of the single courses:

$$R_{\text{buckling}} \sim E_{\text{ma,eff}} = \frac{n}{\sum_{i=1}^{n} w_i \frac{1}{E_{\text{ma,course},i}}} \qquad \textit{Eq. 6-30}$$

The selection of suitable weights w_i, which depend on the moment distribution, is not considered here. Eq. 6-30 only serves the purpose of interpreting the results next.

In the case of material failure, single weak "units" can lead to failure of the whole wall if there are no adjacent stronger "units" that enable stress redistribution. This issue causes a reduction of the mean load-bearing capacity R_{m} compared to a homogeneous wall. For walls failing due to buckling, this consideration is not valid since it is no longer the material strength but the stiffness that is relevant. However, it can be observed that the ratio $R_{\text{m}} / R_{\text{det}}$ does not converge to one. Eq. 6-30 delivers the corresponding explanation: The harmonic mean is always smaller than the arithmetic mean if at least one value differs from the others. Thus, the expectation R_{m} of the load-bearing capacity is smaller than the deterministic load-bearing capacity R_{det} calculated based on mean material properties. Nevertheless, the ratio $R_{\text{m}} / R_{\text{det}}$ remains higher than for the walls with material failure.

Based on these considerations, walls failing due to either material failure or buckling can be compared to the idealised systems from Section 2.5.5. A wall failing due to material failure is closer to a series system since single weak "units" initiate the failure. In contrast, a wall failing due to buckling is closer to a parallel system since the load-bearing capacity

depends on the overall stiffness of the wall, which does not differ greatly from an average of the stiffnesses of the single "units" within the wall.

The results of the parameter study are also displayed in Table 6-8. In addition to the results presented before, the goodness-of-fit of the log-normal, normal, and Weibull distribution is shown. For the investigated cases, either the Weibull or the normal distribution provides the best fit.

Table 6-8 Results for varying slenderness

$E_{ma,m}$ / $f_{ma,m}$	λ	R_m / R_{det}	v_R	$v_{R,5\%}$	R_a / R_{det}	Significance level p			Best fit
						Log-Normal	Normal	Weibull	
Geometrically linear		0.777	0.051	0.059	0.678	$7.9 \cdot 10^{-3}$	0.055	0.057	W
10,000	0.18	0.784	0.051	0.056	0.687	0.012	0.069	0.037	N
1,500	0.46	0.823	0.046	0.052	0.730	$2.8 \cdot 10^{-3}$	0.015	0.163	W
550	0.75	0.872	0.039	0.044	0.786	$3.2 \cdot 10^{-3}$	0.012	0.156	W
300	1.02	0.904	0.034	0.037	0.829	0.468	0.639	$1.6 \cdot 10^{-3}$	N
150	1.44	0.905	0.036	0.040	0.825	0.381	0.583	$3.6 \cdot 10^{-3}$	N
75	2.04	0.888	0.037	0.039	0.811	0.278	0.475	$8.3 \cdot 10^{-3}$	N

To derive approximate functions for the relationship between R_m and $v_{ma,spat}$ as well as between v_R and $v_{ma,spat}$ that are suitable for walls failing due to buckling, the previously investigated wall with $E_{ma,m} / f_{ma,m} = 150$ is also simulated for different unit-to-unit CoVs of the material properties. Approximate relationships can then be formulated equivalently to those defined in Section 6.3.4 for the reference wall with varying CoVs (see Eq. 6-22 to Eq. 6-24). Utilising the method of least squares, suitable parameter values are found to be $a = 0.92$, $b = 1.86$, $c = 0.13$, and $d = 0.12$. The resulting approximate values $R_{m,appr}$ and $v_{R,appr}$ excellently match the simulation results, as demonstrated by Fig. 6-17.

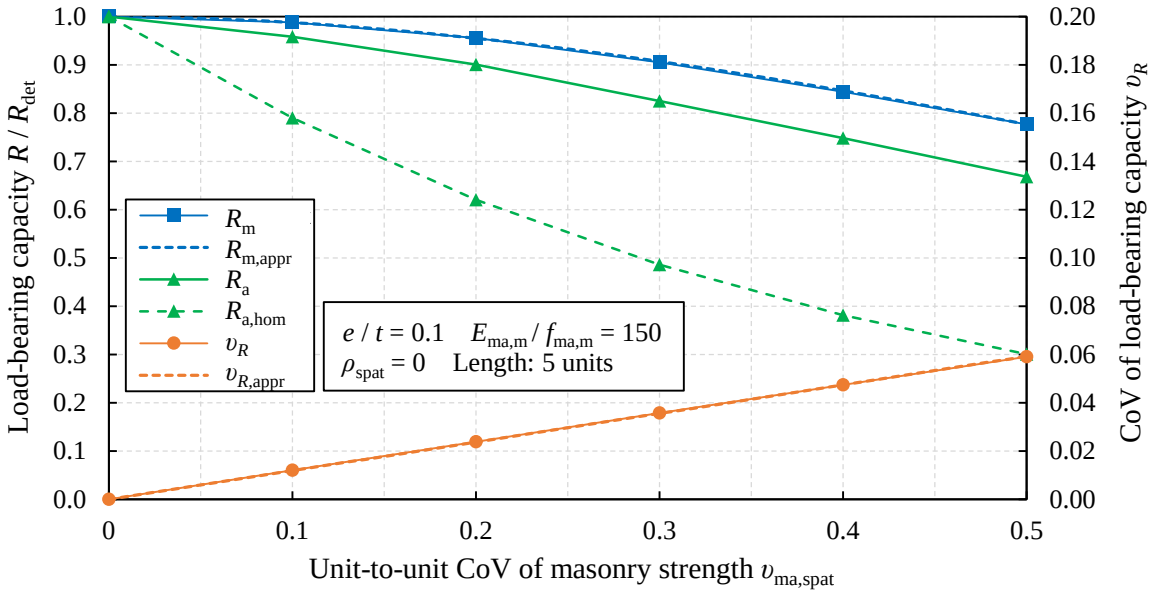

Fig. 6-17 Simulation results for a slender wall and varying coefficients of variation of the material properties

6.3.8 Influence of Load Eccentricity

No eccentricity of the compression loading is considered in the investigation of the reference wall. Therefore, the following parameter study is conducted to investigate the influence of load eccentricity on the probability distribution of the load-bearing capacity. Three different cases are examined. In the first case, the eccentricity of the compression loading at the top and bottom is the same, and the simulations are conducted without considering geometrical nonlinearity. Hence, the resulting bending moment is constant over the wall height (see Fig. 6-18). The second case is equal to the first case, but the simulations are conducted considering geometrical nonlinearity. Finally, in a third case conducted without considering geometrical nonlinearity, the bottom eccentricity is contrary to the eccentricity at the top. Hence, the moment distribution along the wall height is not constant but linear, with the same absolute value at top and bottom (i.e. $e_{top} = -e_{bottom}$). This case is important for engineering practice, as contrary moments at the top and bottom of a wall are usually induced by the rotation of the adjacent slabs; see Annex C of EN 1996-1-1 (2012).

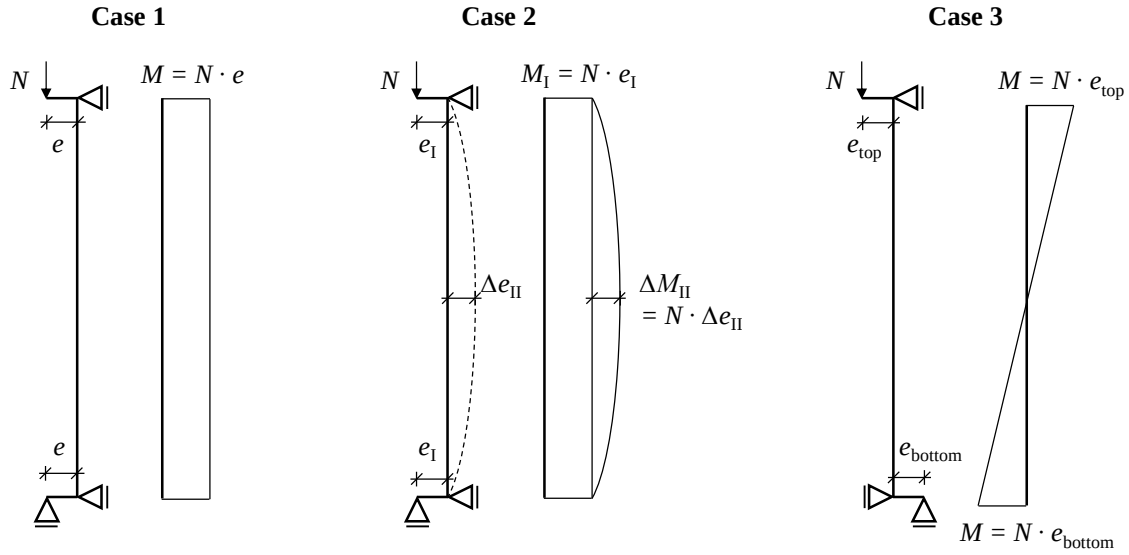

Fig. 6-18 Structural systems of the three investigated cases

The results of the parameter study are displayed in Fig. 6-19. All results for the mean load-bearing capacity R_m and the assessment load-bearing capacity R_a are given in relation to the deterministic load-bearing capacity R_{det}, which is obtained in a simulation with mean material properties. In the determination of R_{det} for the geometrically nonlinear case, a very small initial first order eccentricity of $e_I / t = 0.0005$ is applied. This small eccentricity is negligible in a geometrical linear simulation but is required for the development of the second-order moment in the geometrically nonlinear case.

Fig. 6-19 shows that an eccentricity of $e / t = 0$ leads to the lowest ratios R_m / R_{det}. This effect can be explained by the resulting stress distribution within a cross-section. For

$e / t = 0$, the stress is uniformly distributed over the cross-section. Therefore, the compressive strength of a weak "unit" is reached at all points of its cross-section simultaneously. As a result, the stresses acting on the whole area of this "unit" start to decline and have to be redistributed to other "units". In contrast, the compressive stress increases towards the more compressed edge for $e / t > 0$. Hence, the compressive strength of a weak "unit" is only reached locally in this case, and the force that has to be redistributed to other "units" is smaller. The stress in the remaining area of the weak "unit" can still be increased. As a result, the relative decrease in the mean load-bearing capacity R_m caused by spatial variability is smaller for $e / t > 0$. In the geometrically linear case with constant eccentricity, the CoV v_R is approximately constant for varying eccentricity. Consequently, the relative assessment load-bearing capacity R_a / R_{det} is higher if the load is applied with eccentricity.

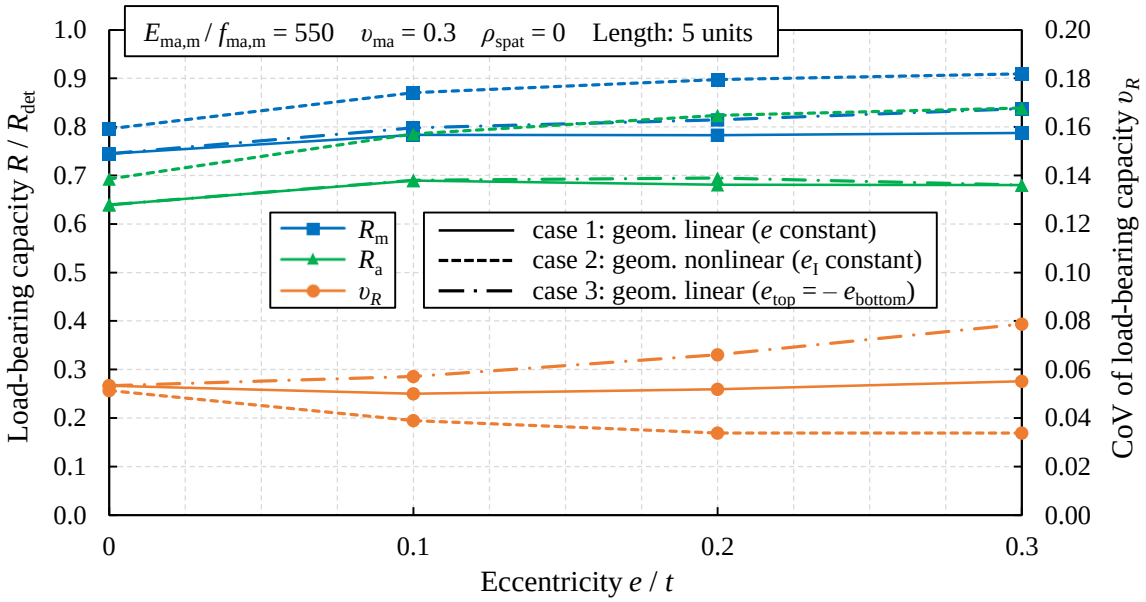

Fig. 6-19 Simulation results for varying load eccentricity

Comparing the geometrically nonlinear case with the geometrically linear case shows that geometrical nonlinearity leads to higher ratios R_m / R_{det}, lower CoVs v_R, and, thus, higher ratios R_a / R_{det}. This effect is identical to the positive effect for increasing slenderness that was observed in Section 6.3.7. With increasing eccentricity, the difference between the geometrically linear and nonlinear case grows. This is due to the growing influence of second-order effects for walls with greater eccentricity, which leads to a transition between material and stability failure at lower slenderness λ (see Glock 2004).

In the third case with contrary eccentricity at the top and bottom ($e_{top} = - e_{bottom}$), the ratio R_m / R_{det} is higher than for the first case with constant eccentricity. If the moment distribution is linear over the wall height and eccentricity is increased, the parts of the wall that are relevant for the load-bearing capacity become smaller. This is because the cross-section at mid-height is almost only subjected to a compressive force, whereas the same compressive

force is accompanied by a moment at the top and bottom (see Fig. 6-18). Therefore, only the strength in the upper and lower part of the wall is critical. As the probability of extraordinarily weak "units" within this smaller region is lower than within the whole wall, R_m / R_{det} is higher for a linear than for a constant moment distribution. This effect is accompanied by an increase in the CoV v_R since a lower number of "units" is effectively involved, and a lower number of elements usually increases the CoV of the load-bearing capacity of a structural system (see Section 2.5.5).

Comparing the relative assessment values R_a / R_{det} for all three cases and varying eccentricity shows that the reference case (e / t = 0, geometrically linear) is the most critical. The choice of geometrical linearity and no eccentricity for the reference case is hence appropriate for making generally valid, conservative statements regarding the effect of spatially variable material properties on the load-bearing capacity of solid clay brick masonry walls.

It is pointed out that no spatial variability of the material properties within a single unit is considered in the present investigations. However, spatial variability at this lower level can influence the probability distribution for the load-bearing capacity of walls with high eccentricity since only a part of the cross-section is subjected to high compressive stress in this case. This limitation of the stochastic model confirms that the results for walls without eccentricity are most appropriate for further developing a method for assessing existing masonry walls.

The previously presented results and the results of Anderson-Darling tests for goodness-of-fit are displayed in Table 6-9. Depending on the specific case, either the Weibull or the normal distribution is the most appropriate distribution type.

Table 6-9 Results for varying eccentricity

Case	Eccentricity e / t	R_m / R_{det}	v_R	$v_{R,5\%}$	R_a / R_{det}	Significance level p			Best fit
						Log-Normal	Normal	Weibull	
1: constant eccentricity, geometrically linear	0	0.745	0.053	0.065	0.640	$2.3 \cdot 10^{-4}$	$4.3 \cdot 10^{-3}$	0.851	W
	0.1	0.784	0.050	0.055	0.689	$1.2 \cdot 10^{-3}$	$9.1 \cdot 10^{-3}$	0.125	W
	0.2	0.783	0.052	0.060	0.681	0.023	0.112	0.060	N
	0.3	0.788	0.055	0.063	0.680	$6.1 \cdot 10^{-3}$	0.040	0.170	W
2: constant eccentricity, geometrically nonlinear	0	0.796	0.051	0.060	0.693	$1.2 \cdot 10^{-5}$	$1.8 \cdot 10^{-4}$	0.199	W
	0.1	0.870	0.039	0.044	0.786	$3.2 \cdot 10^{-3}$	0.012	0.156	W
	0.2	0.898	0.034	0.037	0.824	0.470	0.655	$8.3 \cdot 10^{-3}$	N
	0.3	0.909	0.034	0.035	0.839	0.388	0.523	$2.6 \cdot 10^{-4}$	N
3: contrary eccentricity, geometrically linear	0	0.745	0.053	0.065	0.640	$2.3 \cdot 10^{-4}$	$4.3 \cdot 10^{-3}$	0.851	W
	0.1	0.798	0.057	0.062	0.690	0.014	0.101	0.291	W
	0.2	0.815	0.066	0.068	0.695	0.101	0.386	0.041	N
	0.3	0.838	0.079	0.089	0.680	0.134	0.521	0.030	N

6.3.9 Influence of Masonry Bond

Since mainly masonry walls arranged in cross bond are investigated in the previous parameter studies, simulation results for a single wythe masonry wall are compared to those for the cross-bonded reference wall here. Except for the bond type, the investigated single wythe masonry wall is identical to the reference wall: It also has 36 courses with five units per course and is investigated without considering geometrical nonlinearity and without load eccentricity. It should be noted that the comparison focuses on the influence of spatial variability and does not aim at making statements about the general, deterministic effect of the bond type on masonry strength. As before, the results for the load-bearing capacity are related to the corresponding mean masonry compressive strength $f_{ma,m}$, which, in the case of the wall in cross bond, already includes a reduction compared to the compressive strength for single wythe masonry (see Section 3.5.3). The results are displayed in Fig. 6-20.

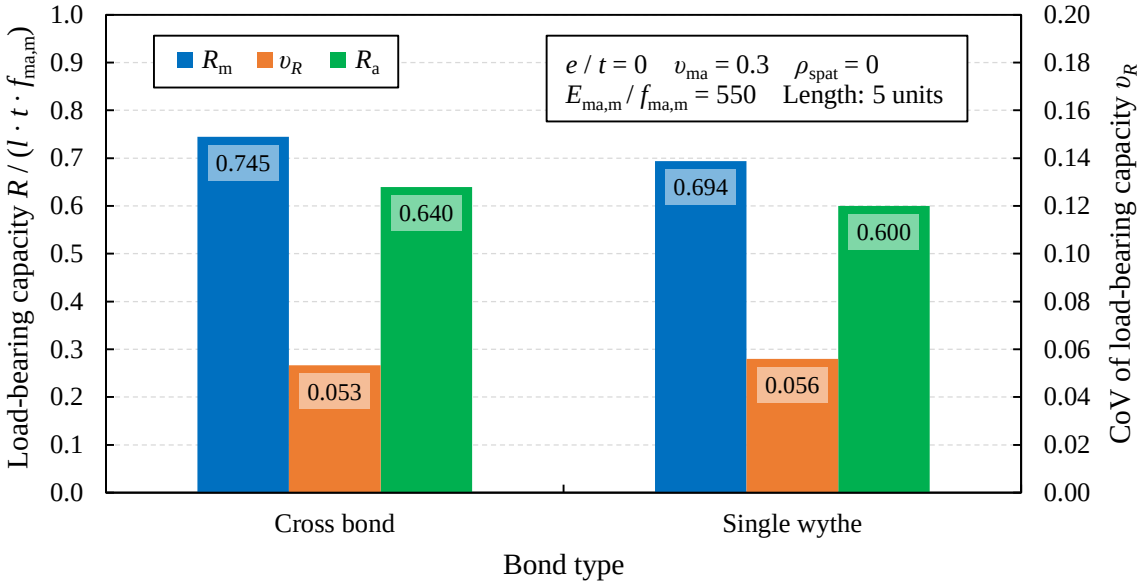

Fig. 6-20 Simulation results for cross bonded and single wythe masonry walls

The influence of spatially variable material properties is slightly more critical for the single wythe masonry wall, which is mainly due to the lower mean load-bearing capacity R_m. Although both walls contain five units per course, the wall arranged in cross bond possesses a higher stress redistribution capability since the cross-section is more compact than the cross-section of the single wythe wall. Thus, each "unit" has more adjacent "units" to which stresses can be redistributed easily. For bonded masonry walls with a thickness of more than two unit widths, it is expected that the stress redistribution capability is further increased since the cross-section is even more compact. Despite the more critical behaviour of single wythe walls, the wall in cross bond is a more appropriate reference case for developing an assessment procedure since existing solid clay brick masonry is very rarely constructed as single wythe masonry.

6.3.10 Influence of Unit Format

The previous parameter studies are conducted based on unit dimensions according to the German standard format NF. Within this last parameter study, the unit format is varied. Thereby, the combined influence of the unit number and dimensions resulting from the selected unit format is investigated. Since units with larger dimensions are usually used for constructing single wythe masonry, the investigated wall in this parameter study is a single wythe masonry wall. No eccentricity of the compression load is considered, and the simulations are conducted without considering geometrical nonlinearity. The wall height is equal to the reference wall (h = 3 m), the length is l = 1 m, and the thickness is determined by a unit width of 0.115 m. Based on these constant overall dimensions, the number of units within the wall is varied by changing the unit dimensions (see Fig. 6-21). The selected dimensions correspond to the standardised unit dimensions DF, NF, 2 DF, 4 DF, and 8 DF according to DIN 20000-401 (2017). The selected unit dimensions result in the following unit numbers (vertical x longitudinal direction): 48 x 4, 36 x 4, 24 x 4, 12 x 4, and 12 x 2.

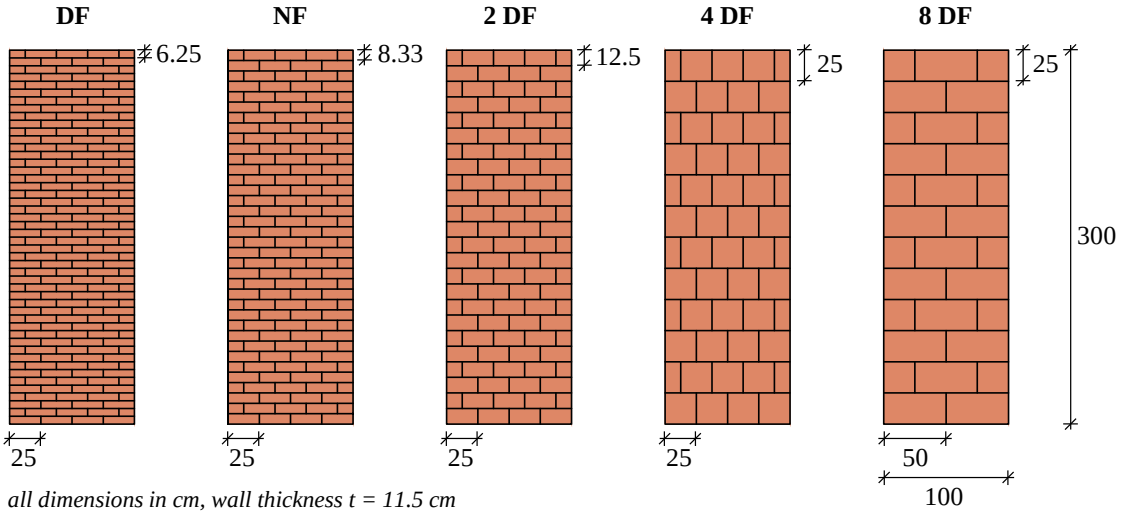

Fig. 6-21 Dimensions of the expanded units and resulting wall arrangement for investigating the influence of the unit format

The number of finite elements per "unit" with format NF is chosen as in the reference wall. When the "unit" dimensions are changed, the element size is kept constant, which leads to a constant total number of elements within the wall, but a varying number of elements per "unit". Consequently, the compressive fracture energy G_{fc}, which results from the stress-strain distribution and the equivalent element length (see Eq. 5-8), is not changed within this parameter study, as the element size is constant.

From Fig. 6-22, it is evident that the resulting mean load-bearing capacity R_m is not very sensitive to the unit format. A higher number of units leads to more potential weak spots within the wall. However, this effect is compensated for by a better stress redistribution capability, as more "units" are engaged in stress redistribution. Furthermore, the positive

effect due to the restraint of weaker “units” by adjacent stronger “units” above and below and the resulting multi-axial compression state is more significant for “units” with a lower height. This compensates for the higher number of potential weak spots in the vertical direction. As a result, there is a slight tendency for the mean load-bearing capacity to decrease with an increase in the unit dimensions.

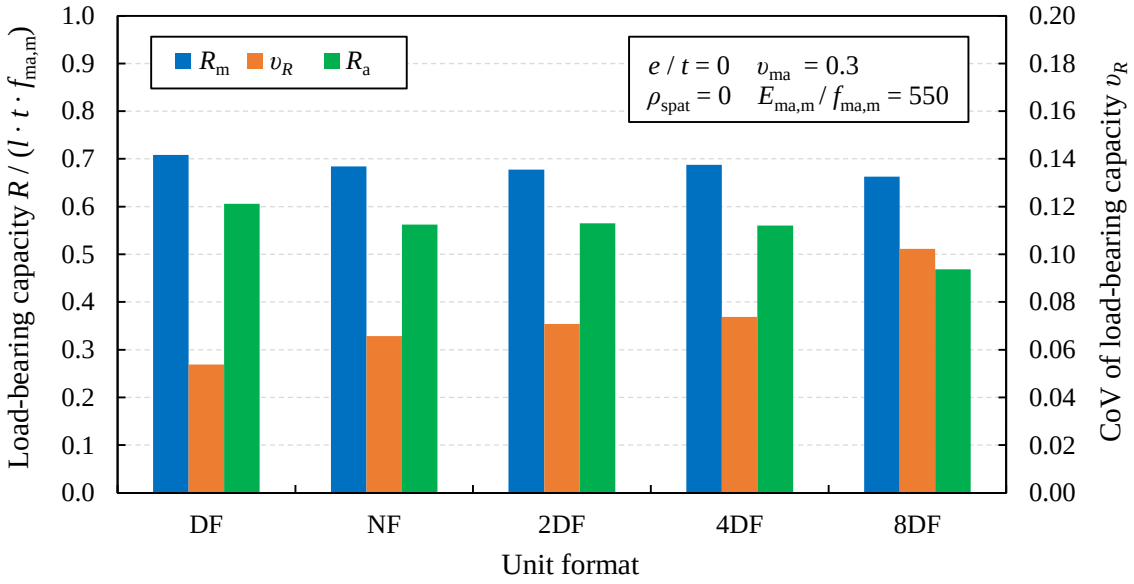

Fig. 6-22 Simulation results for varying unit dimensions

Concerning the CoV v_R of the load-bearing capacity, an increasing trend is evident for a decreasing number of units in the wall. This effect is very common for the load-bearing capacity of structural systems (see Section 2.5.5). As a result of the influence of the unit dimensions on R_m and v_R, the assessment values R_a slightly decrease with increasing unit dimensions. Therefore, small brick dimensions, which are typical for historical solid clay brick masonry, are beneficial for the theoretical assessment value of masonry compressive strength and the resulting reliability of the masonry wall.

Since the results are not strongly sensitive to the unit format, the conclusions for bricks with German standard format NF can be considered valid also for slightly different formats. The findings are thus considered applicable for all typical historical formats of small-sized solid clay bricks, such as the *Reichsformat* (see Section 3.2).

6.4 Summary

In this chapter, extensive investigations of the influence of spatially variable material properties on the load-bearing capacity of solid clay brick masonry walls under compression were carried out. In the investigations, the spatial variability of the compressive strength, modulus of elasticity, and flexural tensile strength of masonry was modelled as unit-to-unit variability. The developed procedure for generating random material properties enables

modelling correlation between the compressive strength and the modulus of elasticity and spatial correlation between the compressive strengths and moduli of elasticity at different units within the wall. Monte Carlo simulations utilising the finite element model presented in Chapter 5 were performed for various boundary conditions to quantify the influence of particular parameters on the probability distribution of the load-bearing capacity. The following conclusions can be drawn from the parameter studies:

- With increasing spatial variability of the material properties within the wall, the mean load-bearing capacity R_m decreases. An approximate equation was found to describe this relationship (see Eq. 6-22). However, the CoV v_R of the resulting load-bearing capacity is much smaller than the input CoV of the spatially variable material properties. The relationship between v_R and the CoV $v_{ma,spat}$ of spatially variable masonry compressive strength can be approximately described by Eq. 6-24.
- Long walls perform better than short walls if material properties are spatially variable, which is reflected in a higher normalised mean load-bearing capacity R_m and a lower CoV v_R of the load-bearing capacity. In principle, this influence confirms the need for a reduction factor for walls with a small cross-section as defined in EN 1996-1-1 (2012).
- For walls with high slenderness, the relative reduction of the mean value R_m caused by spatially variable material properties is smaller than for walls with low slenderness, which can be explained by the influence of the different failure modes. The behaviour of walls with material failure is closer to a weakest-link behaviour since the weakest spots in the wall strongly affect the load-bearing capacity. In contrast, average material properties are more relevant for walls failing due to buckling.
- For walls with eccentric compression loading, the reduction of the mean load-bearing capacity R_m due to spatial variability is smaller than for concentrically loaded walls.
- Single wythe masonry walls are more critical with regard to spatially variable material properties than bonded walls, such as the reference wall arranged in cross bond.
- The variation of the unit dimensions demonstrated that the resulting mean load-bearing capacity R_m is not very sensitive to the unit format. However, if the unit-to-unit CoV $v_{ma,spat}$ of masonry compressive strength is constant for different unit dimensions, the resulting CoV of the load-bearing capacity v_R is smaller for a higher number of units in the wall (i.e. smaller unit dimensions).

The results provide valuable and novel insights into the effects of spatial variability on the probability distribution of the load-bearing capacity of masonry walls under compression. Furthermore, the results provide a broad basis for developing a method for determining suitable assessment values of masonry compressive strength (see Chapter 8).

7 BAYESIAN FRAMEWORK FOR STATISTICAL UNCERTAINTY AND PRIOR MODELLING

7.1 Introduction

If the results of tests on the material properties of existing masonry are used for determining characteristic values or partial factors for structural assessment, the statistical uncertainty caused by the limited number of tests has to be considered. Neither the true mean value nor the true variance of a tested material property is known with certainty, and overestimating the mean of masonry strength or underestimating its variance can lead to a dangerous misjudgement concerning the reliability of a masonry structure under assessment. The issue of statistical uncertainty is addressed by a Bayesian approach in the method developed in this thesis. By utilising Bayesian statistics, prior information from previously assessed masonry buildings can be integrated into the assessment procedure, which reduces statistical uncertainty.

In Section 7.2, the general Bayesian framework that is utilised for the method developed in Chapter 8 is presented. In the framework, prior information regarding the variability of unit and mortar compressive strength can be considered. With the aim of modelling prior information by prior probability distributions, data from tests on the material properties of existing masonry was collected and compiled in a database. In Section 7.3, the composition of the database is described in more detail and observations regarding the material properties of typical existing masonry are made. Based on the test data, prior information on the variability of unit and mortar compressive strength in existing solid clay brick masonry is modelled by prior distributions in Section 7.4. In addition, the test data is used to determine the correlation of unit strengths and of mortar strengths at a specific sampling location within a building. Furthermore, a prior for the variability of masonry compressive strength is obtained based on the priors of unit and mortar compressive strength.

7.2 Bayesian Framework

In the statistical framework, unit and mortar compressive strength are modelled by log-normal distributions. Therefore, the logarithms of unit and mortar strength, $\ln f_b$ and $\ln f_j$, are normally distributed, and the Bayesian procedures developed for normally distributed random variables can be applied. See Section 2.4 for a summary of the general principles of Bayesian statistics. In the following illustration of the Bayesian framework, the random variable X represents the logarithm of unit or mortar strength. Thus, a realisation x_i is the logarithm of a single test result for either unit or mortar compressive strength.

The general procedure for updating the probability distribution for mean μ and variance σ^2 of X is given by Bayes' theorem:

$$f''(\mu,\sigma^2 \mid \mathbf{x}) \propto L(\mu,\sigma^2 \mid \mathbf{x})\, f'(\mu,\sigma^2) \qquad \textit{Eq. 7-1}$$

where $f'(\mu, \sigma^2)$ is the prior distribution, and $f''(\mu, \sigma^2 \mid \mathbf{x})$ is the posterior distribution obtained by the update based on the vector $\mathbf{x}$ containing the observed values x_i. The likelihood L contains the information of the acquired data used for the update and is defined as the joint probability density for the occurrence of the observed values x_i:

$$\begin{aligned} L(\mu,\sigma^2 \mid \mathbf{x}) &= \prod_{i=1}^{n} f\left(x_i \mid \mu,\sigma^2\right) = \prod_{i=1}^{n} \frac{1}{\sqrt{2\pi\sigma^2}} \exp\left(-\frac{\left(x_i-\mu\right)^2}{2\sigma^2}\right) \\ &\propto \frac{1}{\sigma^n} \exp\left(-\frac{\left(n-1\right)s^2 + n\left(\mu-m\right)^2}{2\sigma^2}\right) \end{aligned} \qquad \textit{Eq. 7-2}$$

where m and s^2 are the arithmetic mean and the sample variance of the observed values, respectively, defined as

$$m = \frac{1}{n}\sum_{i=1}^{n} x_i \qquad \textit{Eq. 7-3}$$

$$s^2 = \frac{1}{n-1}\sum_{i=1}^{n}\left(x_i - m\right)^2 \qquad \textit{Eq. 7-4}$$

In the framework, the prior distribution is chosen to be non-informative regarding the mean of X but informative regarding its variance. A similar approach can be found in Caspeele and Taerwe (2012) for the assessment of concrete compressive strength. The approach is selected, as it is expected that the range of mean values for unit and mortar compressive strength is wide, but the corresponding coefficients of variation (CoVs) are in a narrower range. Due to the wide range of possible values for the mean compressive strength of unit and mortar, modelling the available prior information does not lead to prior distributions that are very informative regarding the mean value. The prior distribution for the mean neither substantially reduces the corresponding statistical uncertainty nor greatly influences the posterior probability distribution. However, it would make the methodology more complicated and would limit the general applicability. In contrast, modelling the available prior information about the variance σ^2 leads to much more informative prior distributions and, therefore, a more significant reduction of the corresponding statistical uncertainty. It is noted that the variances $\sigma_{\ln,b}^2$ and $\sigma_{\ln,j}^2$ of the logarithms of strength are entirely defined if the CoVs v_b and v_j of strength are provided since, for a given CoV of strength, the variance of the logarithm of strength does not depend on the absolute value of strength:

$$\sigma_{\ln,b}^2 = \ln\left(1+v_b^2\right) \quad \text{and} \quad \sigma_{\ln,j}^2 = \ln\left(1+v_j^2\right) \qquad \textit{Eq. 7-5}$$

Thus, prior information about the CoV of strength can be expressed by a prior distribution on the variance of the logarithm of strength.

It is decided to use a conjugate prior distribution for the variance, as this makes it possible to perform the Bayesian update analytically. Furthermore, no other distribution type appears to be naturally suited to modelling the prior information. By choosing a conjugate prior, the Bayesian update reduces to an update of the distribution parameters, which is shown in the following. In the general case of a normally distributed random variable with unknown mean μ and unknown variance σ^2, the conjugate joint prior distribution of μ and σ^2 is a normal-inverse-χ^2 distribution (see Section 2.4.2). This means that the conditional distribution of the mean μ given σ^2 is normal, and the marginal distribution of σ^2 is scaled inverse-χ^2 distributed. The joint prior distribution of μ and σ^2 can be written as the product of the conditional distribution of mean μ given σ^2 and the marginal distribution of σ^2:

$$f'(\mu,\sigma^2) = f'(\mu \mid \sigma^2)\, f'(\sigma^2)$$
$$\propto \frac{1}{\sigma} \exp\left(-\frac{n'\left(\mu - m'\right)^2}{2\sigma^2} \right) \frac{1}{\sigma^{\nu'+2}} \exp\left(-\frac{\nu'\, s'^2}{2\sigma^2} \right) \qquad \textit{Eq. 7-6}$$

where m' and n' are the prior hyperparameters for defining the prior distribution of the mean, and ν' and s'^2 are the prior hyperparameters for the variance. Choosing a prior that is non-informative regarding the mean is equivalent to $n' \to 0$, that is, no hypothetical prior test series for the mean (see Section 2.4). This results in an improper uniform prior:

$$f'(\mu \mid \sigma^2) \propto \text{constant} \qquad \textit{Eq. 7-7}$$

Thus, the conjugate joint prior distribution that is non-informative regarding the mean and informative regarding the variance is given by only the right term of Eq. 7-6:

$$f'(\mu,\sigma^2) \propto \frac{1}{\sigma^{\nu'+2}} \exp\left(-\frac{\nu'\, s'^2}{2\sigma^2} \right) \propto f'(\sigma^2) \qquad \textit{Eq. 7-8}$$

The posterior distribution is then obtained by inserting Eq. 7-2 and Eq. 7-8 into Eq. 7-1.

$$f''(\mu,\sigma^2 \mid \mathbf{x}) \propto \frac{1}{\sigma^n} \exp\left(-\frac{(n-1)\, s^2 + n\left(\mu - m\right)^2}{2\sigma^2} \right) \frac{1}{\sigma^{\nu'+2}} \exp\left(-\frac{\nu'\, s'^2}{2\sigma^2} \right)$$
$$= \frac{1}{\sigma} \exp\left(-\frac{n\left(\mu - m\right)^2}{2\sigma^2} \right) \frac{1}{\sigma^{n+\nu'+1}} \exp\left(-\frac{(n-1)\, s^2 + \nu'\, s'^2}{2\sigma^2} \right) \qquad \textit{Eq. 7-9}$$
$$= \frac{1}{\sigma} \exp\left(-\frac{n''\left(\mu - m''\right)^2}{2\sigma^2} \right) \frac{1}{\sigma^{\nu''+2}} \exp\left(-\frac{\nu''\, s''^2}{2\sigma^2} \right)$$

The last conversion step leads to an expression equivalent to Eq. 7-6. Hence, the posterior distribution obtained by using the prior that is non-informative concerning the mean and informative concerning the variance is of the same type as the informative prior. Therefore,

the update can be performed by merely updating the hyperparameters. According to the last conversion step in Eq. 7-9, the posterior hyperparameters n'', m'', v'', and s''^2 are obtained as follows:

$$n'' = n \qquad \textit{Eq. 7-10}$$

$$m'' = m \qquad \textit{Eq. 7-11}$$

$$v'' = v' + n - 1 \qquad \textit{Eq. 7-12}$$

$$s''^2 = \frac{v'\, s'^2 + (n-1)\, s^2}{v''} \qquad \textit{Eq. 7-13}$$

Eq. 7-12 and Eq. 7-13 illustrate why the hyperparameters v' and s' can be understood as the degrees of freedom and sample variance of a hypothetical prior test series. The $n - 1$ degrees of freedom of the actual test series are increased by the v' degrees of freedom of the hypothetical prior test series. Furthermore, the posterior hyperparameter s''^2 is equivalent to an average of the sample variance s^2 and the variance of the hypothetical prior test series s'^2, each being weighted by the respective degrees of freedom.

Based on Eq. 7-9, the posterior predictive distribution (i.e. the distribution of X that includes the remaining statistical uncertainty after the update) can be determined by integrating out the uncertain parameters according to their posterior distribution (see Section 2.4.2). Solving the integral shows that the posterior predictive distribution of X is a Student's t-distribution with v'' degrees of freedom, location m'', and scale s'' $(1 + 1 / n'')^{0.5}$. Consequently, p fractiles x_p of the logarithm of strength can be determined as follows:

$$x_p = m'' + t_{v'',p}\; s'' \sqrt{1 + \frac{1}{n''}} \qquad \textit{Eq. 7-14}$$

where $t_{v'',p}$ is the p fractile of Student's t-distribution with v'' degrees of freedom. Using informative prior distributions for the variance causes an increase in the degrees of freedom of the posterior predictive distribution. Compared to an entirely non-informative approach, which corresponds to $n' = 0$ and $v' = 0$, the degrees of freedom of the t-distribution are increased by v' (see Eq. 7-12). Hence, the utilisation of prior information leads to a predictive distribution with less weight in the tails (see Section 2.3.4).

The predictive posterior distributions for the logarithm of unit and of mortar compressive strength, as defined by Eq. 7-14, are used in the method developed in Chapter 8 to determine characteristic values and partial factors for the compressive strength of masonry. For the framework to be applied in practice, the hyperparameters v' and s'^2 of the prior distribution must be determined, which is presented in Section 7.4 based on the test database presented in Section 7.3.

7.3 Test Database for Material Properties of Existing Masonry

To be able to model prior information about the variability of unit and mortar strength by prior distributions, a test database for the material properties of existing masonry was established. The database contains the results of compressive strength tests on unit and mortar specimens that were extracted from existing masonry structures. The tests were not conducted for the present investigation specifically but became necessary in the context of structural assessments. In most cases, the assessment was necessary due to a planned conversion or extension. The tests were conducted by the Institute of Concrete and Masonry Structures at the Technical University of Darmstadt and five private testing labs, which are located throughout Germany and generously made their testing data available.

In total, 2784 unit and 3014 mortar compressive strength test results for 171 structures (168 buildings, two bridges, and one retaining wall) were received. Since buildings represent the majority of the structures, all types of structures are referred to as "buildings" in the following. In the first step of data preparation, the data is reduced to 140 buildings containing solid clay brick masonry. The large share of buildings containing solid clay brick masonry indicates the high importance of this masonry type in assessing existing masonry structures. It should be noted that the testing labs were asked to limit the data to masonry made of artificial units – natural stone masonry was not part of the data collection – but not to solid clay brick masonry. However, much less data was received for other artificial unit types, such as perforated clay bricks, calcium silicate bricks, or (lightweight) concrete blocks. These other unit types gained importance in construction practice much later than solid clay bricks (see Section 3.2) and appear to play a smaller role in the assessment of existing structures. Regarding the activities of the testing labs, this effect is increased because, for younger buildings, construction documents providing information regarding the strength of masonry exist far more often, which makes material testing unnecessary in many cases.

The considered buildings are located throughout Germany. Due to the amount of data received from the different testing labs, a slight emphasis lies on the regions around Berlin (postal code 1xxxx) and around Munich (postal code 8xxxx), each representing about one-third of the database. The other third mainly consists of projects in Baden-Württemberg, Hesse, Hamburg, and the rest of Bavaria. Fig. 7-1 displays the geographical distribution of the 140 buildings containing solid clay brick masonry with respect to the first number of the postal code. Although the data is not perfectly distributed over Germany, the database contains test results obtained for buildings from many different regions. Therefore, conclusions drawn from the database are considered representative of existing solid clay brick masonry in Germany in general. For about 80 % of the buildings, it was possible to add an estimate for the year of construction. The database can be considered representative for the

period between 1850 and 1950 since the construction year of more than 80 % of the buildings falls into this range (see Fig. 7-1).

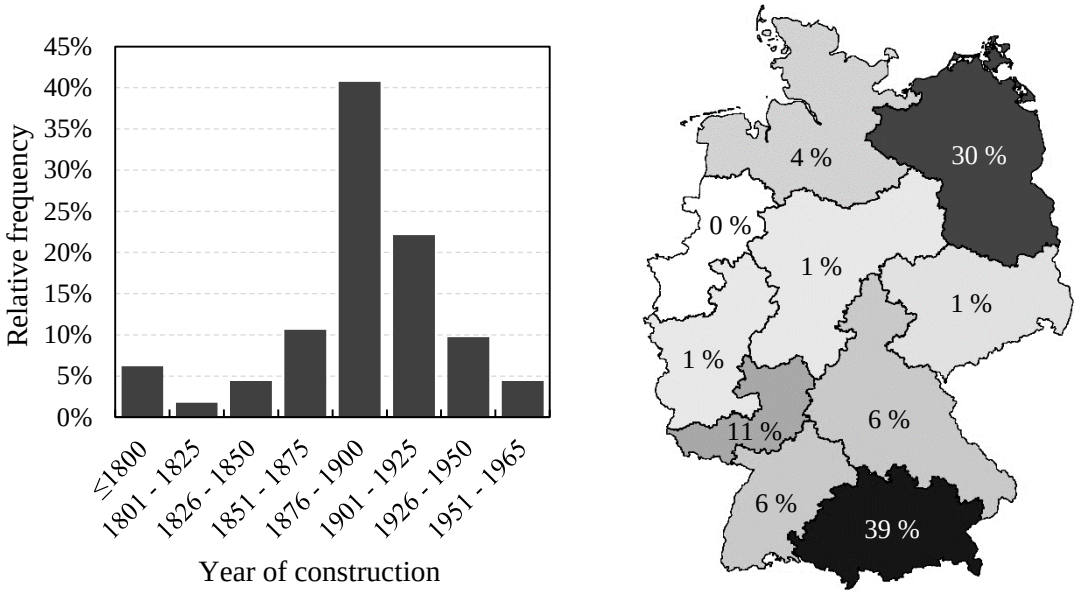

Fig. 7-1 Relative frequencies of construction time and the postal code region of all the buildings containing solid clay brick masonry

In the next step, the testing data received for a particular building is split if the masonry members in this building belong to different masonry populations. In this context, one *population of masonry* is defined as masonry that appears to be of the same type of masonry regarding unit type, mortar type, and workmanship. More than one masonry population for a particular building is assumed if any of the following applies:

- The building consists of different parts being built at different times.
- The testing lab documented a change of masonry type (e.g. due to a change in brick dimensions).
- The average mortar or unit compressive strength in one building significantly changes between floors, indicating a change in the mortar type or unit quality.

Regarding the last criterion, the significance of the difference in average strength is checked by a two-sample *t*-test. The general procedure of the two-sample *t*-test is described in Section 2.3.8. In all cases, where the test data for one building is split into two or more populations, the hypothesis of equal population means is rejected based on $p < 0.05$. By splitting the data for some of the buildings into two or more populations, 167 populations are obtained for the 140 buildings that contain solid clay brick masonry. In total, the database contains 2364 unit compressive strength test results and 2575 mortar compressive strength test results for solid clay brick masonry.

For the solid clay brick masonry populations in the database, Fig. 7-2 shows the relative frequencies of the number of sampling locations per masonry population and the average

number of tests per sampling location. In this context, a *sampling location* is defined as the locally bounded part of a masonry wall from which one or more test specimens are taken (WTA 7-4 2021). The number of sampling locations per population varies greatly, which is due to different sizes of the corresponding buildings, different expected structural utilisation of the assessed masonry walls, and different assessment approaches of the engineers. In the majority of cases, three unit specimens were taken from each sampling location. Concerning the number of mortar tests per sampling location, the approaches of the testing labs vary more strongly. Some testing labs prefer to perform fewer tests on mortar specimens than on unit specimens since unit compressive strength has a stronger influence on the compressive strength of masonry. In some cases, it was decided to perform no mortar tests at all, which is illustrated by the relative frequency of zero mortar sampling locations in Fig. 7-2. In contrast, other labs usually test more mortar samples than unit samples since extracting a high number of mortar specimens is less invasive. However, in most cases, the number of mortar specimens per sampling location was also three.

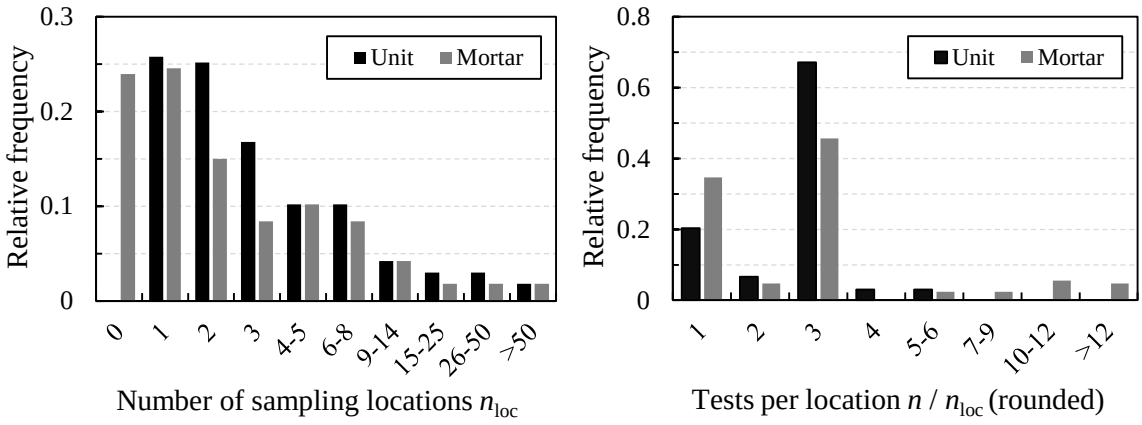

Fig. 7-2 Frequencies of the numbers of sampling locations and the tests per sampling location for the solid clay brick masonry populations in the database

The unit compressive strength tests were either performed according to EN 772-1 (2011) on whole bricks or parts of bricks, or conducted according to DIN 105-1 (1982) on halved bricks, with one half laid upon the other with a thin, intermediate cement mortar layer. In the case of tests according to EN 772-1 (2011), the individual test results were adjusted by corresponding shape factors. All mortar compressive strength tests were double punch tests performed according to DIN 18555-9 (2019). In almost all cases, procedure III of this standard was applied. When test results for mortar compressive strength are presented in the following, correction factors for transforming the double punch test results into standardised mortar strengths are already included. These correction factors are adopted from the testing labs, which mostly decided to use a correction factor of either 1 or 0.7 when testing according to procedure III. A correction factor of 0.7 implies that the specified standardised mortar strengths are smaller than the mortar strengths obtained by double punch tests on specimens extracted from masonry. However, the correction factor for mortar strength is

not relevant for modelling the prior distribution in the following, as the correction factor does not change the CoV of the test results for a particular masonry population.

In Section 7.4, the prior distributions are modelled for two cases:

1. Prior distributions that represent typical CoVs of unit and of mortar strength considering all masonry members in a building that belong to the same type of masonry (i.e. prior distributions that correspond to a masonry population as defined above)
2. Prior distributions that represent typical CoVs of strength at a single sampling location

In the second case, typical CoVs are assumed to be lower than in the first case since the strengths at one sampling location are expected to be correlated. To model the first case, only those populations are considered for which at least $n = 3$ test results in total for at least $n_{loc} = 2$ sampling locations are available. As a result, the number of populations reduces to 119 for unit compressive strength and 79 for mortar compressive strength. For modelling the second case, only sampling locations can be considered for which at least $n = 2$ test results were received. Concerning the number of data points, the process of data preparation can be summarised as follows:

- Total number of buildings in database: 171
- Buildings containing solid clay brick masonry: 140
- Populations of solid clay brick masonry
  - Total number: 167
  - $n_{loc} \geq 2$ and $n \geq 3$ for unit strength: 119
  - $n_{loc} \geq 2$ and $n \geq 3$ for mortar strength: 79
- Sampling locations (solid clay brick masonry)
  - $n \geq 2$ for unit strength: 653
  - $n \geq 2$ for mortar strength: 519

In Annex C, the database is displayed with the sample size, the mean, and the CoV of unit and mortar compressive strength for the 167 populations of solid clay brick masonry. In addition, the first number of the postal code of the respective building location and, if possible, an estimate for the construction year are provided.

In Fig. 7-3, arithmetic means and sample CoVs of unit and mortar compressive strength are displayed using scatterplots. Each point refers to the sample mean and CoV for one of the solid clay brick masonry populations and is based on $n \geq 3$ test results for $n_{loc} \geq 2$ sampling locations. The four scatterplots are arranged to show possible relationships between (a) mean values of unit and mortar strength, (b) CoVs of unit and mortar strength, (c) mean and CoV of unit strength, and (d) mean and CoV of mortar strength. In each of the four scatterplots, linear regression lines are provided.

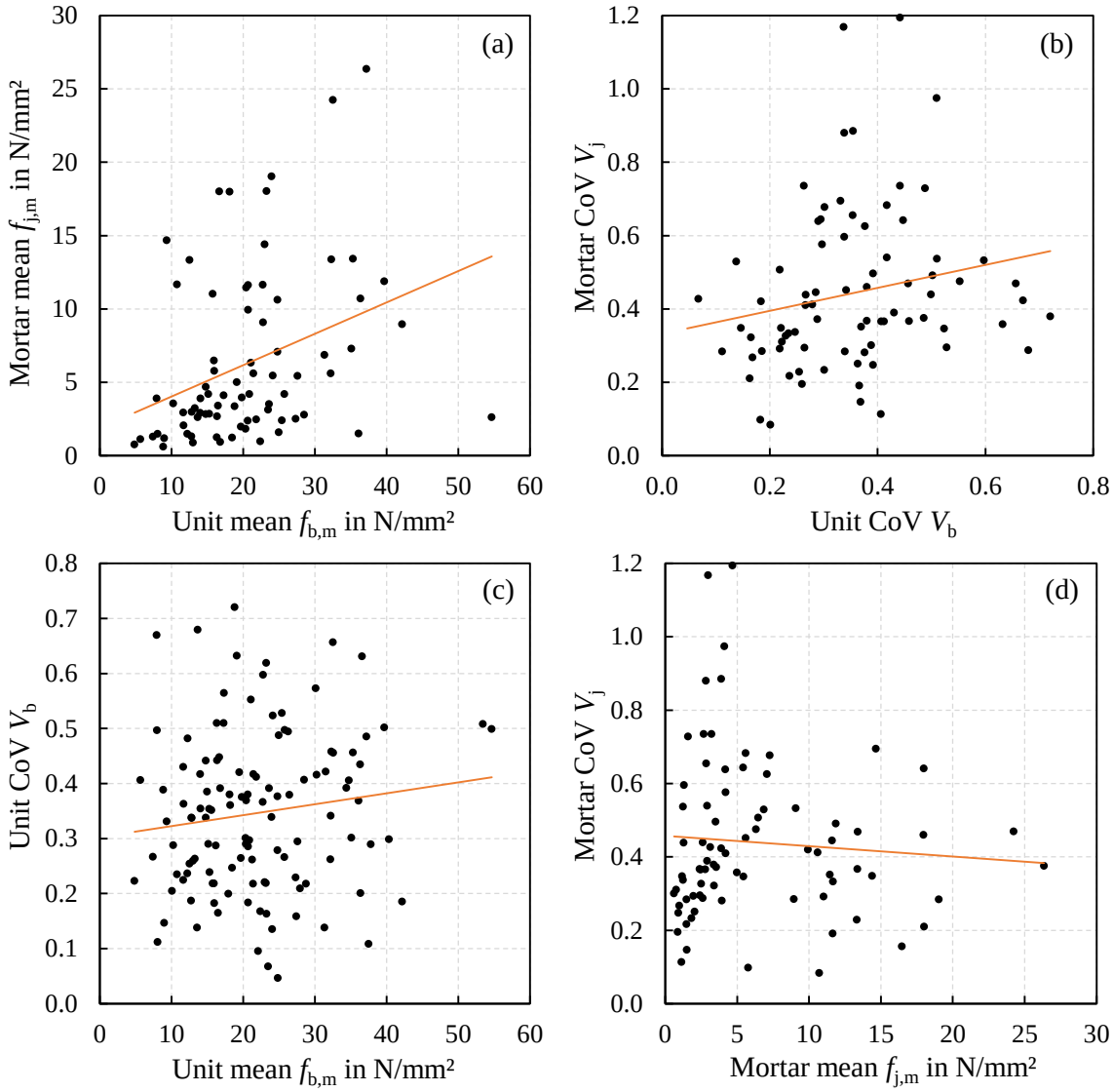

Fig. 7-3 Sample means and CoVs of unit and mortar compressive strength for different solid clay brick masonry populations

Based on Fig. 7-3, the following observations and conclusions can be made:

(a) A wide range of arithmetic means of unit and mortar compressive strength can be observed. The intervals given by the respective 5 % and 95 % fractiles are (8.1 N/mm², 37.8 N/mm²) for mean unit compressive strength and (0.9 N/mm², 18.0 N/mm²) for mean mortar compressive strength. The medians of the arithmetic mean are 20.7 N/mm² and 3.9 N/mm² for unit and mortar strength, respectively. A correlation coefficient of $r = 0.34$ between the means of unit and mortar compressive strength is observed, indicating that bricks with high compressive strength only slightly tend to be combined with mortar types that also show relatively high strength.

(b) The median sample CoV of mortar strength (38 %) is slightly higher than the median CoV of unit strength (34 %). Furthermore, the range of observed CoVs is also higher

for mortar strength. The correlation between the sample CoVs of unit and mortar strength for the same masonry population is quite low (r = 0.20). Therefore, this correlation is considered negligible, and independent prior distributions for the variability of unit and of mortar compressive strength can be modelled in the following.

(c) The CoV of unit compressive strength appears to be independent of the mean of unit compressive strength. This is contrary to observations for concrete compressive strength, in which the CoV decreases with increasing mean compressive strength (JCSS 2002) and, instead, the standard deviation of strength is commonly assumed to be independent of mean strength. In EN 1992-1-1 (2010), for example, the relationship between the characteristic compressive strength f_{ck} and mean compressive strength f_{cm} of concrete is stated as $f_{cm} = f_{ck} + 8$ N/mm², indicating the assumption of an approximately constant standard deviation of about 5 N/mm². Since the CoV of unit strength appears independent of its mean, modelling the prior distribution for the standard deviation of the logarithm of unit strength, which is equivalent to modelling a prior for the CoV of unit strength (see Eq. 7-5), is favoured over modelling a prior for the standard deviation of unit strength itself.

(d) The observations and conclusions for unit compressive strength also apply to mortar compressive strength: The CoV of mortar compressive strength is assumed to be independent of the corresponding mean value in the following.

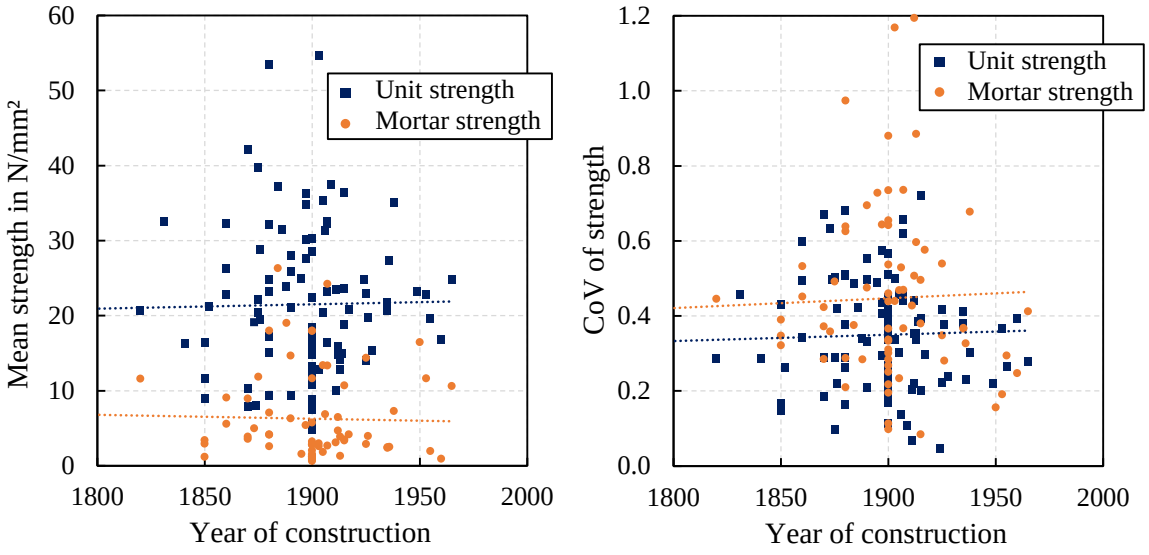

Fig. 7-4 Sample means and CoVs of unit and mortar compressive strength for different solid clay brick masonry populations arranged by year of construction

As shown in Fig. 7-1, most of the existing buildings in the database were constructed between 1850 and 1950, making the database representative for this period. In Fig. 7-4, the sample means and CoVs of unit and mortar compressive strength observed for the solid clay brick masonry populations are displayed again. Here, the data points are arranged over the estimated construction year. Although common production techniques for bricks and

typical types of mortar have changed over time (see Section 3.2), the year of construction does not seem to have a notable influence on the mean values or CoVs of unit or mortar compressive strength in the database, which is indicated by the almost horizontal regression lines in Fig. 7-4.

7.4 Modelling Prior Distributions

7.4.1 General

Informative prior distributions for distribution parameters can be interpreted in two ways (Gelman et al. 2013). On the one hand, there is the *knowledge interpretation*, according to which the knowledge about the particular parameter is limited. Therefore, the parameter is a random realisation of the prior distribution that represents this limitation in knowledge. On the other hand, there is the *population interpretation*. According to this second interpretation, the prior distribution describes a population of parameters from which the parameter of current interest is drawn. The following approach is in line with the population interpretation. It is assumed that each building features a particular CoV for unit strength and a particular CoV for mortar strength that are specific to this building. All of the building-specific CoVs together form a population. Thus, there is one population of unit strength CoVs and one of mortar strength CoVs that can both be described by a corresponding prior distribution. The CoV of unit strength and the CoV of mortar strength for a particular building can be considered as randomly drawn from these two populations.

Instead of formulating the prior distributions for the CoVs of unit and mortar strength directly, they are formulated in terms of the variances $\sigma_{\ln,b}^2$ and $\sigma_{\ln,j}^2$ of the logarithms of the respective strengths since the common Bayesian framework for updating the conjugate priors of normally distributed random variables can then be applied. The prior distributions for the variance are thus chosen to be scaled inverse-χ^2 distributions (see Section 7.2). The two hyperparameters ν' and s', defining the prior distributions, are determined by maximum likelihood estimation in the following. In Section 7.4.2, the methodology for estimating the prior hyperparameters is described.

As previously mentioned, the prior hyperparameters are determined for two different cases:

1. "Building-related" prior distributions display the typical variance if all samples from the building belonging to one masonry type are considered collectively. As a result, the posterior predictive distribution represents the variability of unit or mortar compressive strength for this masonry type over the whole building.
2. "Location-related" prior distributions display the typical variance at one sampling location. These prior distributions can be updated using the test results from one sampling location. Therefore, the resulting posterior predictive distribution represents the variability of mortar or unit compressive strength at only this sampling location.

The building-related and location-related prior hyperparameters are estimated in Sections 7.4.3 and 7.4.4, respectively. The building-related variability originates from both the variability of the material properties within a sampling location and the variability between sampling locations. Thus, the building-related variability is usually higher than the location-related variability; the strengths at one sampling location are correlated. In Section 7.4.5, correlation coefficients for unit and for mortar compressive strengths at one sampling location are estimated. In Section 7.4.6, the precision with which the prior hyperparameters are estimated is quantified through bootstrap confidence intervals. Finally, in Section 7.4.7, a prior distribution for the variability of masonry compressive strength is modelled based on the prior distributions for unit and mortar strength.

7.4.2 Procedure for Estimating the Prior Hyperparameters

Based on the data presented in Section 7.3, the hyperparameters v' and s' for the prior distributions are found by maximum likelihood estimation. The prior distributions are meant to describe the distribution of the true population variances $\sigma_{\ln,b}^2$ and $\sigma_{\ln,j}^2$ of the logarithms of unit and mortar strength. The database, however, only contains sample variances $s_{\ln,b}^2$ and $s_{\ln,j}^2$, which correspond to limited sample sizes n, and, thus, cannot be considered as directly drawn from the prior distribution. Instead, for a given population variance σ_i^2, the observed sample variance s_i^2 for a particular building or sampling location is a random variable, which, after normalisation, is χ^2-distributed (see Section 2.3.6):

$$v_i \frac{s_i^2}{\sigma^2} \sim \chi_{v_i}^2 \qquad \textit{Eq. 7-15}$$

where $v_i = n_i - 1$ are the degrees of freedom in determining the sample variance s_i^2 for the building or sampling location indexed by i. The indices “ln,b” and “ln,j” are omitted here for more brevity.

The additional variability resulting from the limited sample size n_i makes the distribution of the sample variances s_i^2 wider than the distribution of the true population variances σ_i^2. This effect must be considered by the likelihood function because, otherwise, the resulting prior distribution would be too wide. The likelihood function is therefore defined by the product of the marginal probability densities of the observed sample variances:

$$L(s', v' \mid \mathbf{s^2}, \mathbf{v}) = \prod_i f(s_i^2 \mid v_i, s', v') \qquad \textit{Eq. 7-16}$$

where $\mathbf{s^2}$ and $\mathbf{v}$ are vectors containing the sample variances and corresponding degrees of freedom from the database. The marginal probability density function (PDF) of the sample variance s_i^2 can be determined by first defining the joint PDF of s_i^2 and σ_i^2, which is the product of the PDF of s_i^2 given σ_i^2 and the PDF of σ_i^2:

$$f(s_i^2, \sigma_i^2 \mid \nu_i, \nu', s') = f(s_i^2 \mid \sigma_i^2, \nu_i)\, f(\sigma_i^2 \mid \nu', s') \qquad \textit{Eq. 7-17}$$

The PDF of s_i^2 given σ_i^2 is that of a χ^2-distribution with parameter ν_i (see Eq. 7-15) and the PDF of σ_i^2 is the prior distribution, which is a scaled inverse-χ^2 prior distribution with parameters s' and ν'. The marginal distribution for s_i^2 is obtained by integrating the joint PDF of s_i^2 and σ_i^2 over σ_i^2 as follows:

$$\begin{aligned} f(s_i^2 \mid \nu_i, s', \nu') &= \int_0^\infty f(s_i^2 \mid \sigma_i^{\,2}, \nu_i)\, f(\sigma_i^{\,2} \mid s', \nu')\, d\sigma_i^2 \\ &= \int_0^\infty \frac{\left(\frac{\nu_i}{2}\frac{s_i^2}{\sigma_i^2}\right)^{\frac{\nu_i}{2}} \exp\left(-\frac{\nu_i\, s_i^2}{2\,\sigma_i^2}\right)}{s_i^2\,\Gamma\left(\frac{\nu_i}{2}\right)} \frac{\left(\frac{\nu'\, s'^2}{2\,\sigma_i^2}\right)^{\frac{\nu'}{2}} \exp\left(-\frac{\nu'\, s'^2}{2\,\sigma_i^2}\right)}{\sigma_i^2\,\Gamma\left(\frac{\nu'}{2}\right)} d\sigma_i^2 \\ &= \frac{\left(s_i^2\right)^{\frac{\nu_i}{2}-1}\left(\frac{\nu_i}{2}\right)^{\frac{\nu_i}{2}}\left(\frac{\nu'}{2}\, s'^2\right)^{\frac{\nu'}{2}}\Gamma\left(\frac{\nu_i}{2}+\frac{\nu'}{2}\right)}{\left(\frac{\nu_i}{2}\, s_i^2+\frac{\nu'}{2}\, s'^2\right)^{\frac{\nu_i}{2}+\frac{\nu'}{2}}\Gamma\left(\frac{\nu_i}{2}\right)\Gamma\left(\frac{\nu'}{2}\right)} \end{aligned} \qquad \textit{Eq. 7-18}$$

The marginal distribution for the sample variances given by Eq. 7-18 can be inserted in Eq. 7-16 to determine the likelihood for any pair of values for the hyperparameters ν' of s'. The hyperparameters can then be estimated as those values for ν' of s' that maximise the likelihood. The corresponding optimisation problem is solved numerically.

A low value for ν' corresponds to a wide probability density function, which represents a high variability of $\sigma_{\ln,b}^2$ (or $\sigma_{\ln,j}^2$) from building to building or from sampling location to sampling location. The prior hyperparameters $s_{\ln,b}'$ and $s_{\ln,j}'$ can be viewed as prior estimates for the standard deviations $\sigma_{\ln,b}$ and $\sigma_{\ln,j}$. For $\sigma_{\ln,b}$ and $\sigma_{\ln,j} < 0.2$, the standard deviations $\sigma_{\ln,b}$ and $\sigma_{\ln,j}$ of the logarithms of unit and mortar strength are approximately equal to the CoVs v_b and v_j. Therefore, the resulting prior PDFs are displayed as functions of the standard deviations $\sigma_{\ln,b}$ and $\sigma_{\ln,j}$ instead of the respective variances in the following since the results can then be understood more intuitively.

7.4.3 Building-Related Prior Distributions

First, the building-related data is used to determine corresponding prior hyperparameters. Following the previously described procedure, the parameters are obtained as $\nu_b' = 7.7$ and $s_{\ln,b}' = 0.33$ for unit compressive strength as well as $\nu_j' = 4.2$ and $s_{\ln,j}' = 0.40$ for mortar compressive strength. In Fig. 7-5, the corresponding prior distributions of $\sigma_{\ln,b}$ and $\sigma_{\ln,j}$ are illustrated. Due to the lower value of the parameter ν', the probability density of the standard deviation $\sigma_{\ln,j}$ for mortar strength is wider, which represents a higher building-to-building

variability of the CoV of mortar compressive strength. Since the consistency of mortar strength between separate mortar mixes depends not only on the production process but also on the workmanship on site, this result is comprehensible. Consequently, the prior for mortar is less informative than for unit strength. Furthermore, the mean variability is higher for mortar strength.

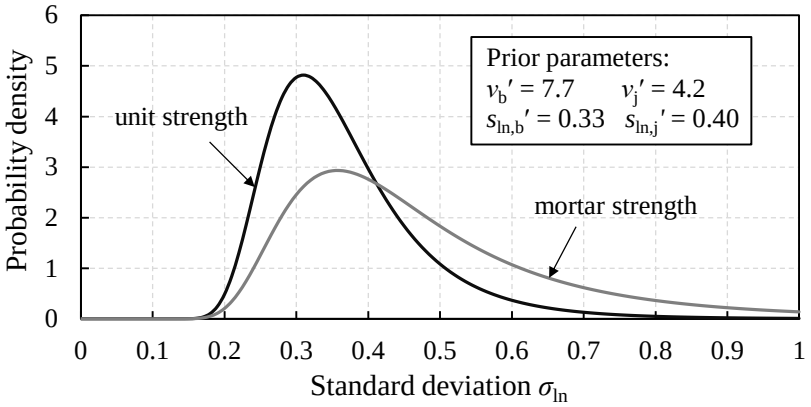

Fig. 7-5 Building-related prior distributions for the standard deviations of the logarithms of unit and mortar compressive strength

To check the consistency of the prior distributions with the corresponding data, the single data points (119 for unit and 79 for mortar), each consisting of a sample standard deviation $s_{ln,i}$ and a corresponding sample size n_i, are illustrated in Fig. 7-6. In addition to the data points, fractiles of the marginal distribution of the sample standard deviation s_{ln} (Eq. 7-18) are provided based on the obtained prior hyperparameters for unit and mortar. The theoretical lower and upper fractiles of the sample standard deviation draw closer to each other with an increase in sample size. The same effect can be seen for the data: Very high and, in particular, very low values of $s_{ln,i}$ tend to occur only for small sample sizes. This observation demonstrates that the utilised procedure, which considers the sample sizes of the standard deviations, is indeed needed to estimate the prior hyperparameters realistically. The data points match the theoretical marginal distribution very well as the median line ($s_{50\%}$) approximately splits the number of data points in half. Furthermore, about 10 % of the data points lie outside the interval provided by the 5 % and 95 % fractiles $s_{5\%}$ and $s_{95\%}$.

For further illustration, the marginal probability density function for the sample standard deviation $s_{ln,b}$ of unit compressive strength is displayed for different sample sizes in Fig. 7-7. The curve with sample size $n \to \infty$ corresponds to the prior distribution. For comparison, relative frequencies of the sample standard deviations in the database are given in the right part of Fig. 7-7. Grouping them by underlying sample size n_i demonstrates that, in accordance with the theoretical marginal distribution, relatively low sample standard deviations only occur for small sample sizes.

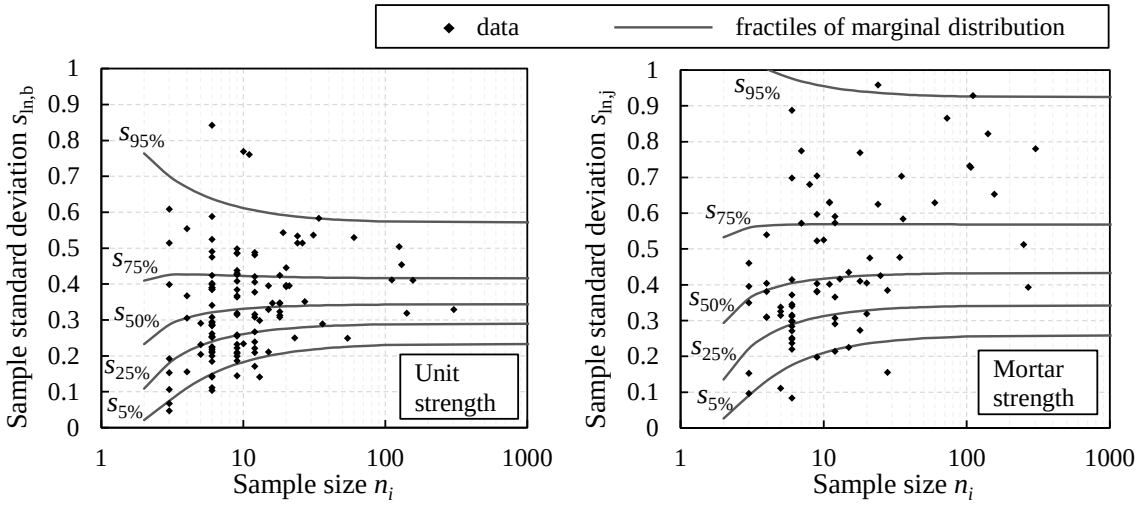

Fig. 7-6 Building-related sample sizes and sample standard deviations of the logarithm of unit (left) and mortar (right) compressive strength

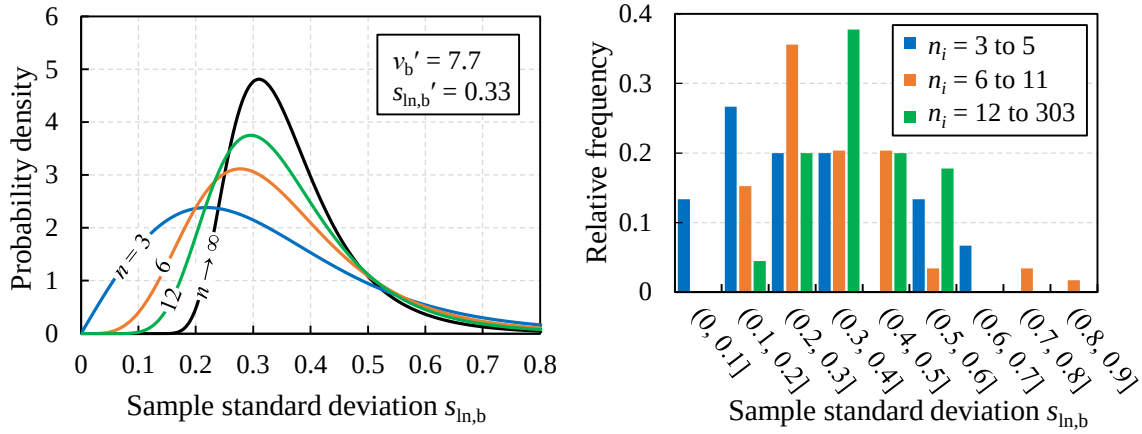

Fig. 7-7 Marginal distribution (left) and relative frequencies (right) of the building-related sample standard deviation of the logarithm of unit compressive strength

7.4.4 Location-Related Prior Distributions

In a second step, the location-related data is used to determine corresponding prior hyperparameters. Based on the same procedure as for the building-related prior, the prior hyperparameters are found to be $\nu_b' = 3.8$ and $s_{ln,b}' = 0.21$ for unit compressive strength as well as $\nu_j' = 6.1$ and $s_{ln,j}' = 0.24$ for mortar compressive strength. It is noted that this prior distribution represents the variability of $\sigma_{ln,b}$ and $\sigma_{ln,j}$ between different sampling locations of different buildings. The corresponding prior distributions are displayed in Fig. 7-8.

The mean location-related variability of both unit and mortar strength is lower than the mean building-related variability, which is due to the correlation of compressive strengths at a single sampling location. Corresponding correlation coefficients are determined in Section 7.4.5. For the location-related data, the value of the degree of freedom parameter ν' for mortar compressive strength is higher than for unit strength.

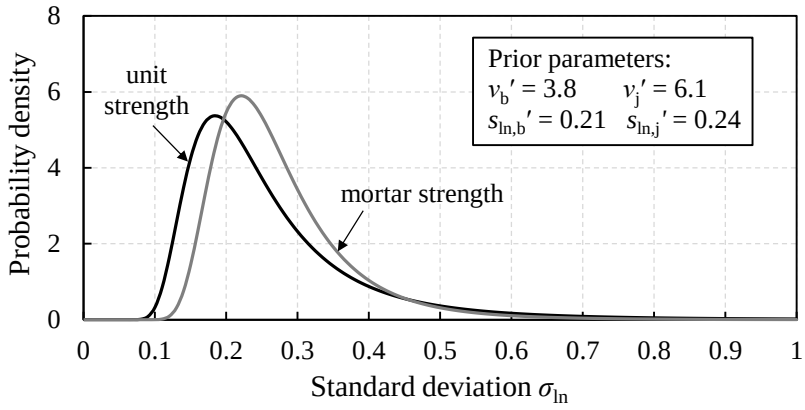

Fig. 7-8 Location-related prior distributions for the standard deviations of the logarithms of unit and mortar compressive strength

The data points (656 for unit and 519 for mortar) from which the location-related prior hyperparameters are obtained are shown in Fig. 7-9. Again, fractiles of the marginal distribution of the sample standard deviation based on the obtained prior hyperparameters are also displayed. In principle, the same effects regarding the sample size can be observed as for the building-related data in the previous section.

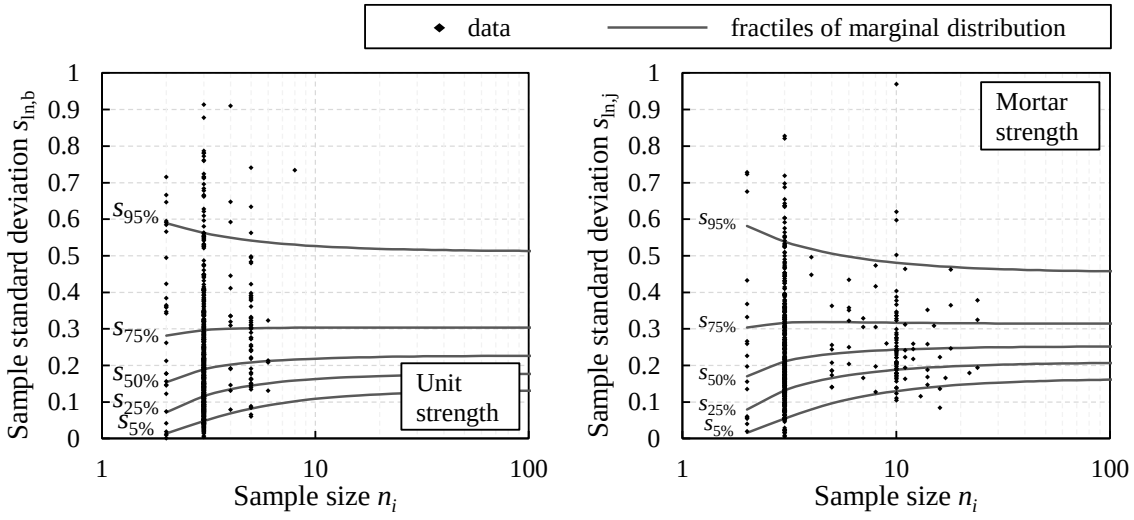

Fig. 7-9 Location-related sample sizes and sample standard deviations of the logarithm of unit (left) and mortar (right) compressive strength

The high number of data points with $n_i = 3$ makes it possible to examine the data for this specific sample size more closely. Fig. 7-10 can be considered as a section through Fig. 7-9 at $n_i = 3$. It demonstrates the excellent agreement between the theoretical marginal PDFs, which are based on the obtained prior distributions, and the relative frequencies of the sample standard deviations. This agreement is particularly remarkable since the distribution type of the prior is not chosen due to a good fit but for mathematical practicality. The conjugate form of the prior distribution can thus be considered excellently suited also beyond its practicality.

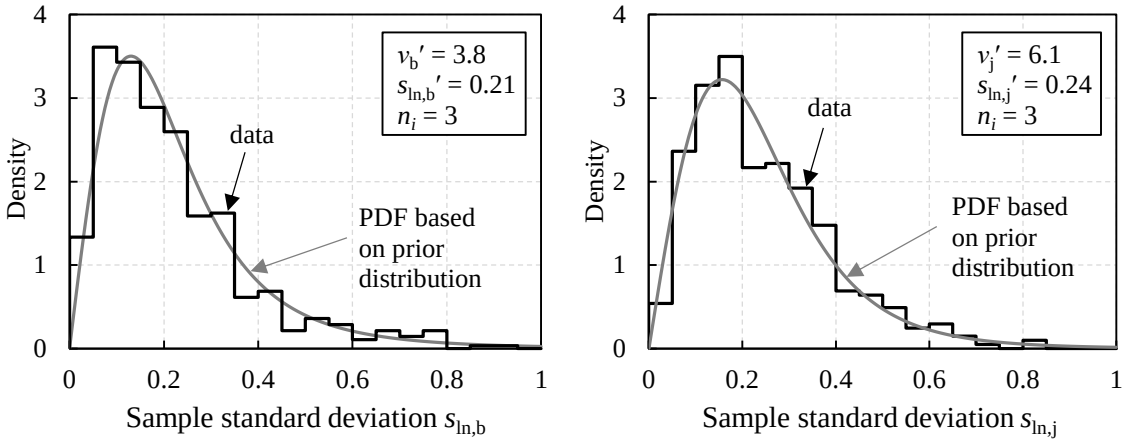

Fig. 7-10 Marginal distributions and relative frequencies of location-related standard deviations for sample size n = 3 (left: unit strength, right: mortar strength)

7.4.5 Correlation of Strength at a Sampling Location

Details about the spatial correlation of material properties within one structural member are needed to incorporate the results of Chapter 6 regarding the influence of spatial variability in the development of a method for determining assessment values of masonry compressive strength. Therefore, the spatial correlation at one sampling location, represented by the correlation coefficient ρ_{loc}, is determined for both unit and mortar compressive strength.

In the following, the spatial correlation is described by a fixed (i.e. deterministic) correlation coefficient. Therefore, instead of describing this parameter by a probability distribution, a specific value for ρ_{loc} is obtained. The correlation coefficient can be determined via the ratio of the average location-related variability to the average building-related variability. For this purpose, the average variability is determined as the average sample variance of the logarithm of unit and mortar compressive strength since the sample variance is an unbiased estimator for the population variance (see Section 2.3.6). The averages of the variances $s_{ln,b}^2$ and $s_{ln,j}^2$ of the logarithm of strength are shown in Table 7-1. The averaged sample variances are taken as estimates for typical population variances $\sigma_{ln,b}^2$ and $\sigma_{ln,j}^2$, which are then transformed to the corresponding CoVs v_b and v_j of unit and mortar compressive strength based on Eq. 7-5. The correlation coefficient can subsequently be determined following the principle of Eq. 6-26, leading to the following equation for determining the correlation coefficient ρ_{loc}:

$$\rho_{loc} = \frac{1 - \frac{v_{location}^2}{v_{building}^2}}{1 + v_{location}^2} \qquad \textit{Eq. 7-19}$$

The correlation coefficients for a sampling location are obtained as $\rho_{loc} = 0.39$ and 0.46 for unit and mortar compressive strength, respectively (see Table 7-1).

Table 7-1 Building- and location-related variability

Material property	Average variance s_{ln}^2		CoV v		Correlation	
	Building	Location	Building	Location	ρ_{loc}	$\rho_{ln,loc}$
Unit compressive strength f_b	0.137	0.081	0.383	0.291	0.392	0.409
Mortar compressive strength f_j	0.244	0.125	0.525	0.364	0.459	0.489

Alternatively, the correlation coefficient can also be determined for the logarithms of unit and mortar compressive strength, which is required for some applications. Based on Eq. 2-40, the correlation coefficient of the normally distributed logarithms of strengths at a particular sampling location can be determined as follows:

$$\rho_{ln,loc} = 1 - \frac{s_{ln,location}^2}{s_{ln,building}^2} \qquad \textit{Eq. 7-20}$$

As evident from Table 7-1, the correlation coefficient $\rho_{ln,loc}$ for the logarithm of strength does not differ significantly from the correlation coefficient ρ_{loc} for strength.

The value $\rho_{loc} \approx 0.4$, which is found for the correlation of unit compressive strength at one sampling location, is interpreted as ρ_{spat} in the subsequent investigations, that is, as the spatial correlation coefficient within a wall (see Section 6.2.1). There are two reasons for choosing the correlation coefficient ρ_{loc} of unit compressive strength instead of the value for mortar compressive strength. First, the spatial correlation coefficient ρ_{spat} is related to the spatial correlation of masonry compressive strength, which is mainly influenced by unit compressive strength. Second, ρ_{spat} refers to the spatial correlation within the whole masonry wall, whereas the obtained correlation coefficient ρ_{loc} of mortar compressive strength at a sampling location represents only a part of the masonry wall. Taking mortar samples from one sampling location (i.e. from a limited area within one wall) usually leads to receiving samples from a single mortar mix, whereas several mortar mixes are used for constructing a wall. In contrast, the correlation coefficient ρ_{loc} for unit compressive strength can be considered representative for the whole masonry wall since there is usually no change of the unit batch within a masonry wall and the units of one batch are placed in the wall arbitrarily.

7.4.6 Statistical Uncertainty in the Estimation of Prior Hyperparameters

As the size of the test database is limited, the estimation of the prior hyperparameters is connected with statistical uncertainty itself. Therefore, the uncertainty in the estimation of the prior hyperparameters is determined in this section to check whether a further increase of the test database might be beneficial. Utilising the bootstrap method (see Section 2.3.6), the standard error in estimating the prior hyperparameters and the corresponding confidence intervals are obtained.

Concerning the application of the bootstrap, the present data features the special characteristic that it does not only consist of the observed values (i.e. the variances s_i^2), but each of the variances belongs to a particular number of tests n_i. In ordinary bootstrapping, a new sample is created by resampling from the observed values with replacement. Here, associated pairs of the values s_i^2 and n_i would have to be resampled together. As a result, the bootstrap samples would each have a different composition regarding the relative share of high and low numbers n_i of respective tests. However, variances s_i^2 belonging to a high n_i have a larger influence on the estimated prior hyperparameters since the shape of the marginal distribution of s^2 more strongly depends on the prior hyperparameters s' and v' for a high number of tests n. In other words, if n_i is high, the value s_i^2 carries more information about the prior hyperparameters. To keep the total amount of information in the bootstrap samples constant, a parametric bootstrap procedure is performed. Instead of directly resampling from the data points (i.e. from the variances s_i^2), random values are generated based on the marginal distribution of s^2 according to Eq. 7-18, with the parameters v' and s' according to their maximum likelihood estimates. The values n_i are kept identical to the original sample and, for each of these values n_i, an accompanying variance s_i^{2*} is generated using the marginal distribution of the variance s^2 for the particular n_i.

The bootstrap sample consisting of the values n_i and the resampled values s_i^{2*} is then used to re-estimate the prior hyperparameters v' and s' following the same maximum likelihood method as for the original sample. In total, 100,000 bootstrap samples are generated, and, thus, 100,000 bootstrap estimates for v' and s' are acquired (see Fig. 7-11). These estimates form the corresponding bootstrap distributions, and the respective standard deviations are the bootstrap standard errors in estimating the parameters v' and s'. Based on the bootstrap distributions for v' and s', bootstrap confidence intervals are determined employing bias-corrected percentile intervals (Efron and Tibshirani 1986; see also Section 2.3.6). In Table 7-2, the maximum likelihood estimates for s' and v', their bootstrap standard errors and their 90 % bootstrap confidence intervals $C_{90\%}$ are listed.

From Table 7-2 and Fig. 7-11, it can be concluded that the prior hyperparameter s' is estimated with high precision. In contrast, the precision in estimating v' could still be improved by increasing the database. This is particularly true for the building-related prior.

Table 7-2 Bootstrap standard errors and confidence intervals for the estimated prior hyperparameters

Type of prior	Component	Degree of freedom parameter v'			Scale parameter s'		
		MLE	SE / MLE	$C_{90\%}$	MLE	SE / MLE	$C_{90\%}$
Building-related	Unit	7.7	26 %	(5.5, 11.1)	0.33	3.6 %	(0.31, 0.35)
	Mortar	4.2	24 %	(3.0, 5.8)	0.40	5.3 %	(0.36, 0.43)
Location-related	Unit	3.8	12 %	(3.2, 4.6)	0.21	3.3 %	(0.20, 0.22)
	Mortar	6.1	16 %	(4.9, 7.8)	0.24	2.8 %	(0.23, 0.25)
MLE = maximum likelihood estimate; SE = standard error							

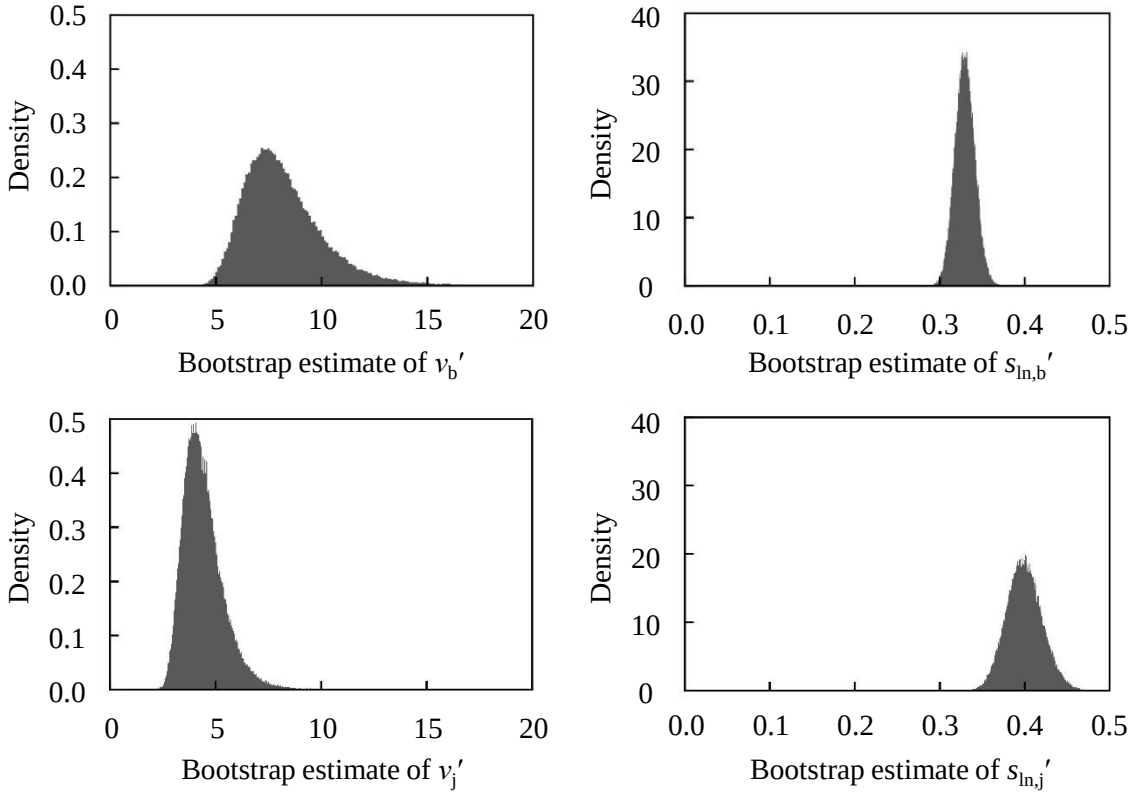

Fig. 7-11 Bootstrap distributions of s′ and v′ for the building-related prior distribution (top row: unit, bottom row: mortar)

Theoretically, the additional statistical uncertainty in the estimation of the prior hyperparameters could be included in the assessment procedure by modifying the bootstrap method such that the bootstrap distributions may be interpreted as the posterior distributions of the prior hyperparameters (see Rubin 1981). Instead of the original prior distribution for the variance, a predictive prior distribution for the variance could then be used that incorporates the statistical uncertainty in the prior hyperparameters s' and v'. This predictive prior distribution could be approximated by a scaled inverse-χ^2 distribution to maintain the benefits of the conjugate form of the prior distribution.

However, the approach of additionally considering the statistical uncertainty in the hyperparameters is not followed here for two reasons. First, the achieved accuracy in estimating the prior hyperparameters is considered sufficient. Therefore, taking into account the statistical uncertainty at this level would unnecessarily over-complicate the procedure. Second, when setting up a safety concept for structural design in engineering practice, it is unusual to consider the statistical uncertainty in the underlying stochastic models if these models are based on a reasonable amount of data. Even when statistical uncertainty in the stochastic parameters of a material property is considered by prior distributions – as, for example, in Rackwitz (1983) and JCSS (2002) regarding concrete strength –, the additional statistical uncertainty at the level of hyperparameters is not explicitly considered. In ISO

2394 (2015), where a procedure for deriving prior hyperparameters is specified, there also is no provision for considering the statistical uncertainty at the level of hyperparameters. Therefore, the approach in the following does not consider the statistical uncertainty in the hyperparameters s' and ν', which originates from the limitation of the test database in this chapter. It only incorporates the statistical uncertainty in the parameters μ and σ^2, which is introduced by different conditions in each structure to be assessed and by the limited sample size for this particular structure.

7.4.7 Prior Distribution for the Compressive Strength of Masonry

The previously determined prior hyperparameters are valid for either unit or mortar compressive strength. Thus, the corresponding prior distributions can be used if units and mortar are tested separately. Since procedures for directly testing masonry compressive strength on composite specimens are currently gaining practical importance, corresponding prior hyperparameters are also determined. However, results of tests on composite masonry specimens were received for only 11 buildings, all performed by the same testing lab (see Annex C). Therefore, the prior distribution for the variance of the logarithm of masonry strength is determined based on the previously obtained prior distributions for the variance of the logarithm of unit and mortar strength. For this purpose, the following relationship is used, which is based on the power equation for masonry compressive strength (see Section 3.5.3):

$$\sigma_{\ln,ma}^2 = \alpha^2 \, \sigma_{\ln,b}^2 + \beta^2 \, \sigma_{\ln,j}^2 \qquad \textit{Eq. 7-21}$$

where α and β are the exponents of the power equation, which, according to EN 1996-1-1 (2012), are set to 0.7 and 0.3. The variances $\sigma_{\ln,b}^2$ and $\sigma_{\ln,j}^2$ are random variables that are scaled inverse-χ^2 distributed with prior hyperparameters ν' and s' as previously obtained. Unfortunately, the linear combination of scaled inverse-χ^2 distributed random variables does not result in a random variable of the same distribution type. Therefore, the prior distribution for $\sigma_{\ln,ma}^2$ is determined as follows. First, 10 million random values for both $\sigma_{\ln,b}^2$ and $\sigma_{\ln,j}^2$ are drawn. Second, Eq. 7-21 is applied to each pair of random values. Third, a scaled inverse-χ^2 distribution is fitted to the results using maximum likelihood estimation. In this stochastic simulation, $\sigma_{\ln,b}^2$ and $\sigma_{\ln,j}^2$ are considered independent, which is assumed to be appropriate according to the observations in Section 7.3.

The prior hyperparameters for the composite material masonry are obtained as $\nu_{ma}' = 9.2$ and $s_{\ln,ma}' = 0.28$ based on the building-related prior hyperparameters for unit and mortar. The simulation results and the fitted prior distribution are displayed in Fig. 7-12. Although mathematically, the simulation results are not perfectly scaled inverse-χ^2 distributed, they can still be excellently described by the fitted scaled inverse-χ^2 distribution.

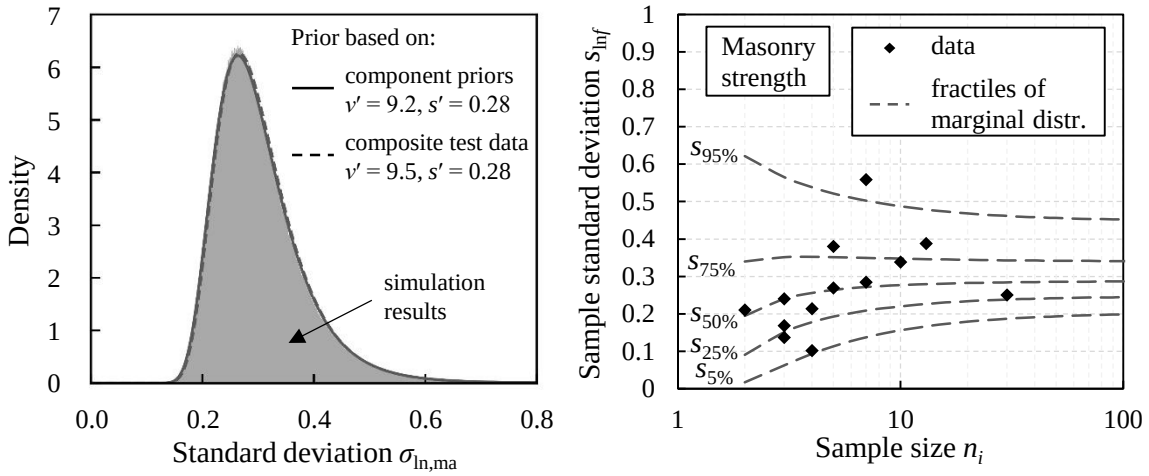

Fig. 7-12 Left: Simulation results and probability densities for the building-related prior distribution of the variability of masonry compressive strength
Right: Building-related sample sizes and standard deviations of the logarithm of masonry compressive strength

For comparison, the little available data for composite tests on masonry specimens from 11 buildings is also used to determine prior hyperparameters. The tests were conducted on masonry cores according to Helmerich and Heidel (Heidel 1989; see also Section 3.4.4) and are also displayed in Annex C. The corresponding sample standard deviations and sample sizes are displayed in the right diagram of Fig. 7-12. Based on the composite test data, the prior hyperparameters are obtained as $\nu_{ma}' = 9.5$ and $s_{ln,ma}' = 0.28$. As in the previous sections, fractiles of the corresponding marginal distributions of the sample standard deviation for different sample sizes are also displayed in Fig. 7-12 (right). The prior distribution corresponding to the hyperparameters obtained from the composite test data is additionally presented in Fig. 7-12 (left).

The two independently obtained prior distributions for the variability of masonry compressive strength agree excellently. Again, this demonstrates that the power equation for masonry compressive strength is suitable for stochastic extension (see Section 3.5.4). To some extent, the almost perfect agreement is a coincidence, especially concerning the parameter ν_{ma}', since, due to the low number of data points (only 11), the estimation of ν_{ma}' based on the composite test results contains much uncertainty. In contrast, the hyperparameters obtained by utilising the component priors are based on a much larger dataset. Therefore, the corresponding estimates for the prior hyperparameters ($\nu_{ma}' = 9.2$, $s_{ln,ma}' = 0.28$) are used in the following.

7.5 Summary

In this chapter, a Bayesian framework for considering statistical uncertainty in evaluating the compressive strength of existing masonry was presented. The framework is incorporated in the assessment method, which is developed in Chapter 8. For the application of the framework, prior hyperparameters need to be determined, which was achieved utilising an extensive database containing test results for unit and mortar compressive strength of existing masonry.

First, the Bayesian framework was described in detail in Section 7.2. Unit and mortar compressive strength are both modelled as log-normal random variables. Thus, the logarithms of these properties are normally distributed. The corresponding parameters, mean and variance, are modelled by prior distributions, which can be updated if test data is available. For the prior distribution of the mean, a non-informative distribution is selected, whereas, for the variance, the prior distribution is chosen to be informative. To reduce the updating of the prior distribution to an update of the corresponding hyperparameters, the conjugate form of the prior distribution is chosen for the variance, which is a scaled inverse-χ^2 distribution.

In Section 7.3, the structure of the test database was described. The database contains results of about 5,800 compression tests on unit and mortar specimens, which were taken from 171 existing buildings. For modelling prior distributions, only samples originating from solid clay brick masonry were considered. The data was arranged so that prior distributions for the variance of unit and mortar strength could be modelled for both building-related variability and variability related to single sampling locations.

The hyperparameters for the building- and the location-related prior distribution were estimated in Section 7.4 using the maximum likelihood method. Furthermore, the correlation of compressive strengths at one sampling location was determined for both unit and mortar compressive strengths. The precision in estimating the prior hyperparameters was quantified by bootstrap standard errors and confidence intervals in Section 7.4.6. Finally, a prior distribution for the variability of masonry compressive strength was determined in Section 7.4.7 based on the previously obtained prior distributions for the variability of unit and mortar compressive strength.

8 METHOD FOR DETERMINING ASSESSMENT VALUES OF MASONRY COMPRESSIVE STRENGTH

8.1 Introduction

Based on the previous findings, the development of the final method for determining suitable assessment values $f_{ma,a}$ of masonry compressive strength is presented in this chapter. These assessment values are equivalent to design values $f_{ma,d}$ for the design of new structures. The different term is chosen to emphasise the differences between the assessment of existing structures and the design of new structures. The developed method can also be used to determine characteristic values $f_{ma,k}$ of masonry compressive strength and structure-specific partial factors γ_M separately. However, this two-step procedure of first estimating the characteristic compressive strength $f_{ma,k}$ and then determining adjusted partial factors γ_M is not required since the assessment values $f_{ma,a}$ can be determined in one step. Nevertheless, results for characteristic values and partial factors γ_M are also presented for better comparability with the approaches for new structures.

First, the general approach and assumptions underlying the method are explained in Section 8.2. Since only material and statistical uncertainties are addressed in the preceding chapters, Section 8.3 deals with model uncertainties. The model uncertainty connected with the prediction of masonry compressive strength based on unit and mortar compressive strength is quantified. Furthermore, a stochastic model for the uncertainty in the resistance model for clay brick masonry walls under compression loading is selected.

In Section 8.4, model uncertainty, statistical uncertainty, and material variability, including the effects introduced by spatial variability, are combined via stochastic simulations to obtain predictive posterior distributions for the vertical resistance of masonry walls. For the practice-oriented final method, approximations have to be made concerning the probability distribution type and the influence of spatial variability. These approximations are made based on a comparison with the simulated distributions. In addition, special considerations are made for slender masonry walls failing due to buckling as well as for masonry walls with a small cross-section and, thus, reduced stress redistribution capability. Although the focus of this chapter lies on a method that can be used in the case of indirect testing of masonry compressive strength (i.e. separate testing of unit and mortar), the same principles are also applied to direct testing.

Finally, the developed method is validated through reliability analyses in Section 8.5. In addition to evaluating the obtained reliability level through Monte Carlo simulations (MCS), analyses by means of the first-order reliability method (FORM) are conducted to determine the sensitivity factors of the basic variables.

8.2 Approach and Assumptions

8.2.1 General

The method enables engineers to directly determine assessment values $f_{ma,a}$ of masonry compressive strength. The assessment values are based on the posterior predictive distribution for masonry compressive strength. Using a fixed sensitivity factor α_R for deriving suitable assessment values $f_{ma,a}$, the method follows the simplified level II approach as introduced by König and Hosser (1982). The method is developed with a particular focus on solid clay brick masonry. It includes statistical prior information for this masonry type (see Chapter 7) and is validated based on the respective assumptions for the stress redistribution capability within the wall (see Chapter 6). However, there is also the option to use the method with a non-informative prior. Hence, it is also possible to apply the method for other types of masonry if the corresponding stress redistribution capability is assumed to be similar or higher than for solid clay brick masonry. The underlying assumptions of the developed method are noted in the following sections.

8.2.2 Selection of Populations, Material Sampling, and Testing

Following the proposed method, the assessment value $f_{ma,a}$ of masonry compressive strength is obtained for a particular population of masonry from which a sample of material specimens is taken and tested. As defined in this thesis, a population of masonry consists of all masonry members in a structure that belong to the same type of masonry and for which the same assessment value $f_{ma,a}$ shall be applied in the verification of the structure. In this context, a specific type of masonry is defined as uniform in terms of the used materials, unit dimensions, masonry bond, and quality of execution (WTA 7-4 2021). A population of masonry can consist of one or more masonry members. If all masonry members in a particular structure are made of the same type of masonry, and no significant deviation of strength between different structural members is found, it is recommended to consider all masonry members of the structure as one population. This choice is convenient for structural verification and reduces statistical uncertainty, as all test results can be considered collectively.

Following the recommendations in WTA 7-4 (2021), specimens from at least two sampling locations should be tested. However, more than two sampling locations per population may be beneficial to ensure that the decision of which members belong to a population is justified. This decision-making process can be assisted by non-destructive testing (see Sýkora et al. 2018). Ultimately, deciding how to subdivide a structure into masonry populations and choosing suitable sampling locations very much depends on the specific project and, to a large extent, on engineering judgement.

The standard case in the following considerations is that information on masonry compressive strength is gained by destructive indirect testing. The testing uncertainty, which is the uncertainty introduced by the testing process itself, is not considered in this case as it is assumed to be negligible compared to the other uncertainties involved in the assessment. If whole units are tested, the observed variability directly corresponds to the unit-to-unit variability as considered in Chapter 6. If only parts of units are tested, the coefficient of variation (CoV) is expected to be slightly higher due to size effects (see Wolf et al. 2008). For simplification, this effect is not considered, which can lead to slightly conservative results. The same applies to double punch mortar testing according to DIN 18555-9 (2019), in which the specimens are much smaller than the whole volume of a mortar joint beneath one unit, which is the reference volume for the investigations in Chapter 6. This simplification can also lead to slightly conservative results. However, since the variability of mortar strength is less influential, neglecting this effect is not expected to have a considerable influence.

In the Bayesian update of the prior distribution utilising the test results, the spatial correlation of the compressive strengths at one sampling location (see Section 7.4.5) is not explicitly considered, as this would significantly complicate the practice-oriented method. In principle, performing the Bayesian update with consideration of the spatial correlation structure is possible as demonstrated by Geyer et al. (2021). However, this would lead to different characteristic values and assessment values of masonry compressive strength for different structural members, whereas the goal of the method is to obtain one assessment value of masonry compressive strength for the whole population under consideration. Since spatial correlation is not considered in the Bayesian update, it is essential that the tested specimens are taken from more than one sampling location. Thereby, the actual amount of information obtained by testing increases, and the risk of underestimating the variance of masonry strength is reduced.

8.2.3 Definition of Safety Elements

The method for determining assessment values $f_{\mathrm{ma,a}}$ of masonry compressive strength is developed to be consistent with the safety elements as defined in EN 1990 (2010) and EN 1996-1-1 (2012). According to EN 1996-1-1 (2012), the characteristic value $f_{\mathrm{ma,k}}$ of masonry compressive strength is the 5 % fractile of the corresponding probability distribution function $F_{f_{\mathrm{ma}}}$:

$$f_{\mathrm{ma,k}} = F_{f_{\mathrm{ma}}}^{-1}\left(0.05\right) \qquad \textit{Eq. 8-1}$$

The model uncertainty in predicting masonry compressive strength based on unit and mortar properties increases the uncertainty connected with this material property. Therefore, this component of model uncertainty, represented by the model uncertainty factor θ_f in the

following, is considered in the determination of $f_{ma,k}$ by including it in the distribution function $F_{f_{ma}}$.

In EN 1996-1-1 (2012), the design value R_d of the vertical resistance of a masonry wall is defined as

$$R_d = \Phi_{red}\ A\ f_{ma,d} = \frac{1}{\gamma_M}\Phi_{red}\ A\ f_{ma,k} \qquad \textit{Eq. 8-2}$$

where Φ_{red} is a capacity reduction factor accounting for the effects of slenderness and eccentricity of loading, and A is the cross-sectional area. Strictly speaking, the partial factor γ_M as defined in Eq. 8-2 is not a partial factor for the compressive strength of masonry but for the vertical resistance of a masonry wall (see Section 3.7). Hence, the design value of masonry compressive strength, which is obtained as $f_{ma,k} / \gamma_M$, should address all effects related to the uncertainty of the vertical resistance of a masonry wall. The design and the assessment value of masonry compressive strength are thus defined as

$$f_{ma,d} = \frac{R_d}{\Phi_{red}\ A}, \qquad f_{ma,a} = \frac{R_a}{\Phi_{red}\ A} \qquad \textit{Eq. 8-3}$$

The partial factor γ_M is defined as the product of the partial factor γ_m, accounting for the variability of the material properties, and the partial factor γ_{Rd}, considering the uncertainty of the resistance model:

$$\gamma_M = \gamma_m\ \gamma_{Rd}, \qquad \gamma_M = \gamma_m\ \gamma_{Ra} \qquad \textit{Eq. 8-4}$$

where γ_{Ra} is equivalent to γ_{Rd} but follows the nomenclature for structural assessment. The design and assessment values of the resistance that do not consider the resistance model uncertainty are denoted as R_d^* and R_a^* in the following:

$$R_d = \frac{R_d^*}{\gamma_{Rd}}, \qquad R_a = \frac{R_a^*}{\gamma_{Ra}} \qquad \textit{Eq. 8-5}$$

The developed method follows the simplified level II approach, as proposed by NABau (1981) and König and Hosser (1982) and currently included in EN 1990 (2010); see Section 2.5.4. According to this approach, the assessment value of the resistance is defined by

$$P\left(R \le R_a^*\right) = \Phi\left(-\alpha_R\ \beta_t\right) \qquad \textit{Eq. 8-6}$$

where β_t is the target reliability index, α_R is the sensitivity factor for the resistance and $\Phi(\cdot)$ is the cumulative distribution function (CDF) of the standard normal distribution. Hence, R_a^* can be determined via the CDF F_R of R:

$$R_a^* = F_R^{-1}\left[\Phi\left(-\alpha_R\ \beta_t\right)\right] \qquad \textit{Eq. 8-7}$$

Following the simplified level II approach, the sensitivity factor α_R is fixed. EN 1990 (2010) defines $\alpha_R = 0.8$ for typical design situations regarding the uncertainties of load effects and resistances, which is usually applied in combination with a target reliability index $\beta_{t,50a}$ for a reference period of 50 years. In the following, a sensitivity factor $\alpha_{R,1a} = 0.7$ is used in combination with a target reliability index $\beta_{t,1a}$ for a reference period of one year (see Section 2.5.4). Setting α_R in Eq. 8-7 to $\alpha_{R,50a} = 0.8$ or $\alpha_{R,1a} = 0.7$ implies that the uncertainty of the resistance is not dominated by the uncertainty of the resistance model (see NABau 1981). By utilising Eq. 8-7, the assessment value $f_{ma,a}$ can be obtained directly. For explicitly determining partial factors γ_M, the partial factor γ_m can be calculated as

$$\gamma_m = \frac{F_{f_{ma}}^{-1}\left(0.05\right) A \, \Phi_{red}}{F_R^{-1}\left[\Phi\left(-\alpha_R \, \beta_t\right)\right]} \qquad \textit{Eq. 8-8}$$

Section 8.4 shows that the assessment value of the resistance can approximately be determined by utilising the probability distribution $F_{f_{ma}}$ of masonry compressive strength instead of the probability distribution F_R of the resistance as long as the cross-sectional area of a masonry wall is larger than 0.1 m². Furthermore, the posterior predictive distribution for masonry strength is approximated by a log-normal distribution. Therefore, Eq. 8-8 simplifies to

$$\gamma_m = \frac{F_{f_{ma}}^{-1}\left(0.05\right)}{F_{f_{ma}}^{-1}\left[\Phi\left(-\alpha_R \, \beta_t\right)\right]} = \exp\left[\left(\alpha_R \, \beta_t - 1.645\right) \sigma_{ln,ma}\right] \qquad \textit{Eq. 8-9}$$

where $\sigma_{ln,ma}$ is the standard deviation of the logarithm of masonry compressive strength, which is set to a value that accounts for material variability, statistical uncertainty due to limited sample size, and the uncertainty in the prediction of masonry compressive strength (see Section 8.4). Eq. 8-7 for directly determining R_a^* can be simplified accordingly:

$$\begin{aligned} R_a^* &= \exp\left(\mu_{ln,ma} - \alpha_R \, \beta_t \, \sigma_{ln,ma}\right) \Phi_{red} \, A \\ &= f_{ma,m} \exp\left(-0.5 \, \sigma_{ln,ma}^2 - \alpha_R \, \beta_t \, \sigma_{ln,ma}\right) \Phi_{red} \, A \end{aligned} \qquad \textit{Eq. 8-10}$$

Based on a log-normally distributed model uncertainty factor θ_R, the partial factor γ_{Ra} for the uncertainty in the resistance model can be determined by

$$\gamma_{Ra} = \frac{\exp\left(0.4 \, \alpha_R \, \beta_t \, v_{\theta R}\right)}{\mu_{\theta R}} \qquad \textit{Eq. 8-11}$$

where the factor 0.4 considers that the model uncertainty is assumed to be a non-dominant basic variable (see NABau 1981). The parameters $\mu_{\theta R}$ and $v_{\theta R}$ are the mean and the CoV of the model uncertainty factor θ_R, which corresponds to the ratio of experimental resistance R_{exp} to the calculated resistance R_{cal}. A value of $\mu_{\theta R} > 1$ represents a conservative bias of the resistance model, which leads to a reduction of the partial factor γ_{Ra}. Here, the resistance

model is defined as the model for determining the vertical resistance based on a known value of masonry compressive strength. The resistance model uncertainty factor θ_R is assumed to cover typical deviations in the overall dimensions of the wall.

8.2.4 Consideration of Statistical Uncertainty

In principle, the consideration of statistical uncertainty follows the approach in Annex D of EN 1990 (2010), according to which the characteristic value and the design value of a material property are determined as specified fractiles of the corresponding posterior predictive distribution (see also Section 2.6.4). In contrast to this approach, which is based on non-informative prior distributions, the use of informative prior distributions for the variance of material strength is incorporated in the presented method to reduce statistical uncertainty. A similar approach can be found in Val and Stewart (2002), in which a general framework for deriving partial factors based on the posterior predictive distributions of the respective material properties is presented. Instead of tabulated fractile factors k_n and $k_{d,n}$ as specified in EN 1990 (2010), statistical uncertainty is considered within the parameter $\sigma_{ln,ma}$ in the proposed method, which is demonstrated in more detail in Section 8.4.

8.2.5 Target Reliability

The target reliability index β_t is an input parameter of the developed method and can be chosen as required by the relevant building authority, the owner, or other relevant parties. For high relative costs of safety measures, which is typical in the assessment of existing structures, and moderate consequences of failure, corresponding to consequence class CC 2 in EN 1990 (2010), a target reliability index $\beta_{t,1a} = 3.3$ for a one-year reference period is specified in JCSS (2001a) and ISO 2394 (2015) based on economic optimisation. Therefore, $\beta_{t,1a} = 3.3$ is applied as an example in this chapter. In particular cases, the required reliability level may be higher due to human safety criteria. More information on appropriate target reliability levels for existing structures can be found in Section 2.6.2.

8.2.6 Partial Factors for Actions

The focus of the developed method is on suitable characteristic values, partial factors, and assessment values for the compressive strength of existing masonry. However, in typical assessment situations, adjusting the partial factors for actions may also be appropriate. This is the case if additional structure-specific information regarding the variability of the actions is acquired, or the target reliability level is different from that for the design of new structures (fib bulletin 80 2016). In typical assessment cases, no additional information regarding the variability of actions is available. However, if the target reliability level is chosen to be lower than for the design of new structures, the partial factors for actions should also be reduced. For this purpose, it is recommended to apply the adjusted partial factor method (APFM; see Section 2.6.3).

In the APFM as illustrated in fib bulletin 80 (2016), partial factors are adjusted relative to a target reliability index $\beta_t' = 3.8$ for a reference period of 50 years. The target reliability level β_t'' for existing structures is applied for a reference period corresponding to the remaining service life. If target reliability levels β_t'' are specified on an annual basis instead, the APFM should be adapted as described next. It is assumed that the current set of partial factors defined by the Eurocodes approximately leads to an average annual reliability index of $\beta_{1a} = 4.2$ (see Section 2.5.1; Meinen and Steenbergen 2018). This reliability index is equal to the target reliability index $\beta_{t,1a}$ in JCSS (2001a) and ISO 2394 (2015) for normal costs of safety measures and moderate failure consequences. Hence, $\beta_{t,1a}' = 4.2$ can be defined as a reference value if annual target reliability levels are specified. Furthermore, the sensitivity factor for action variables is changed from $\alpha_E = -0.7$ to $\alpha_{E,1a} = -0.8$ to consider that a target reliability index for a one-year reference period is applied (see Section 2.5.4). Consequently, Eq. 2-109 and Eq. 2-110 for calculating the adjustment factors ω_γ for permanent and imposed loads can be rewritten as follows:

$$\omega_{\gamma,G} = \frac{\gamma_{\mathrm{Ea},G}\left(\beta_{\mathrm{t,1a}}''\right)}{\gamma_{\mathrm{Ea},G}\left(\beta_{\mathrm{t,1a}}'\right)} \frac{1-\alpha_{E,1a}\,\beta_{\mathrm{t,1a}}''\,v_G''}{1-\alpha_{E,1a}\,\beta_{\mathrm{t,1a}}'\,v_G'} = \frac{1+0.32\,\beta_{\mathrm{t,1a}}v_{\theta G}}{1+0.32\cdot 4.2\,v_{\theta G}} \frac{1+0.8\,\beta_{\mathrm{t,1a}}v_G''}{1+0.8\cdot 4.2\,v_G'} \qquad \textit{Eq. 8-12}$$

$$\begin{aligned}\omega_{\gamma,Q} &= \frac{\gamma_{\mathrm{Ea},Q}\left(\beta_{\mathrm{t}}''\right)}{\gamma_{\mathrm{Ea},Q}\left(\beta_{\mathrm{t}}'\right)} \frac{1-v_{Q,1a}''\left[0.45+0.78\ln\left(-\ln\left(\Phi\left(-\alpha_{E,1a}\beta_{\mathrm{t,1a}}''\right)\right)\right)\right]}{1-v_{Q,1a}'\left[0.45+0.78\ln\left(-\ln\left(\Phi\left(-\alpha_{E,1a}\beta_{\mathrm{t,1a}}'\right)\right)\right)\right]} \\ &= \frac{1+0.32\,\beta_{\mathrm{t,1a}}v_{\theta Q}}{1+0.32\cdot 4.2\,v_{\theta Q}} \frac{1-v_{Q,1a}''\left[0.45+0.78\ln\left(-\ln\left(\Phi\left(0.8\,\beta_{\mathrm{t,1a}}''\right)\right)\right)\right]}{1-v_{Q,1a}'\left[0.45+0.78\ln\left(-\ln\left(\Phi\left(0.8\cdot 4.2\right)\right)\right)\right]}\end{aligned} \qquad \textit{Eq. 8-13}$$

with $v_G' = 0.1$, $v_{\theta G} = 0.065$, and $v_{\theta Q} = 0.11$ according to the suggestions in fib bulletin 80 (2016). The suggested CoV $v_{Q,50a}' = 0.25$ of the maximum imposed load for a reference period of 50 years can be transformed to a CoV for a one-year reference period if, as an approximation, independence of the extreme values in subsequent years is assumed. According to the principles for Gumbel-distributed random variables, the standard deviation remains constant if the reference period is changed to one year, whereas the mean value reduces (see Eq. 2-32 in Section 2.3.4). This results in a CoV of $v_{Q,1a}' = 1.05$. If no additional information regarding the variability of the actions is available, then $v_{Q,1a}'' = v_{Q,1a}'$ and $v_G'' = v_G'$. For the target reliability index $\beta_{t,1a}'' = 3.3$, the following partial factors for permanent and imposed load are obtained:

$$\gamma_G''\left(\beta_{\mathrm{t,1a}}'' = 3.3\right) = \omega_{\gamma,G}\,\gamma_G' = 0.93\cdot 1.35 = 1.26 \qquad \textit{Eq. 8-14}$$

$$\gamma_{Q,\mathrm{imp}}''\left(\beta_{\mathrm{t,1a}}'' = 3.3\right) = \omega_{\gamma,Q}\,\gamma_{Q,\mathrm{imp}}' = 0.70\cdot 1.5 = 1.05 \qquad \textit{Eq. 8-15}$$

Although the CoV of variable actions is usually higher than for permanent actions, the adjusted partial factors γ_Q for variable loads can become lower than the partial factor γ_G for permanent loads. The reason is that characteristic values G_k of permanent loads are defined via their mean value, whereas characteristic values Q_k for variable actions are defined as upper fractiles of the extreme values for a specific reference period and thus already containing a safety margin.

In contrast to the approach in DBV-Heft 24 (2013), the possible reduction of the partial factors for actions is not implicitly considered by reducing the partial factor for the resistance variables. This decision is made since actions can also have a favourable effect, and, therefore, the implicit consideration of reduced partial factors for actions in the partial factors for resistance variables is not applicable in all cases. Furthermore, this would also limit the application to specific ratios of the different types of actions.

In Section 8.5, the combined use of the APFM for partial factors of actions and the proposed method for determining assessment values of masonry compressive strength is validated for typical existing masonry structures through reliability analyses.

8.2.7 Further Influences on Masonry Compressive Strength

The following influences on masonry compressive strength are not considered by the developed method and are, therefore, neither explicitly nor implicitly covered by the obtained assessment value $f_{ma,a}$:

- Effects of high sustained loads
- Joint thicknesses considerably differing from standard dimensions
- Unusually high moisture content of masonry
- Bed joints inadequately filled with mortar
- Other structural defects, such as large cracks

If applicable, these influences must be considered separately by utilising appropriate models. According to the German National Annex to Eurocode 6, DIN EN 1996-1-1/NA (2019), the design value of masonry compressive strength $f_{ma,d}$ has to be reduced by a factor of $\zeta = 0.85$ to consider the effect of sustained loads (self-weight, snow, and imposed load) on masonry compressive strength. Since the investigation of the influence of sustained loads on masonry compressive strength is beyond the scope of this thesis, it is recommended to also apply this factor to the assessment value of masonry compressive strength.

As illustrated in Section 3.5.5, the typical variability of bed joint thicknesses does not lead to a significant increase in the variability of masonry strength since the influence of the variability of unit and mortar compressive strength clearly dominates. Therefore, the variability of bed joint thicknesses is not explicitly considered in the developed method. Instead, the resulting variability is covered by the model uncertainty factor θ_f. Although the

variability of mortar joint thicknesses is not explicitly addressed, an average mortar joint thickness that is considerably higher than normatively specified should be considered. Further information and references for considering the influences listed above are provided in Sections 3.3.5 and 3.5.5.

8.3 Model Uncertainties

8.3.1 Uncertainty in the Resistance Model

For the proposed method, the uncertainty in calculating the vertical resistance of a masonry wall must be specified. Therefore, the model uncertainty factor $\theta_R = R_{exp} / R_{cal}$, which is the ratio of experimental to calculated resistance, is quantified by stochastic parameters, namely its mean $\mu_{\theta R}$ and its CoV $v_{\theta R}$. In Table 8-1, values for $\mu_{\theta R}$ and $v_{\theta R}$ stated in the literature are displayed. Furthermore, corresponding partial factors γ_{Ra} based on Eq. 8-11 are given for $\beta_{t,50a} = 3.8$ and $\alpha_R = 0.8$ (i.e. the current standard values for the design of new structures) and for $\beta_{t,1a} = 3.3$ and $\alpha_{R,1a} = 0.7$.

Table 8-1 Stochastic models for resistance model uncertainty in the literature

Reference		Material	Model	Mean $\mu_{\theta R}$	CoV $v_{\theta R}$	γ_{Ra} for $\alpha_R \beta_t$ =	
						$0.8 \cdot 3.8$	$0.7 \cdot 3.3$
Glowienka (2007)		Calcium silicate masonry	Glock (2004)	0.99	0.16	1.23	1.17
		Autoclaved aerated concrete masonry		1.01	0.11	1.13	1.10
Brehm (2011)		Clay brick masonry	Rigid-plastic stress-strain relationship	1.10	0.18	1.13	1.07
Bakeer and Salehi (2019)		Masonry (general)	Bakeer (2016a)	0.969	0.104	1.17	1.14
fib bulletin 80	(a)	Concrete	-	1.0	0.14	1.19	1.14
	(b)			1.0	0.08	1.10	1.08
DIN EN 1996-1-1/NA*		Masonry (general)	-	1.0	0.14	1.19	1.14
* Implicitly included CoV of model uncertainty.							

The values from Brehm (2011) are based on a comparison between the experimental capacity of shear walls failing due to flexural compression and the theoretical resistance obtained by assuming a fully plastic stress-strain relationship. The mean and CoV provided in Glowienka (2007) and Bakeer and Salehi (2019) are obtained by comparing the experimental vertical resistance of walls with varying slenderness to the load-bearing capacity according to the models by Glock (2004) and Bakeer (2016a), respectively. Furthermore, the values for $\mu_{\theta R}$ and $v_{\theta R}$ specified in fib bulletin 80 (2016) for concrete structures are listed; these differentiate between case (a), in which the variability of geometrical properties is significant, and case (b), in which geometrical uncertainty can be neglected.

Furthermore, it is determined which value for $\upsilon_{\theta R}$ is implicitly included in the partial factor $\gamma_M = 1.5$ as specified by DIN EN 1996-1-1/NA (2019). For this purpose, $\mu_{\theta R} = 1$ is assumed, and the CoV for masonry compressive strength is taken as $\upsilon_{ma} = 17$ % according to the recommendation for clay brick masonry in JCSS (2011). This leads to $\gamma_m = 1.27$ for $\beta_t = 3.8$ (Eq. 8-9), which results in $\gamma_{Rd} = \gamma_M / \gamma_m = 1.19$ (Eq. 8-4) and, hence, $\upsilon_{\theta R} = 14$ % (Eq. 8-11). Therefore, the stochastic model implicitly included in DIN EN 1996-1-1/NA (2019) is equivalent to the recommendation in fib bulletin 80 (2016) for case (a); see Table 8-1.

In Fig. 8-1, the partial factors γ_{Ra} resulting from the models for different values of the target reliability index based on Eq. 8-11 are displayed. The partial factor γ_{Ra} obtained for the stochastic model implicitly included in DIN EN 1996-1-1/NA (2019) lies in the upper middle of the other models. Furthermore, it matches with case (a) in fib bulletin 80, and, due to its derivation, it is consistent with DIN EN 1996-1-1/NA (2019). Therefore, $\upsilon_{\theta R} = 14$ % and $\mu_{\theta R} = 1.0$ are adopted in the following.

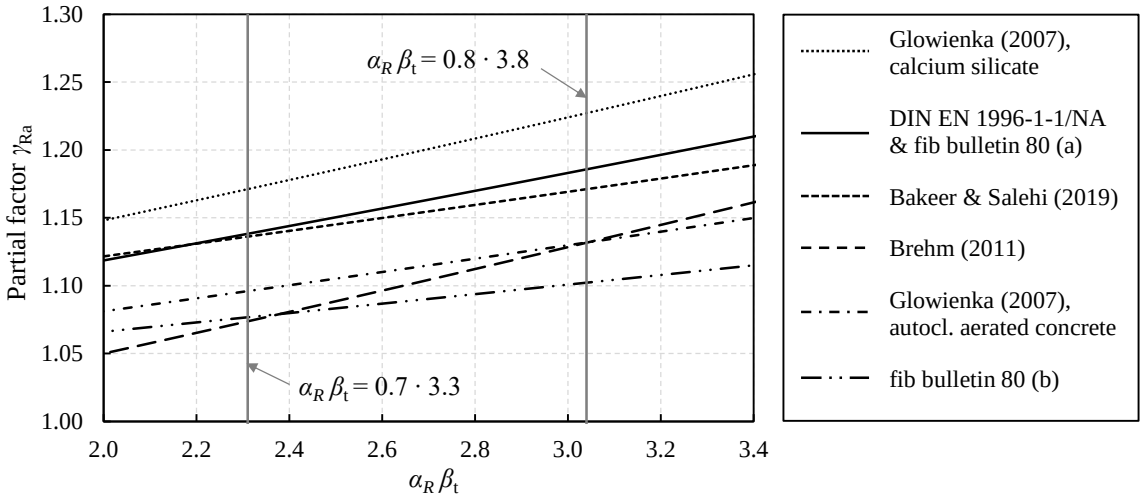

Fig. 8-1 Influence of target reliability and stochastic model on the partial factor γ_{Ra} for resistance model uncertainty

8.3.2 Uncertainty in Masonry Compressive Strength Prediction

In this section, the uncertainty associated with the prediction of masonry compressive strength based on unit and mortar compressive strength is quantified utilising experimental results from the literature. The data from compressive strength tests on solid clay brick masonry, which was compiled for this purpose, consists of experiments from three sources. The first two sources are test databases by Kirtschig and Meyer (1987) and Tschötschel (1990). Both databases contain results of compressive strength tests on laboratory-constructed masonry specimens (RILEM specimens, stack-bonded prisms, single wythe walls, and bonded masonry walls) made of various combinations of unit and mortar. Only tests on solid clay brick masonry with concentric compression loading and at least $n = 3$ repetitions for the same parameter combination are considered. From the database by Tschötschel

(1990), only test results are included that are not part of the test database by Kirtschig and Meyer (1987). This results in 14 combinations of brick and mortar (42 tests in total) from Kirtschig and Meyer (1987) and 11 additional combinations (54 tests) from Tschötschel (1990). The third source are experiments from Lumantarna et al. (2014) consisting of compressive strength tests on three-brick high and one-brick long masonry specimens. These tests were conducted on either prisms directly extracted from existing masonry walls, including head and bed joints, or stack-bonded prisms constructed in the laboratory using solid clay bricks from existing buildings. From Lumantarna et al. (2014), 22 combinations of brick and mortar (120 test results, 45 field-extracted and 75 laboratory-constructed specimens) are added to the compiled test data. For all the tests, the corresponding unit and mortar compressive strength are provided in the referenced literature. In total, the test data for the subsequent investigations contains 216 test results corresponding to 47 combinations of solid clay bricks and mortar. The experimental data is displayed in Annex D.

Since unit, mortar, and masonry compressive strengths were obtained on test specimens with different geometries, the strengths need to be modified to receive standardised strength values. Therefore, unit compressive strength is multiplied by the shape factor according to EN 772-1 (2011). In the databases by Kirtschig and Meyer (1987) and Tschötschel (1990), most of the unit compressive strength results were obtained in tests according to the former German brick standard DIN 105-1 (1982), which required cutting bricks with a height of $h \leq 71$ mm in half. The halves were then laid upon each other with a thin cement mortar layer in between before they were tested. According to this testing procedure, no shape factor was required, which is also followed here.

In the databases by Kirtschig and Meyer (1987) and Tschötschel (1990), mortar strength values correspond to tests on mortar prisms as specified by EN 1015-11 (2019), whereas mortar strength corresponds to tests on cubes of 50 mm length in Lumantarna et al. (2014). The mortar strength results corresponding to both types of testing are directly used as input parameters for masonry compressive strength prediction here since no reliable conversion formula exists. All of the masonry compressive strength results are converted to a height to thickness ratio of $h / t = 5$ following the proposal by Mann (1983); see Eq. 3-12. Test results for bonded masonry (i.e. specimens with mortar joints parallel to the wall face) are additionally adjusted through division by 0.8, as specified in EN 1996-1-1 (2012), to obtain a masonry strength corresponding to single wythe masonry. Strength results obtained on stack-bonded masonry prisms (i.e. masonry specimens without perpend joints) are multiplied by a reduction factor, as the respective strength is higher due to the missing influence of perpend joints. This reduction factor for stack-bonded prisms is chosen as 0.91 according to the evaluation of experimental results in Section 4.3.

The model uncertainty is quantified for the empirical power models in EN 1996-1-1 (2012) and DIN EN 1996-1-1/NA (2019) and the model by Hilsdorf (1969). Although other models with mechanical backgrounds have been developed (see Section 3.5.2), the investigation is limited to Hilsdorf's model as an example since none of the models with a mechanical background is commonly used in current engineering practice. In the model by Hilsdorf (1969), the factor U_u for describing the non-uniformity of the stress distribution is set to 1.5 in this investigation, and unit tensile strength f_{bt} is estimated as 0.04 f_b (Schubert 2010).

The ratio of mean experimental strength $f_{ma,exp}$ to predicted strength $f_{ma,cal}$ is determined for all of the 47 parameter combinations. These ratios can be viewed as random realisations of the model uncertainty factor θ_f, which is defined by

$$\theta_f = \frac{f_{ma,exp}}{f_{ma,cal}} \qquad \textit{Eq. 8-16}$$

For quantification of the model uncertainty, the arithmetic mean $m_{\theta f}$ and the sample CoV $V_{\theta f}$ of the ratios between experimental and predicted strength are determined, which serve as estimates for the expected value $\mu_{\theta f}$ and the coefficient of variation $v_{\theta f}$ of the model uncertainty factor. The CoV $v_{\theta f}$ quantifies the precision of the model, whereas the expected value $\mu_{\theta f}$ specifies the bias. For $\mu_{\theta f} > 1$, the bias is conservative.

The parameters K, α, and β of the empirical power equation (see Eq. 3-19) can be optimised to obtain a model with corresponding arithmetic mean $m_{\theta f} = 1$ and a minimum CoV $V_{\theta f}$. As a result of this procedure, a fourth model is created, which is the optimum power model with regard to model uncertainty based on the employed test data. In the optimisation of the model, $\alpha + \beta = 1$ is chosen as a boundary condition for the reasons explained in Section 3.5.4. Furthermore, with only two independent parameters K and α, the risk of overfitting is also reduced. With the parameter α, the CoV of the model uncertainty factor (the precision) is controlled, whereas the parameter K determines the expected value of the model uncertainty factor (the bias). The optimisation results in $K = 0.71$, $\alpha = 0.76$, and $\beta = 0.24$. The optimised parameter values for α and β align excellently with those obtained by the first-order Taylor approximation of the model by Hilsdorf (1969) in Section 3.5.4, which also resulted in $\alpha = 0.76$ and $\beta = 0.24$.

In Fig. 8-2 (left), the combinations of mortar and unit compressive strengths included in the evaluated test data are displayed. The compiled test data very well covers the range of mortar strengths < 15 N/mm² and unit strengths < 40 N/mm². In Fig. 8-2 (right), the mean experimental strengths $f_{ma,exp}$ are compared to the predictions $f_{ma,cal}$ by the investigated models. It should be noted that the power models from EN 1996-1-1 (2012) and DIN EN 1996-1-1/NA (2019) aim to determine the characteristic masonry compressive strength, whereas the model by Hilsdorf and the power model with optimised parameters aim to determine

the mean value of masonry compressive strength. It is evident that the prediction of masonry compressive strength is connected with a significant model uncertainty that must be considered when masonry compressive strength is determined based on its component strengths. Furthermore, it is worth mentioning that none of the points corresponding to the model in DIN EN 1996-1-1/NA (2019) lies significantly below the experimental strength, which is due to conservatism in the formulation of the corresponding formula.

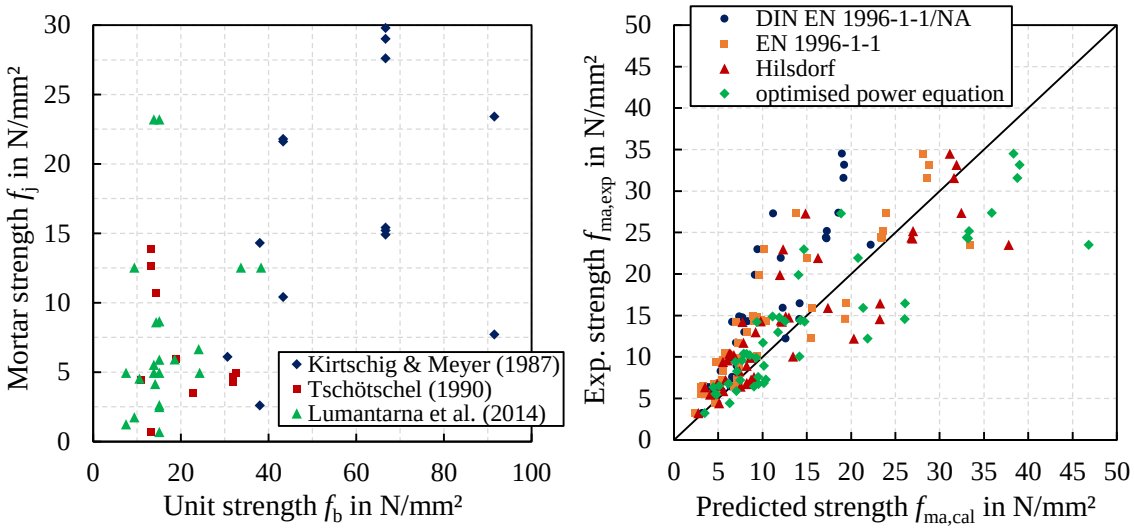

Fig. 8-2 *Left: Combinations of mortar and unit compressive strengths included in the evaluated test data*
Right: Comparison of experimental masonry compressive strengths to the predictions of various models

If the exponents α and β of the power equation are chosen to fulfil $\alpha + \beta = 1$, the power equation can be expressed as a relationship between dimensionless variables:

$$\frac{f_{ma}}{f_j} = K \left(\frac{f_b}{f_j} \right)^{\alpha} \qquad \textit{Eq. 8-17}$$

In logarithmic form, Eq. 8-17 can be written as

$$\ln \frac{f_{ma}}{f_j} = \ln K + \alpha \ln \frac{f_b}{f_j} \qquad \textit{Eq. 8-18}$$

Eq. 8-17 and Eq. 8-18 make it possible to display the power relationship between masonry compressive strength and the component strengths in planar view if the condition $\alpha + \beta = 1$ is met. In Fig. 8-3, the power equation for solid clay brick masonry from EN 1996-1-1 (2012), the power equation with optimised parameters, and the experimental results are displayed. The illustration in logarithmic form demonstrates that the power equation is very well suited to describe the relationship between masonry, unit, and mortar strength, although the choice of a power equation is not based on mechanical reasons. The parameter α

is the slope of the linear curve in the logarithmic representation, and the parameter K corresponds to the ratio f_{ma} / f_j for $f_b / f_j = 1$.

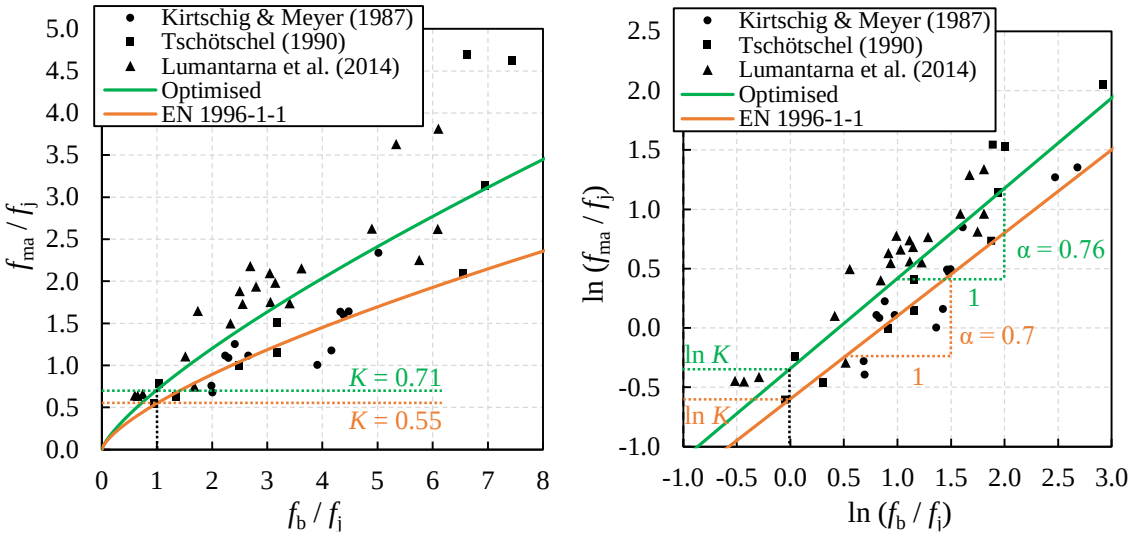

Fig. 8-3 Comparison of experimental masonry compressive strengths and predictions by power equations with $\alpha + \beta = 1$

Table 8-2 displays the model uncertainty statistics for the four investigated models. It can be seen that the CoVs of the model uncertainty are relatively close to each other, with the lowest CoV of 26 % obtained for the power model from DIN EN 1996-1-1/NA (2019). The highest CoV is obtained for the model by Hilsdorf (1969), although it has more input parameters than the power equation. It additionally includes the tensile strength of the unit, which, however, was not directly tested for the investigated specimens, and the ratio of joint thickness to unit height. This indicates that models with a mechanical background may only be favourable over empirical models if additional mechanical input parameters, such as unit tensile strength, are directly tested or uncommon geometrical boundary conditions, such as unusually thick mortar joints, are present. The optimisation of the power equation parameters does not lead to a much lower CoV compared to the existing equations. Compared to the model in DIN EN 1996-1-1/NA (2019), the CoV is even higher, which is due to the additional condition of $\alpha + \beta = 1$ in the optimisation.

Table 8-2 Model uncertainty of masonry compressive strength prediction

Model	Parameters of power equation			Ratio θ_f			
				All data		Lumantarna et. al (2014)	
	K	α	β	Mean	CoV	Mean	CoV
EN 1996-1-1	0.55	0.7	0.3	1.39	29.1 %	1.62	17.2 %
DIN EN 1996-1-1/NA	0.95	0.585	0.162	1.49	25.8 %	1.63	21.6 %
Optimised	0.71	0.76	0.24	1.00	28.6 %	1.18	16.8 %
Hilsdorf (1969)	-			1.18	30.1 %	1.42	19.0 %

As expected, the mean $m_{\theta f}$ of the ratio θ_f is higher for the two normative power equations compared to the two other models since these equations are formulated to determine the characteristic value instead of the mean value of masonry compressive strength. Based on the factor 0.8, which is usually stated as the conversion factor $f_{\mathrm{ma,k}} / f_{\mathrm{ma,m}}$ between characteristic and mean value included in the power equation (see Section 3.5.3), a mean ratio of 1 / 0.8 = 1.25 would be expected. However, the mean ratios of $m_{\theta f}$ = 1.39 and 1.49 are higher. These results indicate two possibilities. First, the normative power equations may include a higher characteristic-to-mean reduction factor than usually stated. Second, the evaluated test data may contain masonry compressive strength results that are systematically higher on average than those included in the test database used for deriving the normative parameters.

One reason for the relatively high CoVs of θ_f are the different types of test specimens in the evaluated test data, whose influence cannot be entirely captured by corresponding conversion factors. Another reason is potentially different boundary conditions in the tests since they were conducted by various researchers. To obtain a more accurate estimate of the model uncertainty, only the test results by Lumantarna et al. (2014) are considered in a second evaluation of the model uncertainty statistics. Therefore, all tests in the evaluation are conducted by only one research team and, hence, according to similar testing conditions. Furthermore, the test results by Lumantarna et al. (2014) cover a range of unit and mortar strengths that is very representative of existing masonry from before 1950 (see Fig. 8-2 and Fig. 7-3). As evident from Table 8-2, the evaluation of only the data from Lumantarna et al. (2014) leads to much lower CoVs. For the model in EN 1996-1-1 (2012), for example, the CoV decreases from 29.1 % to 17.2 %.

It is noted that some of the 47 combinations of unit and mortar compressive strength (see Fig. 8-2, left) lie outside the application range of the power equation as specified in EN 1996-1-1 (2012) and DIN EN 1996-1-1/NA/A1 (2014). However, considering only the combinations within the application range (38 and 32, respectively) does not lead to a significant reduction of the CoVs.

The CoV of the ratio θ_f in Table 8-2 still includes uncertainties in the testing procedure, such as measurement errors and geometrical imperfections. Furthermore, unit, mortar, and masonry compressive strength were only tested on a limited number of specimens. Hence, the average test results for unit and mortar compressive strength may deviate from the average unit and mortar strength in the tested masonry specimens. According to Ellingwood et al. (1980), the actual CoV $v_{\theta f}^{*}$ of model uncertainty can be obtained by

$$v_{\theta f}^{*} = \sqrt{v_{\theta f}^{2} - v_{\mathrm{test}}^{2} - v_{\mathrm{spec}}^{2}} \qquad \textit{Eq. 8-19}$$

where v_{test} is the CoV representing testing uncertainties. The term v_{spec} represents uncertainties related to differences between the strength of the separately tested brick and mortar samples and the actual strength in the test specimens. It also represents deviations of the actual geometrical dimensions of the tested specimens from the nominal or measured geometrical dimensions.

The stochastic model for the uncertainty in masonry compressive strength prediction is meant to include the effect of typical geometrical deviations in the ratio of bed joint thickness to unit height. Since the application of Eq. 8-19 also aims to remove these variations, no further reduction is made at this point. Therefore, the CoV of the model uncertainty in predicting masonry compressive strength is set to $v_{\theta f} \approx 17$ % in the following. A conservative bias, which is found for the normative equations, is not considered. This keeps the developed method open for new, advanced models that predict masonry strength with higher precision and less bias. Thus, the mean of the model uncertainty factor is set to $\mu_{\theta f} = 1$. The model uncertainty factor θ_f is assumed to be log-normally distributed in the following. This choice is advantageous because, as a consequence, multiplying the log-normally distributed masonry compressive strength by θ_f yields a product that is also log-normally distributed.

In the quantification of model uncertainty above, the prediction of masonry compressive strength is, in most cases, based on mortar compressive strengths determined by standard testing on prisms or cubes (i.e. tests on masonry samples that did not cure within masonry). The only exception are those tests by Lumantarna et al. (2014) that were performed on masonry samples directly taken from existing buildings. It is expected that a prediction based on the actual mortar strength in the joint (e.g. obtained by double punch testing) increases the accuracy since the curing conditions are implicitly taken into account (see Sections 3.4.3 and 4.2.2). However, the existing empirical models are based on standard mortar strengths, and too few test results are available to derive an empirical power equation based on the actual mortar strength in the joint. Therefore, the mortar compressive strength determined by double punch tests on samples extracted from masonry joints must be converted to the standard prism strength before being used as an input value for the power equation. By this conversion, additional uncertainty is introduced. It is assumed that this additional uncertainty is compensated for by the increase in accuracy through implicitly taking the curing conditions into account. Hence, the model uncertainty determined above can be considered suitable also for predictions based on mortar samples extracted from masonry.

8.4 Combination of the Different Types of Uncertainty and Approximation

8.4.1 General

In the previous chapters, the different types of uncertainty (spatial material variability, statistical uncertainty, and model uncertainty) were investigated separately. Next, these uncertainties are combined to determine assessment values of masonry compressive strength that include all the corresponding effects. First, probability distributions of the resistance of masonry walls are determined by stochastic simulation. These simulations are performed for the case of indirect testing of masonry compressive strength and are based on

- the relationship between the probability distribution of spatially variable masonry compressive strength and the resulting distribution of the wall resistance (see Chapter 6),
- the Bayesian framework and prior distributions for unit and mortar compressive strength presented in Chapter 7, and
- the findings for model uncertainty from Section 8.3.

Then, suitable assessment values can be determined as fractiles of the simulated posterior predictive distribution. Since the aim is to develop a method for engineering practice, the results of the stochastic simulations need to be approximated. Finding an approximation that is both sufficiently exact and easy to use includes answering the following questions:

- Should the effects caused by the spatial variability of material properties be considered, or can they be neglected?
- How can the predictive log-*t* distributions for unit and mortar compressive strength be combined to a predictive distribution for masonry compressive strength?
- Is the strength reduction factor for walls with a small cross-section defined in EN 1996-1-1 (2012) also suitable for the assessment of existing masonry walls?
- Is it necessary to define a different procedure for slender masonry walls that fail due to buckling?

8.4.2 Simulation Procedure for Combining the Different Types of Uncertainty

The procedure of the stochastic simulation is illustrated by a flowchart in Fig. 8-4. The single steps are based on the findings from the previous chapters and explained in the following. The flowchart is based on the assumption that the resistance of the considered masonry wall is mainly dependent on masonry compressive strength. For slender walls failing due to buckling, a slightly altered procedure is described in Section 8.4.5.

Several times during the procedure, the expectation μ_X and CoV υ_X of log-normal random variables X needs to be transformed to the expectation $\mu_{\ln X}$ and variance $\sigma_{\ln X}{}^2$ of the logarithm of the random variables (and vice versa). This conversion is always done according to Eq. 2-26 and Eq. 2-27 in Section 2.3.4.

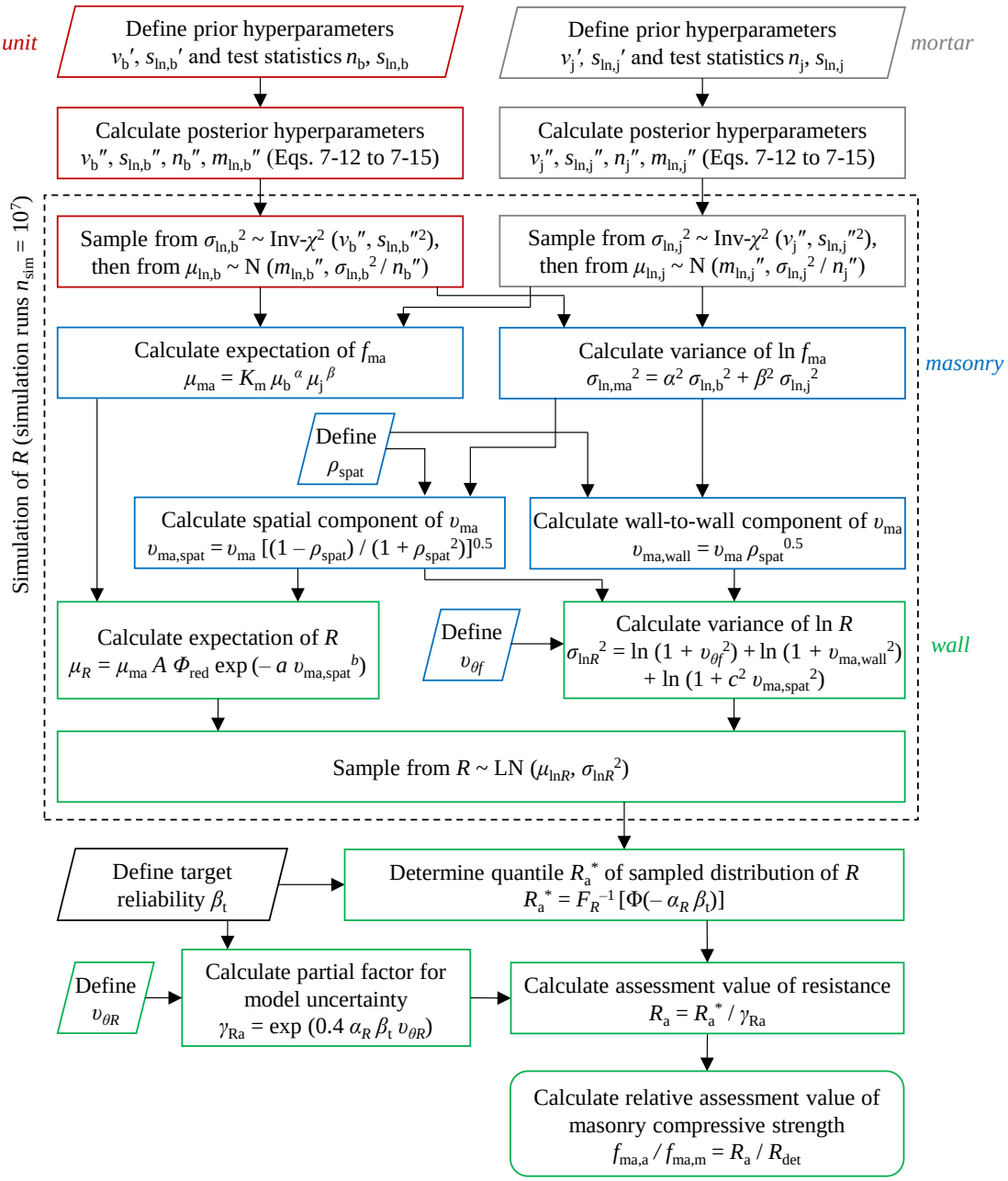

Fig. 8-4 Flowchart for simulating assessment values of masonry compressive strength

First, sample sizes n_b and n_j of unit and mortar compressive strength tests and corresponding standard deviations $s_{ln,b}$ and $s_{ln,j}$ of the test results need to be defined. The arithmetic means of the test results do not need to be explicitly specified, as the results are finally normalised by the compressive strength $f_{ma,m}$, which is the masonry compressive strength calculated based on the arithmetic means of the test results. Given the outcome of the test results, the posterior hyperparameters for the mean and variance of the logarithm of unit and mortar strength are calculated following the Bayesian framework presented in Section 7.2. Thereby, the posterior distributions for the means $\mu_{ln,b}$ and $\mu_{ln,j}$ and the variances $\sigma_{ln,b}^2$ and $\sigma_{ln,j}^2$ of the components are defined, and corresponding random values can be generated.

Based on the random values for the variances $\sigma_{\ln,b}^2$ and $\sigma_{\ln,j}^2$ of the logarithms of unit and mortar strength, the variance $\sigma_{\ln,ma}^2$ of the logarithm of masonry compressive strength is obtained by utilising the power equation with parameters $\alpha = 0.7$ and $\beta = 0.3$ defined in EN 1996-1-1 (2012).

The CoV υ_{ma} of masonry compressive strength can then be split into a component $\upsilon_{ma,spat}$ accounting for spatial variability and a component $\upsilon_{ma,wall}$ addressing wall-to-wall variability (see Eq. 6-25 and Eq. 6-26). It is assumed that the model uncertainty factor θ_f corresponds to an overall model uncertainty for the compressive strength of an entire wall. This is equivalent to perfect spatial correlation (i.e. $\rho_{spat} = 1$) for θ_f. Thus, in analogy to wall-to-wall material variability, the model uncertainty factor θ_f is not subjected to effects resulting from spatial variability. Hence, the overall variance $\sigma_{\ln R}^2$ of the logarithm of the wall resistance can be obtained as follows (see Eq. 6-28):

$$\sigma_{\ln R}^2 = \ln\left(1+\upsilon_{\theta f}^2\right) + \ln\left(1+\upsilon_{ma,wall}^2\right) + \ln\left(1+c^2\,\upsilon_{ma,spat}^2\right) \qquad \textit{Eq. 8-20}$$

where c is the parameter derived in Chapter 6 for the ratio between the resulting CoV of the wall resistance and the CoV of spatially variable masonry strength $\upsilon_{ma,spat}$. The model uncertainty factor θ_f and the wall-to-wall component of the variability of strength are log-normally distributed. In contrast, the probability distribution type of the wall resistance that results from spatial variability is undefined (see Fig. 6-1). For the various walls investigated in Chapter 6, different distribution types appeared to be most suitable for describing the distribution of R in the case of $\rho_{spat} = 0$. However, the CoV of the resistance resulting from the spatial component of material variability ($c \cdot \upsilon_{ma,spat}$) is usually much smaller than the CoV of model uncertainty ($\upsilon_{\theta f} = 17$ %). For $\rho_{spat} = 0.4$, as determined in Section 7.4.5, $c \cdot \upsilon_{ma,spat}$ is also much smaller than the component $\upsilon_{ma,wall}$. Therefore, the log-normally distributed components in Eq. 8-20 clearly dominate. The distribution of R can thus be modelled as log-normally distributed without significant loss of accuracy.

The expectations of masonry compressive strength and the load-bearing capacity are denoted as μ_{ma} and μ_R (instead of $f_{ma,m}$ and R_m) here to better distinguish them from the arithmetic mean values of a sample. The expectation μ_{ma} of masonry compressive strength is determined based on μ_b and μ_j using the power equation with $\alpha = 0.7$, $\beta = 0.3$, and K_m. The parameter K_m is meant to be calibrated such that the power equation yields a mean value of masonry compressive strength instead of a characteristic masonry strength (see Section 3.5.3). Due to the final normalisation, the choice of a specific value for K_m does not influence the simulation results. The expectation μ_R of the wall resistance is then obtained as a function of μ_{ma} and $\upsilon_{ma,spat}$ (see Eq. 6-22):

$$\mu_R = \mu_{ma}\; A\,\Phi_{red}\,\exp\left(-a\,\upsilon_{ma,spat}^b\right) \qquad \textit{Eq. 8-21}$$

where *a* and *b* are the parameters derived in Chapter 6 for describing the influence of spatial variability on the mean wall resistance. For the results presented in Section 8.4.3, the parameters *a*, *b*, and *c* are considered as found for the reference wall investigated in Section 6.3.4. For the considerations in Sections 8.4.4 and 8.4.5, the parameters derived for walls with small cross-sections and slender walls are used, respectively (see Sections 6.3.6 and 6.3.7).

With $\mu_{\ln R}$ and $\sigma_{\ln R}{}^2$, the distribution of the wall resistance is defined. For each randomly generated pair μ_R and $\sigma_{\ln R}{}^2$, one random value for the wall resistance is generated. The generation of random values is repeated 10^7 times for each set of boundary conditions. R_a^* can then be determined as a specific fractile of these simulated resistances (see Eq. 8-7). R_a is obtained by applying the partial factor γ_{Ra}, which is determined according to Eq. 8-11. Therefore, the actual stochastic simulation only considers the uncertainties contributing to γ_m.

Finally, the ratio of the assessment value $f_{ma,a}$ to the value $f_{ma,m}$ of masonry compressive strength is calculated. The parameter $f_{ma,m}$ represents the masonry compressive strength obtained by applying the arithmetic means $f_{b,m}$ and $f_{j,m}$ of unit and mortar compressive strength as input values in the prediction of masonry compressive strength. If the power equation is used for calculating the masonry compressive strength, $f_{ma,m}$ is defined as

$$f_{ma,m} = K_m \; f_{b,m}^{\alpha} \; f_{j,m}^{\beta} \qquad \textit{Eq. 8-22}$$

The ratio $f_{ma,a} / f_{ma,m}$ is equal to R_a / R_{det}, where R_{det} is the deterministic load-bearing capacity that is calculated based on the arithmetic means of unit and mortar compressive strength:

$$R_{det} = K_m \; f_{b,m}^{\alpha} \; f_{j,m}^{\beta} \; A\,\Phi_{red} = f_{ma,m} \; A\,\Phi_{red} \qquad \textit{Eq. 8-23}$$

This leads to the following expression:

$$\frac{R_a}{R_{det}} = \frac{f_{ma,a} \; A\,\Phi_{red}}{f_{ma,m} \; A\,\Phi_{red}} = \frac{f_{ma,a}}{f_{ma,m}} \qquad \textit{Eq. 8-24}$$

It is noted that the simulation is only required in the case of a limited sample size *n*. In the theoretical case of $n \to \infty$, assessment values can also be determined analytically, as demonstrated in Section 6.3.5. The simulation procedure displayed in Fig. 8-4 makes it possible to determine assessment values of masonry compressive strength that can be used in the verification of existing masonry structures. However, such a stochastic simulation is not feasible in engineering practice. Therefore, an approximate procedure is derived in the following based on an analysis of simulation results for different boundary conditions.

8.4.3 Simulation Results and Approximation for the Reference Case

In Fig. 8-5, simulation results for the ratio $f_{ma,a} / f_{ma,m}$ are displayed as a function of the spatial correlation coefficient ρ_{spat}. The correlation coefficient ρ_{spat} specifies what share of material variability can be attributed to spatial variability within a wall and what share to wall-to-wall variability. For $\rho_{spat} = 0$, all the variability of material properties is spatial variability, whereas for $\rho_{spat} = 1$, the material properties within each wall are homogeneous since material variability completely corresponds to variability between walls. The results are obtained for a target reliability level of $\beta_{t,1a} = 3.3$ combined with a sensitivity factor $\alpha_{R,1a} = 0.7$ and sample standard deviations $s_{ln,b} = s_{ln,j} = 0.35$.

First, only material uncertainty is considered. This means that the sample standard deviations for unit and mortar compressive strength are considered equal to the respective population standard deviations, and the CoVs for model uncertainty are set to zero. In this case, spatial variability leads to a positive effect: The ratio $f_{ma,a} / f_{ma,m}$ is considerably higher for $\rho_{spat} = 0$ than for $\rho_{spat} = 1$. This positive effect matches the results of the MCS in Chapter 6 (see Fig. 6-10).

Then, statistical uncertainty is introduced by defining a limited sample size $n_b = n_j = 6$ for tests on unit and mortar. Prior information is considered via the building-related priors from Section 7.4.3 with $v_b' = 7.7$, $s_{ln,b}' = 0.33$, $v_j' = 4.2$, and $s_{ln,j}' = 0.40$. Furthermore, model uncertainty is included according to the stochastic model for the uncertainty in predicting masonry compressive strength derived in Section 8.3.2 and the partial factor γ_{Ra} for resistance model uncertainty (see Section 8.3.1). By additionally considering statistical and model uncertainty, the positive effect of spatial variability disappears: The curve for $f_{ma,a} / f_{ma,m}$ becomes nearly horizontal.

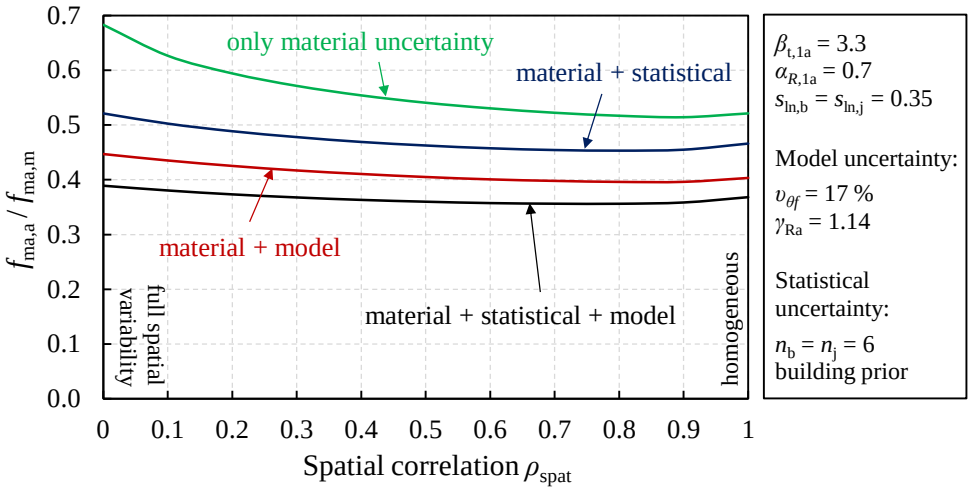

Fig. 8-5 Influence of spatial variability on the assessment value

The loss of the positive effect of considering spatial variability is caused by neither model nor statistical uncertainty alone, as Fig. 8-5 demonstrates. The curve for $f_{ma,a} / f_{ma,m}$ also

tends to become horizontal if either model or statistical uncertainty are considered separately in addition to material uncertainty. The reason for the loss of the positive effect can be explained with support from Fig. 8-6. In the left diagram, the probability density functions (PDFs) of the wall resistance for $\rho_{spat} = 0$ and 1 are given for the case, where only material uncertainty is considered. It is evident that the positive effect of considering spatial variability, which is given by a smaller area under the left tail of the PDF, is caused by the very low variability for $\rho_{spat} = 0$, which overcompensates for the reduction in the expectation μ_R.

If model uncertainty is introduced, both PDFs are widened. However, the effect on the PDF for $\rho_{spat} = 0$ is much more pronounced since the initial CoV is low. It is noted that the PDF in the right diagram of Fig. 8-6 only includes the model uncertainty for predicting masonry compressive strength, as the uncertainty in the resistance model is not considered in the simulation directly but by applying the partial factor γ_{Ra}. Introducing statistical uncertainty also has a more substantial effect in the case of $\rho_{spat} = 0$. Due to the reduction of the expectation μ_R with higher spatial variability, statistical uncertainty in the variance $\sigma_{ln,ma}^2$ also leads to an uncertainty in μ_R. Thus, the PDF is widened, and its kurtosis is also further increased. In total, introducing model and statistical uncertainty leads to the effect that the left tails of the PDFs become close (see Fig. 8-6, right).

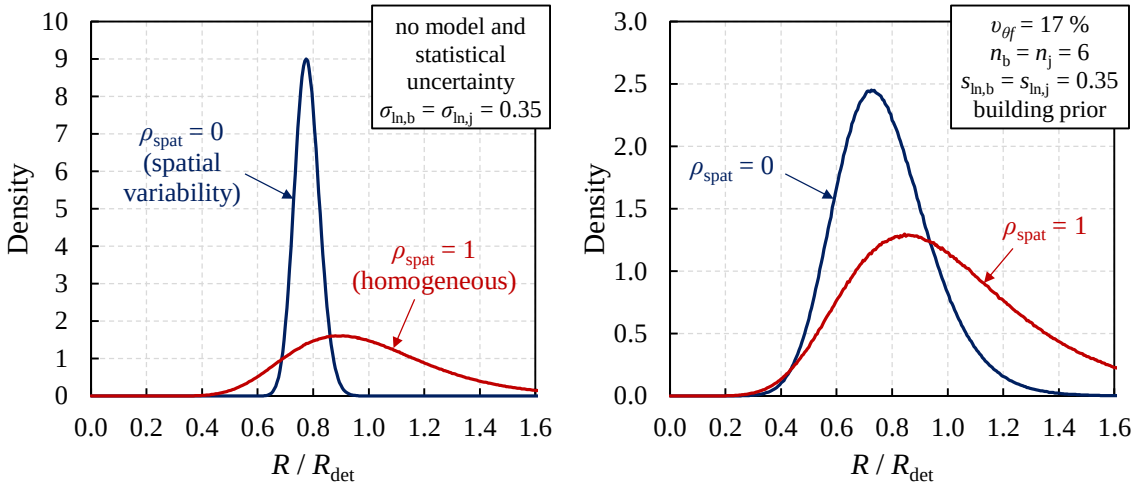

Fig. 8-6 Probability density of the wall resistance for $\rho_{spat} = 0$ and 1 (left: only material uncertainty; right: material, model, and statistical uncertainty)

The results presented in Fig. 8-5 and Fig. 8-6 indicate that the consideration of spatial variability may be negligible. Not explicitly addressing the influence of spatial variability would make the procedure for determining assessment values of masonry compressive strength much more convenient. Therefore, it is investigated whether the influence of spatial variability may also be neglected for other boundary conditions. The sample size is varied between $n_b = n_j = 3$ and $n_b = n_j = 30$, which is considered a typical range in the assessment of existing structures. The target reliability is chosen as $\beta_{t,1a} = 3.3$, which is the

example value for the assessment of existing structures; as $\beta_{t,1a} = 4.2$, which can be applied if the target reliability should not be reduced in comparison to the design of new structures; and as $\beta_{t,1a} = 3.7$ to define an intermediate value. In ISO 2394 (2015), $\beta_{t,1a} = 3.7$ corresponds to the target reliability both for high relative costs of safety measures and large failure consequences and for medium relative costs of safety measures and minor failure consequences. The standard deviations of the test results for the logarithms of unit and mortar strength are set to $s_{ln,b} = s_{ln,j} = 0.2$, 0.35, and 0.5, which correspond to a low, typical, and high variability of strength (see Section 7.3).

These subsequent simulations are performed for two different situations. The first case, which is assumed to be more common, corresponds to a situation where the same assessment value of masonry compressive strength is to be determined for several walls that are made from the same type of masonry. Therefore, tests are performed on specimens from more than one wall. In this case, the correlation of material properties within one wall is set to $\rho_{spat} = 0.4$ (see Section 7.4.5), and the building-related prior is used for both components. Then, a second situation is investigated where a single wall is assessed, meaning that the considered population of masonry consists of only one wall. In this case, the spatial correlation coefficient is set to $\rho_{spat} = 0$, as the observed CoVs do not include a wall-to-wall variability but only the spatial variability within the wall. In this case, the location-related prior is used to evaluate unit compressive strength since this prior distribution is representative of the variability within one wall. For mortar compressive strength, however, the building-related prior is used since the location-related prior for mortar strength cannot be considered representative of the variability within an entire wall, which is usually made of several mortar mixes (see Section 7.4.5). The simulation results for assessing several walls are presented in Fig. 8-7, and the results for assessing a single wall are displayed in Fig. 8-8.

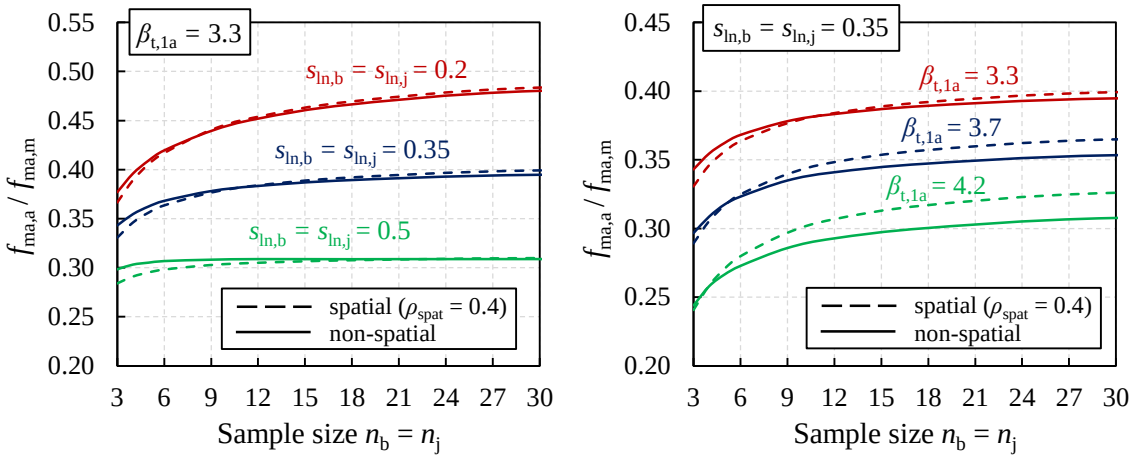

Fig. 8-7 *Assessment values $f_{ma,a}$ of masonry compressive strength obtained by spatial and non-spatial simulation (assessment of several walls, building-related prior)*

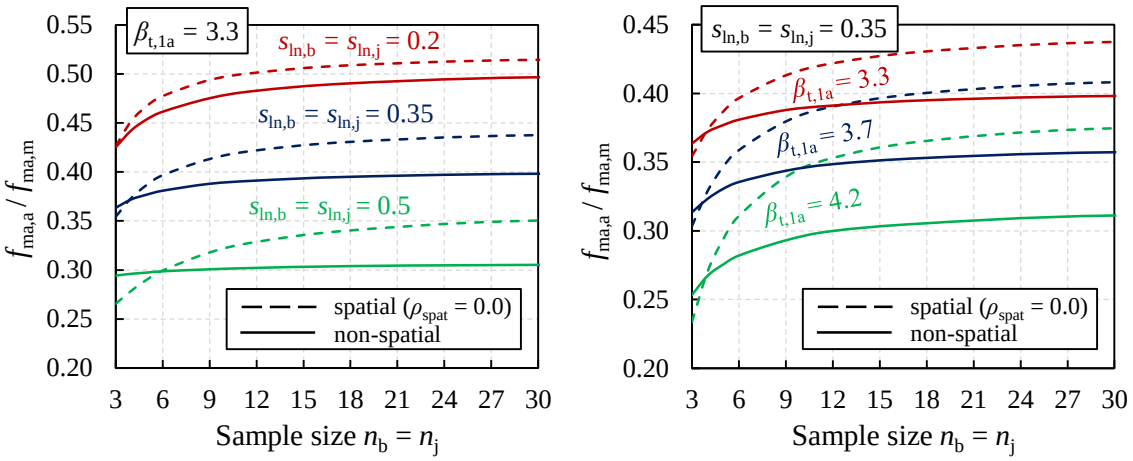

Fig. 8-8 *Assessment values $f_{ma,a}$ of masonry compressive strength obtained by spatial and non-spatial simulation (assessment of a single wall, location-related prior for unit, building-related prior for mortar)*

Based on Fig. 8-7 and Fig. 8-8, the following observations can be made:

- For both assessment situations and almost all boundary conditions, the difference between the spatial ($\rho_{spat} < 1$) and non-spatial ($\rho_{spat} = 1$) analysis is relatively low.
- If the sample size is at least $n_b = n_j = 6$, considering spatial variability never leads to an assessment value that is more than 3 % lower than the assessment value obtained by non-spatial analysis.
- If a single wall is investigated and the sample size is large, considering spatial variability can lead to an increase in the assessment value of more than 10 %. However, large sample sizes are rather uncommon if a single masonry wall is investigated.
- Comparing the non-spatial results for the two different assessment situations (single wall vs several walls), which only differ in the prior distribution for unit compressive strength, reveals only slight differences. In most cases, an assessment based on the location-related prior for unit compressive strength leads to slightly higher assessment values since, in this case, the prior estimate s' for the variability of unit compressive strength is smaller.

It can be concluded that the influence of spatial variability can be neglected without obtaining results that are either too conservative or too unsafe. Furthermore, the building-related prior information can conservatively be used in all assessment situations as it leads to lower assessment values in most cases. Choosing the location-related prior hyperparameters for unit strength is included in the proposed method as an additional option for assessing a single wall.

In addition to neglecting spatial variability, further approximations are needed to obtain an analytical method for determining suitable assessment values of masonry compressive strength. One obstacle for the analytical solution is that the predictive distributions for unit

and mortar compressive strength are log-*t* distributed. As shown in Section 3.5.4, the power equation for masonry compressive strength based on unit and mortar compressive strength is equivalent to a linear combination of the logarithms of strength:

$$\ln f_{\mathrm{ma}} = \ln \theta_f + \ln K_{\mathrm{prob}} + \alpha \ln f_{\mathrm{b}} + \beta \ln f_{\mathrm{j}} \qquad \textit{Eq. 8-25}$$

Therefore, the random variable for the logarithm of masonry compressive strength is a linear function of three random variables (i.e. $\ln \theta_f$, $\ln f_b$, and $\ln f_j$), with $\ln f_b$ and $\ln f_j$ being *t*-distributed. Unfortunately, the sum of two *t*-distributed random variables leads to a random variable with an unspecified distribution type. The predictive log-*t* distributions for f_b and f_j are approximated by log-normal distributions to overcome this obstacle. According to JCSS (2002), a predictive *t*-distribution can be approximated by a normal distribution if the corresponding standard deviation is chosen as

$$\sigma = s'' \sqrt{\frac{n''}{n''-1} \frac{\nu''}{\nu''-2}} \qquad \textit{Eq. 8-26}$$

where s'', n'', and ν'' are the posterior hyperparameters according to the Bayesian framework presented in Section 7.2. In JCSS (2002), it is stated that the approximation is suitable for ν'' and $n'' > 10$.

The example in Fig. 8-9 shows the goodness of the approximation for $m = m'' = 0$, $s = s'' = 1$, and $n = n'' = \nu'' + 1$. This corresponds to a non-informative prior and a predictive distribution that converges to a standard normal distribution for $n \to \infty$. In the left diagram, the PDF is shown, and in the right diagram, the left tail of the CDF is illustrated. It can be seen that the approximation improves for higher *n*. For low values of *n*, the goodness of the approximation is limited, as the normal distribution always has an excess kurtosis $\gamma_2 = 0$, whereas γ_2 is higher than zero for the *t*-distribution. Thus, the approximation slightly overestimates *p* fractiles with low *p*.

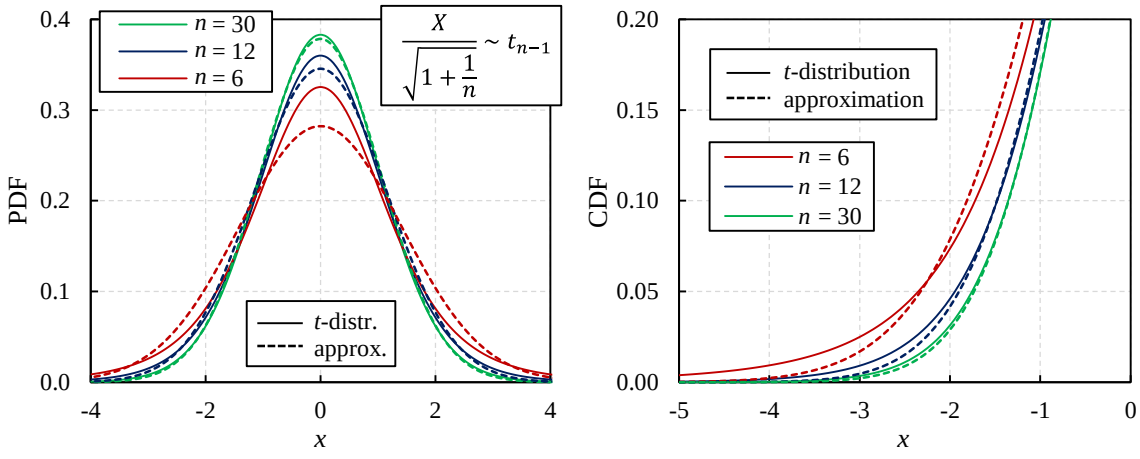

Fig. 8-9 Approximation of posterior predictive distribution

Based on the approximation provided by Eq. 8-26, the variance of the logarithm of masonry compressive strength can be determined as

$$\sigma_{\ln,ma}^2 = \sigma_{\ln \theta f}^2 + \alpha^2 \, s_{\ln,b}''^2 \left(\frac{n_b''}{n_b'' - 1} \frac{v_b''}{v_b'' - 2} \right) + \beta^2 \, s_{\ln,j}''^2 \left(\frac{n_j''}{n_j'' - 1} \frac{v_j''}{v_j'' - 2} \right) \qquad \textit{Eq. 8-27}$$

Thereby, the statistical uncertainty caused by the limited sample size for unit and mortar compressive strength is included in $\sigma_{\ln,ma}^2$, which can be inserted in Eq. 8-9 to obtain partial factors γ_m. Furthermore, assessment values of masonry compressive strength can be determined based on fractiles of the log-normal distribution with $\sigma_{\ln,ma}^2$ according to Eq. 8-27:

$$f_{ma,a} = \frac{1}{\gamma_{Ra}} \exp\left(-\alpha_R \, \beta_t \, \sigma_{\ln,ma} - 0.5 \, \sigma_{\ln,ma}^2\right) f_{ma,m} \qquad \textit{Eq. 8-28}$$

The previously presented simulation results (non-spatial analysis, building-related prior) are compared to the analytical approximation for the assessment value $f_{ma,a}$ of masonry compressive strength to check whether the approximation is sufficiently precise. Fig. 8-10 demonstrates that the approximation leads to very accurate results for the desired application, which is also the case for $n'' < 10$. The slight differences are negligible.

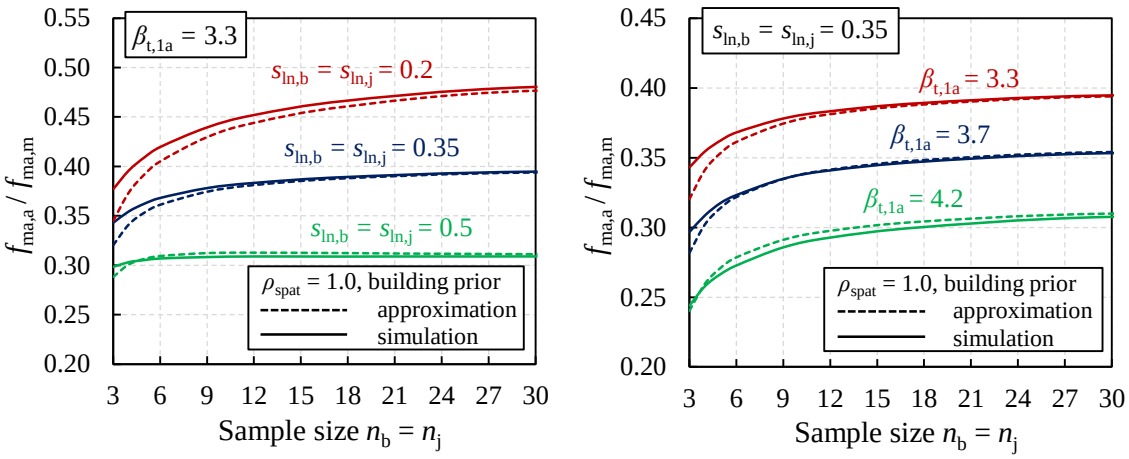

Fig. 8-10 Comparison of assessment values for masonry compressive strength obtained by simulation and analytical approximation

8.4.4 Considerations for Walls with Small Cross-Sections

In the simulations presented in the preceding section, the influence of spatial variability is considered as observed for the reference wall in Chapter 6, having five units per course. As demonstrated in Section 6.3.6, the assessment values of masonry compressive strength should be lower for walls with fewer units per course due to reduced stress redistribution capability. In EN 1996-1-1 (2012), this effect is considered by reducing the design value of masonry compressive strength by a factor of $0.7 + 3\,A$ (with A being the cross-sectional

area in m²) if A is smaller than 0.1 m². In the following, it is checked whether this reduction factor is also suitable for assessing existing masonry structures.

The cross-sectional area of one expanded unit in the finite element simulations of Chapter 6 is equal to 0.25 x 0.12 m² = 0.03 m². The cross-sectional areas A of the investigated walls with one, two, and three units per course are thus below 0.1 m². Therefore, the assessment values $f_{ma,a}$ for these walls are determined by stochastic simulation as described in Section 8.4.2. The results are then related to the reference assessment strength $f_{ma,a,ref}$ obtained for walls with five units per course.

In Fig. 8-11, the simulation results are presented and compared to the reduction factor defined by EN 1996-1-1 (2012). The simulation results are obtained for different boundary conditions: varying sample sizes n_b and n_j, different sample standard deviations $s_{ln,b}$ and $s_{ln,j}$, and different target reliability indices β_t. The spatial correlation coefficient is set to $\rho_{spat} = 0.4$ because, usually, destructive material testing is not performed on specimens from the wall with a small cross-section itself, as this would significantly weaken the considered wall. Hence, the assessment situation corresponds to determining an assessment value of masonry compressive strength for several walls collectively. In a subsequent step, the assessment values $f_{ma,a}$ of walls with $A < 0.1$ m² need to be multiplied by the specified reduction factor.

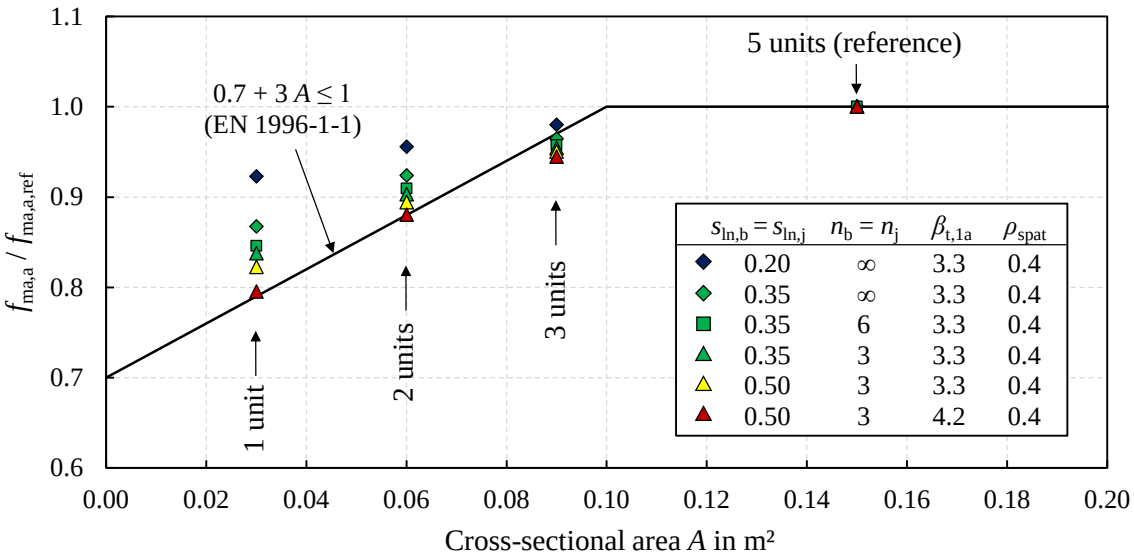

Fig. 8-11 Normative and theoretically required reduction of the design and assessment value of masonry compressive strength for walls with small cross-sections

As illustrated by Fig. 8-11, the theoretically required reduction depends on the chosen boundary conditions. In most cases, the reduction factor specified by EN 1996-1-1 (2012) is slightly conservative. The results indicate that the required reduction increases with higher target reliability indices β_t, higher sample standard deviations $s_{ln,b}$ and $s_{ln,j}$, and lower

sample sizes n_b and n_j. However, even for very low sample sizes $n_b = n_j = 3$ combined with high sample standard deviations $s_{ln,b} = s_{ln,j} = 0.5$ and a target reliability index $\beta_{t,1a} = 4.2$, the normative equation is found to be well suited.

The simulation results show a nonlinear relationship between the cross-sectional area A and the required reduction factor. It is noted that the reference wall does not correspond to the area of $A = 0.1$ m², below which the assessment strength must be reduced. This discrepancy is chosen to obtain more relevant results for the reference case, which must also cover walls with a much larger cross-sectional area. The normative equation can thus be viewed as a bilinear approximation of the actual nonlinear relationship. Consequently, the theoretical assessment values for walls with a cross-sectional area close to 0.1 m² can be slightly lower than obtained by the normative equation. However, the difference is negligible.

In summary, it can be stated that the existing normative equation matches sufficiently well with the more detailed and accurate simulation results. Therefore, the approach from EN 1996-1-1 (2012) can be adopted for the developed method without any modification.

8.4.5 Considerations for Slender Walls

The developed method shall also be applicable to slender masonry walls failing due to buckling. As mentioned in Section 3.7, the partial factor γ_M as defined in EN 1996-1-1 (2012) for the vertical resistance of masonry walls must account for both the influence of the variability of masonry compressive strength f_{ma} and the variability of the elastic modulus E_{ma}. If a masonry wall fails due to buckling, the load-bearing capacity is not affected by its compressive strength but only by its stiffness, which is mainly determined by E_{ma}, (see Section 3.3.3). Concerning suitable partial factors γ_M or assessment values $f_{ma,a}$ for slender masonry walls, the following must be considered:

- For walls that fail due to buckling, consideration of the spatial variability of material properties has a much more positive influence than for walls experiencing material failure (see Section 6.3.7).
- However, the material variability of the elastic modulus of masonry E_{ma} is usually higher than the variability of masonry compressive strength f_{ma} (see Section 6.2.2).
- In addition to predicting masonry compressive strength f_{ma}, the modulus of elasticity E_{ma} must be estimated for slender masonry walls.

This section investigates whether the assessment value $f_{ma,a}$ for masonry compressive strength that is determined based on test results for unit and mortar compressive strength can also be applied to slender masonry walls. For this purpose, the ratio between $R_{a,slender} / R_{det,slender}$ for a slender masonry wall and $R_{a,ref} / R_{det,ref}$ for the reference wall is determined via simulation. Due to the definition of the safety elements (see Section 8.2.3), this ratio is equivalent to $f_{ma,a,slender} / f_{ma,a,ref}$ if the mean strength $f_{ma,m}$ is equal for both walls:

$$\frac{\frac{R_{\mathrm{a,slender}}}{R_{\mathrm{det,slender}}}}{\frac{R_{\mathrm{a,ref}}}{R_{\mathrm{det,ref}}}} = \frac{\frac{\Phi_{\mathrm{red,slender}}\ A_{\mathrm{slender}}\ f_{\mathrm{ma,a,slender}}}{\Phi_{\mathrm{red,slender}}\ A_{\mathrm{slender}}\ f_{\mathrm{ma,m}}}}{\frac{\Phi_{\mathrm{red,ref}}\ A_{\mathrm{ref}}\ f_{\mathrm{ma,a,ref}}}{\Phi_{\mathrm{red,ref}}\ A_{\mathrm{ref}}\ f_{\mathrm{ma,m}}}} = \frac{f_{\mathrm{ma,a,slender}}}{f_{\mathrm{ma,a,ref}}} \qquad \textit{Eq. 8-29}$$

If the simulated assessment value $f_{\mathrm{ma,a,slender}}$ is greater than $f_{\mathrm{ma,a,ref}}$, which is the assessment value for the non-slender reference wall, the general method can also be conservatively applied to slender masonry walls.

In principle, the assessment value $f_{\mathrm{ma,a,slender}}$ of masonry compressive strength for slender masonry walls is determined as described in Section 8.4.2. The parameters *a*, *b*, and *c* for the influence of spatial variability are applied as derived in Section 6.3.7 for masonry walls failing due to buckling. Some further modifications and additional assumptions have to be made. In accordance with the MCS in Chapter 6, the CoV υ_E of the elastic modulus of masonry is taken as 1.3 times the CoV υ_{ma} of masonry compressive strength (see Section 6.2.2). It is further assumed that, in the homogeneous case, the resistance is proportional to the elastic modulus E_{ma} (see Section 3.3.3). The deterministic reduction factor Φ_{red} for considering the influence of eccentricity and slenderness at the middle height of the wall is a function of the ratio $E_{\mathrm{ma}} / f_{\mathrm{ma}}$. For the subsequent investigation, $E_{\mathrm{ma}} / f_{\mathrm{ma}}$ is supposed to be the ratio of the corresponding mean values, that is, $E_{\mathrm{ma,m}} / f_{\mathrm{ma,m}}$. It is assumed that the uncertainty in estimating the modulus of elasticity E_{ma} is equivalent to the uncertainty in predicting the compressive strength f_{ma}. Hence, the corresponding CoV $\upsilon_{\theta E}$ of model uncertainty is equal to $\upsilon_{\theta f}$. Eq. 8-20 can thus be modified to the following expression for slender masonry walls:

$$\sigma^2_{\ln R,\mathrm{slender}} = \ln\left(1+\upsilon^2_{\theta f}\right) + \ln\left(1+1.3^2\ \upsilon^2_{\mathrm{ma,wall}}\right) + \ln\left(1+c^2\ \upsilon^2_{\mathrm{ma,spat}}\right) \qquad \textit{Eq. 8-30}$$

Assuming that the uncertainty in predicting the elastic modulus of masonry is equivalent to the uncertainty in predicting masonry strength requires that the elastic modulus is estimated carefully. According to EN 1996-1-1 (2012), the modulus of elasticity is estimated via specified ratios $E_{\mathrm{ma}} / f_{\mathrm{ma}}$. However, the ratios $E_{\mathrm{ma}} / f_{\mathrm{ma}}$ for existing solid clay brick masonry can greatly differ from the recommended values in EN 1996-1-1 (2012) or DIN EN 1996-1-1/NA (2019), as described in Section 3.3.2. The prediction uncertainty could be reduced by defining appropriate ratios $E_{\mathrm{ma}} / f_{\mathrm{ma}}$ for further sub-types of masonry. Another option for improving the prediction accuracy is to utilise spring models based on the elastic moduli of unit and mortar (see Section 3.3.2). If neither of these options is feasible, assessing engineers need to make conservative assumptions based on previous experience.

In Fig. 8-12, the corresponding simulation results are presented. The resulting ratio $f_{\mathrm{ma,a,slender}} / f_{\mathrm{ma,a,ref}}$ is given as a function of the spatial correlation coefficient ρ_{spat}. The simulation is performed for different boundary conditions, with $n_{\mathrm{b}} = n_{\mathrm{j}} = 6$, $\beta_{\mathrm{t,1a}} = 3.3$, and

$s_{ln,b} = s_{ln,j} = 0.35$ constituting a reference case. Starting from this reference case, the sample size, the sample standard deviation, and the target reliability are altered one by one.

For $\rho_{spat} = 1$, the theoretical assessment value $f_{ma,a}$ is lower for slender walls since the CoV of the elastic modulus is higher than the CoV of masonry compressive strength. As the spatial correlation coefficient ρ_{spat} is reduced, the positive effect of considering spatial variability appears. For $\rho_{spat} = 0$, the theoretically required assessment value $f_{ma,a}$ is significantly higher for slender masonry walls. As discussed in Section 8.4.3, either $\rho_{spat} = 0$ or $\rho_{spat} = 0.4$ may be relevant in the assessment of existing masonry structures. In this range, $f_{ma,a,slender}$ is higher than $f_{ma,a,ref}$. Hence, the developed method, originally derived for non-slender walls with material failure, may conservatively be applied to slender masonry walls with stability failure. The very positive effect of considering spatial variability for slender walls compensates for the higher CoV of the modulus of elasticity compared to the compressive strength of masonry.

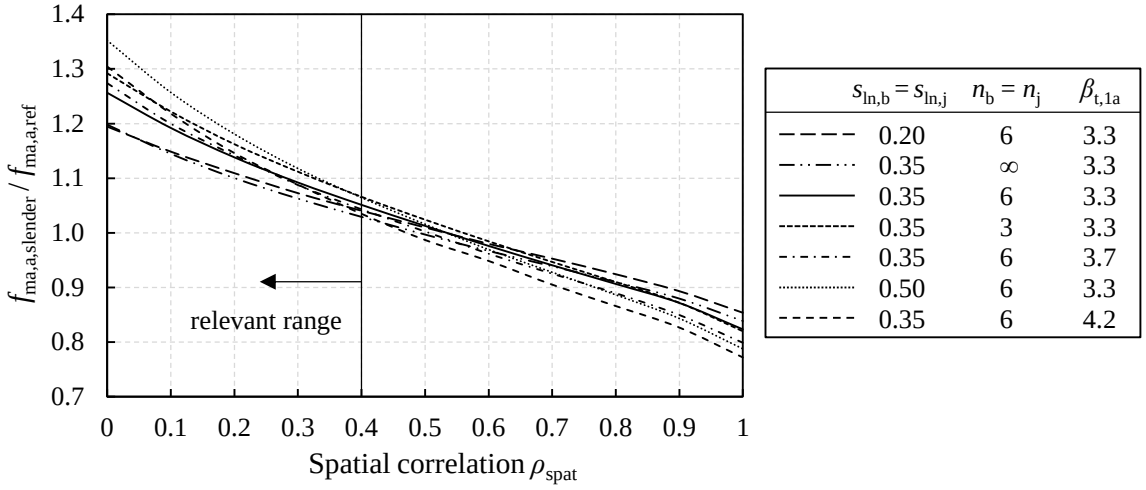

Fig. 8-12 Ratio of the theoretical assessment value $f_{ma,a,slender}$ for a slender wall to the assessment value $f_{ma,a,ref}$ for the non-slender reference wall

8.4.6 Considerations for Direct Testing of Masonry Compressive Strength

In the previous sections, the method for determining assessment values of masonry compressive strength is developed for separate tests on unit and mortar specimens. Here, consideration is given to how the approach can be adopted for direct compression tests on masonry specimens. In this context, direct testing refers to all procedures in which tests on composite specimens are performed, and, therefore, no application of a model for predicting masonry compressive strength based on the component properties is necessary. This type of testing includes, among other procedures, the testing of masonry cores according to Helmerich/Heidel (Heidel 1989) and the testing of masonry prisms according to Gunkler (1993). For a description of these testing procedures, see Section 3.4.4.

Direct testing has the advantage that there is no model uncertainty in predicting masonry compressive strength based on the component properties. However, conversion factors usually have to be applied to obtain a masonry strength that corresponds to the standardised compressive strength obtained on RILEM specimens as defined by EN 1052-1 (1998). Suitable relationships for converting the strength obtained on alternative composite specimens into the standardised strength are still the subject of ongoing research (see Section 3.4.4). The uncertainty associated with these testing procedures, which mainly results from this conversion, can be considered significantly smaller than the uncertainty corresponding to indirect testing and subsequent application of the power equation (see Fig. 3-6; Gigla 2020). However, the corresponding testing uncertainty is not as small as in the case of tests according to EN 1052-1 (1998), for which testing uncertainty is assumed to be negligible compared to material uncertainty. Since suitable models for the conversion between test results on different composite specimens are still subject to research and have only been calibrated for relatively limited boundary conditions, the corresponding testing uncertainty cannot be reliably quantified at present. Therefore, the uncertainty associated with direct testing of alternative masonry specimens is considered via a CoV of 10 %, which should be understood as a preliminary estimate. This estimate considers that the uncertainty lies between the model uncertainty connected with indirect testing (see Section 8.3.2) and the accuracy of compression tests according to EN 1052-1 (1998).

Concerning statistical uncertainty, the same Bayesian framework is applicable as for indirect testing. For the variance of the logarithm of masonry compressive strength, the prior hyperparameters derived in Section 7.4.7 can be used. In general, the procedure for direct testing should be in line with the procedure for indirect testing. Thus, the same approximations are made: Spatial variability is neglected, and the predictive distribution is approximated by a log-normal distribution. The variance of the logarithm of masonry compressive strength can therefore be obtained as

$$\sigma_{\ln,\mathrm{ma}}^2 = \sigma_{\ln\theta f}^2 + s_{\ln,\mathrm{ma}}''^2 \left(\frac{n_{\mathrm{ma}}''}{n_{\mathrm{ma}}'' - 1} \frac{\nu_{\mathrm{ma}}''}{\nu_{\mathrm{ma}}'' - 2} \right) \qquad \textit{Eq. 8-31}$$

where $s_{\ln,\mathrm{ma}}''$, n_{ma}'', and ν_{ma}'' are the posterior hyperparameters for masonry compressive strength. The parameter $\sigma_{\ln\theta f} \approx \upsilon_{\theta f} = 0.1$ considers testing uncertainty, as mentioned above, and is applied instead of the model uncertainty associated with predicting masonry compressive strength.

8.5 Validation of the Developed Method by Reliability Analyses

8.5.1 Procedure of the Reliability Analyses

General procedure and limit state function

The goal of the developed method is to obtain assessment values $f_{ma,a}$ for masonry compressive strength that lead to a reliability level β equal to the target reliability index β_t chosen as the input parameter. Due to the simplifications in the proposed method, such as neglecting spatial variability and following the simplified level II approach with a fixed sensitivity factor α_R, the resulting reliability is not necessarily equal to the target reliability. Therefore, the proposed method is validated by means of reliability analyses to investigate the influence of the approximations on the resulting reliability level.

First, reliability analyses are performed through MCS. In Section 8.5.3, additional reliability analyses are described, utilising FORM to determine the sensitivity factors of the basic variables. The reliability analyses are conducted for the case of indirect testing since this is the most frequent approach in current engineering practice. The procedure of the reliability analyses through MCS is illustrated in Fig. 8-13.

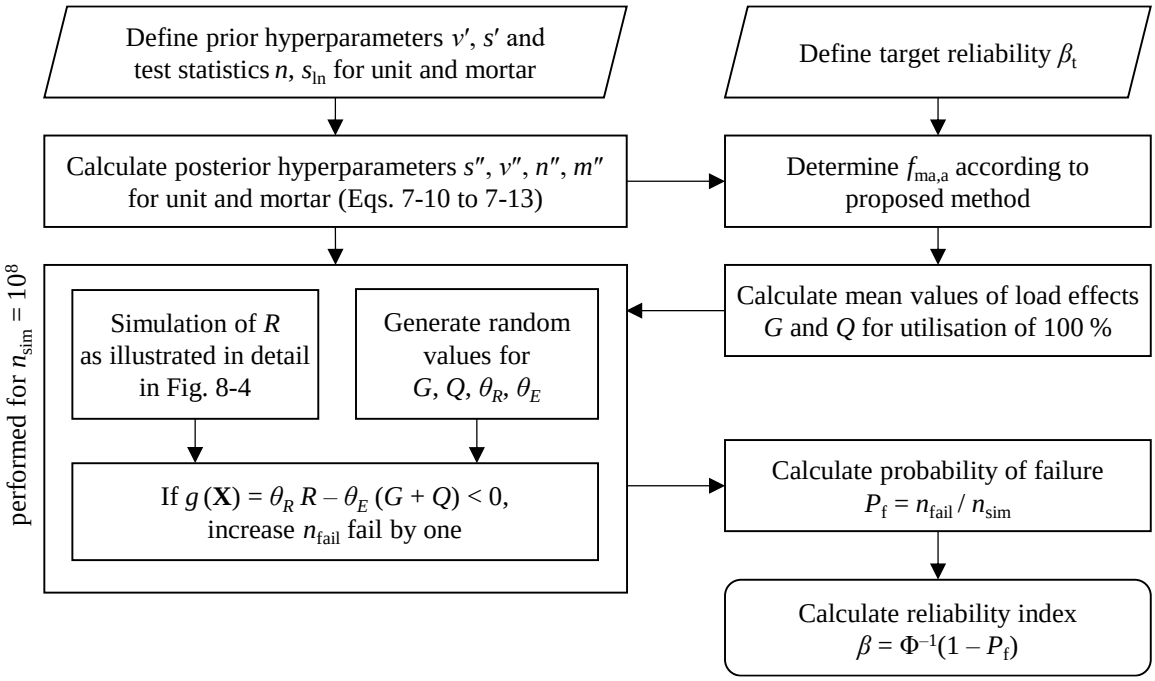

Fig. 8-13 Procedure for the reliability analyses through Monte Carlo simulations

For the validation, the simple case of a non-slender masonry wall under concentric compression resulting from permanent and imposed loads is considered, which leads to the following limit state function:

$$g(\mathbf{X}) = \theta_R \, R - \theta_E \, (G + Q) \qquad \textit{Eq. 8-32}$$

where θ_R is the resistance model uncertainty factor, R the vertical resistance of the wall, θ_E the load effect model uncertainty factor, G the permanent load effect, and Q the imposed load effect.

The reliability analyses are conducted for a reference period of both one and 50 years. Furthermore, the reliability analyses are performed for different test outcomes in terms of obtained sample standard deviations $s_{\ln,b}$ and $s_{\ln,j}$ and corresponding sample sizes n_b and n_j. Based on these test statistics, the posterior hyperparameters for the mean and variance of unit and mortar compressive strength are determined. The resistance R in Eq. 8-32 is modelled according to the posterior predictive distribution of the resistance. In the case of the reliability analyses by MCS, random values of R are thus generated in the same way as in the stochastic simulation of R in Section 8.4 (see Fig. 8-4). For the FORM reliability analyses, the procedure for modelling the posterior predictive distribution of R is explained in 8.5.3. Since spatial variability can be considered in the procedure of the reliability analyses, the influence of neglecting spatial variability in the proposed practice-oriented method can be investigated by performing the reliability analyses with and without considering spatial variability.

The characteristic values G_k and Q_k of the load effects are set to achieve a utilisation of the masonry wall of 100 %. Thus, the following verification criterion is exactly met:

$$A \, f_{ma,a} = G_k \, \gamma_G + Q_k \, \gamma_Q \qquad \textit{Eq. 8-33}$$

where A is the cross-sectional area, $f_{ma,a}$ the assessment value of masonry compressive strength, γ_G the partial factor for permanent loads, and γ_Q the partial factor for imposed loads. It is noted that Equation 6.10a/b in EN 1990 (2010) allows reducing either γ_G = 1.35 by a reduction factor ξ = 0.85 or γ_Q = 1.5 by the combination factor ψ_0, whichever is less favourable. Since the German National Annex does not permit the application of Equation 6.10a/b, this reduction of either γ_G or γ_Q is not made here. In most of the following reliability analyses, the ratio Q_k / G_k is set to 0.5, which is typical for masonry structures (Glowienka 2007). Q_k / G_k = 0.5 corresponds to a ratio of variable characteristic load to total characteristic load of $\chi = Q_k / (G_k + Q_k) = 1/3$. The range of $0.2 < \chi < 0.5$ can be viewed as relevant in practice.

The assessment value $f_{ma,a}$ for the verification criterion is obtained according to the method developed in this chapter (i.e. the method to be validated; see Section 9.2 for a summary of the proposed method, including the respective equations). Thus, the assessment value depends on the chosen target reliability index β_t. In the analyses, the target reliability index is either set to $\beta_{t,1a}$ = 3.3, which is the example target reliability index for the assessment of

existing masonry structures, or to $\beta_{t,1a} = 4.2$, which should lead to a reliability level approximately corresponding to $\beta_{t,50a} = 3.8$ as specified by EN 1990 (2010) for the design of new structures and CC 2 (see Section 2.5.1). The partial factors γ_G and γ_Q are adjusted as described in Section 8.2.6 to account for the different target reliability indices. Hence, γ_G =1.35 and γ_Q =1.5 are applied in the case of $\beta_{t,1a} = 4.2$, and, for $\beta_{t,1a} = 3.3$, γ_G =1.26 and γ_Q =1.05 are used.

Stochastic models for the basic variables

The probability distribution of the wall resistance R is modelled by the corresponding posterior predictive distribution as described by the flowchart in Fig. 8-4. Thus, it depends on test results and includes statistical uncertainty, the uncertainty in masonry compressive strength prediction, and the influence of the spatial variability of material properties. The resistance model uncertainty factor θ_R is modelled according to the considerations in Section 8.3.1 and is intended to also cover geometrical deviations.

The permanent load effect is modelled as a normally distributed random variable with a mean equal to G_k and a CoV of $v_G = 10$ % (fib bulletin 80 2016). In the literature, lower CoVs for the self-weight of masonry structures can also be found. In Glowienka (2007) and Brehm (2011), for example, a CoV of 6 % is specified. However, $v_G = 10$ % is chosen since it can be assumed that the variability of the weight density of historical masonry is higher than that of contemporary masonry. Furthermore, the floors in historical masonry structures are often made of timber, for which $v_G = 10$ % is more appropriate (JCSS 2001b).

The stochastic model for imposed loads is based on information in Rackwitz (1997). Here, the CoV of the corresponding extreme value distribution for a reference period of 50 years and a reference area of 20 m² is stated as 20 % for imposed loads in office buildings and 29 % for imposed loads in residential buildings. Therefore, a Gumbel distribution with an averaged CoV of $v_{Q,50a} = 25$ % is chosen for a reference period of 50 years, which also matches the CoV $v_{Q,50a}$ specified for the APFM in fib bulletin 80 (2016). Based on the assumption of independent extreme values for successive years and following the principles of Gumbel-distributed random variables (see Section 2.3.4), the CoV $v_{Q,1a}$ of the corresponding Gumbel distribution for annual extreme values can be obtained as follows:

$$v_{Q,1a} = \frac{v_{Q,50a}}{1 - \frac{\sqrt{6}}{\pi} v_{Q,50a} \ln 50} = 105\,\% \qquad \textit{Eq. 8-34}$$

The assumption of uncorrelated extreme values of successive years is only a simplification since imposed loads consist of a sustained component and an intermittent component. Usually, the sustained load is approximately constant for several years, whereas intermittent

loads occur every few months for no more than a few days (JCSS 2001b). However, according to Rackwitz (1997), the intermittent component is dominant when considering the mean values of the 50-year extreme value distribution for most types of use, such as office and residential buildings. Hence, the assumption of independence is assumed to be sufficiently precise.

In EN 1990 (2010), the average return period that corresponds to the characteristic value of the imposed load is not explicitly defined. In the literature, different assumptions can be found: Some authors state that the characteristic values for imposed loads correspond to the 95 % fractile of the extreme value distribution for a reference period of 50 years (Grünberg 2004; fib bulletin 80 2016; Meinen and Steenbergen 2018). Others suggest that the characteristic imposed loads correspond to a 98 % fractile of the annual extreme values (Honfi 2014; Tran et al. 2017) or the mode of the 50-year extreme value distribution (Glowienka 2007). Based on the simplified level II approach, the partial factor $\gamma_Q = 1.5$ for imposed loads can be reproduced if it is assumed that the characteristic loads correspond to the 95 % fractile of the 50-year extreme values (fib bulletin 80 2016). However, the characteristic loads defined in EN 1991-1-1 (2009) can be more accurately reproduced by stochastic load simulations if the characteristic values are assumed to be 98 % quantile values of the annual extreme values (Honfi 2014; Tran et al. 2017). This is particularly true for the characteristic imposed loads defined in the German National Annex DIN EN 1991-1-1/NA (2010), which, on average, are slightly lower than the recommended values in EN 1991-1-1 (2009). Therefore, the characteristic imposed load effects are assumed to be 98 % fractiles of the annual extreme values here, which also leads to more conservative results than assuming that they are 95 % fractiles of the 50-year extreme values. Following this definition, the mean-to-characteristic ratios can be obtained as follows (see Eq. 2-31):

$$\frac{\mu_{Q,1a}}{Q_k} = \frac{1}{1 - v_{Q,1a}\left[0.45 + 0.78\ln\left(-\ln\left(0.98\right)\right)\right]} = 0.27 \qquad \textit{Eq. 8-35}$$

$$\frac{\mu_{Q,50a}}{Q_k} = \frac{1}{1 - v_{Q,50a}\left[0.45 + 0.78\ln\left(-\ln\left(0.98^{50}\right)\right)\right]} = 1.13 \qquad \textit{Eq. 8-36}$$

The model uncertainty factor θ_E for calculating load effects is modelled by means of a log-normal random variable with a mean of one and a CoV of 5 %, as recommended for axial forces in JCSS (2002). The stochastic models selected for the basic variables are summarised in Table 8-3.

Table 8-3 Stochastic models for the basic variables

Random variable		Symbol	Distribution	Mean	CoV
Resistance		R	Posterior predictive distribution including effects of (spatial) material variability, strength prediction uncertainty, and statistical uncertainty (see Fig. 8-4)		
Resistance model uncertainty		θ_R	Log-normal	1.0	0.14
Permanent load effect		G	Normal	G_k	0.10
Imposed load effect	one year	Q	Gumbel	0.27 Q_k	1.05
	50 years			1.13 Q_k	0.25
Load effect model uncertainty		θ_E	Log-normal	1.0	0.05

8.5.2 Resulting Level of Reliability

Reliability indices β_{1a} obtained by MCS for different sample standard deviations $s_{ln,b}$ and $s_{ln,j}$ and different input target reliability indices $\beta_{t,1a}$ are displayed in Fig. 8-14 as a function of the sample size $n_b = n_j$. The underlying posterior hyperparameters are calculated based on the building-related priors. The upper left diagram shows the reliability indices obtained in a reliability analysis with $\rho_{spat} = 0.4$ (i.e. under consideration of spatial variability). In contrast, the upper right diagram displays reliability indices determined through a reliability analysis with $\rho_{spat} = 1.0$ (i.e. without considering spatial variability in the reliability analysis). The developed method for obtaining assessment values of masonry compressive strength does not consider spatial variability in either of the two cases. For further illustration, the partial factors γ_M and ratios $f_{ma,k} / f_{ma,m}$ obtained by the proposed method for the investigated input values are displayed in the two lower diagrams of Fig. 8-14.

It is evident from Fig. 8-14 that the proposed method leads to reliability levels β_{1a} that very well match the corresponding input values $\beta_{t,1a}$. Comparing the results for $\rho_{spat} = 0.4$ and $\rho_{spat} = 1$ shows no substantial difference in the obtained reliability level. Again, this demonstrates that neglecting spatial variability is appropriate in assessing an existing masonry wall under compression. With regard to statistical uncertainty, the goal of the proposed method is to obtain resulting reliability indices that are approximately independent of the sample size. Since the curves for the resulting reliability indices plotted over $n_b = n_j$ are almost horizontal, particularly for $\beta_{t,1a} = 3.3$, this goal can be viewed as achieved.

The resulting reliability level should preferably be independent of the sample standard deviations. The small deviations between the reliability indices β_{1a} for $s_{ln,b} = s_{ln,j} = 0.2$, 0.35, and 0.5 can be attributed to the definition of a fixed sensitivity factor α_R by the proposed method. In Section 8.5.3, the actual sensitivity factors α_i of the basic variables are determined utilising an analysis by FORM, which explains the deviations between the results for different sample standard deviations. However, for all investigated scenarios, the deviations from the input target reliability indices $\beta_{t,1a}$ lie within a range of ± 0.5 and can thus

be considered small enough to be accepted. Furthermore, the results demonstrate that the developed method for determining assessment values of masonry compressive strength works well in combination with partial factors γ_G and γ_Q that are modified for a reduced target reliability level using the APFM adapted from fib bulletin 80 (2016).

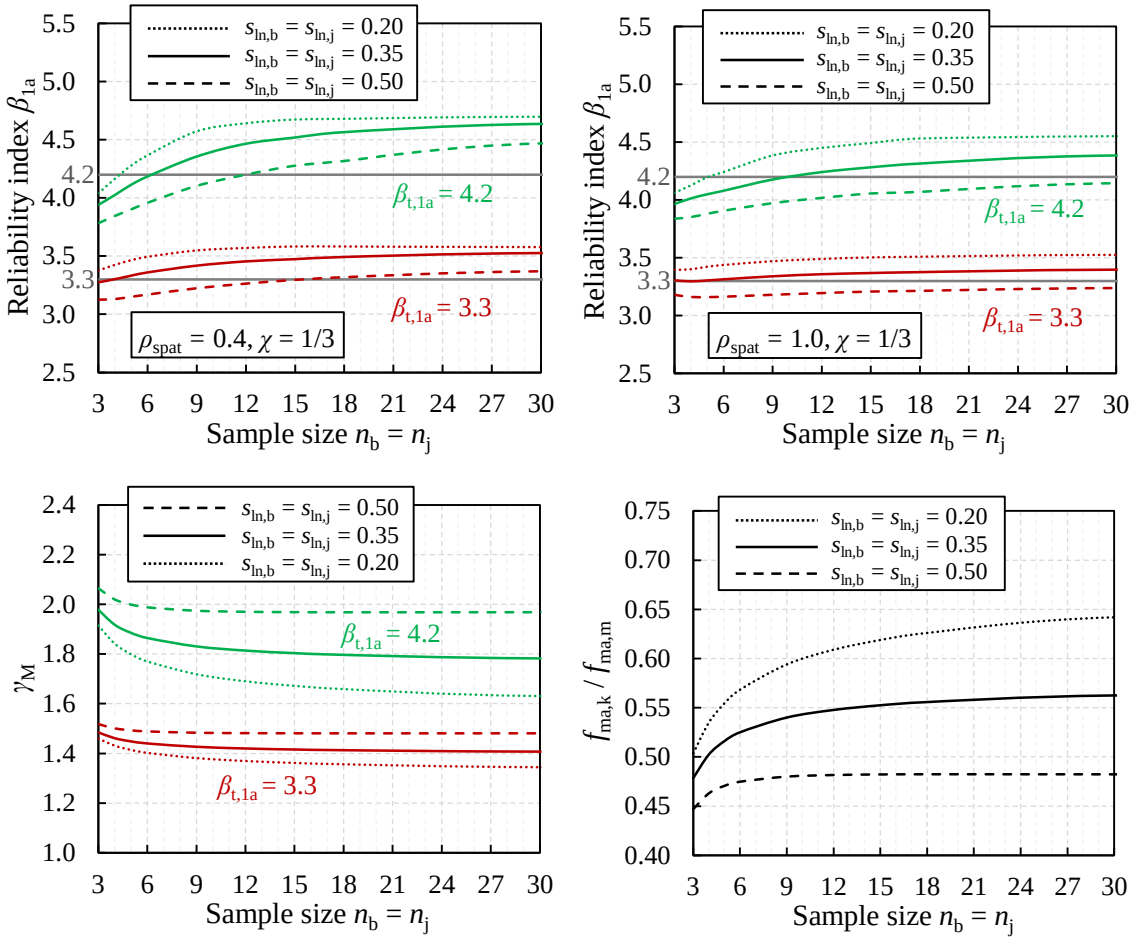

Fig. 8-14 Resulting reliability indices β_{1a} for a one-year reference period (top), corresponding partial factors γ_M (lower left), and ratios $f_{ma,k}/f_{ma,m}$ (lower right)

For further comparison, reliability indices β_{50a} for a reference period of 50 years are displayed in the left diagram of Fig. 8-15. The target reliability indices are still defined for one year (as $\beta_{t,1a} = 3.3$ and $\beta_{t,1a} = 4.2$), which means that the applied assessment values of masonry compressive strength and the partial factors for actions are the same as in Fig. 8-14. However, the time-dependent stochastic parameters for the imposed load are applied for a reference period of 50 years, which results in reliability indices β_{50} that also correspond to a period of 50 years. For the investigated boundary conditions in Fig. 8-15 (left), the choice of $\beta_{t,1a} = 4.2$ leads to $\beta_{50a} = 3.8$, and $\beta_{t,1a} = 3.3$ leads to $\beta_{50a} = 2.8$, on average. In the right diagram of Fig. 8-15, the ratio χ of imposed to total characteristic load is varied while the sample sizes are fixed at $n_b = n_j = 6$. For $\chi = 0$, no time-dependent basic variables are present, which leads to $\beta_{1a} = \beta_{50a}$. For increasing χ, the gap between β_{1a} and β_{50a} increases. In

the range between χ = 0.2 and 0.5, which is most relevant in practice, the resulting reliability indices β_{1a} are very close to the specified target values $\beta_{t,1a}$. Therefore, the proposed method is well suited for achieving the required reliability level.

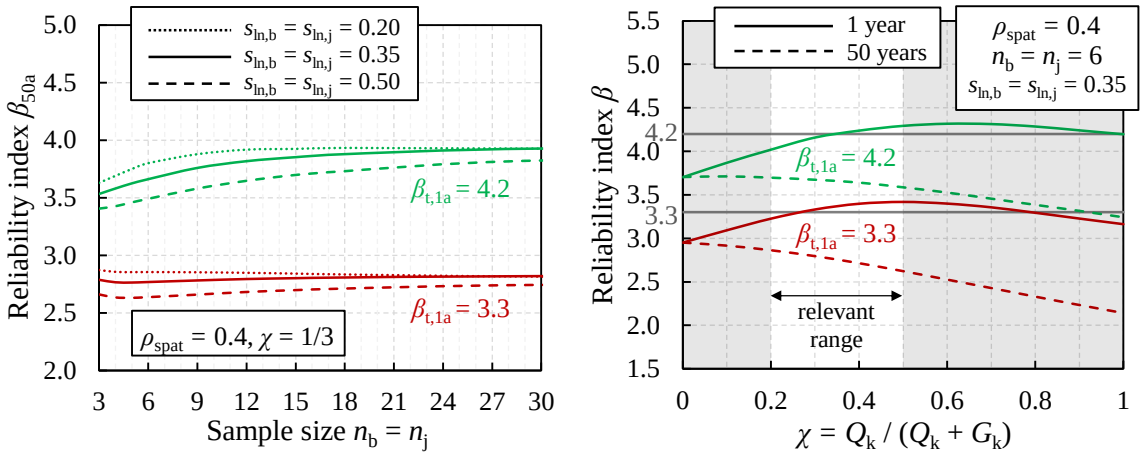

Fig. 8-15 *Left: Resulting reliability indices β_{50a} for a reference period of 50 years*
Right: Influence of the load effect ratio χ on the resulting reliability indices for reference periods of one and 50 years

8.5.3 FORM Sensitivity Factors

Reliability analyses are also conducted utilising FORM to determine corresponding sensitivity factors. To perform a FORM analysis, a different representation of the resistance R in the limit state function is needed. If the spatial variability of material properties is not considered, R can be written as

$$R = A\, f_{ma} = A\,\theta_f\, K_{prob}\, f_b^{\alpha}\, f_j^{\beta} = A\,\theta_f\, K_{prob}\, \exp\left(\alpha \ln f_b + \beta \ln f_j\right) \qquad \textit{Eq. 8-37}$$

where A is the deterministic cross-sectional area of the wall, θ_f is the model uncertainty factor for predicting masonry compressive strength, α and β are the parameters of the power equation, f_b is the unit compressive strength, and f_j is the mortar compressive strength. K_{prob} is the parameter K of the power equation that is suitable in the case of probabilistic application. K_{prob} is set to K_m in the following analysis, which is a slightly conservative approximation (see Section 3.5.4). Both random variables f_b and f_j include statistical uncertainty in their parameters μ_{ln} and σ_{ln}, which is considered in the reliability analysis. Therefore, ln f_b is formulated as

$$\ln f_b = m_{ln,b} + Z_{\mu,b}\,\frac{\sigma_{ln,b}}{\sqrt{n_b}} + Z_b\,\sigma_{ln,b} \qquad \textit{Eq. 8-38}$$

where $m_{ln,b}$ is the arithmetic mean of the logarithms of unit compression test results represented by a deterministic variable. The deviation of the arithmetic mean $m_{ln,b}$ from the population mean $\mu_{ln,b}$ is covered by the standard normal random variable $Z_{\mu,b}$, multiplied by

$\sigma_{\ln,b} / n_b^{0.5}$, which is the standard deviation of the posterior distribution of $\mu_{\ln,b}$ given $\sigma_{\ln,b}$ (see Section 2.4.2). The actual material variability (i.e. the deviation of ln f_b from its mean $\mu_{\ln,b}$) is represented by the standard normal variable Z_b multiplied by $\sigma_{\ln,b}$. The standard deviation $\sigma_{\ln,b}$ of the logarithm of unit compressive strength is a random variable with $\sigma_{\ln,b}^2$ being scaled inverse-χ^2 distributed according to the posterior hyperparameters ν_b'' and $s_{\ln,b}''^2$. The logarithm of mortar strength can be formulated accordingly. Hence, the resistance R can be expressed as

$$R = A\,\theta_f\,K_m\,\exp\left[\begin{array}{l}\alpha\left(m_{\ln,b} + Z_{\mu,b}\,\dfrac{\sigma_{\ln,b}}{\sqrt{n_b}} + Z_b\,\sigma_{\ln,b}\right)\\ +\beta\left(m_{\ln,j} + Z_{\mu,j}\,\dfrac{\sigma_{\ln,j}}{\sqrt{n_j}} + Z_j\,\sigma_{\ln,j}\right)\end{array}\right] \qquad \textit{Eq. 8-39}$$

To take the influence of spatially variable material properties into account, a reduction of the mean value and the variability of the resistance compared to a homogeneous wall must be considered (see Chapter 6). For this purpose, a factor δ for reducing the mean and a factor ξ for reducing the variability are introduced:

$$R = \delta\,A\,\theta_f\,K_m\,\exp\left[\begin{array}{l}\alpha\left(m_{\ln,b} + Z_{\mu,b}\,\dfrac{\sigma_{\ln,b}}{\sqrt{n_b}} + Z_b\,\xi\,\sigma_{\ln,b}\right)\\ +\beta\left(m_{\ln,j} + Z_{\mu,j}\,\dfrac{\sigma_{\ln,j}}{\sqrt{n_j}} + Z_j\,\xi\,\sigma_{\ln,j}\right)\end{array}\right] \qquad \textit{Eq. 8-40}$$

The factor ξ, which reduces the material variability to obtain the resulting variability of the resistance, can be calculated as follows:

$$\xi = \frac{\sqrt{c^{*2}\,\sigma_{\ln,ma,spat}^2 + \sigma_{\ln,ma,wall}^2}}{\sigma_{\ln,ma}} = \sqrt{c^{*2}\left(1-\rho_{spat}\right) + \rho_{spat}} \qquad \textit{Eq. 8-41}$$

The factor δ addresses the reduction of the mean wall resistance μ_R in relation to the deterministic resistance R_{det} based on mean masonry compressive strength. It is obtained as

$$\delta = \exp\left(-a^*\,\sigma_{\ln,ma,spat}{}^{b^*}\right) = \exp\left[-a^*\,\sqrt{\left(1-\rho_{spat}\right)\left(\alpha^2\,\sigma_{\ln,b}^2 + \beta^2\,\sigma_{\ln,j}^2\right)}^{b^*}\right] \qquad \textit{Eq. 8-42}$$

For the final expressions in Eq. 8-41 and Eq. 8-42, the unit-to-unit component $\sigma_{\ln,ma,spat}$ and the wall-to-wall component $\sigma_{\ln,ma,wall}$ of the standard deviation are determined based on Eq. 2-40 (see Section 2.3.5). In contrast to the previous section, the correlation coefficient ρ_{spat} refers to the correlation of the logarithms of strength, which, however, does not deviate strongly from the correlation coefficient of the strengths (see Section 7.4.5). Hence,

ρ_{spat} = 0.4 is also applied here. As noted before, only the unit-to-unit component $\sigma_{ln,ma,spat}$ of the standard deviation leads to a reduction of the mean resistance and is itself reduced by the effects of spatial variability. For ρ_{spat} = 1, the component $\sigma_{ln,ma,spat}$ is zero, which leads to ξ = 1 and δ = 1. The parameters a^*, b^*, and c^* are equivalent to the parameters a, b, and c in the equations derived for approximating the influence of spatial variability in Section 6.3.4. However, the formulae are expressed as a function of the standard deviation $\sigma_{ln,ma}$ instead of formulating it for the CoV of strength v_{ma}, which is more convenient here:

$$\mu_R = R_{det} \exp\left(-a^* \sigma_{ln,ma,spat}^{\ b^*}\right) \qquad \textit{Eq. 8-43}$$

$$\sigma_{\ln R,spat} = c^* \sigma_{ln,ma,spat} \qquad \textit{Eq. 8-44}$$

Based on the results of the MCS for investigating the influence of spatial variability in Section 6.3.4, the method of least squares yields a^* = 1.85, b^* = 1.51, and c^* = 0.21 as suitable parameter values for Eq. 8-43 and Eq. 8-44.

The expression of R according to Eq. 8-40 is finally inserted in the limit state function as previously defined in Eq. 8-32. Then, the reliability analyses are performed by applying the Rackwitz-Fiessler algorithm as described in Section 2.5.2. Except for the different formulation of the resistance R, the stochastic models are equivalent to those used in the reliability analyses by MCS. In Fig. 8-16, the reliability indices obtained by FORM and MCS are compared. The results obtained by the two different methods match very well.

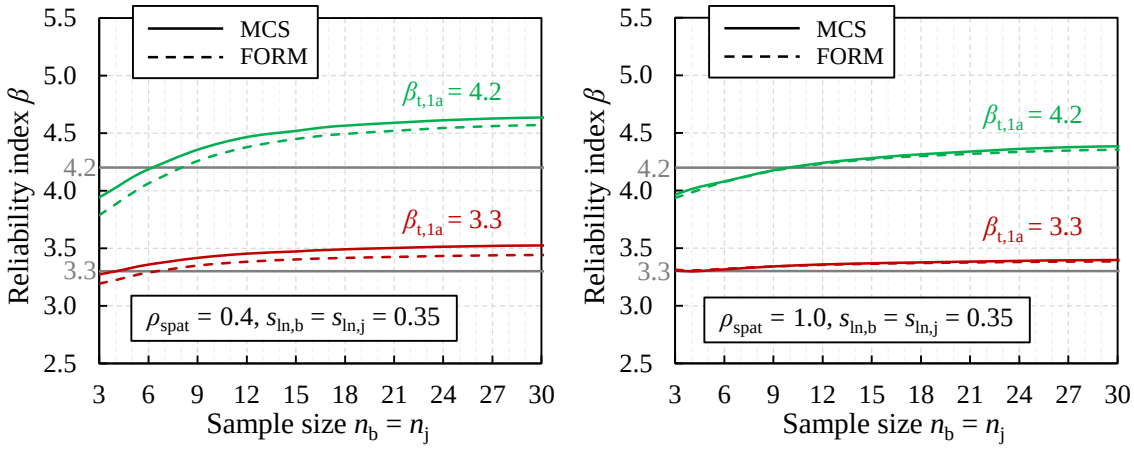

Fig. 8-16 Comparison of reliability indices obtained via the first-order reliability method (FORM) and Monte Carlo simulations (MCS)

In Fig. 8-17, the squared sensitivity factors α_i^2 are illustrated for varying sample sizes $n_b = n_j$. The presented results are obtained for ρ_{spat} = 0.4, $\beta_{t,1a}$ = 3.3, and $s_{ln,b} = s_{ln,j}$ = 0.35. The sensitivity factors for the material variability of f_b and f_j correspond to those for the basic variables Z_b and Z_j, respectively. The squared sensitivity factors for the statistical uncertainty in f_b and f_j are the sum of the values α_i^2 for the basic variables $Z_{\mu,b}$ and $\sigma_{ln,b}$ and

for $Z_{\mu,j}$ and $\sigma_{ln,j}$, respectively. The sum of the squared sensitivity factors for f_b, f_j, and θ_f yields the squared sensitivity factor $\alpha_R{}^2$ for the resistance R.

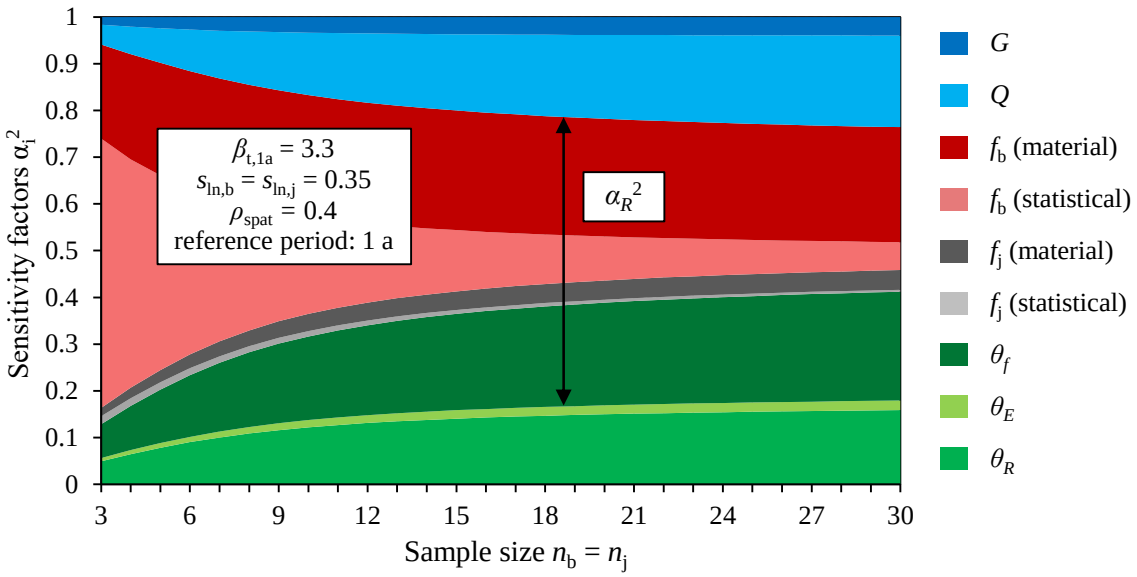

Fig. 8-17 Influence of sample size on the sensitivity factors of the basic variables

As evident from Fig. 8-17, the sensitivity factor for the resistance R is much higher than those for the other basic variables G, Q, θ_E, and θ_R. The composition of the sensitivity factor α_R depends on the sample size: For low sample sizes, the statistical uncertainty in f_b is dominating, whereas, for larger sample sizes, the uncertainty in masonry strength prediction represented by θ_f and the material variability of unit compressive strength f_b are almost equally influential. Compared to unit compressive strength, the sensitivity factors related to mortar compressive strength are much smaller.

In Fig. 8-18, the sensitivity factor α_R is displayed for different sample standard deviations $s_{ln,b} = s_{ln,j}$, sample sizes $n_b = n_j$, and target reliability indices $\beta_{t,1a}$. In the left diagram, the results for $\rho_{spat} = 0.4$ are shown (i.e. spatial variability is considered), whereas the right diagram presents the results for $\rho_{spat} = 1.0$ (i.e. without considering spatial variability).

In both cases, the sensitivity factor α_R decreases with a larger sample size, which is due to the reduction of statistical uncertainty in R. If spatial variability is considered ($\rho_{spat} = 0.4$), the sensitivity factor α_R for larger sample sizes is lower than if spatial variability is not considered ($\rho_{spat} = 1.0$). The lower sensitivity factors α_R for $\rho_{spat} = 0.4$ can be attributed to the reduced material-related variability of the resistance if spatial variability is taken into account.

As expected, the sensitivity factors α_R are higher for high sample standard deviations $s_{ln,b}$ and $s_{ln,j}$. If the sample sizes are small, the difference between the sensitivity factors α_R for different sample standard deviations is smaller than for large sample sizes. This can be explained by the fact that the posterior predictive distribution of masonry strength, which

is the basis for the reliability analyses, is not strongly affected by the sample standard deviation but by the prior distribution if the sample size is small.

Statistical uncertainty results in a higher kurtosis of the probability distribution of R or, in other words, more weight in the tails of the distribution. The higher the target reliability index, the more important the tails of the distribution of the basic variables become. Hence, for small sample sizes n, the sensitivity factor α_R is larger in the case of the higher target reliability index $\beta_{t,1a} = 4.2$.

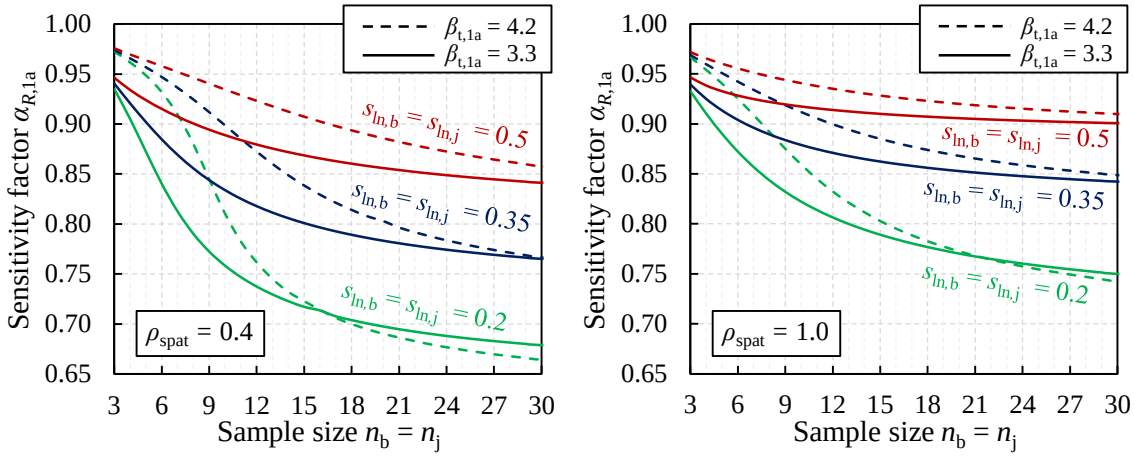

Fig. 8-18 Influence of sample size and sample standard deviation on the sensitivity factor $\alpha_{R,1a}$

In the proposed method, a fixed sensitivity factor α_R is applied. The differences between the actual sensitivity factors α_R in Fig. 8-18 are one reason for the differences in the resulting reliability levels for varying sample sizes and sample standard deviations as obtained in the previous section (see Fig. 8-14). The fixed sensitivity factor $\alpha_{R,1a} = 0.7$, which is not specified for existing masonry structures in particular but for structures in general, is exceeded in most investigated cases, which is due to statistical uncertainty and the high material variability of historical masonry. However, the exceedance of the fixed sensitivity factor $\alpha_{R,1a}$ does not automatically lead to unsafe results since the sensitivity factor α_R is accompanied by sensitivity factors α_G and α_Q, which, in absolute values, are much lower than those that are either explicitly or implicitly considered in the derivation of the partial factors γ_G and γ_Q for actions. When the concept of fixed sensitivity factors was introduced by König and Hosser (1982), a deviation of the resulting reliability index β from the target reliability index β_t of ± 0.5 was considered acceptable (see Section 2.5.4). As this limit is not exceeded (see Fig. 8-14 and Fig. 8-15), there is no need to specify fixed sensitivity factors particularly suited for assessing existing masonry structures.

8.6 Summary

In this chapter, the final method for determining assessment values of masonry compressive strength was developed and validated. In Section 8.2, the general approach and underlying assumptions of the method were noted. The method can be applied if compression tests on either unit and mortar specimens or composite masonry specimens are performed. The assessment values of masonry compressive strength are obtained as fractiles of the respective posterior predictive distribution, which is acquired through a Bayesian update. Assessment values of masonry compressive strength are obtained directly, which means that the determination of characteristic values and partial factors is not necessarily required. The proposed method is mainly suitable for existing solid clay brick masonry. It is based on the influence of spatial variability as quantified for solid clay brick masonry in Chapter 6, and it enables the use of prior distributions obtained for this masonry type in Chapter 7. However, there is also the option to apply the method in combination with a non-informative prior distribution. Thereby, the application range is extended to other masonry types for which a stress redistribution capability at least as good as that of solid clay brick masonry can be assumed.

Section 8.3 dealt with the two considered types of model uncertainty: first, the resistance model uncertainty associated with calculating the load-bearing capacity of a masonry wall and second, the uncertainty in predicting masonry compressive strength based on the compressive strengths of unit and mortar. For the resistance model uncertainty, the stochastic model was selected based on a literature study. The uncertainty in the prediction of masonry strength was quantified based on compressive strength tests from the literature.

In Section 8.4, the posterior predictive distribution of the resistance of a masonry wall under compression was obtained through stochastic simulations, in which, in addition to the statistical and model uncertainty, the influence of spatially variable material properties was considered. The simulation results showed that the assessment values differ only slightly if the influence of spatial variability is neglected and homogeneity (i.e. perfect spatial correlation within a wall) is assumed instead. Therefore, the proposed method can be based on the posterior predictive distribution of masonry compressive strength instead of considering the distribution of the wall resistance. Furthermore, it was shown that the developed method leads to conservative results for slender masonry walls if the ratio between the modulus of elasticity and the compressive strength of masonry is accurately estimated and explicitly considered by the applied resistance model. It was further demonstrated that the reduction factor defined in EN 1996-1-1 (2012) for walls with a small cross-sectional area is also suitable for the assessment of existing solid clay brick masonry.

Finally, the developed method was validated through reliability analyses in Section 8.5. It was shown that the resulting reliability indices differ only slightly from the target reliability

that is selected as the input of the method. Furthermore, the sensitivity factors of the basic variables were determined for a deeper understanding and to enable a comparison with the fixed sensitivity factor for the resistance that is applied according to the simplified level II approach.

9 PRACTICE-ORIENTED PROPOSAL FOR DETERMINING ASSESSMENT VALUES AND PARTIAL FACTORS

9.1 Introduction

In this chapter, the previously developed method for determining characteristic values $f_{ma,k}$, structure-specific partial factors γ_M, and assessment values $f_{ma,a}$ for the compressive strength of existing masonry is presented in its final form. First, Section 9.2 summarises the proposed method and provides the equations that are needed to apply the method in engineering practice. As an alternative, the proposed method can be applied via diagrams, which are introduced in Section 9.3. Typical results of the proposed method are illustrated in Section 9.4. Finally, Section 9.5 provides guidance on assessing existing masonry structures in the absence of test results.

9.2 General and Equations for Determining Assessment Values

The proposed method can be applied if compression tests on specimens extracted from existing masonry are conducted. Masonry compressive strength can be tested either indirectly (i.e. by performing separate compression tests on unit and mortar specimens) or directly (i.e. by conducting tests on composite masonry specimens). The single masonry members of the structure must be assigned to suitable populations. The extracted specimens should be representative of the population of masonry for that the assessment value $f_{ma,a}$ of masonry compressive strength is evaluated. If all the masonry in a structure appears to be of the same type, it is advised to consider all masonry members as one population. For each masonry population, a minimum number of either $n_b \geq 6$ tests on unit and $n_j \geq 6$ tests on mortar specimens or $n_{ma} \geq 5$ tests on composite masonry specimens is recommended, as specified by WTA 7-4 (2021). The specimens should be taken from more than one sampling location. If the considered population consists of more than one masonry member, these sampling locations should belong to several members.

The target reliability index β_t is to be chosen according to the requirements of the building authority, the owner, or other relevant parties. In the case of high relative costs of safety measures and moderate failure consequences, a target reliability index of $\beta_{t,1a} = 3.3$ for a reference period of one year is suitable according to ISO 2394 (2015) based on economic optimisation (see Section 2.6.2).

Before the proposed method can be applied, the mean value of masonry compressive strength $f_{ma,m}$ must be estimated. If indirect tests are performed, the power equation can be utilised with the arithmetic means $f_{b,m}$ and $f_{j,m}$ of unit and mortar strength as the input parameters. If the parameters K, α, and β for the power equation are taken from EN 1996-1-1 (2012) or DIN EN 1996-1-1/NA (2019), the parameter K should be increased by a factor

of 1.25 to obtain an estimate for the mean value of masonry strength (see Section 3.5.3). If the application limits of the empirical equations are exceeded, the utilisation of models with a mechanical background can be beneficial (see Section 3.5.2). If necessary, the estimation of masonry compressive strength $f_{ma,m}$ should additionally account for structural defects, such as mortar joints that are not adequately filled, unusually high moisture content of masonry, or mortar joints significantly thicker than normatively specified (see Sections 3.3.5 and 3.5.5).

Then, the assessment value $f_{ma,a}$ of masonry compressive strength is obtained as follows:

1. Calculate the arithmetic mean m and the variance s^2 of the logarithms of the test results for unit and mortar compressive strength (or masonry compressive strength if direct tests are performed):

$$m = \frac{1}{n}\sum_{i=1}^{n} \ln f_i \qquad \textit{Eq. 9-1}$$

$$s^2 = \frac{1}{n-1}\sum_{i=1}^{n} \left(\ln f_i - m\right)^2 \qquad \textit{Eq. 9-2}$$

   where f_i are the single test results converted to standardised unit, mortar, or masonry compressive strengths, respectively.

2. Determine the posterior hyperparameters v'' and s''^2 for both unit and mortar compressive strength (or masonry compressive strength) based on prior information and the variance s and number n of the test results:

$$v'' = v' + n - 1 \qquad \textit{Eq. 9-3}$$

$$s''^2 = \frac{v'\, s'^2 + (n-1)\, s^2}{v''} \qquad \textit{Eq. 9-4}$$

   Suitable prior hyperparameters v' and s' for solid clay brick masonry constructed before 1950 are defined in Table 9-1 (see Section 7.4 for the derivation of the parameters). For masonry types other than historical solid clay brick masonry, the procedure can be applied using non-informative prior distributions, which is equivalent to $v' = 0$, resulting in $v'' = n - 1$ and $s'' = s$.

Table 9-1 Prior hyperparameters

Parameter	Solid clay brick masonry (constructed before 1950)			Other masonry types
	Unit*	Mortar	Masonry	Unit, mortar, masonry
v'	7.7	4.2	9.2	0
s'	0.33	0.40	0.28	-

**If a single masonry wall is assessed and all test results are obtained on specimens from this wall, the prior hyperparameters for unit compressive strength may be taken as v' = 3.8 and s' = 0.21.*

3. Determine the variance $\sigma_{\ln,ma}^2$, which includes material variability, statistical uncertainty, and model (or testing) uncertainty in determining masonry compressive strength. In the case of indirect testing, $\sigma_{\ln,ma}^2$ is obtained as

$$\sigma_{\ln,ma}^2 = \sigma_{\ln\theta f}^2 + \alpha^2 \, s_{\ln,b}''^2 \, \frac{n_b}{n_b - 1} \frac{v_b''}{v_b'' - 2} + \beta^2 \, s_{\ln,j}''^2 \, \frac{n_j}{n_j - 1} \frac{v_j''}{v_j'' - 2} \qquad \textit{Eq. 9-5}$$

where α and β are the parameters of the power equation, which should be applied as $\alpha = 0.7$ and $\beta = 0.3$ according to EN 1996-1-1 (2012) here. For considering model uncertainty, $\sigma_{\ln\theta f} \approx v_{\theta f} = 0.17$ shall be applied. The indices "b", "j", and "ma" indicate that the parameters s'', n, and v'' correspond to unit, mortar, or masonry compressive strength, respectively. In the case of direct testing, $\sigma_{\ln,ma}^2$ is obtained as

$$\sigma_{\ln,ma}^2 = \sigma_{\ln\theta f}^2 + s_{\ln,ma}''^2 \, \frac{n_{ma}}{n_{ma} - 1} \frac{v_{ma}''}{v_{ma}'' - 2} \qquad \textit{Eq. 9-6}$$

For considering testing uncertainty, $\sigma_{\ln\theta f} \approx v_{\theta f} = 0.10$ is recommended if the masonry specimens for direct testing do not fulfil the specifications of EN 1052-1 (1998). If the specifications are met, testing uncertainty may be neglected.

4. Determine the assessment value of masonry compressive strength:

$$f_{ma,a} = \frac{1}{\gamma_{Ra}} \exp\left(-\alpha_R \, \beta_t \, \sigma_{\ln,ma} - 0.5 \, \sigma_{\ln,ma}^2\right) f_{ma,m} \qquad \textit{Eq. 9-7}$$

If a target reliability index $\beta_{t,1a}$ for a reference period of one year is applied, a sensitivity factor $\alpha_{R,1a} = 0.7$ should be used. If the target reliability index is specified for a reference period of 50 years, the sensitivity factor $\alpha_R = 0.8$, as provided in EN 1990 (2010), should be applied. The partial factor γ_{Ra} addressing the uncertainty of the resistance model is obtained from

$$\gamma_{Ra} = \exp\left(0.4 \, \alpha_R \, \beta_t \, v_{\theta R}\right) \qquad \textit{Eq. 9-8}$$

where the factor of 0.4 considers that model uncertainty is a non-dominant basic variable. The CoV for model uncertainty should be taken as $v_{\theta R} = 14$ %. To ensure that the assumption of the model uncertainty being non-dominant is fulfilled, $\sigma_{\ln,ma}$ should not be taken smaller than $v_{\theta R}$. For $\alpha_{R,1a} = 0.7$ and $\beta_{t,1a} = 3.3$, Eq. 9-8 yields $\gamma_{Ra} = 1.14$.

5. The effect of sustained loads on masonry compressive strength is to be considered additionally. If applicable, it is recommended to reduce the assessment value by a factor of $\zeta = 0.85$ as specified by DIN EN 1996-1-1/NA (2019).

6. For walls with a cross-sectional area of $A < 0.1$ m², the obtained assessment value is to be reduced by a factor of

$$0.7 + 3A \qquad \textit{Eq. 9-9}$$

where A is the cross-sectional area A in m².

If the characteristic value $f_{ma,k}$ and the partial factor γ_M shall be determined separately, the following equations can be used:

$$f_{ma,k} = \exp\left(-1.645\,\sigma_{ln,ma} - 0.5\,\sigma_{ln,ma}^2\right) f_{ma,m} \qquad \textit{Eq. 9-10}$$

$$\gamma_M = \gamma_m\,\gamma_{Ra} \qquad \textit{Eq. 9-11}$$

$$\gamma_m = \exp\left[\left(\alpha_R\,\beta_t - 1.645\right)\sigma_{ln,ma}\right] \qquad \textit{Eq. 9-12}$$

with $\sigma_{ln,ma}$ according to Eq. 9-5 or Eq. 9-6, respectively.

The same procedure may be applied for assessing slender walls, whose resistance is mainly influenced by the modulus of elasticity E_{ma}. However, special care should then be taken in the estimation of the ratio E_{ma} / f_{ma}, which is an input parameter for determining the capacity reduction factor Φ_{red} at the middle height of the wall. The ratio E_{ma} / f_{ma} should be applied via the corresponding mean material properties (i.e. as $E_{ma,m}$ / $f_{ma,m}$). The mean value $E_{ma,m}$ of the modulus of elasticity of masonry is to be determined by utilising a suitable model or by conservative estimation based on previous experience with similar types of masonry. It is noted that the values for the ratio E_{ma} / f_{ma} recommended in EN 1996-1-1 (2012) or DIN EN 1996-1-1/NA (2019) are, in general, not suitable for historical solid clay brick masonry.

9.3 Diagrams for Determining Assessment Values

As an alternative to determining the assessment value of masonry compressive strength by applying the equations defined in Section 9.1, the diagrams in Fig. 9-1, Fig. 9-2, and Fig. 9-3 can be used to obtain suitable characteristic values, partial factors, and assessment values for masonry compressive strength. The diagrams are based on the target reliability level $\beta_{t,1a}$ = 3.3 combined with the sensitivity factor $\alpha_{R,1a}$ = 0.7.

Again, the mean value of masonry compressive strength $f_{ma,m}$ is to be determined first. Then, the sample CoVs of the test results must be determined since, together with the respective sample sizes n, they are the input parameters for the diagrams. In the case of indirect testing, the sample CoVs V_b and V_j of unit and mortar compressive strength are needed. If masonry compressive strength is tested directly, the sample CoV V_{ma} of masonry compressive strength must be calculated. A conversion of the sample CoVs V_b, V_j, and V_{ma} of the test results into the sample standard deviations $s_{ln,b}$, $s_{ln,j}$, and $s_{ln,ma}$ of the logarithms of the test results is included in the diagrams utilising the following relationship:

$$s_{ln}^2 \approx \ln\left(1+V^2\right) \qquad \textit{Eq. 9-13}$$

Eq. 9-13, which is based on the respective relationship between the parameters of a log-normal distribution (see Eq. 2-27), is only an approximation in the case of a limited sample size. The exact relationship between V and $s_{\ln}$ depends on the single test results. It is noted that $s_{\ln}^2$ is an unbiased estimator of the variance $\sigma_{\ln}^2$, whereas the right part of Eq. 9-13 is not. This bias leads to a slight underestimation of $\sigma_{\ln}^2$ for small sample sizes on average, which can be neglected in practical applications. If Eq. 9-13 is exactly fulfilled, the application of the diagrams leads to the same results as the equations in Section 9.2. In principle, it is also possible to display the diagrams with the standard deviations of the logarithms of the test results ($s_{\ln,b}$, $s_{\ln,j}$, and $s_{\ln,ma}$) as input parameters. For practical application, however, a representation via the CoVs is more intuitive, which is why this type of illustration is chosen.

Fig. 9-1 and Fig. 9-2 can be used in the case of indirect testing. The only difference between the two figures is that Fig. 9-1 utilises the previously obtained prior hyperparameters, whereas Fig. 9-2 is based on a non-informative prior. In the upper left and the lower right part of the upper diagram, the updates of the prior estimates s' are performed for mortar and unit compressive strength, respectively. Furthermore, the updated variances s''^2 are modified so that they can be applied as the parameters of a log-normal distribution that approximates the resulting predictive log-t distribution (see Eq. 8-26):

$$s''^2_{\ln,\mathrm{mod}} = s''^2_{\ln} \frac{n}{n-1} \frac{\nu''}{\nu''-2} \qquad \textit{Eq. 9-14}$$

Hence, this modification leads to variances $s_{\ln,\mathrm{mod}}''^2$ that account for statistical uncertainty. These modified variances are then converted back into a CoV based on Eq. 9-13, which yields the CoVs v_j and v_b that are the results of the upper left and lower right part of the diagram. These CoVs are denoted identically to population CoVs since, due to the consideration of statistical uncertainty, they can be applied in the same way.

The ratio $f_{ma,a} / f_{ma,m}$ can then be obtained from the upper right part of the upper diagram based on the intersection of a horizontal and a vertical line at v_j and v_b, respectively. The location of the intersection with respect to the displayed contour lines provides the required value $f_{ma,a} / f_{ma,m}$. Based on v_j and v_b, the ratio $f_{ma,k} / f_{ma,m}$ and the partial factor γ_M are obtained accordingly using the two diagrams at the bottom. However, both values are not necessarily required since the assessment value can be determined from $f_{ma,a} / f_{ma,m}$ alone.

For illustration, the diagrams are employed for two example cases. In the first case, only the recommended minimum number of unit and mortar specimens is tested ($n_b = n_j = 6$), and the sample CoVs are $V_b = V_j = 55$ %. This corresponds to a relatively high CoV, which, however, still sometimes occurs in typical assessment situations (see Fig. 7-6). In the second case, 30 specimens of unit and mortar are tested, and the sample CoVs are $V_b = V_j = 15$ %. This CoV is relatively low for existing solid clay brick masonry constructed

before the year 1950. However, it is a realistic value for younger masonry. In Fig. 9-1 and Fig. 9-2, the determination of the required values is highlighted for the two examples. The corresponding results are listed in Table 9-2.

As evident, the resulting ratios $f_{ma,k} / f_{ma,m}$ between characteristic and mean value and the obtained partial factors γ_M are strongly dependent on the particular conditions. If the sample size is small and the sample CoVs are high, as in the first case, the utilisation of prior information leads to much higher assessment values. This is caused by two effects. First, the utilisation of prior information reduces the overall statistical uncertainty. Second, the estimates $s_{ln,b}$ and $s_{ln,j}$ for the standard deviations are reduced through the Bayesian update ($s_{ln}'' < s_{ln}$). If the sample CoVs are unusually low for existing solid clay brick masonry, the use of prior information can lead to a lower assessment value, as, for example, in the second case. Here, the estimates for the standard deviations are increased through the Bayesian update ($s_{ln}'' > s_{ln}$). However, the overall statistical uncertainty is still reduced, which partly compensates for the higher value of s_{ln}''. In summary, it can be stated that prior information leads to a narrower range of resulting characteristic values, partial factors, and assessment values for masonry compressive strength.

Table 9-2 Example results from applying the proposed method

Sample size $n_b = n_j$	Sample CoV $V_b = V_j$	Type of prior	Ratio $f_{ma,k} / f_{ma,m}$	Partial factor γ_M	Ratio $f_{ma,a} / f_{ma,m}$
6	55 %	Informative	0.46	1.51	0.30
		Non-informative	0.33	1.67	0.20
30	15 %	Informative	0.66	1.33	0.50
		Non-informative	0.70	1.31	0.53

In the case of direct testing, Fig. 9-3 can be employed for determining characteristic values $f_{ma,k}$, partial factors γ_M, and assessment values $f_{ma,a}$ for masonry compressive strength. Since the number of input parameters reduces from four to two – namely, to the sample CoV V_{ma} and the corresponding sample size n – applying the diagrams is more straightforward than in the case of indirect testing. The limiting values in Fig. 9-3 are caused by the condition that $\sigma_{ln,ma}$ must not be lower than the CoV $\upsilon_{\theta R} = 0.14$ of resistance model uncertainty. If the prior hyperparameters for solid clay brick masonry are applied, this limiting value does not become relevant in practical cases. In the case of the non-informative prior distribution, the limiting value for $\sigma_{ln,ma}$ can become relevant for a sample CoV V_{ma} smaller than 10 % if testing uncertainty is considered via $\upsilon_{\theta f} = 0.10$ (see Fig. 9-3). The actual limiting value for V_{ma} depends on the number of tests. In addition to ensuring that the assumption of model uncertainty being non-dominant is valid, the limiting value for the CoV is helpful as it prevents an overestimation of the appropriate assessment value caused by a randomly obtained sample CoV that is much lower than the actual CoV.

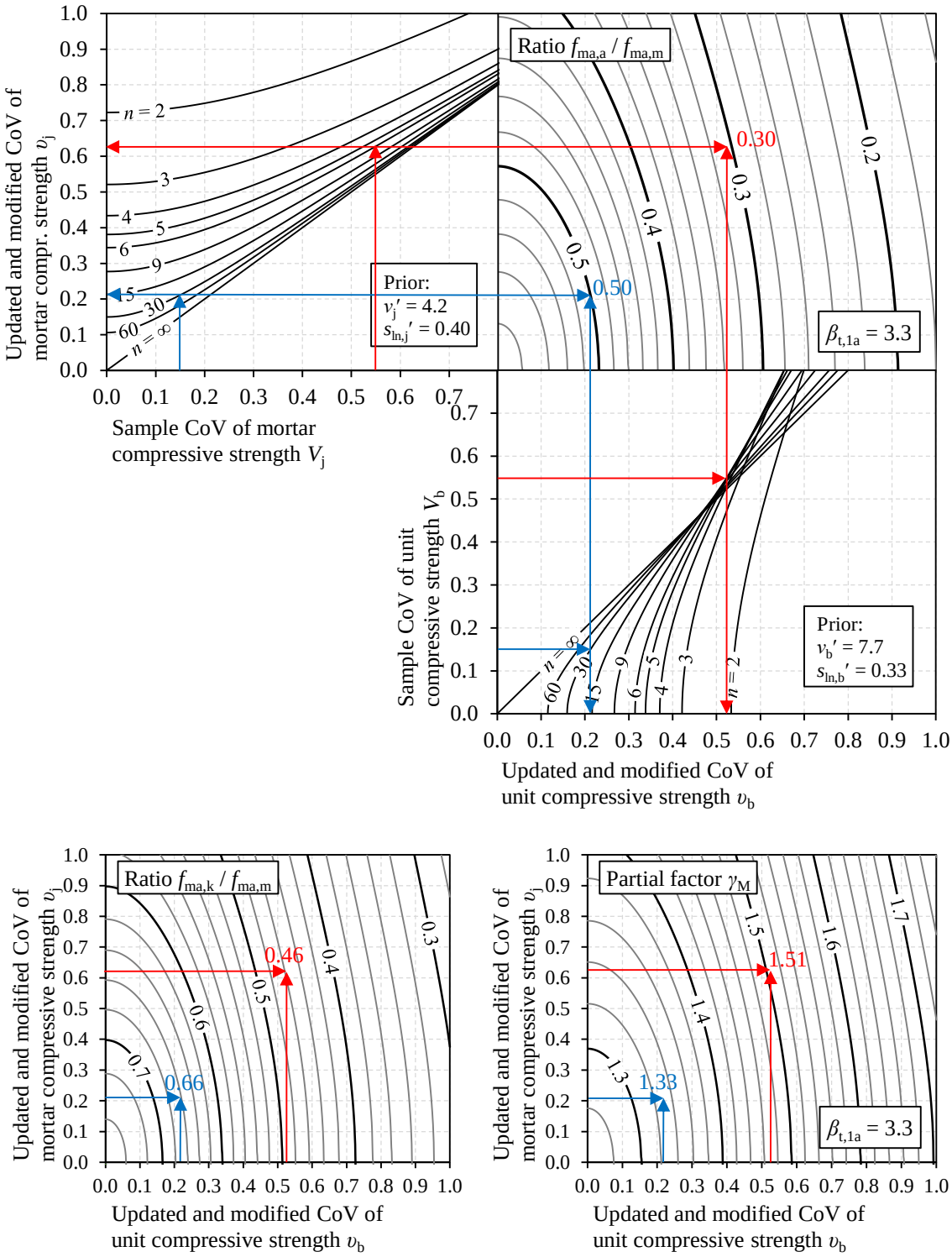

Fig. 9-1 Diagrams for determining assessment values, characteristic values, and partial factors for masonry compressive strength (informative prior)

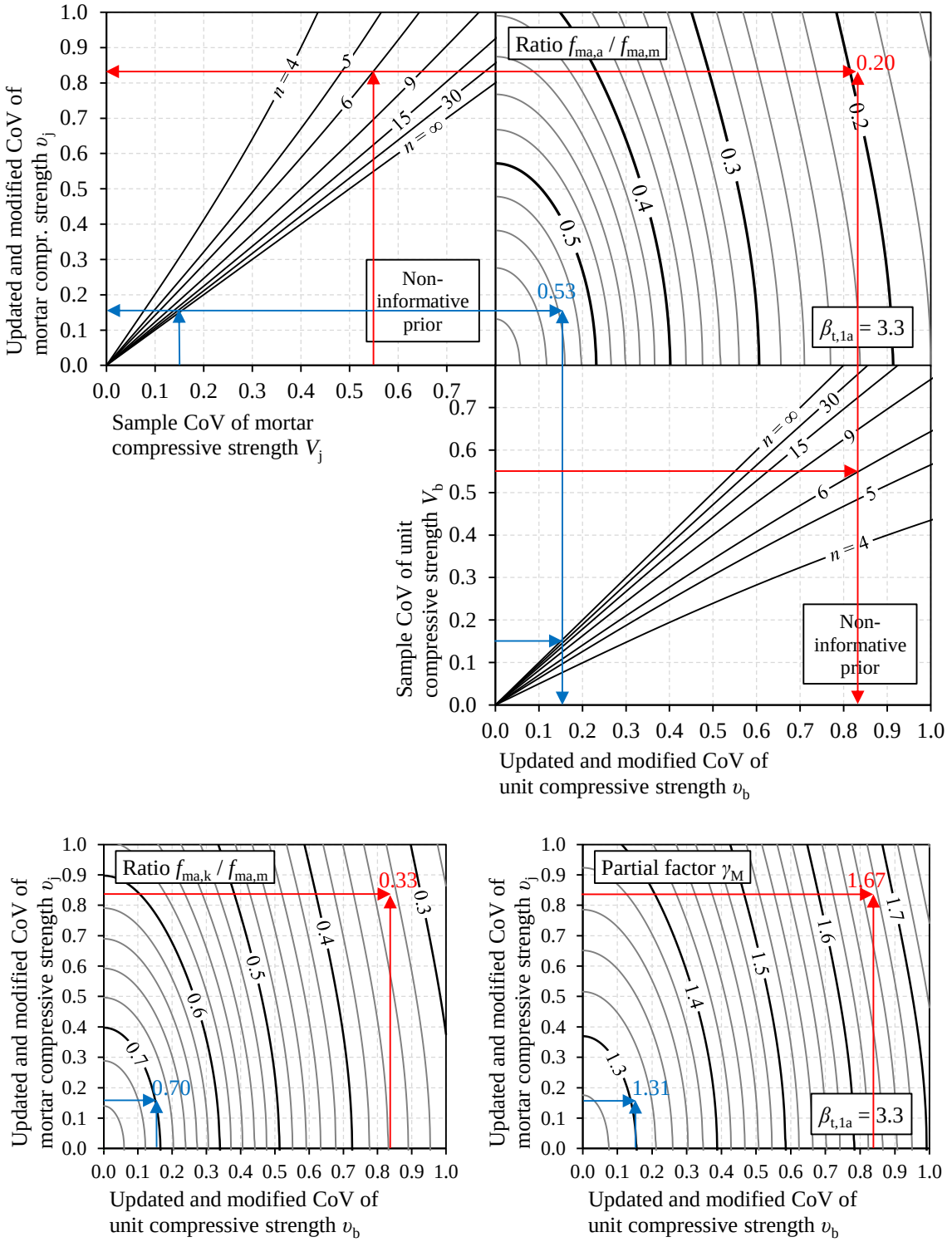

Fig. 9-2 Diagrams for determining assessment values, characteristic values, and partial factors for masonry compressive strength (non-informative prior)

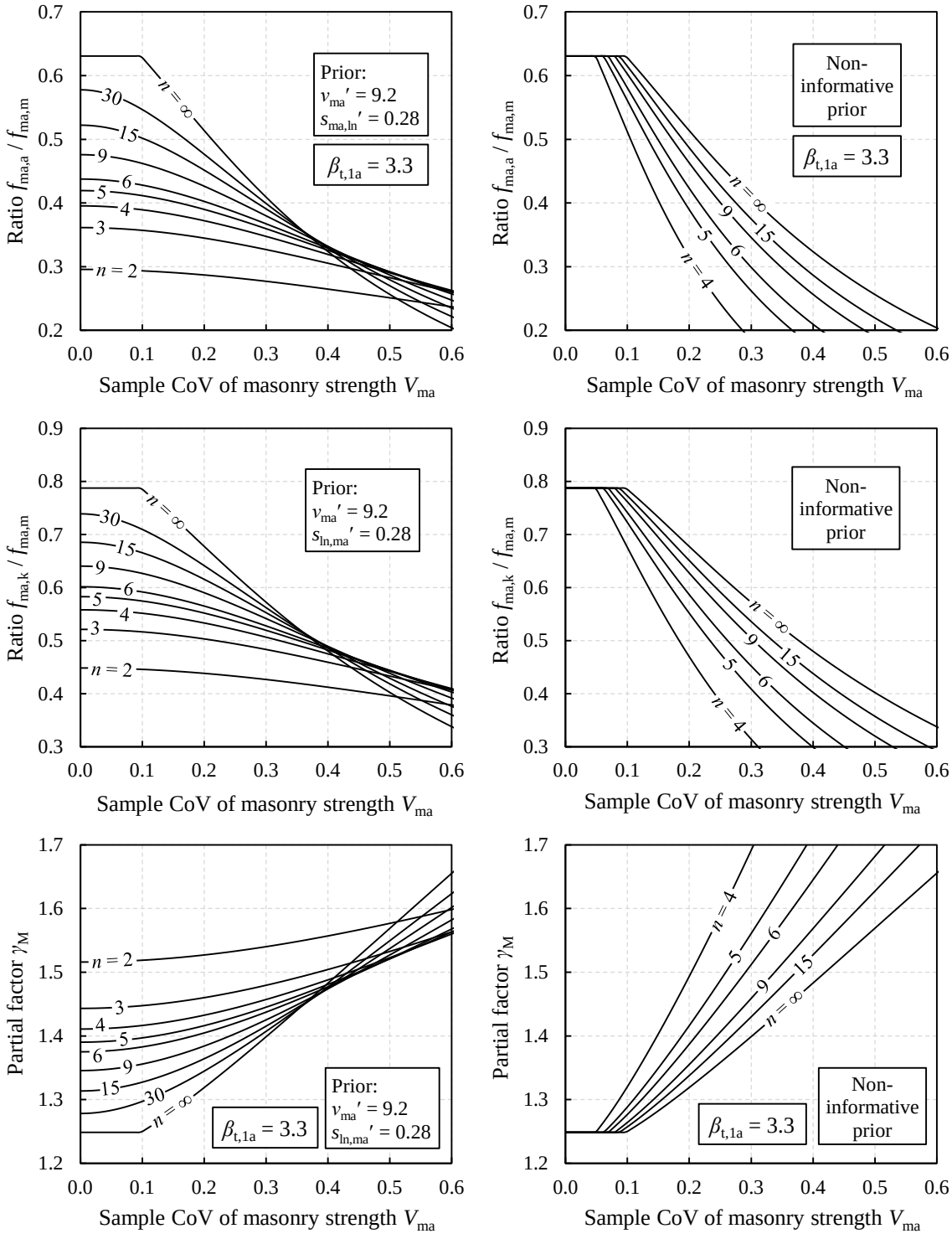

Fig. 9-3 Diagrams for determining assessment values, characteristic values, and partial factors for masonry compressive strength in the case of direct testing (left: informative prior, right: non-informative prior)

As already illustrated by the example for indirect testing, Fig. 9-3 demonstrates that the use of an informative prior leads to higher assessment values of masonry compressive strength $f_{ma,a}$ if the sample CoV is high. In the case of a relatively low sample CoV, the use of prior

information can lead to lower assessment values of masonry compressive strength. Nevertheless, the use of the presented prior hyperparameters is generally recommended when assessing existing solid clay brick masonry constructed before 1950 since this prevents the application of unrealistically low CoVs in the determination of the assessment strength. However, if other masonry types are assessed, utilising the non-informative prior is recommended if prior hyperparameters for this type of masonry are not available.

9.4 Typical Characteristic-to-Mean Ratios and Partial Factors

The proposed method is applied to the existing buildings in the database presented in Section 7.3. Thereby, it can be illustrated which results are typically obtained by the proposed method. Concerning indirect testing, 78 masonry populations are investigated, for which at least three unit and three mortar specimens from at least two different masonry walls are tested. Hence, the populations are defined to include all masonry walls in a building that belong to the same masonry type. Regarding direct testing, data from 11 buildings with at least two test results per building are used for the investigation (see Section 7.4.7). Only solid clay brick masonry is considered. By using the test results from the database, both the typical range of material variability and a typical range for the number of conducted tests are covered. For determining partial factors, two cases are considered. First, the reduced target reliability index $\beta_{t,1a} = 3.3$ is applied in combination with a fixed sensitivity factor $\alpha_{R,1a} = 0.7$. Second, the target reliability index $\beta_{t,50a} = 3.8$ for the design of new structures and CC 2 according to EN 1990 (2010) is applied with $\alpha_R = 0.8$.

The relative frequencies of the results are displayed in Fig. 9-4. The characteristic-to-mean ratios $f_{ma,k} / f_{ma,m}$ lie between 0.37 and 0.60. The partial factors are obtained in the range between 1.37 to 1.61 for $\beta_{t,1a} = 3.3$ and between 1.76 and 2.46 for $\beta_{t,50a} = 3.8$. No significant differences between the results for direct and indirect testing are present. It is evident that selecting the appropriate ratio of characteristic to mean value has a more substantial influence on the resulting assessment value than choosing the appropriate partial factor. The ratio of maximum to minimum value is 1.64 for $f_{ma,k} / f_{ma,m}$ and, thus, higher than the maximum-to-minimum ratio for γ_M, which is 1.17 for $\beta_{t,1a} = 3.3$ and 1.40 for $\beta_{t,50a} = 3.8$.

In the case of $\beta_{t,50a} = 3.8$, $\gamma_M = 1.99$ is obtained on average, which is much higher than the value $\gamma_M = 1.5$ defined in DIN EN 1996-1-1/NA (2019). The main reason for the higher partial factors is that the typical material variability of existing solid clay brick masonry built before 1950 is higher than that of contemporary masonry. However, if the reduced target reliability index $\beta_{t,1a} = 3.3$ is chosen, most of the resulting partial factors are lower than $\gamma_M = 1.5$. In this case, an average partial factor of $\gamma_M = 1.45$ is obtained for both indirect and direct testing.

In the case of $\beta_{t,1a}$ = 3.3, the resulting partial factors γ_M should be applied in combination with reduced partial factors for the action variables. Instead of γ_G = 1.35 for permanent load and γ_Q = 1.5 for imposed load, γ_G = 1.26 and γ_Q = 1.05 can be used (see Section 8.2.6). In the case of a combination of unfavourable permanent load G and imposed load Q with a load effect ratio of Q_k / G_k = 0.5, this enables more than 20 % higher utilisation of existing masonry walls on average if compared to applying the fixed partial factors γ_G = 1.35, γ_Q = 1.5, and γ_M = 1.5.

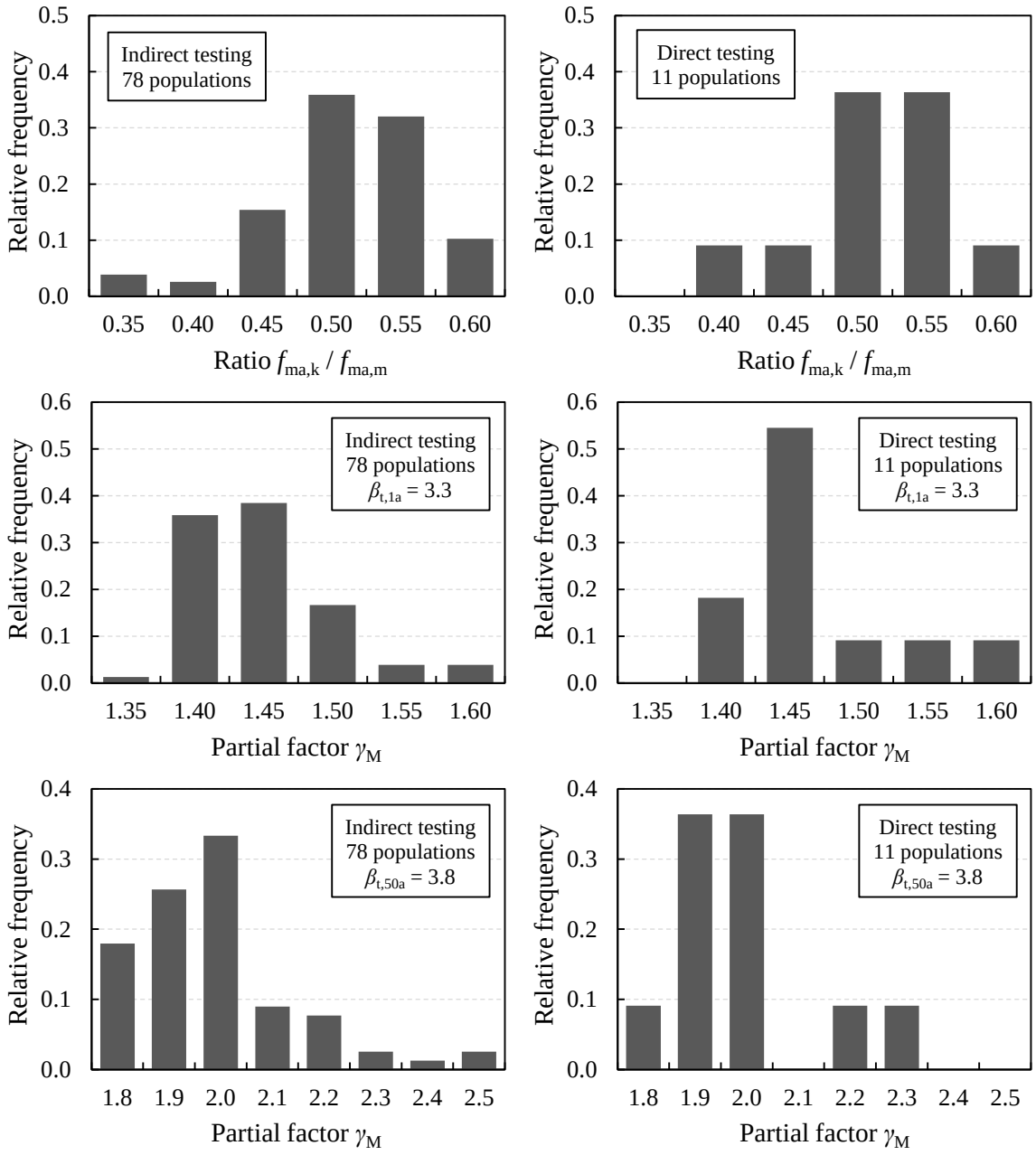

Fig. 9-4 Frequencies of the ratios $f_{ma,k} / f_{ma,m}$ and the partial factors γ_M obtained for the solid clay brick masonry populations in the test database

9.5 Alternative Assessment Procedures in the Absence of Test Results

The proposed method for determining assessment values of masonry compressive strength, as presented in the previous sections, can only be applied if results of compressive strength tests on either unit and mortar or masonry specimens are available. However, in practice, there is sometimes a desire to avoid material testing for economic reasons or to preserve cultural heritage, for example. Therefore, some suggestions on alternative assessment procedures in the case that no tests have been conducted are made here. The remarks should be understood as pragmatic recommendations for engineering practice that are not based on the same scientific rigour as the proposed test-based method. Furthermore, a high level of expertise is needed in some of the following approaches.

If no test results are available, a distinction between the following two cases must be made:

1. The investigated population of masonry was constructed according to particular material and design standards, and documents specifying the standardised compressive strength of unit and mortar (or masonry) are available.
2. The investigated population of masonry is too old to be built according to specific standards, or no documents specifying the material strength are available.

Case 1

In the first case, the specified unit and mortar compressive strength (or masonry compressive strength) can be used to verify structural safety. However, this always requires at least a visual check that the available construction documents – particularly the included information about the unit and mortar types – match the existing structure in its actual condition. In Germany, the structural safety of existing members that must resist increased load effects due to an extension of the building may be verified according to the standards in force at the time of construction if these members themselves are kept unchanged (ARGEBAU 2008). Nevertheless, verification according to the current standards (i.e. the Eurocodes) is also possible. If masonry compressive strength is only given in terms of an allowable stress σ_0 according to the former German standard DIN 1053 (e.g. DIN 1053-1 1990), Graubner et al. (2020) recommend applying a characteristic value $f_{ma,k}$ of 2.64 times σ_0.

If the verification according to former or current standards is not fulfilled, it can be helpful to reduce the current partial factors provided by the Eurocodes to consider a lower target reliability level compared to the design of new structures. Regarding the partial factors for actions, the adjusted partial factor method (APFM) as presented in fib bulletin 80 (2016) can be applied; see also Sections 2.6.3 and 8.2.6. In principle, the APFM can also be applied to the partial factor γ_M for the compressive strength of masonry to account for a reduced target reliability index without conducting tests. However, due to the high diversity of dif-

ferent masonry types and the wide range of partial factors γ_M defined by the National Annexes to EN 1996-1-1 (2012), as presented in Section 3.7, a modification of the partial factor γ_M without additional information from material testing is not recommended in general cases. It is noted that material testing is not only beneficial regarding a more precise modification of the partial factor but also since the in-situ compressive strength of unit and mortar might strongly deviate from the specified strengths in the construction documents.

Case 2

No information about the strength of unit, mortar, or masonry is available from construction documents in the second case. Therefore, reliable information about the in-situ strength can only be obtained by testing. After testing, the proposed method for determining assessment values of masonry compressive strength can be applied.

The testing of material properties can only be avoided entirely in this second case if it is obvious that the compressive strength of the investigated masonry members is sufficiently high to provide resistance against the expected load effects (see also WTA 7-4 2021). This decision can only be made by experts with much experience in assessing existing masonry structures. In addition, the results presented in Fig. 9-5 can be helpful if solid clay brick masonry is investigated.

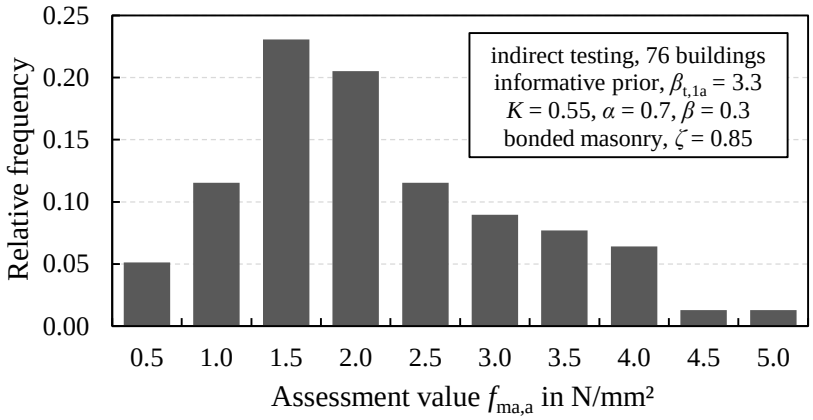

Fig. 9-5 Assessment values $f_{ma,a}$ of masonry compressive strength for the solid clay brick masonry populations in the test database obtained by applying the proposed method and the power equation from EN 1996-1-1 (2012)

Fig. 9-5 displays the relative frequencies of assessment values $f_{ma,a}$ obtained by applying the proposed method to the masonry populations in the test database introduced in Section 7.3. The assessment values are based on the results of indirect testing, an informative prior distribution, and a target reliability index of $\beta_{t,1a}$ = 3.3. Only 54 of the 78 building-related masonry populations lie within the application range of the power equation as specified in DIN EN 1996-1-1/NA (2019). Mainly populations with low mortar compressive strengths are excluded from the application of the respective power equation, as mortar compressive

strengths of $f_{j,m} < 2.5$ N/mm² are not covered. Therefore, the masonry compressive strengths in Fig. 9-5 are based on the power equation with parameters from EN 1996-1-1 (2012); only two populations with $f_{j,m} > 20$ N/mm² are excluded from the investigation due to the application conditions specified in EN 1996-1-1 (2012). The values displayed in Fig. 9-5 are valid for bonded masonry; that is, they include a reduction factor of 0.8 for masonry with vertical joints parallel to the face of the wall. Furthermore, they include a reduction factor of $\zeta = 0.85$ to consider the influence of sustained loading. With values between $f_{ma,a} = 0.54$ N/mm² and 4.8 N/mm², the range of obtained assessment values is relatively large. If the required assessment value of masonry compressive strength is lower than $f_{ma,a} = 0.5$ N/mm², it can be assumed that typical solid clay brick masonry in Germany without significant defects fulfils this requirement.

In some practical cases, only the compressive strength of the units is tested (see Section 7.3), whereas the compressive strength of mortar $f_{j,m}$ is estimated through expert judgement based on the age of the building, visual inspection, and resistance to scratching. This pragmatic – but not very accurate – approach can be suitable since unit compressive strength has much more influence on masonry compressive strength than mortar compressive strength (see e.g. Sections 3.5.3 and 8.5.3). The method presented in Section 9.2 can then be adapted as follows. The informative prior distribution is used for mortar compressive strength, and the number of tests is set to $n_j = 2$, which is the lowest possible value for applying the method. The choice of $n_j = 2$ supposes that the expert estimation of mortar compressive strength is as precise as two destructive tests. Since this cannot be assumed in general, the estimation of mortar compressive strength $f_{j,m}$ needs to be conservative. As no information regarding the variability of mortar strength is obtained by testing, the respective posterior parameters are set equal to the prior parameters (i.e. $\nu_j'' = \nu_j' = 4.2$ and $s_{ln,j}'' = s_{ln,j}' = 0.4$; see Section 7.4). Concerning the parameters for unit strength, the actual values for n_b and $s_{ln,b}$ from testing should be used to determine ν_b'' and $s_{ln,b}''$ as described in Section 9.2. If the application of diagrams instead of equations is preferred to determine characteristic values, partial factors, and assessment values for masonry compressive strength, the diagrams presented in Annex E can be used.

Stepwise approach

It follows from the above that the most suitable procedure to avoid material tests in the assessment of existing masonry structures is given by a stepwise approach (see also WTA 7-4 2021). The flowchart in Fig. 9-5 displays such a step-by-step procedure. Depending on the outcome of the verification attempts at the different steps, required testing is increased from no tests at all, to tests on units only, to tests on units and mortar. If the verification based on tests on unit and mortar is not fulfilled, either the number of tests on unit and mortar specimens can be increased, or tests on composite masonry specimens can be performed. Finally, if the structural safety of an assessed masonry member cannot be verified

in this last step, strengthening measures must be taken, the loads must be reduced, or the member must be replaced.

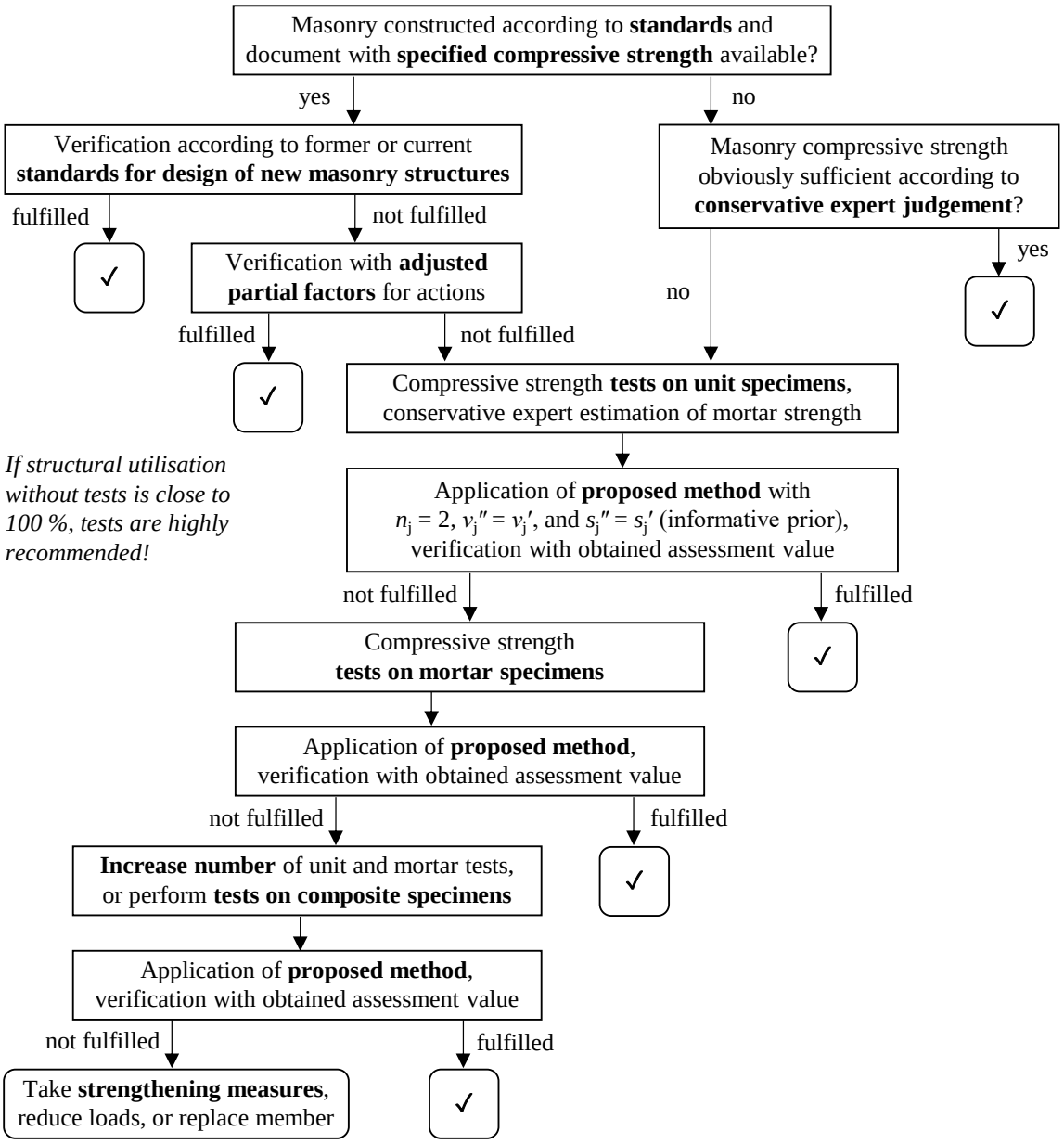

Fig. 9-6 Iterative assessment procedure for avoiding material tests

Although performing no material tests is sometimes possible (see Fig. 9-6), the question is whether conducting no tests is indeed the optimal decision in these cases. The additional information obtained by testing decreases the present uncertainty and can thus lead to better decision-making (i.e. decisions resulting in a higher expected benefit or lower expected costs; see also Section 2.6.2). This *value of information* obtained by performing tests often compensates for the testing costs. For example, it might be observed that the strength specified by construction documents does not match the structure as built, and a potential failure can hence be avoided by testing. A complete description of the concept behind the term

"value of information" and a corresponding study to optimise the number of tests is beyond the scope of this thesis. It is thus referred to Sykora et al. (2022), where the concept is described in detail, and the results of a case study dealing with a historic masonry structure are presented. Regarding the value of information, Sykora et al. (2022) demonstrate that destructive compressive strength testing is particularly beneficial concerning the value of information if the structural utilisation before performing destructive tests is around 100 %. Therefore, performing destructive tests on specimens from the investigated masonry population is also highly recommended here if the structural utilisation of one or more members of this population is close to 100 %.

10 SUMMARY AND OUTLOOK

The main objective of this thesis was to develop a method for determining suitable assessment values of the compressive strength of existing masonry if test results for either unit and mortar compressive strength or masonry compressive strength are available. For this purpose, the influence of spatially variable material properties on the load-bearing capacity of masonry walls under compression had to be quantified, which was accomplished by experimental, numerical, and analytical investigations. To consider the statistical uncertainty introduced by small sample sizes in material testing, a Bayesian framework was established, including suitable prior distributions for the stochastic parameters of unit, mortar, and masonry compressive strength. Concerning the influence of spatial variability and the obtained prior distributions, the focus of the investigations was on solid clay brick masonry. Finally, a practice-oriented method was proposed, which allows for determining characteristic values, partial factors, and assessment values for masonry compressive strength. Hence, the developed method is an essential and valuable tool for evaluating existing masonry structures and making appropriate decisions concerning the need for retrofitting measures if, for example, the respective building is extended or converted.

In Chapter 2, the relevant background regarding statistics and structural reliability was introduced. Particular emphasis was placed on Bayesian statistics, the calibration of partial factors, and the reliability assessment of existing structures. Appropriate target reliability levels for the assessment of existing structures were discussed. For the assessment of typical masonry structures with moderate consequences in case of failure, a target reliability index of $\beta_{t,1a} = 3.3$ for a reference period of one year, which is specified in ISO 2394 (2015) based on economic optimisation for large relative costs of safety measures, can be considered appropriate.

Chapter 3 dealt with the basics of masonry construction. After a brief illustration of the history of masonry construction, an overview of the state of the art regarding the load-bearing behaviour of masonry under compression was given. Then, the different procedures for testing the compressive strength of masonry were discussed. A distinction must be made between direct testing of masonry compressive strength on composite specimens and indirect testing, which is the separate testing of unit and mortar compressive strength. In the latter case, masonry compressive strength needs to be predicted based on the component strengths using a suitable model. The most common model is the empirical power equation specified in EN 1996-1-1 (2012), which was therefore analysed in detail. The analysis demonstrated that the power equation is also suited for probabilistic applications. The chapter closed with a description of strategies for the finite element modelling of masonry and a discussion of the safety format for the design of masonry structures according to EN 1996-1-1 (2012).

In Chapter 4, experimental investigations on the stress redistribution capability of masonry walls under compression loading were presented. The tests were conducted on solid clay brick masonry in which weaknesses were intentionally inserted through either a missing brick or a specified percentage of perforated bricks. The tests showed a reasonably good – but not perfect – capability of stress redistribution. In addition to the main tests on masonry walls, accompanying tests on unit and mortar were conducted. Regarding mortar strength, double punch tests according to DIN 18555-9 (2019) on mortar specimens extracted from masonry and standard compressive strength tests on mortar prisms according to EN 1015-11 (2019) were performed. The results indicate that the curing conditions within solid clay brick masonry lead to much higher mortar strengths than the curing conditions for standard mortar prisms.

Chapter 5 described the developed finite element model for masonry walls under compression loading. The model follows the simplified micro-modelling approach. The inelastic behaviour of masonry under compression is assigned to expanded units, whereas the discrete cracking in the mortar joints under tensile stresses is modelled by interface elements between these expanded units. It was shown that the experimental results on masonry walls with weak spots from Chapter 4 can be well reproduced with the developed finite element model.

In Chapter 6, Monte Carlo simulations of the load-bearing capacity of masonry walls under compression were presented. For these investigations, the validated finite element model was utilised, and the spatial variability of the compressive strength and the elastic modulus of masonry was modelled as unit-to-unit variability. In parameter studies, the relationship between the probability distribution of the material properties and the probability distribution of the wall resistance was investigated for various boundary conditions. It was observed that the mean wall resistance decreases with an increase in the spatial variability of the material properties. However, the resulting variability of the wall resistance is significantly smaller than the underlying spatial variability of the material properties within the wall. Considering only material variability, this results in a positive effect of taking spatial variability into account: If assessment values of masonry compressive strength are determined considering the effects of spatial variability on the distribution of the wall resistance, they are higher than the results of a direct calculation based on the probability distribution of masonry compressive strength. The parameter studies revealed that this positive effect is more pronounced for slender masonry walls failing due to buckling than for non-slender walls with cross-sectional failure. Furthermore, longer walls show a more favourable behaviour than short walls if subjected to spatial variability of material properties.

Chapter 7 first defines the Bayesian framework for considering statistical uncertainty. The framework allows the inclusion of prior distributions for the variances of the logarithms of unit, mortar, and masonry compressive strength. A test database for the material properties

of existing masonry was compiled to enable the modelling of prior distributions. The database contains test results for unit and mortar compressive strength of 140 existing buildings made of solid clay brick masonry. More than 2,000 test results for both unit and mortar compressive strength are included. Based on this data, the hyperparameters of the prior distributions were obtained by maximum likelihood estimation. Moreover, the hyperparameters of the prior distribution for masonry compressive strength were determined based on the respective prior distributions for unit and mortar via stochastic simulations utilising the power equation for masonry compressive strength.

In Chapter 8, the method for determining suitable assessment values of masonry compressive strength was finally developed. At first, the underlying principles, conditions, and assumptions were explained in detail. The method follows the simplified level II approach, which means that a fixed sensitivity factor α_R of the resistance is applied. The developed method can be used if results of either direct or indirect tests of masonry compressive strength for a particular masonry population are available. If the method is applied to solid clay brick masonry, the prior distributions determined in Chapter 7 can be used. For other types of masonry, the method can be employed using non-informative prior distributions. The target reliability index β_t is an input parameter of the method and can hence be selected as required in a specific case. Although assessment values of masonry compressive strength can be determined directly, the method also allows for the separate calculation of characteristic values of masonry compressive strength and partial factors for the resistance of masonry. The model uncertainties to be considered in assessing the resistance of a masonry wall were evaluated. This included the uncertainty of the model for calculating the load-bearing capacity of a masonry wall for a given masonry compressive strength and the uncertainty in predicting masonry compressive strength in the case of indirect testing.

In the next step, the different types of uncertainty (i.e. spatial material variability, model uncertainty, and statistical uncertainty) were combined via stochastic simulations. Thereby, posterior predictive distributions for the resistance of a masonry wall were obtained, based on which suitable assessment values for various boundary conditions were determined. These investigations served the purpose of deriving suitable approximations for engineering practice. It was shown that, in typical cases, it only makes a slight difference whether assessment values are determined based on the distribution of the wall resistance or based on the distribution of masonry compressive strength. The positive effect of considering spatial variability, which was observed in Chapter 6, disappears almost entirely if statistical and model uncertainty are considered in addition to material variability. Hence, for more convenience, the spatial nature of the variability of material properties can be neglected. Additional stochastic simulations demonstrated that the proposed method is not only suitable for the reference case of non-slender masonry walls with cross-sectional failure but also for slender walls failing due to buckling. Furthermore, it was shown that the strength

reduction factor specified by EN 1996-1-1 (2012) for walls with small cross-sections is also appropriate for the assessment of existing masonry walls. Finally, reliability analyses were conducted to validate the proposed method. It was demonstrated that the reliability level that results from applying the proposed method matches well with the selected target reliability index.

In Chapter 9, the proposed method for determining characteristic values, partial factors, and assessment values for masonry compressive strength was presented in its final, practice-oriented form. In addition to step-by-step instructions for applying the method via equations, diagrams for determining suitable assessment values, characteristic values, and partial factors were provided. Moreover, typical results from applying the proposed method to solid clay brick masonry were shown in terms of resulting characteristic-to-mean ratios for masonry compressive strength and partial safety factors γ_M for the resistance of masonry under compression. For the buildings in the test database presented in Chapter 7, an average partial factor $\gamma_M = 1.45$ was obtained based on a target reliability index of $\beta_{t,1a} = 3.3$. Finally, suggestions for alternative assessment procedures in the absence of test results were made.

Although a wide range of aspects concerning the probabilistic assessment of existing masonry structures was addressed in this thesis, there are still many open issues. Further research is needed on the following topics:

- Although the test database presented in Chapter 7 is quite extensive, further extension of the database would be beneficial. Thereby, prior distributions for masonry types other than solid clay brick masonry could be determined precisely. In addition, further differentiation of the prior distributions, such as according to specific geographic regions or narrower time periods, would be enabled.
- The procedures for testing the compressive strength of existing masonry should be further developed. The application limits of the available procedures for directly testing masonry compressive strength on relatively small composite specimens, such as masonry cores, should be widened. Therefore, research is needed concerning a precise conversion of the test results to the reference strength according to EN 1052-1 (1998). Regarding indirect testing, one shortcoming of the empirical power equation is its derivation based on the mortar compressive strength determined on standard prims, which differs from the strength determined on mortar specimens extracted from masonry. An empirical equation formulated directly via the mortar strength of specimens extracted from masonry would be beneficial. However, no sufficient database is currently available for this purpose.
- In this thesis, the focus was on the assessment of existing masonry walls under compression loading. A similar method is required for assessing masonry walls under shear

loading, where several potential failure modes need to be considered, such as flexural failure, sliding shear failure, and diagonal tension failure. These failure modes differ regarding the influential material properties, which have to be tested or estimated, and in terms of the influence of the respective spatial variability.

- Research is also needed on practice-oriented tools for decision-making regarding suitable populations, representative sampling locations, and optimal sample sizes when testing material properties of existing structures. In this context, it should be investigated how destructive and non-destructive testing methods can be combined optimally.

REFERENCES

Ahnert, R.; Krause, K. H. (2009): Typische Baukonstruktionen von 1860 bis 1960 – zur Beurteilung der vorhandenen Bausubstanz – Band 1. Siebte Auflage. Berlin: Huss-Medien.

Anderson, T. W.; Darling, D. A. (1952): Asymptotic Theory of Certain "Goodness of Fit" Criteria Based on Stochastic Processes. Annals of Mathematical Statistics 23 (2), pp. 193–212.

Ang, A. H.; Tang, W. H. (1984): Probability concepts in engineering planning and design – Volume 2: Decision, Risk, and Reliability. New York: John Wiley & Sons.

ARGEBAU (2008): Hinweise und Beispiele zum Vorgehen beim Nachweis der Standsicherheit beim Bauen im Bestand. Fachkommission Bautechnik der Bauministerkonferenz.

ASTM C1314 (2018): Standard Test Method for Compressive Strength of Masonry Prisms. West Conshohocken: ASTM International.

Au, S.-K.; Beck, J. L. (2001): Estimation of small failure probabilities in high dimensions by subset simulation. Probabilistic Engineering Mechanics 16 (4), pp. 263–277.

Bakeer, T. (2015): Stability of masonry walls. Habilitation thesis. Technische Universität Dresden.

Bakeer, T. (2016a): Empirical estimation of the load bearing capacity of masonry walls under buckling – Critical remarks and a new proposal for the Eurocode 6. Construction and Building Materials 113, pp. 376–394.

Bakeer, T. (2016b): Reliability assessment of vertically loaded masonry walls. Structural Safety 62, pp. 47–56.

Bakeer, T.; Salehi, H. (2019): Determination of a model partial safety factor for unreinforced masonry walls under buckling. Mauerwerk 23 (1), pp. 32–39.

Bayes, T. (1763): An Essay towards Solving a Problem in the Doctrine of Chances. Philosophical Transactions of the Royal Society 53, pp. 370–418.

BBSR (2020): Strukturdaten zur Produktion und Beschäftigung im Baugewerbe – Berechnungen für das Jahr 2019. BBSR-Online-Publikation 15/2020. Bonn: Bundesinstitut für Bau-, Stadt- und Raumforschung.

Bender, W. (2004): Vom Ziegelgott zum Industrieelektroniker – Geschichte der Ziegelherstellung von den Anfängen bis heute. Bonn: Bundesverband der Deutschen Ziegelindustrie e. V.

Berger, F. (1987): Zur nachträglichen Bestimmung der Tragfähigkeit von zentrisch gedrücktem Ziegelmauerwerk. In Wenzel (Ed.): Erhalten historisch bedeutsamer Bauwerke. Jahrbuch 1986 des SFB 315. Berlin: Ernst & Sohn, pp. 231–248.

Binda, L. (Ed.) (2008): Learning from failure – Long-term behaviour of heavy masonry structures. International Series on Advances in Architecture 23. Southampton, Boston: WIT Press.

BMVBS (2011): Richtlinie zur Nachrechnung von Straßenbrücken im Bestand (Nachrechnungsrichtlinie). Berlin, Bonn: Bundesministerium für Verkehr, Bau und Stadtentwicklung.

Brameshuber, W.; Graubohm, M.; Meyer, U. (2012): Druckfestigkeit von Ziegelmauerwerk – aktuelle Auswertungen zur Festlegung von charakteristischen Mauerwerkdruckfestigkeiten in DIN EN 1996. Mauerwerk 16 (1), pp. 10–16.

Brehm, E. (2011): Reliability of Unreinforced Masonry Bracing Walls – Probabilistic Approach and Optimized Target Values. Dissertation. Technische Universität Darmstadt.

Breitung, K. (1984): Asymptotic Approximations for Multinormal Integrals. Journal of Engineering Mechanics 110 (3), pp. 357–366.

Bucher, C. G. (1988): Adaptive sampling – an iterative fast Monte Carlo procedure. Structural Safety 5 (2), pp. 119–126.

Bucher, C. G.; Bourgund, U. (1990): A fast and efficient response surface approach for structural reliability problems. Structural Safety 7 (1), pp. 57–66.

Bundesverband Kalksandsteinindustrie e.V. (2018): Kalksandstein Planungshandbuch – Planung, Konstruktion, Ausführung. Düsseldorf: Verlag Bau+Technik.

Caspeele, R.; Sykora, M.; Allaix, D. L.; Steenbergen, R. (2013): The Design Value Method and Adjusted Partial Factor Approach for Existing Structures. Structural Engineering International 23 (4), pp. 386–393.

Caspeele, R.; Taerwe, L. (2012): Bayesian assessment of the characteristic concrete compressive strength using combined vague-informative priors. Construction and Building Materials 28 (1), pp. 342–350.

Cischinsky, H.; Diefenbach, N. (2018): Datenerhebung Wohngebäudebestand 2016 – Datenerhebung zu den energetischen Merkmalen und Modernisierungsraten im deutschen und hessischen Wohngebäudebestand. Darmstadt: Institut Wohnen und Umwelt.

ČSN 73 0038 (2019): Hodnocení a ověřování existujících konstrukcí – doplňující ustanovení. Prague: Úřad pro technickou normalizaci, metrologii a státní zkušebnictví.

Daniels, H. E. (1945): The statistical theory of the strength of bundles of threads. Proceedings of the Royal Society of London. Series A, Mathematical and Physical Sciences 183 (995), pp. 405–435.

DBV-Heft 24 (2013): Begründung eines reduzierten Zuverlässigkeitsindexes und modifizierter Teilsicherheitsbeiwerte für das Bauen im Bestand. Abschlussbericht zum DBV-Forschungsvorhaben 294. Berlin: Deutscher Beton- und Bautechnik-Verein e.V.

DBV-Merkblatt (2013): Modifizierte Teilsicherheitsbeiwerte für Stahlbetonbauteile. Berlin: Deutscher Beton- und Bautechnik-Verein e.V.

Der Kiureghian, A.; Ditlevsen, O. (2009): Aleatory or epistemic? Does it matter? Structural Safety 31 (2), pp. 105–112.

Destatis (2020): Baufertigstellungen von Wohn- und Nichtwohngebäuden (Neubau) nach überwiegend verwendetem Baustoff – Lange Reihen ab 2000. Statistisches Bundesamt.

Diamantidis, D. (Ed.) (2001): Probabilistic assessment of existing structures – JCSS Report. A publication of the Joint Committee on Structural Safety (JCSS). Cachan: RILEM Publications.

DIANA FEA (2019): DIANA Documentation – Release 10.3. Delft: DIANA FEA BV.

DIN 105 (1922): Mauerziegel (Backsteine). Berlin: Beuth Verlag.

DIN 105 (1952): Mauerziegel – Vollziegel und Lochziegel. Berlin: Beuth Verlag.

DIN 105-1 (1982): Mauerziegel – Vollziegel und Hochlochziegel. Berlin: Beuth Verlag.

DIN 1053 (1937): Berechnungsgrundlagen für Bauteile aus künstlichen und natürlichen Steinen. Berlin: Beuth Verlag.

DIN 1053-1 (1990): Mauerwerk – Teil 1: Rezeptmauerwerk; Berechnung und Ausführung. Berlin: Beuth Verlag.

DIN 1053-2 (1984): Mauerwerk; Mauerwerk nach Eignungsprüfung; Berechnung und Ausführung. Berlin: Beuth Verlag.

DIN 106 (1952): Kalksandsteine (Mauersteine). Berlin: Beuth Verlag.

DIN 18555-9 (2019): Prüfung von Mörteln mit mineralischen Bindemitteln – Teil 9: Bestimmung der Fugendruckfestigkeit von Festmörteln. Berlin: Beuth Verlag.

DIN 20000-401 (2017): Anwendung von Bauprodukten in Bauwerken – Teil 401: Regeln für die Verwendung von Mauerziegeln nach DIN EN 771-1:2015-11. Berlin: Beuth Verlag.

DIN 4172 (1951): Maßordnung im Hochbau. Berlin: Beuth Verlag.

DIN 4172 (2015): Maßordnung im Hochbau. Berlin: Beuth Verlag.

DIN EN 1991-1-1/NA (2010): Nationaler Anhang – National festgelegte Parameter – Eurocode 1: Einwirkungen auf Tragwerke – Teil 1-1: Allgemeine Einwirkungen auf Tragwerke – Wichten, Eigengewicht und Nutzlasten im Hochbau. Berlin: Beuth Verlag.

DIN EN 1996-1-1/NA (2019): Nationaler Anhang – National festgelegte Parameter – Eurocode 6: Bemessung und Konstruktion von Mauerwerksbauten – Teil 1-1: Allgemeine Regeln für bewehrtes und unbewehrtes Mauerwerk. Berlin: Beuth Verlag.

DIN EN 1996-1-1/NA/A1 (2014): Nationaler Anhang – National festgelegte Parameter – Eurocode 6: Bemessung und Konstruktion von Mauerwerksbauten – Teil 1-1: Allgemeine Regeln für bewehrtes und unbewehrtes Mauerwerk; Änderung A1. Berlin: Beuth Verlag.

DIN EN 1996-3/NA (2019): Nationaler Anhang – National festgelegte Parameter – Eurocode 6: Bemessung und Konstruktion von Mauerwerksbauten – Teil 3: Vereinfachte Berechnungsmethoden für unbewehrte Mauerwerksbauten. Berlin: Beuth Verlag.

Drucker, D. C.; Prager, W. (1952): Soil mechanics and plastic analysis for limit design. Quarterly of Applied Mathematics 10 (2), pp. 157–165.

DS/EN 1996-1-1 DK NA (2013): National Annex to Eurocode 6: Design of masonry structures – Part 1-1: General rules for reinforced and unreinforced masonry structures. Copenhagen: Danish Standards Foundation.

Efron, B. (1979): Bootstrap Methods: Another Look at the Jackknife. The Annals of Statistics 7 (1), pp. 1–26.

Efron, B. (1987): Better Bootstrap Confidence Intervals. Journal of the American Statistical Association 82 (397), pp. 171–185.

Efron, B.; Tibshirani, R. (1986): Bootstrap Methods for Standard Errors, Confidence Intervals, and Other Measures of Statistical Accuracy. Statistical Science 1 (1), pp. 54–75.

Efron, B.; Tibshirani, R. (1993): An Introduction to the Bootstrap. Monographs on statistics and applied probability 57. New York: Chapman and Hall.

Egermann, R. (1992): Zur nachträglichen Bestimmung der mechanischen Eigenschaften von Mauerziegeln. In Wenzel (Ed.): Erhalten historisch bedeutsamer Bauwerke. Jahrbuch 1990 des SFB 315. Berlin: Ernst & Sohn, pp. 159–182.

Egermann, R.; Mayer, K. (1989): Die Entwicklung der Ziegelherstellung und ihr Einfluss auf die mechanischen Eigenschaften von Mauerziegeln. In Wenzel (Ed.): Erhalten historisch bedeutsamer Bauwerke. Jahrbuch 1988 des SFB 315. Berlin: Ernst & Sohn, pp. 107–130.

Ellingwood, B. R. (1996): Reliability-based condition assessment and LRFD for existing structures. Structural Safety 18 (2–3), pp. 67–80.

Ellingwood, B. R.; Galambos, T. V.; MacGregor, J. G.; Cornell, C. A. (1980): Development of a Probability Based Load Criterion for American National Standard A58. Washington, DC: U.S. Government Printing Office.

EN 1015-11 (2019): Methods of test for mortar for masonry – Part 11: Determination of flexural and compressive strength of hardened mortar. Brussels: European Committee for Standardization.

EN 1052-1 (1998): Methods of test for masonry – Part 1: Determination of compressive strength. Brussels: European Committee for Standardization.

EN 13791 (2019): Assessment of in-situ compressive strength in structures and precast concrete components. Brussels: European Committee for Standardization.

EN 1990 (2010): Eurocode – Basis of structural design. EN 1990:2002 + A1:2005 + A1:2005/AC:2010. Brussels: European Committee for Standardization.

EN 1991-1-1 (2009): Eurocode 1: Actions on structures – Part 1-1: General actions – Densities, self-weight, imposed loads for buildings. EN 1991-1-1:2002 + AC:2009. Brussels: European Committee for Standardization.

EN 1992-1-1 (2010): Eurocode 2: Design of concrete structures – Part 1-1: General rules and rules for buildings. EN 1992-1-1:2004 + AC:2010. Brussels: European Committee for Standardization.

EN 1996-1-1 (2012): Eurocode 6: Design of masonry structures – Part 1-1: General rules for reinforced and unreinforced masonry structures. EN 1996-1-1:2005 + A1:2012. Brussels: European Committee for Standardization.

EN 1996-3 (2009): Eurocode 6: Design of masonry structures – Part 3: Simplified calculation methods for unreinforced masonry structures. EN 1996-3:2006 + AC:2009. Brussels: European Committee for Standardization.

EN 459-1 (2015): Building lime – Part 1: Definitions, specifications and conformity criteria. Brussels: European Committee for Standardization.

EN 772-1 (2011): Methods of test for masonry units – Part 1: Determination of compressive strength. Brussels: European Committee for Standardization.

Faber, M. H. (2005): On the Treatment of Uncertainties and Probabilities in Engineering Decision Analysis. Journal of Offshore Mechanics and Arctic Engineering 127 (3), pp. 243–248.

Ferretti, D. (2020): Dimensional analysis and calibration of a power model for compressive strength of solid-clay-brick masonry. Engineering Structures 205, 110064.

fib (2016): Bulletin 80 – Partial factor methods for existing concrete structures. Lausanne: Fédération internationale du betón.

fib (2020): Model Code 2020 (draft). Lausanne: Fédération internationale du betón.

Fienberg, S. (2006): When did Bayesian inference become "Bayesian"? Bayesian Analysis 1 (1), pp. 1–40.

Fischer, K.; Viljoen, C.; Köhler, J.; Faber, M. H. (2019): Optimal and acceptable reliabilities for structural design. Structural Safety 76 (3), pp. 149–161.

Förster, V. (2018): Tragfähigkeit unbewehrter Druckglieder aus Beton und Mauerwerk bei zweiachsig exzentrischer Beanspruchung. Dissertation. Technische Universität Darmstadt, Darmstadt. Institut für Massivbau.

FprEN 1996-1-1 (2020): Eurocode 6: Design of masonry structures – Part 1-1: General rules for reinforced and unreinforced masonry structures: European Committee for Standardization.

Francis, A. J.; Horman, C. B.; Jerrems, L. E. (1971): The Effect of Joint Thickness and Other Factors on the Compressive Strength of Brickwork. In West, Speed (Eds.): Proceedings of the Second International Brick Masonry Conference. Stoke-on-Trent: British Ceramic Research Association, pp. 31–37.

Franke, L.; Goretzky, W. (2004): Tragfähigkeit von druckbeanspruchtem Mauerwerk aus festigkeits- und verformungsstreuendem Material. Bauingenieur 79 (3), pp. 136–144.

Franke, L.; Schumann, I. (1998): Schadensatlas – Klassifikation und Analyse von Schäden an Ziegelmauerwerk. Europäische Kommission, Schutz und Erhalt des europäischen Kulturerbes. Forschungsbericht Nr. 8, Band 2. Stuttgart: Fraunhofer IRB Verlag.

Franzoni, E.; Gentilini, C.; Graziani, G.; Bandini, S. (2015): Compressive behaviour of brick masonry triplets in wet and dry conditions. Construction and Building Materials 82 (2), pp. 45–52.

Gelman, A.; Carlin, J. B.; Stern, H. S.; Dunson, D. B.; Vehtari, A. (2013): Bayesian Data Analysis. Third edition. Boca Raton, London, New York: CRC Press.

Geyer, S.; Papaioannou, I.; Straub, D. (2021): Characteristic values of spatially varying material properties in existing structures. In Chen, Ruan, Frangopol (Eds.): Life-Cycle Civil Engineering: Innovation, Theory and Practice. Proceedings of the 7th International Symposium on Life-Cycle Civil Engineering (IALCCE 2020). London: CRC Press.

Ghiassi, B.; Lourenço, P. B. (Eds.) (2019): Long-term Performance and Durability of Masonry Structures. Duxford, Cambridge, Kidlington: Woodhead Publishing.

Gigla, B. (2020): Bestimmung der Druckfestigkeit von vorhandenem Mauerwerk. Mauerwerk 24 (4), pp. 215–226.

Glock, C. (2004): Traglast unbewehrter Beton- und Mauerwerkswände – Nichtlineares Berechnungsmodell und konsistentes Bemessungskonzept für schlanke Wände unter Druckbeanspruchung. Dissertation. Technische Universität Darmstadt.

Glowienka, S. (2007): Zuverlässigkeit von Mauerwerkswänden aus großformatigen Steinen – Probabilistische Analyse von großformatigem Mauerwerk aus Kalksandstein und Porenbeton mit Dünnbettvermörtelung. Dissertation. Technische Universität Darmstadt.

Gooch, L. J.; Masia, M. J.; Stewart, M. G. (2021): Application of stochastic numerical analyses in the assessment of spatially variable unreinforced masonry walls subjected to in-plane shear loading. Engineering Structures 235, 112095.

Goretzky, W. (2000): Tragfähigkeit druckbeanspruchten Mauerwerks aus festigkeits- und verformungsstreuenden Mauersteinen und -mörteln. Dissertation. Technische Universität Hamburg-Harburg.

Graubner, C.-A.; Brehm, E.; Förster, V.; Ostendorf, D.; Purkert, B.; Schermer, D.; Schmidt, U.; Scheller, E. (2020): Eurocode 6 – DIN EN 1996 mit Nationalen Anhängen: Bemessung und Konstruktion von Mauerwerksbauten. Kommentierte Fassung. Berlin: Beuth, Ernst & Sohn.

Graubner, C.-A.; Koob, B. (2015): Analysis and comparison of the NDPs of various national annexes of Eurocode 6 / Analyse und Vergleich der NDPs verschiedener nationaler Anhänge zu Eurocode 6. Mauerwerk 19 (6), pp. 427–440.

Graubohm, M.; Brameshuber, W. (2016): Determining the masonry compressive strength / Bestimmung der Druckfestigkeit von Mauerwerk. Mauerwerk 20 (5), pp. 340–351.

Gregorczyk, P.; Lourenço, P. B. (2000): A Review on Flat-Jack Testing. Engenharia Civil 9, pp. 39–50.

Grimm, C. T. (1988): Brick Masonry Workmanship Statistics. Journal of Construction Engineering & Management 114 (1), pp. 147–149.

Grünberg, J. (2004): Grundlagen der Tragwerksplanung – Sicherheitskonzept und Bemessungsregeln für den konstruktiven Ingenieurbau. Erläuterungen zu DIN 1055-100. Berlin: Beuth Verlag.

Gumbel, E. J. (1958): Statistics of Extremes. New York: Columbia University Press.

Gunkler, E. (1993): Zur nachträglichen Erhöhung der Biegetragfähigkeit von Mauerwerkswänden durch bewehrte Ergänzungsschichten. Dissertation. Technische Universität Braunschweig.

Hall, W. B. (1988): Reliability of Service-Proven Structures. Journal of Structural Engineering 114 (3), pp. 608–624.

Hasofer, A. M.; Lind, N. C. (1974): Exact and Invariant Second-Moment Code Format. Journal of the Engineering Mechanics Division 100 (1), pp. 111–121.

Hedderich, J.; Sachs, L. (2020): Angewandte Statistik. Berlin, Heidelberg: Springer.

Heffler, L. M.; Stewart, M. G.; Masia, M. J.; Correa, M. R. S. (2008): Statistical Analysis and Spatial Correlation of Flexural Bond Strength for Masonry Walls. Masonry International 21 (2), pp. 59–70.

Heidel, R. (1989): Ermittlung der Materialkennwerte von Mauerwerk als Grundlage zur Beurteilung der Tragfähigkeit von Mauerwerkskonstruktionen. Dissertation. Technische Hochschule Leipzig.

Henkel, J. (2016): Evaluation of the quality of historic brickwork. Mauerwerk – European Journal of Masonry 20 (5), pp. 391–406.

Henkel, J.; Neuwald-Burg, C. (2021): Das Fugenbohrkernverfahren nach Helmerich/Heidel bzw. UIC-Kodex 778-3 zur Bestimmung der Druckfestigkeit von Bestandsmauerwerk. Mauerwerk 25 (2), pp. 53–62.

Henzel, J.; Karl, S. (1987): Determination of Strength of Mortar in the Joints of Masonry by Compression Tests on Small Specimens. In König, Reinhardt, Walraven (Eds.): Darmstadt Concrete. Darmstadt: Institut für Massivbau, pp. 123–136.

Hesterberg, T. C. (2015): What Teachers Should Know About the Bootstrap: Resampling in the Undergraduate Statistics Curriculum. The American statistician 69 (4), pp. 371–386.

Hierl, J.; Pfeiffer, H.; Rasch, C.; Schneider, H.; Schnell, W. (1973): Dauerstandfestigkeit von Mauerwerk – Festigkeit, Schwinden und Kriechen von Hohlblock-Mauerwerk. Berlin: Ernst & Sohn (Berichte aus der Bauforschung, 89).

Hilsdorf, H. (1965): Untersuchungen über die Grundlagen der Mauerwerksfestigkeit. Bericht Nr. 40. München: Materialprüfungsamt für das Bauwesen der Technischen Universität München.

Hilsdorf, H. K. (1969): Investigation into the failure mechanism of brick masonry loaded in axial compression. In Johnson (Ed.): Designing, Engineering and Constructing with Masonry Products. Houston: Gulf Publishing Company, pp. 34–41.

Hohenbichler, M.; Rackwitz, R. (1983): Reliability of Parallel Systems under Imposed Uniform Strain. Journal of Engineering Mechanics 109 (3), pp. 896–907.

Honfi, D. (2014): Serviceability floor loads. Structural Safety 50 (4), pp. 27–38.

IRS 70778-3 (2017): Recommendations for the inspection, assessment and maintenance of masonry arch bridges. Paris: International Union of Railways (UIC).

Isfeld, A. C.; Stewart, M. G.; Masia, M. J. (2021): Stochastic finite element model assessing length effect for unreinforced masonry walls subjected to one-way vertical bending under out-of-plane loading. Engineering Structures 236, 112115.

ISO 13822 (2010): Bases for design of structures – Assessment of existing structures. Geneva: International Organization for Standardization.

ISO 2394 (1998): General principles on reliability for structures. Geneva: International Organization for Standardization.

ISO 2394 (2015): General principles on reliability for structures. Geneva: International Organization for Standardization.

Jäger, W.; Pflücke, T. (2006): Einfluss der Schlankheit auf die Druckfestigkeit von Mauerwerksprüfkörpern nach EC 6. Forschungsbericht T 3106. Stuttgart: Fraunhofer IRB Verlag.

JCSS (2001a): Probabilistic Model Code – Part 1: Basis of Design. Joint Committee on Structural Safety. Available online at www.jcss-lc.org/jcss-probabilistic-model-code, checked on 15/10/21.

JCSS (2001b): Probabilistic Model Code – Part 2: Load Models. Joint Committee on Structural Safety. Available online at www.jcss-lc.org/jcss-probabilistic-model-code, checked on 15/10/21.

JCSS (2002): Probabilistic Model Code – Part 3: Material Properties. Joint Committee on Structural Safety. Available online at www.jcss-lc.org/jcss-probabilistic-model-code, checked on 15/10/21.

JCSS (2011): Masonry Properties. In: Probabilistic Model Code. Joint Committee on Structural Safety. Available online at www.jcss-lc.org/jcss-probabilistic-model-code, checked on 15/10/21.

JSCE (2010): JSCE Guidelines for Concrete No. 15. Standard Specifications for Concrete Structures – 2007 – "Design". Tokyo: Japan Society of Civil Engineers.

Kaushik, H. B.; Rai, D. C.; Jain, S. K. (2007): Stress-Strain Characteristics of Clay Brick Masonry under Uniaxial Compression. J. Mater. Civ. Eng. 19 (9), pp. 728–739.

Khan, A.; Lemmen, C. (2014): Bricks and urbanism in the Indus Valley rise and decline. Available online at arxiv.org/pdf/1303.1426v2.pdf, checked on 15/10/21.

Khoo, C.-L. (1972): A Failure Criterion for Brickwork in Axial Compression. Dissertation. University of Edinburgh.

Kirtschig, K.; Meyer, J. (1987): Auswertung von Mauerwerksversuchen zur Festlegung von zulässigen Spannungen und charakteristischen Mauerwerksfestigkeiten. Heft 54. Hannover: Institut für Baustoffkunde und Materialprüfung der Universität Hannover.

Kirtschig, K.; Meyer, J. (1989): Baukostendämpfung durch Ermittlung des Einflusses der Güte der Ausführung auf die Druckfestigkeit von Mauerwerk. Bauforschungsbericht F 2141. Stuttgart: IRB Verlag.

Kirtschig, K.; Meyer, J. (1990): Zur Sicherheit von Wänden und Pfeilern im Mauerwerksbau. Bauforschungsbericht F 2161. Stuttgart: IRB Verlag.

König, G.; Hosser, D. (1982): The simplified level II method and its application on the derivation of safety elements for level I. In CEB (Ed.): Bulletin No. 147 – Conceptional Preparation of Future Codes. Paris: Comité euro-international du béton.

König, G.; Hosser, D.; Schobbe, W. (1982): Sicherheitsanforderungen für die Bemessung von baulichen Anlagen nach den Empfehlungen des NABau – eine Erläuterung. Bauingenieur 57, pp. 69–78.

Kurapkat, D. (2017): Bauwissen im Neolithikum Vorderasiens. In Renn, Osthues, Schlimme (Eds.): Wissensgeschichte der Architektur – Band I: Vom Neolithikum bis zum Alten Orient. Berlin: Edition Open Access, pp. 57–127.

Larbi, J. A. (2004): Microscopy applied to the diagnosis of the deterioration of brick masonry. Construction and Building Materials 18 (5), pp. 299–307.

Lemaire, M. (2009): Structural reliability. London, Hoboken: ISTE, Wiley.

Li, J.; Masia, M. J.; Stewart, M. G.; Lawrence, S. J. (2014): Spatial variability and stochastic strength prediction of unreinforced masonry walls in vertical bending. Engineering Structures 59, pp. 787–797.

Limpert, E.; Stahel, W. A.; Abbt, M. (2001): Log-normal Distributions across the Sciences: Keys and Clues. Biometrika 51 (5), pp. 341–352.

Lind, N. (2002): Social and economic criteria of acceptable risk. Reliability Engineering & System Safety 78 (1), pp. 21–25.

Loga, T.; Stein, B.; Diefenbach, N.; Born, R. (2015): Deutsche Wohngebäudetypologie – Beispielhafte Maßnahmen zur Verbesserung der Energieeffizienz von typischen Wohngebäuden. Zweite erweiterte Auflage. Darmstadt: Institut Wohnen und Umwelt.

Lourenço, P. J. B. B. (1996): Computational strategies for masonry structures. Dissertation. TU Delft.

Lumantarna, R.; Biggs, D. T.; Ingham, J. M. (2014): Uniaxial Compressive Strength and Stiffness of Field-Extracted and Laboratory-Constructed Masonry Prisms. J. Mater. Civ. Eng. 26 (4), pp. 567–575.

Maes, M. A.; Schueremans, L.; Van Balen; K. (1999): Reliability based assessment of existing masonry structures. In Melchers, Stewart (Eds.): 8th International Conference on Applications of Statistics and Probability (ICASP8). Amsterdam: Balkema, pp. 689–695.

Maier, J. (2012): Handbuch Historisches Mauerwerk. Untersuchungsmethoden und Instandsetzungsverfahren. Zweite Auflage. Berlin: Springer Verlag.

Mann, W. (1983): Druckfestigkeit von Mauerwerk. Eine statistische Auswertung von Versuchsergebnissen in geschlossener Darstellung mit Hilfe von Potenzfunktionen. In Funk (Ed.): Mauerwerk-Kalender 1983. Berlin: Ernst & Sohn, pp. 687–699.

Mann, W.; Betzler, M. (1996): Auswirkungen verschiedener Fomen von Probekörpern zur Prüfung der Druckfestigkeit von Mauerwerk. In Funk (Ed.): Mauerwerk-Kalender 1996. Berlin: Ernst & Sohn, pp. 607–613.

Marastoni, D.; Pelà, L.; Benedetti, A.; Roca, P. (2016): Combining Brazilian tests on masonry cores and double punch tests for the mechanical characterization of historical mortars. Construction and Building Materials 112, pp. 112–127.

Meinen, N. E.; Steenbergen, R. D. J. M. (2018): Reliability levels obtained by Eurocode partial factor design – A discussion on current and future reliability levels. Heron 63 (3), pp. 243–302.

Melchers, R. E.; Beck, A. T. (2018): Structural reliability analysis and prediction. Third edition. Hoboken, New Jersey: Wiley.

Meyer, U.; Schubert, P. (1992): Spannungs-Dehnungs-Linien von Mauerwerk. In Funk (Ed.): Mauerwerk-Kalender 1992. Berlin: Ernst & Sohn, pp. 615–622.

MIL-HDBK-17-1F (2002): Composite Materials Handbook – Volume 1. Polymer Matrix Composites – Guidelines for Characterization of Structural Materials. US Department of Defense.

Mojsilović, N.; Stewart, M. G. (2015): Probability and structural reliability assessment of mortar joint thickness in load-bearing masonry walls. Structural Safety 52 (2), pp. 209–218.

Moses, F.; Lebet, J. P.; Bez, R. (1994): Applications of Field Testing to Bridge Evaluation. J. Struct. Eng. 120 (6), pp. 1745–1762.

NABau (1981): Grundlagen zur Festlegung von Sicherheitsanforderungen für bauliche Anlagen. Normenausschuss Bauwesen im DIN. Berlin: Beuth-Verlag.

Neumann, H.-H. (2017): Ziegelmauerwerk im Wandel der Zeit. Bausubstanz 8 (4), pp. 42–49.

Neuwald-Burg, C.; Bohne, D. (1999): Zum Trag- und Verformungsverhalten historischen Ziegelmauerwerks. In Wenzel (Ed.): Erhalten historisch bedeutsamer Bauwerke. Jahrbuch 1996 des SFB 315. Berlin: Ernst & Sohn, pp. 111–136.

Noor-E-Khuda, S.; Albermani, F. (2019): Mechanical properties of clay masonry units: Destructive and ultrasonic testing. Construction and Building Materials 219 (8), pp. 111–120.

Nowak, A. S.; Collins, K. R. (2013): Reliability of structures. Second edition. Boca Raton: CRC Press.

Ohler, A. (1986): Zur Berechnung der Druckfestigkeit von Mauerwerk unter Berücksichtigung der mehrachsigen Spannungszustände in Stein und Mörtel. Bautechnik 63 (5), pp. 163–168.

Olsson, A. M. J.; Sandberg, G. E. (2002): Latin Hypercube Sampling for Stochastic Finite Element Analysis. J. Eng. Mech. 128 (1), pp. 121–125.

Osthues, W. (2017): Bauwissen im Antiken Rom. In Renn, Osthues, Schlimme (Eds.): Wissensgeschichte der Architektur – Band II: Vom Alten Ägypten bis zum Antiken Rom. Berlin: Edition Open Access, pp. 265–422.

Page, A. W. (1981): The biaxial compressive strength of brick masonry. Proc. Instn. Civ. Engrs., Part 2 71, pp. 893–906.

Pearson, K. (1900): On the criterion that a given system of deviations from the probable in the case of a correlated system of variables is such that it can be reasonably supposed to have arisen from random sampling. Philosophical Magazine 50 (302), pp. 157–175.

Pech, A.; Gangoly, H.; Holzer, P.; Maydl, P. (2018): Ziegel im Hochbau. Basel: Birkhäuser.

Pelà, L.; Canella, E.; Aprile, A.; Roca, P. (2016): Compression test of masonry core samples extracted from existing brickwork. Construction and Building Materials 119 (4), pp. 230–240.

prEN 1990 (2020): Eurocode – Basis of structural and geotechnical design. Brussels: European Committee for Standardization.

prEN 1990-2 (2021): Eurocode – Basis of assessment and retrofitting of existing structures: general rules and actions (final draft). Brussels: European Committee for Standardization.

Probst, P. (1981): Ein Breitrag zum Bruchmechanismus von zentrisch gedrücktem Mauerwerk. Dissertation. Technische Universität München.

Rackwitz, R. (1983): Predictive distribution of strength under control. Matériaux et Construction 16, pp. 259–267.

Rackwitz, R. (1997): Einwirkungen auf Bauwerke. In Mehlhorn (Ed.): Der Ingenieurbau. Berlin: Ernst & Sohn 1997.

Rackwitz, R. (2000): Optimization – the basis of code-making and reliability verification. Structural Safety 22 (1), pp. 27–60.

Rackwitz, R. (2002): Optimization and risk acceptability based on the Life Quality Index. Structural Safety 24 (2-4), pp. 297–331.

Rackwitz, R.; Fießler, B. (1976): Note on discrete safety checking when using non-normal stochastic models for basic variables. In: Berichte zur Sicherheitstheorie der Bauwerke Nr. 14. München: Labor für Konstruktiven Ingenieurbau, pp. 85–100.

Raiffa, H.; Schlaifer, R. (1961): Applied statistical decision theory. Boston: Harvard Business School.

Riechers, H.-J.; Schubert, P.; Deutler, T. (1998): Prüfung der Druckfestigkeit von Mauermörtel – Formfaktoren für den Vergleich der unterschiedlichen Prüfverfahren. Mauerwerk 2 (3), pp. 102–106.

RILEM (1994): Technical Recommendations for the testing and use of construction materials: E & FN Spon.

Rubin, D. B. (1981): The Bayesian Bootstrap. The Annals of Statistics 9 (1), pp. 130–134.

Rubinstein, R. Y.; Kroese, D. P. (2017): Simulation and the Monte Carlo Method. Third edition. Hoboken, New Jersey: John Wiley & Sons.

Rupp, E.; Friedrich, G. (1993): Die Geschichte der Ziegelherstellung. Dritte Auflage. Bonn: Bundesverband der Deutschen Ziegelindustrie e. V.

Rüsch, H. (1960): Researches Toward a General Flexural Theory for Structural Concrete. ACI Journal 57 (1), pp. 1–28.

Sassoni, E.; Franzoni, E.; Mazzotti, C. (2015): Influence of Sample Thickness and Capping on Characterization of Bedding Mortars from Historic Masonries by Double Punch Test (DPT). Key Engineering Materials 624, pp. 322–329.

Sassoni, E.; Mazzotti, C.; Pagliai, G. (2014): Comparison between experimental methods for evaluating the compressive strength of existing masonry buildings. Construction and Building Materials 68, pp. 206–219.

Schlegel, R. (2004): Numerische Berechnung von Mauerwerksstrukturen in homogenen und diskreten Modellierungsstrategien. Dissertation. Bauhaus-Universität Weimar.

Schmidt, U.; Schubert, P. (2004): Festigkeitseigenschaften von Mauerwerk – Teil 2: Biegezugfestigkeit. In Irmschler, Jäger, Schubert (Eds.): Mauerwerk-Kalender 2004. Berlin: Ernst & Sohn, pp. 31–63.

Schneider, J. (1996): Sicherheit und Zuverlässigkeit im Bauwesen: Grundwissen für Ingenieure. Zweite, überarbeitete Auflage. Zürich: vdf Hochschulverlag AG.

Schneider, R.; Fischer, J.; Bügler, M.; Nowak, M.; Thöns, S.; Borrmann, A.; Straub, D. (2015): Assessing and updating the reliability of concrete bridges subjected to spatial deterioration – principles and software implementation. Structural Concrete 16 (3), pp. 356–365.

Schubert, P. (1995): Beurteilung der Druckfestigkeit von ausgeführtem Mauerwerk aus künstlichen Steinen und Natursteinen. In Funk (Ed.): Mauerwerk-Kalender 1995. Berlin: Ernst & Sohn, pp. 687–701.

Schubert, P. (2010): Eigenschaftswerte von Mauerwerk, Mauersteinen, Mauermörtel und Putzen. In Jäger (Ed.): Mauerwerk-Kalender 2010. Berlin: Ernst & Sohn, pp. 3–25.

Schueremans, L. (2001): Probabilistic evaluation of structural unreinforced masonry. Dissertation. KU Leuven.

Segura, J.; Pelà, L.; Roca, P. (2018): Monotonic and cyclic testing of clay brick and lime mortar masonry in compression. Construction and Building Materials 193, pp. 453–466.

Segura, J.; Pelà, L.; Roca, P.; Cabané, A. (2019): Experimental analysis of the size effect on the compressive behaviour of cylindrical samples core-drilled from existing brick masonry. Construction and Building Materials 228, 116759.

SIA 269 (2011): Grundlagen der Erhaltung von Tragwerken. Zürich: Schweizerischer Ingenieur- und Architektenverein.

SIA 269/6-2 (2014): Erhaltung von Tragwerken – Mauerwerksbau, Teil 2: Mauerwerk aus künstlichen Steinen. Zürich: Schweizerischer Ingenieur- und Architektenverein.

Sievertsen, U. (2017): Bauwissen im Alten Orient. In Renn, Osthues, Schlimme (Eds.): Wissensgeschichte der Architektur – Band I: Vom Neolithikum bis zum Alten Orient. Berlin: Edition Open Access, pp. 131–280.

Smirnov, N. (1948): Table for Estimating the Goodness of Fit of Empirical Distributions. Annals of Mathematical Statistics 19 (2), pp. 279–281.

Song, J.; Kang, W.-H. (2009): System reliability and sensitivity under statistical dependence by matrix-based system reliability method. Structural Safety 31 (2), pp. 148–156.

Spaethe, G. (1992): Die Sicherheit tragender Baukonstruktionen. Zweite, neubearbeitete Auflage. Vienna: Springer.

Steenbergen, R. D. J. M.; Sýkora, M.; Diamantidis, D.; Holický, M.; Vrouwenvelder, T. (2015): Economic and human safety reliability levels for existing structures. Structural Concrete 16 (3), pp. 323–332.

Steenbergen, R. D. J. M.; Vrouwenvelder, A. C. W. M. (2010): Safety Philosophy for Existing Structures and Partial Factors for Traffic Loads on Bridges. Heron 55 (2), pp. 123–140.

Stephens, M. A. (1974): EDF Statistics for Goodness of Fit and Some Comparisons. Journal of the American Statistical Association 69 (347), pp. 730–737.

Stephens, M. A. (1977): Goodness of Fit for the Extreme Value Distribution. Biometrika 64 (3), pp. 583–588.

Stephens, M. A. (1986): Tests Based on EDF Statistics. In D'Agostino, Stephens (Eds.): Goodness-of-Fit Techniques. New York and Basel: Marcel Dekker, pp. 97–194.

Streck, M. (2006): Die Stadt, an deren Freuden man nicht satt wird – Babylon: Ein Mythos über die Jahrtausende. In: DAMALS – Antike Metropolen. Darmstadt: Wissenschaftliche Buchgesellschaft, pp. 11-28.

Sudret, B.; Der Kiureghian, A. (2000): Stochastic Finite Element Methods and Reliability – A State-of-the-Art Report. Berkeley: University of California.

Sykora, M.; Diamantidis, D. (2021): fib TG 3.1 Developments Concerning Semi-Probabilistic Format. Presentation at the JCSS Workshop on Assessment of Existing Structures (28–29 January 2021). Available online at folk.ntnu.no/jochenk/JCSSWS2101/21Diamantidis.pdf, checked on 15/10/21.

Sykora, M.; Diamantidis, D.; Müller, D.; Sousa, H. (2022): A practical guide on the quantification of value of information gained by structural health monitoring and application to historic masonry structures. Structure and Infrastructure Engineering 18 (4), pp. 441–455.

Sýkora, M.; Diamantidis, D.; Holický, M.; Marková, J.; Rózsás, Á. (2018): Assessment of compressive strength of historic masonry using non-destructive and destructive techniques. Construction and Building Materials 193, pp. 196–210.

Tanner, P.; Hingorani, R. (2015): Acceptable risks to persons associated with building structures. Structural Concrete 16 (3), pp. 314–322.

Thamboo, J. A.; Dhanasekar, M. (2019): Correlation between the performance of solid masonry prisms and wallettes under compression. Journal of Building Engineering 22 (3), pp. 429–438.

Tran, N. L.; Grziwa, U.; Graubner, C.-A. (2015): Spatial variability of material properties and its influence on structural reliability of UHPC columns. In Stang, Braestrup (Eds.): Concrete – Innovation and Design. 13th fib Symposium Proceedings. Copenhagen, 18-20 May 2015.

Tran, N. L.; Müller, D.; Graubner, C.-A. (2017): Floor Live Loads of Building Structures. In Caspeele, Taerwe, Proske (Eds.): 14th International Probabilistic Workshop. Cham: Springer International Publishing.

Tschötschel, M. (1990): Zuverlässigkeitstheoretisches Konzept zur Bemessung von Mauerwerkskonstruktionen. Dissertation. Technische Hochschule Leipzig.

Val, D. V.; Stewart, M. G. (2002): Safety Factors for Assessment of Existing Structures. Journal of Structural Engineering 128 (2), pp. 258–265.

van der Pluijm, R. (1999): Out-of-Plane Bending of Masonry – Behaviour and Strength. Dissertation. Eindhoven University of Technology.

Vanmarcke, E. (1983): Random Fields: Analysis and Synthesis. Cambridge: The MIT Press.

Vasanelli, E.; Calia, A.; Colangiuli, D.; Micelli, F.; Aiello, M. A. (2016): Assessing the reliability of non-destructive and moderately invasive techniques for the evaluation of uniaxial compressive strength of stone masonry units. Construction and Building Materials 124, pp. 575–581.

Vereecken, E.; Botte, W.; Lombaert, G.; Caspeele, R. (2020): Bayesian decision analysis for the optimization of inspection and repair of spatially degrading concrete structures. Engineering Structures 220 (2), 111028.

Verstrynge, E. (2010): Long-term behaviour of monumental masonry constructions: modelling and probabilistic evaluation. Dissertation. KU Leuven.

Wasserman, L. (2011): All of Statistics. A Concise Course in Statistical Inference. New York, London: Springer.

Weibull, W. (1939): A statistical theory of the strength of materials. Ingeniörsvetenskapsakademiens handlingar nr 151. Sockholm: Generalstabens litografiska anstalts förlag.

Wenzel, F.; Gigla, B.; Kahle, M.; Stiesch, G. (2000): Erhalten historisch bedeutsamer Bauwerke – Empfehlungen für die Praxis. Karlsruhe: Sonderforschungsbereich 315.

Westfall, P. H. (2014): Kurtosis as Peakedness, 1905 – 2014. R.I.P. The American statistician 68 (3), pp. 191–195.

Witzany, J.; Cejka, T.; Zigler, R. (2010): The Effect of Moisture on Significant Mechanical Characteristics of Masonry. Engineering Structures and Technologies 2 (3), pp. 79–85.

Wolf, S.; Walther, H.; Langer, P.; Stoyan, D. (2008): Statistische Untersuchung der Druckfestigkeit von Porenbeton – Größeneffekt und Umrechnungsfaktoren. Mauerwerk 12 (1), pp. 19–24.

WTA Wissenschaftlich-Technische Arbeitsgemeinschaft für Bauwerkserhaltung und Denkmalpflege e.V. (2021): Merkblatt 7-4 Ermittlung der Druckfestigkeit von Bestandsmauerwerk aus künstlichen kleinformatigen Steinen. Stuttgart: Fraunhofer IRB Verlag.

Annex

ANNEX

Annex A – Documentation of Experiments on Masonry Walls 267

Annex B – Derivation of Formulae for Generating Correlated Material Properties 279

Annex C – Database of Component and Composite Strengths of Existing Masonry.....282

Annex D – Data for Evaluating the Uncertainty in Masonry Strength Prediction 287

Annex E – Diagrams for Determining Assessment Values Based on Unit Tests Only...288

Annex A – Documentation of Experiments on Masonry Walls

In the following, the results of the experiments on masonry walls are documented by providing one page of information for each type of tested masonry wall, including

- an example picture of one wall belonging to this wall type,
- the tabulated test data, including the testing age, wall dimensions, corresponding unit and mortar compressive strength, maximum applied load, strength (= maximum load related to gross cross-section), modulus of elasticity $E_{ma,0\text{-}33}$ (= secant modulus at one-third of strength with strain determined via the average displacement of the LVDTs related to measurement length), and stress-strain parameter k (calculated according to Eq. 4-1),
- the stress-strain curve, where the stress is the applied load related to the gross cross-sectional area, and the strain is the average displacement of the LVDTs related to the measurement length,
- the vertical strain under maximum load as obtained by digital image correlation (only the middle area is shown for single wythe walls since the test setup did not allow to capture a wider angle),
- and one picture from each individual wall showing one or several of the most prominent cracks after testing.

Solid clay brick reference wall, single wythe (sw-sol)

Before testing

Test data

		1	2	3
Age	d	35	36	40
Length	mm	1,266	1,265	1,255
Thickness	mm	115	115	115
Height	mm	1,122	1,112	1,115
Unit strength f_b	N/mm²	25.7	25.7	25.7
Mortar strength f_j	N/mm²	2.77	2.77	2.77
Maximum load	kN	1,004	1,089	1,136
Strength	N/mm²	6.90	7.49	7.87
$E_{ma,0\text{-}33}$	N/mm²	2,561	2,786	3,311
k		2.18	2.16	2.60

Stress-strain curve

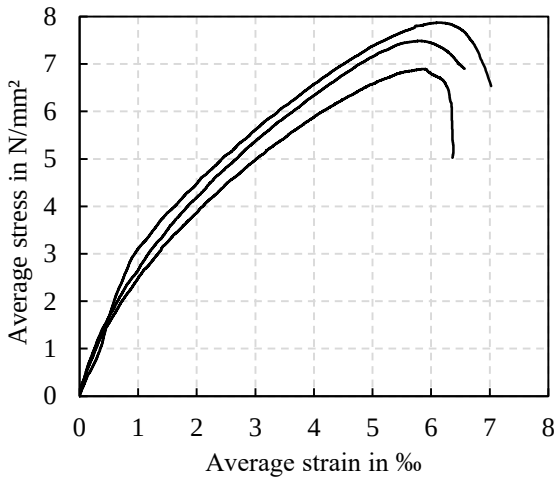

Vert. strain at max. load (sw-sol-2)

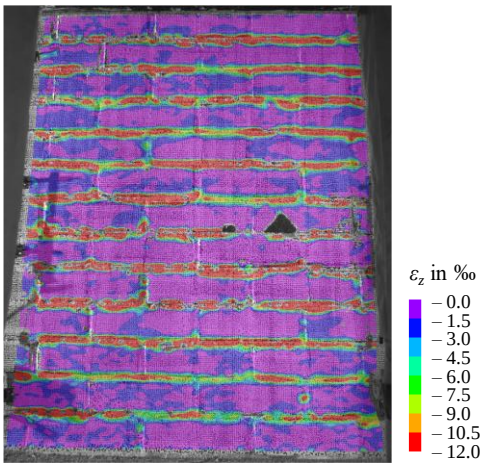

After testing (left: sw-sol-1, centre: sw-sol-2, right: sw-sol-3)

Perforated clay brick reference wall, single wythe (sw-perf)

Before testing

Test data

		1	2
Age	d	34	37
Length	mm	1,234	1,245
Thickness	mm	110	111
Height	mm	1,077	1,086
Unit strength f_b	N/mm²	12.0	11.4
Mortar strength f_j	N/mm²	2.80	2.24
Maximum load	kN	437	423
Strength	N/mm²	3.22	3.06
$E_{ma,0\text{-}33}$	N/mm²	2,540	2,143
k		1.98	1.40

Stress-strain curve

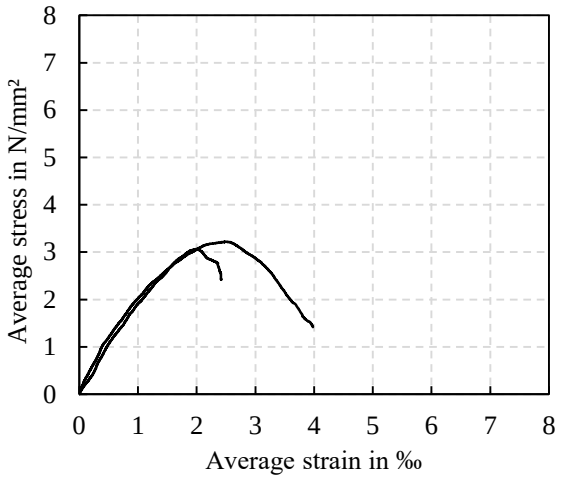

Vert. strain at max. load (sw-perf-2)

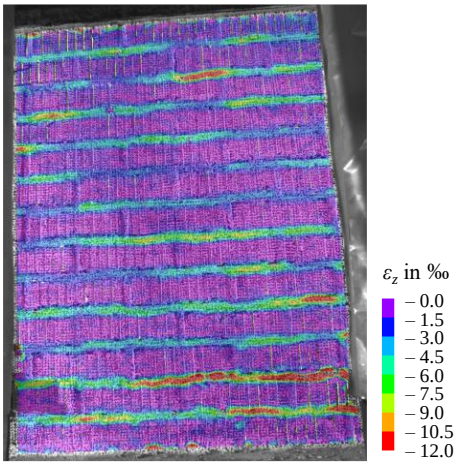

After testing (left: sw-perf-1, right: sw-perf-2)

Wall with missing brick, single wythe (sw-hole)

Before testing

Test data

		1	2
Age	d	40	41
Length	mm	1,245	1,250
Thickness	mm	115	115
Height	mm	1,110	1,112
Unit strength f_b	N/mm²	23.6	23.6
Mortar strength f_j	N/mm²	2.4	2.4
Maximum load	kN	814	799
Strength	N/mm²	5.68	5.56

Stress-strain curve

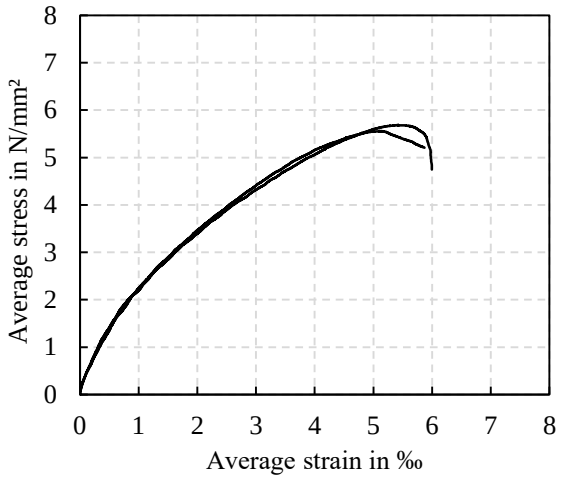

Vert. strain at max. load (sw-hole-1)

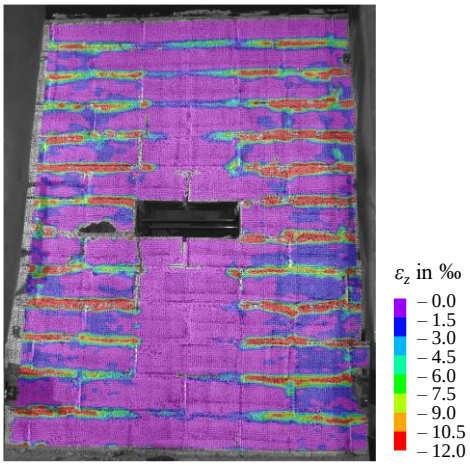

After testing (left: sw-hole-1, right: sw-hole-2)

Wall with 25 % perforated bricks, single wythe (sw-25)

Before testing

Test data

		1	2
Age	d	36	35
Length	mm	1,247	1,248
Thickness	mm	113	113
Height	mm	1,108	1,119
Unit strength f_b	N/mm²	24.6 / 12.0	24.6 / 12.0
Mortar strength f_j	N/mm²	2.30	2.03
Maximum load	kN	681	736
Strength	N/mm²	4.83	5.22
$E_{ma,0-33}$	N/mm²	2,561	2,805
k		1.69	1.94

Stress-strain curve

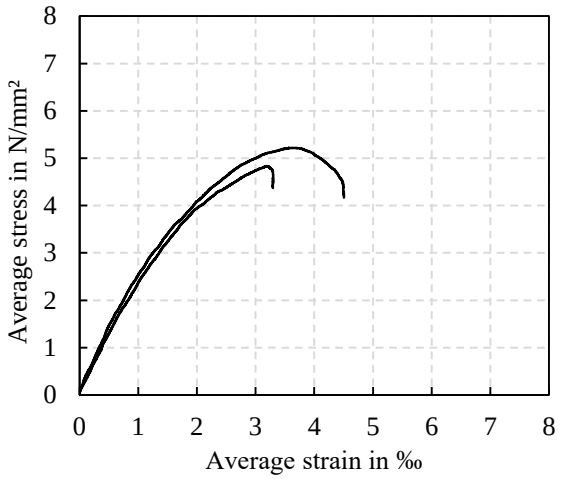

Vert. strain at max. load (sw-25-1)

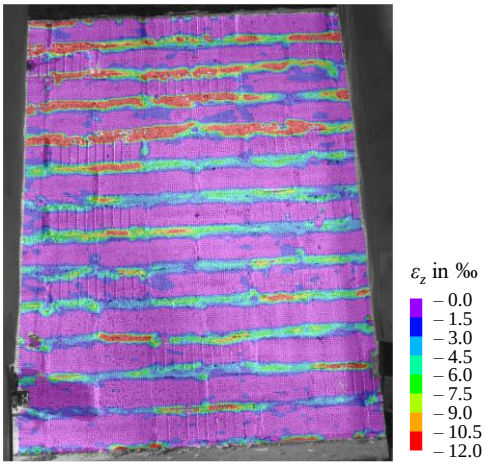

After testing (left: sw-25-1, right: sw-25-2)

Wall with 50 % perforated bricks, single wythe (sw-50)

Before testing

Test data

		1	2
Age	d	36	36
Length	mm	1,246	1,248
Thickness	mm	113	113
Height	mm	1,112	1,105
Unit strength f_b	N/mm²	24.6 / 12.0	24.6 / 12.0
Mortar strength f_j	N/mm²	2.16	2.03
Maximum load	kN	565	568
Strength	N/mm²	4.01	4.03
$E_{ma,0-33}$	N/mm²	3,023	2,430
k		1.79	1.56

Stress-strain curve

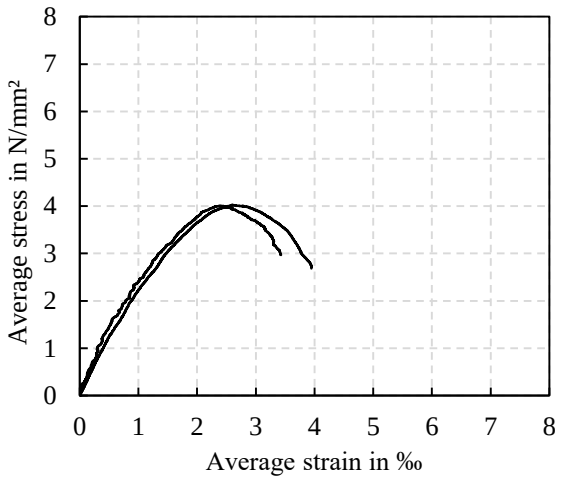

Vert. strain at max. load (sw-50-1)

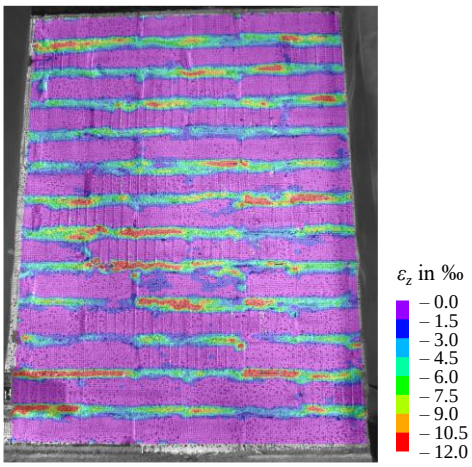

After testing (left: sw-50-1, right: sw-50-2)

Solid clay brick reference wall, cross bond (cb-sol)

Before testing

Test data

		1	2	3
Age	d	32	39	37
Length	mm	620	629	625
Thickness	mm	241	241	240
Height	mm	1,121	1,091	1,110
Unit strength f_b	N/mm²	25.2	23.1	24.0
Mortar strength f_j	N/mm²	2.76	2.89	2.85
Maximum load	kN	943	826	1,093
Strength	N/mm²	6.31	5.45	7.29
$E_{ma,0\text{-}33}$	N/mm²	3,014	2,958	3,309
k		2.79	2.40	1.95

Stress-strain curve

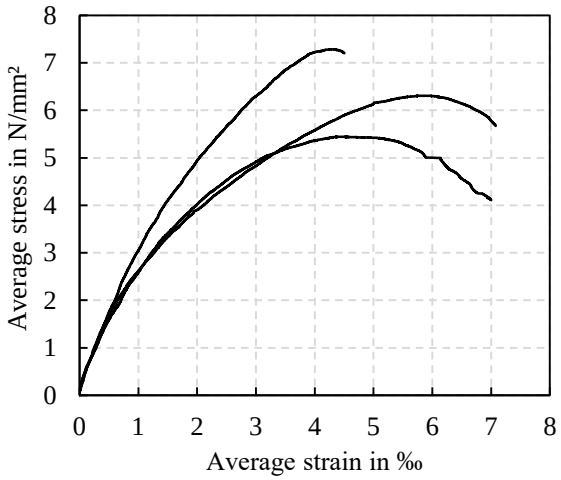

Vert. strain at max. load (cb-sol-1)

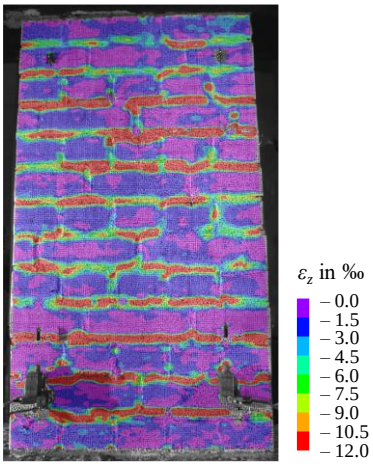

After testing (left: cb-sol-1, centre: cb-sol-2, right: cb-sol-3)

Perforated clay brick reference wall, cross bond (cb-perf)

Before testing

Test data

		1	2
Age	d	38	41
Length	mm	622	621
Thickness	mm	239	239
Height	mm	1,084	1,083
Unit strength f_b	N/mm²	11.4	11.4
Mortar strength f_j	N/mm²	2.90	3.11
Maximum load	kN	391	394
Strength	N/mm²	2.63	2.66
$E_{ma,0-33}$	N/mm²	2,090	2,191
k		2.14	1.94

Stress-strain curve

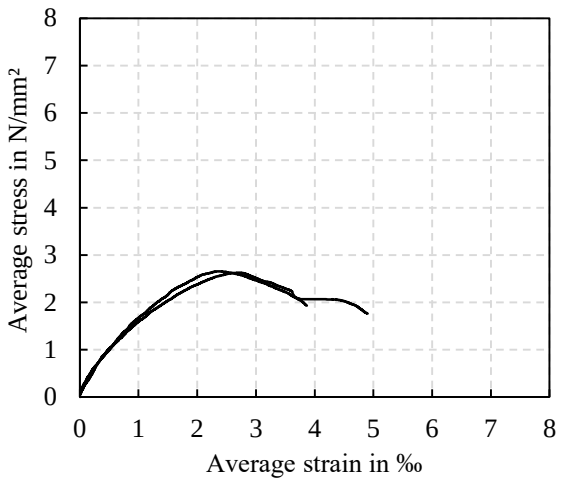

Vert. strain at max. load (cb-perf-1)

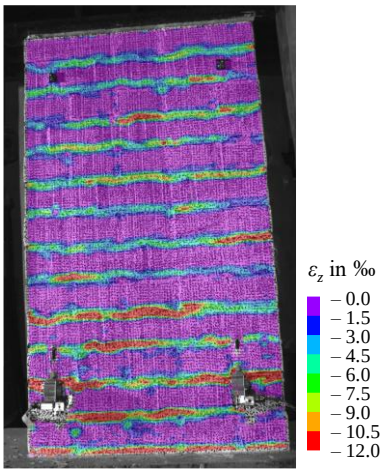

After testing (left: cb-perf-1, right: cb-perf-2)

Wall with missing stretcher, cross bond (cb-str)

Before testing

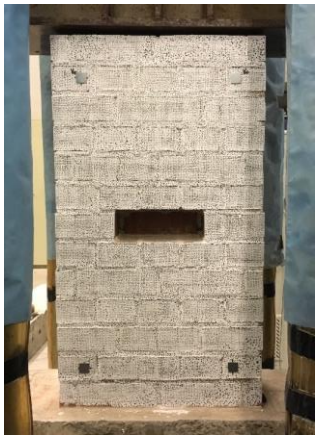

Test data

		1	2
Age	d	33	34
Length	mm	623	624
Thickness	mm	242	241
Height	mm	1,114	1,116
Unit strength f_b	N/mm²	25.2	25.2
Mortar strength f_j	N/mm²	2.76	2.76
Maximum load	kN	694	651
Strength	N/mm²	4.61	4.33

Stress-strain curve

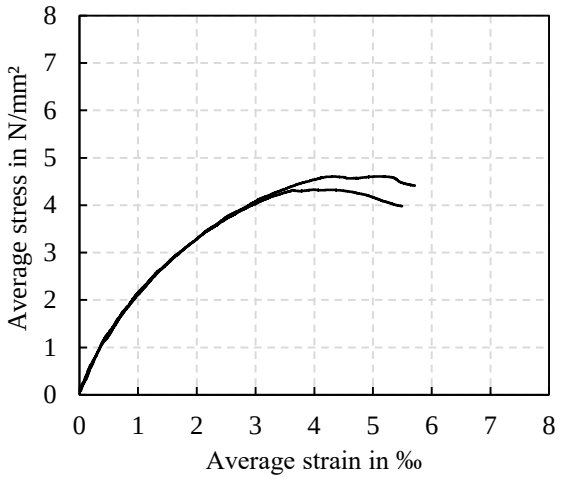

Vert. strain at max. load (cb-str-2)

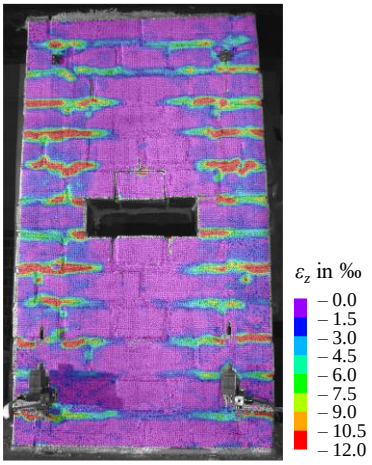

After testing (left: cb-str-1, right: cb-str-2)

Wall with missing header, cross bond (cb-head)

Before testing

Test data

		1	2
Age	d	35	36
Length	mm	617	622
Thickness	mm	242	242
Height	mm	1,115	1,117
Unit strength f_b	N/mm²	25.2	25.2
Mortar strength f_j	N/mm²	2.76	2.76
Maximum load	kN	748	732
Strength	N/mm²	5.01	4.86

Stress-strain curve

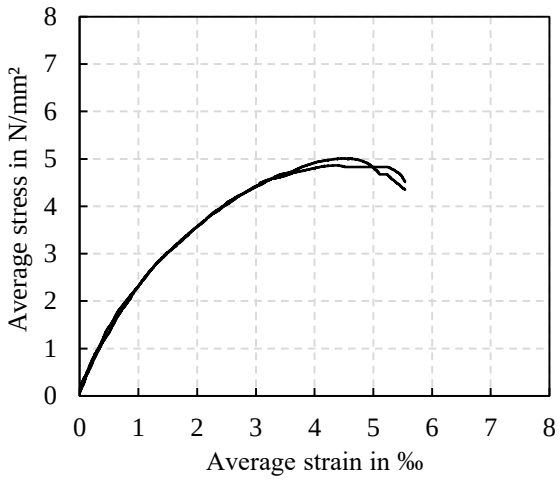

Vert. strain at max. load (cb-head-2)

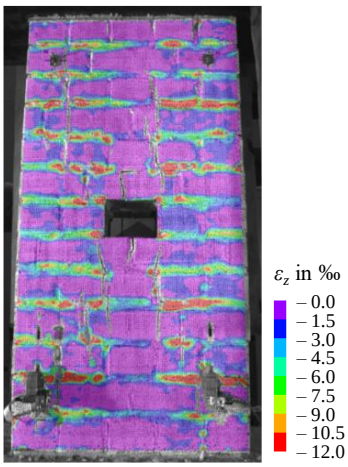

After testing (left: cb-head-1, right: cb-head-2)

Wall with 25 % perforated bricks, cross bond (cb-25)

Before testing

Test data

		1	2
Age	d	41	42
Length	mm	624	622
Thickness	mm	239	240
Height	mm	1,098	1,101
Unit strength f_b	N/mm²	24.0 / 11.4	24.0 / 11.4
Mortar strength f_j	N/mm²	3.13	2.73
Maximum load	kN	721	703
Strength	N/mm²	4.83	4.71
$E_{ma,0\text{-}33}$	N/mm²	2,548	2,766
k		1.67	1.91

Stress-strain curve

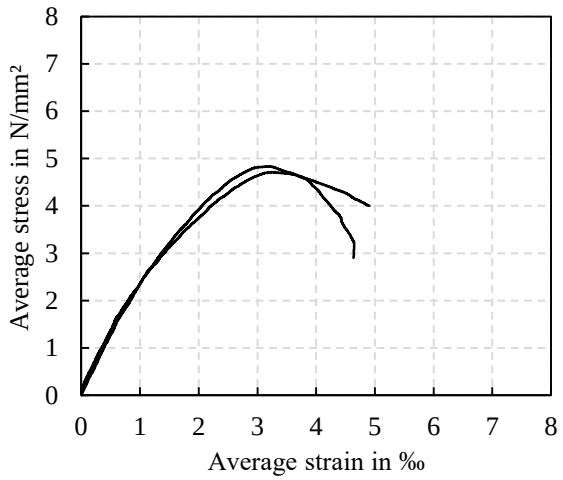

Vert. strain at max. load (cb-25-1)

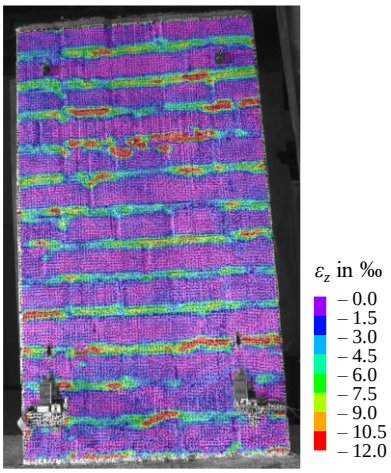

After testing (left: cb-25-1, right: cb-25-2)

Wall with 50 % perforated bricks, cross bond (cb-50)

Before testing

Test data

		1	2
Age	d	42	43
Length	mm	620	622
Thickness	mm	239	240
Height	mm	1,093	1,095
Unit strength f_b	N/mm²	24.0 / 11.4	24.0 / 11.4
Mortar strength f_j	N/mm²	3.14	2.90
Maximum load	kN	501	485
Strength	N/mm²	3.38	3.25
$E_{ma,0-33}$	N/mm²	2,669	2,043
k		2.26	1.90

Stress-strain curve

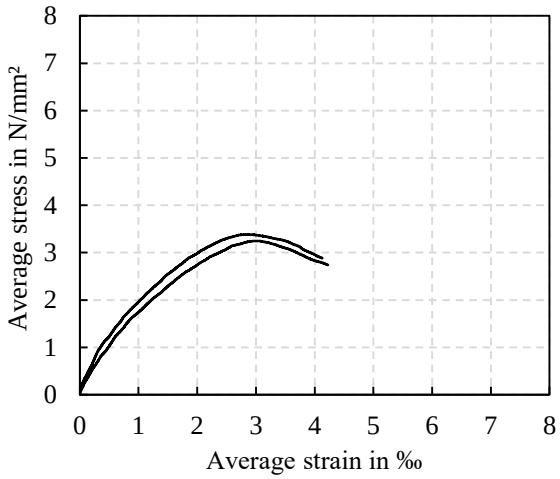

Vert. strain at max. load (cb-50-1)

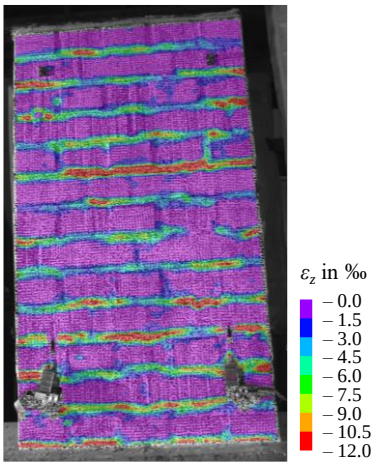

After testing (left: cb-50-1, right: cb-50-2)

Annex B – Derivation of Formulae for Generating Correlated Material Properties

In this Annex, the derivation of Eq. 6-4 to Eq. 6-9, which yield the CoVs of the auxiliary variables for generating correlated log-normal material properties, is illustrated.

At first, two random variables X and Y are considered that result from a product of two independent random variables, sharing the random variable Z as a common factor:

$$Z\,X^{*} = X \qquad \textit{Eq. B-1}$$

$$Z\,Y^{*} = Y \qquad \textit{Eq. B-2}$$

The covariance of X and Y can be determined following the general expression of the covariance (see Eq. 2-14), which can then be transformed using the relationships for the stochastic moments of a product (see Eq. 2-19):

$$\begin{aligned}
&\mathrm{Cov}\left(X,Y\right) = \mathrm{E}\left[\left(X-\mu_X\right)\left(Y-\mu_Y\right)\right] \\
&= \mathrm{E}\left[\left(Z\,X^{*}-\mu_Z\,\mu_{X^{*}}\right)\left(Z\,Y^{*}-\mu_Z\,\mu_{Y^{*}}\right)\right] \\
&= \mathrm{E}\left[Z^2\,X^{*}Y^{*}-Z\,X^{*}\,\mu_Z\,\mu_{Y^{*}}-Z\,Y^{*}\,\mu_Z\,\mu_{X^{*}}+\mu_Z^2\,\mu_{X^{*}}\,\mu_{Y^{*}}\right] \\
&= \mathrm{E}\left[Z^2\,X^{*}Y^{*}\right]-\mathrm{E}\left[Z\,X^{*}\,\mu_Z\,\mu_{Y^{*}}\right]-\mathrm{E}\left[Z\,Y^{*}\,\mu_Z\,\mu_{X^{*}}\right]+\mathrm{E}\left[\mu_Z^2\,\mu_{X^{*}}\,\mu_{Y^{*}}\right] \\
&= \left(\mu_Z^2+\sigma_Z^2\right)\mu_{X^{*}}\,\mu_{Y^{*}}-\mu_Z^2\,\mu_{X^{*}}\,\mu_{Y^{*}}-\mu_Z^2\,\mu_{X^{*}}\,\mu_{Y^{*}}+\mu_Z^2\,\mu_{X^{*}}\,\mu_{Y^{*}} \\
&= \sigma_Z^2\,\mu_{X^{*}}\,\mu_{Y^{*}}
\end{aligned} \qquad \textit{Eq. B-3}$$

The relationship $\mathrm{E}\left(Z^2\right) = \mu_Z^2 + \sigma_Z^2$, which is needed for the above transformation, is provided in Melchers and Beck (2018), for example. If the covariance is converted to a correlation coefficient $\rho_{X,Y}$ (see Eq. 2-14), it follows:

$$\rho_{X,Y} = \frac{\mathrm{Cov}\left(X,Y\right)}{\sigma_X\,\sigma_Y} = \frac{\sigma_Z^2\,\mu_{X^{*}}\,\mu_{Y^{*}}}{\sigma_X\,\sigma_Y} = \frac{\upsilon_Z^2\,\mu_Z^2\,\mu_{X^{*}}\,\mu_{Y^{*}}}{\upsilon_X\,\mu_X\,\upsilon_Y\,\mu_Y} = \frac{\upsilon_Z^2\,\mu_X\,\mu_Y}{\upsilon_X\,\mu_X\,\upsilon_Y\,\mu_Y} = \frac{\upsilon_Z^2}{\upsilon_X\,\upsilon_Y} \qquad \textit{Eq. B-4}$$

Hence, the correlation coefficient of two random variables that result from a product of independent variables is equal to the squared coefficient of variation (CoV) of the shared factor divided by the product of the CoVs of the random variables. This principle can be applied to determine the CoVs of the auxiliary random variables required for generating correlated random material properties (see Section 6.2.3). The equations for generating the material properties are Eq. 6-2 and Eq. 6-3, which are repeated here:

$$f_{\mathrm{ma},i} = W\;f_{\mathrm{w}}\;U_i\;f_{\mathrm{u},i} \qquad \textit{Eq. B-5}$$

$$E_{\mathrm{ma},i} = W\;E_{\mathrm{w}}\;U_i\;E_{\mathrm{u},i} \qquad \textit{Eq. B-6}$$

The spatial correlation coefficient ρ_{spat} between the masonry compressive strength $f_{ma,i}$ at "unit" i and $f_{ma,j}$ at "unit" j results from the shared factors W and f_w. Following the principle of Eq. B-4, ρ_{spat} can be expressed via the squared CoV of the product $W f_w$ divided by the squared CoV of masonry compressive strength:

$$\rho_{spat} = \frac{v_{W \cdot f_w}^2}{v_{ma}^2} \quad \Leftrightarrow \quad v_{W \cdot f_w} = v_{ma} \sqrt{\rho_{spat}} \qquad \textit{Eq. B-7}$$

Since ρ_{spat} also represents the spatial correlation coefficient between the elastic moduli at different "units", the equivalent expression follows for the elastic modulus:

$$\rho_{spat} = \frac{v_{W \cdot E_w}^2}{v_E^2} \quad \Leftrightarrow \quad v_{W \cdot E_w} = v_E \sqrt{\rho_{spat}} \qquad \textit{Eq. B-8}$$

If no spatial variability was considered, the random variables U_i, $f_{u,i}$, and $E_{u,i}$ would not be required. In this case, compressive strength and elastic modulus could be generated via $f_{ma} = W f_w$ and $E_{ma} = W E_w$ (if the mean values of f_{ma} and E_{ma} were included in f_w and E_w instead of $f_{u,i}$ and $E_{u,i}$). The auxiliary variable W then serves the purpose of creating the correlation between E_{ma} and f_{ma}, represented by the correlation coefficient $\rho_{f,E}$:

$$\rho_{f,E} = \frac{v_W^2}{v_{W \cdot f_w} \, v_{W \cdot E_w}} \quad \Leftrightarrow \quad v_W = \sqrt{\rho_{f,E} \, v_{W \cdot f_w} \, v_{W \cdot E_w}} \qquad \textit{Eq. B-9}$$

Inserting Eq. B-7 and Eq. B-8 in Eq. B-9 yields the final expression for the CoV of W:

$$v_W = \sqrt{\rho_{spat} \, \rho_{f,E} \, v_E \, v_{ma}} \qquad \textit{Eq. B-10}$$

In the general case with spatial variability, the correlation between the compressive strength and elastic modulus at one "unit" i is created through the shared variables W and U_i:

$$\rho_{f,E} = \frac{v_{W \cdot U_i}^2}{v_{ma} \, v_E} = \frac{v_W^2 + v_{U_i}^2 + v_W^2 \, v_{U_i}^2}{v_{ma} \, v_E} \quad \Leftrightarrow \quad v_{U_i} = \sqrt{\frac{\rho_{f,E} \, v_{ma} \, v_E - v_W^2}{1 + v_W^2}} \qquad \textit{Eq. B-11}$$

Inserting Eq. B-10 in Eq. B-11 and subsequent transformation yields the final expression for the CoV of U_i:

$$v_{U_i} = \sqrt{\frac{\rho_{f,E} \, v_{ma} \, v_E - \rho_{spat} \, \rho_{f,E} \, v_E \, v_{ma}}{1 + \rho_{spat} \, \rho_{f,E} \, v_E \, v_{ma}}} = \sqrt{\frac{\rho_{f,E} \, v_E \, v_{ma} \left(1 - \rho_{spat}\right)}{1 + \rho_{spat} \, \rho_{f,E} \, v_E \, v_{ma}}} \qquad \textit{Eq. B-12}$$

For determining the CoV of the auxiliary variable f_w, Eq. B-7 is first transformed as follows:

$$\rho_{spat} = \frac{v_{W \cdot f_w}^2}{v_{ma}^2} = \frac{v_W^2 + v_{f_w}^2 + v_W^2 \, v_{f_w}^2}{v_{ma}^2} \quad \Leftrightarrow \quad v_{f_w} = \sqrt{\frac{\rho_{spat} \, v_{ma}^2 - v_W^2}{1 + v_W^2}} \qquad \textit{Eq. B-13}$$

Inserting Eq. B-10 in Eq. B-13 yields the final expression for the CoV of f_w:

$$v_{f_w} = \sqrt{\frac{\rho_{spat}\, v_{ma}^2 - \rho_{spat}\, \rho_{f,E}\, v_E\, v_{ma}}{1+\rho_{spat}\, \rho_{f,E}\, v_E\, v_{ma}}} = \sqrt{\frac{\rho_{spat}\left(v_{ma}^2 - \rho_{f,E}\, v_E\, v_{ma}\right)}{1+\rho_{spat}\, \rho_{f,E}\, v_E\, v_{ma}}} \qquad \textit{Eq. B-14}$$

The final expression for the CoV for E_w can be found equivalently by first transforming Eq. B-8 and then inserting Eq. B-10:

$$\begin{aligned} &\rho_{spat} = \frac{v_{W\cdot E_w}^2}{v_E^2} = \frac{v_W^2 + v_{E_w}^2 + v_W^2\, v_{E_w}^2}{v_E^2} \\ &\Leftrightarrow \quad v_{E_w} = \sqrt{\frac{\rho_{spat}\, v_E^2 - v_W^2}{1+v_W^2}} = \sqrt{\frac{\rho_{spat}\left(v_E^2 - \rho_{f,E}\, v_E\, v_{ma}\right)}{1+\rho_{spat}\, \rho_{f,E}\, v_E\, v_{ma}}} \end{aligned} \qquad \textit{Eq. B-15}$$

The CoV of $f_{u,i}$ ensures that the desired overall CoV of f_{ma} is obtained. The CoV of f_{ma} is given by the following expression:

$$\begin{aligned} v_{ma}^2 &= v_{W\cdot f_w\cdot U_i\cdot f_{u,i}}^2 \\ &= v_W^2 + v_{f_w}^2 + v_{U_i}^2 + v_{f_{u,i}}^2 + v_W^2\, v_{f_w}^2 + v_W^2\, v_{U_i}^2 + v_W^2\, v_{f_{u,i}}^2 + v_{f_w}^2\, v_{U_i}^2 + v_{f_w}^2\, v_{f_{u,i}}^2 + v_{U_i}^2\, v_{f_{u,i}}^2 \\ &+ v_W^2\, v_{f_w}^2\, v_{U_i}^2 + v_W^2\, v_{f_w}^2\, v_{f_{u,i}}^2 + v_W^2\, v_{U_i}^2\, v_{f_{u,i}}^2 + v_{f_w}^2\, v_{U_i}^2\, v_{f_{u,i}}^2 + v_W^2\, v_{f_w}^2\, v_{U_i}^2\, v_{f_{u,i}}^2 \end{aligned} \qquad \textit{Eq. B-16}$$

Solving for the CoV of $f_{u,i}$ yields:

$$v_{f_{u,i}} = \sqrt{\frac{v_{ma}^2 - v_W^2 - v_{f_w}^2 - v_{U_i}^2 - v_W^2\, v_{f_w}^2 - v_W^2\, v_{U_i}^2 - v_{f_w}^2\, v_{U_i}^2 - v_W^2\, v_{f_w}^2\, v_{U_i}^2}{1+v_W^2 + v_{f_w}^2 + v_{U_i}^2 + v_W^2\, v_{f_w}^2 + v_W^2\, v_{U_i}^2 + v_{f_w}^2\, v_{U_i}^2 + v_W^2\, v_{f_w}^2\, v_{U_i}^2}} \qquad \textit{Eq. B-17}$$

The final expression for the CoV of $f_{u,i}$ is obtained by inserting Eq. B-10, Eq. B-12 and Eq. B-14 in Eq. B-17, followed by several steps of simplification:

$$v_{f_{u,i}} = \sqrt{\frac{\left(v_{ma}^2 - \rho_{f,E}\, v_E\, v_{ma}\right)\left(1-\rho_{spat}\right)}{\left(1+\rho_{spat}\, v_{ma}^2\right)\left(1+\rho_{f,E}\, v_E\, v_{ma}\right)}} \qquad \textit{Eq. B-18}$$

The CoV of $E_{u,i}$ ensures that the desired overall CoV of E_{ma} is received. Thus, it is obtained equivalently to the approach for the CoV of $f_{u,i}$. This yields:

$$v_{E_{u,i}} = \sqrt{\frac{\left(v_E^2 - \rho_{f,E}\, v_E\, v_{ma}\right)\left(1-\rho_{spat}\right)}{\left(1+\rho_{spat}\, v_E^2\right)\left(1+\rho_{f,E}\, v_E\, v_{ma}\right)}} \qquad \textit{Eq. B-19}$$

Annex C – Database of Component and Composite Strengths of Existing Masonry

In Table C-1, the test database for unit and mortar compressive strengths of existing masonry that is evaluated in Chapter 7 is given in a condensed form. All of the displayed data corresponds to solid clay brick masonry. The results of unit and mortar compressive strength tests are presented with regard to the number of tests, the arithmetic mean of the test results, and the corresponding coefficient of variation (CoV). The tests on unit specimens were performed according to either EN 772-1 (2011) or DIN 105-1 (1982), whereas all the tests on mortar specimens were performed following DIN 18555-9 (2019). The presented unit compressive strengths already include a conversion into the normalised unit compressive strength via shape factors (see Section 3.4.2). Likewise, the listed mortar compressive strengths contain a factor for converting the obtained strengths into standard prism strengths (see Section 3.4.3). Both factors are adopted as chosen by the testing labs that provided the respective data. The corresponding structures, in most cases buildings, are characterised by their type of use. Furthermore, their location is specified via the first number of the respective postal code, and, if possible, an estimate for the construction year is added. In the case of a construction period of several years, the middle year of the period is given. Where the test data for one building is split into separate populations, it is indicated by the letters (“a”, “b”,…) behind the number of the building.

Table C-2 presents the direct test results for the compressive strength of existing solid clay brick masonry that are evaluated in Section 7.4.7. The tests were performed on drilled cores according to Helmerich/Heidel (see Section 3.4.4; Heidel 1989).

Table C-1 Test data of component compressive strengths of existing masonry

#	Type of building	Year of construction	Postal code area	Unit compr. strength test results f_b			Mortar compr. strength test results f_j		
				Number	Mean in N/mm²	CoV	Number	Mean in N/mm²	CoV
1	Concert hall	1880	6	4	23.3	16 %	15	18.0	21 %
2	Retaining wall	-	6	3	17.8	41 %	24	3.2	37 %
3	Hospital	1915	3	10	18.8	72 %	20	3.4	38 %
4	Residential/commercial	1905	6	12	35.3	46 %	107	13.4	47 %
5	Residential	1950	6	4	23.9	37 %	16	19.7	9 %
6	Residential	1950	6	2	32.6	30 %	28	16.5	16 %
7	Residential	1950	6	2	22.0	7 %	11	14.9	21 %
8	Residential	1950	6	2	27.2	67 %	33	20.9	13 %
9a	School	1911	6	3	11.3	10 %	11	24.7	16 %
9b	School	1911	6	3	7.8	17 %	11	4.9	32 %
10	Residential	-	6	15	21.4	42 %	73	5.6	68 %
11	Agricultural	1925	6	3	14.0	42 %	28	2.9	54 %
12	School	1870	6	4	26.8	35 %	48	4.7	27 %
13	Barracks	1938	6	18	35.1	30 %	105	7.3	68 %
14a	Office	1907	1	156	16.4	44 %	156	2.7	74 %
14b	Office	1903	1	141	12.8	34 %	141	3.0	117 %
14c	Office	1912	1	111	14.8	44 %	111	4.7	119 %

Table C-1 Test data of component compressive strengths of existing masonry (continued)

#	Type of building	Year of con-struction	Postal code area	Unit compr. strength test results f_b			Mortar compr. strength test results f_j		
				Number	Mean in N/mm²	CoV	Number	Mean in N/mm²	CoV
14d	Office	1913	1	303	14.1	35 %	303	3.9	88 %
15	Agricultural	-	1	3	19.6	27 %	-	-	-
16	Residential	1900	1	12	12.2	24 %	12	1.5	22 %
17	Residential	1900	1	18	14.8	34 %	18	2.8	88 %
18	Residential	1900	1	6	13.0	26 %	6	0.9	20 %
19a	Train station	1935	1	6	20.6	38 %	6	2.4	37 %
19b	Train station	1955	1	12	19.7	26 %	12	2.0	29 %
20	Agricultural	1902	1	3	28.0	18 %	3	0.7	12 %
21	Residential	1850	1	9	9.0	15 %	9	1.2	35 %
22	Residential	1900	1	12	4.8	22 %	12	0.8	31 %
23	Hotel	1900	1	12	8.8	39 %	12	0.6	30 %
24	Prison	-	1	6	12.5	25 %	6	13.3	23 %
25	Residential/commercial	1900	1	1	12.1	-	3	0.4	25 %
26	Bridge	1880	1	3	34.1	10 %	3	37.1	6 %
27	Residential	1900	1	6	13.3	26 %	6	3.2	73 %
28	Agricultural	1900	1	9	5.7	41 %	5	1.1	11 %
29	Residential	1900	1	3	16.0	18 %	3	5.8	10 %
30	Residential	1900	1	18	11.7	36 %	18	2.1	25 %
31a	Residential	1900	2	6	10.8	24 %	6	11.7	33 %
31b	Residential	1900	2	24	16.3	51 %	21	1.2	54 %
32	Restaurant	1900	1	6	7.4	27 %	6	1.3	44 %
33	Residential	1890	1	9	9.3	33 %	9	14.7	69 %
34	Industrial	1913	1	9	12.8	34 %	24	1.3	60 %
35	Residential	1900	1	6	8.1	11 %	6	1.5	28 %
36a	Post office	1900	1	6	28.5	41 %	6	2.8	37 %
36b	Post office	1920	1	3	48.2	27 %	3	26.4	5 %
37	Hospital	1880	1	3	33.2	44 %	3	2.0	16 %
38	Concert hall	1820	1	18	20.7	29 %	18	11.6	44 %
39	Residential	1900	1	12	15.3	35 %	12	2.9	65 %
40	Residential	1900	1	6	22.4	17 %	6	1.0	27 %
41	School	1935	1	9	21.8	41 %	9	2.5	37 %
42a	Office	1895	1	24	25.0	49 %	24	1.6	73 %
42b	Office	1895	1	3	30.4	42 %	3	11.9	13 %
43	Residential	1900	1	9	18.4	25 %	9	1.2	34 %
44a	Post office	1960	1	3	15.1	14 %	3	4.9	14 %
44b	Post office	1960	1	6	16.8	39 %	6	0.9	25 %
45	Industrial	-	2	6	24.2	52 %	6	5.5	35 %
46	Residential	1905	1	6	20.3	30 %	6	1.8	23 %
47	Castle	1185	1	3	12.0	14 %	3	7.2	10 %
48	Industrial	1888	2	4	24.0	34 %	6	19.0	28 %
49	Bar	1900	1	3	12.0	11 %	3	1.3	23 %
50	School	1910	2	3	17.8	44 %	3	2.9	15 %
51	Residential	1775	1	3	7.5	5 %	3	1.9	7 %
52	Residential	1910	1	3	14.1	8 %	3	0.8	20 %
53	School	1874	9	18	8.0	50 %	-	-	-
54a	Industrial	1880	1	6	13.6	68 %	6	2.6	29 %
54b	Industrial	1880	1	6	24.8	38 %	7	7.1	63 %
54c	Industrial	1880	1	6	15.1	29 %	6	4.2	64 %
55	Residential	1880	1	60	17.3	51 %	60	4.1	97 %
56	Residential	1900	1	31	17.3	56 %	-	-	-
57	Residential	1850	1	20	11.6	43 %	20	2.9	39 %
58	University	1917	1	36	20.9	30 %	36	4.2	58 %

Table C-1 Test data of component compressive strengths of existing masonry (continued)

#	Type of building	Year of construction	Postal code area	Unit compr. strength test results f_b			Mortar compr. strength test results f_j		
				Number	Mean in N/mm²	CoV	Number	Mean in N/mm²	CoV
59a	Residential	1915	1	20	23.6	39 %	12	3.5	50 %
59b	Residential	1915	1	6	36.4	20 %	6	10.7	8 %
60a	Residential	1870	1	5	10.2	29 %	4	3.6	37 %
60b	Residential	1870	1	5	42.2	19 %	5	8.9	28 %
60c	Residential	1870	1	11	7.9	67 %	11	3.9	42 %
61a	Office	1907	2	125	32.5	66 %	250	24.2	47 %
61b	Office	1907	2	130	32.3	46 %	270	13.4	37 %
62a	Residential	1912	2	23	15.9	22 %	35	6.5	51 %
62b	Residential	1912	2	4	61.2	14 %	5	9.2	26 %
63	-	-	7	54	25.7	27 %	34	4.2	41 %
64	-	-	7	10	21.4	22 %	2	9.6	6 %
65a	Office	1925	6	5	23.0	22 %	6	14.4	35 %
65b	Office	1925	6	3	10.0	63 %	3	30.0	15 %
65c	Office	1925	6	3	6.8	19 %	3	8.7	13 %
66	Barracks	1890	7	27	21.1	55 %	25	6.3	48 %
67	Agricultural	1900	7	9	16.7	45 %	9	18.0	64 %
68	Residential	1965	5	3	69.0	2 %	3	32.6	2 %
69	Hospital	1860	6	9	32.2	34 %	9	5.6	45 %
70a	Residential	-	8	18	20.4	37 %	13	11.4	35 %
71	Granary	1900	7	15	18.1	38 %	15	18.0	46 %
72	Residential	1953	6	9	22.7	37 %	9	11.6	19 %
73	Barracks	1897	7	6	30.1	57 %	-	-	-
74	Barracks	1897	7	3	22.4	23 %	-	-	-
75	Barracks	1897	7	9	34.7	41 %	-	-	-
76	Barracks	1897	7	9	36.3	43 %	-	-	-
77	-	-	8	3	12.3	48 %	-	-	-
78a	Office	-	8	3	27.4	16 %	1	6.8	-
78b	Office	-	8	2	59.4	41 %	1	8.0	-
79	Residential	1900	8	9	17.9	20 %	-	-	-
80	School	1692	8	4	10.2	31 %	-	-	-
81	Residential	-	8	6	18.2	36 %	-	-	-
82	Office	1841	8	6	16.2	29 %	-	-	-
83	Market hall	1912	8	4	15.6	35 %	-	-	-
84	Bridge	1710	8	6	13.6	14 %	-	-	-
85a	Restaurant	-	8	3	42.5	26 %	2	34.2	19 %
85b	Restaurant	-	8	4	38.5	33 %	-	-	-
86	Residential	1924	9	3	24.8	5 %	-	-	-
87	Restaurant	-	8	3	20.1	42 %	1	13.8	-
88	Spinning/weaving mill	1852	8	9	21.2	26 %	-	-	-
89a	School	1863	8	1	30.6	-	1	3.2	-
89b	School	1863	8	2	53.4	58 %	2	31.8	28 %
90	Residential	-	8	9	34.4	39 %	-	-	-
91	Distillery	1880	8	9	32.2	26 %	-	-	-
92	School	1909	9	3	37.5	11 %	2	5.6	3 %
93	Residential/commercial	1280	8	15	15.8	22 %	5	11.0	29 %
94	Residential/commercial	1890	8	9	28.0	21 %	-	-	-
95	Residential	-	8	3	15.6	8 %	-	-	-
96	Brewery	1850	9	12	16.5	16 %	5	3.4	32 %
97	Residential	-	9	2	40.0	14 %	2	1.9	18 %
98	Workshop	1949	8	9	23.2	22 %	-	-	-
99	School	1914	8	6	15.0	39 %	-	-	-
100	Agricultural	1781	8	9	11.6	22 %	-	-	-

Table C-1 Test data of component compressive strengths of existing masonry (continued)

#	Type of building	Year of construction	Postal code area	Unit compr. strength test results f_b			Mortar compr. strength test results f_j		
				Number	Mean in N/mm²	CoV	Number	Mean in N/mm²	CoV
101	Residential/commercial	-	8	3	45.0	45 %	3	5.4	27 %
102	Residential	1965	8	12	24.8	28 %	4	10.6	41 %
103	Hotel	1907	8	4	23.2	62 %	1	12.4	-
104	Brewery	1831	8	12	32.6	46 %	-	-	-
105	Residential/commercial	1886	8	6	31.5	42 %	-	-	-
106	Distillery	1880	8	3	53.5	51 %	1	1.3	-
107a	Industrial	-	9	3	23.2	2 %	1	2.6	-
107b	Industrial	-	9	6	12.8	19 %	2	4.1	9 %
108	School	1876	8	16	19.5	42 %	-	-	-
109	School	1897	8	13	27.6	29 %	7	5.4	64 %
110	Residential	1926	8	12	19.8	38 %	4	3.9	28 %
111a	Church	1875	8	6	22.1	10 %	1	3.1	-
111b	Church	1875	8	6	20.4	29 %	1	8.0	-
112	Hospital	1928	8	6	15.3	24 %	2	2.6	17 %
113	Military	1860	8	9	26.3	49 %	-	-	-
114	Residential	-	8	6	37.8	29 %	-	-	-
115	Brewery	1911	8	6	10.1	20 %	-	-	-
116	Brewery	1706	8	9	36.1	37 %	3	1.5	15 %
117	Residential	-	8	6	36.6	63 %	-	-	-
118	School	1914	9	2	68.9	34 %	2	1.7	26 %
119	Commercial	1860	8	26	22.8	60 %	11	9.1	53 %
120	Agricultural	1870	8	3	23.3	7 %	3	10.8	10 %
121	Police station	1936	9	12	27.3	23 %	4	2.5	33 %
122	Residential	-	8	3	26.3	11 %	1	1.4	-
123	Office	1812	8	3	35.9	26 %	1	7.0	-
124a	-	-	8	6	24.1	14 %	-	-	-
124b	-	-	8	3	22.8	19 %	-	-	-
125	School	1876	8	3	22.5	9 %	-	-	-
126	Residential/commercial	-	8	6	26.5	38 %	-	-	-
127a	School	1911	8	3	23.5	7 %	3	3.1	43 %
127b	School	1911	8	1	28.9	-	1	2.9	-
128	Gymnasium	-	9	6	40.4	30 %	-	-	-
129	Residential/commercial	1890	8	6	25.8	50 %	2	22.9	14 %
130	Residential	1884	8	9	37.2	49 %	4	26.4	38 %
131	Post office	1906	8	13	31.3	14 %	10	6.9	53 %
132a	Residential	1873	8	12	19.1	63 %	3	5.0	36 %
132b	Residential	1873	8	3	17.0	10 %	-	-	-
132c	Residential	1873	8	3	17.4	15 %	1	7.2	-
133	Monastery	-	8	19	25.4	53 %	6	2.4	29 %
134	Hospital	1903	0	34	54.7	50 %	11	2.6	44 %
135	Office	1875	0	20	39.7	50 %	8	11.9	49 %
136	Residential	1900	8	21	30.2	42 %	-	-	-
137	Commercial	-	8	1	25.9	-	3	14.2	9 %
138	Agricultural	1876	8	6	28.8	22 %	-	-	-
139	Residential	-	8	9	20.7	18 %	3	9.9	42 %
140	Office	1959	8	1	18.4	-	-	-	-

Table C-2 Test data of the compressive strength of existing masonry

#	Type of building	Year of construction	Postal code area	Masonry compressive strength test results f_{ma}		
				Number	Mean in N/mm²	CoV
1	Industrial	1888	2	4	9.8	10 %
2	Hotel	-	2	4	5.4	22 %
3	Residential/commercial	1900	1	3	2.0	14 %
4	-	1900	1	2	6.6	21 %
5	Residential/commercial	1900	1	5	4.0	27 %
6	Brewery	1925	1	13	7.8	34 %
7	Residential/commercial	1900	2	30	4.9	24 %
8	Residential	1900	1	7	2.7	32 %
9	Residential	1900	1	3	0.9	16 %
10	School	1910	2	7	4.3	62 %
11	Residential	1958	1	3	3.3	24 %

Annex D – Data for Evaluating the Uncertainty in Masonry Strength Prediction

In Table D-1, the data used in Section 8.3.2 to evaluate the model uncertainty in predicting masonry compressive strength is presented.

Table D-1 Data for evaluating the uncertainty in masonry strength prediction

Reference	Specimen Type	Length	Thickness	Height	Unit height	Bed joint thickness	Unit strength	Normalised unit strength f_b	Mortar strength f_j	Number of tests	Average masonry strength	Standardised masonry Strength
		mm	mm	mm	mm	mm	N/mm²	N/mm²	N/mm²		N/mm²	N/mm²
Kirtschig & Meyer (1987)	Bonded	490	240	1250	114	12	42.0	43.3	10.4	3	9.73	12.20
	Bonded	490	240	1250	114	12	42.0	43.3	21.6	3	11.63	14.58
	Bonded	1240	240	2500	114	12	42.0	43.3	21.8	3	11.83	16.47
	Single wythe	490	120	600	70	12	66.7	66.7	15.4	3	25.17	25.17
	Single wythe	490	120	600	70	12	66.7	66.7	14.9	3	24.40	24.40
	Single wythe	490	120	600	70	12	66.7	66.7	15.2	3	24.30	24.30
	Single wythe	490	120	600	70	12	66.7	66.7	27.6	3	34.50	34.50
	Single wythe	490	120	600	70	12	66.7	66.7	29.8	3	33.17	33.17
	Single wythe	490	120	600	70	12	66.7	66.7	29.0	3	31.57	31.57
	Single wythe	490	120	600	72	12	38.0	38.0	14.3	3	15.93	15.93
	Single wythe	490	120	600	72	12	38.0	38.0	2.6	3	10.07	10.07
	Single wythe	490	120	600	70	12	91.5	91.5	23.4	3	23.50	23.50
	Single wythe	490	120	600	70	12	91.5	91.5	7.7	3	27.37	27.37
	Stack-bonded	240	120	670	72	12	30.6	30.6	6.1	3	15.53	14.25
Tschötschel (1990)	Bonded	1300	255	2190	71	12	18.9	18.9	5.9	3	6.70	8.93
	Single wythe	1300	122	1650	71	12	18.9	18.9	5.9	4	5.65	6.86
	Bonded	235	235	732	71	12	32.5	32.5	4.9	3	18.77	22.97
	Bonded	1500	240	2500	71	12	22.9	22.9	3.5	5	5.24	7.29
	Bonded	490	240	435	71	12	32.0	32.0	4.3	3	16.38	19.87
	Bonded	1250	240	2500	71	12	32.0	32.0	4.6	3	10.37	14.43
	Bonded	490	240	425	71	12	13.2	13.2	0.7	5	4.57	5.54
	Bonded	490	240	425	71	12	13.2	13.2	12.6	5	8.16	9.90
	Bonded	490	240	425	71	12	13.2	13.2	13.9	4	6.26	7.60
	Single wythe	490	115	415	71	12	14.5	14.5	10.7	16	6.85	6.74
	Single wythe	490	115	425	71	12	11.0	11.0	4.4	3	4.49	4.42
Lumantarna et al. (2014)	Single wythe	228 (average)	112 (average)	264 (average)	78 (average)	between 12 and 18 (assumed average: 15)	8.5	7.5	1.2	5	3.31	3.22
	Single wythe						12.0	10.6	4.5	6	6.98	6.80
	Single wythe						15.7	13.8	5.5	6	10.70	10.42
	Single wythe						16.0	14.1	4.1	6	7.39	7.19
	Single wythe						16.3	14.4	8.6	6	6.59	6.42
	Single wythe						17.1	15.1	2.6	4	6.06	5.90
	Single wythe						21.1	18.6	5.9	6	12.05	11.73
	Single wythe						27.3	24.1	6.7	6	14.70	14.31
	Stack-bonded						8.5	7.5	5.0	5	6.19	5.48
	Stack-bonded						10.6	9.3	1.8	5	7.17	6.35
	Stack-bonded						10.6	9.3	12.5	5	9.35	8.28
	Stack-bonded						15.7	13.8	5.0	6	10.82	9.59
	Stack-bonded						15.7	13.8	23.2	6	16.78	14.87
	Stack-bonded						17.1	15.1	0.7	7	7.35	6.51
	Stack-bonded						17.1	15.1	2.5	6	10.63	9.42
	Stack-bonded						17.1	15.1	5.0	4	11.71	10.37
	Stack-bonded						17.1	15.1	5.9	4	11.52	10.21
	Stack-bonded						17.1	15.1	8.7	7	16.07	14.24
	Stack-bonded						17.1	15.1	23.2	5	16.68	14.78
	Stack-bonded						27.5	24.2	5.0	6	14.66	12.99
	Stack-bonded						38.2	33.7	12.5	5	30.79	27.28
	Stack-bonded						43.4	38.3	12.5	4	24.77	21.94

Annex E – Diagrams for Determining Assessment Values Based on Unit Tests Only

In Section 9.5, alternative assessment procedures in the absence of test results were presented. This included an approach for the case that only test results for unit compressive strength are available, combined with conservative expert estimation of mortar compressive strength. For this particular case, Fig. E-1 provides diagrams for determining characteristic values, partial factors, and assessment values for masonry compressive strength. The diagrams are constructed analogously to those in Section 9.3.

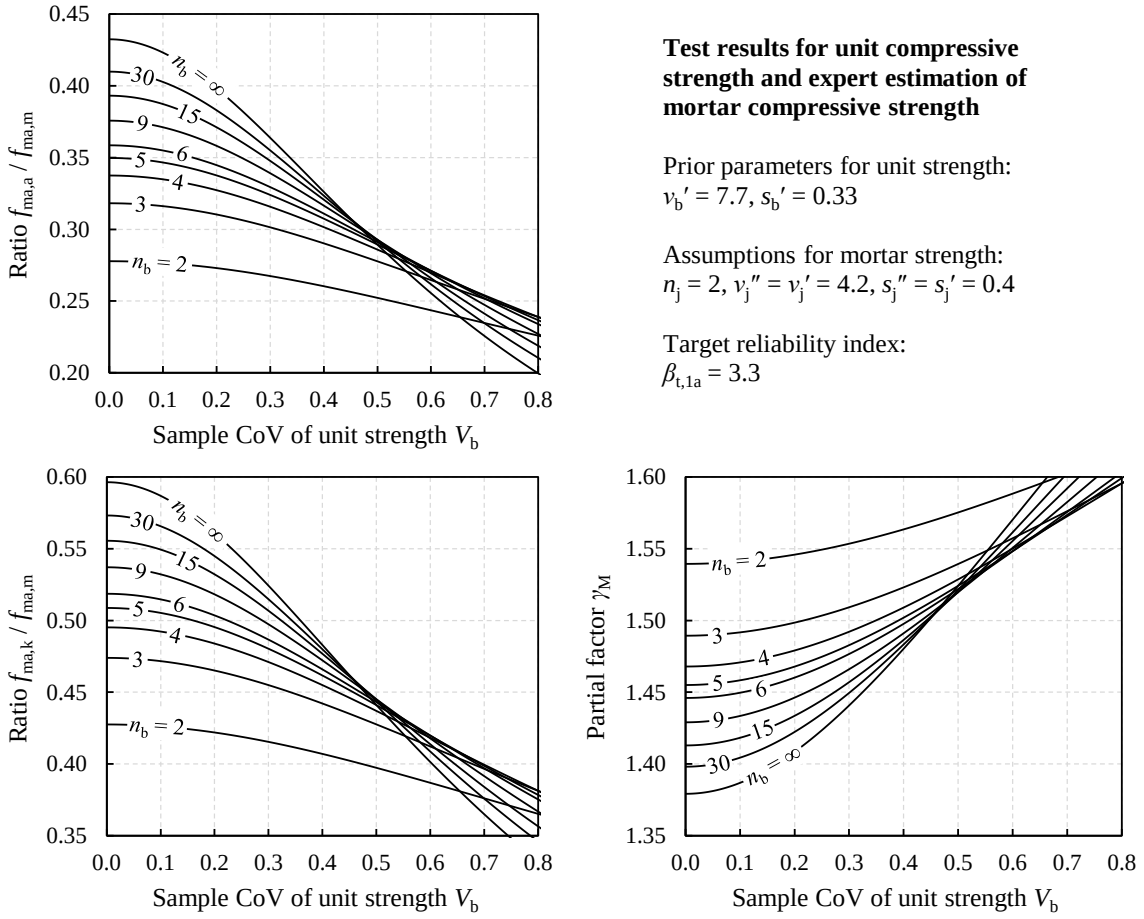

Fig. E-1 Diagrams for determining assessment values, characteristic values, and partial factors for masonry compressive strength (unit tests only)

Dissertationsreihe

Prof. Dr.-Ing. Carl-Alexander Graubner

Institut für Massivbau
Technische Universität Darmstadt

Heft 1: **Stefan Kempf (2001)**
Technische und wirtschaftliche Bewertung der Mindestbewehrungsregeln für Stahlbetonbauteile

Heft 2: **Katja Reiche (2001)**
Nachhaltigkeitsanalyse demontagegerechter Baukonstruktionen – Entwicklung eines Analysemodells für den Entwurf von Gebäuden

Heft 3: **Michael Six (2001)**
Sicherheitskonzept für nichtlineare Traglastverfahren im Betonbau

Heft 4: **Eric Simon (2002)**
Schubtragverhalten von Mauerwerk aus großformatigen Steinen

Heft 5: **Holger Schmidt (2003)**
Versagenswahrscheinlichkeit unbewehrter Wand-Decken-Verbindungen bei Gasexplosionen im Fertigteilbau

Heft 6: **Andreas Bachmann (2003)**
Ein wirklichkeitsnaher Ansatz der böenerregten Windlasten auf Hochhäuser in Frankfurt/Main

Heft 7: **Duy Tien Nguyen (2004)**
Rotationskapazität von biegebeanspruchten Stahlbetonbauteilen mit Schubrissbildung

Heft 8: **Gert Wolfgang Riegel (2004)**
Ein softwaregestütztes Berechnungsverfahren zur Prognose und Beurteilung der Nutzungskosten von Bürogebäuden

Heft 9: **Christian Glock (2004)**
Traglast unbewehrter Beton- und Mauerwerkswände – Nichtlineares Berechnungsmodell und konsistentes Bemessungskonzept für schlanke Wände unter Druckbeanspruchung

Heft 10: **Kati Herzog (2005)**
Lebenszykluskosten von Baukonstruktionen – Entwicklung eines Modells und einer Softwarekomponente zur ökonomischen Analyse und Nachhaltigkeitsbeurteilung von Gebäuden

Heft 11: **Andreas Garg (2006)**
Spannungszustände in Fahrbahnplatten weit gespannter Stahlverbundbrücken – Empfehlungen für die Herstellung der Ortbeton-Fahrbahnplatte von Talbrücken mit der Schalwagenmethode

Heft 12: **Tilo Proske (2007)**
Frischbetondruck bei Verwendung von Selbstverdichtendem Beton – Ein wirklichkeitsnahes Modell zur Bestimmung der Einwirkungen auf Schalung und Rüstung

Heft 13: **Simon Glowienka (2007)**
Zuverlässigkeit von großformatigem Mauerwerk – Probabilistische Analyse von großformatigem Mauerwerk aus Kalksandstein und Porenbeton mit Dünnbettvermörtelung

Heft 14: **Alexander Renner (2007)**
Energie- und Ökoeffizienz von Wohngebäuden – Entwicklung eines Verfahrens zur lebenszyklusorientierten Bewertung der Umweltwirkungen unter besonderer Berücksichtigung der Nutzungsphase

Heft 15: **Guido Hausmann (2007)**
Verformungsvorhersage vorgespannter Flachdecken unter Berücksichtigung der stochastischen Eigenschaften

Heft 16: **Stefan Daus (2007)**
Zuverlässigkeit des Klebeverbundes von nachträglich verstärkten Betonbauteilen – Sicherheitskonzept für den Verbundnachweis von oberflächig geklebter Bewehrung

Heft 17: **Thomas Kranzler (2008)**
Tragfähigkeit überwiegend horizontal beanspruchter Aussteifungsscheiben aus unbewehrtem Mauerwerk

Heft 18: **Lars Richter (2009)**
Tragfähigkeit nichttragender Wände aus Mauerwerk – Ein nichtlineares Berechnungsmodell und Bemessungsverfahren für biegebeanspruchte Innen- und Außenwände

Heft 19: **Markus Spengler (2010)**
Dynamik von Eisenbahnbrücken unter Hochgeschwindigkeitsverkehr – Entwicklung eines Antwortspektrums zur Erfassung der dynamischen Tragwerksreaktion

Heft 20: **Ngoc Linh Tran (2011)**
Berechnungsmodell zur vereinfachten Abschätzung des Ermüdungsverhaltens von Federplatten bei Fertigträgerbrücken

Heft 21: **Carmen Schneider (2011)**
Steuerung der Nachhaltigkeit im Planungs- und Realisierungsprozess von Büro- und Verwaltungsgebäuden – Entwicklung eines Instrumentes zur Vorbewertung und Optimierung der Nachhaltigkeitsqualität

Heft 22: **Frank Ritter (2011)**
Lebensdauer von Bauteilen und Bauelementen – Modellierung und praxisnahe Prognose

Heft 23: **Benjamin von Wolf-Zdekauer (2011)**
Energieeffizienz von Anlagensystemen zur Gebäudekühlung – Ein nutzenbezogener Bewertungsansatz

Heft 24: **Eric Brehm (2011)**
Reliability of Unreinforced Masonry Bracing Walls – Probabilistic Approach and Optimized Target Values

Heft 25: **Carolin Roth (2011)**
Lebenszyklusanalyse von Baukonstruktionen unter Nachhaltigkeitsgesichtspunkten – Ein Beitrag zur Beurteilung der Nachhaltigkeit von Gebäuden bei ungewissem Lebensweg

Heft 26: **Kay-Uwe Thorn (2013)**
Neuentwicklung eines Ladungsrückhaltesystems aus textilbewehrten Betonfertigteilen

Heft 27: **Andreas Greck (2013)**
Straßenbrücken mit einteiligem Verbundquerschnitt – Optimierung des Betonierablaufs der Fahrbahnplatte und Entwicklung eines Vorschlags zur vereinfachten globalen Systemberechnung beim Einsatz mehrerer Schalwagen

Heft 28: **Martin Heimann (2013)**
Tragwerkszuverlässigkeit hochbeanspruchter Druckglieder aus ultrahochfestem Beton

Heft 29: **Torsten Mielecke (2013)**
Nachhaltigkeitsbewertung von Einfamilienhäusern – Ein Beitrag zur Beurteilung und Optimierung der Nachhaltigkeitsqualität von kleinen Wohngebäuden

Heft 30: **Sebastian Pohl (2013)**
Nachhaltigkeit im Gebäudebetrieb – Ein Vorschlag zur Diversifizierung des bau- und immobilienwirtschaftlichen Zertifizierungsregimes in Deutschland

Heft 31: **Stefan Hainer (2015)**
Karbonatisierungsverhalten von Betonen unter Einbeziehung klinkerreduzierter Zusammensetzungen – Ein Modell zur Abschätzung des Karbonatisierungsfortschrittes

Heft 32: **Achim Knauff (2016)**
Heizwärmeerzeugung mit Solarthermie, Geothermie und Photovoltaik für Büro- und Verwaltungsgebäude

Heft 33: **Ulf Grziwa (2017)**
Zuverlässigkeit schlanker UHPC-Druckglieder mit räumlich streuenden Materialeigenschaften

Heft 34: **Björn Freund (2017)**
Frischbetondruck lotrechter, geneigter und gekrümmter Betonbauteile bei Verwendung von Betonen mit hoher Fließfähigkeit

Heft 35: **Gökhan Uysal (2017)**
Kostenrisiken von Industriebauten mit flexiblen Nutzungsszenarien – Ein Berechnungsmodell für die Investitionsentscheidung unter Verwendung probabilistischer Methoden

Heft 36: **Moien Rezvani (2017)**
Shrinkage model for concrete made of limestone-rich cements – An approach from cement paste to concrete

Heft 37: **Claudia Weißmann (2017)**
Effizienter Einsatz erneuerbarer Energieträger in vernetzten Wohnquartieren – Entwicklung eines simulationsbasierten Verfahrens zur energetischen, ökologischen und ökonomischen Bewertung

Heft 38: **Markus Blatt (2017)**
Beitrag zum Trag- und Verformungsverhalten von Stahlbetondeckenknoten

Heft 39: **Michael Schmitt (2017)**
Tragfähigkeit ausfachender Mauerwerkswände unter Berücksichtigung der verformungsbasierten Membranwirkung

Heft 40: **Valentin Förster (2018)**
Tragfähigkeit unbewehrter Beton- und Mauerwerksdruckglieder bei zweiachsig exzentrischer Beanspruchung

Heft 41: **Ngoc Linh Tran (2018), Habilitationsschrift**
Shear strength of slender reinforced concrete members without shear reinforcement – A mechanical model

Heft 42: **Jaroslav Kohoutek (2018)**
Zuverlässigkeit integraler Straßenbrücken in Massivbauweise

Heft 43: **Jochen Zeier (2019)**
Thermisch getrennte Stützen-Decken-Anschlüsse im Stahlbetonbau – Ein Modell zum Tragverhalten bei großen Fugendicken

Heft 44: **Katharina Fritz (2019)**
Qualifizierte Beurteilung der sektoralen Ressourceninanspruchnahme im deutschen Bauwesen

Heft 45: **Patrick Wörner (2020)**
Einfluss des Nutzerverhaltens auf den Stromverbrauch in Wohngebäuden – Entwicklung eines komplexen Simulationsmodells für energetische Analysen

Heft 46: **Martina Lohmeier (2020)**
Nachhaltigkeitsvergleich von Projektvarianten für Außerortsstraßen − Ein Vorschlag für den Abwägungs- und Entscheidungsprozess in der Vorplanung

Heft 47: **Larissa Krieger (2020)**
Tragverhalten textilbewehrter Fertigteilplatten aus hochfestem Carbonbeton – Einfluss der Ausbreitung konzentrierter Einzellasten auf die Biegetragfähigkeit

Heft 48: **Sarah Steiner (2020)**
Carbonation of concrete made of limestone-rich cement − CO_2 diffusivity and alteration of the hydrate phases

Heft 49: **Redouan El Ghadioui (2020)**
Bemessung carbonbewehrter Betonbauteile unter besonderer Betrachtung des Gebrauchszustandes – Entwicklung eines Modells zur wirklichkeitsnahen Verformungsberechnung

Heft 50: **Sebastian Hofmann (2021)**
Rissentwicklung in Betonbauteilen mit Basaltfaserkunststoffbewehrung bei wirklichkeitsnaher Betrachtung des Verbundverhaltens – Ein Modell zur Berechnung der Rissbreite im Grenzzustand der Gebrauchstauglichkeit

Heft 51: **Dominik Müller (2022)**
Probabilistic Assessment of Existing Masonry Structures – The Influence of Spatially Variable Material Properties and a Bayesian Method for Determining Structure-Specific Partial Factors

TECHNISCHE UNIVERSITÄT DARMSTADT
INSTITUT FÜR MASSIVBAU
PROF. DR.-ING. CARL-ALEXANDER GRAUBNER

Dominik Müller

Probabilistic Assessment of Existing Masonry Structures

For the assessment of existing masonry structures, a safety concept is required that takes into account the differences compared to the design of new masonry structures, such as the possibility of material testing, high variability of material properties, and a potentially reduced target reliability level. Therefore, a method for determining characteristic values, structure-specific partial factors, and assessment values for the compressive strength of existing masonry is developed.

For this purpose, the influence of spatially variable material properties within a masonry wall is investigated first: Based on experiments on clay brick masonry, a finite element model is developed and then used in Monte Carlo simulations for quantifying the effect of spatial material variability on the probability distribution of the load-bearing capacity of masonry walls under compression. The statistical uncertainty resulting from small sample sizes in material testing is considered through Bayesian statistical procedures. Prior distributions for unit, mortar, and masonry compressive strength are modelled utilising a test database for existing solid clay brick masonry. Finally, the findings are implemented in a practice-oriented method for determining assessment values of masonry compressive strength, which is validated through reliability analyses.

ISBN 978-3-942886-28-4